TABLE OF CONTENTS

Saturday, September 14, 2019

Saturday, September 14, 2019

Acoustics of Wind Instruments and Organs - Pipe Organ 25 year Culmination

Saturday, September 14, 2019

Acoustics of Wind Instruments and Organs: Flutes

Saturday, September 14, 2019

Directivity of Musical Instruments: String ensembles

Saturday, September 14, 2019

Directivity of Musical Instruments: Sound fields

Saturday, September 14, 2019

Posters

Saturday, September 14, 2019

Design & Playing: Fingering & articulation

Saturday, September 14, 2019

Design & Playing: Room acoustics

Saturday, September 14, 2019

Acoustics of Wind Instruments and Organs: Pipe organs

Saturday, September 14, 2019

Acoustics of Wind Instruments and Organs: Clarinet and single reeds

Sunday, September 15, 2019

Sunday, September 15, 2019

Strings: Non-western instruments

Sunday, September 15, 2019

Strings: Guitar, modeling, and modes

Sunday, September 15, 2019

Virtual Prototyping of Musical Instruments: Design and player control

Sunday, September 15, 2019

Virtual Prototyping of Musical Instruments: Numerical exploration

Sunday, September 15, 2019

Acoustics of Wind Instruments and Organs: Numerical improvements

Monday, September 16, 2019

Monday, September 16, 2019

Reeds: Clarinet

Monday, September 16, 2019

Live Stream: Reeds

Monday, September 16, 2019

Mixed

Monday, September 16, 2019

Modelling: Modelling techniques

Monday, September 16, 2019

Modelling: Modelling strings

Monday, September 16, 2019

Virtual Prototyping of Musical Instruments: Virtual instruments and data bases

Monday, September 16, 2019

Virtual Prototyping of Musical Instruments: Instrument design

Monday, September 16, 2019

Instrument Building

Monday, September 16, 2019

Timbre and Perception

Monday, September 16, 2019

Live Stream: Timbre and Perception

PROCEEDINGS of ISMA 2019
International Symposium on Music Acoustics

13 - 17 September 2019 in Detmold, Germany

25 years applied pipe organ research at Fraunhofer IBP in Stuttgart

Judit ANGSTER[(1)], Péter RUCZ[(2)], András MIKLÓS[(1)]

[(1)] Fraunhofer Institute for Building Physics, Germany, judit.angster@ibp.fraunhofer.de

[(2)] Budapest University of Technology and Economics, Hungary

Abstract

Throughout the world, musical instruments are deeply rooted in cultural traditions. They are part of our cultural heritage, and their preservation and further development deserves our utmost attention. For many years, the Fraunhofer Institute for Building Physics IBP has been engaged in the research of European musical instruments, the pipe organ in particular. To preserve its sound, to give support in building instruments as well as to contribute to the further development by integrating modern technologies are the focus of the joint research with other research institutions and a multitude of European organ building enterprises.

In 25 years, 9 common European and several other research projects were carried out. Some examples of the topics will be mentioned like development of 1) different kinds of new wind systems, methods and software for the design, 2) design methods, tools and software with applying computer simulations for flue and reed organ pipes, 3) innovative swell shutters, 4) design methods and comprehensive tools for matching the instrument on the acoustics of the room. The procedure of research, way of communication with instrument builders, the method of demonstration and dissemination of the research results will be discussed.

Keywords: Music, Pipe organ, acoustics

1 INTRODUCTION

The Research Group of Musical Acoustics of the Fraunhofer IBP in Stuttgart, Germany deals mostly with pipe organ research [1–6]. The manufacturing of pipe organs is a traditional European industrial sector, which should be preserved. Nevertheless, innovative design methods and technologies can be applied in the daily practice, without endangering the valuable traditions. As Judit Angster comes from a well-known organ builder factory “Josef Angster and Son” [7, 8], she decided to help the small organ builder enterprises in Europe to overcome their practical problems. Organ builders are artisans, who do not have the capacity to consider and treat an instrument as a complex physical system to be able to surmount special problems. Thus the main goal of the research and development work at the IBP has been to carry out applied research so that the results can directly be used in practice. Nonetheless, fundamental research also had to be carried out to be able to focus then on the application.

2 WAY OF COMMUNICATION WITH INSTRUMENT BUILDERS

The first challenge when trying to set up a research project in cooperation with instrument builders is the “translation” of the practical problems to the “language” of scientific research. The instrument makers explain their problems from the viewpoint of the practical work. Acoustical phenomena will be described by artistic expressions. The issues have to be formulated in a special scientific way so that the answers to the questions raised can be given by means of scientific research. This is always a pretty hard mission to accomplish in a project application. Furthermore, one has to be careful during the implementation of the work so that the instrument maker partners can understand how research has to be done. Otherwise the project partners—who generally support the work—lose the sense of the participation.

Generally it is “easy” to solve physical problems by means, as an example, of solving differential equations. Nevertheless you never can report for an instrument maker about such theoretical solutions. Hence the next step is to translate the research results to the language of the craftsmen. Doing so by meetings, organ builders have been amazed about how physics can be so simple and understandable. That's why it became possible to carry out several research projects with numerous European organ builder firms [9].

There appears a disadvantage by such applied research projects. The applicable results are owned by the enterprises and so they should not be published for several years after finishing the work. For this reason the authors of the present paper plan to summarize the most important outcomes of earlier confidential European projects in a book. Nevertheless, the dissemination of knowledge has been carried out as soon as possible in the form of workshops organized for organ builder enterprises. These workshops have been the only possibility internationally for organ builders to learn about the acoustics of the organ and getting instructed for the application of research results, design methods, and software.

3 EXAMPLES OF RESEARCH TOPICS

3.1 Scaling of labial organ pipes

In organ building, pipe scaling is a complicated process. All geometrical dimensions of a labial pipe, such as diameter, flue width, cut-up etc. (Figure 1), have to be determined so that its sound fulfills the requirements defined by the organ builder: each pipe stop (consists of about 60 pipes with the same sound character, e.g. “Diapason”, “Chimney flute”, “Salicional”) has a characteristic timbre that should be balanced and clearly recognizable over the whole rank from low to high notes. Sound at the audience position, however, is strongly influenced by room acoustics. When planning an organ, the organ builder judges the specific room properties and determines all pipe diameters needed for an adequate sound power. Then, a uniform volume and sound distribution is hopefully achieved when playing the organ. If a room amplifies low and dampens high frequencies, for example, the diameters of low pipes and thus their sound power have to be decreased and those of high pipes have to be increased in order to balance the influence of the room [10, 11].

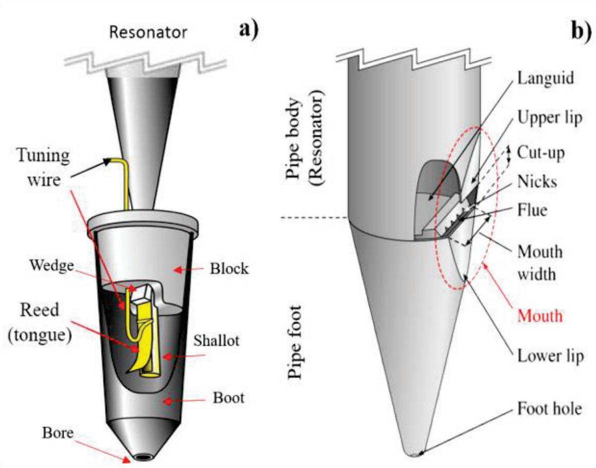

Figure 1. The parts of a reed (lingual) **a)** and a flue (labial) **b)** organ pipe.

3.1.1 Scaling of chimney pipes

Chimney pipes are semi-open flue organ pipes whose resonator consists of two main parts: a straight cylindrical main part and a shorter and thinner chimney attached to its top (Figure 2a). The length and the diameter of the chimney may vary, which allows the organ builder to adjust the timbre of the pipe. Chimney pipes in baroque-style pipe organs should have a sound rich in the pure fifth (third harmonic), while romantic-style instruments require more major third (fifth harmonic) in the sound. To be able to fulfill these requirements, special design rules are needed for determining the dimensions of the pipes so that the desired character of the sound can be achieved. The process of determining the appropriate geometrical dimensions of organ pipes with the purpose of attaining a predefined timbre is referred to as “sound design.”

In the study initiated by the organ builders and performed by the authors of this article, a novel methodology for the sound design of chimney pipes was established and implemented in a software tool. Acoustic measurements have been carried out in the anechoic chamber of the Fraunhofer IBP in Stuttgart (Figure 3).

The idea of the proposed sound design approach is to tune the eigenfrequencies of the resonator such that they become coincident with the frequencies of predefined harmonic partials of the sound [12, 13]. The eigenfrequencies of the resonator have been specified by means of a transfer function measurement as shown in Figure 2b. When a harmonic partial overlaps with an eigenfrequency, the corresponding eigenmode gets excited very efficiently and hence the amplification of the harmonic can be expected. By computer simulation, the so-called input admittance (i.e., the ratio of the acoustic volume velocity and the acoustic pressure at the mouth of the pipe) is calculated [12]. The peaks of the input admittance correspond to the peaks of natural resonances.

The performance of the developed software tool was tested by building experimental chimney pipes with the dimensions calculated by the software and by comparing their measured sound spectra with the results of the computer simulations. The measured steady state sound spectra and the calculated input admittances are displayed in Figure 4a–c. In each diagram, the sound pressure spectrum measured at the pipe mouth and the calculated input admittance are displayed by the black and red lines, respectively. The broad peaks in the sound spectra correspond to the natural acoustical resonances of the pipe, while the sharp peaks are the harmonic partials of the pipe sound. The design method is successful when one of the peaks of the red curves in Figure 4b–c matches the partial to be enhanced.

Figure 4a shows the sound spectrum of the reference pipe (a chimney pipe with the usual dimensions) with the amplitude of the first seven harmonics, indicated by the numbers on the blue background. The reference pipe has a strong fundamental component in its sound while the higher harmonics are very weak. Figure 4b and c display the results of the chimney pipes optimized for the third and fifth harmonics, respectively. The numbers on the green background indicate the amplification of the targeted harmonic partial compared with the levels measured in the case of the reference pipe. The numbers on the yellow background show the same changes in the levels of the other harmonics. As can be seen, the optimized resonators can enhance the targeted harmonics by more than 15 dB while keeping the fundamental constant. This amplification can be considered substantial if one takes into account that the experimental pipes only differed in the geometry of their resonators. The developed software tool is being used in the practical work of the organ builder partners of the project [14].

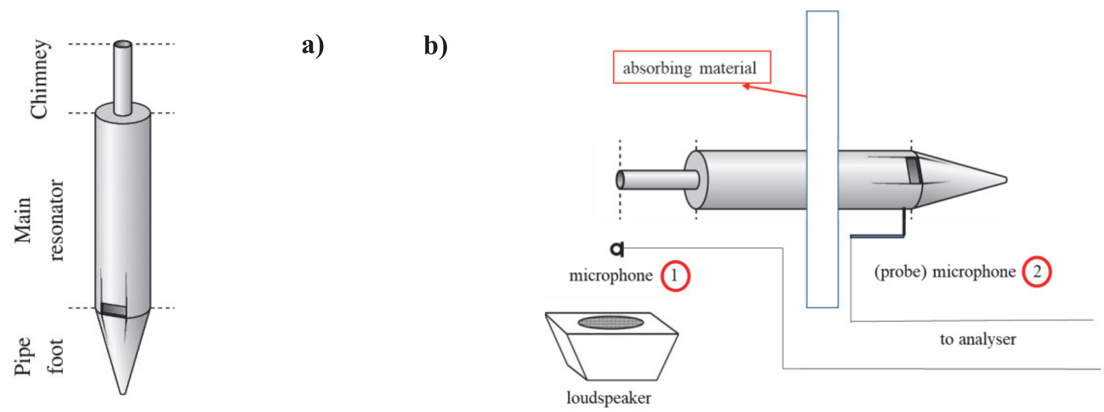

Figure 2. a) Sketch of a chimney organ pipe. b) Measurement of the transfer function: the pipe resonator was excited by a loudspeaker; (probe) microphone 2 is in the resonator against the pipe mouth

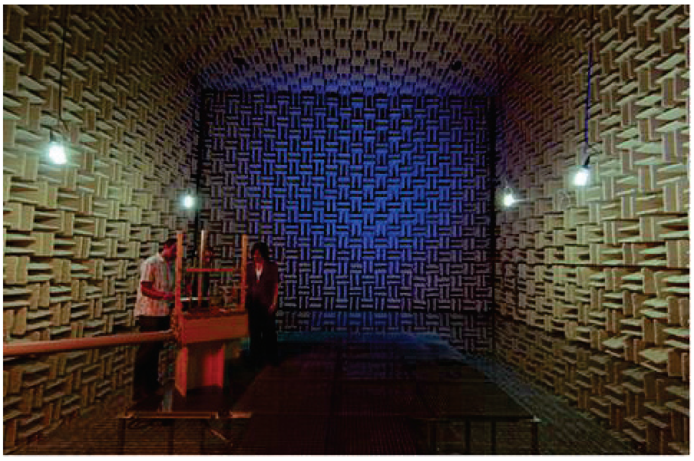

Figure 3. Acoustic measurements in the anechoic room of the Fraunhofer IBP in Stuttgart

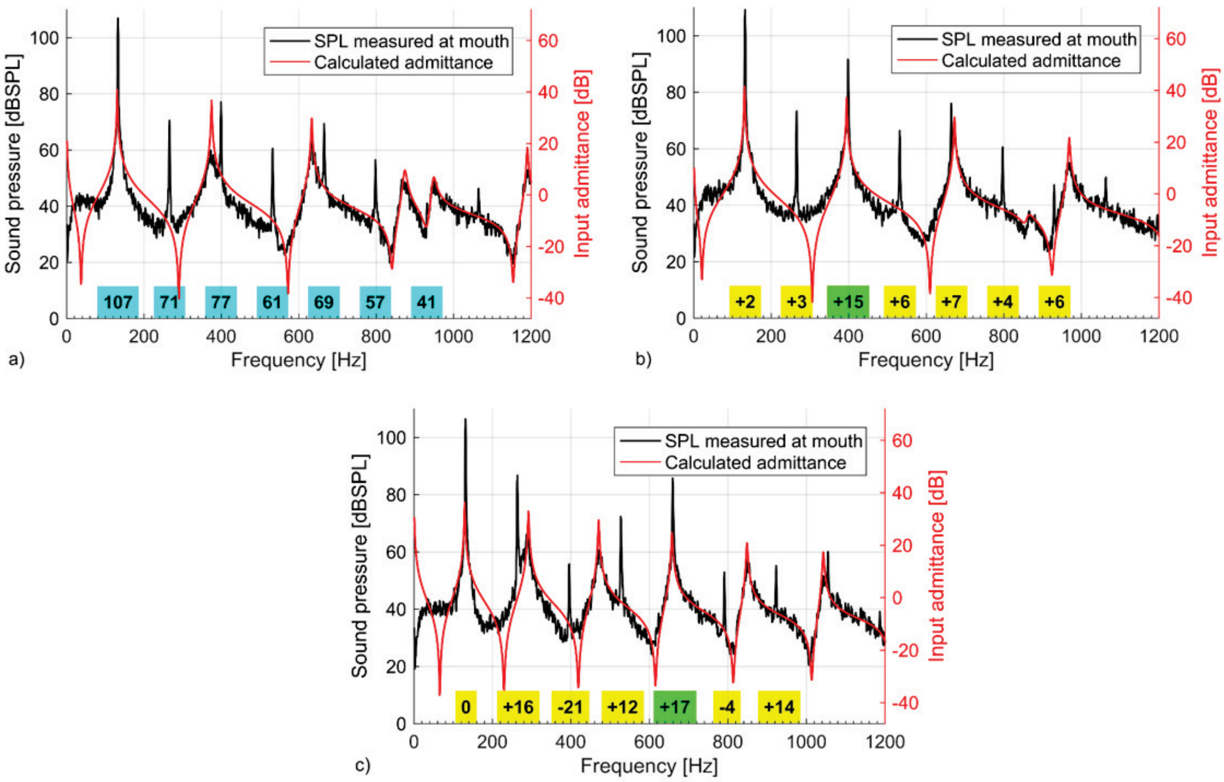

Figure 4. **a–c)** Measured spectra (black) and calculated input admittance (red) of the experimental chimney pipes. **a)** Reference chimney pipe design. Numbers on the blue background are the amplitudes of the first seven harmonic partials. **b)** Optimized design enhancing the third harmonic (pure fifth) by 15 dB. **c)** Optimized design enhancing the fifth (major third) by 17 dB. Numbers on the green and yellow backgrounds show the relative levels of the harmonics compared with the reference pipe.

3.1.2 Scaling of wooden pipes

Research partners in the European research projects wanted to build the large wooden pedal pipes narrower than so far without deteriorating the character of the sound. Frequently, there is only little space for these pipes. Moreover, in the case of narrower pipes, the wind chest could be built in shorter form and thus in a more cost-efficient manner. Wooden pipes always have a rectangular cross section. Their mouth widths (= pipe widths) are equal to those of the reference pipes (circular metal pipes with the same pitch and similar timbre). Their depths are traditionally calculated such that the rectangular cross section $A_{w,trad}$ equals the circular cross section A_{ref} of the reference pipes (Figure 5a). As mentioned before, the widths become too large sometimes so that the total width of a whole pipe rank does not fit into the available space within the organ. Therefore a new calculation method was developed. Here the organ builder first scales down the widths until the pipe rank fits into the available space. In order to avoid an essential change of the timbre, their depths are then calculated, such that instead of the cross sections the energy losses or quality factors Q (Figure 5b) of the traditional and new wooden pipes become equal [10, 14].

The new calculation and design method was tested by building and measuring experimental pipes, proving the applicability of the proposed method. Thus, it is now possible to build narrower wooden flue pipes which maintain the sound quality of the pipes with standard dimensions.

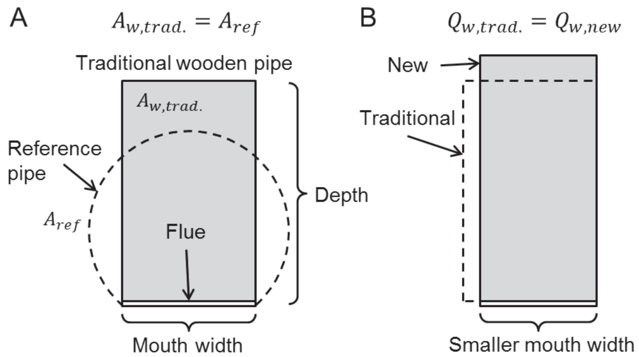

Figure 5. A: Traditional scaling of wooden pipes with equal cross sections, B: innovative scaling of wooden pipes with equal losses (quality factors).

3.2 Scaling of reed (lingual) organ pipes

The sound generation mechanism of reed organ pipes is a complex physical phenomenon. The reed pipe consists of three main parts: the boot, the block with the shallot and the reed, and the resonator, as it is depicted in Figure 1a. When the pipe is played air flows through the bore and the reed is forced into motion by the pressure forces acting on it. Under playing conditions the motion becomes periodic by means of an aerodynamic-acoustic feedback loop [15].

The pitch of the pipe is determined by the coupling of two oscillating systems, the vibrating reed and the acoustic resonator-shallot system [16]. The strength of the coupling varies in a wide range for different pipe ranks. Trumpet pipes are characterized by strong interaction between the resonator and the reed, whereas in case of stops such as the Vox humana the coupling is weak typically. In both cases, the resonator has a great effect on the timbre of the pipe. In case of weak coupling the resonator acts as a filter, which can reinforce or suppress certain harmonic partials in the pipe sound.

Discussions with organ builder partners in the framework of a European project [17] have shown that there are no common rules for the design of reed pipe resonators. Also measurements prove that design rules of thumb applied currently in practice do not fully exploit the capabilities of the resonator. Thus, the aim of our research has been to achieve an optimal scaling of reed pipe resonators, which can lead to cost and effort reduction in practice. Therefore a methodology has been committed, which combines a one-dimensional analytical model with three-dimensional finite element simulation in order to predict the acoustic behavior of reed pipe resonators. The proposed method is validated by means of comparisons with measurements and it is shown that the technique is capable of calculating the eigenfrequencies of the resonator accurately [18].

As an example the scaling method of reed pipes is presented on a "Vox humana" pipe, which imitates the human voice. This is a so-called beating lingual pipe, as by sounding the reed (tongue) beats periodically on the shallot. The resonator consists of three sections (Figure 6a):

1. the shallot continues in a straight neck, which has a length of 2/5 of that of the complete resonator,
2. a flaring section, nearly as long as the neck, where the diameter increases greatly,
3. a tapering section, which is open at the top.

Figure 6b shows the setup of the transfer function measurement of the pipe resonator. The simulation arrangement and the waveforms at the first four eigenfrequencies of the Vox humana resonator are displayed in Figure 7a and b, consequently. The comparison of the measured transfer function and the calculated input admittance function using analytical and FEM impedance models of a Vox humana pipe are shown in Figure 8. As seen, by applying the FEM for the simulation of the radiation impedance, the model is optimized and the calculated eigenfrequencies match the measured frequencies well.

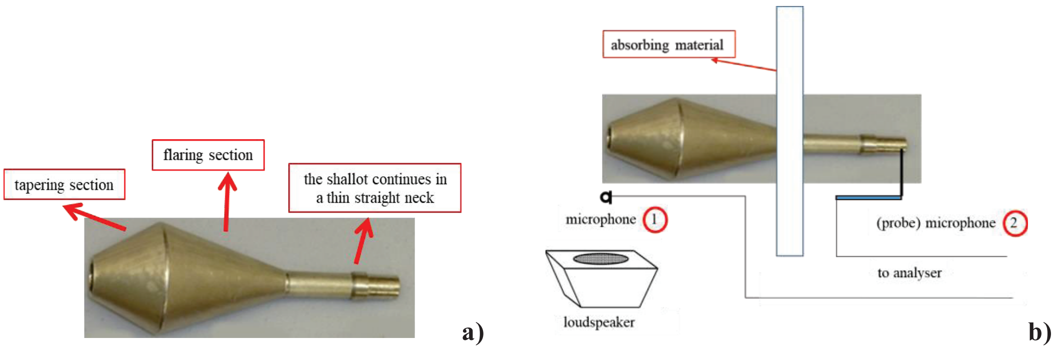

Figure 6. **a)** The resonator of a Vox humana pipe **b)** Measurement of the transfer function: the pipe resonator was excited by a loudspeaker with a sweep signal. Microphone 1 is at the end of resonator against the loudspeaker, (probe) microphone 2 is in the neck [18]

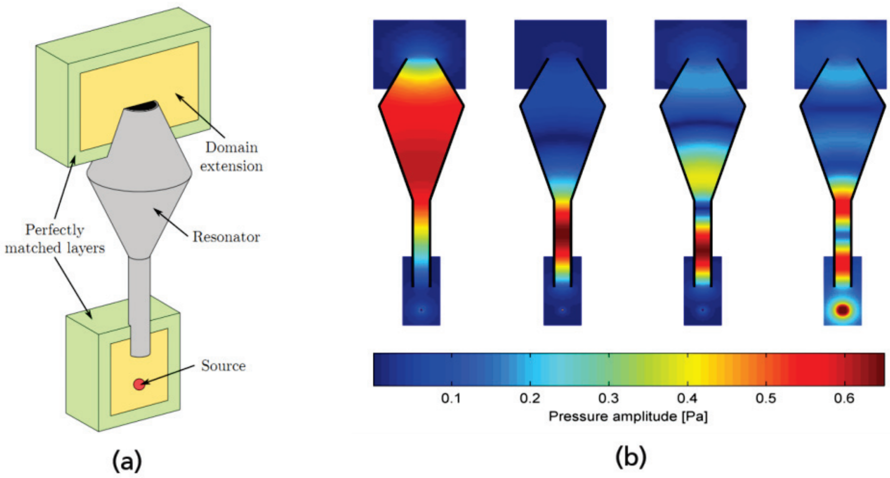

Figure 7. Simulation arrangement **(a)** and the first four eigenmodes **(b)** of the Vox humana resonator

Based on the measurement and simulation results a software tool has been developed for the design of reed pipes. In the following it is demonstrated how organ builders can use this method for dimensioning reed pipes. The main window of the software and the most important controls are shown in Figure 9. The resonator can be constructed individually as shown in the figure. In our example Figure 10a shows that by using the original resonator dimensions the strongest partial is not the third, which would be desired. By changing the resonator dimensions (the conical part near to the open end has been elongated) the frequency of the 1st natural resonance is tuned to the 3rd partial of the sound (Figure 10b).

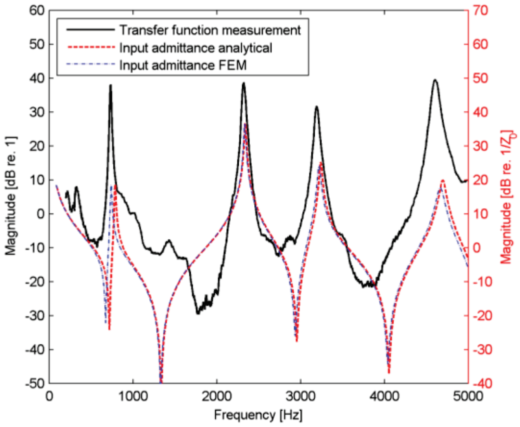

Figure 8. The measured transfer function and the calculated input admittance of a Vox humana resonator

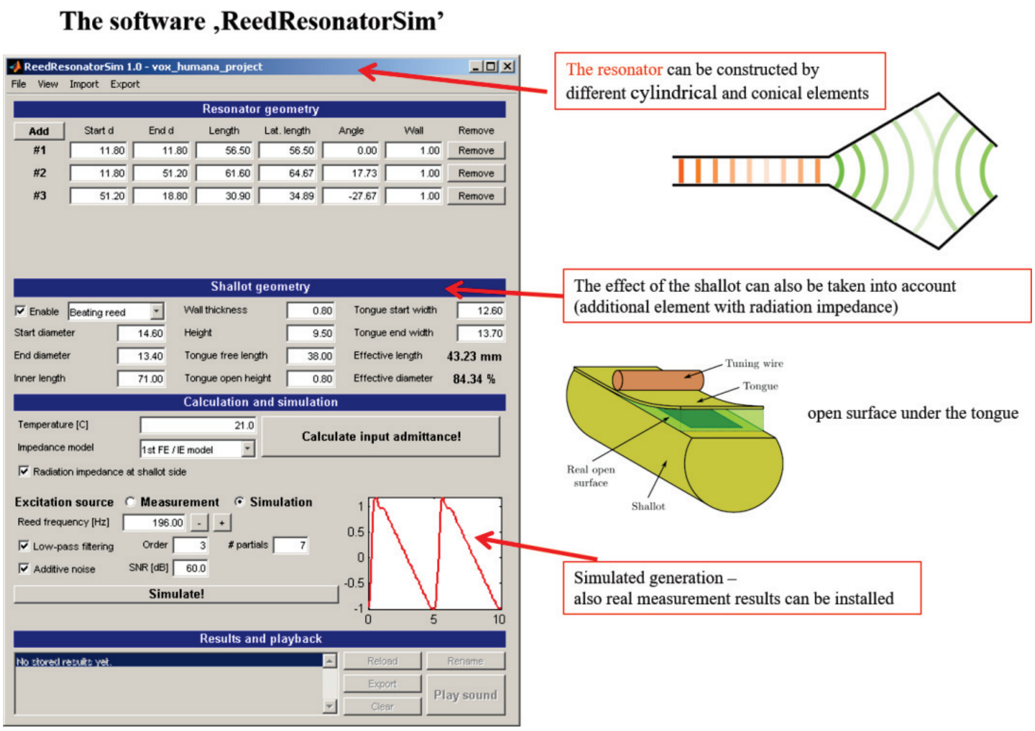

Figure 9. The main window of the software tool and the most important controls. The function shows the simulated excitation, which was adjusted on the basis of laser vibrometer and probe microphone measurements to make them as realistic as possible [18].

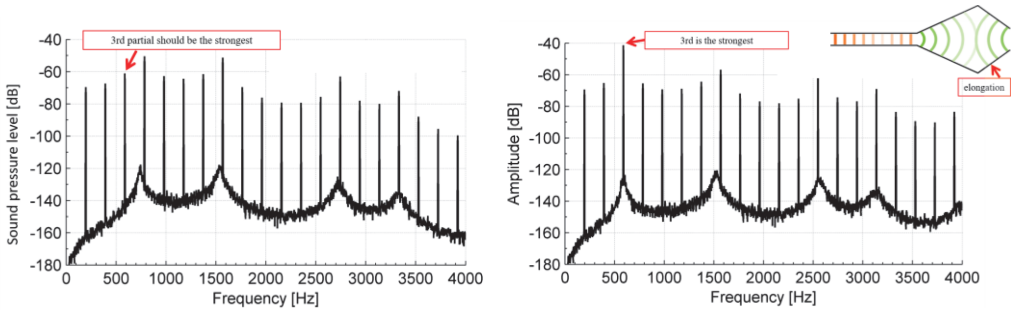

Figure 10. Simulation of the steady state sound spectrum of a Vox humana pipe **a)** with the original resonator dimensions **b)** with optimized resonator dimensions [18]

4 RESEARCH ORGAN AT THE FRAUNHOFER IBP

In the year 2011 a research pipe organ was built at the Fraunhofer IBP by the Werkstätte für Orgelbau Mühleisen, Leonberg for the scientists (Figure 11a). The pipe organ was financed by the state of Baden-Württemberg. Its transparent and unique scope of design allows the demonstration of research results, the investigation of technical and acoustical problems in organ building as well as the audible testing of ideas on organ sound. This organ contributes to further develop our knowledge on sound; it also allows new connections of art and science, of music and physics [19].

In this context it is now discussed why the research organ was necessary, which research results can be demonstrated, what are the specific characteristics of the research organ, and what significance does this instrument have for future research.

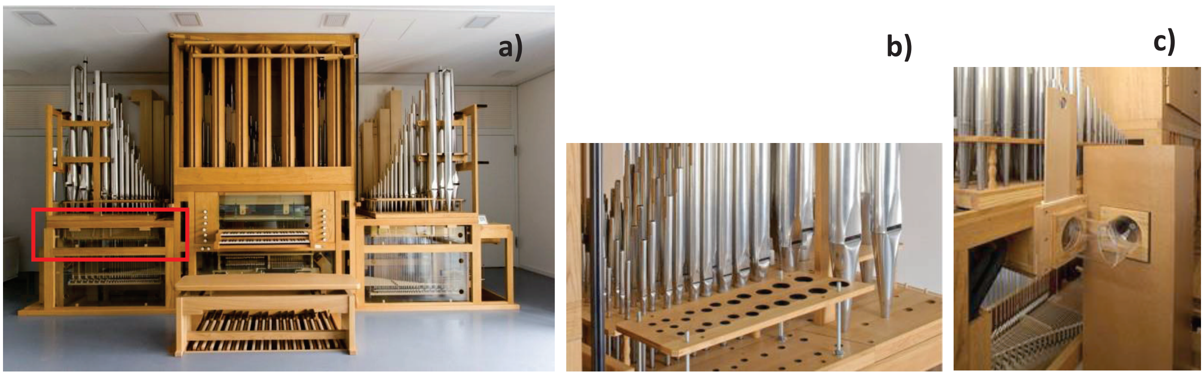

Figure 11: **a)** Research organ of the Fraunhofer IBP (built in 2011 by Werkstätte für Orgelbau Mühleisen, Leonberg). The red frame denotes the exchangeable wind chest. **b)** To test newly designed stops a blind slider is available with a pipe rack, which can be adjusted in height **c)** the outlet valve mounted as part of the innovative wind system.

4.1 Why a research organ?

The research organ serves as a demonstrator for numerous research results as well as it allows the investigation of problems on technology and sound directly at a real instrument. Moreover, it simplifies the dissemination of the knowledge in the field of organ research. In former times, new developments had to be tested at a church organ. It was difficult to obtain the permission for these measurements. In the majority of cases, first of all the instrument had to be modified by an organ builder. For example, several holes have to be drilled for the different detectors necessary for the measurements. Most measurements could only be carried out at night, since the ambient noise would have been too loud in the church during the day. These business trips always involved intricacies, as unexpected problems frequently occurred.

The details of the design of this pipe organ can only be partially described in this publication. They are gained from the results of many projects conducted by organ researchers at the IBP during the last 25 years [20]. The symbiosis of scientific and technological knowledge and instrument building broadens our knowledge of sound and creates new connections of physics and music, science and art.

4.2 Specific characteristics

- The pipe organ is transparent to the greatest possible extent to make visible and demonstrate the functioning of the mechanics.
- One wind chest of a division can be exchanged to allow the testing of new wind chests, valve constructions as well as pipe layouts (Figure 11a).
- The keyboard is prepared for the mounting contacts for electric controllable valves.
- The toe boards can be exchanged for experiments.
- To test new stops a blind slider is available with a pipe rack, whose height can be adjusted (Figure 11b).
- There are some blind grooves to analyze the effect of the wind flow, of the resonances in the grooves as well as of different outlet holes on the pipe sound.
- Two different wind systems are available: a traditional one and an innovative design with outlet valve system (Figure 11c) [21, 22]. The system can be switched from the traditional to the innovative one.
- Blowers are controlled by a frequency converter for continuous adjustment of the wind pressure.
- Removable swell shutters, developed by the IBP, are mounted in the swell organ (see details in Section 4.3).
- To visualize the air jet motions of flue pipes a groove is equipped for CO_2 connection.
- The motion of a beating as well as a free reed can be visualized by means of a stroboscope installed.
- Special wind chests are used for experiments as well as demonstration. Especially, a transparent wind chest with tone valves is operable either manually or by keyboard. A wind chest with cone valves and with membrane valves is also available.
- Besides the demonstration of different valve systems investigations of different wind chests can be conducted. They can also be used for the demonstration of innovative pipes.
- The metal pedal pipes are made of organ metal (tin-lead alloy) on the left side and of zinc on the right side of the instrument. Thereby it can be directly tested whether an influence of the material on the pipe sound can be heard.

4.3 Examples of innovations applied in the research organ

Several results of the pipe organ research of the IBP are applied in the research organ. For example, the design method, the construction and the control mechanism of the outlet valves of the innovative new wind systems have been developed in the course of two subsequent EU research projects [21, 22]. The dimensions of large wooden pedal pipes, furthermore both the chimney and reed pipes have been designed and optimized by means of software developed at the Fraunhofer IBP (Figure 12a and b). The application of different materials (lead-tin alloy vs. zinc) for the metal pedal pipes is based on the results of an earlier research project commissioned by the Grillo-Werke Aktiengesellschaft [23, 24].

Besides the innovations gained from EU-supported research other innovations have also been applied. For example, innovative removable swell shutters developed in cooperation with the organ building company of Mühleisen in Leonberg are mounted in the swell organ allowing better sound radiation and higher dynamics of organ music. The traditional (a) and innovative (b) swell shutters are depicted in Figure 13. The swell organ front is removable, therefore other swell shutter constructions can also be tested [25].

This swell shutter construction has been developed earlier in the course of a bilateral cooperation between IBP and Mühleisen. Models of the traditional and innovative swell shutter constructions were investigated in the anechoic room of the IBP. A loudspeaker with pink noise served as a sound source. The directional sound radiation characteristics of the two constructions are represented at 2500 Hz in Figures 14a and b. The traditional swell shutters radiate the sound asymmetrically. The innovative swell shutters have an acoustically more favorable symmetrical sound radiation.

a)

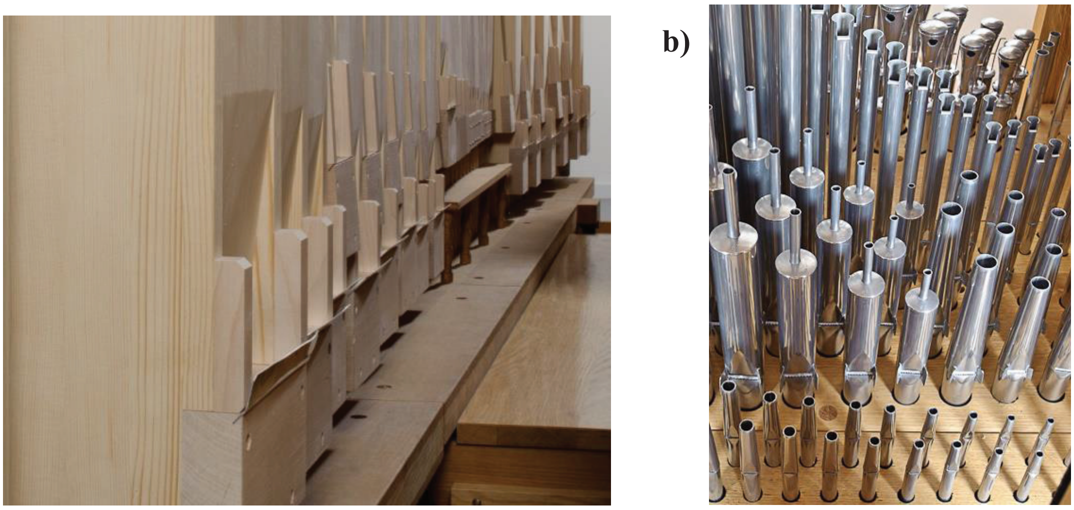

Figure 12: The dimensions and sound of wooden pipes **a)** and of chimney pipes **b)** have been optimized by means of software developed at the IBP.

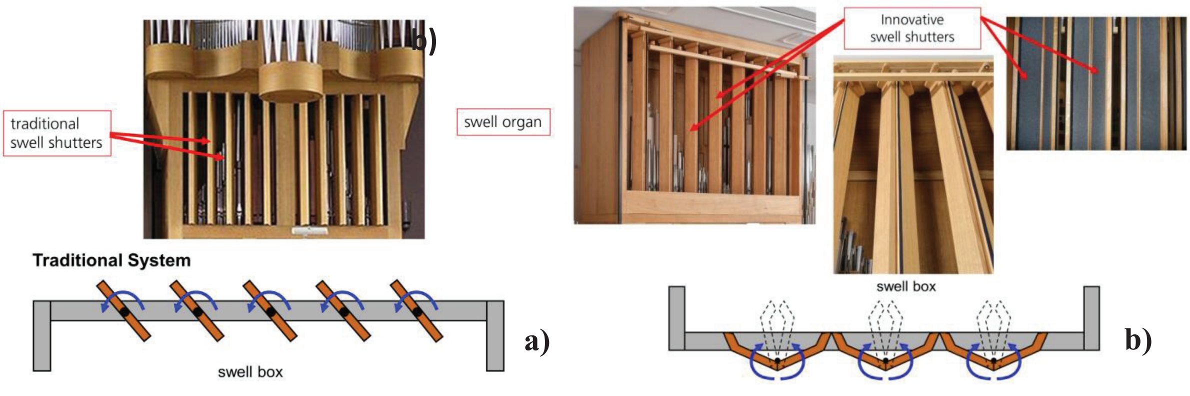

Figure 13: Traditional (a) and innovative (b) swell shutters. The innovative, removable swell shutters are mounted in the swell organ (b).

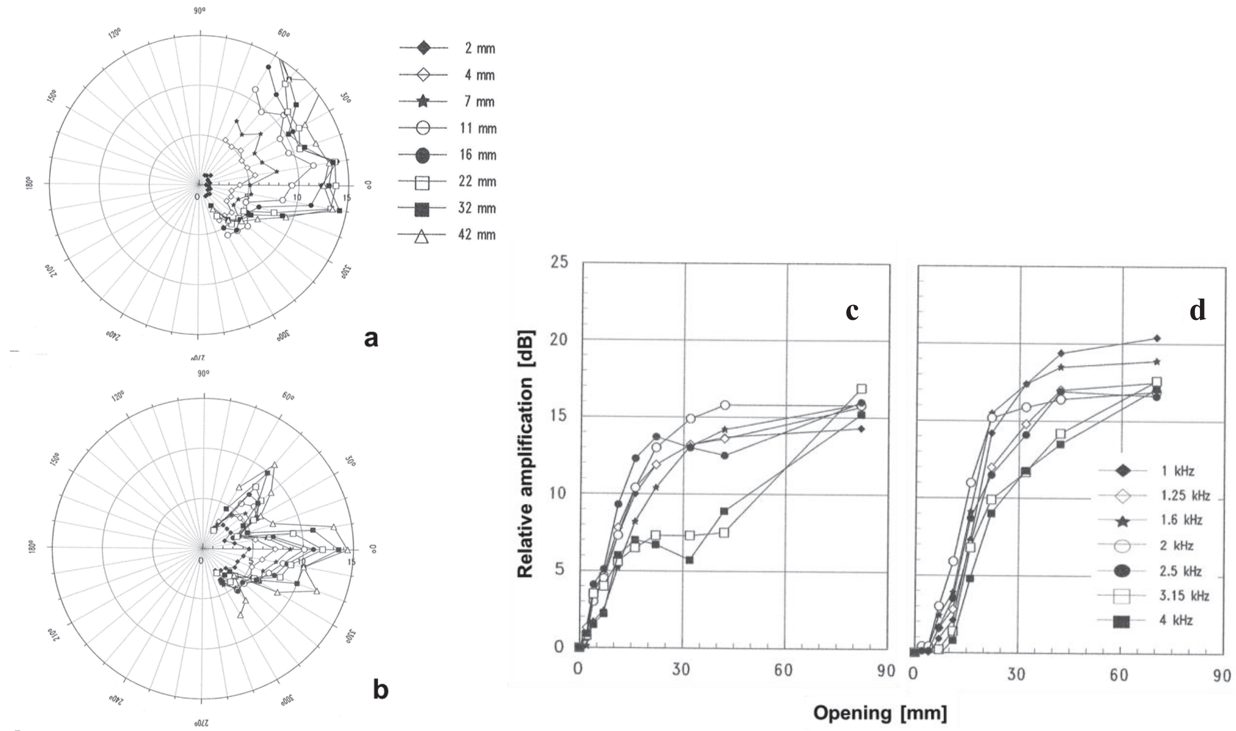

Figure 14: Directional sound radiation characteristics of the traditional (a) and innovative (b) swell shutters as a function of the opening at 2500 Hz. Sound amplification of the traditional (c) and innovative (d) swell shutters at 0 degree in different frequency ranges.

In Figure 14c the relative sound amplification referred to the closed situation of the traditional and innovative swell shutters at 0 degree in different frequency ranges is shown. The innovative construction (Figure 14d) achieves a significantly (by approx. 5 dB) higher relative sound amplification. In addition, the dynamics can be influenced in smaller steps (especially at the beginning of the opening) than with the traditional swell shutters.

5 DISSEMINATION OF RESEARCH RESULTS

The dissemination of research results is a very important task of the Fraunhofer IBP. The developed software and the results of the European research projects are primarily passed on to the organ building companies participating in the projects in form of project meetings and training. After a few years, however, the right to use these results is conferred by the partners and thus can be disseminated to other organ experts by intensive courses and workshops lasting several days. These events are being organized by using the research organ. Organ concerts are performed as well as concerts with organ and other musical instruments accompanied by generally understandable explanations of the physics of the presented musical instruments.

6 SUMMARY AND OUTLOOK

It has been shown, how the knowledge of the acoustics of the pipe organ is being adopted in applied research for supporting organ builders. Computer simulation optimized and verified by comparison with measurement results can be used for supporting organ builder companies in dimensioning the pipes. Software for optimizing the wind system (here not shown) and pipe organ sounds have been developed.

It was mentioned that by realizing applied research projects the applicable results are owned by the enterprises and so they should not be published for several years after finishing the work. For this reason the authors of the present paper plan to summarize the most important outcomes of earlier confidential European projects in a book. Nevertheless, as soon as possible the dissemination of knowledge has been carried out in the form of workshops organized for organ builder enterprises. These workshops have been the only possibility internationally for organ builders to learn about the acoustics of the organ and getting instructed for the application of research results, design methods, and software.

Furthermore, the extensive knowledge attained on the sound generation of organ pipes can serve as a guideline in improving the physical models of sound generation of flue and reed wind instruments.

At last but not least, our research organ will hopefully have the effect of creating new combinations of physics and music, science and art for the benefit and delight of people.

ACKNOWLEDGEMENTS

Acknowledgements to the European Commission for the support of the several research projects.

Acknowledgements to the organ builder firms taking part and supporting the European research projects at the Fraunhofer IBP:

Werkstätte für Orgelbau Mühleisen GmbH, Leonberg, Germany,
Societé de Construction d'Orgues Muhleisen sarl, Strasbourg, France,
Fagmilia Artigiana Fratelli Ruffatti S.n.c., Padova, Italy,
Orgelbau Schumacher GmbH, Baelen, Belgium,
Blancafort, orgueners de Montserrat S. L., Collbato, Spain,
Oficina e Escola de Organaria, LDA, Esmoriz (Porto), Portugal,
Organ Work Manufacture of Pécs, Pécs, Hungary,
Flentrop Orgelbouw B.V., Zaandam, The Netherlands,
Johannes Klais Orgelbau GmbH &Co. KG, Bonn, Germany,
Orgelmakerij Boogaard, Rijssen, Niederlande,
Marcussen & Son, Orgelbyggeri A/S, Aabenraa, Denmark,
Orgelwerkstatt Christian Scheffler, Sieversdorf (Frankfurt/Oder), Germany,
Restaurierungwerkstatt für Orgeln Kristian Wegscheider, Dresden, Germany,
Gerhard Grenzing S.A., Papiol, Spain,
Pels-D'Hondt Orgelbouw bvba, Herselt, Belgium,
Mander Organs, London, Great Britain,
Marc Garnier Orgues Sarl, Morteau, France.

P. Rucz acknowledges the support of the Bolyai János research grant provided by the Hungarian Academy of Sciences. P. Rucz is also supported by the ÚNKP-18-4 New National Excellence Program of the Ministry of Human Capacities.

REFERENCES

[1] Angster, J.; Miklós, A.; Leistner, Ph.: Survey of the musical acoustics research at the Fraunhofer IBP in Stuttgart, Germany. Musical Acoustics: Xiangshan Science Conferences; the 401st session. Beijing, 2011, pp. 80–85.

[2] Angster, J.: Musical Acoustics Research at the Fraunhofer IBP in Stuttgart, Germany (in Chinese), In: 2016' The Fifth Symposium of Musical Instrument of China, 3–5 December, Beijing; 2016, pp. 38–39.

[3] Angster, J.; Rucz, P.; Miklós, A.: Acoustics of Organ Pipes and Future Trends in the Research. Acoustics Today. 13(1), 2017, pp. 10–18 Online: https://acousticstoday.org/wp-content/uploads/2017/01/Acoustics-of-Organ-Pipes-and-Future-Trends-in-the-Research-Judit-Angster-1.pdf

[4] Außerlechner, H.; Trommer, Th.; Angster, J.; Miklós, A.: Experimental jet velocity and edge tone investigations on a foot model of an organ pipe. J. Acoust. Soc. Am. 126(2), 2009, pp. 878–886. DOI: 10.1121/1.3158935

[5] Trommer, Th.; Angster, J. and Miklós, A.: Roughness of organ pipe sound due to frequency comb. J. Acoust. Soc. Am. 131 (1), 2012, pp 739–748. DOI: 10.1121/1.3651242

[6] Paál, Gy.; Angster, J.; Garen, W.; Miklós, A.: A combined LDA and flow-visualization study on flue organ pipes. Experiments in Fluids 46(6), 2006, pp. 825–835, DOI: 10.1007/s00348-006-0114-0

[7] Plitnik, G.: The Josef Angster Story. ISO Journal. Magazin of International Society of Organ Builders, No. 6, 1999, pp. 56–64

[8] Metz, F.: Josef Angster. Das Tagebuch eines Orgelbauers. Verlag der Donauschwäbischen Kulturstiftung, München, 2004

[9] Ruffatti, F.; Angster, J.: Organbuilders and research: Two points of view. The Diapason, 2010, pp 24–27. Online: https://sgcweb.s3.wasabisys.com/thediapason/s3fs-public/webJan10p24-27.pdf

[10] Pitsch, S.; Rucz, P.; Angster, J.; Miklós, A.; Kirschmann, J.: Scaling software for labial organ pipes. AIA–DAGA Conference, Merano, Italy, 2013, pp. 299–302.

[11] European Research Project in the Sixth Framework Program of the European Union; GROWTH program; CRAFT: Innovative Design Method for Matching the Pipe Organ to the Acoustics of the Room (INNOPIPEORG); Contract No: COOP-CT-2005-017712, 2005–2008

[12] Rucz, P.; Trommer, Th.; Angster, J.; Miklós, A.; Augusztinovicz, F.: Sound design of chimney pipes by optimization of their resonators. J. Acoust. Soc. Am. 133 (1), 2013, pp. 529–537. DOI: 10.1121/1.4770236

[13] Angster, J.; Miklos, A.; Rucz, P.; Augusztinovicz, F.: The physics and sound design of flue organ pipes. J. Acoust. Soc. Am. 132(3), 2012, p. 2069, DOI: 10.1121/1.4755627

[14] Seventh Framework Program of the European Union; Research for SMEs (FP7-SME-2007-1): Innovative Methods and Tools for the Sound Design of Organ Pipes; (INNOSOUND) Contract No: INNOSOUND-222104, 2008–2010

[15] Miklós, A.; Angster, J.; Pitsch, S.; Rossing, T. D.: Reed vibration in lingual organ pipes without the resonators. J. Acoust. Soc. Am. 113(2), 2003, pp. 1081–1091, DOI: 10.1121/1.1534101

[16] Miklós, A.; Angster, J.; Pitsch, S.; Rossing, T.D.: Interaction of reed and resonator by sound generation in a reed organ pipe. J. Acoust. Soc. Am. 119(5), 2006, pp. 3121–3129, DOI: 10.1121/1.2188372

[17] Seventh Framework Program of the European Union; Research for SMEs (FP7-SME-2007-1): Innovative Sound Design of Reed Organ Pipes (REEDDESIGN); Contract No: REEDDESIGN-286539, 2011-2013

[18] Angster, J.; Rucz, P.; Miklós, A.: Detailed measurements on lingual organ pipes for developing innovative methods and software for the pipe design. 171st meeting of the Acoustical Society of America, Salt Lake City, USA, 2016. Special Session: Hot topics. DOI: 10.1121/1.4950306 Online: https://www.youtube.com/watch?v=ct-wHcbRpyY

[19] Verbindungen von Physik und Musik, von Wissenschaft und Kunst durch die Forschungsorgel am Fraunhofer IBP, Forschung im Fokus, Januar 2012, Online: https://www.ibp.fraunhofer.de/de/presse-medien/forschung-im-fokus/koenigin-der-instrumente.html

[20] Homepage Fraunhofer IBP Musical Acoustics: http://www.ibp.fraunhofer.de/de/Kompetenzen/akustik/musikalische-akustik.html

[21] Development and Modernization of the Wind Supply System of Pipe Organs, EU CRAFT research project, Contract no: BRST-CT98-5247, 1998–2000

[22] Advanced Computer Designed Open Wind Systems for Pipe Organs, EU CRAFT research project, COMPDESORG, Contr. No.: G1ST-CT2001-50139, 2002–2003

[23] Zink im Orgelpfeifenbau – im Auftrag der Grillo-Werke Aktiengesellschaft, Laufzeit: 2009–2010

[24] Angster, J; Dubovski, Z.; Pitsch, S.; Miklós, A.: Impact of the Material on the Sound of Flue Organ Pipes (Acoustic and Vibration Investigations with Modern Measuring Techniques). In: Birnbaum, Clemens (Ed.): Analysis and description of music instruments using engineering methods. Halle (Saale): Stiftung Händel-Haus, 2011, pp. 34–41

[25] Angster, J., Pitsch, S., Dubovski, Z., Leistner, Ph.; Miklós, A.: Research organ for pipe organ research at the Fraunhofer IBP in Stuttgart. AIA–DAGA Conferece, Merano, Italy, 2013, pp. 295–298

PROCEEDINGS of ISMA 2019
International Symposium on Music Acoustics

13 - 17 September 2019 in Detmold, Germany

How do flute players adapt their control to modifications of the flute bore ? *†‡

Benoit FABRE(1), Patricio de la Cuadra(2), Augustin ERNOULT(3)

(1)LAM, Institut d'Alembert 7190, Sorbonne Universite, Paris France, E-mail 1

(2)Electrical Engineering and Music dpt. Pontificia Universidad Catolica de Chile, Santiago, Chile, E-mail 2

(3)Magique 3D Team, Inria, Bordeaux Sud-Ouest, France, E-mail 3

Abstract

Skilled players can adapt their control parameters according to the response of the instrument they are playing. In the case of the flute, the lip and face position relative to the mouthpiece is the main adjustment used for a fine control of the pitch, while the detailed geometry of the flute bore determines the intonation profile of the instrument along its tessiture. Using the negative bore concept, we apply controlled modifications of the intonation profile of the flute. Skilled players are then invited to play on different profiles of the same instrument while the geometrical and hydrodynamical control parameters are monitored.

Keywords: Flute, Negative bore, Control, Adaptation

1 INTRODUCTION

Analysis of the acoustical response of wind instruments through the calculated or measured input impedance has become very popular during the last decades. Excellent results have been achieved in the case of reed instruments like the clarinet, while the tuning of brass instruments has also been studied with great success. In the case of the recorder and the flue organ pipe, the question of the exact prediction of the acoustical influence of the geometry at the blowing end has recently been studied by Ernoult, providing excellent quantitative prediction of the passive resonance frequencies.

Despite these promising results, the prediction of the passive resonances on flute-like instruments where the jet is formed between the lips provides limited information: calculation of the resonance frequencies from the input impedance for transverse flute, quena or shakuhachi predicts pitches from one to several semitones sharper than the notes played! The reason for this discrepancy is the presence of the lips and face of the player at the blowing end of the instrument. This changes drastically the radiation properties, and therefore the radiation impedance or the acoustic length correction associated with the imaginary part of the radiation impedance.

Indeed, the adjustment of the lips and face position appears to be the main resource used by flute players to fine-tune their instruments. In real-time flutists adjust their lips position to fine-tune the pitch they are hearing, closing a controlled feedback loop. From this perspective, the pitch of a note played is the result of the intonation of the flute itself together with the influence of the player's control strategy [1].

In order to analyse the players control strategy, we carry global modifications of the intonation profile of the flute over its entire compass and observe the adaptation of flute players.

2 Experiment

In order to study the adaptation of the control of the flute player, the first question to answer is how to modify the global acoustical response of the instrument, without changing important details such as the precise geometry of the blowing hole. The next step is to define the control parameters that need to be monitored during playing. Last, since the player is engaged in a continuous real-time adjustment including sound perception, the playing task needs to be carefully designed.

*benoit.fabre@sorbonne-universite.fr

†pcuadra@uc.cl

‡augustin.ernoult@gmail.com

2.1 How to modify the global response of the flute ?

Modern Boehm flute are built starting from a 19mm diameter cylinder. Only the mouthpiece shows a finely tuned tapering, from 17mm at the embouchure hole to 19mm diameter at the slide connecting the mouthpiece to the rest of the instrument. Because of its position at the input of the instrument, this tapering affects all the notes of the tessitura, in pitch, sound quality and dynamic response of the instrument.

We developed the *negative bore* concept in order to allow a controled modification of the flute's bore. This is achieved by using a cylindrical mouthpiece in which a spine shaped plug is inserted. The inserted plug is calculated in order to obtain the same open passage as would provide a tapered bore. For a cylindrical mouthpiece of radius R, the radius of the negative plug $r_n(x)$ equivalent to a tapered bore of radius $r_b(x)$ writes as:

$$r_n^2 = R^2 - r_b^2 \tag{1}$$

Figure 1. The *negative* bore concept: a negative plug is inserted in a cylindrical bore in order to provide the same open passage as that in a tapered bore. *up:* the geometry of a standard headjoint; *down:* a *negative* equivalent headjoint with the inserted plug.

Figure 1 presents the negative bore concept. It is interesting to note that the concept allows for bores with profiles that are difficult to build using traditional instrument making tools and techniques. The *negative* allows to modify only the flute bore, without altering any other part of the instrument, such as the shape of the blowing hole.

The method was validated by creating mouthpieces with *negatives* that emulate several existing headjoints. Flute players were asked compare *negatives* and original headjoints on one single flute body. Informal tests showed that, while *negative* mouthpieces were different from originals in the detailed geometry of the blowing hole, they were perceived as similar in their overall pitch structure.

Thus, for this paper three different *negative* inserts were built and labelled as follows:

- *c*: is a thick and long insert. It corresponds to a mouthpiece with diameter variations much stronger than usual
- *m*: corresponds to a standard bore, designed after measurements on several brands of flutes
- *f*: is a thin and rather short insert. It corresponds to a mouthpiece with almost cylindrical bore.

2.2 Control parameters

We follow here the work presented by de la Cuadra [1], [4] and Ernoult [2], the control parameters analysed in order to study the adaptation of the player to different flute bores are summarized in figure **??**:

- the blowing pressure p_m as measured in the players mouth
- the lips to edge distance W as estimated through automatic image analysis. This distance corresponds to the jet length.
- the coverage angle β is also estimated by means of automatic image analysis.

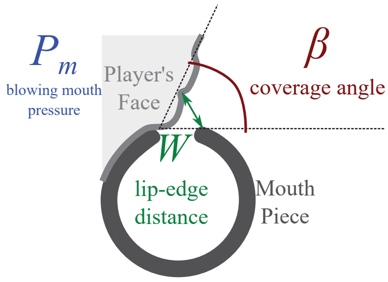

Figure 2. The main control parameters analyzed throughout the study are the blowing pressure, the lip-edge distance and the coverage angle.

The sound produced by the instrument and the player is also recorded, first as the inner acoustic pressure field, allowing for amplitude and spectral estimations, and second as the radiated acoustic pressure. Pitch, spectra and amplitudes are then calculated from the acoustic signals.

2.3 Playing task

Two players with formal training in classical flute playing and an extensive concert experience have been invited to play on a cylindrical mouthpiece with negative inserts mounted on a Yamaha YFL-382 flute body. They were asked to play different musical excerpts, and the analysis carried in this paper is focused on the scale task shown in figure 3. They were presented the tool used to modify the flute acoustic response and were allowed to practice in order to get used to the set-up. When starting the measurements, the negative insert was changed and the players were not informed of which negative insert was plugged in the flute.

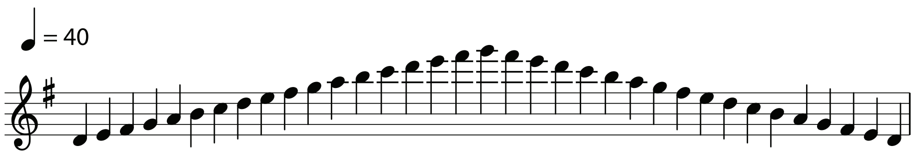

Figure 3. The musical excerpt analysed in this study.

The musical task analysed in this paper is a G-major scale, played slowly, with an emphasis on intonation. For this excerpt, a Korg OT-120 tuner is placed in view of the player to help with intonation. G major scale was chosen in order to avoid C sharp, known to show intonation difficulties. The reference pitch of the tuner is adjusted according to the intonation of $A3$. Due to warm summer conditions, this tuning was found sharp, up to $446Hz$. Because some players tend to use alternate fingerings for pitch correction, players were here asked to use only standard fingerings.

3 Results

Preliminary results are discussed, comparing data obtained with the three negative inserts for each player. First the sounding result is discussed, then the control data.

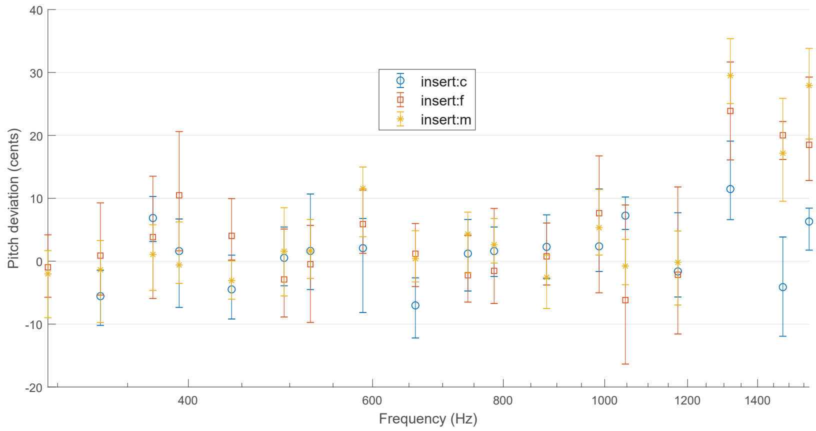

Figure 4. For each note of the scale played, the frequency detected is compared to the frequency corresponding to the equal temperament. The ratio of these frequencies is expressed in cents.

Analysis of the intonation is presented for one player on figure 4. It shows that, independently of the insert plugged, the player managed to maintain the intonation within ± 10 cents of the equal temperament, except for the three higher notes (E to G). It is interesting to note that insert *c* allows the player to maintain the expected intonation even for these three higher notes. A spectral centroid of the sound produced was also estimated throughout the scale, and showed small enough differences, indicating that the players did somehow produce a standard tone quality. This indicates that the three negative inserts used offered "playable" conditions, allowing to compare the control data.

The analysis of the control data indicate that the blowing pressure pattern used by the players is not affected when changing the acoustics response of the instrument. Changes are mainly concentrated on the two geometrical parameters, the jet to labium distance W as shown on figure 5, and on the coverage angle β as shown on figure 6.

As discussed by de la Cuadra, the dimensionless jet velocity $\theta = U_j/fW$, with U_j the jet velocity and f the playing frequency, is a good indication of the player's strategy. The two players maintain their individual target in terms of dimensionless blowing velocity, as can be seen for one of them on figure 7, related to only small changes in sound production. The dimensionless jet velocities show individual profile for each player, independent of the flute bore: it is a nice summary of each player's idea. This observation is in line with the observation on the sound production: despite changes in some of the control parameters in order to adapt to the modifications of the flute response, the players maintain a similar global hydrodynamical control of the sound production, resulting in a similar sound production.

4 PERSPECTIVES

The study presented should be considered as a preliminary study, intended at testing hypothesis on the balance between different parameters in the sound production in flute playing. The main hypothesis is that the player, whenever it is possible, compensates for changes in the instrument's response. The data analyzed indicate that this compensation can be tracked, mainly in terms of geometrical parameters.

This study also validates the set-up used and the efficiency of the *negative bore* concept, allowing for further experiments, involving more players and a developed musical task.

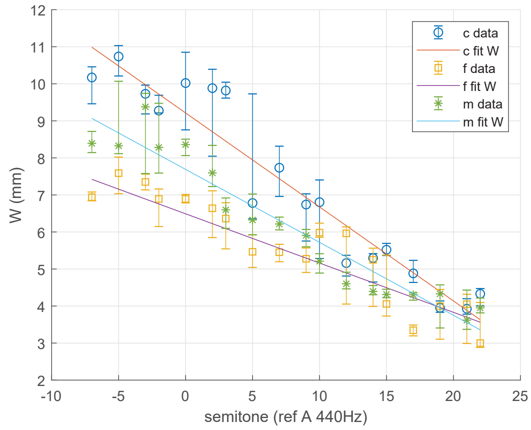

Figure 5. For each note of the scale played, the lip-edge distance W is estimated from image analysis. The player changes this distance to adapt to the acoustic response of the instrument.

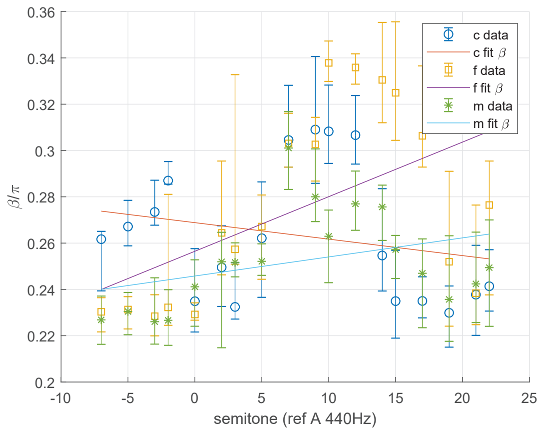

Figure 6. For each note of the scale played, the coverage angle β is estimated from image detection. The player shows quite different strategies to adapt to changes in the acoustic response of the flute.

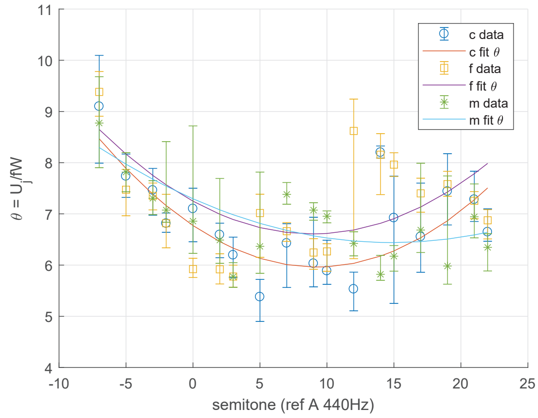

Figure 7. For each note of the scale played, the dimensionless velocity θ is estimated. The player shows quite similar patterns, independently of the acoustic response of the flute.

The experiment presented rises questions regarding the reference each player has in mind: indeed, the results are related to the "distance" between the configuration proposed and each players' individual usual conditions, for example in terms of the global tuning of the instrument. Experimentation with different bores shows that the different configurations can be adapted to different goals like, for instance "fast playing" (possibly corresponding to the smallest possible changes in control), or "sound tonal balance" over the tessitura. This also rises the question of the direction in which standard bores go.

ACKNOWLEDGEMENTS

The authors would like to thank Laurent Quartier, Valentine Laporte and Matthias Fama for help in the conception and selection of the different negative inserts used in this study. This work is supported by CONICYT through FONDECYT Project No.1161464.

REFERENCES

[1] De la Cuadra, P.; Ernoult, A. , Balosso-Bardin C., Fabre B., Playability in flute-like instruments: Investigating the relation between flute making and instrumental control The Journal of the Acoustical Society of America 141, 3874 (2017); https://doi.org/10.1121/1.4988664

[2] A. Ernoult, P. De La Cuadra, and B. Fabre. An Inclined Plane: A Simple Model for the Acoustic Infuence of the Flutist's Face. Acta Acustica united with Acustica, 104(3):496-508,May 2018. doi: 10.3813/AAA.919192.

[3] C. Vauthrin, B. Fabre, and I. Cossette. How Does a Flute Player Adapt His Breathing and Playing to Musical Tasks? Acta Acustica united with Acustica, 101(2):224-237, March 2015. doi: 10.3813/AAA.918821.

[4] De la Cuadra P., Fabre B., Montgermont N., Chafe C. *Analysis of flute control parameters: a comparison between a novice and an experienced flautist* Acustica / Acta Acustica No.5 p. 740 September/October [2008].

[5] Balosso-bardin, C., De la Cuadra, P., Vauthrin, C. and Fabre, B., An interdisciplinary study of the 1832 Boehm flute: history, geometry and acoustics (2017). Musique et Technique, 7 . pp. 11-24. ISSN 2496-2333

PROCEEDINGS of ISMA 2019
International Symposium on Music Acoustics

13 - 17 September 2019 in Detmold, Germany

Experimental study on the temporal fluctuation of harmonics in flute sounds

Keita ARIMOTO[1]

[(1)] YAMAHA Corp. R&D, Japan, keita.arimoto@music.yamaha.com

Abstract

There are some studies on the temporal fluctuation of harmonics in flute sounds. However, it is still unclear whether it is due to the fluctuation coming from human player or the nature of the sounding mechanism. In this study, an experiment was conducted to investigate temporal fluctuations purely due to the sounding mechanism of the flute. For this purpose, an artificial blowing system was built in order to yield flute sounds by a constant air flow as well as by adjusting the angle, offset, length and velocity of the jet. The temporal fluctuation for a harmonic component was computed by a standard deviation for a series of instantaneous harmonic amplitudes obtained from a short-time audio analysis. The result shows that the temporal fluctuation increases as the average harmonic amplitude decreases, and vice versa. The effect of the temporal fluctuation on perceptual impression was finally confirmed by a synthesis experiment where flute sounds were re-synthesized with controlling the amount of the temporal fluctuation.

Keywords: flute, fluctuation, artificial blowing

1 keita.arimoto@music.yamaha.com

PROCEEDINGS of ISMA 2019
International Symposium on Music Acoustics

13 - 17 September 2019 in Detmold, Germany

Experimental investigation for effects of jet angle on the harmonic structure in the flute

Onogi KIMIE[1]; Ai NATSUBORI[2]; Hiroshi YOKOYAMA[3]; Akiyoshi IIDA[4]; Keita ARIMOTO[5]

(1) Toyohashi University of Technology, Japan, onogi@aero.me.tut.ac.jp
(2) Toyohashi University of Technology, Japan
(3) Toyohashi University of Technology, Japan, h-yokoyama@me.tut.ac.jp
(4) Toyohashi University of Technology, Japan, iida@me.tut.ac.jp
(5) Yamaha Corporation, Japan, keita.arimoto@music.yamaha.com

Abstract

To clarify the effects of jet angle on the radiated sound from the flute, the radiated sound and jet fluctuations were experimentally investigated. An artificial blowing device with an artificial oral cavity was used to change the jet angle and the geometric jet offset (the relative height of the vertical line of the cavity exit center from the edge) independently. The actual jet offset (the relative height of the jet fluctuation center from the edge) was estimated based on the velocity profile measured by a hot-wire anemometer. Under the condition that the geometric jet offset is zero, the actual jet offset changed with the jet angle. Also, the sound of the second/third mode radiated more/less intensely with larger actual jet offset, while the radiated sound of the first mode remained almost the same level. These results indicate that the variation of the jet angle affects the actual jet offset, which affects the harmonic structure.

Keywords: Flute, Jet angle, Jet offset

PROCEEDINGS of ISMA 2019
International Symposium on Music Acoustics

13 - 17 September 2019 in Detmold, Germany

Kora-Som: An interface that converts a player's beating heart into a real-time metronome

Leonardo FUKS[1]; Gabriel MOURA[2]; Frederico JANDRE[3]

(1) UFRJ- Escola de Música, Brazil, fuks.leonardo@gmail.com
(2) UFRJ- Escola Politécnica, Brazil, gabrielgm@poli.ufrj.br
(3) UFRJ- Programa de Engenharia Biomédica, Brazil, frederico.jandre@poli.ufrj.br

Abstract

The heartbeat is a central timing reference in life and in music. Several composers and players along history have mentioned the heart rate as a measure for the musical pulse. On the other hand, it is known that listening and playing music affects the heartbeat frequency, besides other physiological signals. The purpose of this project consists of building a device that detects, measures and replicates a subject's heartbeat and makes it available in real-time for musical research and performance. The Kora-Som system employs a commercial heart rate sensor, widely used in sports. The data from this meter are received and decoded by a remote sensor, connected to an Arduino and a portable computer. A piece of software generates and plays sounds from wavetables, melodic sequences, midi files and other formats and protocols. A player may literally play with his/her own heart, which opens a large range of composing and improvising fields. A whole musical group is able to play to/with a certain listener, such as a hospital patient, in a very touching and stimulating situation. All timing and performing data is recorded and made available for eventual processing and evaluation.

Keywords: Heartbeat, Metronome, Music, Performance, Ensemble

PROCEEDINGS of ISMA 2019
International Symposium on Music Acoustics

13 - 17 September 2019 in Detmold, Germany

A liquid sloshing vibrato mechanism for the Symbaline; an active wine glass instrument *†‡

Lior ARBEL(1), Yoav Y. SCHECHNER(2), Noam AMIR(3)

(1)Faculty of Architecture and Town Planning, Technion - Israel Institute of Technology, Haifa, Israel
(2)Viterbi Faculty of Electrical Engineering, Technion - Israel Institute of Technology, Haifa, Israel
(3)Department of Communication Disorders, Sackler Faculty of Medicine, Tel-Aviv University, Tel-Aviv, Israel

Abstract

The Symbaline is an active instrument consisting of water tuned wine glasses excited by electromagnets. Its timbre is characterized by steady overtones and a smooth attack-decay envelope. In this demonstration we present an electromechanical system for adding vibrato to the Symbaline's sound. The system consists of a pendulum with a magnetic bob, submerged inside the liquid in the wine glass. Infra-sound signals are sent to an electromagnet external to the glass, generating a magnetic field which puts the pendulum into oscillation. As a result of the pendulum's movement the liquid in the glass sloshes and the water level fluctuates in a periodic manner. Audio frequency signals are sent to the same electromagnet, in parallel, inducing vibrations in the wine glass itself, by exciting a small magnet on the glass's surface. While the glass is radiating sound, its resonance frequencies are altered by the changing water levels, resulting in frequency and intensity modulation.
Keywords: Active, Liquid, Vibrato, Electromechanic, Wineglass

(a)

(b)

Figure 1. (a) The Symbaline, consisting of a set of tuned wine glass actuated by electromagnets. The Symbaline is played by an amplified auxiliary musical instrument (not shown). (b) The vibrato mechanism in mid oscillation. The pendulum is excited to oscillation by the electromagnet placed outside the glass. The water is sloshing, periodically altering the glass resonance frequencies and modulating the wine glass tone.

*lior51@campus.technion.ac.il
†yoav@ee.technion.ac.il
‡noama@tauex.tau.ac.il

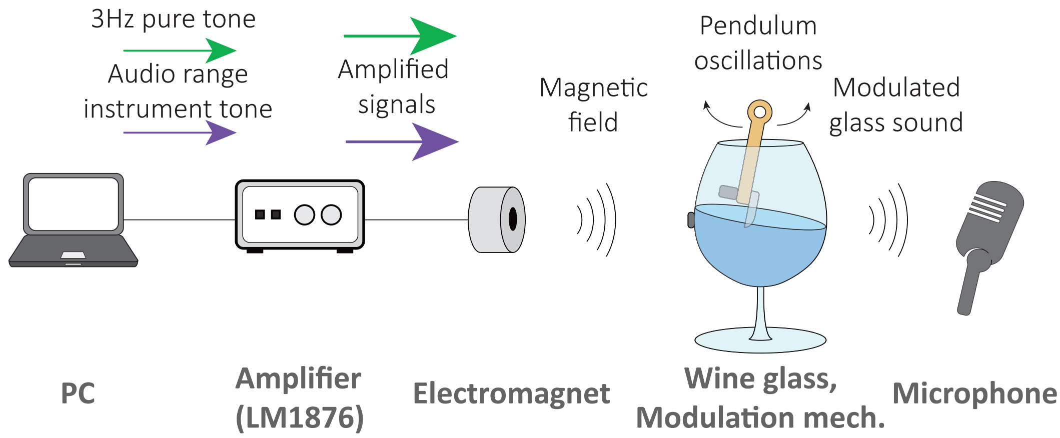

Figure 2. Block diagram of the modulation mechanism setup. The PC generates both a low-frequency tone and an audio range tone sampled from a musical instrument. The signals are amplified and routed to the electromagnet, where they are converted to a magnetic field. The audio range signal excites wine glass tones, and the low-frequency signal oscillates the pendulum. The pendulum oscillations generate water sloshing which modulates the wine glass radiated sounds.

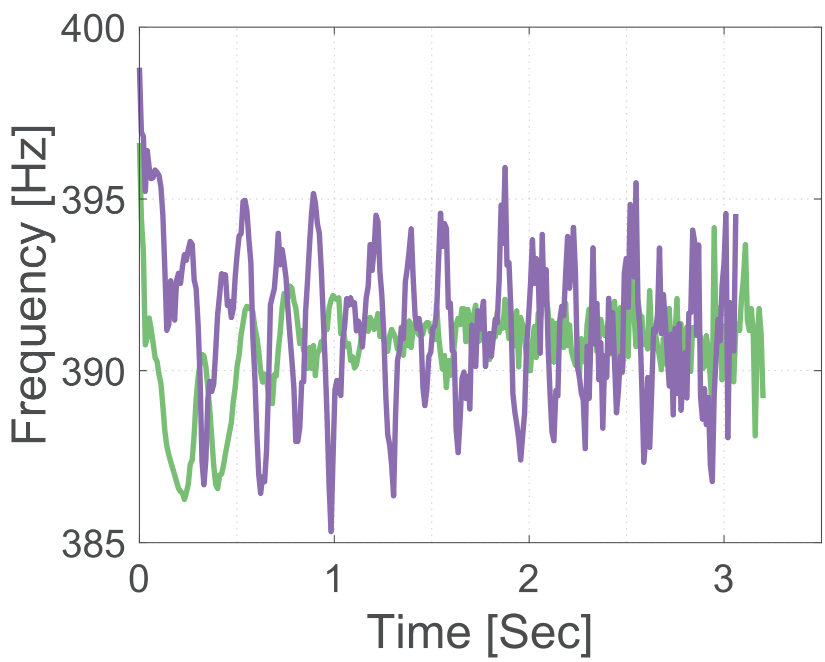

Figure 3. Analysis of the fundamental frequency of a wine glass tone excited by a classical guitar signal. The wine glass tone is modulated by activating the pendulum. A plot of the resulting wine glass fundamental frequency over time is shown in *purple*. The fundamental frequency of the non-modulated tone is shown in *green* for comparison.

PROCEEDINGS of ISMA 2019
International Symposium on Music Acoustics

13 - 17 September 2019 in Detmold, Germany

A real-time feedback system for vocal tract tuning

Marie JEANNETEAU[1], Noel HANNA[1], John SMITH[1], Joe WOLFE[1]

[1] School of Physics, UNSW Sydney, Australia

Abstract

The first resonance of the vocal tract (R1, an impedance minimum when measured at the lips) is tuned by some singers: all of the sopranos we have studied, whether trained or not, tune R1 to f_o over the range roughly C5 to C6; altos and tenors sometimes tune it to one of the lower harmonics in their upper range. Sopranos who sing in the range substantially above about C6 tune the second resonance R2 to f_o. The first purely acoustic impedance maximum is tuned by saxophonists and clarinettists under some conditions. This paper introduces a public version of software that can be used in a system to teach vocal tract tuning using a nearly real-time display and a graphical user interface. Our first use of it was to teach R2: f_o tuning to sopranos. In a one-hour session, most subjects learned tuning over a limited range, but only while the interface provided visual feedback. One of the authors (MJ) spent several weeks with the system and learned to extend her range of R2 variation and could use R2: f_o tuning over from F5 to E6, with and without the visual feedback. Training resonance tuning on saxophone is also proposed.

Keywords: Resonance tuning, Vocal tract, Feedback system

1 INTRODUCTION

In speech, the fundamental frequency f_o of the vibrating vocal folds, and hence that of the voice, is typically ~100-300 Hz and usually falls below the range of the resonances of the vocal tract, which typically lie above about 300 Hz. Further, the frequency response of the vocal tract is controlled independently of f_o and is used for a largely unrelated phonetic purpose: the first two resonances, R1 and R2, produce formants F1 and F2, which are broad peaks in the spectral envelope. Regions on the (F2,F1) plane identify vowels, and the trajectories F1(t) and F2(t) contribute to identifying consonants [*e.g.* 1].

In performance on wind musical instruments, it is possible to achieve a degree of competence without adjusting vocal tract resonances as a function of f_o, (which here means the fundamental frequency of the note being played). This is not surprising: With regard to the pressure difference acting across a reed or a brass player's lips, the acoustic impedances of the bore and the vocal tract are in series. Usually, the impedance of the bore of reed or wind instruments is rather greater than that of the vocal tract, so that the latter has only a modest effect.

Nevertheless, there are important circumstances in which both singers and some wind instrumentalists tune the vocal tract, as we explain below. In some cases, the tuning is counter-intuitive. In others, there may be no simple auditory feedback. For these reasons, visual feedback may be helpful in learning the art of resonance tuning. For that purpose, high precision in the feedback is not necessarily required, and so techniques rather simpler than those used in an acoustics research lab may suffice. For that reason, we decided to make a public version of software that, with relatively simple and easily obtained hardware, provides feedback in nearly real time of the frequencies of vocal tract resonances. This paper first introduces resonance tuning, then describes the new, simple system, then summarises the results of a preliminary study using it.

1.1 Resonance tuning in singing

In normal nomenclature, tract resonances correspond to resonant modes having a pressure node near the open lips and a pressure antinode near the larynx: such a resonance acts as an effective impedance matcher from the high impedance at the glottis to the low impedance of the radiation field at the lips. Resonance R1 has no pressure node between the two ends, R2 has one and Rn has $n-1$.

The normal range of the soprano voice, from about C4 (middle C) to nearly C6 (a soprano's 'high C'), covers approximately the range of R1. A soprano who varied R1 independently of f_o (in other words, one who allowed the librettist rather than the composer to specify the vocal tract shape) would often pay the penalty of losing the

[1] jeanneteau.marie@gmail.com, N.Hanna@unswglobal.unsw.edu.au, john.smith@unsw.edu.au, j.wolfe@unsw.edu.au

loudness boost provided by the impedance matching possibility of R1, and perhaps also risk vocal instabilities because of the phase of the acoustic load at the larynx [2].

Observations of sopranos [3,4] and direct measurements of their resonance [5] showed that, over this range, they tune R1 very near to f_o: what we call R1:f_o tuning. Untrained as well as trained sopranos use this technique: the auditory feedback of producing a louder sound with less effort is apparently enough for singers to learn it. Altos and tenors sometimes use R1:f_o tuning in their upper range and altos, tenors and baritones use R1:nf_o tuning occasionally: *i.e.* they tune R1 to one of the harmonics of the voice [6,7].

Because of the vocal tract's length and the limit to the ability to open the lip aperture, it is difficult to increase R1 much above 1 kHz, which corresponds roughly to the typical upper limit of pitch range for most sopranos, *i.e*. about C6 or 'high C'.

A minority of sopranos sing pitches well above C6. In a study of those who do use this range [8], we found that most make a transition, in the region of C6, to R2:f_o tuning: they tune the tract's second resonance to the fundamental of the voice. This may be counter-intuitive: in spite of having learned (whether taught or not) to increase the lip aperture when ascending a scale, they would need suddenly to reduce the aperture to go higher. This observation led us to wonder whether the difficulty in learning R2:f_o tuning might be a cause of the upper limit to the range of most sopranos. This in turn was one incentive for the current project.

1.2 Resonance tuning in wind instrument performance

Reed instruments usually operate at a frequency very near to a maximum in the impedance spectrum of the bore[2]. To access the second register (operated by the second resonance and second impedance peak), players usually open a small register hole, which weakens and detunes the first resonance, making it unplayable. For higher registers, either more register holes are used, or some of the tone holes serve that purpose.

Saxophones have a larger cone angle than other reed instruments. This has the intended consequence of making them louder, but makes the third impedance peak too weak to drive the reed [9]. For that reason, many saxophonists are limited to the first two registers, giving a pitch range of about two octaves and a fifth.

To access the third and higher registers (known to saxophonists as *altissimo*), players learn to tune an impedance peak[3] of the vocal tract to the frequency of the desired note [10,11]. The series combination of bore and tract impedance then drives the reed at that frequency. Clarinettists also use vocal tract tuning to access the *altissimo* registers [12].

Both clarinettists and saxophonists also use tract tuning for pitch glides [12] and for controlling multiphonics [13].

Providing feedback that might teach resonance tuning to reed players was a second motivation for this project and we are continuing with work on that aspect.

2 MEASUREMENTS

2.1 Measuring resonance tuning in and outside the laboratory

For both singing and reed playing, we have measured vocal tract impedance spectra using the capillary method: a broadband source with a high output impedance and a microphone are combined in an impedance head. This is first calibrated to remove the frequency response of the source. The different experimental details are described elsewhere [12] and a schematic is shown in Fig 1. Briefly, a synthetic broadband signal, synthesised on a computer, is output via an interface to an audio power amplifier and then to a horn driver. An inverted horn matches it to a flexible tube, next to which is attached a microphone. The microphone is connected via a preamplifier to the audio interface and thence to the computer.

Measuring the frequency of resonances for singers has the challenge of ecological relevance: it is possible to make precise measurements of the vocal tract (and trachea) using a multiple microphone system in a duct sealed to the lips [14,15], but this has the disadvantage of making normal singing impossible. For this reason, we have used a flexible pipe as the source and bound a microphone to it—Fig 1. This makes a simple impedance head that, held to touch the lower lip, can measure the frequency of resonances with little inhibition of normal singing.

For measurements on clarinet and saxophone players, we install the source and the microphone in the mouthpiece, which then becomes an impedance head. For lip reed instruments, two thin tubes are inserted in the corner of the mouth of the player; these then become the impedance head [16,17].

---

[2] Reed instruments resemble the voice in that the bore resonances have a pressure antinode at the source and a node near the bell or the start of the array of open tone holes. Of course, the qualitative difference is that, in instruments, it is the resonator and not the source that largely determines the pitch—inadvertent squeaks excepted.

[3] In the notation used for the voice, an impedance peak at the voice would be an antiresonance, though the term resonance is sometimes used for both maxima and minima in acoustic impedance.

2.2 Hardware

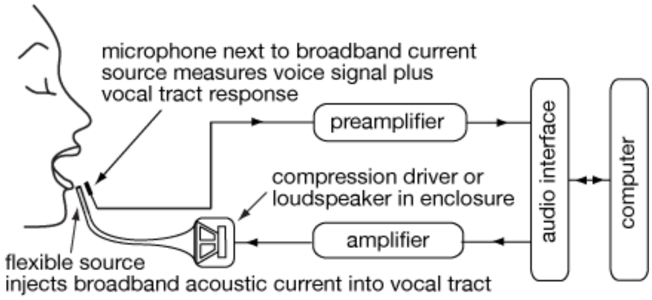

Figure 1 – A schematic (not to scale) of the hardware used for resonance feedback in singing.

In the lab, we use research-quality microphones, preamplifiers and audio interfaces. For the purposes of providing feedback, less expensive items may be used. A key element is a horn driver that delivers significant power at the lower frequencies of interest; many commercial options are available. Linearity in the microphone is important, so a low sensitivity microphone is desirable. However, we have in the past used cheap tie-clip microphones with acceptable, though not good, results. A 3D print design for the horn, along with other information, will be posted soon to our web site. As this contribution is submitted as a demonstration presentation, details will be available at the demonstration.

2.3 Calibration

For singing, we ask subjects to hold the source and microphone at the lower lip, with the mouth closed. We then inject a broad band signal comprising a sum of sine waves whose magnitudes and relative phases are adjusted to improve the dynamic range. The spectral envelope of the microphone signal then exhibits the frequency-dependent gain of the source, microphone and amplifiers, and the acoustic impedance of the radiation field at the lips, baffled by the face. To 'flatten' this curve, a new output signal is generated having Fourier components proportional to the reciprocals of those of the first measurement [18]. When this is output, the linear gain of the entire system is compensated and the next pressure signal measured (under the same conditions) is close to flat. A further iteration is often helpful to compensate for nonlinear effects in microphone or speaker. The flattened signal measured with closed lips we call p_{closed}.

For measuring the tracts of wind players, our calibration load is an acoustically infinite waveguide, into which the impedance head is inserted. Ideally these ducts should be straight to avoid reflections, so we have them installed in the ceiling space of the building. However, less precise measurements are possible using calibrations made on a long coil of pipe, provided precautions are taken to avoid crosstalk between loops of the coil [19].

2.4 Measurements

The calibration using infinite pipes, whose impedance is a pure resistance, means that the pressure measurements made with this source calibration are proportional to the acoustic impedance (provided that the measured impedance is small compared to the output impedance of the source). For the measurements in the mouths of wind players, maxima in the measured probe signal give the vocal tract impedance maxima.

For singing, the source is calibrated on the radiation impedance, as described above. When this calibrated signal is output during singing, the current source is loaded with the acoustic impedance of the vocal tract, as measured at the lower lip, in parallel with the radiation field, still baffled by the face, albeit with an altered geometry. We call this microphone signal p_{open}. We then plot the ratio $\gamma = p_{open}/p_{closed}$. Both calibration and measurement are shunted by the radiation impedance, the source is approximately a current source for these loads, so γ is approximately equal to the ratio of their impedance. At low frequencies, maxima in γ are a good approximation to the resonances of the tract, with precision usually much greater than that given by formant estimations. However, neither this technique nor formant estimation gives a good measurement of resonance amplitude or bandwidth.

Measurements of singers and players have the serious complication that the harmonics of the note played or sung usually have a much greater amplitude than the response of the system to the probe signal. Figure 2 gives an example for a measurement of p_{open}/p_{closed} on a singer. Here, the harmonics at nf_o are prominent. Peaks in the broadband signal indicate the resonances, as marked. Observe that the fifth harmonic falls close to R2 and thus receives an amplitude boost, called the formant F2. In this case, however, the R1 resonance falls between the second and third harmonic, so no harmonic is boosted by this resonance: R1 does not produce a formant F1 in this case.

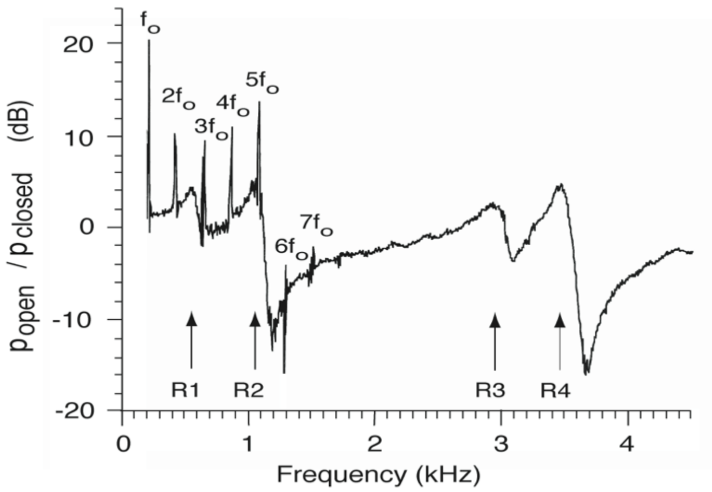

Figure 2 – A plot of the measured pressure ratio, mouth open to mouth closed.

We note that the approximations made above in interpreting p_{open}/p_{closed} are less accurate at high frequencies and that peaks in γ correspond less well with resonances. This limitation does not apply to measurements made with the lips sealed around a duct-type impedance head [*e.g.* 14,15]. However, the geometry in that case precludes ecological articulation.

3 SOFTWARE INCLUDING GRAPHICAL USER INTERFACE

3.1 Shareware software

The shareware software has a graphical user interface (GUI) with panels for measurement parameters, calibration, display, recording and editing and a number of other features. These are described in more detail elsewhere [20].

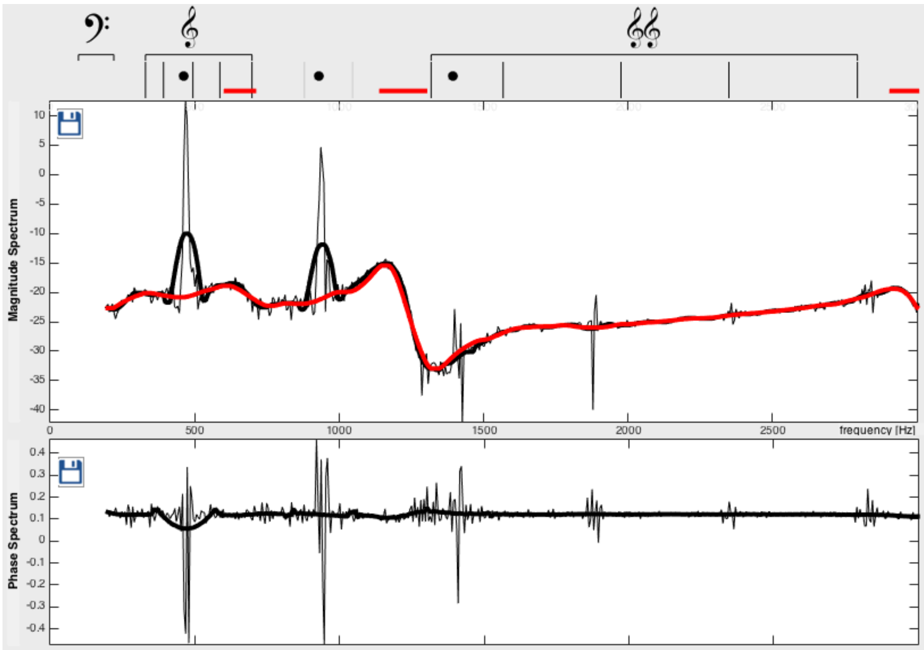

Figure 3 – A panel from a screen grab during a singing measurement.

Figure 3 shows a panel from a screen grab. The two graphs show the magnitude and phase of p_{open}/p_{closed} during a sung note (Bb4). The ordinates are dB and radians. The abscissa in the middle is frequency in Hz. Above the graph this is converted to pitch using the three clefs, bass, treble and supertreble (two octaves above treble). The fine black line is the raw p_{open}/p_{closed} signal, which is smoothed to give the thick black trace. The harmonics are then removed and interpolated to give the red line, which is thus the response of the vocal tract to the injected signal. On the music staves are shown horizontal red bars, which are estimates of the resonance frequencies, including error bars.

The singer in question is not tuning resonances—the pitch is towards the lower end of the range over which sopranos practise resonance tuning. In a tuning exercise, the singer would sustain the note while making an articulatory change and simultaneously watch the positions of the horizontal bars, adjust articulation to move one of the bars (R1 or R2) to overlap with one of the harmonics (nf_o), thus to achieve the desired Rn: nf_o tuning.

4 EXAMPLES OF USE

4.1 Teaching basic articulation skills

For some learning exercises, it is helpful to learn the articulatory gestures while miming, with glottis closed and with velum raised (*i.e.* without nasalisation). Figure 4 shows the effects of these separately. In the 'normal' condition, with glottis closed and velum raised (top left), R1, R2 and R3 are visible. Opening the glottis (top right) then adds the trachea below the glottis. One would expect this roughly to double the length of the duct, with an open end approximating the remote end where the trachea branches rapidly. This would roughly double the number of expected resonances in a given frequency range [15]. One extra resonance does indeed appear at ~1 kHz. The higher whole-duct resonances have not appeared probably because the glottis was only partly open and the inertia of the air in the glottis was large enough to isolate the two tracts at high frequencies. Finally, lowering the velum gives a single strong resonance in the range viewed. (For measurements at the lips, and with the velum completely lowered, it makes little difference whether the glottis is open or closed.)

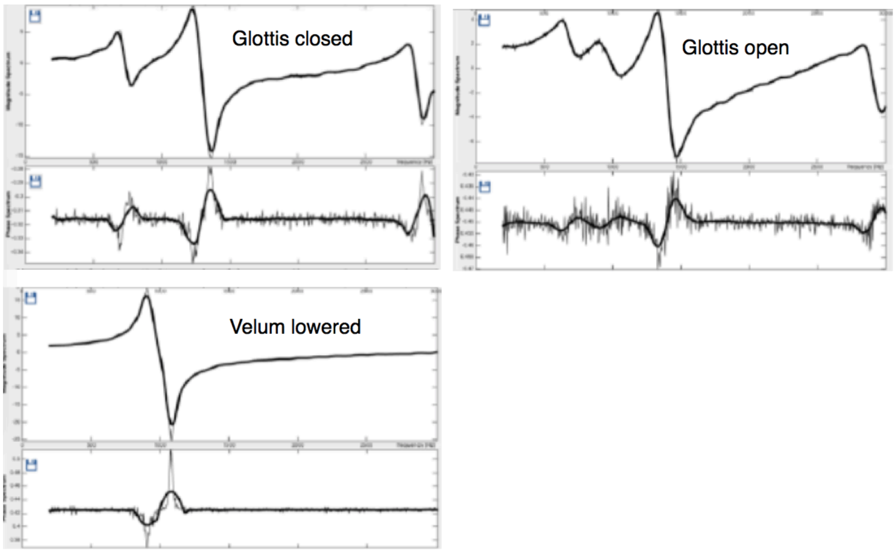

Figure 4 – Three screen grabs with the gestures indicated. Again, the frequency axis is from 0 to 3 kHz.

4.2 Training R2:f_o tuning

Can visual feedback teach resonance tuning? We conducted a preliminary experiment using this interface.
As mentioned above, sopranos do not need help to learn R1:f_o tuning. But those who sing in the range well above high C usually use R2:f_o tuning. Could we teach this skill? A formal account of this project has been submitted elsewhere, but the simple results will be described here.
Eight sopranos came to the lab for a one-hour session each. All of them had a self-described range with an upper limit near high C (C6). Using the hardware and software described above, each of them first tried to learn how to control glottis and velum while miming (see Fig 4). In the next stage, they mimed the vowel /*a*/, then gradually adjusted the vocal gesture to put R2 (the second red bar in Fig 3) at a pitch near G5. Then they heard that note on a glockenspiel, and attempted to sing it, without changing the mouth or tongue shape. Those that achieved the goal then sang up a scale, tuning R2 as they went.

4.3 Training results

Of the eight subjects, six learned to control the glottis and velum when miming—the other two had difficulty in closing the glottis. Once these two did close the glottis, they then had difficulty sealing the nasal tract with the velum.
One of these two was never able to completely seal the velum when miming. The other seven were able to use the visual feedback to lower R2 to a desired value while miming: one could lower it as far as D5.
Of the six subjects with good independent control of glottis and velum, five learned to lower R1 when singing.
However, only two learned how to perform R2:f_o using the visual feedback in the one-hour session (see Fig 5).
After the training, subjects sang an ascending scale while R1 and R2 were measured by the experimenter, without displaying visual feedback. In these measurements, all eight subjects were observed to use R1:f_o tuning over

the suitable range, but none spontaneously switched to R2:f_o near the top of their range. Evidently, one hour is not enough time to teach what is, for sopranos, a counter-intuitive technique: to reduce the lip aperture on an ascending step in a scale.

Just one soprano has used this interface for a sustained period. One of the authors (MJ), a soprano with no formal training, spent an estimated half an hour per day over a period of three months while developing the software used here. It took her about 4 weeks to have competent and independent control of the glottis, velum and vocal tract gesture.

After three months, she was able to use R1:f_o up to C#6 and R2:f_o over the range from E5 to E6, without needing to use the feedback system. Further, she extended her comfortable range by a fifth (A5 to E6) and her absolute upper limit to F#6, the range D6 to F#6 being only possible with R2:f_o tuning. The results of the study summarized here will (we hope) appear in more detail later.

5 CONCLUSIONS

Doing precise measurements of vocal tract resonances requires sophisticated hardware and has, until recently, required software that has gradually evolved for research purposes and was not widely available. New software has been written for use in feedback applications and is available as shareware. Simple versions of the hardware and software suitable for singing will be available for demonstration in the conference demonstration session. Software download and details are at http://www.phys.unsw.edu.au/jw/broadband.html

ACKNOWLEDGEMENTS

We thank the Australian Research Council for its support and our volunteer subjects.

REFERENCES

1. Clark J, Yallop C, Fletcher J. An introduction to phonetics and phonology. Blackwell, Oxford 2007.
2. Titze IR. Nonlinear source-filter coupling in phonation: Theory. J Acoust Soc Am. 2008; 123: 2733–2749.
3. Sundberg J. Formant technique in a professional female singer Acustica 1975; 32: 89–96.
4. Sundberg J, Skoog J. Dependence of jaw opening on pitch and vowel in singers. J. Voice 1997; 11:301–306.
5. Joliveau E, Smith J, and Wolfe J. “Vocal tract resonances in singing: The soprano voice,” J Acoust Soc Am 2004; 116:2434–2439.
6. Henrich N, Smith J, Wolfe J. Vocal tract resonances in singing: Strategies used by sopranos, altos, tenors, and baritones. J Acoust Soc Am. 2011; 129: 1024-1035.
7. Henrich N, Kiek M, Smith J, Wolfe J. Resonance strategies in Bulgarian women's singing. Logopedics Phoniatrics Vocol. 2007; 32: 171-177.
8. Garnier M, Henrich N, Smith J, Wolfe J. Vocal tract adjustments in the high soprano range. J Acoust Soc Am. 2010; 127: 3771-3780.
9. Chen JM, Smith J, Wolfe J. Saxophone acoustics: introducing a compendium of impedance and sound spectra. Acoust. Aust. 2009; 37: 18-23.
10. Chen JM, Smith J, Wolfe J. Experienced saxophonists learn to tune their vocal tracts. Science 2008; 319: 726.
11. Scavone GP, Lefebre A, Da Silva AR. Measurement of vocal-tract influence during saxophone performance. J Acoust Soc Am 2008; 123: 2391–2400.
12. Chen JM, Smith J, Wolfe J. Pitch bending and glissandi on the clarinet: roles of the vocal tract and partial tone hole closure. J Acoust Soc Am. 2009; 126: 1511-1520.
13. Chen JM, Smith J, Wolfe J. Saxophonists tune vocal tract resonances in advanced performance techniques. J Acoust Soc Am. 2011; 129: 415-426.
14. Hanna N, Smith J, Wolfe J. Frequencies, bandwidths and magnitudes of vocal tract and surrounding tissue resonances, measured through the lips during phonation. J Acoust Soc Am. 2016; 139: 2924–2936.
15. Hanna N, Smith J, Wolfe J. How the acoustic resonances of the subglottal tract affect the impedance spectrum measured through the lips. J Acoust Soc Am. 2018; 143: 2639-2650.
16. Tarnopolsky A, Fletcher N, Hollenberg L, Lange B, Smith J, Wolfe J. Vocal tract resonances and the sound of the Australian didjeridu (yidaki) I: Experiment. J Acoust Soc Am. 2006; 119: 1194-1204.
17. Boutin H, Fletcher N, Smith J, Wolfe J. Relationships between pressure, flow, lip motion, and upstream and downstream impedances for the trombone. J Acoust Soc Am. 2015; 137: 1195-1209.
18. Epps J, Smith JR, Wolfe J. A novel instrument to measure acoustic resonances of the vocal tract during speech. Measurement Sci. Tech. 1997; 8: 1112-1121.
19. Dickens P, Smith J, Wolfe J. Improved method of measuring reflection or impedance spectra using adapted signal spectra and resonance-free calibrations. Int. Cong. Acoust., Sydney. 2010. M. Burgess, ed.
20. Music Acoustics. http://www.phys.unsw.edu.au/jw/broadband.html UNSW 2019.

PROCEEDINGS of ISMA 2019
International Symposium on Music Acoustics

13 - 17 September 2019 in Detmold, Germany

Experimental setup for real-time control of a single-reed woodwind instrument model

Alex Hofmann[1]; Sebastian Schmutzhard[2]; Vasileios Chatziioannou[3]

(1) Department of Music Acoustics, University of Music and Performing Arts Vienna, Austria
(2) Acoustics Research Institute, Austrian Academy of Sciences, Vienna, Austria
(3) Department of Music Acoustics, University of Music and Performing Arts Vienna, Austria

Abstract

This paper demonstrates an experimental setup for music acoustic experiments and contemporary music performance following a hybrid physical modelling approach. In this setup, a clarinet mouthpiece with a sensor-equipped reed is coupled to a virtual tube [1]. A C++ implementation of a tube model is presented in the form of a Csound opcode which runs on the ultra low-latency audio platform Bela [2]. The coupling is realised with an actuator that acts on the sensor-reed. The actuator is driven by the virtual pressure at the closed end of the tube model, whereas the sensor-reed signal is fed back to the model as volume flow. The experimenter can modify the parameters for length, radius, conicity, end-reflection and air density of the tube model, and is also given control over the coupling between reed and actuator in real time. This setup allows to explore acoustic phenomena that are usually either enclosed (reed-resonator coupling) or static (e.g. resonator shape) in conventional acoustic instruments and may also be useful for music acoustics training.

Keywords: Physical Modelling, Woodwinds, Realtime Audio, Haptic feedback, Bela, Csound

REFERENCES

[1] A. Hofmann, V. Chatziioannou, S. Schmutzhard, G. Erdogan, and A. Mayer, "The half-physler: an oscillating real-time interface to a tube resonator model," in *Proceedings of the international conference on new interfaces for musical expression*, Porto Alegre, Brazil, 2019, p. 130–133.

[2] Schmutzhard, S., Chatziioannou, V., & Hofmann, A. (2017). Parameter Optimisation of a Viscothermal Time-Domain Model for Wind Instruments. In *Proceedings of the 2017 International Symposium on Musical Acoustics* (pp. 27–30). Montreal, CA: McGill University.

1 hofmann-alex@mdw.ac.at
2 sschmutzhard@kfs.oeaw.ac.at
3 chatziioannou@mdw.ac.at

PROCEEDINGS of ISMA 2019
International Symposium on Music Acoustics

13 - 17 September 2019 in Detmold, Germany

ODESSA – Orchestral Distribution Effects in Sound, Space and Acoustics: An interdisciplinary symphonic recording for the study of orchestral sound blending

Martha de Francisco(1), Malte Kob(2), Jean-François Rivest(3), Caroline Traube (4)

(1)McGill University, Canada, martha.defrancisco@mcgill.ca

(2)Detmold University of Music, Germany, kob@hfm-detmold.de

(3)Université de Montreal, Canada, jean-francois.rivest@umontreal.ca

(4)Université de Montreal, Canada, caroline.traube@umontreal.ca

Abstract

ODESSA is a collaborative project between the Université de Montréal, McGill University and Detmold University of Music aiming to study orchestral blending effects, examining how instrumental sounds are sculpted by the conductor, the musicians and the hall acoustics and how the sound changes when heard and recorded from different perspectives. This project is realized in the context of the ACTOR (Analysis, Creation, and Teaching of Orchestration) Partnership, which involves a diverse international team of composers, music theorists, musicologists, computer and signal processing scientists, psychologists, acousticians, sound recordists and conductors. ACTOR's main goals are to develop a perceptually based theory of orchestration and to create new tools for music analysis, composition, teaching and mediation.

Keywords: orchestral blending, timbre, ACTOR, concert hall acoustics

1 INTRODUCTION

ODESSA – an acronym for "Orchestral Distribution Effects in Sound, Space and Acoustics" is a project created jointly by members of the Université de Montréal, McGill University and Detmold University of Music aiming to study orchestral blending effects. Approaches to achieve this goal consist of investigations on how instrumental sounds are sculpted by the conductor, the musicians and the hall acoustics and how the sound changes when heard and recorded from different perspectives. The framework of this project is the 7-year project ACTOR (Analysis, Creation, and Teaching of Orchestration), a partnership, which involves a diverse international team of composers, music theorists, musicologists, computer and signal processing scientists, psychologists, acousticians, sound recordists and conductors.

At the core of the ODESSA project is a complex multitrack recording of the Orchestre de l'Université de Montréal performing excerpts from Tchaikovsky's Sixth Symphony, "Pathétique". More than 50 microphones are used in a combination of close microphone pick-up and ambient recording. Concurrently, the acoustical balance of the instruments is examined employing techniques such as 3D intensity probes and an acoustic camera. Excerpts of the recording of varying instrumental combinations are used as listening test stimuli with the purpose of investigating timbral blending effects.

1.1 ODESSA GROUP

Under the combined leadership of four researchers of the ACTOR Partnership, the ODESSA project consists of a complex multitrack recording, a joint music production and evaluation of an orchestral recording realized at Salle Claude-Champagne, Université de Montréal's concert hall, on September 29-30, 2018. Under the baton of conductor Jean-Francois Rivest, the Orchestre de l'Université de Montréal performed excerpts from Tchaikovsky's Sixth Symphony, "Pathétique". Led by recording producer (Tonmeister) Martha de Francisco a multimicrophone recording of the rehearsal was realized with more than 50 microphones used in a combination of close microphone pick-up and ambient recording. Concurrently, the balance of room acoustics and musical instruments was examined by acoustician Malte Kob with the students Cosima Riemer, Caspar Ernst and Stefanos Ioannou from Detmold University of Music and Dorothea Lincke from TU Berlin employing techniques such as 3D intensity probes and an acoustic camera. Excerpts of the recording of varying instrumental combinations are used as listening test stimuli with the purpose of investigating timbral blending effects. Caroline Traube contributed with the study of the performers' role in the shaping of instrumental timbre and to the sound analysis and perceptual evaluation of the recorded excerpts. She also led the complex organisation of the event, which involved coordinating several teams of technicians and students, as well as the research equipment provided by the three collaborating institutions. An online resource and a video recording from the "Music mediation" programme of the University of Montreal document the entire project [1, 2].

1.2 RESEARCH OBJECTIVES

The ODESSA project's interdisciplinary character establishes an array of diverse research questions and objectives. Approaching the main topic of "orchestral blending" from different perspectives will provide insight in music composition, musical performance, musical acoustics, psychoacoustics, room acoustics and sound recording. With the combined data from the recording, the various audio tracks and microphone groups, the acoustical measurements from the hall and the timbre analysis of the whole process, we intend to offer to the ACTOR community in particular (and to the musical world at large) a vast array of tools to study the combination of timbres and orchestral instruments, as well as the interaction between instruments and the surrounding acoustics.

One of the main objectives of this project is to trace instrumental blending in an orchestra by listening to and analyzing the sound of instruments as recorded from different perspectives. The aim is to present the research community with audible information of the sound of single instruments and orchestral sections in the close range, as well as the sounds that are heard at more distant perspectives with the help of group, main and ambient microphones. By comparing the close-microphone pick-up and the ambient recordings the researchers aim at shedding light at the importance of reflected sound for our perception of instrumental blend.

The study of the acoustical balance of the instruments of the orchestra as well as the distribution of the sound energy on stage and in the hall will be used to verify and confirm orally established findings of instrumental nuances and the detail of ambient characteristics of the symphonic sound in the space as perceived by the conductor and the recording professionals.

2 METHODOLOGY

2.1 Selection of excerpts from the Pathetique Symphony

The Pathétique symphony lasts about 45 minutes and it has the following instrumentation:
- Woodwinds: 3 flutes (3rd doubling piccolo), 2 oboes, 2 clarinets, 2 bassoons
- Brass: 4 horns, 2 trumpets, 3 trombones, 1 tuba
- Percussion: timpani, bass drum, cymbals, tam-tam
- Strings (string strength on the recording day): 9 violins I, 8 violins II, 5 violas, 7 celli, 4 double basses (32 in total).

Prof. Jean-François Rivest developed a list of music segments for the recording which present different thematic complexes such as orchestral groups, compositional groups, composite melodic line, and the aggregation of individual instruments in a section. Here are a few examples of the excerpts that were recorded, as described by Maestro Rivest:

> "In order to listen individually to different orchestral groups, we recorded certain passages with only the winds, only the brass, the percussion instruments or the strings and finally we recorded the whole tutti. This is the simplest yet most important way to delve into the construction of the orchestration of the symphony. The coda of the 3rd movement or the fugal development at bar 270 in the 1st movement are good examples. One will be able to hear each of these sections separately and in various 'takes' and microphone settings."
>
> "Often, the composer will combine various instruments from different families into one melodic line and other instruments will perform the countersubject or harmony and the accompaniment. This

describes an orchestration by compositional groups. For example, we recorded the beginning of the 4th movement with the countersubject alone (with its haunting combination of high bassoon, low flutes and progressively added clarinets and oboes). Then, we recorded the main musical element in the whole string section and finally we recorded the tutti. Another good example is the re-exposition of the second theme of the 1st movement, at bar 305 (arguably the most well-known melody of the Pathétique). We recorded the harmony only (double-basses, trombones, timpani, horns, cellos and violas), then the counter-melody only (oboes, clarinets, bassoons and added violas and cellos at bar 309), then the melody itself (violins, flutes and added bassoons and clarinets, from bar 311), and finally the whole tutti."

"One of the most striking orchestration features of the Pathétique is the invention of the composite melodic line in the violins at the beginning of the 4th movement. The listener hears a descending scale, but individual violins take turns with weird leaps exchanging the relevant notes that form this scale. We therefore recorded each violin section separately (with their very strange broken lines) and then both sections together to demonstrate Tchaikovsky's trait of genius. The recording of this passage was asked for by many of our colleagues from ACTOR."

"Finally, another interesting aspect of orchestration is the building or aggregation of individual instrumentalists to form a string section: many individuals playing the same line become one line of music. We wanted to show that on the one hand there is a clear de-individualization and grouping effect that takes place the more violins play together, but on the other hand we wanted to illustrate the fact that there is a lower limit, a number under which it is not possible for a few violins to sound and blend like a section. In order to explore that, we used the same melody, the second theme of the 1st movement in the first violins (from bar 89) recording the same melody with one violin (the solo concertmaster), 2 violins, 3 violins, 4 violins, 6 violins, and finally the whole section. We even did a recording where the front of the section leads and one where the back of the section leads, which showed us interesting psychological aspects of orchestration."

A short summary of the musical excerpts that have been performed in the frame of ODESSA is given in Table 1.

Table 1. Selected excerpts and their related research question or characteristic orchestral gesture.

Excerpt	Subject
MOV. I, bars 305-309	How a poetic demand from the conductor can change the orchestra's playing
MOV. I, bars 305-313	Hyper-romantic counterpoint, a study of orchestration strata
MOV. I, bars 89-97	The perception of individual violins or of a section of violins
MOV. I, bars 170-185	Counterpoint and orchestration as a way to enhance energy
MOV. I, bars 284-304	Hyper-romantic counterpoint and the building of a climax
MOV. III, bars 196-256	Contrast between pointillistic motives and linear horizontal ascending energy lines
MOV. III, bars 221-229	Alternating sections between strings and woodwinds
MOV. IV, bars 19-23	Composite violin line (only violins)

2.2 Recording the ODESSA project

The complex sonorities of a symphony orchestra, as a result of a cooperation of the playing technique of the musicians, the sound radiation of the instruments and the acoustic influences of the room, represent a major challenge for recording professionals [3].

In order to create a sonically convincing recording of a large ensemble performing in a concert hall, skilled recording engineers learn to discern the acoustic components that appear almost simultaneously when music is being played, the direct sound as well as the sound reflections that result as the waves emanating from the sound sources expand and bounce off the walls, floor and ceiling in multiple reflections, developing a diffuse sound field. The sequence in the right proportions of direct sound, early reflections and the ensuing reverberation are important for the tonal impression of a musical performance [4]. Learning to discern the nuances of close and reflected sound in various layers of its expansion constitutes one of the main practices of expert recording engineers for classical music, and it marks a point of departure for the recording of the ODESSA project.

The ODESSA recording is based on a number of arrays of microphones placed in various distances of the musical instruments in order to reconstruct the natural sonic sequence in the hall. A team led by Jack Kelly and Diego Quiroz from McGill University prepared a recording system with 50 studio microphones and digital recording technology in HD at 96 kHz, 24 bit. The microphones have been carefully positioned and fine-tuned by ear. In Figures 1 and 3 the microphone positions of the orchestra recording are indicated.

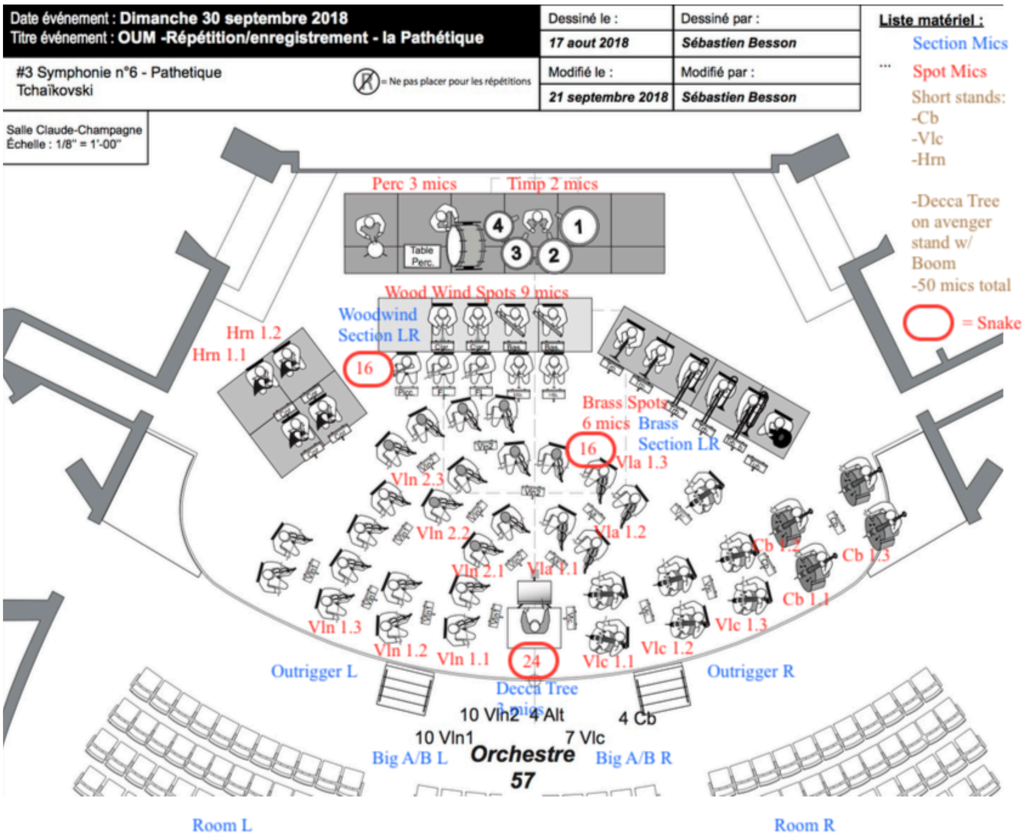

Figure 1. Orchestra seating arrangement and microphone placement.

The main array consists of a modified “Decca Tree” [5] suspended above the conductor with flanking microphones (outriggers). This array of omnidirectional studio microphones is responsible for the capture of the general, balanced and blended sound of the full orchestra. Besides, a large number of spot microphones in the close range of the orchestra provides a near sound picture of each instrument meant to increase the definition of their sound and to intensify their tonal characteristics. Additionally, two further levels of distance, the AB microphones (in front of the first row of the audience) and the furthest room microphones (on the balcony) define the most distant layers of sound. In postproduction the recorded material is edited and mixed to resemble the closest representation of a natural listening experience in the concert hall. The recorded material (in multitrack, stereo and binaural) will be presented to the research community for evaluation. The online resource will serve as a conduit [1].

Figure 2. ODESSA recording session: the Orchestra of the University of Montreal (OUM) recorded under an extensive cloud of microphones. In the foreground the acoustic camera. Colour code for microphones: red = Decca Tree, green = Outriggers, blue = AB, yellow = Spot microphones.

2.3 ACOUSTIC MEASUREMENTS

Along with the orchestra recordings an extensive assessment of acoustical properties of the Salle Claude Champagne was performed. The aim of such investigations is the characterization of the acoustic boundary conditions that musicians and conductors experience when performing music as well as the assessment of acoustic measures that correlate with the perception of music listeners. Earlier studies indicate that acoustic conditions not only affect the listeners' impression of music [6, 7] and can be described by acoustic measures [8], but also significantly impact on the musicians' performance [9, 10, 11, 12, 13, 14, 15]. A number of useful parameters have been proposed in [8] which can be derived using impulse response and sound level measurements. To allow the evaluation of these and more complex parameters, the following measurements have been provided:

- Reverberation time (EDT, T20, T30)
- SDM measurements with intensity probe and sweeps [16]
- Speech transmission index (STIPA) from musicians' positions to other musicians' and listeners' positions
- Noise criterion curves according to ANSI/ASA 12.2-2008

Several loudspeaker (omnidirectional and directive) and microphone positions have been used to evaluate the parameters. Their positions are indicated in Fig. 3. Using the SDM analysis the direction of sound impact at specific locations can be visualised. Among other interesting findings the statement that the balcony position is Martha de Francisco's favourite listening position could be confirmed: At this position a very good balance of direct sound and listeners' envelopment could be observed due to the ceiling reflection (see Fig. 4).
During the orchestra performance additional measurements have been performed:

- Acoustic camera recordings
- Contact microphone recordings on first violins

The acoustic camera allows a visualisation of the orchestral balance and sound pressure distribution at the listener's location and is used to validate and extend earlier findings related to sound propagation and perception within ensembles [17, 18].

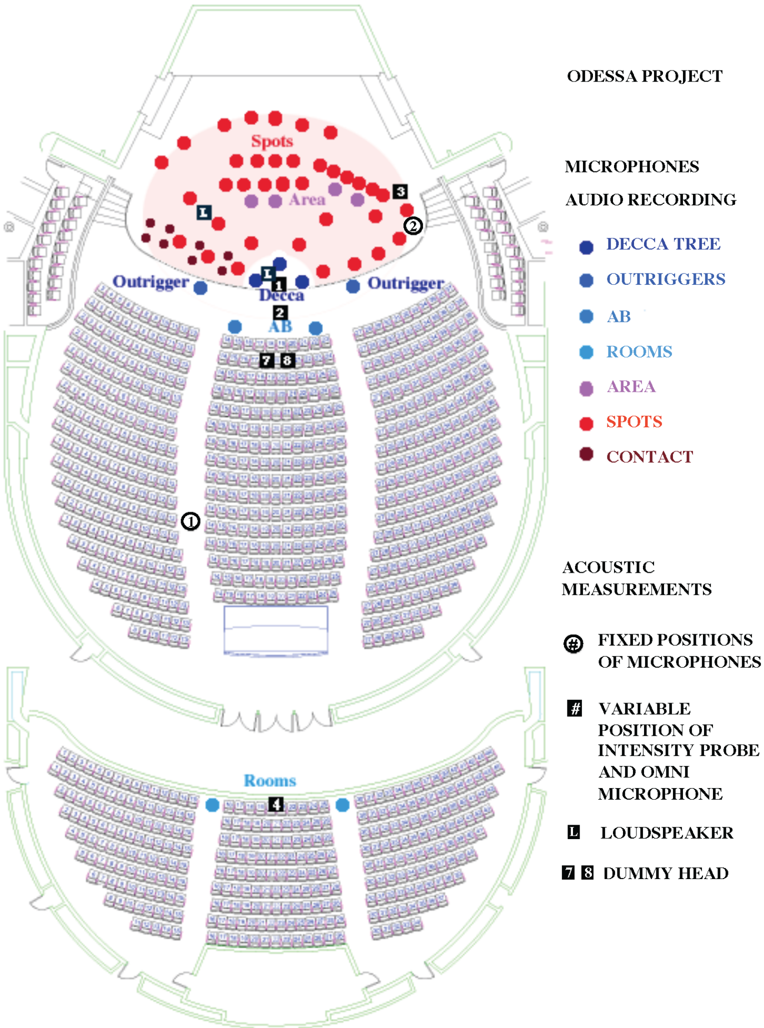

Figure 3. Location of loudspeakers and microphones for the acoustic evaluation.

The contact microphones were used to investigate the coherence among single instruments within an ensemble, see next section and [19].

A third set of measurements is currently performed under laboratory conditions in Detmold and other places: Directivity measurements of instruments. Since the sound radiation from musical instruments can be very complex in various domains (space, time, frequency), the effect of the instruments' orientation, construction, playing style and fingering techniques have a a strong impact on the perception of musical sounds. This research area also impacts on the virtualisation of orchestration using computer programs and virtual acoustic environments [20] as planned in the ACTOR project. An upcoming research interest is the relevance of directivity data on the evaluation of acoustic measures [21].

For future studies in other concert halls a set of measurements is currently developed for an acoustic description of recording environments. Directives for such a recommendation would be, among others: ease of acquisition and interpretation, high reproducibility, good correlation with subjective cues.

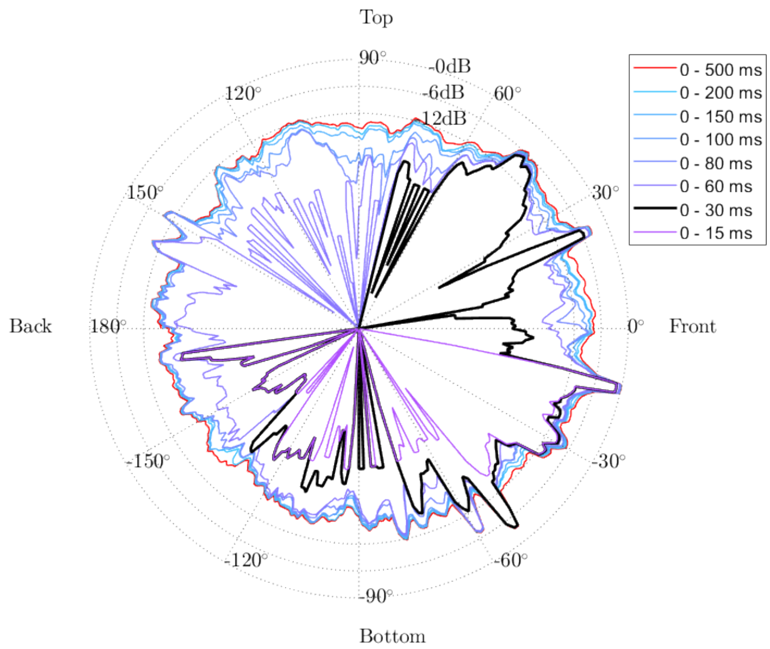

Figure 4. Direction of sound incidence from the stage to the balcony, visualised for various time frames using the SDM method [16], calculation by Dorothea Lincke using a Matlab script by Sebastià Amengual [22].

2.4 Perceptual evaluation

On a perceptual level, timbre blend can be defined as the auditory fusion of concurrent instrumental sounds. When blending occurs, the individual sounds become less distinct [23]. Some instruments of the orchestra blend more easily than others. For example, the horn is generally considered as an easily blendable instrument [24]. The oboe, on the other hand, does not blend easily because of a prominent formant structure which makes its timbre stand out [25, 24, 26]. Blending effect also depends on other factors. It increases drastically when instruments are played in unison and with synchronized attacks. Performance-related factors include tuning, pitch modulation (as vibrato) and articulation. When instruments are played on different notes, blending depends on which instrument is assigned to the higher voice [23].

The degree of perceived blend can be measured in several ways. One approach consists in deducing blend from increasing confusion in the identification of instruments in a mixture [25]. A more direct measure is done through rating scales [25, 24, 26, 27].

In the context of a student work a first study on the perception of blend was undertaken by Stefanos Ioannou, who investigated the conditions that perceptually contribute to the impression of a blended sound, based upon a listening test using the recordings of Mov. 1 bars 89-97. In this movement, the violins were captured by microphones placed at different distances from the stage (including contact microphones) and in groups of various sizes (from 1 to 8). For this segment, the results are given in [19].

In the next stage of this project, performance-related factors will be investigated such as the pitch and timbre tuning which occurs when violinists attempt to achieve blending within their section. Fundamental frequency (mean value as well as modulation depth and rate) and acoustic descriptors related to timbre (such as spectral centroid) will be tracked over time. Finally, blending effect on dyads and triads will also be analyzed on the basis of previous research [23], exploring the role of the extensity (auditory size as a dimension of timbre [28]) and of the instrument directivity and radiation into the acoustic surrounding space.

3 CONCLUSIONS

The ODESSA project "Orchestral Distribution Effects in Sound Space and Acoustics", allows insight in how orchestral sound works as examined in a multidisciplinary context of music performance, acoustics, perception and audio engineering. It enables researchers to investigate timbral blending effects, and it demonstrates the impact of the acoustics on our perception of music. In addition to the Performance Axis' activities that enabled the recording of the project, in the Musical Analysis Axis of the ACTOR partnership the researchers will realize perceptually relevant analysis of the recorded data. Detailed kinds of analysis will be performed: sound analysis, perceptive analysis and an analysis of how the instrumental and orchestral sound changes with the distance.

The ODESSA project brings together an array of experts in different disciplines who for the first time join forces to explore their research topics. In an unprecedented way, an intense convergence of several types of expertise and technical means developed over many years have come together to give insight into how orchestral sound works in all its complexity.

ACKNOWLEDGEMENTS

The ODESSA project was supported by the Social Sciences and Humanities Research Council of Canada (SSHRC) through the ACTOR partnership, the Fonds de recherche du Québec – Société et Culture (FRQSC), the Faculté de musique et Vice-rectorat – Recherche, Découverte, Création, Innovation, at Université de Montréal, the Schulich School of Music at McGill University, the Erich Thienhaus Institute of Detmold University of Music, the Canada foundation for innovation (CFI), the Center for Interdisciplinary Research in Music, Media and Technology (CIRMMT) and the Observatoire interdisciplinaire de création et de recherche en musique (OICRM). We warmly thank the members of the different technical teams involved, as well as all the students who participated in the project, as research assistants in sound recording, musical acoustics and "médiation de la musique" and as musicians of the Orchestre de l'Université de Montréal.

REFERENCES

[1] Online resource (documentation/audio examples) of the ODESSA project: www.actorproject.org/odessa

[2] Video documentary of the ODESSA project: www.youtube.com/watch?v=yD9kdz03tDQ

[3] Meyer, J. The Sound of the Orchestra, J. Audio Eng. Soc. 41(4), 1993, 203-213.

[4] Meyer, J. Acoustics and the Performance of Music: Manual for Acousticians, Audio Engineers, Musicians, Architects and Musical Instrument Makers, 5th ed., trans. Uwe Hansen, New York: Springer, 2009, 196-201.

[5] Görne, T. Tontechnik. 1. Ed., Carl Hanser Verlag, Leipzig, 2006, ISBN 3-446-40198-9.

[6] Weinzierl, S. & Vorländer, M. Room acoustical parameters as predictors of room acoustical impression: What do we know and what would we like to know? Acoustics Australia, 2015, 1–8.

[7] Sahin, B. Investigating listeners' preferences in Detmold Concert Hall by comparing sensory evaluation and objective measurements. Master's thesis, Detmold University of Music, 2017.

[8] Acoustics – measurement of room acoustic parameters – part 1: Performance spaces, 1st Edition, International Standards Organization, ISO 3382-1, Geneva, Switzerland, 2009.

[9] Winckel, F. F. Optimum acoustic criteria of concert halls for the performance of classical music. J. Acoust. Soc. Amer. 34(1), 1962, 81–86.

[10] Wenmaekers, R. H.; Hak, C. C. & van Luxemburg, L. C. On measurements of stage acoustic parameters: Time interval limits and various source-receiver distances. Acta Acustica/Acustica 98, 2012, 776–789.

[11] Schärer Kalkandjiev, Z. & Weinzierl, S. The influence of room acoustics on solo music performance: An empirical case study. Acta Acustica united with Acustica 99(3), 2013, 433–441, doi:10.3813/AAA.918624Z.

[12] Schärer Kalkandjiev, Z. & Weinzierl, S. The influence of room acoustics on solo music performance. An experimental study. Psychomusicology: Music, Mind, and Brain 25(3), 2015, 195–207, doi:10.1037/pmu0000065.

[13] Schärer Kalkandjiev, Z. The Influence of Room Acoustics on Solo Music Performances. An Empirical Investigation, PhD thesis, TU Berlin, 2015, doi:10.14279/depositonce-4785Z.

[14] Kob, M.; Amengual Garí, S. V. & Schärer Kalkandjiev, Z. Room effect on musicians' performance. In: Binaural understanding, Springer, 2019 (in print).

[15] Amengual Garí, S.V.; Kob, M. & Lokki, T. Analysis of trumpet performance adjustments due to room acoustics. Proceedings of ISRA Amsterdam, 2019.

[16] Tervo, S.; Pätynen, J. & Lokki, T. Spatial decomposition method for room impulse responses. J. Audio Eng. Soc 61(1), 2013, 1–13.

[17] Békésy, G. von Feedback phenomena between the stringed instrument and the musician. The Rockefeller University Review 6(2), 1968.

[18] Ueno K.; Kanamori, T. & Tachibana, H. Experimental study on stage acoustics for ensemble performance in chamber music. Acoust. Sci. & Tech. 4(4), 2005, 345–352.

[19] Ioannou, S. & Kob, M. Investigation of the blending of sound in a string ensemble. Proceedings of ISMA Detmold, 2019.

[20] Kob, M.; Ackermann, D.; Weinzierl, S. & Zotter, F. Analyse und Synthese der dynamischen Richtwirkung von Musikinstrumenten. Akustik Journal, DEGA 2018.

[21] Wenmaekers, R. H. C.; Hak, C. C. J. M.; Hornikx, M. C. J. & Kohlrausch, A. G. Sensitivity of stage acoustic parameters to source and receiver directivity: Measurements on three stages and in two orchestra pits. Applied Acoustics 123 (Supplement C), 2017, 20–28, doi:10.1016/j.apacoust.2017.03.004.

[22] Amengual Garí, S. V. Investigations on the Influence of Acoustics on Live Music Performance using Virtual Acoustic Methods. Doctoral Thesis, University of Music Detmold, 2018.

[23] Lembke, S.-A.; Parker, K.; Narmour, E. & McAdams, S. Acoustical correlates of perceptual blend in timbre dyads and triads, Musicæ Scientiæ, Vol. 23(2), 2019, 250-274, DOI: 10.1177/1029864917731806.

[24] Sandell, G. J. Roles for spectral centroid and other factors in determining "blended" instrument pairings in orchestration. Music Perception, 13, 1995, 209-246.

[25] Kendall, R. A. & Carterette, E. C., Identification and blend of timbres as a basis for orchestration, Contemporary Music Review, Vol. 9, Parts I & 2, 1993, 51-67.

[26] Tardieu, D. & McAdams, S. Perception of dyads of impulsive and sustained instrument sounds. Music Perception, 30(2), 2012, 117-128.

[27] Lembke, S.-A.; Levine, S. & McAdams, S. Blending Between Bassoon and Horn Players: An Analysis of Timbral Adjustments During Musical Performance, Music Perception Vol. 35(2), 2017, 144-164, DOI: 10.1525/mp.2017.35.2.144.

[28] Chiasson, F.; Traube, C.; Lagarrigue, C. & McAdams, S. Koechlin's volume: Perception of sound extensity among instrument timbres from different families. Musicae Scientiae, Vol. 21(1), 2017, 113-131. DOI: 10.1177/1029864916649638.

PROCEEDINGS of ISMA 2019
International Symposium on Music Acoustics

13 - 17 September 2019 in Detmold, Germany

Investigation of the blending of sound in a string ensemble

Stefanos IOANNOU[1], Malte KOB

(1) HfM Detmold, Germany, stefanos@primehome.com

(2) HfM Detmold, Germany, kob@hfm-detmold.de

Abstract

Ensemble sound is a topic where, to date, only little research has been conducted. A fundamental question that still needs to be answered is how many violins are required for a number of violins to blend together in an ensemble.

As part oft the ACTOR project, A violin phrase from Tchaikowsky's 6th Symphony has been recorded with one, two, three, four, six and ten violins over piezo microphones, spot microphones, a decca tree, room microphones and a dummy head. These recordings were used to create a listening test, in which participants had to guess the number of violins playing and state if the recording sounded like an ensemble. Results of this test will be presented.

1 INTRODUCTION

When orchestras were first formed, they were far smaller than the typical modern orchestra. In 1730, J. S. Bach submitted his request for his church orchestra: 3 first violins, 3 second violins, 4 violas, 2 violoncellos, 1 double bass, 6 woodwinds, 3 trumpets and timpani. The first bigger orchestra was the Mannheim court orchestra, which in 1756 could boast with a 10.10.4.4.2. string section. This, however, was far from the norm. Most orchestras of the classical period had around 10 to 20 string players. In the course of the 19th century, orchestras with at least 10 first violins became common. Up to now this is the standard orchestra size for symphonic works (1). Reasons for this increase may vary, but it might be attributed to more wind instruments, such as clarinets and trombones, being used which caused the need for more strings or the tendency to build bigger concert halls, which required more instruments to achieve a full sound.

A string ensemble is extremely complex. It can be considered a number of incoherent sound sources, meaning that no matter how good the musicians are, no static phase relationship will be achieved between two instruments. Moreover, the distribution of the instruments on stage makes it difficult to predict the ensembles' timbre and radiation. Even the individual sound of the instruments is important for the sound of the ensemble as a whole. In a 2012 demonstration in Stuttgart, a violinist recorded a phrase of music multiple times using overdubbing. The resulting sound failed to create the illusion of a real ensemble. When the experiment was repeated using different violins each time, the result was much more natural sounding (1).

Due to the incoherency of the sound sources and the different distances to the microphones, the listener will localize the ensemble around the instrument nearest to him. The normal critical distance (defined as the distance from a sound source where the sound pressure of the direct sound and the reverberant sound are equal) is of little importance concerning the perceived relationship between direct and reverberant sound. A better measure would be the ratio of the direct sound to the closest instrument and the diffuse sound of the whole ensemble.

It is clear, that the transition from single sound sources to ensembles is acoustically very complex, with only little research having been published. This study aims to provide a first analysis of ensemble sound and instrumental blending. A fundamental question that needs to be answered is how many instruments are required for a number of string instruments to be perceived as an ensemble, rather than as individual instruments, as well as the influence the room has on the blending of the sound. For this, a listening test was designed with recordings made at the Salle Claude-Champagnie in Montral with the orchestra of the Université de Montréal. Furthermore, the "imperfections" of the players are to be examined, such as the phase relationship between the instruments and the intonation.

2 SETUP

The data used for the following investigation was collected on the 25th and 26th September 2019 during measurements at the Salle Claude-Champagnie in Montral as part of the ACTOR project. The measurements were made in collaboration with the orchestra of the Université de Montréal as well as researchers from the McGill University in Montreal and the Hochschule für Musik Detmold.

The measurements are based on recordings of P. I. Tchaikovsky’s 6th Symphony in B Minor op. 74; specifically, the phrase of the first violins in the first movement from bar 89 to 97. This excerpt was first played by one violin, then again by 2, 3, 4, 6 and 9 violins.

Figure 1 the violin theme

The first six violins were fitted with small piezo microphones, which were taped onto the tailpiece of the instruments. These were sent to an RME Octamic for amplification and then via Dante to the control room where they were recorded in the Pyramix Digital Audio Workstation.

Traditional recording methods were also implemented; 3 Schoeps MK4 microphones were used as spot microphones, 3 DPA4006 were used for a decca tree, a Neumann KU100 dummy head was placed in the second row and 2 Schoeps MK2S were placed in the balcony as room microphones. These went into RME Micstacy preamps and then via MADI into the control room.

3 Pitch analysis

The piezo microphone signals were used for a pitch analysis of each of the first six violins, to study if an ensemble sound is related to the pitch difference of the individual players. This analysis was done with the software Praat. The first five notes of the phrase where analyzed in each instrument and the mean and standard deviation in Herz and in cent were calculated. The orchestra tuning was 443Hz, so the reference pitches were based on this value. The Data is shown in Tables 1 to 5, with sharp notes (too high) marked in red, correct notes (correct to the nearest Hz) marked in green and flat notes (too low) marked in orange.

The data presented here has to be treated with care, due to the high amount of uncertainty in the measurements. Violinists play with a vibrato, which is done by moving the finger used to determine the length of the string, leading to a fluctuation in pitch. This makes it difficult to determine an exact pitch, as the pitch varies over the duration of the note; hence an average value had to be taken.

Note	Pitch (Hz)	Violin 1	Violin 2	Mean (Hz)	σ (Hz)	σ (cent)
f#	745.0	750	750	750.0	0.0	0.0
e	663.8	664	671	667.5	4.9	12.8
d	591.3	591	596	593.5	3.5	10.3
b	497.3	501	503	502.0	1.4	4.9
a	443.0	443	443	443.0	0.0	0.0
f#	372.5	373	375	374.0	1.4	6.5

Table 1 Pitch 2 violins

When only two violins play (table 1), the first violin plays most of its notes correctly and some to sharp, whereas the second violin generally plays a bit sharp. The standard deviation ranges from 0 to 12.8 cents, depending on the note played.

Note	Pitch (Hz)	Violin 1	Violin 2	Violin 3	Mean (Hz)	σ (Hz)	σ (cent)
f#	745.0	754	749	748	750.3	3.2	7.4
e	663.8	668	666	668	667.3	1.2	3.0
d	591.3	592	592	593	592.3	0.6	1.7
b	497.3	501	505	502	502.7	2.1	7.2
a	443.0	444	446	444	444.7	1.2	4.5
f#	372.5	376	375	376	375.7	0.6	2.7

Table 2 Pitch 3 violins

When three violins played (table 2), they all played quite sharp. There is not a single note where all violins had the exact same pitch. The range of the standard deviation was from 0.6 to 7.4 cents.

Note	Pitch (Hz)	Violin 1	Violin 2	Violin 3	Violin 4	Mean (Hz)	σ (Hz)	σ (cent)
f#	745.0	750	752	747	748	749.3	2.2	5.1
e	663.8	670	670	670	666	669.0	2.0	5.2
d	591.3	591	595	591	595	593.0	2.3	6.7
b	497.3	500	501	504	498	500.8	2.5	8.6
a	443.0	444	445	446	446	445.3	1.0	3.7
f#	372.5	376	374	378	375	375.8	1.7	7.9

Table 3 Pitch 4 violins

When four violins played (table 3), the tendency again was to play quite sharp, with only a few notes spot on. The range of the standard deviation was again reduced, ranging from 3.7 to 8.6 cents.

Note	Pitch (Hz)	Violin 1	Violin 2	Violin 3	Violin 4	Violin 5	Violin 6	Mean (Hz)	σ (Hz)	σ (cent)
f#	745.0	752	749	754	753	740	749	749.5	5.1	11.7
e	663.8	665	664	670	670	660	669	666.3	4.0	10.4
d	591.3	589	589	593	593	590	594	591.3	2.3	6.6
b	497.3	502	501	504	502	492	504	500.8	4.5	15.5
a	443.0	443	444	445	444	442	445	443.8	1.2	4.6
f#	372.5	375	376	375	377	368	372	373.8	3.3	15.3

Table 4 Pitch 6 violins

When six violins played (table 4), it can be seen that the 5th violin was consistently flat. However, again the general tendency was rather sharp, with a few correct notes. While during the increase from two to four violins, the range of the standard deviation was decreasing, in this measurement the range of the standard deviation increases dramatically, ranging from 4.6 to 15.5 cents. This is mainly due to the fifth violin playing flat.

Note	Pitch (Hz)	Violin 1	Violin 2	Violin 3	Violin 4	Violin 5	Violin 6	Mean (Hz)	σ (Hz)	σ (cent)
f#	745.0	743	753	750	750	741	745	747.0	4.7	10.8
e	663.8	662	663	668	672	662	675	667.0	5.6	14.4
d	591.3	590	590	591	593	590	594	591.3	1.8	5.1
b	497.3	503	496	502	500	501	498	500.0	2.6	9.0
a	443.0	443	442	444	447	443	446	444.2	1.9	7.5
f#	372.5	373	377	376	379	372	372	374.8	2.9	13.5

Table 5 Pitch all violins

The last recording was of all nine violins (table 5). Only the first six had piezo pickups, which could be used to evaluate the pitch. When all nine violins played, only violin 4 was always sharp. The standard deviation in pitch ranged from 5.1 to 13.5 cents, which is similar to the range when only six violins played.

Number of Violins	Minimum	Maximum	Range
2	0	12.8	12.8
3	0.6	7.4	6.8
4	3.7	8.6	4.9
6	4.6	15.5	10.9
9 (only 6 in measurement)	5.1	13.5	8.4

Table 6 Pitch summary

An interesting observation is the fact that the minimum standard deviation in pitch of a single tone is constantly rising. This suggests that the more instruments there are, the greater the range of pitches that is played. Up to four violins, the maximum standard deviation increases, but then increases again as more violins play. Especially the increase of the minimum standard deviation may suggest that an ensemble sound can be defined by this spread of different pitches played by each instrumentalist. Especially when one considers that each player's vibrato is slightly different, it might be possible that the spread of pitches heard at the same time is even larger than these measurements revealed.

4 Listening Test

4.1 Design

In order to answer the question of how many violins are needed to create the feeling of an ensemble a listening test was performed. The test consisted of 24 different examples in random order of the recorded violin phrase with different microphones and different numbers of musicians. The piezo microphones were not used, as they did not offer a natural sound similar to what can be heard in a room. The 24 variations consisted of 1, 2, 3, 4, 6 or 9 musicians and the spot microphones, decca tree, dummy head and room microphones. All examples were in stereo, except the ones recorded with the spot microphones, which were in mono.

The examples consisted of almost no mixing. The spot microphones were all mixed together at the same level. The three microphones of the decca tree were also mixed together at the same level, with the left microphone only on the left channel, the right microphone only on the right channel and the center microphone on both channels at −3dB. The dummy head and room microphone examples consisted of the left and right microphones panned to the left and right channel respectively.

For each example, the test subjects had to estimate the number of violins and state whether or not it sounded like an ensemble. The first question was to determine the accuracy to which one can hear the number of instruments – the lower the accuracy, the less individual instruments can be identified, hence sounding more like an ensemble. The second question was to determine how many violins are needed for the listener to conceive an ensemble, making it a more subjective question. The term "ensemble" was purposefully not defined, so as to not influence the listener in terms of what parameters are criteria for an ensemble sound.

The listening test was hosted with an online provider, allowing participation from all over the world. The instructions stated that the participants should take the test with headphones, as the examples from the dummy head are binaural. Over a period of five weeks, 54 people participated in the listening test, 13 of who only partially completed the test.

Participants came from all over Europe and North America.

4.2 Results

4.2.1 Spot microphones

Violins	Mean	StdDev	Mode	%Correct	EnsembleYes%	EnsembleNo%	Min	Max
1	1.0	0.1	1	98.1	3.7	96.3	1	2
2	2.1	0.3	2	90.7	13.0	87.0	1	3
3	3.1	0.9	3	51.9	35.2	64.8	1	5
4	4.1	1.8	4	25.9	77.8	22.2	1	10
6	4.4	1.5	3 and 4	7.4	74.1	25.9	2	8
9	5.2	2.5	3	1.9	88.9	11.1	1	15

Table 7 Spot microphone results

As the number of violins increases, the percentage of test subjects who felt that the example sounded like an ensemble playing also increases. The biggest difference is between three and four violins – whereas only 35% thought three violins sound like an ensemble, 78% thought that four violins sound like an ensemble. Interestingly, fewer people thought that six violins sound like an ensemble than that four violins sound like an ensemble.

As the number of violins increases from one to four, the mode (most common answer) from the test matches the number of violins. Also, the mean is extremely close to the correct number of violins, with the standard deviation increasing as the number of violins increases. This is also due to the fact that the number of participants whose estimate was correct decreases as the number of violins increases. While for one and two violins over 90% of participants were correct, only 52% and 26% were correct for three and four violins respectively.

For six and nine violins, the number of violins was vastly underestimated as, on average, 4.4 and 5.2 violins respectively. The mode was also much lower, between 3 and 4 and the number of correct estimates was negligible.

4.2.2 Decca Tree

Violins	Mean	StdDev	Mode	%Correct	EnsembleYes%	EnsembleNo%	Min	Max
1	1.0	0.2	1	95.7	4.4	95.6	1	2
2	2.1	0.5	2	73.3	15.6	84.4	1	3
3	3.4	2.3	2	26.1	43.5	56.5	1	10
4	3.8	1.4	3	28.3	66.0	34.0	1	8
6	4.6	2.8	3	8.7	73.9	26.1	1	12
9	5.7	2.4	5	0.0	97.8	2.2	1	12

Table 8 Decca tree results

With the decca tree microphones, the number of subjects perceiving an ensemble also increased as the number of violins increases. The biggest increase was from two to three violins (from 16% to 44%) and from six to nine violins (74% to 98%). It is noteworthy, that with all nine violins playing, almost all subjects stated that they perceived an ensemble.

For one and two violins, both the mean and the mode match the number of violins playing. However, for two violins the accuracy of the test subjects was a lot lower than for one violin.

For three and four violins, the number of correct estimates is significantly lower (26% and 28% respectively). Also, the mode is too small in both cases. However the mean is still well within one standard deviation of the actual number of violins. This suggests that while subjects found it difficult to guess the correct number of violins, they were not far off.

For six and nine violins, the number of correct guesses is negligible. As with the spot microphones, the number of violins was underestimated in both cases. With six violins, the mean is still within one standard deviation of the correct number of violins, but with nine violins this is not the case. This may explain the large difference in ensemble perception between six and nine violins.

4.2.3 Dummy Head

Violins	Mean	StdDev	Mode	%Correct	EnsembleYes%	EnsembleNo%	Min	Max
1	1.2	0.5	1	87.5	10.0	90.0	1	4
2	2.5	1.9	2	64.1	15.4	84.6	1	12
3	3.3	2.5	2 and 3	25.0	50.0	50.0	1	12
4	4.1	1.9	4	37.5	85.0	15.0	1	10
6	4.2	2.2	3	10.0	75.0	25.0	1	10
9	5.3	2.8	5 and 6	0.0	87.5	12.5	1	12

Table 9 Dummy head results

The dummy head is a head model with microphones in the ears. This way head related transfer functions (HRTFs) are included in the recording (2). When listening over headphones, one can hear almost exactly what could have been heard in that place in the room. Due to this, the dummy head is the microphone that most exactly represents what a listener in the concert hall would have heard.

For one and two violins, the mean is further away from the correct number of violins than in with the previous microphones, however it is still quite accurate and within one standard deviation. However the standard deviation is also larger. The percentage of subjects correctly estimating the number of violins is also a lot less.

For three and four violins, the mean is also quite accurate; however, the number of correct estimates is a lot lower. At three violins, half the subjects perceived the sound as an ensemble, while at four violins 85% of the subjects stated that the examples sounds like an ensemble.

As in the previous section, for six and nine violins the number of violins was underestimated and very few estimates where correct. Surprisingly, more people thought that four violins sounded like an ensemble than six.

4.2.4 Room Microphones

Violins	Mean	StdDev	Mode	%Correct	EnsembleYes%	EnsembleNo%	Min	Max
1	1.0	0.2	1	97.5	0.0	100.0	1	2
2	2.0	0.6	2	67.5	10.0	90.0	1	4
3	2.4	1.0	2	20.0	12.8	87.2	1	6
4	3.0	1.3	3	30.0	40.0	60.0	1	7
6	4.1	2.2	3	5.0	69.2	30.8	1	10
9	4.4	1.8	3	2.5	71.8	28.2	1	9

Table 10 Room microphones results

The room microphone examples follow the general tendency of the other microphones. However, for four or more violins, the number of violins was ever more underestimated than in the other examples. Also, even with all nine violins playing, only 72% of test subjects perceived the sound to be that of an ensemble. The maximum estimates for how many violins were playing were also lower. Even though test subjects could not accurately say how many violins were playing, they still did not perceive the sound as an ensemble. This suggests that just because one cannot distinguish individual instruments, this does not mean that an ensemble sound can be presumed.

4.2.5 Summary

The recordings made with the decca tree showed the best results for ensemble sound for when all violins played. The decca tree, due to its large distances between the microphones, may produce extremely uncorrelated signals, which are known to give a good feeling of envelopment (3). However, uncorrelated stereo signals alone do not seem to be enough, as the room microphones are also very uncorrelated, but do not prove useful for creating an ensemble sound. The decca tree is also the only microphone system, which due to its proximity to the orchestra has a relatively large percentage difference in distance from one desk to the next, causing a good depth perception (the last violin desk has a multiple of the distance to the decca tree that the first desk has). Perhaps it is this depth that may cause this ensemble sound.

Except from the room microphone examples, four violins seem to be enough to create a feeling of an ensemble in at least half the test subjects. However the more instruments play, the more subjects get this feeling. In the dummy head and spot microphones, four violins sounded to more test subjects like an ensemble than 6 violins. A pitch analysis showed that when six violins played, the range of pitches was larger than when nine violins played, suggesting slightly worse intonation. This might be the cause for this effect, as the deviation in intonation of the players could lead to the group sounding less homogenous, and hence less like an ensemble.

The reason for the worse ensemble sound in the room microphones might be because of the apparent width of the ensemble. The room microphones are so far away, that the angle between the left and right edge of the stage becomes small. This leads to a reduced width during reproduction, which opposes the idea of many instruments spread over the stage.

While one violin playing had a very high rate of correct prediction no matter the microphone setup, only the spot microphones had a high rate of correct prediction for two violins. Also, for three and four violins the mean was closest to the correct number of violins with very small standard deviations. The spot microphones were the closest to the individual violins and as a result recorded less reverberant room sound and more playing sounds such as bowing. This might make individual violins more distinguishable.

Six and nine violins are often estimated as being a lot less. This suggests saturation at four violins, at which point one cannot distinguish individual violins. Perhaps, even when more violins play, one can distinguish a few violins out of the whole, and hence the responses yielded such low numbers.

5 CONCLUSION

The transition between being able or not to estimate the correct number of violins or at least come close to the correct number seems to be about at six violins, regardless of the microphone setup. However, for the listener to perceive an ensemble, more violins lead to better result. The microphone setup also influences this, with the decca tree offering the most ensemble-like sound, while the room microphones were the worst.

Intonation may influence the listeners' perception, as six violins have in some examples received a lower ensemble rating than four violins, which could be due to the larger deviation in intonation. If this is the reason for this effect, an ensemble sound can be achieved through good intonation, meaning that sounds will little deviation in frequency blend better together.

The terms blending and ensemble sound do not seem to be the interchangeable. Especially with the room microphones it can be seen that while the number of violins cannot be accurately estimated (high blending of individual instruments), the result still does not sound like an ensemble to all listeners. However, to achieve an ensemble sound, a high amount of blending seems to be required.

The results of this study apply to the recordings done by the orchestra of the Université de Montréal in the Salle Claude-Champagnie. For definitive results, this study would need to be replicated with different orchestras in different concert halls. Especially interesting would be a study with a professional orchestra which has been playing together for years, in order to analyze their intonation and phase relationships and the effect this has on the listener's perception. Also, while the mean estimate for four violins is about the correct value, six violins are largely underestimated. In future studies, examples with five violins playing the theme should also be included.

REFERENCES

[1] Meyer, J. (2015): Akustik und musikalische Aufführungspraxis. Bergkirchen: PVVMEDIEN

[2] Boré G., Peus S. (1999): Microphones. Berlin, Neumann GmbH

[3] Wittek, H. (2015): Stereo, 5.1 and 3D-Audio, Tonmeistertagung 2014

PROCEEDINGS of ISMA 2019
International Symposium on Music Acoustics

13 - 17 September 2019 in Detmold, Germany

Sounds like melted chocolate: How musicians conceptualize violin sound richness

Charalampos SAITIS[1,2], Claudia FRITZ[3], Gary P. SCAVONE[4]

[1]Centre for Digital Music, Queen Mary University of London, United Kingdom
[2]Chair of Acoustic and Haptic Engineering, TU Dresden, Germany
[3]Lutheries-Acoustique-Musique, Sorbonne Université, UMR CNRS 7190, France
[4]Computational Acoustic Modeling Laboratory, CIRMMT, Schulich School of Music, McGill University, Canada

Abstract

Results from a previous study on the perceptual evaluation of violins that involved playing-based semantic ratings showed that preference for a violin was strongly associated with its perceived sound richness. However, both preference and richness ratings varied widely between individual violinists, likely because musicians conceptualize the same attribute in different ways. To better understand how richness is conceptualized by violinists and how it contributes to the perceived quality of a violin, we analyzed free verbal descriptions collected during a carefully controlled playing task (involving 16 violinists) and in an online survey where no sound examples or other contextual information was present (involving 34 violinists). The analysis was based on a psycholinguistic method, whereby semantic categories are inferred from the verbal data itself through syntactic context and linguistic markers. The main sensory property related to violin sound richness was expressed through words such as full, complex, and dense versus thin and small, referring to the perceived number of partials present in the sound. Another sensory property was expressed through words such as warm, velvety, and smooth versus strident, harsh, and tinny, alluding to spectral energy distribution cues. Haptic cues were also implicated in the conceptualization of violin sound richness.

Keywords: Violin, Semantics, Perception, Acoustics

1 INTRODUCTION

The overall goal of the research presented here is to better understand how musicians evaluate violins within the wider context of finding relationships between measurable vibrational properties of instruments and their perceived qualities. Contrary to the typical approach of beginning with a physical hypothesis based on structural dynamics measurements [1, 2] or audio feature extraction [3, 4], a method that relies on theoretical assumptions about cognitive-semantic categories and how they relate to natural language [5, 6] was used to identify and categorize concepts of violin sound richness emerging in spontaneous verbal descriptions. These were collected during a carefully controlled playing experiment [7] and in an online survey where no sound examples or other contextual information was present.

Using the same method in earlier violin playing experiments, whereby skilled string players ranked a set of instruments based on preference and described their criteria through free verbalization tasks [8], we previously explored how violin quality in general is conceptualised by the musician [9, 6]. Specifically, eight semantic categories (concepts or meta-criteria) were identified: 1) TEXTURE (distribution of spectral content); 2) RESONANCE (intensity "under the ear" and via "felt" vibrations); 3) PROJECTION (intensity "at a distance"); 4) RESPONSE (ease of playing and responsiveness); 5) CLARITY (lack of audible artifacts in the sound); 6) BALANCE (of sound and response across strings and registers); 7) INTEREST (affective-hedonic reactions); 8) RICHNESS (amount of spectral content). The latter emerged as a key perceptual factor in assessing violin quality. A statistical analysis of the preference judgments collected in the same and subsequent experiments corroborated that violin preference is strongly associated with perceived richness in the sound [10, 8, 11, 12, 7].

Importantly, it was shown that while perceived variations in violin quality rely on variations in style and the expertise of different musicians, the broader semantic categories emerging from verbal descriptions remain common across diverse musical profiles, thus reflecting a shared perception of acoustic information. This allowed us to develop a musician-driven framework for understanding how the dynamic behavior of a violin might relate to its perceived quality [6]. Furthermore, the verbal data revealed that vibrations from the violin body and the bowed string (via the bow) are used as extra-auditory cues that not only help to better control the played sound but also contribute to its perceived qualities. Indeed, recent research on the evaluation of violin and piano quality has revealed that an increase in the vibrations felt at the left hand of violinists and the fingertips of pianists can lead to an increase in the perceived richness as well as loudness of the sound [13].

Here we further investigated the perceptual and cognitive processes involved when violinists evaluate violins by focusing on how they describe perceptions of sound richness. Verbalizations were analyzed on the basis of semantic proximities in order to identify emerging concepts that could be coded under broader categories acting as psychologically relevant descriptors of violin sound richness. Semantic proximities were inferred from syntactic context and linguistic markers (e.g., reformulation, explanation, comparison, negation). The coding process was based on the inductive principle of Grounded Theory, where a system of ideas is constructed not starting from a hypothesis (or a set of hypotheses) but from the data itself [14].

2 METHOD

2.1 Online survey

Taking into account the lingual diversity of Québec, where this research took place, bilingual questions in English and French were compiled, and participants were invited to respond in the language they felt most comfortable with. Similarly to our previous work [6], very general open-ended questions were formed to avoid confining the responses into pre-existing categories. Two respondents chose to reply in French and it was decided not to translate their responses but include them in the analysis directly.

Thirty-four violinists (20 female; average age = 42 yrs, SD = 17 yrs, range = 19–73 yrs) provided written responses to the questions (French version is given in parentheses) **Q1:** ***What does richness mean for you?*** (*Qu'est-ce que la richesse signifie pour vous?*) and **Q2:** ***How would you evaluate a violin in terms of richness?*** (*Comment évalueriez-vous un violon en termes de richesse?*). Respondents had at least 14 years of violin experience (average years of violin training = 31 yrs, SD = 15 yrs, range = 14–65 yrs), with 13 describing themselves as professional musicians. Musical profile information for each violinist is reported in Table 1.

2.2 Playing experiment

2.2.1 Musicians, violins and controls

Sixteen violinists participated in the playing experiment (8 female; average age = 32 yrs, SD = 8 yrs, range = 21–55 yrs). They had at least 15 years of violin experience (average years of violin training = 25 yrs, SD = 8 yrs, range = 17–48 yrs) and were remunerated for their participation. Eleven participants described themselves as professional musicians. Musical profile information for each violinist is reported in Table 2. Musicians #10 and #11 had previously participated in the online survey (respondents #25 and #23 in Table 1, respectively).

Five violins of different make (Europe, North America, China), year of fabrication (1914–2011) and price ($2.7k–$71k) were chosen from two luthier workshops in Montreal, Canada, in order to form, as much as possible, a set of instruments with a wide range of characteristics [7]. The respective luthiers provided the price estimates and tuned the instruments for optimal playing condition based on their own criteria. Participants' own violins were not included in the set of instruments in order to avoid possible preference biases caused by the mere exposure effect [15] by which familiarity with a stimulus object increases preference toward it.

Low light conditions and dark sunglasses were used to help hide the identity of the instruments as much as possible and thus circumvent the potential impact of visual information on judgment while ensuring a certain level of comfort for the musicians, as well as safety for the violins. To avoid the potential problems of using a common bow across all participants (e.g., musicians being uncomfortable with a bow they are not familiar with, bow quality), each violinist used their own bow. Furthermore, violinists were given the option to either use a provided shoulder rest (Kun Original model), or use their own, or use no shoulder rest. Sessions took place in

Table 1. Musical profile of online survey respondents and semantic categories they used.

	Musical profile			Semantic categories							
	Practice (yrs)	Skill	Style of music	Fu	Wa	Reso	Cl	Vi	Resp	Ba	In
1	17	Amateur	Classical, Folk	✗	✗					✗	✗
2	16	Amateur	Classical	✗	✗					✗	
3	14	Amateur	Classical	✗	✗						✗
4	16	Amateur	Classical	✗	✗	✗	✗		✗		✗
5	18	Amateur	Classical, Jazz, Folk	✗		✗			✗		✗
6	23	Professional	Classical, Jazz	✗	✗	✗					✗
7	44	Professional	Classical, Contemporary	✗	✗	✗	✗			✗	
8	23	Amateur	Classical, Baroque	✗							✗
9	20	Amateur	Classical, Jazz, Folk	✗				✗		✗	
10	17	Professional	Classical, Contemporary	✗		✗	✗	✗	✗		
11	20	Professional	Classical, Baroque, Contemporary	✗	✗	✗	✗		✗		✗
12	39	Professional	Classical, Contemporary	✗	✗	✗			✗	✗	✗
13	45	Amateur	Classical	✗	✗			✗			
14	50	Professional	Classical, Contemporary	✗							
15	34	Amateur	Classical	✗	✗	✗					✗
16	35	Amateur	Classical	✗							
17	25	Amateur	Classical	✗	✗						
18	56	Amateur	Classical, Contemporary	✗			✗				
19	19	Professional	Classical, Jazz	✗	✗	✗	✗	✗			✗
20	15	Amateur	Classical, Jazz	✗		✗					
21	15	Amateur	Classical, Folk	✗	✗	✗					
22	27	Professional	Classical, Baroque	✗	✗		✗				✗
23	25	Professional	Jazz, Folk	✗	✗	✗			✗		
24	31	Professional	Classical, Baroque	✗		✗					✗
25	48	Professional	Classical, Folk	✗	✗						✗
26	18	Professional	Classical, Baroque	✗		✗					
27	44	Professional	Classical	✗							✗
28	30	Amateur	Classical	✗		✗					✗
29	65	Amateur	Classical, Baroque		✗						
30	40	Amateur	Classical, Contemporary		✗	✗		✗			
31	50	Amateur	Classical, Baroque	✗	✗		✗				✗
32	60	(not reported)	Classical, Baroque	✗							
33	38	Amateur	Classical, Folk	✗	✗						
34	22	Amateur	Classical	✗							✗

acoustically dry rooms to help minimize the effects of room reflections on the direct sound from the violins.

2.2.2 Tasks and procedure

In the playing experiment, musicians were asked to "rank-rate" the five violins in terms of richness in two tasks. In each task, violinists simultaneously rated each of the violins using separate, identical on-screen sliders, thus providing a ranking of the instruments at the same time. They were instructed to always rate their top choice as 1 and their lowest as 0, and were not allowed to assign the same rank-rating to two or more instruments. Musicians were instructed to maximise evaluation speed and accuracy, and were encouraged to play their own violin whenever they needed a reference point during the experiment. To minimise fatigue, violinists were encouraged to take breaks between trials whenever needed.

The first task involved playing the eight notes of the chromatic scale *G2* $\rightarrow$ *D3 détaché*, first *without vibrato*

Table 2. Musical profile of playing test participants and semantic categories they used.

	Musical profile			Semantic categories							
	Practice (yrs)	Skill	Style of music	Fu	Wa	Reso	Cl	Vi	Resp	Ba	In
1	21	Professional	Classical	✗	✗	✗				✗	✗
2	23	Professional	Classical	✗	✗		✗				✗
3	21	Professional	Classical	✗		✗					
4	18	Professional	Contemporary	✗		✗		✗			
5	17	Amateur	Classical					✗			✗
6	30	Professional	Classical	✗							
7	26	Professional	Classical	✗		✗				✗	
8	20	Amateur	Classical	✗						✗	
9	25	Amateur	Jazz	✗							
10	48	Professional	Classical	✗	✗	✗					✗
11	22	Amateur	Classical	✗	✗	✗		✗			✗
12	34	Professional	Classical	✗		✗	✗				✗
13	17	Professional	Folk	✗							
14	20	Amateur	Classical	✗	✗		✗				
15	32	Professional	Classical, Folk	✗		✗				✗	
16	28	Professional	Classical		✗						✗

followed by a repetition *with vibrato*. Violinists were instructed to follow a 50 bpm tempo and use the whole bow. The second task involved playing the opening solo passage from Max Bruch's Violin Concerto No. 1 in *G* Minor, Op. 26 (Movement I: Prelude). The particular excerpt was chosen because it incorporates the whole range of the instrument (as opposed to the first task) as well as a variety of techniques and dynamics. Violinists were instructed to follow the temporal and expressive markings as much as possible (i.e., a certain degree of personal interpretation was expected).

Upon completing the second task, participants provided written responses to the same two questions as in the online survey. Two violinists chose to reply in French and it was decided not to translate their responses but include them in the analysis directly.

2.3 Analysis

Following the data coding steps that form the constant comparison method within the Grounded Theory framework [14, 6], our analysis started from the verbalizations collected in the online survey. First, groups of words indicating a concept of violin sound richness, henceforth called verbal units, were extracted from musicians' responses to the first question and classified in semantic categories. Inter-categorical associations were then established, at which point a tentative core for our conceptual framework had been formed. We next scanned the verbal responses to the second question. New concepts were identified and the core was updated to fit with the new data. The analysis was then extended to the verbal responses collected in the playing experiment on the basis of the updated core, wherein no further concepts emerged. Consequently coding was stopped as theoretical saturation had been reached.

Each verbal unit corresponded to a semantically distinct violin quality characteristic. Semantic proximities were assessed through syntactic context and linguistic markers such as the use of apposition, opposition, reformulation, explanation, comparison, or negation. For example, the phrase *"a complex and pleasant sound"* contained two verbal units, namely "complex" and "pleasant," whereas the phrase *"resonant sound that is not weak"* constituted a single unit which, however, comprised two manifestations of the same quality characteristic with opposite meanings, namely "resonant" (positive connotation or desirable quality) and "weak" (negative connotation or undesirable quality).

3 RESULTS

3.1 Semantic categories

In total, 211 verbal units were extracted from the responses collected in the online survey (34 violinists, 6 units per respondent on average) and 75 units in the playing experiment (16 violinists, 5 units per respondent on average), and were classified in eight distinct semantic categories, revealing a common framework for semantic features given to "rich" as a qualifier of violin timbre and sound quality:

1. A strong consensus was observed with the use of *full* (*plein* in French), describing a certain sensory property referring to the perceived amount of spectral content as in the perceived number of partial frequencies present in a violin note. This sensory property was also described, with some approximation, by other semantically related sensory adjectives such as *deep*, *dark* (*sombre* in French), *dense*, *complex*, *big* (*ample* in French), *wide* (*large* in French), and *thick*, or semantic opposites like *thin*, *narrow*, *small*, *light*, and *nasal*. Some musicians described this characteristic of a rich violin sound in acoustical (i.e., technical) terms—*lots of/an abundance/variety of harmonics/overtones/dynamics*)—while others tried to qualify a rich violin sound by referring to the *ease/flexibility* of the instrument to produce *a variety/palette of colours/timbres* and to *react a lot in terms of sound changes, colours*, thus *enabling a violinist to create appropriate sounds for the chosen repertoire* and having *a shimmering quality whereby the sound changes constantly as one draws the bow*. Along the same line of conceptualization, one violinist described a rich sound as being *generous* (*généraux* in French).

2. Another sensory property was expressed through words such as *warm*, *velvety*, *smooth*, *round*, *sweet*, and *mellow*, versus *strident*, *harsh*, *tinny*, *brassy*, *squeaky*, *metallic*, and *bright*—borrowed from the semantic field of texture. Also referring to spectral content, such conceptualizations direct to the distribution of spectral energy between the bass, midde, and treble registers in a played note; undesirable qualities are associated with disproportionately more treble or not enough bass frequencies (*mellow tone on lower strings, no stridency on upper ones*). This sensory property of a rich violin sound was also described in acoustical terms by some performers: *evenness of projection across the frequency range*; *the sound has to contain a particular amount of energy in the different range of frequencies*; *combined with a good dose of lower frequencies for warmth*.

3. Strong consensus was also observed with the use of *resonant*, *strong*, *ringing*, *powerful*, *sonorous*, *sustained*, *lively*, and *projective*, versus *weak*, *muffled*, and *closed*. The semantic field summarizing these verbalizations can be described as action-presence [6] and suggests an evaluation of "how much sound" comes out of the violin based on estimated intensity and spatial attributes (*a rich sound has to vibrate naturally and to go far without forcing*), but also on the "amount of felt vibrations" from the body-bow system (*how much you feel the sound in your body when you hear it*) [13].

4. Yet another sensory property associated with a rich violin sound was expressed through words and phrases such as *clarity*, *pure*, *precise*, *focus*, *speakability* or *how freely each string speaks*, *the sound can take a lot of pressure without cracking*, *lack of grainy tonality*, and *direction* (as in *focus*). Here violinists tried to describe a violin tone perceived as having more distinct and well-defined spectral components, especially in the low register where different notes may be heard as "blending into each other" or "unfocused" due to overlapping overtones. Some violinists specifically referred to a clear sound as lacking audible artifacts such as a wolf tones (oscillating beat when note frequency too close to the resonance frequency of the violin body).

5. Some musicians tried to qualify a rich violin sound as *varying with/responding to vibrato* and offering *lots/nuances of vibrato* or *un vibrato nerveux, ample, leger ou inexistant* (*a vibrato that is nervous, full, light or non-existent*).

Table 3. Distribution of categories within and across responses to questions ($N =$ total units; # = coded units; % = proportion).

	Online survey						Playing experiment					
	Q1 ($N = 132$)		Q2 ($N = 79$)		ALL ($N = 211$)		Q1 ($N = 46$)		Q2 ($N = 29$)		ALL ($N = 75$)	
	#	%	#	%	#	%	#	%	#	%	#	%
Fu	69	52	19	24	88	42	20	44	8	28	28	37
Wa	30	23	7	9	37	18	8	17	5	17	13	17
Reso	9	7	23	29	32	15	7	15	7	24	14	19
Cl	5	4	10	13	15	7	5	11	-	-	5	7
Vi	3	2	4	5	7	3	-	-	3	10	3	4
Resp	-	-	6	8	6	3	-	-	-	-	-	-
Ba	1	1	5	6	6	3	1	2	3	10	4	5
In	15	11	5	6	20	10	5	11	3	10	8	11

6. Some violinists qualified a rich violin sound by referring to the responsiveness of the instrument (i.e., how quickly the violin responds to different bowing gestures): *if the violin answers tenderly to the bow*; *I pay attention to reactions to different strokes*; *it is important that* [the violin] *responds quickly and evenly*; *the sensitivity/response of the violin is helpful*; *it is important that it responds quickly and evenly*; *il faut sentir la sensibilité jusqu'au bout des doigts* (*you have to feel the sensitivity right down to your fingertips*.

7. Some violinists qualified a rich violin sound as being *well-balanced for both low and high notes* or *stable (if the sound is good in all the ranges)*, or having *equal resonance on all strings... thus making the richness of tone consistent throughout*. In particular, some musicians explicitly referred to the responsiveness of the violin in higher positions on the lower strings (G and D). As one violinist put it, *I often find a rich sounding violin starts to get a weak sound as I strain the string by going higher*.

8. Finally, many musicians referred to global affective-hedonic qualities that do not reflect the perception of certain physical parameters and could thus qualify any sensory property irrespective of modality: *beautiful*; *pleasant/not irritating*; *has personality*; *unmusical tonality*; *the heart-melting sound*; *richness is the difference between butter and margarine*; *richness is indulgence*; *the instrument blooms... has the sensation that you can sink in to it*. Or as one violinist said: *I judge richness based on how much the sound reminds of melted chocolate.*

Table 1 reports the musical profile of each respondent in the online survey along with information on whether they used verbal expressions within a given category (Fu = fullness; Wa = warmth; Reso = resonance; Cl = clarity; Vi = vibrato; Resp = responsiveness; Ba = balance; In = interest). Corresponding information for the musicians in the playing experiment is reported in Table 2. No obvious relationship between having a certain style and/or level of experience and attending to particular attributes was observed. Consequently, Table 3 summarizes the across-musicians distribution of semantic categories within each and over all responses to the different questions. Occurrences were further summarized across questions due to similar trends.

3.2 Discussion

In order to identify how the definitions of violin sound richness proposed by the experts (i.e., the violinists) position themselves in relation to dictionary definitions of the adjective *rich* in English, we have noted definitions and synonyms from two sources:

- Oxford English Dictionary (OED; 2nd Edition): 1) Of things: Powerful, strong. 2) Wealthy in, having abundance of, amply provided with, some form of property or valuable possessions. 3) Of choice or superior quality; esp. of articles of food or drink with reference to their stimulative or nourishing effects. 4) Of a full, ample, or unstinted nature; highly developed or cultivated. 5) Of colour: Strong, deep, warm. 6) Of musical sounds: Full and mellow in tone. 7) Of odours: Full of fragrance.

- WordNet (www.wordnet.princeton.edu; a large network of semantic relations between words based on psycholinguistic and computational theories of human lexical memory [16]): 1) Having an abundant supply of desirable qualities or substances. 2) Fat, fertile, productive (marked by great fruitfulness). 3) Deep (strong; intense). 4) [Of wine, food, etc.] full-bodied, racy, robust (marked by richness and fullness of flavor). 5) [Of sound] pleasantly full and mellow. 6) Ample, copious, plenteous, plentiful (affording an abundant supply).

It appears that rich is conceptualized in a highly similar fashion across sensory modalities (taste, smell, vision, audition) but also in more abstract nonsensory domains (wealth, strength, abundance). Central to all conceptualizations of *rich* is the idea of "affording an abundant supply" of one or more “desirable qualities,” which is reflected in the first semantic category identified in the experts discourse (*full sound*; *lots of harmonics/overtones*). Furthermore, qualifying a rich violin sound as *resonant/powerful/strong* (third semantic category) and as offering *lots/nuances of vibrato* (fifth semantic category) can be regarded in the same light as the global "lots of" definition of *rich*. The agreement of OED and WordNet in how *rich* is defined for sounds suggests that its qualification as both *full* and *mellow* (second semantic category) is considered beyond violin sound to any auditory scenario.

The semantic categories of *clear/focused* and *balanced* are more specific to musical sound and to the violin in particular, where tones in the middle and low registers should not be “muddy” or “blurry”, and those in the high register should not be “thinner” or “weaker” (cf. [6]). Characterizations of a rich violin sound as *beautiful*, *pleasant*, *heart-melting*, and *reminding of melted chocolate* assume a cognitive evaluation of the subjective-affective state of the musician in response to their imaginary (online survey) or physical (playing experiment) interaction with the violin and its sound.

Descriptions of responsiveness (of the instrument) were the least recurrent in both the imaginary and physical situations. In fact, this semantic category did not emerge at all in the playing experiment, while in the online survey it emerged only in responses to the question *How would you evaluate a violin in terms of richness?* (Q2). It is plausible that, for the violinists who responded to the online survey, the type of question at hand may have affected how different facets of *rich* are negotiated. That is, the use of the word “evaluate” in Q2 could have evoked notions of musician-instrument interaction and playability, whereas the formulation of Q1 led to a prioritization of primarily sound attributes. Similarly, the violinists who took part in the playing experiment were asked to first respond to the question *How and based on which criteria did you make your preference ranking?* before answering Q1 and Q2. A look at those responses, which is beyond the scope of the present analysis, indeed reveals descriptions of responsiveness.

4 CONCLUSIONS

The present analysis provides further evidence that metaphorical linguistic structures such as *rich sound* are central to the process of conceptualizing timbre by allowing the musician to meaningfully perceive and communicate subtle acoustic variations in terms of other, more commonly shared experiences [17].

While individual conceptualizations of violin sound richness are very subtle and can overlap, the broader semantic categories emerging from the collected verbalizations reflect a shared representation of what a rich violin sound may mean. This can be seen as a first step in translating the semantics of violinists’ expressions into perceptually meaningful descriptors of violin sound quality. Importantly, it demonstrates that violin players with different levels of experience and expertise share a common framework for differentiating the sensory meanings of auditory cues.

We expect that there are variations of the language (i.e., the specific lexicon and its meaning) used by musicians from place to place (sometimes resulting from a strong influence by one or more particular teachers in an area). The present analysis might thus be biased toward a verbal tradition specific to the Montreal region. Nevertheless, this research provides a resource that should be consulted by any researchers planning to conduct perceptual studies of violin quality (i.e., when designing the language used in their experiments).

REFERENCES

[1] Bissinger, G. Structural acoustics of good and bad violins. J. Acoust. Soc. Am., 124, 2008, pp 1764–1773.

[2] Fritz C.; Cross I.; Moore B. C. J.; Woodhouse J. Perceptual thresholds for detecting modifications applied to the acoustical properties of a violin, J. Acoust. Soc. Am., 122, 2007, pp 3640–3650.

[3] Štěpánek J.; Otčenášek Z. Rustle as an attribute of timbre of stationary violin tones. Catgut Acoust. Soc. J. (Series II), 3, 1999, pp 32–38.

[4] Łukasik E. Matching violins in terms of timbral features. Archives of Acoustics, 31, 2006, pp 227–233.

[5] Dubois D. Categories as acts of meaning: The case of categories in olfaction and audition. Cognitive Science Quarterly, 1, 2000, pp 35–68.

[6] Saitis C.; Fritz C.; Scavone G. P.; Guastavino C.; Dubois D. Perceptual evaluation of violins: A psycholinguistic analysis of preference verbal descriptions by experienced musicians. J. Acoust. Soc. Am., 141, 2017, pp 2746–2757.

[7] Saitis C.; Scavone G. P.; Fritz C.; Giordano B. L. Effect of task constraints on the perceptual evaluation of violins. Acta Acust. united Ac., 101, 2015, pp 382–393.

[8] Saitis C.; Giordano B. L.; Fritz C.; Scavone G. P. Perceptual evaluation of violins: A quantitative analysis of preference judgments by experienced players. J. Acoust. Soc. Am., 132, 2012, pp 4002–4012.

[9] Saitis C.; Fritz C.; Guastavino C.; Scavone G. P. Conceptualization of violin quality by experienced performers. Proceedings of the 2013 Stockholm Music Acoustics Conference (SMAC), Stockholm, Sweden, 2013, pp 123–128.

[10] Saitis C.; Giordano B. L.; Fritz C.; Scavone G. P. Investigating the origin of inter-individual differences in the preference for violins. Proceedings of the 2011 Forum Acusticum, Aalborg, Denmark, 2011, pp 497–501.

[11] Saitis, C.; Scavone, G. P.; Fritz, C.; Giordano, B. L. Evaluating violin quality: A comparison of player reliability in constrained vs. unconstrained tasks. Proceedings of the 2013 Stockholm Music Acoustics Conference (SMAC), Stockholm, Sweden, 2013, pp 109–114.

[12] Saitis, C.; Scavone, G. P.; Fritz, C.; Giordano, B. L. Perceptual evaluation of violins: A comparison of intra-individual agreement in playing vs. listening tasks for the case of richness. Proceedings of Meetings on Acoustics, 19, 2013, p 035029.

[13] Saitis C.; Järveläinen H.; Fritz C. The role of haptic cues in musical instrument quality perception. In: Papetti S.; Saitis C. (eds) Musical Haptics, Springer, Cham, 2018, pp 73–93.

[14] Strauss A. L.; Corbin J. M. Basics of qualitative research: Techniques and procedures for developing grounded theory. Sage Publications Inc., Thousand Oaks (CA), 2nd edition, 1998.

[15] Zajonc R. B. Attitudinal effects of mere exposure. J. Pers. Soc. Psychol., 9, 1968, pp 1–27.

[16] Miller G. A. WordNet: A lexical database for English. Communications of the ACM, 38, 1995, pp 39–41.

[17] Saitis C.; Weinzierl S. The semantics of timbre. In: Siedenburg K.; Saitis C.; McAdams S.; Popper AN.; Fay RR. (eds) Timbre: Acoustics, Perception, and Cognition. Springer, Cham, 2019, pp 119–149.

PROCEEDINGS of ISMA 2019
International Symposium on Music Acoustics

13 - 17 September 2019 in Detmold, Germany

External sound field simulations and measurements of woodwind resonators

Erik Alan PETERSEN(1), Romane ROSSER(1)

(1)Aix Marseille Univ, CNRS, Centrale Marseille, LMA, UMR 7031, Marseille, France, petersen@lma.cnrs-mrs.fr

Abstract

The input impedance is a useful quantity to characterize the acoustic response of woodwind instruments and is efficiently simulated using the Transfer Matrix Method (TMM). However, the TMM does not calculate intermediate variables that are convenient for simulating the external sound field. Recent work by Lefebvre et al proposes the Transfer Matrix Method with external Interactions (TMMI) which accounts for the mutual radiation impedance of toneholes radiating into the same space and uses the acoustic flow through each aperture as the reference variable. Treating the flow through each tonehole as a source in a linear array, it is possible to calculate the external sound field such as the waveforms at a given receiver location and directivity patterns. Additionally, the efficiency of a resonator can be calculated as the ratio of the power at the input of the resonator and the sum of the power radiating from each aperture. This is a useful step towards understanding the competition between the energy that is retained within a resonator and facilitates the auto-oscillation of the reed, and that which radiates from the resonator. This topic is explored through simulation and measurements using simplified cylindrical resonators.

Keywords: Musical acoustics, radiation, cutoff frequency, clarinet.

1 INTRODUCTION

The tonehole lattice cutoff frequency is a well-known property of the clarinet and is generally considered to have an influence on the “character” of a given instrument [1]. However, it is not precisely known how the cutoff frequency influences the sound production and radiation. Recent work has shown that the cutoff frequency has a relatively small effect on the production of sound, primarily changing the spectral content of internal waveforms above the cutoff frequency [2]. It is hypothesized that the cutoff frequency will also change the radiation of a given resonator, an effect that could also determine the timbrel properties of an instrument. An early development of this idea is provided in the current paper where simplified resonators are excited at acoustically linear levels by a compression chamber. The pressure inside the resonators and at external points are measured in anechoic conditions. Transfer functions are then calculated and used to compare resonators with different cutoff frequencies and validate simulations.

2 SIMULATION OF EXTERNAL SOUNDFIELD

In order to predict the radiating characteristics of a resonator, the transfer function between a source inside the resonator and an external observation point is simulated. The simulation relies on the Transfer Matrix Method with external Interactions (TMMI) [3], a variant of the classic Transfer Matrix Method (TMM). The TMMI is designed to simulate the input impedance of a resonator by assuming a fictitious flow source U^s, and calculates the resulting pressure and flow P_n and U_n at each n^{th} radiating aperture, accounting for the mutual radiation load between sources that radiate into the same space. Therefore, the transfer function between the source flow U^s and each hole is simply

$$H_{u,n} = U_n/U^s, \tag{1}$$

where U^s has equal amplitude and phase for all frequencies.

The TMMI is readily exploited for radiation calculations because, in the process of simulating the input impedance, it provides the flow from each hole, already accounting for external interactions. Ignoring the presence of the body of the resonator, the holes can then be treated as an array of monopole sources. The pressure at some

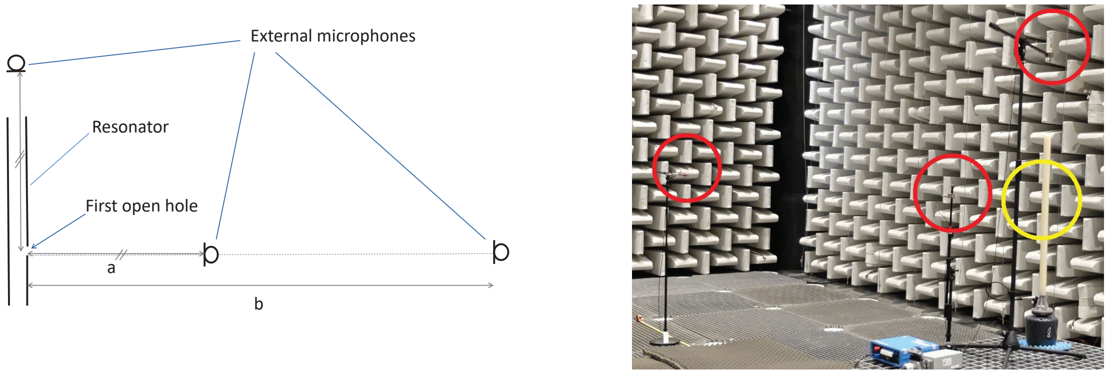

Figure 1. Three microphones (right, in red) are positioned around the resonator. The first two microphones are at the level of the first open hole (right, in yellow) and at a distance of b = 4 m and a = 0.7 m, respectively. The third is positioned above the end of the resonator at a distance a = 0.7 m from the first open hole.

observation point M is proportional to the time derivative of the summation of the contributions of each U_n, accounting for a propagation delay and spherical spreading:

$$P_M = \frac{d}{dt} \sum_{n=1}^{N} \frac{H_{u,n} U^s}{r_n} e^{-j\omega r_n / c}, \tag{2}$$

where r_n is the distance between the n^{th} hole and M, ω is the angular frequency, and c is the speed of sound in air. This model assumes anechoic conditions and ignores absorption in air.

Because this is a linear model, at each step we have the option to choose the acoustic variables P or U, related by the impedance. It is numerically equivalent to consider pressure sources P^s and P_n, from which the external pressure P_M is calculated. Therefore, equations 1 and 2 can just as easily be written in terms of pressure sources, which is less physical but more convenient when comparing with measurements because a microphone measures pressure inside resonator.

3 MEASUREMENTS

3.1 EXPERIMENTAL RESONATORS

The resonators used in this work are designed to have the same first impedance resonance, but different tonehole lattice cutoff frequencies [2]. The global cutoff frequency is fixed by choosing the geometry of each cell to have an equivalent local cutoff frequency [4]. Three resonators $\mathscr{R}_{1.0}, \mathscr{R}_{1.5}$, and $\mathscr{R}_{2.0}$ are used in the current work. All have first impedance peaks at 185 Hz, and cutoff frequencies at 1000, 1500, and 2000 Hz, respectively. The distance between toneholes is the same for all three resonators, and the cutoff frequency is changed only by varying the radius of the toneholes.

3.2 EXPERIMENTAL DESIGN

The transfer function in pressure from inside the resonator to the external sound field was measured experimentally. The resonators were connected to a compression chamber using a 3D printed adapter piece with a 6 cm cylindrical portion in which the microphone is mounted. The pressure measured by this microphone is treated as the source pressure P^s in Section 2. The pressure was measured at three external locations, the positions of which are shown in Fig. 1.

Pure sinusoidal excitation signals were used to force the resonator from 100 Hz to 4000 Hz in steps of 10 Hz.

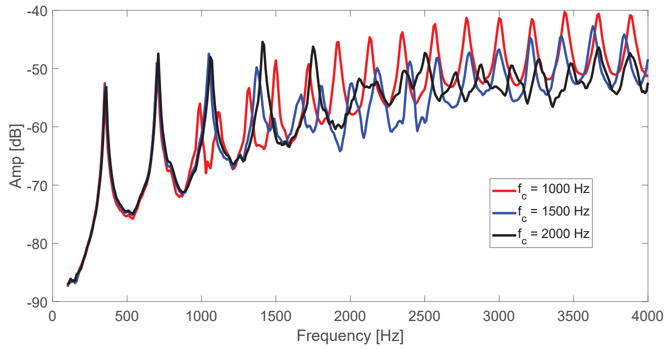

Figure 2. Transfer function between interal pressure and external pressure at the overhead microphone location. The resonators with f_c = 1000, 1500, and 2000 Hz are shown in red, blue, and black, respectively.

This signal choice was chosen instead of a frequency sweep because the radiation from the resonator, particularly at frequencies corresponding to the impedance troughs, is very weak. The coherence function calculated using a sweep type signal was only robust in the vicinity of the impedance peaks.

The measured signals are band filtered from 50 Hz to 6000 Hz and windowed to retain only the stable portion of the signal. Peak amplitudes of the i^{th} harmonics are extracted using synchronous detection

$$P_M(\omega_i) = |2 < p_m(t) \cdot e^{-j\omega_i t} >|. \tag{3}$$

This method is valid because the frequencies are precisely known and stable. In the following analysis only the fundamental frequency ($i = 1$) is considered.

3.3 MEASURED TRANSFER FUNCTION FOR THREE RESONATORS

The transfer function between internal pressure and three external observation points described in Section 3.2 was measured for all three resonators. Figure 2 shows the transfer function between the internal pressure and the microphone that is located 0.7 m above the first open hole for each of the three resonators. All three resonators radiate similarly at frequencies below the tonehole lattice cutoff frequency, with peaks that are harmonically related to the first peak. This is because at low frequencies the main acoustic source of the resonator is the first open tonehole, which radiates as a monopole. As the frequency increases up to and past the cutoff frequency of a given resonator, the transfer functions become more complicated. This transition is particularly abrupt for resonator $\mathscr{R}_1$, where the cutoff frequency happens to coincide with an existing peak.

3.4 COMPARISON WITH SIMULATION

The simulated and measured transfer functions between internal pressure and all three microphone locations is shown in Fig. 3 for $\mathscr{R}_1$. Because the simulation is normalized (ie the flow source $U^s = 1$), the amplitude of the simulation is shifted so that the minimal point between the first two peaks is at the same amplitude as the measurement. The peak amplitude was not chosen as the reference point because the measurements (in steps of 10 Hz) do not fully resolve the peak.

The simulation matches the measurements at low frequencies. At high frequencies, the shape of the simulation aligns reasonably well with the measurements, but the amplitude is not adequately captured. The simulation under-predicts the amount of radiation. This is also noticed in the impedance measurements (not shown). Around the cutoff frequency there is a marked shift in frequency between the simulation and measurement. This may be an interesting topic for further developing the model.

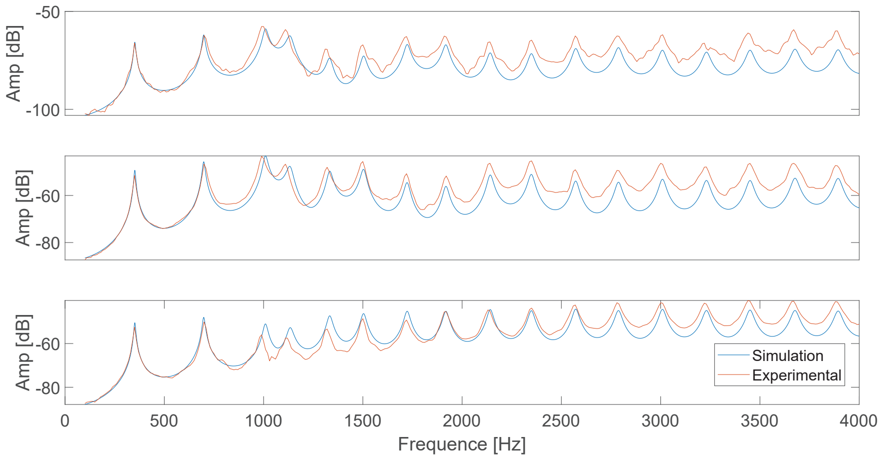

Figure 3. Simulated and measured transfer function for resonator $\mathscr{R}_1$ between internal pressure and external pressure at three microphone locations (see Fig. 1).

4 CONCLUSIONS

The effect on radiation of the tonehole lattice cutoff frequency is investigated. It is found that the cutoff frequency has a considerable impact on the transfer function between internal pressure and pressure at multiple points external to the resonator. This implies that the cutoff frequency could act as a filter of the sound that is radiated from an instrument, irrespective of its influence on sound production. It is also found that it is possible to extend the TMMI calculation to simulate external pressure waveforms. This use of the TMMI is adequate at low frequencies but is only approximate at high frequencies. This is a logical place to search for an improved model. Future work could involve repeating the experiment at sound pressure levels that are high enough to induce nonlinear effects. This would be done with a compression chamber or artificial blowing machine.

ACKNOWLEDGEMENTS

The authors would like to thank Patrick Sanchez and Clément Rabau for their help with the experimental aspect of this work, and in particular for designing the adapter piece that connects the compression chamber and the resonators. We would also like to thank Guy Rabau for piercing the resonators. Finally, we acknowledge the many helpful discussions with Marc Pachebat, Fabrice Silva, and Philippe Guillemain. This work has been partly supported by the French Agence Nationale de la Recherche (ANR16-LCV2-0007-01 Liamfi project.)

REFERENCES

[1] Benade, A. H., Fundamentals of Musical Acoustics Oxford University Press, London (1976).

[2] Petersen, E. A.; Guillemain, G.; Kergomard, J.; Colinot, T., The effect of the cutoff frequency on sound production of clarinet-like instruments, Journ. Acoust. Soc. Am (to appear, accepted 2019).

[3] Lefebvre, A.; Scavone, G. P.; Kergomard, J., “External tonehole interactions in woodwind instruments,” Acta Acustica united with Acustica **99**, 975-985 (2013).

[4] Moers, E.; Kergomard, J., “On the cutoff frequency of clarinet-like instruments. Geometrical versus acoustical regularity,” Acta Acustica united with Acustica **97**, 984-996 (2011).

PROCEEDINGS of ISMA 2019
International Symposium on Music Acoustics

13 - 17 September 2019 in Detmold, Germany

Impact of free field inhomogenity on directivity measurements due to the measurement set-up

Malte Kob(1), Alexis Baskind(2)

(1)Detmold University of Music, Germany, kob@hfm-detmold.de

(2)alexis baskind music production, Germany, a@alexisbaskind.net

Abstract

Measurements in an-echoic conditions are affected by the measurement set-up itself. The presence of grids, stands, turntables and the human body introduces reflections, diffraction, absorption and more changes to the ideally free field conditions. The impact of such equipment on directivity measurements is often neglected, and artifacts are are easily misinterpreted as features of the source directivity. In an an-echoic chamber several setups are compared with respect to changes in the measured directivity of a simplified musical instrument. The differences of the 1/r amplitude decay as well as the resulting directivity functions are presented and discussed.

Keywords: free field, reflections, directivity, set-up

1 INTRODUCTION

Measurements of musical instruments are often performed in an-echoic chambers to avoid any impact of reflections or other acoustic sources on sound recordings. Measurements of instrument directivity usually require complex set-ups including a turntable, a microphone array, excitation devices or a human player. These devices and the human body modify the transfer path between instrument and sensor/microphone due to superposition of reflected sound waves, diffraction or shadowing effects. Further deviations from ideal free field conditions are size and damping quality of the an-echoic chamber and its borders.

Depending on the size of the structures the effects depend on frequency. In earlier studies the impact of a music stand has been investigated [1, 2]. Whereas for frequencies that correspond to wavelengths that are much longer than the stand diameter the impact of the stand reflections can be neglected whereas the sound pressures from reflected waves of higher frequencies can be of same magnitude as the direct sound waves.

1.1 FUNDAMENTALS

At low frequencies and for omnidirectional sources the assumption of a point source radiation characteristics of a musical instrument is justified. For such a source the function of the sound pressure with respect to the distance r is defined as

$$p(t,r) = \frac{\hat{p}}{r} e^{j(\omega t - kr)}$$

with the peak value

$$\hat{p} = \frac{j\omega\rho_0\hat{Q}}{4\pi},$$

angular frequency ω, wave number k, density ρ_0 and volume velocity $\hat{Q}$. For each wave of unique frequency the amplitude decreases with distance according to the $\frac{1}{r}$ law.

Musical instruments that emit sound from one location only, i.e. a bell or one side of a vibrating plate, can be approximated by a point source when the dimensions of the opening or oscillating structure are small with respect to the wave length [3].

For higher frequency or larger dimensions of the sound exit the geometrical structure plays an important role for the estimation of the radiation characteristics [4]. For circular openings and membranes the assumption of a baffled piston can be used which exhibits a strong spatial variation of the pressure near field. For very high frequencies or large distance from the source ($kr \gg 1$) the assumption of a plane wave radiation is justified. In this case the amplitude of the sound wave does not follow the $\frac{1}{r}$ law but stays rather constant with respect to distance from the source.

If more than one relatively small opening exist the radiation can be approximated by a number of point sources that superpose taking account their relative amplitudes and phases. For only two openings a dipole source can be assumed, for higher numbers or complex geometries the radiation characteristic can be very complex and is difficult to predict [5, 6, 7].

2 METHODOLOGY

For a validation of the impact of the set-up two experiments have been performed. One series of measurements was used to test the validity of the $\frac{1}{r}$ law, the other one intended to quantify the room impact on FRF function during directivity measurements.

2.1 FRF OF A LOUDSPEAKER

In Figure 1 the loudspeaker position is shown with microphone array and turntable installed.

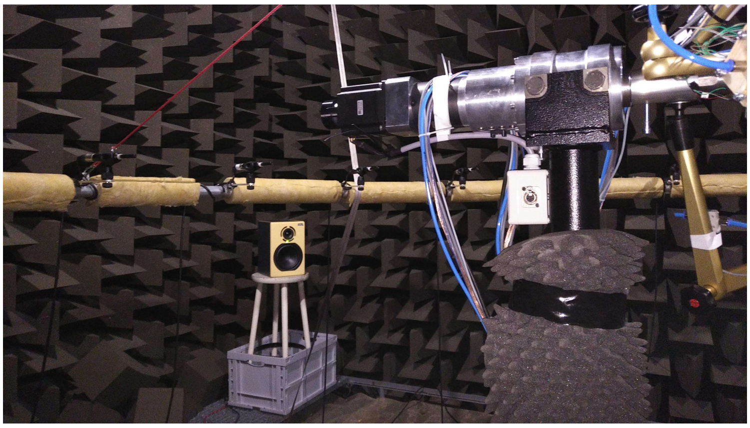

Figure 1. Set-up of loudspeaker in an-echoic chamber with turntable and microphone array.

2.1.1 Measurements

In Figures 2a and 2b the frequency response functions (FRFs) of a loudspeaker in an an-echoic chamber is shown. Figure 2a displays the FRFs measured in various distances, ranging from 25 cm to 7.33 m using the set-up shown in Figure 1. They seem to be rather similar but differ in some details. When the SPL is normalised to one measurement at 1.29 m distance the similarity of the functions is less obvious. In Figure 2b the calculated SPLs for the measured distances are added to the graphs.

This representation illustrates that the FRFs vary strongly at low frequencies below 200 Hz and also exhibit up to 5 dB variation throughout the whole frequency range. The level variation with distance below 200 Hz can be described as a low shelf filter for $r < 1.29m$ and a high-pass filter if increasing order for larger values of r.

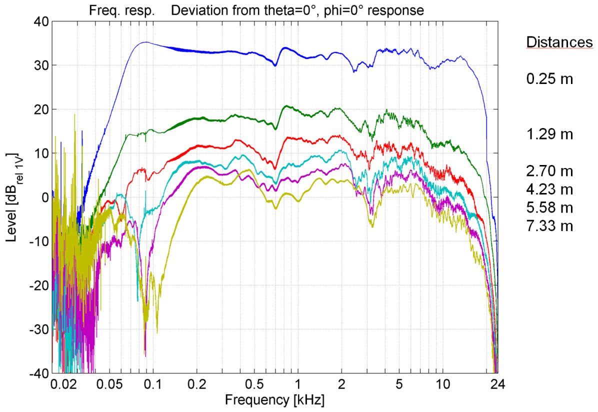

(a) Overlay of FRFs without normalisation.

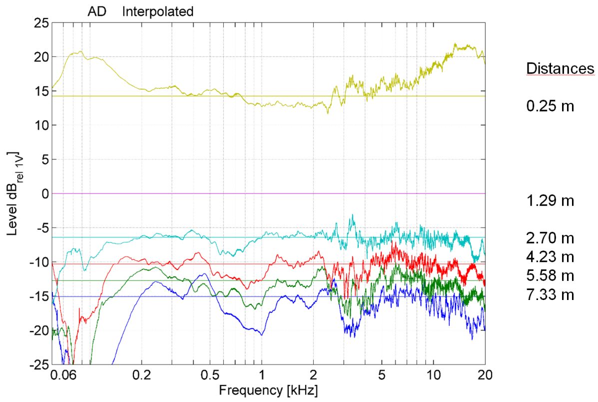

(b) FRFs normalised to the FRF in 1 m distance.

Figure 2. Measurement of a loudspeaker frequency response function in various distances.

2.2 DIRECTIVITY OF A TROMBONE BELL

In this experiment the directivity of a bell that was removed from a King Trombone Model 2104 4B was investigated using different set-ups of a Fouraudio ELF turntable, mounted in the an-echoic chamber of the OWL University of Applied Sciences and Arts. In all cases the bell was excited with swept sine signals emitted by a horn driver directly attached to the small end of the bell. These were the set-ups for the directivity measurements:

1. Bell without any other object than turntable and microphone
2. Bell as above with additional microphone array
3. Bell as above with additional mannequin

In Figure 3 the set-up with just the bell mounted on the turntable is shown. This set-up shall allow directivity measurements of the directivity with a minimum of artefacts. Due to the length of the bell it was mounted

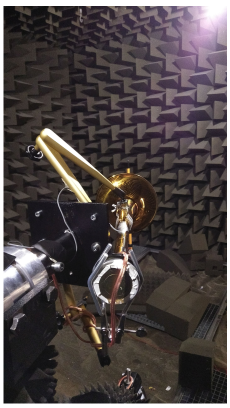

Figure 3. Directivity measurement set-up of trombone bell with neither mannequin nor microphone array

slightly off-axis with respect to the vertical axis of the turntable. In the second set-up shown in Figure 4a a 24 channel microphone array was installed in the an-echoic chamber. It is used for simultaneous assessment

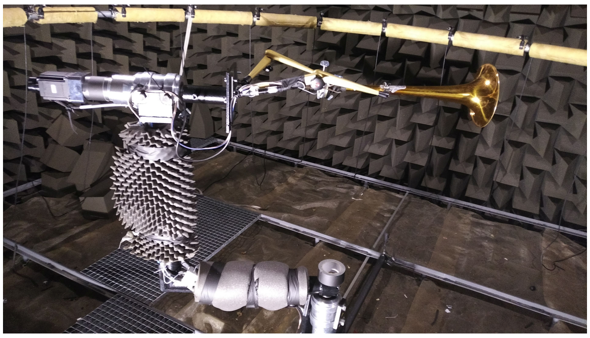

(a) Directivity measurement set-up without mannequin but with microphone array

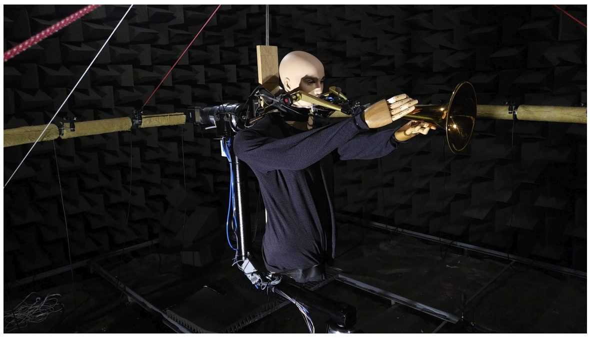

(b) Directivity measurement set-up with mannequin and microphone array

Figure 4. Directivity measurement of a trombone bell with and without a mannequin

of the sound radiated in the horizontal plane. The array was not used as a sensor in this investigation but rather as an obstacle which potentially introduced artefacts to the measurements. In the last set-up a mannequin was attached to the bell that was turned together with the bell for all measurements. It shall mimic the acoustic effect of a human player with respect to diffraction and absorption of sound from the bell. This set-up is shown in Figure 4b.

2.2.1 Results

A comparison of measurements of the set-up with mannequin in horizontal direction and 12 different values of vertical orientation is shown in Figure 5. The variation of the vertical angle of the mannequin and the bell

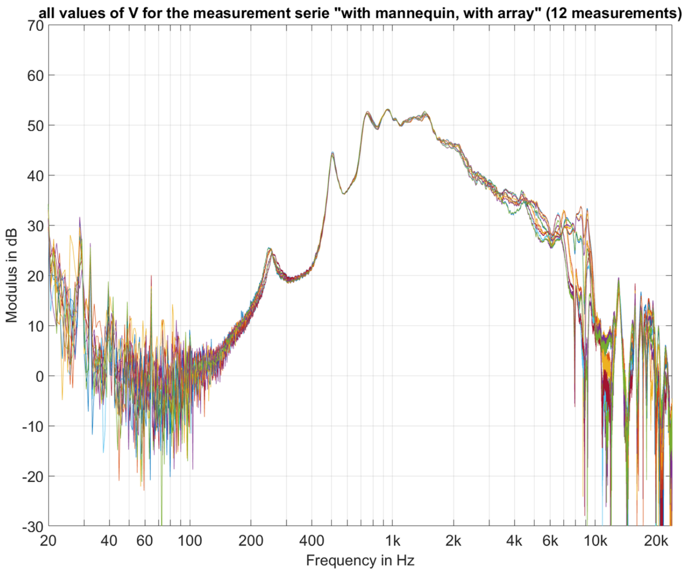

Figure 5. Frequency response function between horn driver and recording microphone for 0° horizontal and varied vertical angle of the instrument with mannequin attached

should not have any impact on the measurement in an ideal an-echoic environment since due to symmetry considerations all potential contributions of the turning sound source and the mannequin should be the same on axis, disregard the orientation in space.

However, in Figure 5 differences between the FRFs can be observed in the low frequency range below 200 Hz and in the high frequency range above 4 kHz. In the medium range the deviation is rather small.

Another comparison of measurements of the set-up without any obstacle, with the microphone ring, and with an additional mannequin inside the room is shown in Figure 6. As for the previous measurements, the variation

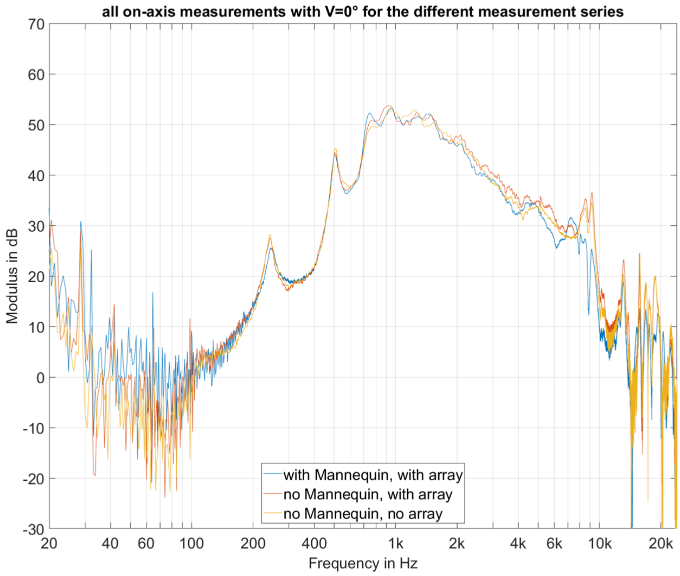

Figure 6. Frequency response functions in 0° vertical and 0° horizontal direction between horn driver and recording microphone for varied configurations of the room and instrument set-ups

of the FRFs is rather small for the frequency range from 200 Hz to 2 kHz. At higher frequencies the mannequin seems to introduce a small level drop up to 7 kHz and more serious level fluctuations for higher frequencies.

3 CONCLUSIONS

From the investigations using FRF measurements of a loudspeaker in an an-echoic chamber the effect of the near field and proximity of the loudspeaker to the walls could be observed. Contrary to the assumption of a point source the sound pressure only approximately followed the $\frac{1}{r}$ law. For low frequencies the lack of room absorption at the walls could explain the level increase with smaller distances: the hard walls of the not anymore an-echoic chamber would increase the SPL near the edge where the loudspeaker was placed. However, the level decay with increasing distance would not be explained with this effect.

The investigations of the FRFs have shown that the presence of obstacles in a room such as microphone arrays or a model of the human body have a small effect on FRF measurements for on-axis measurements. At higher frequencies, however, larger deviations occur that can be attributed to the presence of obstacles in the room. In case of the microphone array the effect seems to be very small, probably the attempts to reduce reflections of the array were not in vain. Measurements with a mannequin revealed larger deviations in SPL at frequencies that correspond to wavelengths of similar order as the mannequin's variation in geometry.

A more detailed investigation of the radiation patterns is planned in the future. A problem to be solved is the transformation of the acoustic centre and axis of rotation for the different set-ups. Due to the change of the opening and axis of the bell with respect to the turntable axes these transformations are needed to avoid artefacts in the radiation pattern calculation.

ACKNOWLEDGEMENTS

These investigations were motivated by the studies of musical instrument directivities in several projects with members of the Ensemble Musikfabrkik in Cologne and students of Detmold University of Music. All musicians are cordially acknowledged for their contribution to the measurements and their interest in the investigations.

REFERENCES

[1] Kob, M. Impact of Excitation and Acoustic Conditions on the Accuracy of Directivity Measurements. Proceedings of the International Symposium on Music Acoustics (ISMA), Le Mans, 2014

[2] Amengual Garí, S. V. & Kob, M.: Investigating the impact of a music stand on stage using spatial impulse responses. 142nd Convention of the Audio Engineering Society, Berlin, 2017

[3] Meyer, J. The Sound of the Orchestra, J. Audio Eng. Soc. 41(4), 1993, 203-213.

[4] Morse, P. M.; Ingard, K. U. Theoretical Acoustics, New York, McGraw-Hill, 1968.

[5] Meyer, J. Acoustics and the Performance of Music: Manual for Acousticians, Audio Engineers, Musicians, Architects and Musical Instrument Makers, 5th ed., trans. Uwe Hansen, New York: Springer, 2009, 196-201.

[6] Kob, M.; Ackermann, D.; Weinzierl, S. & Zotter, F. Analyse und Synthese der dynamischen Richtwirkung von Musikinstrumenten. Akustik Journal, DEGA 2018.

[7] Grothe, T. & Kob, M. High resolution 3D measurements on the bassoon. Proceedings of ISMA 2019, Detmold, 2019, http://pub.dega-akustik.de/ISMA2019

PROCEEDINGS of ISMA 2019
International Symposium on Music Acoustics

13 - 17 September 2019 in Detmold, Germany

Piano strings with reduced inharmonicity

Jean-Pierre DALMONT(1), Sylvain MAUGEAIS(2), ...

(1)Laboratoire d'acoustique de l'Université du Mans (LAUM, UMR CNRS6613), France, Jean-Pierre.Dalmont@univ-lemans.fr
(2)Laboratoire Manceau de Mathématiques, France, Sylvain.Maugeais@univ-lemans.fr

Abstract

The inharmonicity of the lower strings of straight pianos is still rather large especially for the first octave. Consequently, the timber of these strings can be sometimes awful and chords on the first octave highly dissonant. The idea of the present study is to show how this defect can be rectified by using an inhomogeneous winding on the whole string in order to minimize inharmonicity. The problem is solved by using an optimization procedure considering a non uniform linear density. Result show that the inharmonicity can be highly reduced. First results on a real string will be presented and discussed.

Keywords: Piano, String, Inharmonicity

REFERENCES

[1] Dalmont, J.-P.; Maugeais, S. Piano strings with reduced inharmonicity. To be published in Acta Acustica united with Acustica.

PROCEEDINGS of ISMA 2019
International Symposium on Music Acoustics

13 - 17 September 2019 in Detmold, Germany

Non-destructive measurement of the pressure waveform and the reflection coefficient in a flue organ pipe

Viktor HRUŠKA[(1)], Pavel DLASK[(1)], Milan GUŠTAR[(1)]

[(1)]Academy of Performing Arts in Prague, Music Acoustics Research Centre, Czech Republic, hruska.viktor@hamu.cz

Abstract

A multiple-microphone method employed for in-duct acoustics applications is adapted for a flue organ pipe geometry. In order to make the measurement, non-destructive the microphones are replaced by a pressure probe synchronized with a reference signal. Limits of the method regarding the pipe geometry are verified by the numerical calculations. Acoustic pressure waveforms are reconstructed and a framework for the reflection coefficient calculation is designed and tested.

Keywords: flue organ pipes, measurement methods, pressure waveform, reflection coefficient

INTRODUCTION

At present, it is safe enough to state that the qualitative nature of the sounding mechanism of a flue organ pipe is known (see e.g. [4, 1, 3]). However, many questions regarding the subtleties of the pipe design remain not fully resolved. The general problem lies in the inherent nonlinearity of the self-sustained system's dynamics. In order to deal with these questions properly, good and detailed measurements of various aspects of the pipe design are needed. In-depth knowledge of the internal pressure field is among them without any doubt.

Although there were measurement methods approaching this topic [5] it is highly convenient for practical reasons to have a non-destructive technique. To this purpose, we alter the classical multiple microphone method [8] and test it on a pipe well-known from our previous experiments.

The paper is organized as follows. First, the multiple microphone method is briefly reviewed along with its prerequisites (a plane wave region span, a suitable wave number). Then the measurement setup is introduced followed by the experimental results (the pressure waveform reconstruction, the reflection coefficient evaluation). The text is completed with the discussion and some conclusions are finally given.

THEORY

Suppose that plane waves are propagating through the pipe. The axis along the pipe is labeled x and its origin is placed at the open end of the tube (i.e. all pipe interior points have negative x coordinate). The acoustic pressure field is conveniently represented as $p(x,\omega)e^{i\omega t}$. Next, replace the angular frequency $\omega = 2\pi f$ with the frequency f and split the forward and backward propagating waves to obtain

$$p(x,f) = P_+(f)e^{-i\Gamma x} + P_-(f)e^{i\Gamma x}\,, \tag{1}$$

where Γ is the wave number introduced below and P_+, P_- denote the complex amplitudes of the forward and backward propagating waves respectively. When the acoustic pressure is known at multiple locations $p(x_1,f), p(x_2,f), ..., p(x_n,f)$ we may use Eq. (1) to form the set of linear equations

$$\mathbf{A}\mathbf{p} = \mathbf{b}\,, \tag{2}$$

with

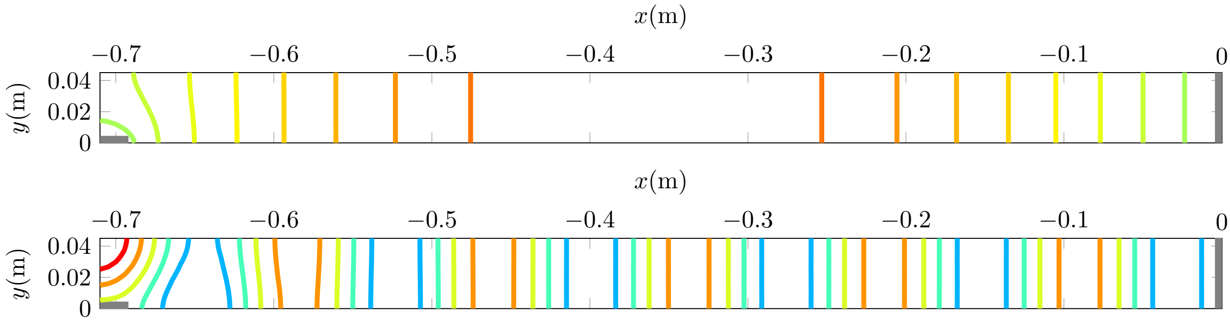

Figure 1. Isolines of the acoustic pressure in the lowest eigenmode (up) and the last eigenmode before the transversal patterns occur (down). The mouth and the open end are marked grey.

$$\mathbf{A} = \begin{bmatrix} e^{-\mathrm{i}\Gamma x_1} & e^{\mathrm{i}\Gamma x_1} \\ e^{-\mathrm{i}\Gamma x_2} & e^{\mathrm{i}\Gamma x_2} \\ \vdots & \vdots \\ e^{-\mathrm{i}\Gamma x_n} & e^{\mathrm{i}\Gamma x_n} \end{bmatrix}, \quad \mathbf{p} = \begin{bmatrix} P_+(f) \\ P_-(f) \end{bmatrix}, \quad \mathbf{b} = \begin{bmatrix} p(x_1, f) \\ p(x_2, f) \\ \vdots \\ p(x_n, f) \end{bmatrix}. \tag{3}$$

The set in Eq. (2) is overdetermined. Therefore the Moore–Penrose pseudoinverse $(\ )^+$ is employed and the complex amplitudes are obtained as follows

$$\mathbf{p} = \mathbf{A}^+\mathbf{b} = \left(\mathbf{A}^{\mathrm{H}}\mathbf{A}\right)^{-1}\mathbf{A}^{\mathrm{H}}\mathbf{b}\,, \tag{4}$$

where $(\ )^{\mathrm{H}}$ denotes the conjugate (Hermitian) transpose. Note that this approach corresponds to the least squares fitting of the Eq. (1) right-hand-side to the experimental data. The reflection coefficient of the open end R is then straightforwardly calculated as

$$R(f) = \frac{P_-(f)}{P_+(f)}\,. \tag{5}$$

The described method is applicable only to the plane waves. When considering the organ pipe, the nonplanar regions are inevitable, at least at the pipe mouth. In order to assess the spatial applicability of the method, the eigenfrequencies and corresponding eigenmodes of the pipe are calculated.

Directly above the flue the relation between the acoustics and the turbulent flow field is strongly nonlinear. However, the turbulent velocities quickly decay leaving much less perturbed flow. Generally, the governing equations linearized around the mean flow would be required. Nevertheless, as it is commented below, the mean flow Mach number, as well as its gradients, are very low. Since we are interested just in an indicative assessment of the wavefront shapes, the simple Helmholtz equation $\nabla^2 p + k_{\mathrm{eig}}^2 p = 0$ is numerically solved employing our own code with the finite volumes discretization. The open end and the inner surface of the mouth region are treated as ideal pressure release surfaces. The full three-dimensional calculation has been conducted, the 2D results from the center cut plane are depicted only for the sake of simplicity. Based on the wavefronts depicted in Fig. 1 we assume that the plane wave region spans from the $x = -0.55$ m to the pipe open end ($x = 0$). The full geometrical length of the pipe is 0.71 m. Therefore we expect to observe the acoustic pressure node at the open end and follow the waveform a bit beyond the antinode of the first resonance.

The least squares fitting that results from Eq. (4) demands knowledge of the wave number Γ relevant for the studied case. Although there is a nonzero mean flow through the pipe, its Mach number (see below) is so low that we do not have to split the wavenumber into the upstream and the downstream part. For the same reasons we neglect the turbulent losses outside the mouth region.

Hence, we are left only with the thermoviscous losses which are expressed in the usual manner [8, 2]

$$\Gamma = \frac{\omega}{c_0} - \mathrm{i}\delta \,, \tag{6}$$

where c_0 is the adiabatic speed of sound and the attenuation parameter δ is defined as

$$\delta = \frac{1}{a}\sqrt{\frac{\omega\nu}{2c_0^2}}\left(1 + \frac{\gamma - 1}{\mathrm{Pr}}\right) \,, \tag{7}$$

where a, ν, γ and Pr denote a ratio of the pipe cross-section to its perimeter, the kinematic viscosity of air, ratio of specific heats and the Prandtl number respectively.

EXPERIMENTAL SET-UP

A transparent open flue organ pipe of the fundamental frequency 208 Hz has been used for measurements. For the above described procedure the transparency is not required but we benefit from our previous Particle Image Velocimetry measurements with the same pipe [7]. Based on them we assess the mean flow through the pipe to have the Mach number $\mathrm{Ma} \approx 10^{-3}$, which allows for neglecting the convective effects on the sound field inside the pipe.

Two major issues have to be overcome when designing an experimental set-up suitable for the above-described procedure: the pressure field inside the pipe should not be distorted by the presence of the microphones and the microphones (or probes in general) must endure strong sound field. The acoustic pressure inside the pipe exhibits amplitudes well over 130 dB, as it is shown below in detail. Hence, an array of common microphones cannot be employed, at least not without significant waveform distortion. A miniature pressure transducer (Kulite XCQ–080) capable of capturing the high amplitudes has been used instead.

In order to keep the internal pressure field as undistorted as possible, just one probe is employed and the measurement is repeated for multiple probe positions. Such procedure relies on the fact that a "well-behaved" organ pipe is constructed to produce the same sound repeatedly. The necessary synchronization is provided by an auxiliary microphone (Sennheiser MKE 2 P–C) placed at half of the pipe length. Its waveform has been used only for determining an instant from which the transducer signal is further analyzed (retaining the correct phase information).

A holder fixes the position of the thin metal tube terminating in the pressure transducer (see Fig. 3). Its legs covered less than 5% of the open end surface. The metal tube occupied 0.3% of the pipe cross-section. Since we have limited our measurements to the plane wave frequencies and the mean flow is too slow to produce significant vortex shedding around the obstacle we expect the effects of the measurement construction presence to be negligibly low.

The measurements took place in an anechoic chamber. The measurement block scheme is depicted in Fig. 2. Two pipe set-ups have been investigated. For the sake of brevity, only the labels S1 and S2 are used henceforth. The voicing parameters are summarized in Tab. 1.

Table 1. Voicing parameters of the investigated pipe set-ups.

	S1	S2
Foot pressure [Pa]	87	134
Cut-up length [mm]	18	11
Flue width [mm]	1.35	1.35

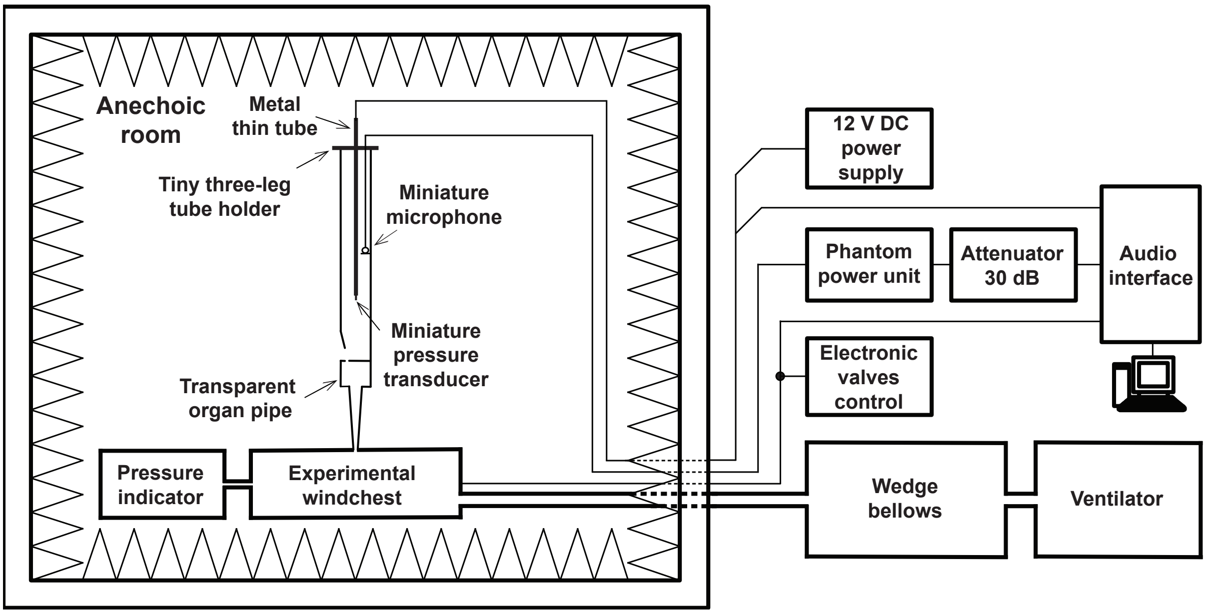

Figure 2. The block scheme of the measurement set-up.

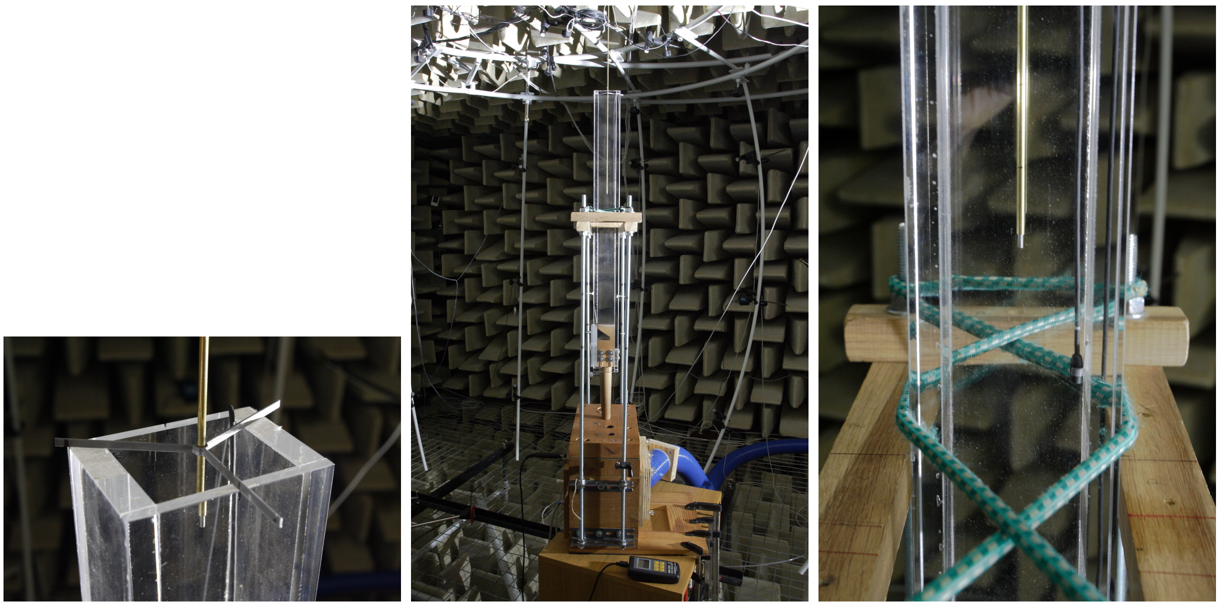

Figure 3. The holder of the pressure transducer tube (left), the transparent organ pipe in the anechoic chamber (middle), the pressure transducer inside the pipe (right).

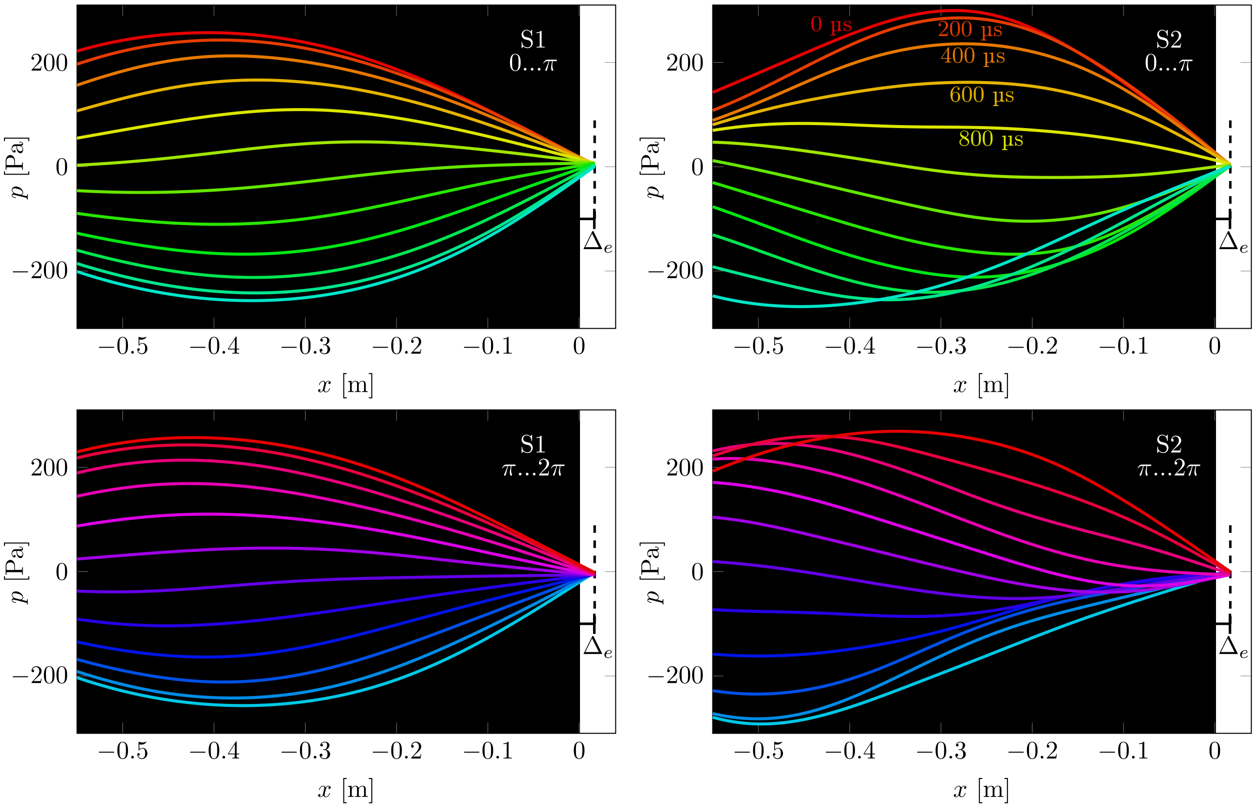

Figure 4. Reconstructed spatial waveforms of the acoustic pressure p in the setups S1 (left column) and S2 (right column). The curves in plots equidistantly divide the sound period into 24 parts (the first half of the period at the top, the second at the bottom). The time sequence is indicated by the HSV color cycle. The black background correspond to the pipe interior, the white one to the free space just above the open end. The end correction Δ_e is indicated.

RESULTS

Eighteen positions inside the pipe ($x = -540$ mm, -510 mm, $\ldots$, -30 mm) were chosen for measurements and long time-averaged spectra of the pressure signal are used henceforth. The cut-off frequency of our rectangular pipe is slightly above 3 kHz.

Spatial waveforms of the reconstructed acoustic pressure are depicted in Fig. 4. The setup S1 exhibits sine-like shape, only little distorted by the relatively weak contribution of other harmonics. On the other hand, the setup S2 is noticeably influenced particularly by the 2nd harmonic that is not in phase with the 1st one. It results in a quite asymmetric waveform. Even though there are no additional local minima or maxima, several inflection points that would not occur on a pure sine wave have taken place.

In accordance with theoretical predictions the acoustic pressure node is not situated at the interface between the pipe interior (marked by the black background in Fig. 4) but it is slightly protruded outside the pipe (the white background). The end correction $\Delta_e = 0.34\sqrt{S_e}$ (with S_e being the open end cross-section – 2475 mm^2) is marked in Fig. 4 as well. Since the open end has a nonzero radiation impedance the curves do not intersect precisely at a single point but evidently the Δ_e provides a very good approximation.

The reflection coefficient of the open end evaluated by Eq. (5) could be expressed as $R = |R|\exp(\mathrm{i}\varphi_R)$, where the magnitude $|R|$ and the phase φ depends on frequency. Both parameters are plotted in Fig. 5. In the low

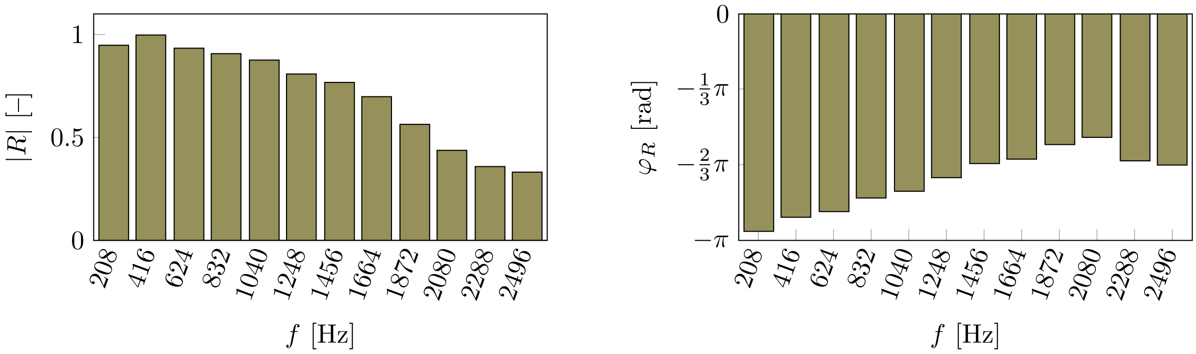

Figure 5. Magnitude (left) and phase (right) of the open end reflection coefficient for the S1 setup.

frequencies, the $|R| \to 1$ and the reflected wave travels with the opposite phase regarding the incident one, which is the textbook case. It suggests that the measurement and the data treatment were conducted properly and the method does not interfere with the nature of the pipe. It is known (see e.g. [9]) that when the mean flow is present the reflection coefficient might even exceed 1 due to the flow-acoustic interactions at the open end. However, given our Mach number, it is not likely to observe such behavior.

DISCUSSION

The reflection coefficient was presented only on the frequencies corresponding to the strong spectral lines and the pressure distribution data were obtained the same way. The reason why all the FFT bins are not used lies in the musically obvious fact that the majority of the pipe acoustic energy is stored in the harmonics. The rest of the spectrum is relatively weak and incoherent between individual spatial measurement points. It follows that the ratio P^-/P^+ resembles a $0/0$ case, which results in considerably uncertain reflection coefficient values. An example of this behavior is depicted in Fig. 6. The broad resonance of the noise on the eigenfrequency of the pipe interferes with the 3rd resonance of the oscillating jet driving, thus causing the spectral peak broadening and weakening (cf. e.g. [3] for more details). The fit according to Eq. (4) becomes less reliable and the resulting value (marked red) is evidently wrong. The same, yet not so pronounced effect takes place on the 6th, 9th and 12th harmonic as well.

Although the pressure amplitudes inside the pipe (ca. 250 Pa $\sim$ 140 dB) would suggest that some finite-amplitude nonlinearities could be present, our measurements have not directly proven any. Very probable reasons lie in the fact that the nonlinear effects do not build up significantly if there is even small detuning of the driving from the resonator eigenfrequencies (see e.g. [6] or when the significant dispersion and dissipation takes place (which would be the case within the generally nonlinear flow-acoustic interactions in the pipe mouth).

For the sake of necessary brevity, a detailed analysis of the measurement errors due to the probe positions (see [8]) is omitted here.

CONCLUSIONS

A non-destructive method of the pressure waveform and the reflection coefficient measurement for flue organ pipes has been tested and discussed. The results exhibit the key features required by theory and verified by other approaches (such as the validity of the end correction or the low limit behavior of the reflection coefficient regardless of the voicing parameters). Therefore we can conclude that the above described method is promising for future application on cases that are "textbook" to a less extent.

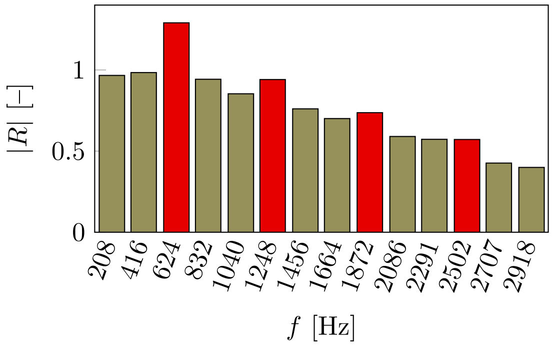

Figure 6. Magnitudes of the reflection coefficient for the S2 setup. The doubtful values are marked red.

Apart from dealing with the issues outlined in the Discussion, future research is intended to cover the comparison with theoretical predictions [9] and focus on the more complex situation regarding the pipes with non-negligible mean flow.

ACKNOWLEDGEMENTS

This work was supported by the MKČR project No. DG18P02OVV014.

REFERENCES

[1] J. Angster, A. Miklós, P. Rucz, and F. Augusztinovicz. The physics and sound design of flue organ pipes. *The Journal of the Acoustical Society of America*, 132(3):2069–2069, sep 2012.

[2] D. T. Blackstock. *Fundamentals of Physical Acoustics*. Wiley & Sons, New York, 2000.

[3] B. Fabre. Flute-like instruments. In *Acoustics of Musical Instruments*. Springer, New York, NY, 2016.

[4] B. Fabre and A. Hirschberg. Physical modeling of flue instruments: A review of lumped models. *Acta Acustica united with Acustica*, 86:599–610, 2000.

[5] F. Fimiani, M. Buiat, D. Bonsi, and D. Stanzial. Scanning a flue organ pipe with a p-v probe. In *Proceedings of the Forum Acusticum*, 2014.

[6] V. Hruška, M. Bednařík, and M. Červenka. Weakly nonlinear oscillations of gas column driven by self-sustained sources. *MATEC Web of Conferences*, 283:06001, 2019.

[7] V. Hruška and P. Dlask. Investigation of the sound source regions in open and closed organ pipes. *Archives of Acoustics*, 2019 [in press].

[8] S.-H. Jang and J.-G. Ih. On the multiple microphone method for measuring in-duct acoustic properties in the presence of mean flow. *The Journal of the Acoustical Society of America*, 103(3):1520–1526, mar 1998.

[9] R. Munt. Acoustic transmission properties of a jet pipe with subsonic jet flow: I. the cold jet reflection coefficient. *Journal of Sound and Vibration*, 142(3):413–436, nov 1990.

PROCEEDINGS of ISMA 2019
International Symposium on Music Acoustics

13 - 17 September 2019 in Detmold, Germany

Temporal acuity - flamenco guitar versus classical Spanish guitar

Robert MORES[1]

Hamburg University of Applied Sciences, Germany

Abstract

Other than classical Spanish guitars, flamenco guitars are capable of projecting rapid beat sequences in pronounced clarity. This relates to what musicians call a fast guitar. This asks for fast attack but also for some kind of damping in between beats, which may follow each other densely by some ten milliseconds in a rasgueado. Temporal features are investigated across guitars of both types to understand whether the flamenco guitar differs from the classical guitar in these aspects. The full data corpus contains impulse responses from more than 60 valuable reference guitars. Attack and decay are extracted from bridge impulse responses and from playing open strings. Additionally, a simple measure represents the speed of sound development across the soundboard. Populations of both types of guitars strongly overlap in these temporal maps and the physics seem to provide only part of the answer, auditory physiology may provide the other part of the answer.

Keywords: flamenco guitar, temporal features

1 INTRODUCTION

Contemporary flamenco and classical Spanish guitars appear to be similar on the first sight, without typical differences for the scale, the plantilla, the volume of the enclosed air, or the strings used. On the contrary, in the times of Torres, the plantillas differed very much from guitar to guitar, and guitars were not necessarily classified flamenco or classical guitars, but rather professional or cheap guitars (1). And even though flamenco *(FG)* and classical Spanish guitars *(CG)* are much more similar today than ever, most of the Andalusian contemporary guitars makers offer them as specific *FG* or *CG* (2). While interviewing some ten different Granadian guitar makers about the differences most of them claim that there is no difference but the action. The action should allow for easy play in both hands: the lasting play of fast pieces should not tire the left hand, and the striking/plugging combined with the golpe should be ergonomically convenient for the right hand. A few guitar makers claim, that the action also determines the sustain and the modulation of tone, i.e. a higher bridge would cause the modulation and sustain that you want for a *CG*. Another difference is the wood used for the ribs and the bottom. While palisander is the typical wood used for *CG*, the much lighter cypress is the typical wood used for *FG*. Some guitar makers say they would even refuse to build a *FG* with palisandro or a *CG* with cypress, some other guitar makers claim that they can use either wood and tune the sound towards either direction.

This brings up the question about desired sound features for *FG* versus *CG*. Interviewing not only guitar makers but also musicians and in particular professional flamenco musicians in Granada, the desired sound features can be summarized in its most simple form as shown in Table 1.

Table 1. Some basic sound features in flamenco versus classical guitars.

guitar	classical *(CG)*	flamenco *(FG)*
main focus	melodic sound	percussive sound
sustain	long	short
sound	rich, full	clear
modulation	strong	no
bass	strong	dry

Apart from that, the *FG* has its own typical sound character that cannot easily be described in words, but can be recognized by many players and listeners. A typical element for the percussive play in flamenco is the rasgueado, that is striking the four fingers in a rapid sequence, with as little as some 20 ms between strokes. A *FG* is expected to project such fast sequence with acuity while a *CG* is not. With a *CG*, the four strokes usually kind of merge to

[1] robert.mores@haw-hamburg.de

just one sound comparable to what a bell does when being hit rapidly. On the other hand, a *CG* can develop a beautiful, modulated and rich tone even while playing only simple melodies or even single notes, whereas a *FG* will not necessarily. And even more, a good *CG* provides a range of voices, or registers, that is, the guitar translates variations of manual action into variations of sound. And while there is an even more differentiated expectation of what a *CG* should provide for different epochs of composition, there is a likewise differentiated view on what a *FG* should do for the three main different flamenco performances: accompanying a singer, playing for dance, and playing solo. There are some 30 to 40 styles of singing and some 200 styles of dancing (3). Some professional musicians claim that these even require three different types of flamenco guitars.

All flamenco musicians interviewed in Spain and in Germany agree that accompanying a singer or playing for dance requires a traditional *FG* made of cypress, whereas the solo play benefits from using palisander wood, referring to the skilled solo play of Paco de Lucia, who strongly developed the solo play and is still a reference for virtuous flamenco. The musicians also agree that the *FG* approaches the *CG* in terms of sound features since the days of Paco. This is where the larger question of this research begins: how did the *FG* evolve over the last 100 years? This raises not only ethnological questions (4) but also acoustical ones. Measurements were taken from more than 60 very good to excellent instruments, including reference instruments of history such as guitars from Barranco, Fleta, Pages, Torres, Simplicio, but also best vintage and contemporary guitars from Barber, Bellido, Conde, Contreras, Devoe, Marin, Reyes, and Wiechmann. In this study, six classical guitars and six flamenco guitars are evaluated, three of each from a Hamburg vintage collection of Andalusian guitars, and three of each from contemporary Granadian guitar makers. For a brief spectral evaluation, these will be referenced against Romantic guitars, early romantic guitars, and Torres' guitars. For temporal discussions, mentioned guitars will be referenced against a vintage guitar from Faustino Conde (Madrid), which reveals features of both types of guitars.

2 MEASUREMENT METHOD AND DATA CORPUS

2.1 Measurement matrix

Acceleration sensors (Kistler Type 8778A500, 0.4 grams) are placed at the bass side and the treble side of the bridge, red marks in Fig. 1. The bridge is driven with an impulse hammer (DYTRAN 5800SL, 9.8 grams) between pairs of string attachment locations, on top of the bone inlay, see blue marks. Radiation is measured by pressure microphones located at the far end of the bridge, see green marks, but 10 ± 0.1 cm above the top. For additional temporal features, the top is excited at 13 different locations and the response measured at the bridge.

Figure 1. Setup with positions for hammer excitation (blue), acceleration sensors (red), and microphones (10 cm above green marks), for structural and radiation response from the bridge (left) and for temporal responses of the top (right).

In order to prevent room acoustics to interfere in radiation responses, a dedicated mobile absorber was used on the ground underneath the guitars, featuring 50% absorption at 100 Hz and close to 100% absorption from 200 Hz (5). Measured guitars were placed in the middle of larger rooms, yielding some 20 ms of reflection-free responses.

2.2 Guitar selection

The various guitars from various collections and museums are listed in Table 2.

Table 2. Investigated guitars and some of their features. All guitars made by Andalusian guitar makers if not noted otherwise. All *FGs* have cypress ribs and back, whereas all *CGs* have palisander ribs and back. The only exception is FC64 with palisander ribs and back while build as a *FG* using golpe plate, low action.

acronym	maker / model [location]	year	epoch	type	remark
JB18	Jesus Bellido	2018	contemporary & vintage	*FG*	workshop products 2018
McB18	Mauricio Bellido	2018		*FG*	
MB18	Manuel Bellido	2018		*FG*	
MB18c	Manuel Bellido /Aurea closed hd.	2018		*CG*	
MB18o	Manuel Bellido /Aurea open head	2018		*CG*	
MB99	Manuel Bellido	1999		*CG*	workshop reference guitar
JLB01	Jose Lopez Bellido	2001		*CG*	private vintage collection, Hamburg
MC71	Manuel Contreras [Madrid]	1971		*CG*	
MLB78	Manuel Lopez Bellido	1978		*CG*	
MC81	Manuel Contreras [Madrid]	1981		*FG*	
GPB71	Germán Pérez Barranco	1971		*FG*	
JLB70	Jose Lopez Bellido	1970		*FG*	
FC64	Faustino Conde [Madrid]	1964		*(FG)*	private collection, Hamburg
T89	Antonio de Torres	1889	Torres, 2nd epoch		Museo Barcelona #12107
T83	Antonio de Torres	1883			Centro Doc. Mus. Andalusia
O78	Francisco Ortega	1878	romantic		collect. Daniel Gil de Avalle
T67	Antonio de Torres	1867	Torres, 1st epoch		collect. Daniel Gil de Avalle
T62	Antonio de Torres	1862			Museo Barcelona #625, paper
T59	Antonio de Torres	1859			Museo Barcelona #626
C40	Benito Campo	1840	romantic		collect. Daniel Gil de Avalle
P37	Francisco Pagés	1837			Museo Barcelona
P06	José Pagés	1806			Museo Barcelona #452
M05	Francisco Martinez	1805	early romantic		12 strings, collect. Romanillos
M03	Manuel Munoa	1803			12 strings, collect. Romanillos

3 META-LEVEL SPECTRAL FINDINGS

The structural response of the guitars in Table 2 is documented and discussed in detail by means of mobility plots for the contemporary and vintage guitars (6), and for the Torres, the Romantic and the early romantic guitars (7). One of the major findings of the study on the vintage and contemporary guitars is, that all but one *FGs* have a systematically wider bandwidth at the air mode A_0 compared to *CGs*, and all but one *FGs* have a systematically narrower bandwidth across the (0,0) top mode and the (0,1) cross mode, compared to *CGs*. This answers, in part, the feature of modulation for the *CG*.

From the mobility plots, tuning parameters can be derived. In the context of mutual coupling between top mode and air mode (8, 9, 10, 11) and the guitar makers' desire to support the lowest E string at 82.4 Hz, the mapping of the (0,0) top mode versus the fundamental air mode A_0 is revealing. Regressions across these major tuning parameters suggest a classification of epochs. The plantilla size for Spanish guitars increased steadily until today, left graph in Fig. 2, and the Helmholtz resonance frequency f_0 of the enclosed cavity, calculated for the rigid, non-flexible box, accordingly declined until today, left graph in Fig. 2. Surprisingly, the fundamental air mode A_0 for the assembled, flexible-plates in contemporary guitars does *not* further tend to even lower frequencies when compared to Torres, as could be assumed from the plantilla size and the 'rigid-body' air cavity frequency f_0. Even though Torres' guitar bodies are small in the light of contemporary guitars, their A_0 their reaches further down. This can be explained by the rather large flexibility of Torres' rather thin tops. Contemporary guitar makers returned to thicker tops in favour of the projection potential. This comes from factors of radiation derived from plate thickness as explained in (7).

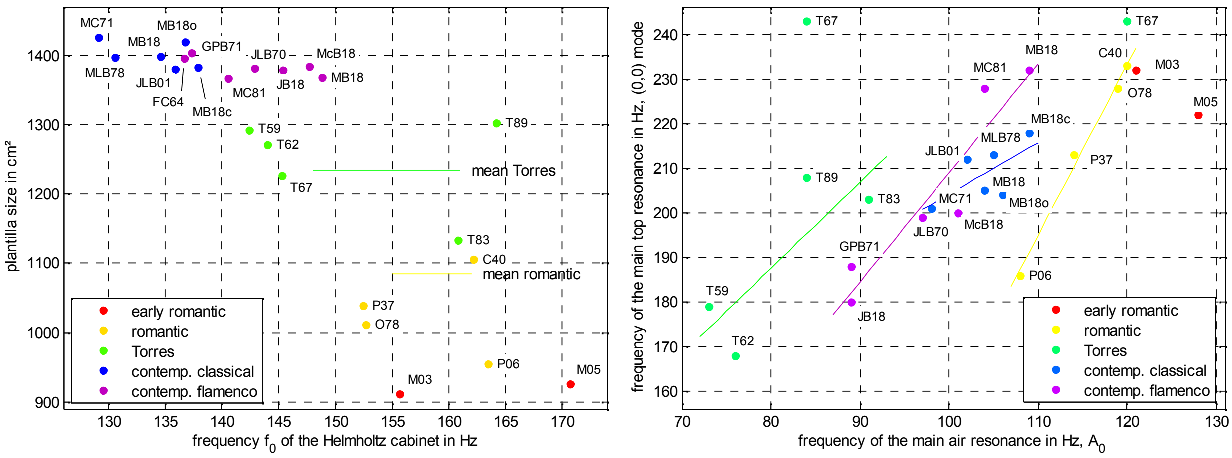

Figure 2. Plantilla size versus frequency f_0 of the 'rigid-body' air cavity for different epochs (left), and frequency of the main top resonance (0,0) versus frequency of the main air resonance A_0 for different epochs. The regression for Torres does not include T67 as there are two very strong peaks in the typical region. Values for mean size of Torres plantillas from (1) for Romantic plantillas from (12).

This brief discussion on meta-level spectral findings has a purpose. As the question is about the evolution of flamenco guitars over the last century, this perspective helps to recognize some fundamental trends. Contemporary flamenco guitars are conceptually very close to contemporary classical guitars. And both are conceptually well distinguishable from guitars of other epochs. So flamenco and classical guitars evolved both into similar directions for the similar reasons, such as bass support or projection. Unfortunately, the author did not find flamenco guitars of the early 20th century in any good condition. The reason is that these guitars initially were cheap guitars for ordinary people; these simple guitars were played extensively with heavy percussive strokes and golpe, and the top was usually typically thinner than that of classical guitars, as it is still the case today. So these guitars had no long future anyway. In lack of reference guitars the discussion about the evolution and the context of the flamenco guitar reduces to a comparison between contemporary classical and flamenco guitars, and only vague trends from vintage to today.

4 TEMPORAL FATURES

From the impulse responses three different temporal features are derived.

4.1 Attack and decay in the radiation impulse response

As outlined in the introduction, the impulses of a fast rasgueado come along in intervals of few 10 ms. In order to expose the distinct impulses, a fast attack and some decay between impulses is assumed to foster temporal acuity. Guitars are now compared along this feature. The attack time is extracted along the conditions of measurement. With few exceptions, there was no way to bring the instruments into free-field conditions. That means that most guitars were measured under semi-reverberant conditions. In most cases, walls and the ceiling were at least somewhat more than 3 m away from the guitar so the first echo is expected around 20 ms after impulse strokes. Reflections from the near-by ground were absorbed by a mobile absorber. While the radiation impulse response lasts longer than 100 ms, the ambient noise floor became the strongest component after some 50 to 100 ms. But after some 50 ms, most of the energy is already radiated. As a measure for the attack time, $T_{r,a}$ represents the time when 50% of the energy is radiated with reference to the total energy radiated over the first 50 ms after strokes. As decay relates to the damping of a signal, the damping of the radiated response is measured. The damping after 20 ms appears to be a telling feature when referencing against the temporal conditions of a rasgueado. The damping is extracted via a 5th order fitting to the logarithm of the envelope. Figure 3 shows attack times versus damping after 20 ms, for the vintage and the contemporary guitars, for both ends of the bridge, bass side and treble side.

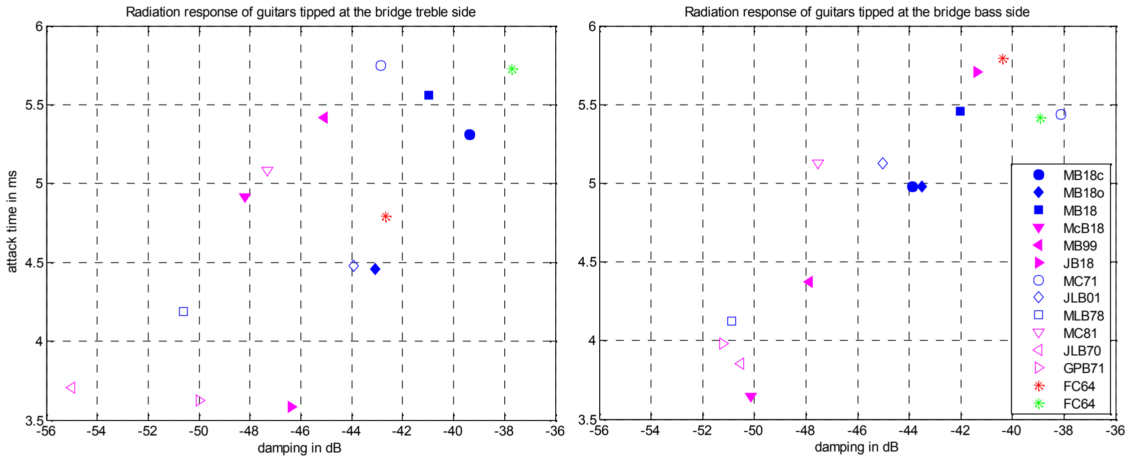

Figure 3. Attack time, i.e. 50% of total energy radiated, versus damping after 20 ms for vintage (non-filled marks) and contemporary guitars (filled marks), classical guitars (blue), and flamenco guitars (purple). The reference guitar FC64 was measured along with other guitars in the various measurement environments, and differences are likely to represent the influence of ambient acoustical conditions.

There are several observations concerning the attack versus damping populations:

(i) Fast attack correlates with damping in a plausible way. The faster the guitar, the more likely the main energy is dissipated early, the larger is the damping. In fact, all guitars rank along the same trend line, well observable in the right graph of Fig. 3.

(ii) There are significant differences between guitars, some radiate 50% of their energy within 3.7 ms others within 5.7 ms. This difference is relevant for the question here, as the rasgueado leaves only some 20 ms between strokes, and a fast attack combined with a fast declining between individual attacks is assumed to sharpen the impulse pattern.

(iii) Populations of *FGs* and *CGs* overlap. There is only a minor tendency to faster *FGs* as compared to *CGs*. In the right graph of Fig. 3, there are four *FGs* clearly faster than five *CGs*. But there is also a rather fast *CG* (MLB78), and there are also two rather slow *FGs* (JB18, MC81).

(iv) Regarding the reproducibility of measurements, the FC64 guitar is a good indicator. This guitar served as reference instrument in a semi-reverberant room (red asterisk in Fig. 3) and in a free-field (green asterisk).

(v) Mentioned tendency for *FGs* is less clear in the left graph of Figure 3, and even less clear when taking the uncertainty of (iv) into account.

(vi) There is likewise no clear tendency whether vintage guitars or contemporary guitars are faster. The populations overlap with the vintage guitars at the faster end and the contemporary guitars at the slower end.

(vii) The FC64, in this representation, is a slow guitar. Interesting to note here, because the same guitar will be at the fast end in another temporal representation.

In conclusion, there is a tendency that *FGs* are somewhat faster than *CGs*, but the employed features are not good enough to clearly separate classes of guitars.

4.2 Spacial coincidence of attack across the top plate

The attack coincidence across the top plate seeks to represent the time it takes to develop the acoustical radiation from the entire top. One would think that the sound velocity of typically more than 5000 m/s in spruce does not leave much room for such a question. Indeed, such speed would imply, that a wave originating from the bridge would reach the far end of the top in less than 0.0001 seconds, which is 2 orders of magnitude smaller than the timelines considered here for musical temporal acuity. However, as has been shown by Bader (13), the waves that travel across the top surrender part of their energy to the ribs, and further on to the back plate. The systemic approach considers an initial phase until the energy is distributed more or less well across the guitar components. The climax of vibration obviously cannot be reached across the entire top at the instant of releasing a string. Indeed, the measurements show that it takes a few milliseconds rather than 100 microseconds to develop the vibrational response at the far end of the top.

This translates to a relevant acoustical cue. The principles of projection suggest that spacial focus grows with the size of a sound source. Of course this is frequency dependent. Secondly, the attack is likely to be more distinct, if the radiation impulse starts concurrently across the entire top. So the size of a guitar top and the concurrency together could be a reasonable temporal feature.

This feature differs from the attack and decay in the radiation impulse response. Of course, the principle of loading a structure with vibrational energy is still the same and the attack and decay should also hold this aspect. However, the bridge impulse response has little chance to represent the concurrency of energy flow and dissipation across a guitar's components.

To derive a useful measure, the vibrational response across the top plate is taken. Assuming that the principle of reciprocal transfer functions applies also for guitar tops, the mechanical impulses are inserted at the various positions across the top while the response is measured at the two positions at the bridge, see the right picture in Figure 1. This measurement approach seemed reasonable, as otherwise the 1 gram heavy sensor on the thin top would impair the results more than applying the same sensor at the rather heavy bridge. The measurement with an acoustical array would be the perfect approach. However, this is impractical: the guitars usually had to stay at the collector's or at the museum's space, and the transport of an entire 100 channel array is more than difficult.

Figure 4 shows the response what is now called local rise time for each of the 13 locations across the top plate. This time is measured beginning with the rising edge of the inserted impulse (50 %), while the impulse is typically 600 to 900 microseconds wide, ending with the peak of the envelope function of the signal measured at the bridge, on either side, bass or treble.

The observations concerning the maps of local rise times are:

(i) The differences between measurements of the FC64 in the semi-reverberant and in the free-field are little. The mean difference across all measurements between semi-reverberant and free-field is 0.21 ms for the FC64.

(ii) The rise time across positions on the soundboard and across guitars ranges from 0.4 to almost 7 ms. Most of the entries are in the range of 2 to 3 ms. Note that even positions 5 and 9 very close to the bridge peak after some 2 ms, for most of the guitars, see brown area rectangles in Fig. 4.

(iii) Propagation is faster along the grain direction / along the direction of bars. This can well be seen with the fast response indicated by entries within black boxes. It is apparent that there is a fast response at the side of the impulse insertion. Positions 3, 4, 6, and 7 for the treble side of the bridge, and positions 7, 8, 10, and 11 for the bass side. It is surprising that even the remote positions 3 and 11 have a shorter rise time than the close-by positions 5 and 9. Note the typical effect of the top plate responding fast in one half and slow in the other half.

(iv) Even the remote positions 2 and 12 show short rise times, see green rectangles in Figure 4. This can be explained by the bars which roughly point in the same direction as the grain of the top plate. The bars act as fast wave guides while vibrations spread through a soundboard.

(v) There is only a slight tendency that *FGs* are faster than *CGs*. For instance, vintage *FGs* in positions 3, 4, 7, and 8 on the bass side are faster than vintage *CGs*. Contemporary *FGs* are faster than contemporary *CGs* only on positions 2 and 4 on the bass side.

(vi) The FC64 is surprisingly fast on both halves, whether the impulse insertion is on the treble side or the bass side. Among all guitars, the FC64 seems to be the fastest. This is evident when checking whether the respective other half is fast as well, e.g. positions 2 and 4 when inserting an impulse at the bass side, or positions 10 or 11 when striking the treble side. Even the remote positions 1 and 13 are surprisingly fast with the FC64. This speed is also very striking when playing the guitar. It is much faster than the other guitars investigated. The fast rise time can be explained by the inverted bracing: the bars of all other guitars are directed towards a crossing point somewhere between the 7th and the 19th fret, the bars of the FC64 are directed towards a crossing point in opposite direction outside the guitar. This means that a bar reaches from a position somewhere between 6 and 7 directly to position 3, and from a position somewhere between 7 and 8 directly to position 11.

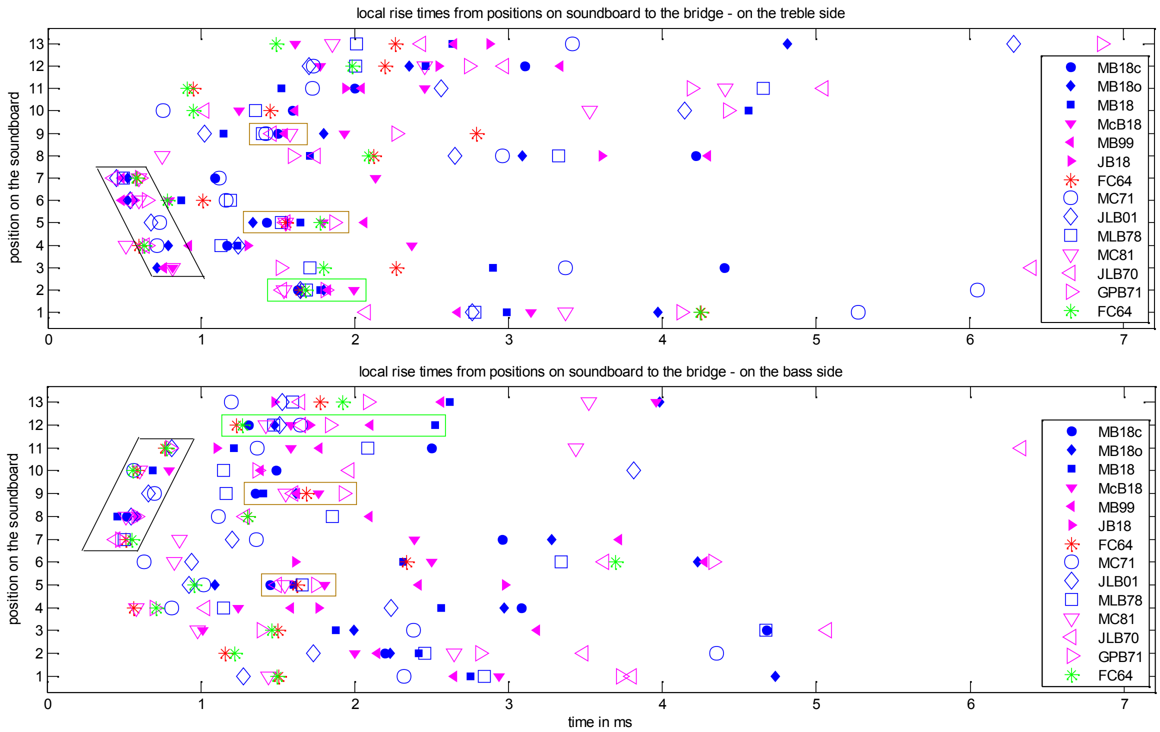

Figure 4. Local rise time for 13 positions across the top plate, or soundboard, for guitars listed in Table 2. Rise time measured from the beginning of the hammer impulse at the specific position to the time of a peaking envelope at the bridge, on either side, bass or treble, see Fig. 1 For details see text. Vintage (non-filled marks) and contemporary guitars (filled marks), *CGs* (blue), and *FGs* (purple). The reference guitar FC64 was measured along with other guitars in the various measurement environments, and differences are likely to represent the influence of ambient acoustical conditions. For rectangles see text.

4.3 Attack and decay in the radiation response to plucked strings

Using the plucked open strings instead of the impulse hammer relates well to the use case of having various impedance matching across strings and guitar bridges. Fig. 5 shows the attack and decay for the contemporary guitars. A comparison with the vintage guitars is not credible due to the strong influence of the room acoustics after 20 ms. All six contemporary guitars were furnished with the same type of new strings on the day of measurement, so the string impedance is the same across guitars. The damping after one second is extracted via a 5th order fitting to the logarithm of the envelope.

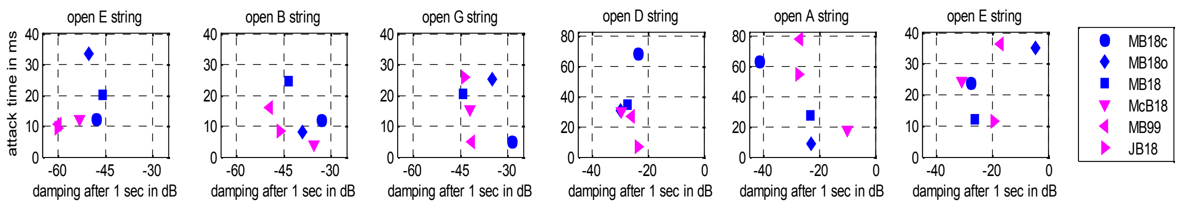

Figure 5. Attack time, maximum of the envelope after releasing open strings at the sound hole, versus damping after 1 sec. for classical guitars (blue) and flamenco guitars (purple).

The *FGs* are clearly faster than the *CGs*, on the treble strings. This can be explained by the somewhat lighter top soundboard in *FGs*. *FG* soundboards are typically some two to four tens of a mm thinner. This difference is more apparent for the treble strings with their lower impedance. The small time advantage may be enough for the ears to perceive the brightness of a *FG*. Reutter (14) studied onset perception and he claims that even tiny temporal advantages in the range of few ms of one spectral band against another one will condition the hearing process such that an advantageous band will dominate even if it is not provided with superior energy.

5 SUMMARY

The meta-level spectral findings suggest that the discussion of flamenco guitars *(FG)* versus classical guitars *(CG)* is a discussion limited to contemporary and vintage guitars, and not to historical guitars from 1900 and before. Three different temporal features lead to various findings: Attack and decay of the bridge impulse radiation responses suggest that *FGs* are somewhat fast than *CGs*, however a clear classification is not supported. Second, the attack in terms of coincidence across the soundboard helps even less in terms of classification. However, this attack measure reveals the function of bracing and it does relate to the guitar's ability to instantaneously translate action into sound. This result relates well to what can be heard across the guitars. Third, attack and decay of plucked open strings support a clear classification. Treble strings on *FGs* have some time advantage. This small advantage may be enough for the ears to perceive the brightness and acuity of a *FG* when taking psychophysics into consideration.

ACKNOWLEDGEMENTS

Guitars were measured from various collections in Spain and Germany. I want to express my honest gratitude to José Luis Romanillos and Marian Harris, to Daniel Gil de Avalle in Granada, to the Museu de la Música de Barcelona, and in particular to Soledad Sánchez Bueno and to Manel Barcons, to the Centro de Documentación Musical de Andalucía in Granada, and in particular to Antonia Riquelme Gómez, for allowing me to measure their Torres guitars and the early romantic guitars. I also thank Hakan Hatay in Hamburg, and Jésus, Mauricio and Manuel Bellido in Granada for allowing me to measure contemporary guitars.

REFERENCES

[1] Romanillos, J. L. Antonio de Torres, guitar maker: his life and work. Bold Strummer Limited. 1997.

[2] Ray, John. The Granada School of Guitar Makers. Publicaciones de Diputación Provincial de Granada. 2014.

[3] Ortega, R. H.: La transcripción musical para guitarra flamenca: Análisis e implementación metodológica, Doctoral dissertation, Universidad de Sevilla, 2011.

[4] Llobet, Francisco Javier Bethencourt. Rethinking Tradition: Towards an Ethnomusicology of Contemporary Flamenco Guitar. Diss. University of Newcastle Upon Tyne, 2011.

[5] Mores, R. Traveler's portable plate absorber for field applications. Proceedings of the TMT, Köln, 2018.

[6] Mores, R. Flamenco Guitar Sound - Documenting the Heritage. Proceedings of the DAGA, Rostock, 2019.

[7] Mores, R. Studying Torres guitars - Part II: acoustics on the path to the modern guitar. Música oral del Sur: revista internacional, número 16, 2019.

[8] Meyer, J. Die Akustik der Gitarre in Einzeldarstellungen, Verlag Erwin Bochinsky, Frankfurt. 1985.

[9] Elie, Benjamin, François Gautier, and Bertrand David. Macro parameters describing the mechanical behavior of classical guitars, JASA 132.6, 2012, 4013-4024.

[10] Elejabarrieta, M. J., A. Ezcurra, and C. Santamarıa. Coupled modes of the resonance box of the guitar, JASA 111.5, 2002, 2283-2292.

[11] Firth, Ian M. Physics of the guitar at the Helmholtz and first top - plate resonances, JASA 61.2, 1977, 588-593.

[12] Dausend, G. Michael (2002). Die klassische Gitarre: (1750-1850). H. Nogatz, 2002.

[13] Bader, Rolf. Computational mechanics of the classical guitar. Springer Science & Business Media, 2006.

[14] Reuter, Christoph. Der Einschwingvorgang nicht-perkussiver Musikinstrumente. Europäische Hochschulschriften, Reihe 36, Musikwissenschaft. 1995.

PROCEEDINGS of ISMA 2019
International Symposium on Music Acoustics

13 - 17 September 2019 in Detmold, Germany

Measurement-based comparison of marimba bar modal behaviour

Douglas BEATON *, Gary SCAVONE †

Computational Acoustic Modeling Laboratory
Centre for Interdisciplinary Research in Music Media and Technology
Schulich School of Music, McGill University, Canada

Abstract

A marimba bar's modal behaviour is governed by the shape of its 'undercut'. Manufacturers typically shape these undercuts to tune up to three modes for specified frequencies. With only three or fewer partials to tune, numerous bar geometries may yield the desired results. Different manufacturers will employ different techniques to arrive at suitable bar geometries. This diversity in tuning approaches, coupled with the natural variability of wood, results in a multitude of undercut shapes. Two bars may produce the same musical note despite plainly visible differences in undercut geometry.

This work uses experimental modal analysis to investigate the variability of marimba bar modal behaviour. Measurements are performed on numerous bars of the same note. Geometric data, including overall dimensions and mass, are recorded for each bar. Several manufacturers are represented in the resulting data set, including Yamaha, Musser and Marimba One.

Variability of the tuned and untuned modal frequencies are of primary interest. Untuned torsional modes may compromise bar performance if their frequencies are near those of the tuned modes. The proximity of these untuned mode frequencies to those of the tuned modes is therefore also investigated. Results are presented comparing bar performance both between brands and within a brand.

Keywords: Marimba, Modal Analysis, Experimental Measurements

1 INTRODUCTION

Marimba bars are tuned by removing material from the underside of the bar to affect its modal behaviour. The resulting *cutaway* or *undercut* is typically shaped to tune up to three modes of vibration. Each of the tuned modes is a flexural mode in a vertical plane. It is common for the first three flexural modes to be tuned to the frequency ratios $(1:4:10)$. The fundamental mode is tuned to the bar's designated musical note. The second flexural mode is tuned two octaves above the fundamental. The third vertical flexural mode is tuned roughly three octaves and a major third above the fundamental.

For some notes, the frequencies of untuned torsional modes may be close to those of the tuned modes. Depending on the difference in frequency, these untuned modes may affect the bar's timbre in a negative way. Marimba manufacturers have described the challenge these untuned modes can present [1].

With only three vibrational modes to tune, any number of cutaway geometries may produce the desired frequency ratios. As a result, bar geometries vary considerably. Different manufacturers may employ different tuning strategies to attempt to tune flexural modes while separating the frequencies of untuned modes. Within a brand, bars of a lower quality designation may have different geometries than those of higher quality, the tuning of which warrant more effort. In fact, it is not uncommon to find visibly apparent geometry variations between adjacent bars on a single instrument.

This work investigates the variability of marimba bar geometry through measurements. Bars of the note F♯3 were taken from a variety of instruments for investigation. Experimental modal measurements were performed on each bar. Outer bar dimensions were also recorded. At the time of writing, efforts are underway to produce 3D scans of select bars.

*douglas.beaton@mail.mcgill.ca
†gary.scavone@mcgill.ca

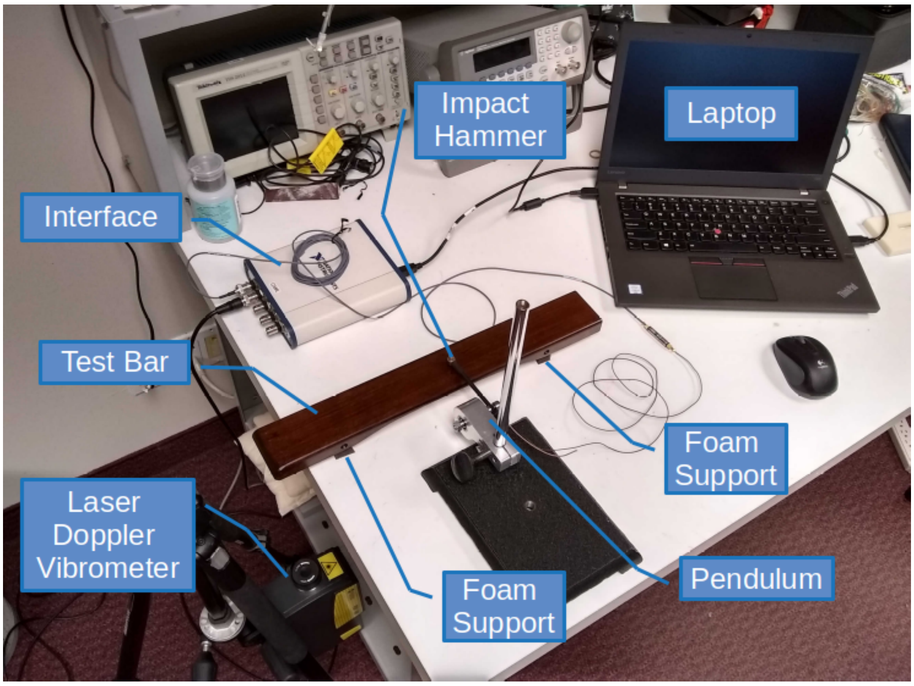

Figure 1. Experimental modal analysis measurement setup.

2 MEASUREMENT PROCEDURE

Bars on a marimba are supported by a cord passing through two holes bored through the bar. These holes are positioned near the nodes of the fundamental mode. During experimental modal measurements, the bar under test was supported on small foam blocks positioned below the bar's bored holes. This approach served to mimic the support conditions of a marimba while ensuring unrestrained bar movement. Each bar was excited using a Brüel & Kjær Type 8203 Impact Hammer. Responses were measured with a Polytec PDV-100 Laser Doppler Vibrometer (LDV).

The LDV was positioned to measure movement on the bar's bottom surface, near a corner. Strike locations were laid out in a grid on the bar's playing surface. Each location was excited using the impact hammer. Three responses were recorded for each point. At the time of writing, it is under consideration to include excitation locations on the sides of some bars, similar to previous work on marimba bar modal analysis [2].

Mode shapes and frequencies were estimated from the measured data using the Complex Mode Indication Function (CMIF) [3]. The modal frequencies presented herein are taken directly from peaks in the CMIF. At the time of writing, it is contemplated to further refine these values by fitting parameterized models to the data.

3 BAR GEOMETRY

Figure 2a gives a view of the F♯3 bar taken from an Adams 5.0-octave marimba. Notable in this geometry is the large asymmetric portion of material removed from the cutaway. This cut nearly intersects the bored holes for the supporting cord. Also notable, though more difficult to see, is a portion of material removed from the flat portion of the bar at the right end, just beyond the stamped letters "MA". These modifications appear to be part of retuning work performed some time after the bar was purchased.

Figure 2b shows the F♯3 bar taken from a Yamaha 4.5-octave marimba. The geometry of this bar is notably symmetric compared to others in the measured set (particularly that of the Adams bar in Figure 2a). It is interesting to contrast the Yamaha bar in Figure 2b to a second Yamaha bar shown in Figure 2c. These bars have essentially the same width and length, though the bar in Figure 2c has slightly thicker ends. The cutaway portion of the bar from Figure 2c is noticeably longer, ending near the cord support holes.

Table 1 provides measured dimensions for the bars assessed at the time of writing. As shown in the table, bar widths and end thicknesses are generally consistent, with the exception of the much older Premier bar. More variation is observable in the bar lengths, with the longest bar a full 50 mm longer than the shortest bar.

(a) Adams 5.0-octave marimba

(b) Yamaha 4.5-octave marimba

(c) Yamaha 5.0-octave marimba

Figure 2. Cutaways of F♯3 bars from the instruments indicated. Note that the bar in (a) appears to have been retuned since its initial manufacture.

Table 1. Measured bar dimensions.

Brand	**Instrument Size (octaves)**	**Length (mm)**	**Width (mm)**	**End Thickness (mm)**	**Mass (g)**
Adams	5.0	404	58	24	366
Marimba One	5.0	416	57	24	418
Musser	4.3	373	56	25	336
Premier	4.0	397	51	26	331
Yamaha	4.0	423	57	22	382
	4.5	423	58	22	390
	5.0	422	57	24	447

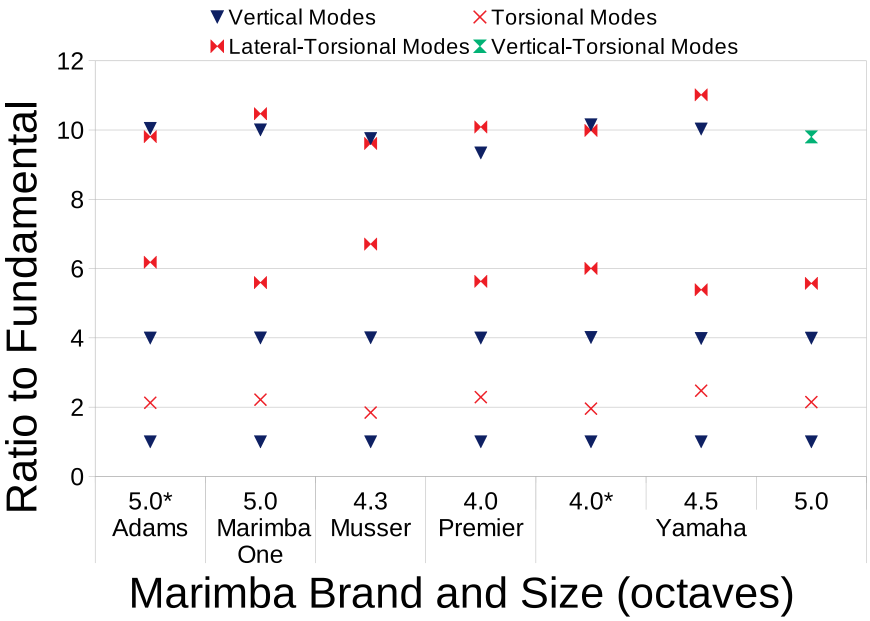

Figure 3. Modal frequency ratios of measured bars. *Indicated bars have been retuned one or more times since purchase.

4 MEASUREMENT RESULTS

Figure 3 displays the experimentally measured modal frequencies of the various bars as ratios of each bar's fundamental mode. The first tuned overtone of all bars is consistently very near the target frequency ratio of 4, two octaves above the fundamental. The second tuned overtone, with a target frequency ratio near 10 shows greater variability between bars. Differences in frequency between the second tuned overtone and the nearest untuned mode varies considerably from bar to bar, even within the same brand. In terms of achieving the desired tuning ratios and separating untuned modes, the F♯3 bar from the Yamaha 4.5-octave marimba is the clear winner from the bars measured at the time of writing.

Removing material from only the bottom of the bar to create the cutaway results in a coupling between lateral and torsional deformations. With the exception of the first torsional mode, lateral and torsional deformations are observed in modes of either type. These two modes types are thus combined into a single lateral-torsional category in Figure 3.

By contrast, the lone vertical-torsional mode appears to be produced from two degenerate modes. The third vertical mode of the Yamaha 5.0-octave marimba bar is so close in frequency to a lateral-torsional mode that the CMIF analysis yields a single mode. The shape of this single mode, shown in Figure 4c, is recognizable as a combination of the third vertical mode (e.g. Figure 4a) and nearby lateral-torsional mode (e.g. Figure 4b) observed in other bars.

5 SUMMARY

At the time of writing, experimental modal analysis has been performed on seven F♯3 marimba bars, with additional bar measurements planned. The following features of the current measured bar set are notable in their variability:

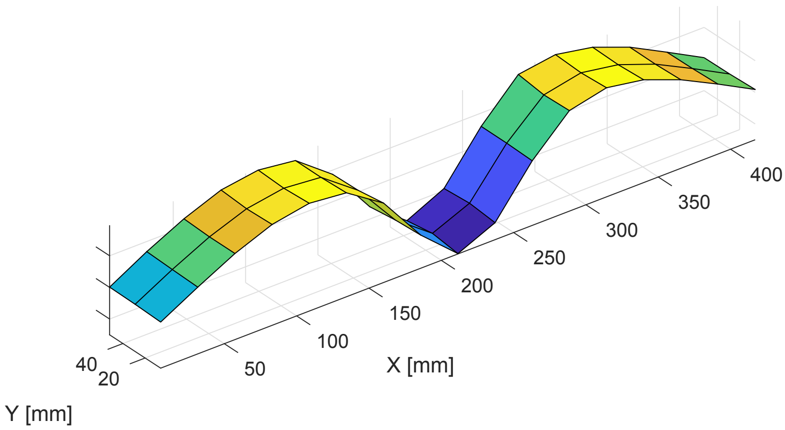

(a) Yamaha 4.5-octave marimba, mode shape 5

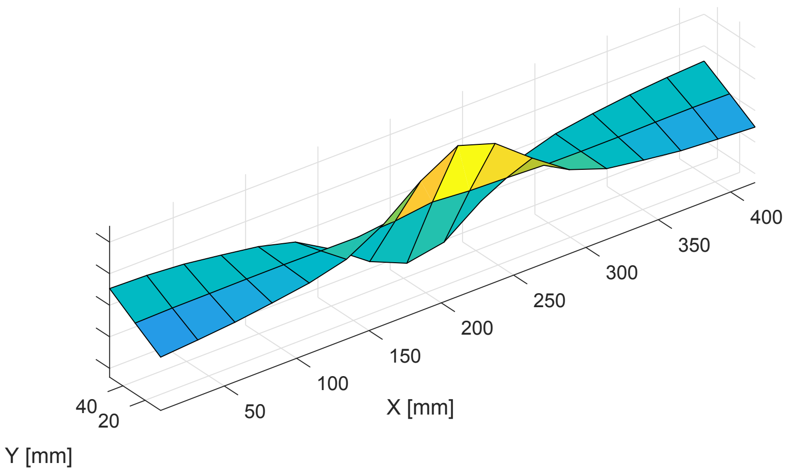

(b) Yamaha 4.5-octave marimba, mode shape 6

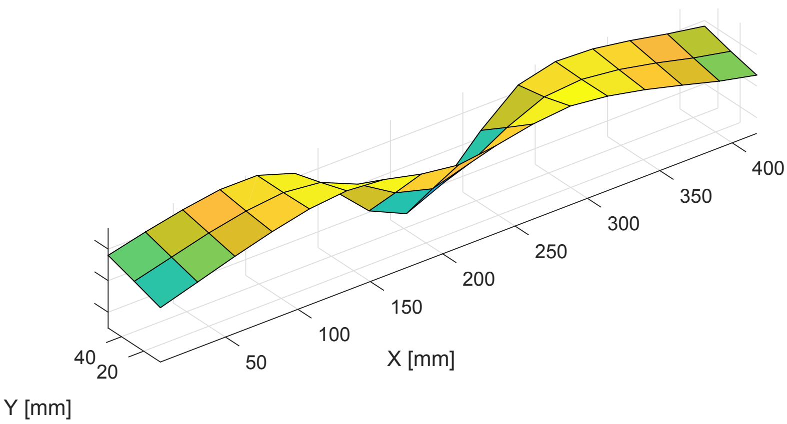

(c) Yamaha 5.0-octave marimba, mode shape 5

Figure 4. Measured mode shapes (vertical component only) of F♯3 marimba bars. Instruments and mode shape numbers as indicated.

- Bar mass and length
- Cutaway geometry
- Ratio of second tuned overtone frequency to fundamental
- Frequency spacing of second tuned overtone and nearest untuned mode

For the F♯3 bar from the Yamaha 5.0-octave marimba, the Complex Mode Indication Function (CMIF) produced a single mode at a frequency around ten times that of the fundamental. For all other bars, the CMIF indicated two modes around the same frequency ratio. The mode shape of this single mode (Figure 4c) appears to be a combination of the two modes (Figures 4a and 4b) near the same frequency ratio for other bars. At the time of writing, further investigation with additional measurement points is contemplated to separate this single mode.

ACKNOWLEDGEMENTS

This work was made possible through financial support from the Vanier Canada Graduate Scholarships Program, the Schulich School of Music, and the Centre for Interdisciplinary Research in Music Media and Technology (CIRMMT). The authors would also like to thank Fabrice Marandola, Martin Daigle and David Brongo at the Schulich School of Music for their insights into marimba performance and access to instruments.

REFERENCES

[1] Stevens, LH. The acoustic complexity of keyboard percussion instruments. Part I: What we know and what we wish we knew. The Journal of the Acoustical Society of America, 138, 2015, pp 1912.

[2] Bork, I.; Chaigne, A.; Trebuchet, LC.; Kosfelder, M.; Pillot, D. Comparison between modal analysis and finite element modelling of a marimba bar. Acta Acustica United With Acustica, 85, 1999, pp 258-266.

[3] Shih, C.; Tsuei, Y.; Allemang, R.; Brown, D. Complex Mode Indication Function and its applications to spatial domain parameter estimation, Mechanical Systems and Signal Processing, 2 (4), 1988, pp 367-377.

PROCEEDINGS of ISMA 2019
International Symposium on Music Acoustics

13 - 17 September 2019 in Detmold, Germany

Analysis of reed vibration and mouthpiece pressure in contemporary bass clarinet playing techniques

Peter Mallinger[(1)*], Montserrat Pàmies-Vilà[(1)], Vasileios Chatziioannou[(1)], Alex Hofmann[(1)†]

[(1)]Dept. of Music Acoustics, University of Music and Performing Arts Vienna, Austria

Abstract

While articulation on the B♭-clarinet has already been a subject in various studies, articulation on the bass clarinet has gotten less attention. Because of the increasing interest for using the bass clarinet, especially in contemporary music, this instrument is emerging from the shadow of the B♭-clarinet. In order to investigate articulation on the bass clarinet an experiment was carried out in an anechoic chamber at the University of Music and Performing Arts Vienna. A professional clarinetist was recorded performing different articulation techniques on a German bass clarinet under controlled performance conditions. Results show that the attack transients on the bass clarinet were about 0.085 s long in staccato articulation. In comparison, attack transients on the B♭-clarinet are 2 to 3 times shorter. This study especially focuses on the slap tonguing technique. Of particular interest is the reed bending signal, which shows the movement of the reed. It has been observed that tones articulated with slap tonguing have a significantly shorter attack transient and are immediately entering the decay phase. Such measurements allow an in-depth analysis of player-instrument interactions with contemporary playing techniques and may support the refinement of physical model parameters but may also support music education.

Keywords : Bass clarinet, articulation, woodwinds, contemporary music, player-instrument interaction

1 INTRODUCTION

Articulation techniques on the bass clarinet require precise control over the blowing pressure, the tongue and the embouchure as well as simultaneous fingering actions. There have been studies on how professional players use their vocal tract [5, 6] and tonguing technique for articulation on single reed instruments [7]. Furthermore, measurements of finger forces during clarinet playing were investigated [1]. However, these studies have primarily been focussing on classical performances on the B♭-clarinet and did neither investigate the playing techniques on the bass clarinet nor contemporary playing techniques like slap tonguing.

Recently, the bass clarinet gets more attention not only in orchestral or chamber music, but especially in contemporary music [2]. Reasons therefore are for example the large pitch range (4 octaves), the possibility of extreme dynamics and the potential of being able to producing a variety of contemporary sound effects. For the production of such sound effects, unique playing techniques are required and some techniques are still under development, usually in a collaboration between clarinetists and composers. Classical articulation techniques, like staccato, legato or portato, mostly require an interaction between the tip of the tongue and the tip of the reed [4].

In contrast, the so called slap tongue requires the player to use a larger area of the tongue to act on a large reed area [3]. During slap tongue, the top side of the tongue is used to create a vacuum between tongue and reed so that it is possible to pull the reed away from the mouthpiece, working against its restoring force. When the tongue is reshaped, it releases the reed, so it snaps back against the mouthpiece. There are three different kinds of slap tonguing: the non-pitched slap, where the player releases the reed without blowing into the instrument, the pitched slap, where the tone actually sounds after the snap of the reed, and the open slap, which is played

*peter.mallinger@students.mdw.ac.at / pet.mall@gmx.at
†hofmann-alex@mdw.ac.at

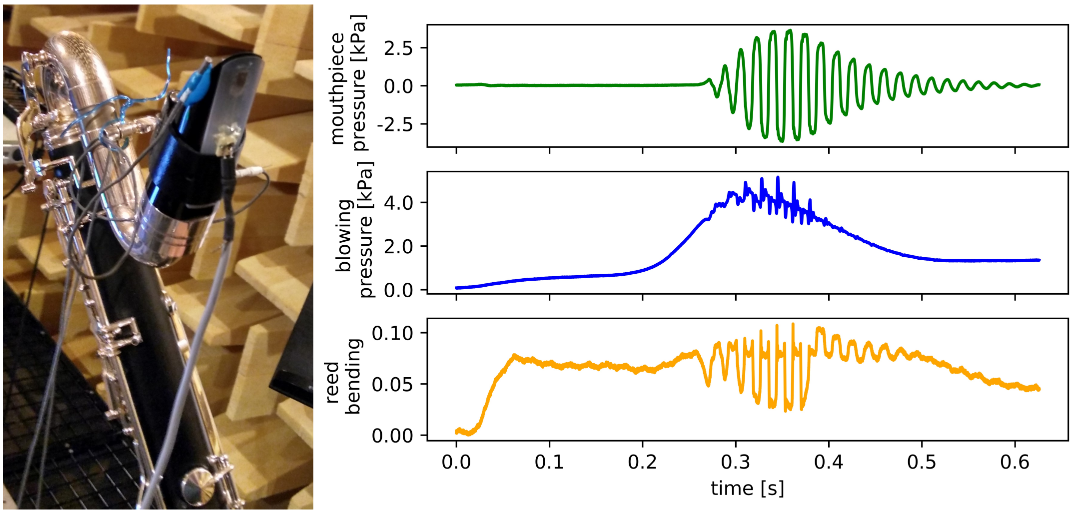

Figure 1. Left: Bass clarinet mouthpiece with two piezo-resistive pressure tranducers to measure blowing pressure (left side of the mouthpiece) and mouthpiece pressure (right side of the mouthpiece). Synthetic reed with strain gauge measures the reed bending. Right: Captured signals during classical staccato articulation of the tone C2 (notated), showing mouthpiece pressure (green), blowing pressure (blue) and reed bending (orange).

by releasing the reed and simultaneously opening the lower jaw.

This study has two aims: a) to compare classical articulations on the bass clarinet with measurements available for the B♭-clarinet and b) to gain more insight into the slap tonguing playing technique.

2 METHODS

2.1 Experimental Setup

For this study a bass clarinet with German system (F. Arthur Uebel B-740) was used. For the measurements, the mouthpiece (MAXTON-KW) and a synthetic reed were equipped with sensors. Because there are no synthetic reeds for bass clarinet with German system, a reed for alto saxophone was used, as it is common practice among professional bass clarinetists. Two piezo-resistive pressure transducers (Endevco 8507C-2) were mounted in a way that they recorded the acoustic pressures in the player's mouth and also inside the mouthpiece. Therefore one transducer was inserted into the mouthpiece via a side hole. The other one was attached to the side of the mouthpiece so that it remains inside the player's mouth while playing. The synthetic reed was equipped with a strain-gauge sensor to measure the bending of the reed. This measurement setup is similar to the one used in [7]. Using the same equipment allows to compare the data of this study with the measured values of the previous study carried out on a B♭-clarinet with German system in the same lab [7].

2.2 Procedure

The experimental aim is to capture data that allows a comparison with articulation techniques on the B♭-clarinet as well as to gain new insights into the slap tonguing techniques on the bass clarinet. To this cause a systematic recording protocol was prepared in the form of a musical score. This score was comprised of a C-major scale and combinations of different intervals (some with slap tonguing sound effects). Instructions were given on the articulation techniques (legato, portato, staccato with and without tonguing), tempi and dynamics on how the score has to be played by a performer.

Pitch (notated)	Articulation	Dynamic	Attack time	Mouthpiece pressure [kPa]	Blowing pressure [kPa]
C2 (58,27 Hz)	staccato	forte	0,085s	3,67	5,19
C2	staccato	piano	0,102s	2,27	3,43
C2	portato	forte	0,102s	2,11	3,45
C2	portato	piano	0,17s	1,25	1,96
C2	without tongue	forte	0,102s	3,42	4,92
C2	without tongue	piano	0,136s	1,87	2,88
Bb3 (207,7 Hz)	staccato	forte	0,024s	2,76	4,38
Bb3	without tongue	forte	0,029s	3,00	4,76

Table 1. Overview of measurements with different articulation techniques and dynamics on a German bass clarinet. Giving details of Attack time, maximum Mouthpiece pressure and maximum Blowing pressure for each analyzed tone.

A professional clarinetist (first author) played the given score on the sensor-equipped bass clarinet. A recording was made in the anechoic chamber of the Department of Music Acoustics at the University of Music and Performing Arts Vienna. The entire recording session lasted approximately 45 minutes, including a 10-minute warm-up phase.

3 RESULTS

3.1 Classical Articulation measurements

Figure 1 (right) shows an exemplary signal of the measurements (captured data was converted into SI units for better comparison). The top panel shows the mouthpiece pressure (green), the middle panel the blowing pressure (blue) and below is the bending signal of the reed (orange). In Figure 1 the lowest tone in the range of the bass clarinet is shown, played with staccato articulation. It was observed that the blowing pressure (blue) increased (0.2-0.28 s) before the tongue released the reed (0.28 s). A tongue release indicates the starting point of the actual tone. After a tongue-release, the observed attack time was about 0.085 s until the maximum amplitude of the oscillations was reached. At the end of the tone when the tongue stops the reed (0.38 s), small vibrations can still be observed in both the mouthpiece pressure (green) and the reed signal (orange). The tone decay time of 0.22 s is the duration of the remaining energy of the standing wave in the tube that gets slowly radiated through the bell of the instrument or lost due to thermal and viscous effects [8].

Table 1 summarizes the results of the measurements of classical articulation techniques. A comparison between the different articulation techniques shows that a tone played on the bass clarinet has the shortest attack time when played with staccato articulation in forte dynamics, because of the higher blowing pressure. Furthermore, a possible influence may be that in staccato-forte playing, the tension of the respiratory system including the tongue may also be higher, compared to other playing techniques like portato or legato.

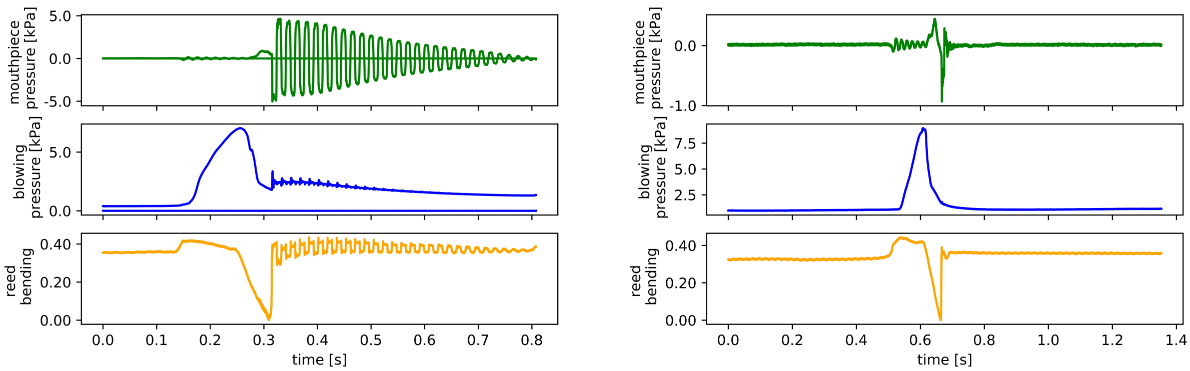

Figure 2. Mouthpiece pressure, blowing pressure and reed bending of a slap tongue tone (notated C2). Left: Slap tongue with giving blowing pressure after the release of the reed. Right: No blowing pressure is applied to the instrument after the reed has been released.

3.2 Contemporary Playing Techniques

Contemporary playing techniques on wind instruments are often created through a new way of player-instrument interactions. Hence, an extraordinary use of the embouchure or unusual tonguing actions are required for these playing techniques. The slap tongue is a prime example for this. Figure 2 shows two slap tonguing tones with a starting transient that has zero attack time. The left panel shows a slap tone with the player giving a blowing pressure to the instrument after the tongue released the reed, whereas in the right panel the reed is released without blowing into the instrument.

In the toned-slap (left), the first period of the tone already reaches the maximum amplitude and then fades out. Specific attention should be given to the reed signal (orange), which depicts how the reed was pulled away from the mouthpiece (0.25–0.3 s) before it suddenly snaps back to the mouthpiece (0.3 s). Compared to classical articulation techniques, the reed bends away from the mouthpiece about four times larger than the equilibrium position. In this case the slap was played in combination of giving a blowing pressure (blue, 0.2–0.3) so that the fingered pitch actually sounded and faded out after the snap. The duration of the fade out is related to the characteristics of the bore resonator.

In the case of mute-slap (Figure 2, right), no such decay was observed, showing that no standing wave was built up in the resonator. The mouthpiece pressure shows an impulse created at reed release (0.68 s). This results in a percussive sound effect.

4 DISCUSSION

Various contemporary playing techniques exist for both the B♭-clarinet and especially for the bass clarinet. This study is a starting point in precisely measuring the player-instrument interactions taking place in such. As this study only scratches the surface of the topic, there is a lot of potential for further studies involving comparisons of similar experiments on different single-reed instruments or even capturing data from different performers.

Moreover, a comparison with a similar procedure carried out on a bass clarinet with french system would be suited to better understand the differences in player-instrument interactions on the two types of popular clarinet systems. Future studies may also involve computer simulations of the captured signals, to gain insight into hidden playing parameters controlled by the player.

REFERENCES

[1] Hofmann, A., Goebl, W. Finger forces in Clarinet playing. *Frontiers in Psychology. Performance Science,* 7(1140), 2016.

[2] Iles, J.B. *The Changing Role of the Bass Clarinet: Support for Its Integration into the Modern Clarinet Studio*, PhD thesis, University of Nevada, Las Vegas, 2015.

[3] Krassnitzer, G. *Multiphonics und andere zeitgenössische Spieltechniken auf der Wiener Klarinette*, Master thesis, University of Music and Performing Arts Vienna, 2000.

[4] Krautgartner, K. *Untersuchungen zur Artikulation bei Klarinetteninstrumenten im Jazz*, PhD thesis, University of Cologne, 1982.

[5] Li, W., Almeida A., Smith J., Wolfe J. How clarinettists articulate: The effect of blowing pressure and tonguing on initial and final transients. *The Journal of the Acoustical Society of America 139 (2)*, 2016, pp 825-838.

[6] Pàmies-Vilà, M., Scavone, G., Hofmann, A., Chatziioannou, V. Investigating vocal tract modifications during saxophone performance. In *Proc. 174th Meeting of the Acoustical Society of America*, New Orleans, Louisiana, (Proceedings of Meetings on Acoustics Vol. 31), 2018.

[7] Pàmies-Vilà, M., Hofmann, A., Chatziioannou, V. Analysis of Tonguing and Blowing Actions During Clarinet Performance. *Frontiers in psychology 9: 617*, 2018.

[8] Schmutzhard, S., Chatziioannou, V., Hofmann, A. Parameter Optimisation of a Viscothermal Time-Domain Model for Wind Instruments. In *Proceedings of the 2017 International Symposium on Musical Acoustics (pp. 27–30)*, Montreal, CA: McGill University, 2017.

PROCEEDINGS of ISMA 2019
International Symposium on Music Acoustics

13 - 17 September 2019 in Detmold, Germany

Relation between subjective evaluation for proficiency, expression or technique and acoustic feature on violin performance

Madoka OKEMOTO[1]; Masanobu MIURA[2]

(1) Graduate School of Engineering, Hachinohe Institute of Technology, Japan, unkomgn@gmail.com
(2) Faculty of Music, Kunitachi College of Music, Japan, miura.masanobu@kunitachi.ac.jp

Abstract

Studies of proficiency estimation for musical performances have been intensively conducted in the field of performance science. In most of the studies, feature parameters are calculated from each sound of performances to estimate performance proficiency. However, most cases in the studies estimated only proficiency score, did not estimated expression or technique scores, although they are thought as important for the proficiency estimation. Therefore, this report tries to clarify a relation of subjective evaluation concerning proficiency, expression or technique to acoustic features on violin performances. Moreover, most important parameter on the three scores are discussed. Firstly, five professional violin players gave scores for proficiency, expression and technique to 100 performances for the simple major scale starting from 261Hz or C3 with vibrato. Then, a set of 106 parameters are calculated from the 100 performances. By using the parameters, scores for proficiency, expression and technique are estimated using the liner regression with relative weights for each parameter, so that we confirm the most effective parameters on the estimation. As the results, most important parameters on each score are: the FM vibrato parameter on proficiency, the strength on attack for each note on expression, and the smoothness on consecutive two notes on technique. At the conference, the authors will explain the results in detail on their presentation.

Keywords: Sound, Music, Performance, Violin, Acoustic parameter

1 INTRODUCTION

Estimating the proficiency of musical performances is difficult for novice musicians but desired for their self-learning. Tuns, computational estimation of performance proficiency has been studied [1,2]. A previous study by the authors examined proficiency estimation by using acoustic parameters that include tone duration, tone pitch, AM vibrato, FM vibrato, and so forth. Estimation accuracy of the study was .78 in terms of correlation coefficient between rated and estimated scores. However, that study focused on only proficiency score and did not focused on expression or technique score, even though they are important for proficiency score. Moreover, previous studies did not examine the relation between the parameters and the scores of proficiency, expression and technique for violin performances.

2 AIMS

This study estimates scores of proficiency, expression and technique with the liner regression using 106 parameters proposed by a previous study, and confirms relations between effective parameters and scores of proficiency, expression and technique for violin performances.

3 RELATIONS BETWEEN PARAMETERS AND SCORES

3.1 Method

Firstly, scores of proficiency, expression and technique are estimated by the liner regression using 106 parameters [2]. Second, the relative weights of the liner regression are calculated to confirm the effectiveness to the scores of proficiency, expression and technique for violin performances. In addition, the algorithm M5[3] is

1 unkomgn@gmail.com
2 miura.masanobu@kunitachi.ac.jp.

employed to conduct the liner regression in this report.

3.2 Violin performance

Employed sheet music is a "C-major scale with A4 = 440Hz master tuning with vibrato". Figure 1 shows the sheet music of the musical task. Numbers in Figure 1 are fingering number. Audio of 100 performances (10 persons * 10 trials) are recorded, on which the ten persons are amateur players.

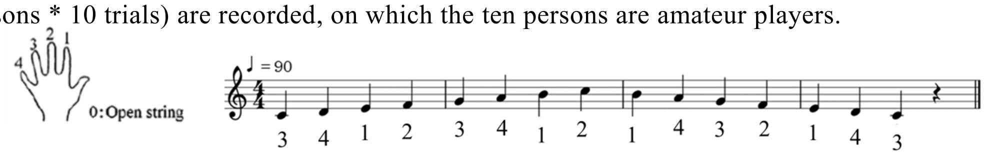

Figure 1. Sheet music

3.3 Scores of proficiency, expression and technique

The scores of proficiency, expression and technique are given by 5 evaluators. The 5 evaluators were graduated from musical university, and are currently players or instructors of the violin as their main work. The recorded audio of the 100 performances were presented in a random order for every task. The experts were asked to evaluate them based on 10 steps from 1 to 10 with the best performance being a 10 about proficiency, expression or technique.

3.4 Parameters

Table 1 shows parameter set. Used parameters by a previous study[2] are combination with acoustics and statistics parameters (the total amount 106 parameters). The acoustic parameters are calculated by each tone in the sheet music, and the statistic parameters are calculated by that calculated the acoustic parameters are calculated to all 11 tones in the sheet music. The acoustic parameters are tone pitch, AM vibrato, FM vibrato, and so forth. The number of the acoustic parameters are 21. The statistic parameters are the average (Ave), the standard deviation (P_0) and 4 parameters (P_0 ~P_4). The 4 statistic parameters (P_0 ~P_4) are parameters relating to tendency curve by 11 tones of the sheet music. The amount of the statistic parameters is 6.

Table 1. Parameter set

	Ave	P_0	P_1	P_2	P_3	P_4
Onset	●	●	●	●	●	●
Duration	●	●	●	●	●	●
St	●	●	●	●	●	●
Tempo	●	●	●	●	●	●
P2P	●	●	●	●	●	●
Diff_peak	●	●	●	●	●	●
Diff_bottom	●	●	●	●	●	●
Relative_SC	●	●	●	●	●	●
Sigma_flux	●	●	●	●	●	●
F0gap	●	●	●	●	●	●
F0gap_slope	●					
F0gap_tgap	●					
Fm_slope	●	●	●	●	●	●
Fm_times	●	●	●	●	●	●
Fm_wid	●	●	●	●	●	●
Am_slope	●	●	●	●	●	●
Am_times	●	●	●	●	●	●
Am_wid	●	●	●	●	●	●

3.5 Results

Results of the calculated relative weights on the liner regression can be confirmed of most closely related parameter at each score (proficiency, expression and technique). From the obtained results, it is clarified that the proficiency score is most closely related to range of tendency curve of FM vibrato parameters. The expression score is closely related to difference in tendency curve between adjacent tones of velocity. The technique score is most closely related to average of the difference in amplitude of the two peaks of two tones. Moreover, estimation accuracy of proficiency is .67, expression is .70, and technique is .68, in terms of correlation coefficient.

3.6 Discussion

Estimation accuracy of proficiency, expression or technique are almost same level (.67, .68 or 0.70). However, the highest ten parameters in terms of relative weights on proficiency, expression or technique are not consistent. Figure 2 shows the ten highest parameters with relative weights for proficiency, expression and technique scores. The vertical axis shows relative weights of each score, and the horizontal axis shows the parameter in the order of rank of relative weights. As can be seen in figure 2, the magnitude of relative weights on the technique score are comparatively high, whereas those on proficiency are low, and those on expression are lowest among the three scores. It implies that evaluation for expression does not depend mainly on several parameters whereas the evaluation for technique depends mainly on specific set of parameters. Therefore, it may suggest the difference of complexity of the evaluations on expression and technique aspects.

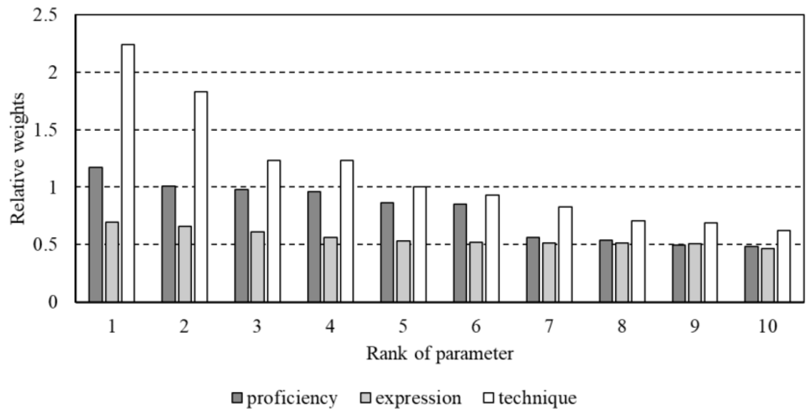

Figure 2. Relative weights on the parameters

4 CONCLUSIONS

Most important parameters on each score are: FM vibrato parameter on proficiency, strength on attack for each note on expression, and smoothness on smooth of two notes on technique. The difference of relative weights on the parameters on the linear regression to estimate the evaluation scores is shown. It may represent the difference of complexity of the evaluations on expression and technique aspects.

REFERENCES

[1] A. Nonogaki, S. Shimazu, N. Emura, M. Miura,S. Akinaga and M. Yanagida, "Use of spline curve to evaluate performance prociency of a Czerny pianopiece", Proceedings of International Symposium on Performance Science, pp.68-74 (2011).

[2] M. Okemoto, M. Miura, "A Proficiency estimation system for violin performance", 15th International Conference on Music Perception and Cognition: Abstract book, p.501 (2018).

[3] H. Akaike, "A new look at the statistical model identification.", Selected Papers of Hirotugu Akaike. Springer, pp.215-222 (1974).

PROCEEDINGS of ISMA 2019
International Symposium on Music Acoustics

13 - 17 September 2019 in Detmold, Germany

Acoustical analysis of stringed instruments without touch

Heidi von Rüden[1] and Anton Schlesinger[2]

[1]State Institute for Music Research of the Prussian Cultural Heritage Foundation, Germany, vRueden@sim.spk-berlin.de

[2]theapro, daberto + kollegen planungsgesellschaft mbh, Germany, a.schlesinger@theapro.de

Abstract

At an abstracted level, the stringed instrument consists of a box with a neck and fastened strings. The design of the resonator determines the sound. Therefore, the acoustic measurement of instruments plays a prime role for functional analysis and digital archiving. In this contribution an acoustical, contact-free measurement method for quantifying the transfer function of guitars is presented. The method assesses the sounding body and its periphery by means of a standard acoustical impulse response measurement (AIR). As a test signal a logarithmic sweep is employed that offers a high signal to noise ratio and the ability to separate potential harmonic distortion of the electronic signal chain from the impulse response of the instrument. The measurement is compared to the hammer probe, which is the current gold standard method for measuring the transfer functions of sounding bodies and the periphery of stringed instruments.

This contribution summarizes an ongoing investigation. Prospectively, AIR is an ideal tool for functional analysis, long term monitoring of instruments as well as quality control. Instruments are not subjected to mechanical stress and do not have to be prepared for play. The sonification of the impulse response allows for aural assessment and may complement the description of stringed instruments in archives.

Keywords: Measurement, stringed instruments

1 INTRODUCTION

In the museum the meaning of an instrument changes from a tool of the musician to an historical artefact. Due to the functionality a musical instrument has always a technical background. A museum not only shows the external appearance of an instrument, further aspects are important to understand how an instrument works, as for example the material, the construction and its manufacturing process.

The requirement for an acoustical measurement technique arose at the museum of musical instruments, which is part of the Stiftung Preussischer Kulturbesitz (Prussian Cultural Heritage Foundation). It is located in Berlin at the State Institute for Music Research (SIM). The museum collects instruments of the European classical music tradition from the 16th to the 21th century. The conservators are in charge of nearly 3200 instruments.

For the staff of the restoration laboratories the preservation of the object is the principal goal. The ICOM code of ethics for museums sets minimum professional standards and encourages the recognition of values shared by the international museum community. *Museums have the duty to acquire, preserve and promote their collections as a contribution to safeguarding the natural, cultural and scientific heritage* [1]. Therefore, a protective environment with a careful monitoring and documentation is essential and part of the museum's work.

Although the museum comprises a vast collection of instruments, only few instruments are in a playable condition. Often the physical maintenance of an instrument as a whole is more important than studying the sound of it. The restoration of an instrument requires different concepts. Heavily used and old materials need special care. Despite due diligence, the new stringing of a lute can still lead to irreversible damages if a joint between soundboard and shell opens or the bridge tears off because of high string tension. The documentation of the acoustical context of an object is therefore being considered more and more often as an alternative to executing sound measurements or recordings with strung instruments. However, fundamental research questions on sound qualities cannot be answered in this way.

Rare but popular with visitors are concert projects and recordings with a limited duration of playing time on instruments of the collection. Concerts with plucked instruments of the museum collection are even more seldom. Guides of the museum generally work with copies of bowed and plucked stringed instruments.

As regards the acoustical description of a string instrument in an archive, the resonances are of prime importance. Among which, the Helmholtz resonance (HR) strongly determines the sound of an instrument, namely the sound volume and sonority. It depends on three parameters, the volume, the size of the sound hole and the stiffness of sound board. The larger the volume, the deeper the resonance. Furthermore, the band width (Q-factor) of the HR is influenced by the material density and flexibility of the sides of the instrument's body. There are further acoustic features in the transfer function that are characteristic to certain models of stringed instruments [2]. The transfer functions are generally captured by the hammer probe method. The excitation by hammer is however problematic for historical instruments, because the applied force can cause damage. Nevertheless, the hammer method is a reliable measuring method for instrument makers in order to monitor acoustic conditions during the construction process. In recent years, the importance of this method has been recognized more and more in the context of organology.

In this contribution, an alternative acoustical probing method for string instruments is presented. The method is purely acoustical, hence contact free and therefore much less destructive than the hammer method. To many people dealing with instruments, the method is already known from the excitation of the HR by singing into the sound hole. In this contribution, this testing method is systemized as an acoustical impulse response method (AIR) and general questions for retrieving reliable results are discussed. This contribution starts with the presentation of the AIR method. Thereafter, the method is validated and discussed.

ACOUSTIC IMPULSE RESPONSE (AIR) METHOD

The proposed method is based on two room impulse response measurements, one with the string instrument present and one without. Subsequently, the room is eliminated by numerical deconvolution, which results in the impulse response of the sounding body of the string instrument alone.

The logarithmic sweep was applied as the measurement signal. This excitation signal for measuring the impulse response is characterized by a high and frequency independent signal-to-noise ratio (SNR) and removes harmonic distortion of the signal chain [3]. In order to get the impulse response of the string instrument h_{i}, two signals are recorded in the time domain[1]

$$y_{\mathrm{r}} = s * h_{\mathrm{r}} \tag{1}$$

$$y_{\mathrm{r,i}} = s * h_{\mathrm{r,i}} \tag{2}$$

with y_{r}, $y_{\mathrm{r,i}}$, s, h_{r} and $h_{\mathrm{r,i}}$ being the convolutional product of the room and s, the convolutional product of the room, the instrument and s, the logarithmic sweep (swept sine), the impulse response of the room and the confounded impulse response of the room and the instrument, respectively. Because $h_{\mathrm{r,i}} = h_{\mathrm{i}} * h_{\mathrm{r}}$ and the possibility of forming the inverse of the logarithmic sweep, the impulse response of the instrument can be retrieved by deconvolving the room impulse response from the confounded impulse response

$$h_{\mathrm{i}} = h_{\mathrm{r,i}} * h_{\mathrm{r}}^{-1} \tag{3}$$

Which is equivalent to

$$h_{\mathrm{i}} = y_{\mathrm{r,i}} * y_{\mathrm{r}}^{-1} \tag{4}$$

Because this calculation of h_{i} contains a collateral dirac (from the deconvolution process of the room) followed or superimposed by the smaller impulse response of the instrument, h_{i} needs further preconditioning before analysis. In this work, the dirac was simply subtracted by

$$\hat{h}_{\mathrm{i}} = h_{\mathrm{i}} - y_{\mathrm{r}} * y_{\mathrm{r}}^{-1} \tag{5}$$

[1]The index t for indicating the time domain representation is dropped in the following formulae for the sake of brevity.

The numerical implementation of the deconvolution process needs a stabilization constant. This constant however amplifies low frequencies noise in the resulting impulse response. As a countermeasure, a high pass filter with a very low cutoff frequency was applied to $\hat{h}_\mathrm{i}$ in this work.

VALIDATION

1.1 Comparision with the hammer probe

The measurements were taken at two different locations, the University of Applied Sciences / Department of Musical Instrument Technology in Markneukirchen and the State Institute for Music Research of the Prussian Cultural Heritage Foundation / Department III: Acoustics and Music Technology and Department I: Museum of Musical Instruments in Berlin. The climatic conditions on both places were similar.[2] Subject of the investigation were two newly built guitars with different design made by the first author. A modern concert guitar and the replica of a 19th century terz guitar. The sound quality and the artistic crafted work of the research objects are comparable with guitars of the museum in Berlin. The instruments allow further investigations on timbral features because they are playable. The material of the classical guitar is very conventional. The back is strongly arched. It has three ribs. The soundboard is made from spruce with fine growth rings with a thickness of 2.2 to 2.5 mm. The guitar has seven fan struts, the outer ones reach down through the crosswise bar into the sound hole area. The shape of the strutting is asymmetrically, the treble side is made stiffer than the bass side. The terz guitar is made from maple and spruce with an inner mold like a violin. The back has four cross ribs, equally divided. The soundboard has also four cross ribs, two above and two underneath the sound hole. The part of the bridge is reinforced. The neck fits with a screw to the body. The fingerboard holds these two parts together. The sound qualities of these two guitars differ highly.

Figure 1. Classical guitar (left) and terz guitar (right) used in the comparison between the AIR method and the hammer probe.

At the Department of Musical Instrument Technology the measurement was taken in a small studio on a table. The guitar was supported in laying position by foam material underneath the area of the end block and the neck block of the body. The strings were damped by hand. The accelerometer was fastened with wax on the soundboard of the guitar, at the point of 6 cm (6,5 cm/ terz guitar) from the bridge-saddle E-string (G-string/

[2]Due to the ethical standards according to ICOM, with very high safety requirements, we choose instruments of private property and not from a museum collection for this project. The transport of the guitars was not air-conditioned. The temperature and relative humidity in the locations in Markneukirchen and Berlin were recorded: In Markneukirchen the relative humidity was 53% at 19,5°C, the premises in Berlin is air conditioned with a humidity of 55% at 21°C

terz guitar) straight to the end of the body. The piezo sensor (model: Piezotronics Model 352B10 with a sensitivity of 10.04 mV/g or 1.024 mV/m/s2) and the hammer (model: PCB 086 B01) were connected to the FFT Analyzer (Ono Sokki CF-7200 FFT Analyzer). The knocking was executed in the middle on the saddle of the bridge by hand and averaged. A coherence function served as a quality criterion of the measurement accuracy.
The presented method AIR was executed in the anechoic room of the SIM for the sake of a controlled environment, predominantly for a reduced acoustical background level. All six surfaces of the room are covered with wedge shaped absorbers. The floor consists of walkable netting with meshes of 60 mm. The room has a volume of around 50 cubic metres. The guitar was placed on the floor, supported by foam material (200 x 80 x 20 mm) on the upper and lower part of the body. The guitars lie very stable in this position. The contact time to the foam material was limited. The object had no other physical contact to the interior or the equipment. Each measurement lasted about 20 min. The guitars were placed on the floor and the omnidirectional microphone was fixed at a height of 1.90 m, perpendicularly above the bridges. The position of the applied omnidirectional loudspeaker was at the opposite corner of the room. The distance between the loudspeaker and the microphone was 3.50 m. The distance between the middle of the guitar body and the loudspeaker was 3.83 m. The strings were damped by polyester fleece.
The applied swept sine had a length of 8 s and a sampling frequency of 48 kHz. During the measurement, the maximum Z-weighted sound pressure level was at 105.4 dB at the microphone. In each measurement, the sweep recording was executed three times and averaged in order to improve the signal to noise ratio (SNR). The recording chain obeyed the requirements for room acoustic measurements in auditoria [4] and consisted of an omnidirectional measurement microphone type NTI M2230 (sensitivity 43.3 mV/Pa), a digital audio interface type RME Fireface UFX II, an amplifier type PA 1000 and a dodecahedron speaker type QSAM QS12. The measurements were executed with Matlab, The Mathworks.
For calculating the power spectrum, the impulse response was analysed with the periodogram technique with a Hamming window, favouring the suppression of the leakage effect rather than an exact representation of the signal's power in the frequency domain.
In order to test the robustness of the AIR method, the locations of sender and receiver were altered. The quasi-omni source, the applied dodecahedron loudspeaker, was turned in steps of 0, 30, 60 and 90 degrees, as it is known that these speakers are not fully omnidirectional. An effect that is pronounced in an anechoic room. As a second variation, the position of the instrument with respect to the microphone and the loudspeaker was changed in three steps on an axis from 0 m (perpendicular below the microphone), to 0,55 m and 1 m. In order to safe time, only four impulse responses for angular rotations of the dodecahedron loudspeaker (0, 30, 60 and 90 degree) were measured to capture the impulse response of the room alone. Figure 2, (a) depicts the comparison for the classical guitar and 2, (b) for the terz guitar. Note, a constant of 150 dB was added to the power spectrum of the AIR method in order to facilitate the comparison. As can be seen the power spectrum of both methods resemble each other in the regions of the acoustic resonances. At higher frequencies there is generally no congruency observed. The resonances lie at around 100 and 200 Hz for the concert guitar and roughly at 180 Hz for the terz guitar. The positioning of sender and receiver leads to a standard deviation of approximately a maximum of 10 dB. However, due to a measurement mistake, the impulse responses of the room (without the instrument, Eq. 1) were acquired for slightly different angular positions of the loudspeaker and a longer sweep signal. Therefore, it was not possible to calculate the impulse response with Eq. 4 but with Eq. 3, which reduces the SNR. Additionally, the mismatch between the angular positions in the impulse response of the room and the confounded impulse response may result into the observed standard deviation.

1.2 Analysis of microphone distance to the sound hole

In 2016 multiple guitars of the SIM collection where measured with the AIR method. As compared to the setup presented above, each measurement was executed with two microphones, a cardioid microphone (type Beyerdynamic TG I53c) directed to the sound hole at an distance of 34 cm and an omni directional microphone (type Beyerdynamic MM1) at a distance of 110 cm to the sound hole. The setup of sender and receiver

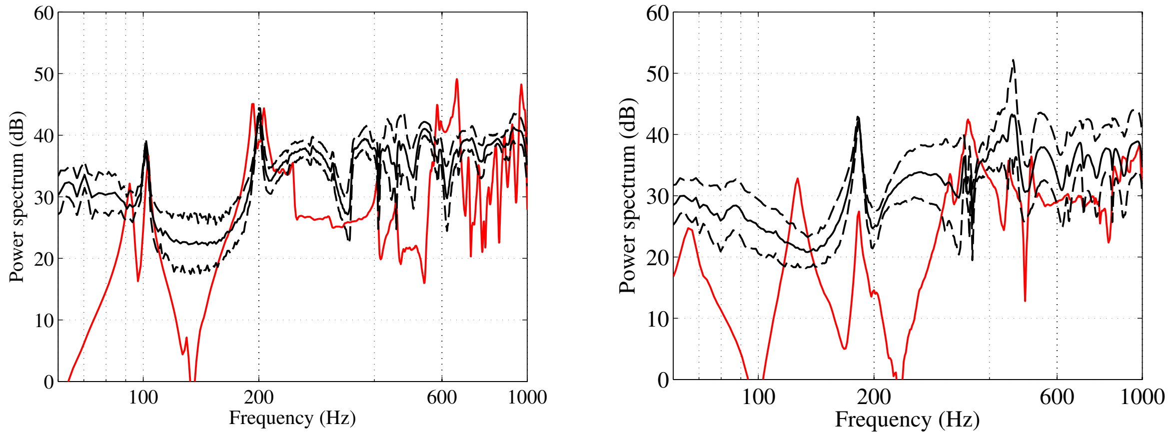

Figure 2. Power spectrum of the classical guitar (left) and the terz guitar (right) measured with the hammer probe (red) and the AIR method (black). The solid lines represent the mean, the dashed lines the mean ± standard deviation.

remained unchanged between measurements of $y_{\mathrm{r,i}}$ and y_{r}. The data is used to study the effect of microphone distance and the usage of y and h in the deconvolution process.
Figure 3 shows the transfer functions of the 1890's Guitar of Salvador Ibanez in Table 1. As can be seen, applying h instead of y reduces the sound power and likewise the signal to noise ratio. Moreover, the fine structure at higher frequencies appears to be lost when applying Eq. 3.
Increasing the distance to 110 cm reduces the signal to noise ratio considerably, to the extent that it becomes difficult to find the resonances of the guitars. Note that the self noise of the Beyerdynamic MM1 is higher than of the microphone NTI M2230, which was employed in the measurement of the previous section with a distance of $\geq$ 1.9 m to the sound hole.
Based on the 34 cm cardioid pickup and the deconvolution process using the microphone signal y, the guitars of Table 1 are analysed in Fig. 3, (b) and 4. The power spectrum allows for a direct readability of the HRs. The lower part of Figure 4 reveals further information on the timbral characteristics, as for example modulation characteristics.

DISCUSSION

From the conducted experiments, the following conclusion can be drawn. The AIR method cannot replace the hammer probe. Primarily because the AIR method does not capture mechanical oscillations. AIR measures the acoustical response of the sounding body. Therefore, the AIR method can assess the HR, harmonics and overtones.
A typical example of insight is derived from the power spectrum acquired with the hammer probe in Fig. 2, (a), which was not possible with the AIR method alone. The neck of the concert guitar is reinforced with two carbon rods. These bars (330 x 12 x 5mm) are not visible in photos. They were glued into two slots under the fingerboard into the cedro wood. They stiffen the neck. As a result, only little energy of the sound is lost to neck vibrations. This is an interpretation for the fairly high resonance of the neck vibration, just shortly before the HR resonance.
The AIR method as executed here, owns methodological weaknesses. First, the recorded sound power of the instrument is low. Decreasing the distance of the measurement location has shown to improve the sound power and more importantly the SNR. The distance of 1.9 m has been chosen in this analysis to measure as far as possible in the far field of the sounding bodies. It is likely that a compromise has to be defined here. Also,

Item	Instrument	Material	Soundboard area [cm^2]	string length [mm]	Helmholtz res. (Hz)
a	Guitar Salvador Ibanez Valencia around 1890	spruce, mahogany, rosewood, cedro	1035	640	120 Hz
b	Guitar Salvador Ibanez Valencia around 1900	spruce, rosewood, cedro	1328	655	90 Hz
c	Guitar Karl Höfer GmbH Bubenreuth 1992	spruce, rosewood	1402	650	100 Hz
d	Guitar Walter J. Vogt, Horb-Mühlen 1983	spruce, rosewood, ebony, mahogany	1415	652	100 Hz
e	Lute (Ud) unknown maker Turkey before 1955	pinewood, walnut, tortoise shell	—	569	130 Hz

Table 1. Guitars of the collection of the State Institute for Music Research.

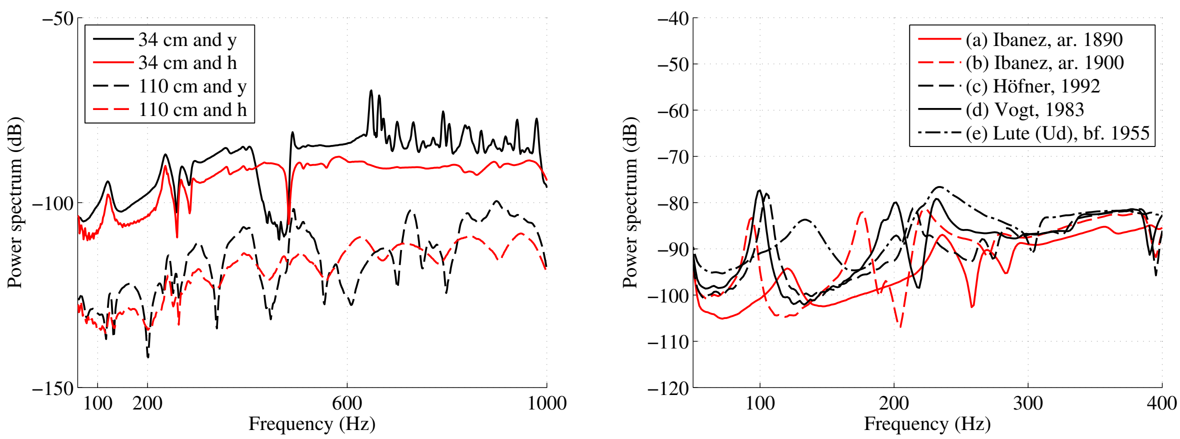

Figure 3. Left: Power spectrum of the guitar of Salvador Ibanez from 1890 measured with the AIR method at difference distances from the sound hole and based on the deconvolution of the recorded signals or the pre-processed impulse responses. Right: Comparison of the acoustic resonances of the guitars in Table 1.

the hammer method measures at a specific point (at the point of 6 cm from the bridge-saddle E-string) and does therefore not give a fully comprehensive image of the spectral behaviour of the guitar. The method is however well defined and using a coherence measure (as available in the software of the measurement software of the Ono Sokki CF-7200 FFT Analyzer), the degree of reproducibility can be assessed. In measurements in Markneukirchen, the coherence was close to one for almost the entire spectrum, hence the reproducability high. As described before, the observed standard deviation in Fig. 2 is likely an effect of the slightly different sender

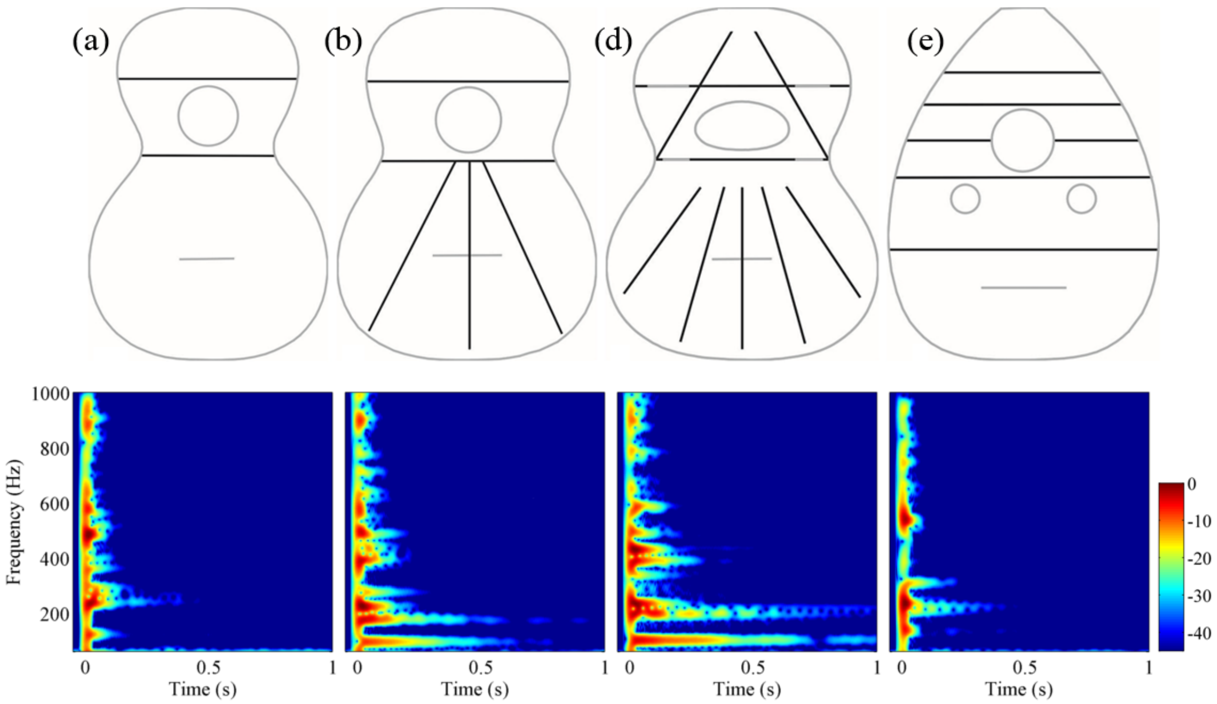

Figure 4. Guitars of the collection of the State Institute for Music Research, with letters corresponding to the rows of Table 1. The upper part of the Figure gives a conceptual drawing of the guitar's composition. The lower part depicts the respective spectro-temporal behavoir.

and receiver locations in the recording of y_{r} and $y_{\mathrm{r,i}}$. An improved measurement procedure of the AIR method should enable a high degree of reproducibility and a high SNR.
The preconditioning of the signal before analysis needs further sophistication. First the path length between the speaker to the microphone and between the loudspeaker via the instrument to the microphone might be arranged in a way that reduces the temporal overlap between the collateral dirac and the impulse response of the instrument. Furthermore, an improved suppression of the collateral dirac in the signal as well as an improved stabilization in the deconvolution process might enhance the signal quality.
Also the AIR method does not assess mechanical oscillations, as for example the oscillation of the fingerboard, it can deliver an acoustical image of the sounding body. The experience of an auralized AIR-measured impulse responses resembles the effect of finger knocking on the sounding body of an instrument. Given this realistic sound impression, the sonification of historical instruments by convolving recorded strings of different notes with the AIR-measured impulse responses represents an attractive tool for organology as well as for the presentation of historical instruments in museums.

CONCLUSION

In this contribution, a method for measuring the acoustical impulse response (AIR) of the sounding body of stringed instruments has been presented. Because it is a contact-free measurement method, historical instruments, which cannot be evaluated with the hammer probe, become analysable in terms of spectro-temporal behaviour of the sounding body. In a comparison with the hammer probe, the method proved successful in indicating the specific acoustic resonances of the instrument. However, there is no correspondence with the

transfer function retrieved with the hammer probe at large, because the latter incorporates the assessment of mechanical oscillations. With the AIR method, mechanical oscillations are rather captured to the degree of their acoustical radiation. This however, might not represent a drawback. The method measures the acoustical spectro-temporal pattern of the instrument and may supplement the existing measurement techniques for describing, documenting and constructing stringed instruments.
The presented AIR method needs further analysis and sophistication. In future work, a setup for the AIR method must be defined that secures data quality and reproducibility. At the same time, the method should be executable in a standard workshop situation or archive with simple equipment in order to be practical for conservators and instrument builders.

ACKNOWLEDGEMENTS

The authors would like to express their gratitude to Prof. Meinel for his support in the preparation of this paper and executing the hammer probe measurements in Markneukirchen.

REFERENCES

[1] ICOM – Internationaler Museumsrat. Ethische Richtlinien für Museen von ICOM. Übersetzt durch ICOM Schweiz et al., 2010.

[2] Anabelle Kiessig, Eberhard Meinel, Thomas Ochs, Heidi von Rüden, Angela Waltner, Akustische Untersuchungen zu klanglichen Eigenschaften von Weißgerber-Gitarren. In: Gitarren von Richard Jacob "Weißgerber". Museum für Musikinstrumente der Universität Leipzig. Andreas Michel (Hrsg.) Katalog. Leipzig 2007, S. 146-149

[3] Hulsebos, E. (2004) Auralization using Wave Field Synthesis. Dissertation, TU Delft

[4] DIN EN ISO 3382-1:2009-10. Akustik - Messung von Parametern der Raumakustik - Teil 1: Aufführungsräume (ISO 3382-1:2009); Deutsche Fassung EN ISO 3382-1:2009. Berlin: Beuth-Verlag, Oktober 2009

PROCEEDINGS of ISMA 2019
International Symposium on Music Acoustics

13 - 17 September 2019 in Detmold, Germany

Digital synthesis to evaluate the role of the cutoff frequency on sound production and radiation

Erik Alan PETERSEN[(1)], Philippe Guillemain, Jean Kergomard[(1)]

[(1)] Aix Marseille Univ, CNRS, Centrale Marseille, LMA, UMR 7031, Marseille, France, petersen@lma.cnrs-mrs.fr

Abstract

The cutoff frequency of the input impedance is a well-known characteristic of woodwind instruments. Benade remarks that the frequency at which cutoff occurs is strongly related to the produced sound of a given instrument and that it correlates to the adjectives musicians use to describe the character of a given instrument. However, it is not known how the cutoff frequency contributes to the competition between the energy that contributes to the auto-oscillation of the reed and the energy that is radiated from the resonator. To evaluate the effects on sound production and radiation, simplified resonators with the same first impedance peak frequency, but different cutoff frequencies, are simulated and experimentally verified. It is found that a rigorous geometrical regularity results if a very strong cutoff behavior. Next, digital synthesis is used to simulate the pressure and velocity waveforms within the mouthpiece which are propagated to the external field. Spectral characteristics of the sound both within and outside the resonators can be used to quantify how the cutoff frequency affects sound production and radiation.

Keywords: Musical acoustics, tonehole lattice cutoff frequency, digital sound synthesis, clarinet.

REFERENCES

[1] Benade, A. H., Fundamentals of Musical Acoustics Oxford University Press, London (1976).

[2] Petersen, E. A.; Guillemain, G.; Kergomard, J.; Colinot, T., The effect of the cutoff frequency on sound production of clarinet-like instruments, Journ. Acoust. Soc. Am (to appear, accepted 2019).

[3] Lefebvre, A.; Scavone, G. P.; Kergomard, J., “External tonehole interactions in woodwind instruments,” Acta Acustica united with Acustica **99**, 975-985 (2013).

[4] Moers, E.; Kergomard, J., “On the cutoff frequency of clarinet-like instruments. Geometrical versus acoustical regularity,” Acta Acustica united with Acustica **97**, 984-996 (2011).

PROCEEDINGS of ISMA 2019
International Symposium on Music Acoustics

13 - 17 September 2019 in Detmold, Germany

On the use of reed-to-room transfer function in bassoon auralizations – a listening test

Timo GROTHE, Stefanos IOANNOU and Sebastià V. AMENGUAL GARI

Hochschule für Musik Detmold, Germany, grothe@hfm-detmold.de

Abstract

The sound of a bassoon in a room can be convincingly synthesized from a reed mouthpiece pressure measurement, if the transfer function between the reed and a room position is known. We present an experimental setup which allows to measure such "reed-to-room" transfer functions, with a bassoon fixed in playing position on stage and a binaural microphone on a seat in a concert hall. With measured mouthpiece pressure signals from a musician playing the fixed bassoon on stage, the synthesis results from convolving source signals with transfer functions can be compared to the corresponding measurements.

We demonstrate results in the form of a listening test to investigate the auditory quality of these auralizations.

Keywords: Sound, Music, Acoustics

PROCEEDINGS of ISMA 2019
International Symposium on Music Acoustics

13 - 17 September 2019 in Detmold, Germany

Substitution of spruce tonewood with composite materials tailored using numerical models: an application to archtop guitar *

Romain VIALA[(1)], Claudia Fritz[(2)], Vincent PLACET[(1)], Emmanuel FOLTÊTE[(1)], Scott COGAN[(1)]

[(1)]Univ. Bourgogne Franche-Comté, FEMTO-ST Institute, CNRS/UFC/ENSMM/UTBM, Department of Applied Mechanics, France

[(2)]Sorbonne Universités, UPMC Univ Paris 06, CNRS, UMR 7190, Institut Jean-Le-Rond-d'Alembert, France

Abstract

Stringed instrument making traditionally requires selected wooden materials, called tonewood. Numerous species are used, especially spruce and maple for domestic species and rosewood, ebony, mahogany and pernambuco for tropical ones. Nowadays, the shortage of sufficiently large trees as well as the impact of climate change has led to current and future supply issues. Multilateral treaties to protect endangered wood species are now including several of the above mentioned species, and may include more in the future. In parallel, during the last decade, composite materials made with natural fibres have increasingly been studied and used. The bio-based composites associate fibres from annually renewable sources and bulk wood cores with epoxy resin to create materials that exhibit adjustable mechanical properties. The long-term objective of this work is to demonstrate that such materials can be tailored to mimic the vibro-acoustical behaviour of tonewoods and seen as a sustainable solution. In this study, numerical models of stringed instruments are used to optimize the architecture of bio-based composites to copy the dynamic behaviour of a spruce archtop guitar soundboard. The dynamic response of the manufactured composite parts are measured and compared to the model predictions in order to validate the model-based recipes of composites.

Keywords: Bio-based composites, Tonewood, Optimisation, Virtual prototyping, Archtop guitars

*romain.viala@univ-fcomte.fr

PROCEEDINGS of ISMA 2019
International Symposium on Music Acoustics

13 - 17 September 2019 in Detmold, Germany

Proposal of a human-instrument interaction model and its basic examination using electromyogram

Ryo ITOIGAWA*

School of Integrative and Global Majors, University of Tsukuba, Japan

Abstract

In the production of musical instruments, prototypes are evaluated by professional performers. It is empirically known that evaluation of musical instruments differs depending on the evaluator. However, the mechanism how human evaluates a musical instrument is not revealed. In this study, I newly proposed a human-instrument interaction model when a person evaluates a musical instrument to reveal its mechanism. For a basic study of the model, I measured human muscle activity and verified its trend when controlling the plucking parameters for the guitar. In the experiment, 5 subjects were asked to play a simple task with a plectrum under control the plucked position and plucking dynamics. Subjects consist 4 experienced amateurs and 1 beginner. EMG of four muscles considered to be involved in the plucking motion using a plectrum and audio from the front magnetic pickup were measured simultaneously. As a result, the muscle activity due to the difference in the position has a large difference for each subject, and no specific trend was observed. The muscle activity due to the difference in the dynamics was found to have a certain tendency among subjects, such as muscle activity also increases and decreases with the increase and decrease of plucking dynamics.

Keywords: Interaction, Guitar, Evaluation, Electromyogram, EMG,

1 INTRODUCTION

How do humans evaluate musical instruments? The physical aspects of various musical instruments have widely investigated in a long history. While it is difficult to reveal the principle of sound production, the evaluation of musical instruments is also full of wonders and unknown things. Because the evaluation of the instrument is considered to be based on the cross- or multi-modal perception of the person who played the instrument, or the person who listened to the instrument, it can not be told only by the physical characteristics of the instrument. Thus, it is also necessary to consider the characteristics of people themselves. For violins as an example, it is suggested that the bias changes the evaluation of the instrument [1] and acoustical or mechanical analysis has been not conclusive to quantify the subjective evaluation of the instruments [2]. The perception related to the evaluation is thought to be not only auditory but also visual and haptic feedbacks. Several models have been proposed for this "performer-instrument interaction", incorporating control engineering insights [3, 4, 5]. In addition to human common perceptual characteristics, in particular, I believe that individual differences in perceptual characteristics are large, due to the difference in the level of performance skill and understanding of music itself in the case of musicians. It is also assumed that the breadth of the physical parameters given to the instrument, such as the velocity of the plectrum, differs depending on the performance skill. Even if the physical parameters given to the instruments are equivalent, the usage of body and muscle may differ due to differences in physique and skill. Its difference in the somatic sensation may affect the evaluation of the instrument.

Based on these points, it is expected that the followings interact with each other in a complex way in the evaluation of musical instruments; (i) Acoustic and physical characteristics of musical instruments and spaces, (ii) Human common physiological and perceptive characteristics (including illusion), (iii) Differences in player's performance skills and sensitivity to feedback from instruments. As for (iii) for example, advanced players may prefer instruments that respond sensitively to their input, but beginners may prefer to enjoy the musical performance itself, with less sensitive instruments where their performance can be heard well.

To clarify these interactions, it is necessary to not only measure physical phenomena and acoustical characteris-

*itoigawa.ryo@gmail.com

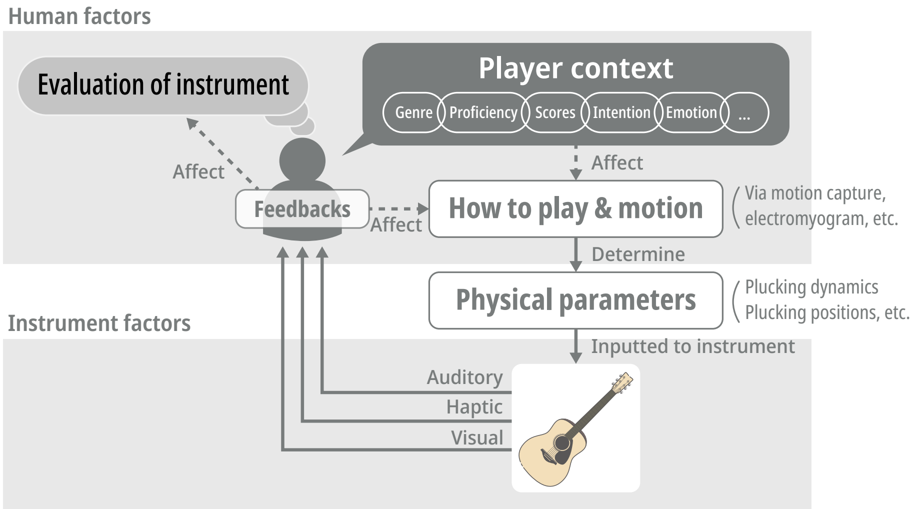

Figure 1. Outline of proposed Human-Instrument Interaction model.

tics of musical instruments but also comprehensively measure various subjective and objective characteristics of players, which includes subjective evaluation of musical instruments. However, there is little related research.

In this study, "Human-Instrument Interaction" which considers the player context is proposed. Figure 1. shows the outline of the Human-Instrument Interaction model. Here, "the player context" is defined as the combination of various implicit parameters such as the player's favorite genre and proficiency level. There is research on the difference in movement due to the difference in proficiency (e.g. [6]), however, a lot of questions about the relationship between the comprehensive player context and the actual human motion/muscle activity remains. (e.g. Does the player who likes a specific genre have a specific motion tendency?) Also, It has been clarified neither that the relationship between human motion and the physical parameters given to the instrument, nor the kinetics and kinematics of playing. By clarifying these relationships, for example, players who like certain genres may be more likely to produce instruments that understand human characteristics, such as being more likely to play certain instruments. Some injuries due to muscle fatigue have also been reported in musical instrument performance [7]. There is also a possibility that understanding the performance movement will lead to failure prevention and efficiency improvement in the performance education scene.

Based on these questions, in this study, I examined how human motion changes when the player context and proficiency differ during an electric guitar playing. The population of a guitarist is very large and the instructions are substantial. However, few mention the relationship between the player context (such as playstyle) and how to play, and intuitive explanations based on the author's rule of thumb are often seen. The acquisition of techniques is often done in one's way, and techniques and movements are not standardized. It may be needed to clarify the relationship mentioned above with how the actual technique is realized. The measurement and systematization of performance techniques and movements can be expected to provide scientific performance proficiency support as well as academic contributions in the related field.

I focused on electromyogram (EMG), which has been used as one of the embouchure measurement indicators in brass instruments [8, 9]. The plucking position and dynamics are set as control conditions. These two are considered to greatly affect timbre and to be relatively easy to be controlled by the player. While changing these conditions, the player's EMG at the time of plucking using a plectrum and the musical sound from the magnetic pick-up on the electric guitar are measured. In this study, the objective is to examine the player's muscle activities using EMG and their tendency during plucking.

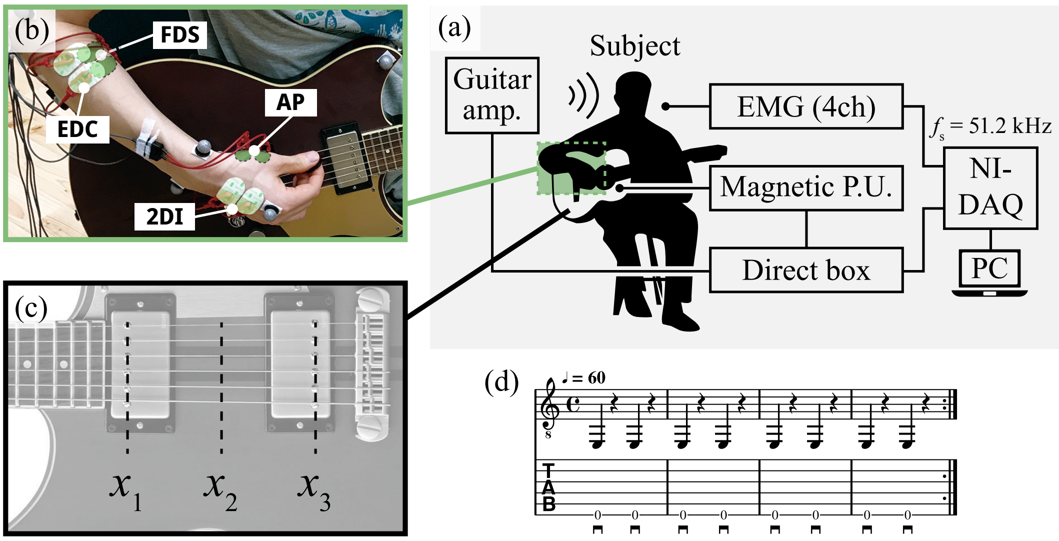

Figure 2. (a) Experimenal system and setup. Four EMG and audio signal from a magnetic pick-up on the electric guitar are measured simultaneously. (b) Four EMG measurement sites from right forearm to hand. (c) Specified plucked positions. (d) The music score for the performance task.

2 METHODS

2.1 Experiment

The experimental system is shown in Figure 2(a). The surface EMG using electromyograph (Wet bipolar EMG sensor, Oisaka Electronic Equipment Ltd.) and electrodes (F-150M, Nihon Kohden) and the signal output from the front pickup when the subject plays a specific task with a plectrum (INFINIX HARD POLISH JAZZ 1.20mm, MASTER 8 JAPAN) and electric guitar (REVSTAR RS820CR, YAMAHA Corp., factory initial condition) via the DI unit (BOSS DI-1, Roland) are measured simultaneously by data acquisition device (cDAQ-9174, NI-9234, National Instruments). A sampling rate was 51.2 kHz.

The measurement sites of EMG were four parts that would be related to the string-picking operation using a plectrum: Adductor pollicis muscle (AP), 2nd Dorsales interossei muscle (2DI), Flexor digitorum superficialis muscle (FDS), and Extensor digitorum muscle (EDC). Since the plucking motion is targeted only for down-picking (picking the strings from top to bottom) in this study, FDS is considered to be an antagonistic muscle during plucking motion. Figure 2(b) also shows the EMG measurement site.

2.2 Experimental setup

2.2.1 Subjects

The subjects of the experiment were a total of five, four amateur players who play the guitar daily and one beginner. The performance genres that each subject performs on a daily basis and the features (i.e. the player context) are shown below.

Subject 1 About 20 years of guitar playing experience. Playing rock or funk. Playing solid body electric guitars using plectrums and often play crisp mute strum with a slightly distorted crunch sound.

Subject 2 About 10 years of guitar playing experience. Playing pops focusing on solo guitar. In many cases, playing acoustic guitars in a fingerstyle. It is rare to use a plectrum, and strumming style is mainly played when using with a plectrum.

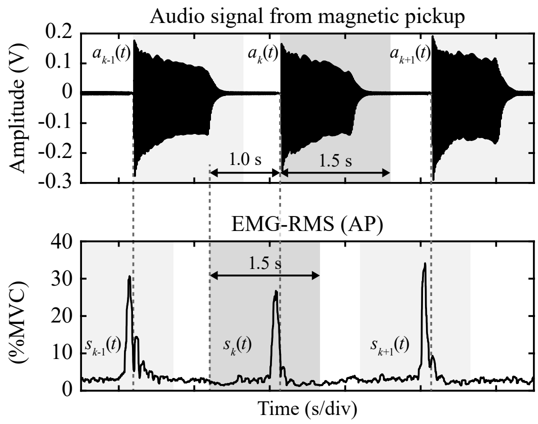

Figure 3. Typical example of audio signal from magnetic pickup and EMG-RMS (at AP). The peak position of the second derivative of the each audio signal is defined as the onset. The signal from the onset to 1.5 sec is used as the audio signal $a_k(t)$, and the corresponding EMG-RMS signal for 1.5 seconds isdefined as $s_k(t)$.

Subject 3 About 10 years of guitar playing experience. Playing modern jazz. Playing electric arched top guitars with plectrums, often playing single tones and chords with clean tones.

Subject 4 More than 10 years of guitar playing experience. Playing hard rock. Playing solid body electric guitars using a plectrum, and often distorting sounds. Holding the plectrum deep.

Subject 5 Beginner of playing the guitar. Having experience of violin.

2.2.2 Protocol

Each subject was informed in advance about the experiment and given a playing time to get used to the experimental guitar for several minutes. The subject can monitor the output of the electric guitar with a guitar amplifier (THR10, YAMAHA Corp.). The settings for the guitar and amplifier were the same throughout all trials.

As shown in the score of Figure 2(d), the subject performed the task of playing the sixth string (E2, approx. 82 Hz) with down-picking according to the 60 bpm metronome. In the rest, the strings were muted in any way.

The task was performed by controlling three levels of plucking dynamics (*p, mf, ff*) and three plucked positions (x_1, x_2, x_3). The dynamics were determined subjectively by each subject. The subject was instructed to play *ff* more strongly than *mf* and play *p* weaker than *mf*. The plucked position was determined as follows. The position of pole piece on the front pickup is x_1, the position of pole piece on the rear pickup is x_3, and their middle position is x_2. Figure 2(c) shows the approximate plucked position described above.

First, the subject performs the task with dynamics *mf* at position x_2. Next, after several seconds of rest, the subject keeps the plucked position x_2 and performs the task with dynamics *p*. Finally, the subject performs with dynamics *ff*. In the same way, the subject then performs the task at the plucked position x_1, and finally the task on the plucked position x_3. After performing the task under all conditions, EMG at maximum voluntary contraction (MVC) [10] was measured for about 3 seconds to normalize each subject EMG.

2.3 Analysis

The obtained EMG was rectified and smoothed by calculating the root mean square (RMS) in 50 ms steps with reference to the muscle activity measurement cases during musical performance [9, 11, 12]. Hereafter this is called EMG-RMS. Figure 3 shows the part of the audio signal from the pickup and EMG-RMS (at adductor pollicis muscle: AP) in a trial under a certain condition. The dotted line in Figure 3 is the peak position of the second derivative of each audio signal, which is defined as the onset of each sound. The signal from the onset to 1.5 sec is used as the audio signal $a_k(t)$. As shown in Figure 3, the corresponding EMG-RMS $s_k(t)$ is taken 1.5 sec from the point of 1 sec before the onset of $a_k(t)$ since the onset of EMG-RMS is thought to precede sounding [13]. For each subject, $S(t)$ shown in the following equation 1 is used as a representative value of EMG-RMS under each plucked dynamics and plucked position.

$$S(t) = \frac{1}{N}\sum_{k=1}^{N} s_k(t) \quad (0 \leq t \leq 1.5) \tag{1}$$

Here, N is the total number of trials (i.e. the number of plucking strings) in one experiment, and it was approximately $N = 16$ in most of the experiment.

3 RESULTS

Figure 4 shows each $S(t)$ under the condition that the plucked position is x_2. The upper part of Figure 5 shows the peak values of $S(t)$ obtained around the onset. The lower part of Figure 5 shows their time difference from the onset.

3.1 Changes in muscle activity due to differences in position: x_1, x_2, x_3

I describe the tendency of $S(t)$ and its peak value and timing when changing the plucked position. From Figure 5, the peak of EMG-RMS from the muscles considered to be related to plucking (i.e. AP, 2DI and EDC) tends to be observed before the onset regardless of the plucked position. However, changes in peak value were not observed among subjects. For example, focusing on the AP, Subject 2 has the highest %MVC at x_2, but Subject 5 has the same %MVC at all positions. Also in 2DI and EDC, there was no common tendency among subjects for peak value among the plucked positions.

3.2 Changes in muscle activity due to differences in dynamics: *p, mf, ff*

I describe the tendency of $S(t)$ and its peak value and timing when changing the plucking dynamics. The peaks of AP, 2DI and EDC also tend to be observed before the onset regardless of the plucking dynamics. In addition, there is common to all subjects that %MVC tends to increase as plucking dynamics increased. However, the gradient of increase varies depending on the subject and muscle. Also, the peak time difference from the onset tends to decrease as plucking dynamics increased.

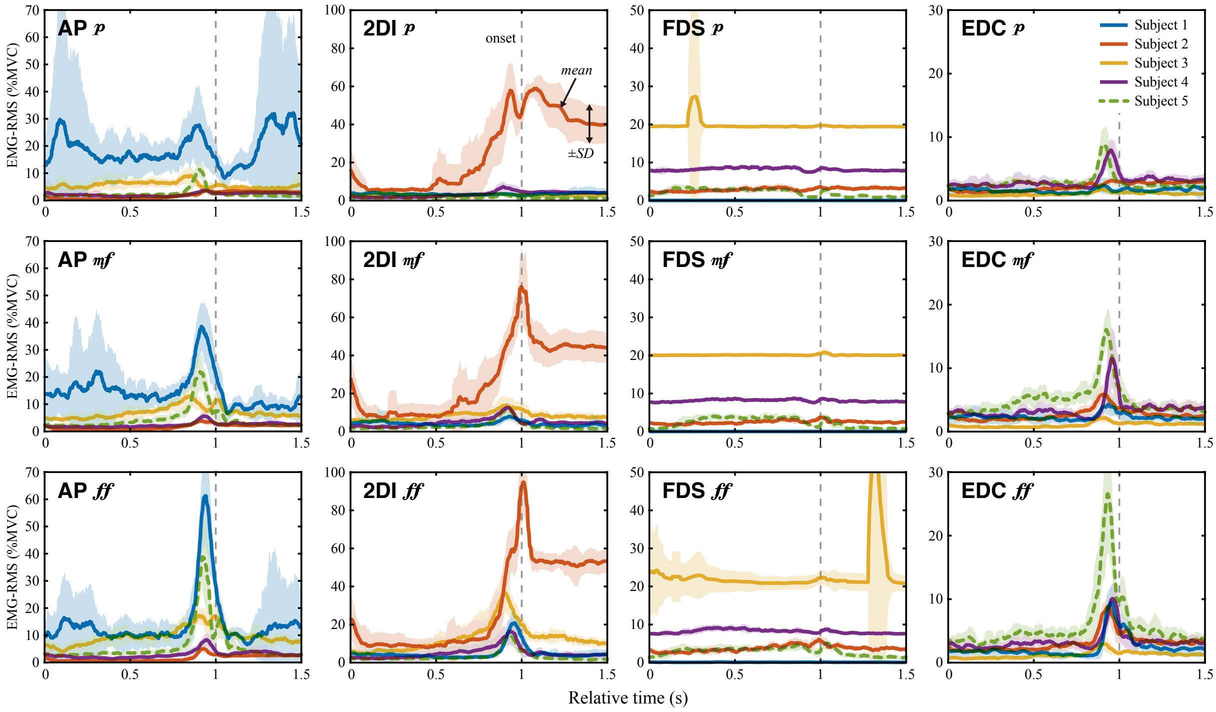

Figure 4. Results of EMG-RMS during plucking under the condition the plucking dynamics changed at position x_2. The colored lines show the $S(t)$ for each subject. Dotted lines at 1 second indicate the audio onset timing.

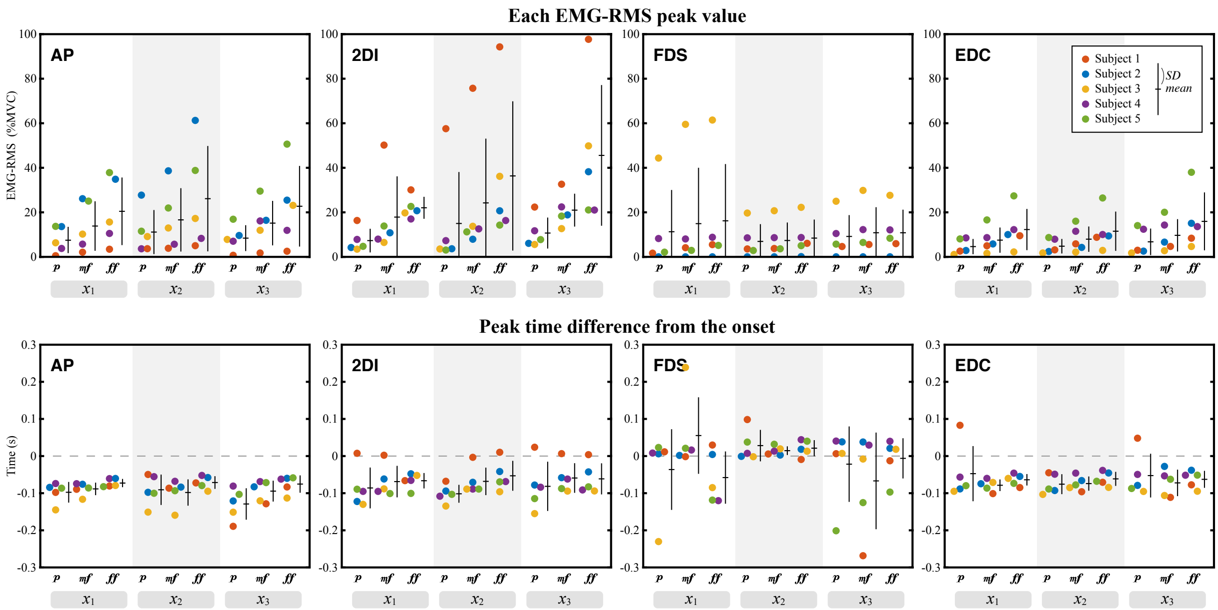

Figure 5. Results for peak values obtained from each EMG-RMS. The upper part shows the %MVC value of the EMG peak at each site, and the lower part shows the time difference from the audio onset of the peak.

4 DISCUSSION

A common tendency was observed among the subjects, with the AP mainly increasing/decreasing the muscle activity as the plucking dynamics increased/decreased. Also, the peak time difference from the onset tends to decrease as plucking dynamics increased. In particular, these tendencies were observed in AP and 2DI, which is considered to have a significant effect on plectrum gripping. On the other hand, there was no common tendency among the subjects about the peak value when the plucked position was changed. This suggests that the difference in the performance of each subject appeared in the muscle activity largely due to the difference in the plucked position. The subjects in this experiment tended to differ in the genres that they perform daily. Therefore, it is assumed that the performance movement differs depending on the daily habituation and the muscle activity is largely dispersed when the plucked position is controlled.

Although it was difficult to observe the feature of FDS throughout the trial, The lower part of Figure 5 shows that there is a peak timing at or after the onset. Since FDS is an antagonistic muscle of EDC, few peaks were observed during down-picking, and no co-contraction has occurred. This suggests that FDS muscle activity is weak during down-picking regardless of the player's years of experience and genre. Moreover, it may be hypothesized that FDS may contribute to fixation of the wrist after down-picking since some peaks are seen at or after the onset.

FDS of Subject 3 always has a high %MVC value, which is assumed to be the superposition of noise due to the misalignment of the EMG measurement electrodes during the experiment. Furthermore, electromyography often gives a restrained feeling to the subject as shown in Figure 2(b). For this reason, the experiment was conducted with a simple performance task in this research. However, an experimental method to eliminate these is important to measure the player's original behavior faithfully.

Besides, it is necessary to simultaneously obtain not only EMG but also to obtain joint displacements and angles using motion capture for detailed kinematics analysis. Simultaneous measurement of physical parameters given to strings by a player would also contribute to the elucidation of interaction. In this study, I targeted people with different player contexts and clarified the tendency of muscle activity at plucking in limited conditions. However, it will be necessary to investigate people with similar player contexts to clarify Human-Instrument Interaction.

5 CONCLUSION

In this paper, the Human-Instrument Interaction model including player context, performance motion, physical parameters given to the instrument, feedback given from the instrument to the player and its outline were presented to reveal a complex interaction between instrument and player. As a basic study, I measured the muscle activity using EMG when controlling the plucked position and plucking dynamics for the guitar. As a result, muscle activity due to the difference in the plucked position was largely different among subjects, and no specific tendency was found. Besides, muscle activity due to the difference in plucking dynamics indicated a certain common tendency among subjects such that the muscle activity increased/decreased with the increase/decrease of plucking dynamics and the peak timing also increased/decreased. Furthermore, it was suggested that the balance between the active muscle parts was different depending on different player contexts.

ACKNOWLEDGEMENTS

I would like to express my gratitude to the R&D department at Yamaha Corporation for cooperation with the experiment.

REFERENCES

[1] Fritz, C.; Curtin, J.; Poitevineau, J.; Morrel-Samuels, P.; Tao, Fan-Chia. Player preferences among new and old violins. *Proceedings of the National Academy of Sciences*, Vol 109, 2012, pp. 760–763.

[2] Bassinger, G. Structural acoustics of good and bad violins. *The Journal of the Acoustical Society of America*, Vol 124 (3), 2008, pp. 1764–1773.

[3] Campbell, D. Murray. Evaluating musical instruments. *Physics Today*, Vol 67, 2014, pp. 35–40.

[4] Berdahl, E.; Smith, J.O.; Niemeyer, G. Feedback control of acoustic musical instruments: Collocated control using physical analogs. *The Journal of the Acoustical Society of America*, Vol 131, 2012, pp. 963–973.

[5] Papetti, S.; Saitis, C. Musical Haptics. Springer, Berlin (Germany), 1st edition, 2018.

[6] Baader, P.A.; Kazennikov, O.; Wiesendanger, M. Coordination of bowing and fingering in violin playing. *Cognitive Brain Research*, Vol 23 (2), 2005, pp. 436–443.

[7] Ranelli, S.; Smith. A.; Straker. L. Playing-related musculoskeletal problems in child instrumentalists: The influence of gender, age and instrument exposure. *International Journal of Music Education*, Vol 29 (1), 2011, pp. 28–44.

[8] Iltis, P.W.; Givens, M.W. EMG characterization of embouchure muscle activity: reliability and application to embouchure dystonia. *Medical Problems of Performing Artists*, Vol 20, 2005, pp. 25–35.

[9] Hirano, T.; Kudo, K.; Ohtsuki, T.; Kinoshita T. Orofacial muscular activity and related skin movement during the preparatory and sustained phases of tone production on the French horn. *Motor Control*, Vol 17, 2013, pp. 256–272.

[10] Merletti, R.; Di Torino, P. Standards for reporting EMG data. *Journal of Electromyography and Kinesiology*, Vol 9 (1), 1999, pp. 3–4.

[11] Fjellman-Wiklund, A.; Grip, H.; Karlsson, J.S.; Sundelin, G. EMG trapezius muscle activity pattern in string players: Part Iis there variability in the playing technique?. *International Journal of Industrial Ergonomics*, Vol 33 (4), 2004, pp. 347–356.

[12] Gotouda, A.; Yamaguchi, T.; Okada, K.; Matsuki, T.; Gotouda, S.; Inoue, N. Influence of playing wind instruments on activity of masticatory muscles. *Journal of Oral Rehabilitation*, Vol 34, 2007, pp. 645–651.

[13] Hodges, P.W.; Richardson, C.A. Relationship between limb movement speed and associated contraction of the trunk muscles. *Ergonomics*, Vol 40 (11), 1994, pp. 1220–1230.

PROCEEDINGS of ISMA 2019
International Symposium on Music Acoustics

13 - 17 September 2019 in Detmold, Germany

The ObieAlto project: Looking for correlations between perceptual properties and constructional data

Claudia Fritz, Valérian Fraisse, Danièle Dubois

Institut Jean Le Rond d'Alembert, Sorbonne Université / CNRS, France

Abstract

While the outline geometry differs slightly between violins, it can vary considerably between violas, which are less standardised. During the 2016 Oberlin workshop (organised by the Violin Society of America), a group of instrument makers have collectively designed the so-called ObieAlto outline. 25 violas were then built following this model (but without any other constraint except for the set of strings) and brought to the 2017 workshop during which two short excerpts (one in the low register, one in the high) were recorded by a professional player in a recording studio. The results of the statistical and linguistical analyses of the listening tests show a large variability between the participants (20 makers and 10 violists) but still show groups of instruments that share relatively consensual features. Very few relationships have been found between these perceptual features and physical parameters (constructional data but as well audio descriptors calculated on the recordings and vibro-acoustical measurements) showing that the multiplicity of the parameters during the building process allow instrument makers to obtain a certain set of perceptual properties with very different strategies.

Keywords: Viola, perceptual properties, constructional data, free categorisation, audio descriptors

PROCEEDINGS of ISMA 2019
International Symposium on Music Acoustics
13 - 17 September 2019 in Detmold, Germany

Tuning of membranophone based on visualization of membrane vibration mode

Eri ZEMPO, Naoto WAKATSUKI*, Koichi MIZUTANI, Yuka MAEDA

University of Tsukuba, Japan

Abstract

Tuning of membranophones is important to design timbre, while it is difficult for inexperienced players, due to the insufficient ability for judgment of pitch difference. In this paper, we propose tuning scheme for membranophones, substituting visual information for auditory information. First, vibration modes shape of the head membrane are visualized, based on the measurement of sound pressure on the head membrane by a circular microphone array, and we estimate the tension distribution of the head membrane, especially unbalance in tightness of the pair of rods on oppositional position, make the nodal line of the (1,1) vibration mode change. Second, we propose a tuning scheme for membranophones based on information on the state of the nodal lines of the mode shapes, visualized based on the microphone measurements, and the difference of eigenfrequencies between the orthogonal modes. We show that the proposed scheme is helpful to make the head tension uniform, as the results of experiments using the vibration of tom-tom with only one side head stretched as an example of actual membranophones. We expect this scheme to train the tuning ability for inexperienced players.

Keywords: Membranophone, Tuning, Vibration mode, Visualization

1 INTRODUCTION

Membranophones are musical instruments that sounds by vibration of a head membrane. Players play mainly by hitting the head. A schematic of the snare drum is shown in Fig. 1, as an example of membranophones. The top and bottom heads are stretched on the cylindrical shell. The Edge of each head is held between by a circular hoop and a shell. Bolts, called *"tension rods,"* equally spaced on the circumference of the hoop apply tension to the head as the hoop approaches the shell. The tightening of multiple rods cause a change in the tension distribution of the head, which is an element that changes the timbre. Therefore, it is important to adjust the tightening of each rod so that the instrument sounds with the desired timbre. This process and the state of the instrument by it, are called *"tuning."*

The player taps the head and tunes while listening to the sound of the instrument. At this time, players are required to have the ability to distinguish slight differences in sounds and to determine which rod needs to be tightened (or loosened) from the differences in the sounds. This is difficult for inexperienced players, and even for well-experienced players, it is difficult to make the tuning repeatable[1] Therefore, a tuning support system for membrane sounding instruments is required.

Typically, one of the standard is to stretch the head so that the membrane tension is uniform[2]. In the circular membrane under non-uniform tension, normal modes, those degenerate under uniform tension, separate into two independent normal modes having slightly different eigenfrequencies. It may cause a beat in the sound generated by hitting, which is considered to be one of the reasons to make the head tension to be uniform.

Players adjust the tightening for each lot to make the head even. The players tap the head near each rod, estimate the tension imbalance of the head by listening to the height of the hitting sound, and adjust the tightening of each rod.

It is known that the tension distribution of the head changes the vibration mode[3]. When the head is in uniform tension, the nodal line of the vibration mode is almost straight and the frequency difference between the orthogonal modes is very small. On the contrary, when the head is in non-uniform tension, the nodal line curves and the frequency difference of the orthogonal mode becomes larger.

*wakatuki@iit.tsukuba.ac.jp

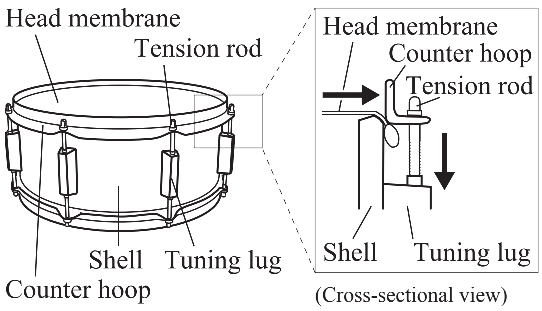

Figure 1. Schematic view of snare drum: Tightning tension rods makes the head membrane streched.

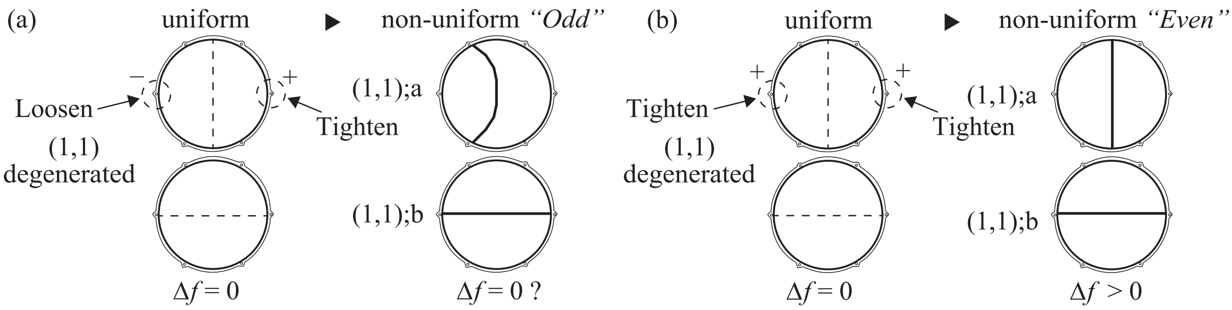

Figure 2. Non-uniform pattern: (a)*"odd"* pattern, (b)*"even"* pattern

When hitting various points on the head, the vibration mode which antinode is near to the hit point, is easy to be excited. Tuning to proceed while listening to the pitch of each point by ear, it is considered to be equivalent to adjusting the frequency difference of this orthogonal mode. Even if the pitches of the sound are made uniform, there may be cases where the unequal spacing of the nodal lines remains and the tension does not become uniform.

In this paper, we propose a method to correct the non-uniformity of the head based on the visualized vibration mode shape, even when it does not appear in the hitting sound in the process of tuning the drum head.

2 TUNING SCHEME

The previous research[3] and our previous experiments[4] imply that the tightening of a pair of opposing rods changing from the uniform condition may raise the eigenfrequency of one normal mode more than the other normal mode and the mode shape may not change. In contrast, the tightening of one rod and the loosening of opposing rod may deform one mode shape, while eigenfrequencies of both mode may not change. Therefore, there are two patterns of the detuning condition as shown in Fig. 2.

Fig. 2(a) shows the change of the mode shape (*"odd"* pattern), when one rod is tightened and the rod opposite to the rod is loosened at the same time. The nodal line of the mode, $(1,1)$, sandwiched by these two rods is curved in the direction surrounding the loosened rod. Frequencies cannot be changed by certain tightening or loosening of both rods. Therefore, the frequency difference of pairs of orthogonal modes may or may not change.

Fig. 2(b) shows the change when two opposing rods are both tightened or loosened (*"even"* pattern). The frequency of the mode, $(1,1)$, with a nodal line between two tightened (or loosened) rods becomes high (or low when loosened), and a frequency difference occurs with its orthogonal mode. The nodal line at this time

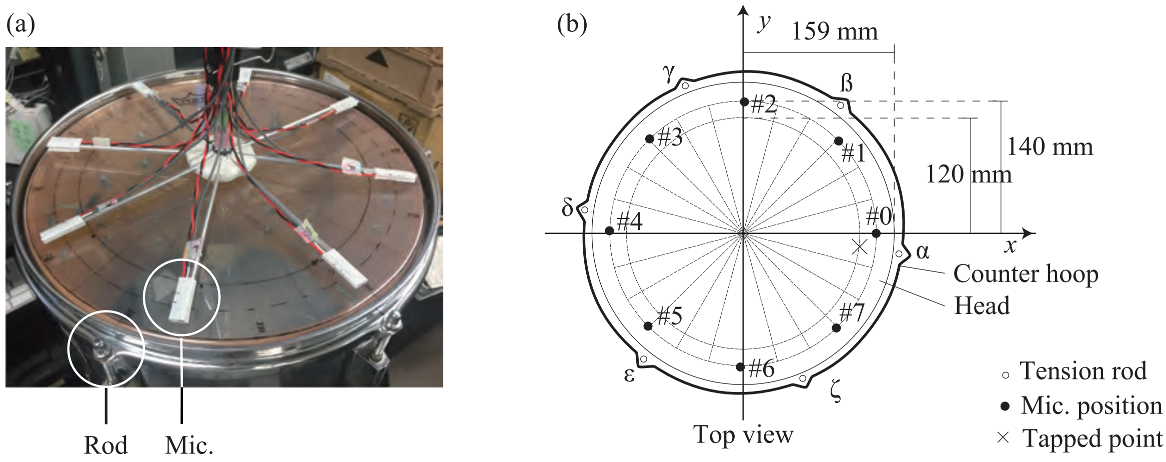

Figure 3. Experimental system: (a)microphone array, (b)positions of microphones on the head

may or may not change because that the curving is caused by the tightening (or loosening) of both rods.

From the above, when curving of a nodal line is observed, tightening of rods sandwiching the nodal line should be adjusted, and when a frequency difference between orthogonal modes is observed, the pair of opposing rods should be tightened or loosened depending on the orientation. Since it is considered that tension non-uniformity can be expressed by superposition of *"odd"* pattern and *"even"* pattern as far as $(1,1)$ mode is concerned, at least, it is expected that the head can be finally tightened by repeating this operation.

3 EXPERIMENTS

3.1 Method

We confirm that the drum head can be adjusted uniformly, by the method described in the previous section. As an example of membranophones, a 13-inch diameter tom-tom with a head extended on one side was used in this experiment. This tom-tom has six rods (rod, $\alpha - \zeta$).

Figure 3 shows the experimental system. A microphone array with eight channels ($f_{si} = 8$), was placed 10 mm from the top of the head, as Fig. 3(a),(b). The tom-tom was placed on the drum stand with the head on top. The drum stand was adjusted so that the head was horizontal at a height of 910 mm from the floor.

First, the rods of tom-tom were adjusted, to make the head tension uniformly. Then, the rod, α was loosened by 180°, and the rod, δ was tightened by 120°. This change is shown in Fig. 4. The experimenter repeated to adjust each rod's tightening, to make the head tension uniformly again, according to the method of the section. At this time, the experimenter referred nodal lines, and orientations and frequency differences of pairs of orthogonal modes, with hitting the point $\times$ of Fig. 3(b).

The sampling frequency for the measurements was 30 kHz. Signals from 0.01 s before beating to 5 s after beating were used for extraction of mode shapes. The order of the autoregressive model used for extraction of mode frequencies, was 400.

3.2 Results

An example of the tuning process obtained in this experiment is shown in Fig. 5. Fig. 5(a) is identical to Fig. 4 <detuned>. The nodal line of the vibration mode curves to the right and there is also a frequency difference of the orthogonal mode.

First, a pair of rods, α and δ, that sandwich the nodal line of the orthogonal mode with low frequency, were

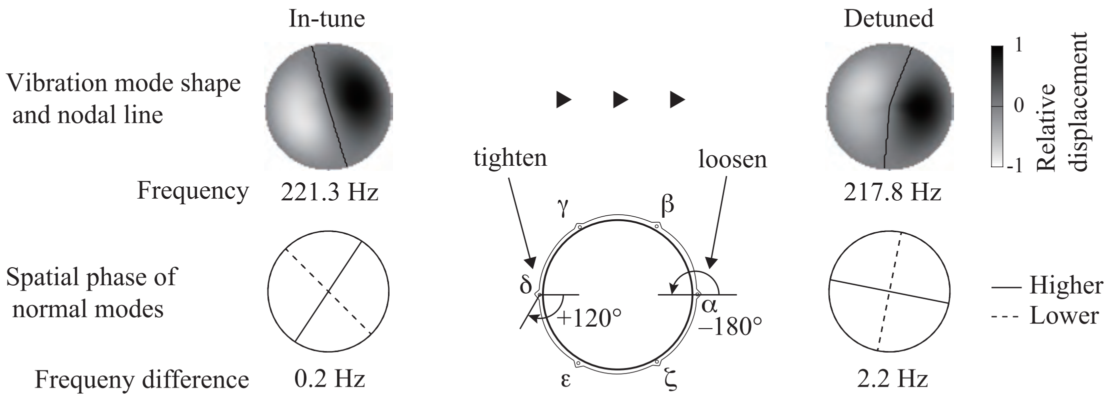

Figure 4. Making tuning problem for experiments

Table 1. Comparison of rotation angles of rods adjustment

Tuning step	α	β	γ	δ	ε	ζ
(a) → (b)	+90°	0°	0°	+90°	0°	0°
(b) → (c)	−45°	0°	0°	−45°	0°	0°
(c) → (d)	0°	0°	+30°	0°	0°	+30°
(d) → (e)	+120°	0°	0°	−150°	0°	0°
(e) → (f)	0°	0°	0°	−60°	0°	0°
(f) → (g)	0°	0°	−30°	0°	0°	−30°
(g) → (h)	0°	+30°	0°	0°	+30°	0°
(a) → (h)	+165°	+30°	0°	−165°	+30°	0°
Fig. 4	−180°	0°	0°	+120°	0°	0°

both tightened by about 90°, to reduce the frequency difference of the orthogonal mode. Then, the rods α and δ were loosened because the frequency of the orthogonal mode was reversed, as shown in Fig. 5(b). The rods γ and ζ were tightened because the orientation of the orthogonal mode has changed, as shown in Fig. 5(c). As a result, the frequency difference was reduced to 0.5 Hz (Fig. 5 (d)).

Second, the rod, α was tightened by about 120° while the δ by about 150°, to correct the curvature of the nodal line, as a pair of rods, α and δ sandwiched the curved nodal line. Then, the curvature of the nodal line became smaller, as shown in Fig. 5(e). However, the rod δ was loosened by about 60° because the nodal line was still curved and the frequency of the orthogonal mode, that the rod α and δ sandwiche, was high. As a result, nodal curvature was no longer seen (Fig. 5(f)).

On the other hand, since the frequency difference of the orthogonal mode was observed, correction was continued by the same method as Fig. 5 (a), (b) and (c). Finally, as shown in Fig. 5(h), the node line was corrected to be almost straight and the frequency difference of the orthogonal mode was small. In other words, the head tension was corrected to be almost uniform.

3.3 Discussion

Table 1 shows the rotation angle of the rod corrected in this experiment. Comparing the rotation angle of the rod changed in Fig. 4, with the rotation angle corrected by the proposed method(“(a)→(h)” in Table 1), it can be confirmed that the changed rods, α and δ, are corrected in the reverse direction. However, the rotation angle is different. In addition, it is also shown that the rod β and ε that were not initially changed, are also corrected.

From this, the correspondence between the tuning that can be regarded as identical by this visualization method and the corresponding tightening of the rod, and its accuracy remain questionable. It is necessary to clarify in the future work whether they become a problem in the process of actual tuning. Moreover, in this paper, we focus only on the (1,1) mode, but it is also necessary to verify whether the tension distribution can be made uniform or if higher order modes should be considered.

4 CONCLUSION

In this paper, we propose tuning scheme for membranophones, referring nodal lines, and orientations and frequency differences of pairs of orthogonal modes. We show that the proposed scheme can correct the head uniformly, as a results of the experiments using the vibration of tom-tom. It is necessary to study in detail the correspondence with the actual tuning process.

REFERENCES

[1] R. Toulson, C. C. Crigny, P. Robinson, and P. Richardson. The perception and importance of drum tuning in live performance and music production. *Journal on the Art of Record Production*, 4:1–7, 2009.

[2] I. DAddario & Company. *How to tune your drum set*, 2006. Tip Sheet.

[3] R. Worland. Normal modes of a musical drumhead under non-uniform tension. *The Journal of the Acoustical Society of America*, 127(1):525–533, 2010.

[4] E. Zempo, N. Wakatsuki, K. Mizutani, and Y. Maeda. Measurement and analysis of effect of tuning on membrane vibration of membranophones. In *Proceedings of the Technical Comittee on Musical Acoustics of the Acoustical Society of Japan*, MA2010–45, volume 37, pages 49–54, Oct. 2018. (In Japanese)

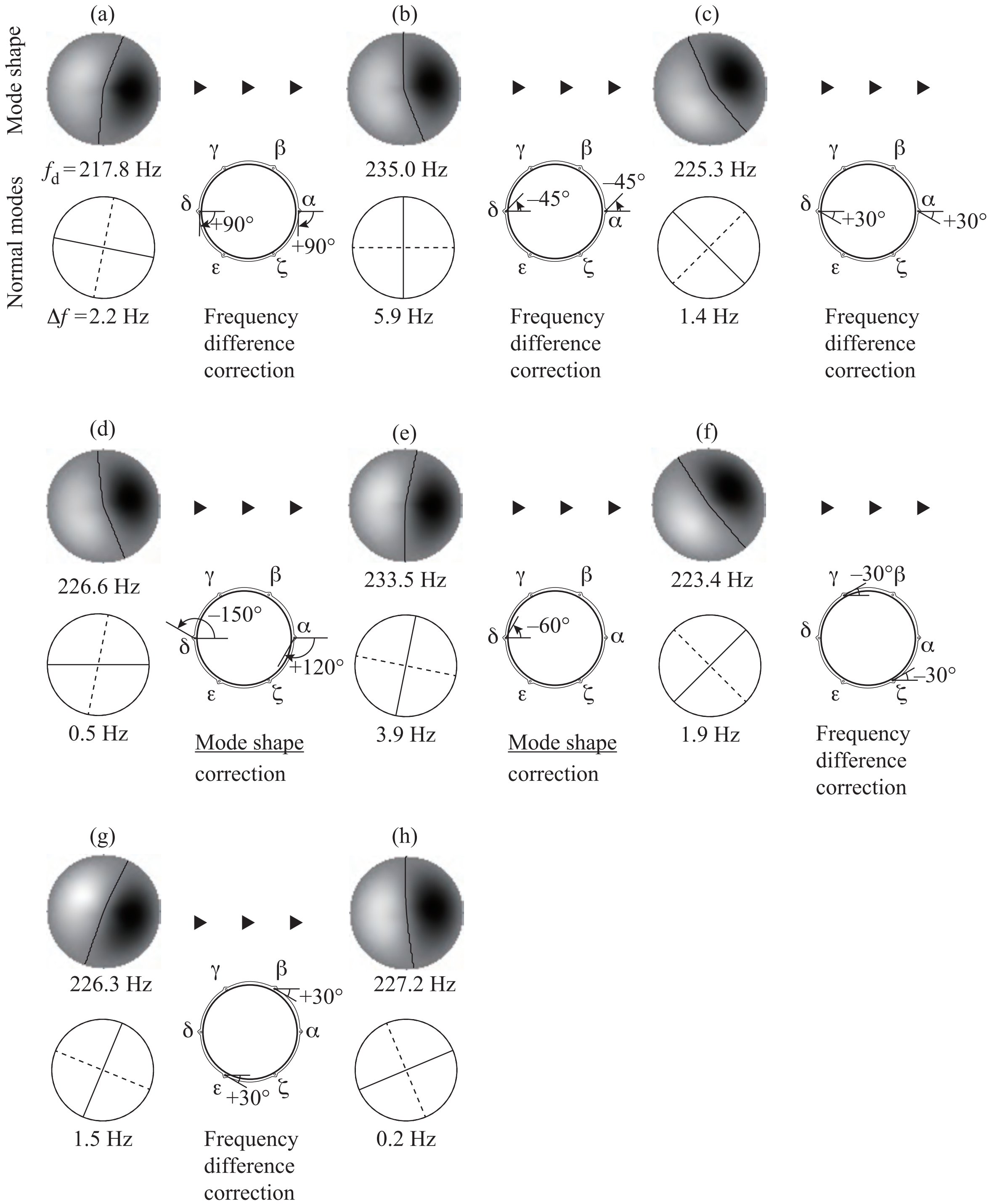

Figure 5. Tuning process with proposed scheme

PROCEEDINGS of ISMA 2019
International Symposium on Music Acoustics

13 - 17 September 2019 in Detmold, Germany

Non-contact measurement of bow force and friction force in bowed string instruments using a camera

Ryodai IZAKI, Naoto WAKATSUKI*, Koichi MIZUTANI, Keiichi ZEMPO

University of tsukuba, Japan

Abstract

Visualizing the mechanical parameters given by the player to the instrument may help to improve the performance technique. Thus, the methods to measure parameters that have less influence on musical performance are required. In this research, we proposed a non-contact measurement method of bow force and friction force using an ordinary camera (not high speed). By using an ordinary camera instead of a high-speed camera, we can obtain the average position of the strings from the blurred image. The process consists of the following 3 steps: (1) Taking the video of illuminated strings with a camera. (2) The position of the strings is calculated from the center of gravity illuminated part. (3) String displacement from a neutral position is converted into bow force and friction force using the relation between position and force in a string. In addition, this method is possible to visualize the bow force and friction force with the proposed method by a verification experiment.

Keywords: bowed string instruments, image processing

1 INTRODUCTION

When playing an instrument, the player gives the instrument mechanical several parameters such as bow speed and bow force. By measuring these parameters and providing feedback in real-time, it is expected that they can be used to support the improvement of performance techniques. Actually, methods using 3D motion capture [1] and methods using armband sensors [2] have been tried as measurement methods for bowed string instruments. Also, a measurement method of bow motion and bow force has been proposed using strain gauges, accelerometers, and resistance wires.[3],[4] However, these methods can not be measured casually because the equipment is large-scale and multiple devices need to be installed. Therefore, we proposed a measurement method of bow motion and bow force using an ordinary camera (not high speed).[5],[6] In this method, it is expected that it is possible to measure bow force, friction force, bow velocity, and bow position simultaneously by performing image processing from the captured image. In addition, it is very easy to measure because it is equipped with one camera. In this paper, among the four parameters, the method of measuring the bow force and friction force was verified.

2 METHOD

2.1 Theory

The definitions of bow force and friction force in this paper are shown in Figure 1. Of the forces applied to the string at the point of contact between the bow and the string, the force parallel to the traveling direction of the bow is the friction force, the bow pressure is perpendicular to that.

The string vibration of the bowed string instruments is represented by the combination of the vibration by Helmholtz movement and the static displacement by the bow force and the friction force. Therefore, it is considered that the displacement due to the bow force and the friction force can be obtained by removing the vibration due to the Helmholtz movement.

For a string of length L that is tensioned at points A and B with a tension T, such as Figure 2, let us consider the bowing motion at point P. It is assumed that the straddling motion is performed parallel to the x-axis, and the point P moves in the x-axis direction u_x and y-axis direction u_y. Assuming that the string has a small amplitude, the bow force F_x and friction force F_y are approximately expressed as Eq 1, 2.

*wakatuki@iit.tsukuba.ac.jp

HfM Detmold HOCHSCHULE FÜR MUSIK
ISMA 2019
DEGA

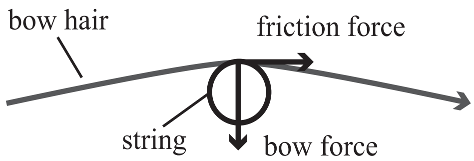

Figure 1. Bow force and bow friction

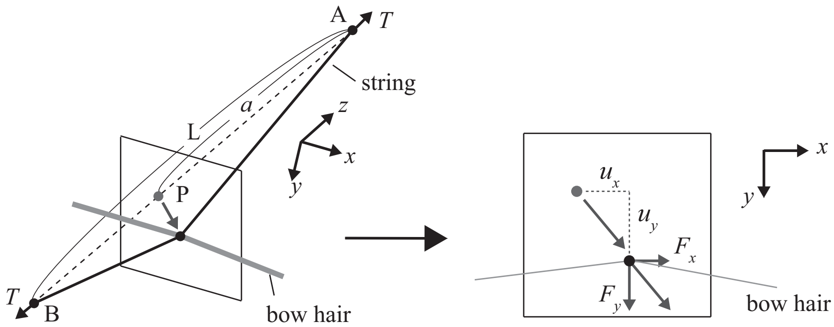

Figure 2. Strings in bow action

$$F_x \approx \frac{T\mathrm{L}}{aL - a^2} u_x \tag{1}$$

$$F_y \approx \frac{T\mathrm{L}}{aL - a^2} u_y \tag{2}$$

Therefore, by obtaining the relationship between displacement and force in advance, it is possible to convert the acquired displacement into bow force and friction force.

2.2 Measurement method

Figure 3 show a flowchart of the proposed method. Arrange the camera at an angle to the strings, and taking the video of illuminated strings by light. Calculate the displacement corresponding to the bow force and friction force by image processing of the video. After that, convert the displacement into bow force and friction force using the relationship between displacement and force.

In this paper, we propose two image processing methods as shown in the Figure 3.

Method (A) is the method for which brightness on the picture isn't used. First, the acquired video is noise reduction and binarization. Next, we obtain the displacement of the string corresponding to the bow force and friction force by calculating the center of gravity of the image. This method is suitable for removing the vibration where mid-range and the average coincide in one cycle.

Method (B) use the brightness of the image. First, the acquired video is noise reduction and binarization. Second, an outline is extracted from the image of the light spot on the image, and a mask is created based on it. Next, we obtain the displacement of the string corresponding to the bow force and friction force by calculating the center of gravity of the image by performing mask processing on the original image. This method is suitable for removing the vibration in which the mid-range and the mean do not match in one cycle.

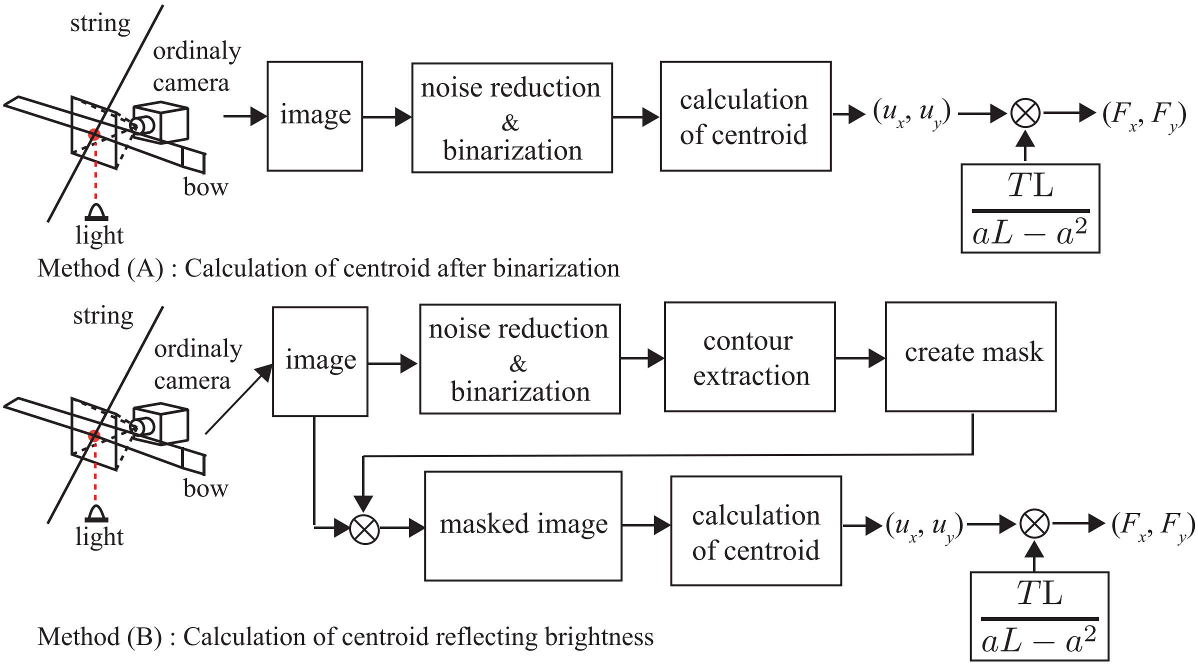

Figure 3. Flow chart of the proposed method

3 SIMULATION

3.1 Experimental method

A simulation was performed to compare Method (A) and Method (B) in image processing. On the image at 500 [pixels] wide by 300[pixels] in height, a pseudo-weighted string was created along the x-axis. Assuming that the string is moving at a sine wave or at a constant velocity, images were generated at 1/4160 intervals. By combining 160 sheets of the image, a blurred image taken at 26 fps was generated. Method (A) and Method (B) were compared using these pictures.

3.2 Result

Figure 4 (a) shows the displacement of the center of gravity when the string is moved to the x-axis with a sine wave with an amplitude of 50 [pixel] and a frequency of 80 [Hz]. The center of gravity of the initial image is taken as the origin. Method (A), the origin was shown without blurring. Because the sine wave is equal in average to the mid-range in one cycle and the cycle of the sine wave is sufficiently faster than the frame rate. On the other hand, Method (B) showed a sine wave with a frequency of about 2 [Hz]. because aliasing has occurred by reflecting the brightness. However, the amplitude of the sine wave is suppressed.

Figure 4 (b) shows the displacement of the center of gravity when the string is moved one pixel per second. Method (A)shows a change like stairs. Because the center of gravity is taken from the binarized image, so displacements less than 1 [pixel] can not be reproduced. On the other hand, Method (B) shows a straight line proportional to time. Because the displacement less than 1 [pixel] can be analyzed by taking the center of gravity in consideration of the luminance.

From the above, Method(A) is excellent for eliminating vibration components whose mean value is equal to the mid-range in one cycle. However, it is not suitable for measuring displacement smaller than one pixel. Method(B) can be smoothed even though some vibration components remain, It has been confirmed that it can cope with even smaller displacements.

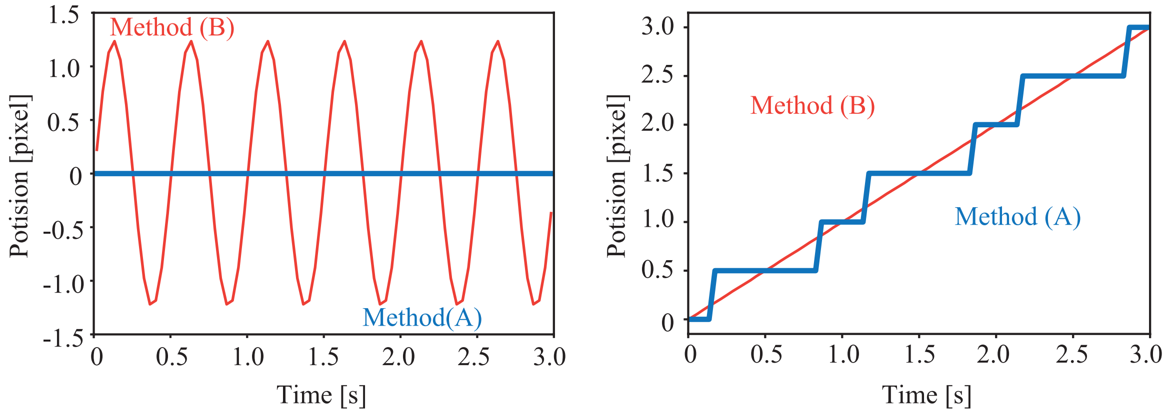

(a) Sine wave

(b) Proportional to time

Figure 4. Displacement by simulation

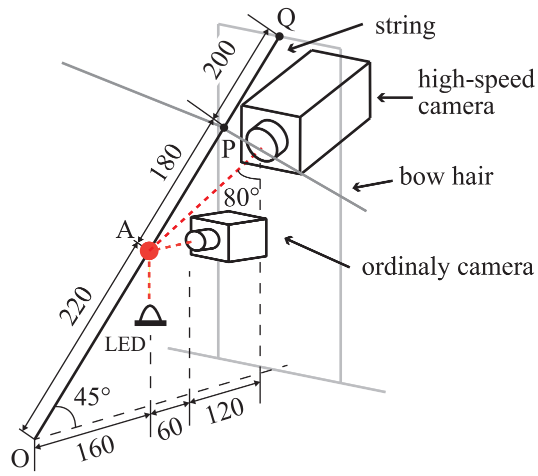

Figure 5. Experimental configuration

4 VERIFICATION EXPERIMENT

4.1 Experimental method

A verification experiment was performed to compare Method (A) and Method (B). Also, as a reference for displacement measurement, simultaneous measurement with a high speed camera (1200fps)was performed. Figure 5 show an experimental device. A string (cello A string, Alloy-steel) of 600 [mm] in length was stretched from point O to point Q in the y-z plane, It was placed so that the angle between the string and the stage was 45 degrees. The LED was given a current of 1.2 [A] and irradiated to point A on the string. The light-receiving surface of an ordinary camera was placed so that the light-receiving surface and the stage were vertical. Then, taking the video of illuminated strings. .Rubbing movement was performed three times at point P.

4.2 Result

Figure 6 shows string vibration measured with a high-speed camera, multiplied by moving average, and those using Method (A) and Method (B). Figure 6 (a) is the displacement corresponding to the friction force, Figure

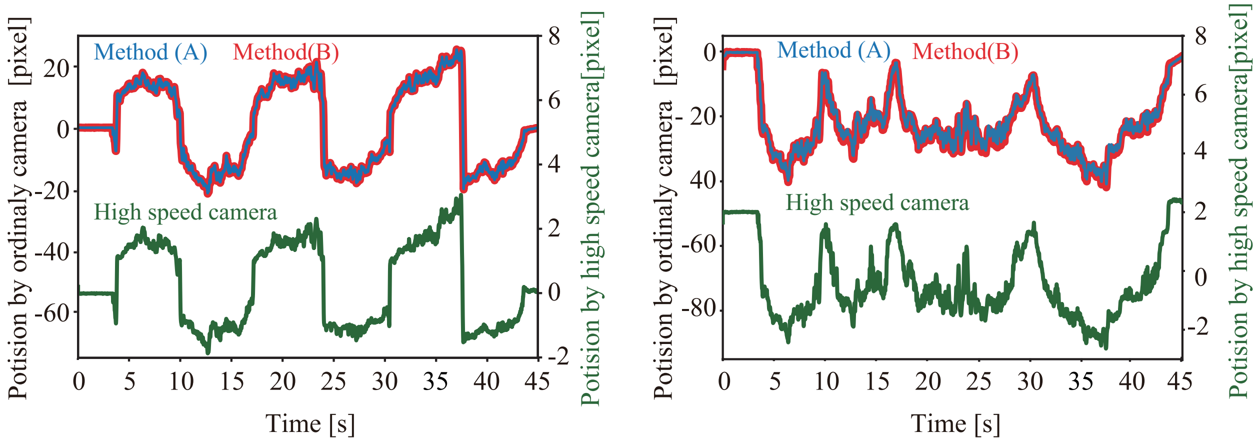

(a) Displacement corresponding to friction force

(b) Displacement corresponding to bow force

Figure 6. Displacement measured by ordinary camera and high speed camera

6 (b) is the displacement corresponding to the bow force. The displacement measured by the high-speed camera and the displacement measured by the proposed method has similar responses. Thus, it is considered possible to measure the displacement corresponding to the bow force and friction force by the proposed method. Also, no significant difference was found in the displacement measured at Method (A) and Method (B). From this, even the proposed method that does not use the brightness of the image may be sufficiently useful for the measurement of the bow force and the friction force.

5 DISCUSSION

In this research, it was found that it is possible to measure the displacement corresponding to the bow force and friction force in the rubbed instrument using an ordinary camera (not high speed). We proposed two methods, one using brightness and the other not using brightness, and as a result of the comparison, it was shown that A without using brightness may be sufficiently useful. This is considered to be the vibration that we want to remove because the Helmholtz motion is equal to the mid-range and average in one cycle. ff Vibrations that differ from the mid-range may occur, such as when the bow is released from the string. In such cases, the analysis method using brightness may be able to measure more accurately. Therefore, it is considered necessary to use two analysis methods according to the purpose of measurement.

Also, Method (A) can process to RealTime, but Method (B) is done by post-processing.

In this paper, we measured the displacement corresponding to the bow force and friction force, but it is possible to convert the displacement into a force. Therefore, when converting to power, it is necessary to examine whether there is any harm.

As a future development, we will convert displacements into forces and check if we can measure them. In addition, we examine the measurement method of bow velocity and bow position, and confirm whether simultaneous measurement using a camera is possible.

6 CONCLUSION

In this paper, we propose a measurement method using an ordinary camera(not high speed) as a measurement method of bow force and friction force in bowed string instruments. It is expected that measuring these parameters will help to improve the performance technique. In this method, the light emitted to the strings is acquired as a movie, and the displacement of the strings corresponding to the bow pressure and the frictional force is calculated by image processings. The bow forces and the friction force are measured by converting this displacement into a force. We proposed two methods, one using brightness and the other not using brightness. As a result of comparison by experiment, it is possible to measure the displacement corresponding to the bow force and the friction force using the camera, and the method without using the brightness is sufficiently useful.

REFERENCES

[1] Kia Ng, Paolo Nesi and Neil Mckenzie, "Technology-enhanced learning for music theory and performance," proceedings of the iadis international conference on e-learning, amsterdam, the netherlands, pp. 66–70, 2008.

[2] Rose Johnson, Janet van der Linden, Yvonne Rogers, "Real-time Feedback for Learning the Violin," Proceedings of the 25th BCS Conference on Human-Computer Interaction, pp 535-538, 2011.

[3] Anders Askenfelt "Measurement of bow motion and bow force in violin playing" The Journal of the Acoustical Society of America 80, 1007, 1986

[4] Matthias Demoucron, Anders Askenfelt and René Causse, "measuring bow force in bowed string performance: theory and implementation of a bow force sensor," acta acustica united with acustica, hirzel verlag, 95 (4), pp. 718-732. 2009.

[5] Ryodai Izaki, Naoto Wakatsuki, Koichi Mizutani and Keiichi Zempo "Real-Time Visualization of Bow-Force and Friction Force in Bowed String Instruments Using Camera", technical report of musical acoustics, Vol. 37, No. 9, MA2018-90, pp. 89–93, 2018. (in Japanese)

[6] Ryodai Izaki, Naoto Wakatsuki, Koichi Mizutani and Keiichi Zempo "Photographing and Image Processing Methods for Improving Accuracy in Bow Pressure and Friction Measurement using a Camera", technical report of musical acoustics, Vol. 38, No. 1, MA2019-03, pp. 13–18, 2019 (in Japanese)

PROCEEDINGS of ISMA 2019
International Symposium on Music Acoustics

13 - 17 September 2019 in Detmold, Germany

Time-domain response measurement of the trumpet, and the room

Timo GROTHE

Hochschule für Musik Detmold, Germany, grothe@hfm-detmold.de

Abstract

The bell of a trumpet is a flaring horn which has two functions: on the one hand, it terminates the resonating bore and therefore controls the sound reflections traveling back to the mouthpiece. On the other hand, the bell controls the impedance match between the narrow downstream bore and the surrounding air in a room, and the radiation directivity. The cylindrical bore downstream of the mouthpiece can favor non- linear wave steepening: The "brassiness" of the sound perceived in the room depends on the amplitude of the pressure peaks inside the mouthpiece. To investigate these phenomena sound pressure measurements have been performed on a trumpet, with sensors inside the mouthpiece, and at different distances from the bell using "musical" excitation signals (generated by a trumpeter) and pulselike technical excitation signals, at various levels.

Keywords: Sound, Music, Acoustics

PROCEEDINGS of ISMA 2019
International Symposium on Music Acoustics
13 - 17 September 2019 in Detmold, Germany

Timbre and Duration of Attack Depend on the Amount of Reverberation

Tor HALMRAST

University of Oslo/Musicology, Norway

ABSTRACT

The attack of a signal is of course best preserved if we hear the direct sound only, but that is not the case in a concert hall. Acousticians often remembers that long reverberation masks the entrance of the next onset, but more astonishing is the perceived and measured difference in timbre due to "smoothening"/"prolongation" of the attack, (also for a first note in a phrase). The paper will discuss general theory regarding how "diffuse field reverberation" influences the attack. The early response of a concert hall, is, however, seldom "diffuse". The paper discusses methods for measuring attack including Rise Time, Steepness etc. of the Integrated (Cumulative) Squared Step Response and also Spectral Flux, for both real halls and simulations (Odeon). Investigations were done for signals of different lengths and for different musical instruments which in itself have slow or fast note-onset. An important question: Is it possible to reduce the smoothening of the attack due to reverberation by adding early reflections? Preserving the attack is important also because listeners nowadays are used to recordings where any wanted amount of direct sound is mixed with a late, long and (too?) smooth, non-correlated, digital reverberation.

Keywords: Attack, Reverberation, Timbre

1 INTRODUCTION

When listening to musicians playing the same pieces of music in different acoustic settings in Stavanger concert hall (see 3.1), the perceived differences were astonishing. However, the measured overall changes in spectrum, level etc., were surprisingly small. Long reverberation of course increases the length of a tone, so that it masks the entrance of the next one, but probably most astonishing was the perceived difference in timbre due to changes of the attack also for a first note in a phrase.

The paper will discuss general theory of how an "ideal, diffuse field reverberation" influences on attack. The early response of a concert hall, is, however, seldom "diffuse". The paper will show measurements and simulations (Odeon) of attack with/without early reflections. Methods for measuring attack in concert halls is not as trivial as measuring Rise Time, Steepness etc. for ordinary electronic filters, and alternative approaches like Integrated (Cumulative) Squared Step Response and Spectral Flux is discussed. The importance of attack has been little discussed in concert hall design, but should be more and more important because listeners nowadays are used to recordings where any wanted amount of direct sound is mixed with a long and (too?) smooth, non-correlated, (digital) reverberation. It is generally assumed that a fast attack is more brilliant, sounds more like if there are more high frequencies present than a "fade in".

First we must remember that a signal of course preserves it attack best if we just hear the direct sound only. This paper will show how reverberation always smoothens/prolongs the attack and discuss how this affects signals of different lengths, different musical instruments which in itself have slow or fast onset of note, and if it is possible to reduce the smoothening of the attack by early reflections.

2 ATTACK IN ROOMS WITH/WITHOUT EXPONENTIAL DECAY

Following Schroeder[1], Jordan[2] discusses rise time etc. of concert halls. Assuming that the decay process in a hall follows the exponential function in eq.1, a corresponding (complementary) build-up process may be written as in eq. 2: (assuming a speed of sound of 344 m/s. I_0 is the intensity at zero time).

$$I_{t,decay} = I_0 e^{-\mathrm{k}t} = I_0 e^{\frac{-13.76t}{\mathrm{RT}}} \qquad (1) \qquad\qquad I_{t,buildup} = I_0(1 - e^{\frac{-13.76t}{\mathrm{RT}}}) \qquad (2)$$

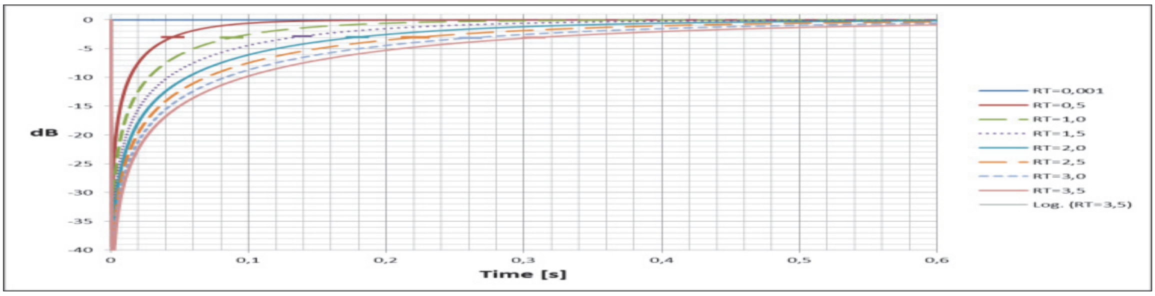

Figure 1 – Attack as a function of reverberation time following Eq.2

The value of **Rise Time** (*TR*) will correspond to the point of time where 50% of the total energy has arrived:

$$\frac{I_{TR}}{I_0} = 0.5 \qquad \text{which is shown to give:} \quad TR \cong 0.05\ RT\ [s] \tag{3}$$

From Jordan[2] we find that:

$$10log\frac{I_{t,buildup}}{I_0} \sim 10log(1 - e^{\frac{-13.76t}{\mathrm{RT}}}) \tag{4}$$

It is further shown that at a level -5 dB below the stationary level, we get a calculated value of Steepness, σ :

$$\sigma_{calc} = \frac{d}{dt}\left(10log\frac{I_{t(-5dB)}}{I_0}\right) = 0.0094\frac{13.76}{RT} \approx \frac{0.13}{\mathrm{RT}[s]}\ \ [\mathrm{dB}\ /\mathrm{ms}] \tag{5}$$

Schroeder[1] states that for enclosures with nearly exponential reverberation*,* the time t_0 at which the sound intensity during the build-up process has reached a level 5 dB below steady state, is typically 1/40 of the reverberation time RT_{60}. Schroeder further states that a more convenient and accurate method of measuring steepness is *'measuring the echo amplitudes of the enclosure near RT_{60}/40 after excitation'*.

For standardised measurements of reverberation time, one often "forgets" the very first part of the decay, and starts the calculations after -5 dB decay. This is of course beneficial for the reproducibility of the measurement results, but we lose a lot of interesting information about possible coloration due to very early reflections etc., see Halmrast[3]. Regarding the shape of the build-up, Jordan[2] states: *'When one considers that the sound paths which are effective in determining the steepness are those which occur early in the build-up process and include the reflections with short time delays, it would seem possible to influence the value of steepness. If, for instance, reflecting surfaces were placed in some sound paths between source and receiver. .... then this would correspond to a reduction of the effective mean free path in an early interval of the build-up process'.*

Several investigations conclude that measuring the Early Decay Time gives a better judgement of the perceived reverberation in a hall (especially for "running music"). Measurements including the first part of the decay, however, often give somewhat different results for different sender positions on stage. Such differences should in fact be considered important. (We should also remember that measurements on an empty stage often gives results that are repeatable, but not practically interesting).

3 LISTENING AND ANALYSING

3.1 Same music performed in different acoustic settings in Stavanger Concert Hall

For the IMS conference on musicology in 2016, the author had the possibility of playing with a group of musicians and recording the same short pieces of music in different acoustic settings in Stavanger Concert Hall (See Halmrast[4]). The same music was played on the same instruments for three settings in the Valen concert hall (a highly flexible hall, with both flexible absorbers on walls and flexible ceiling), and one "jazz-club"-setting in the flexible Zetlitz hall. The settings in Valen was named *2.Chamber* ($T60_{mid.frq}$=1.9s), *4.Amplified* (a setting used for amplified events) ($T60_{mid.frq}$=1.7s) and *6.Concert* ($T60_{mid.frq}$=2.5s). The musicians were instructed to keep same strength for all settings (as good as possible). The recordings were done at the same position on the 8th row, slightly off-centre, with the same recording level for all settings. The main results are given in Halmrast[4]. The music was: classical trumpet a cappella followed by a string quartet (and trumpet) (material from Mahler 5th), jazz piano trio and rock guitar trio, both with trumpet soli. All music was performed without the use of any house amplification (only guitar and bass personal amplifiers with exact the same levels etc. for all the acoustic settings of the hall). Analysing the recordings, we found that the differences, both in level and overall frequency content were surprisingly small. This could of course be discussed regarding "performology", (how the musicians compensate for the acoustics, even when told not to do so), but for this paper, the most interesting result was that the "driest" settings sounded much more "brilliant"/high-frequency than the more reverberant settings. The note lengths were analysed, and the length of each note of course increases with increased reverberation time. For "the same" snare drum stroke, the length was 0,27 s in the dry *5.Zetlitz* setting, increasing to 0,40 (*2.Aplified*), 0,41 (*4.Chamber*) up to 0,44 s for the *6.Concert* setting. The increased length of each note due to reverberation of course gives that one note "masks" the attack of the next one (if the first one is not very, very short or the time between the notes are very long). This "masking" effect of reverberation is well known. The effect reverberation has on the attack also for the "the first note" is not so well known, and the main issue for this paper. (Close inspections on the spectrograms might indicate that in the most reverberate settings, the high frequencies "arrive later", giving additional "smoothing" to the attacks). (see Halmrast[4])

3.2 Convolution of "dry" recordings with impulse responses

We must remember that the general equations for the build-up of the attack in part 2 are only valid for long signals. Noise bursts; very short, longer and much longer, were convolved with Stavanger Concert Hall in most reverberant *6.Concert* setting. Figure 2 shows sound pressure level over time for increasing length of the noise burst. *Black:* dry noise bursts*, Lime:* Convolved with IR measured on stage (close reflections). *Blue:* Convolved with IR from stage to hall in Stavanger (most reverberant setting, *6.Concert*).

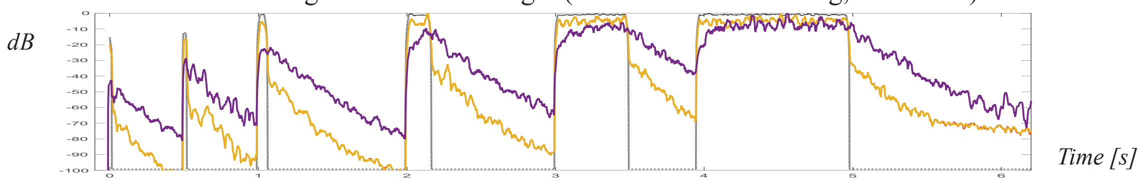

Figure 2 - Noise bursts of increasing length. *Black*=dry, *Lime*=short RT, *Blue*=Long RT

From the left in fig. 2 we see that very short notes are clearly detected without any prolonged attack, because they do not "build-up" in the reverberant room. For the longest reverberation (to the right), the attack for longer notes/bursts are severely prolonged. The decays, however, are similar for all the situations. This simple analysis shows that the room´s influence on the attack not only depends on the reverberation time, but also on the length of the signal (and of course also on the instruments own "onset time"/"attack time"/ "fade in").

The guitar is a good instrument for analysing attack. The guitar did not play any a cappella parts in our tests in Stavanger, but a dry guitar lick (without distortion pedal), was convolved with a very moderate reverberation (like in *5.Zetlitz*), and with the long impulse response measured in *6.Concert.* From figure 3 we clearly see how the reverberation smoothens and prolongs the attack.

Guitar *8 va basso*,

Tempo MM=100

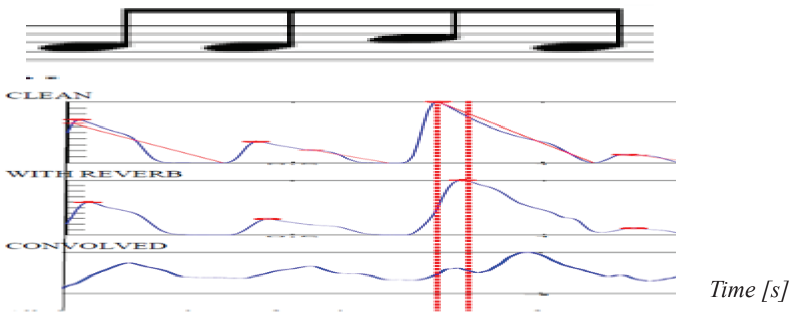

Figure 3 – Guitar Lick. *Upper*=clean/dry, *Middle*=Convolved short RT, *Lower*=Convolved Long RT

4 MEASURING ATTACK

At the moment, a lot of investigations on attack is done, for instance at the Ritmo[5] Centre at Dept. of Musicology at Univ. Oslo. However, most of this work is done regarding rhythm, finding the so-called *p-centre* of the musical event. The effect of attack on timbre is little discussed in literature, but a sharp (short) attack is usually said to be perceived as more "trebly". Hajda[6] mentions attack as: *´that period of the signal in which the global RMS amplitude is rising and the spectral centroid is falling after the initial maximum´……‘In general, three acoustical parameters repeatedly appear as correlates to dimensional solutions in timbre studies: 1. Amplitude-vs-time (temporal) envelope, usually expressed in terms of attack or rise times. 2. Spectral energy* *distribution across frequency components. 3. Spectral variance in terms of the amplitudes of frequency components.* Comment regarding 1*: Log-rise-time = log10(t_{max} − t_{thresh}), where t_{max} is the time from onset to maximum RMS amplitude and t_{thresh} is the time from onset to a threshold taken as 2% of the amplitude at t_{max}'*. Here we see yet another, similar, but not identical definition of Rise Time. (See also Vos[7]).

A big problem when measuring timbre of attack is of course that the attack is fast, but a good frequency analysis requires measurement over a long time ("window"). The next problem is uncertainty about our hearing: How long time do humans actually integrate over, when the sound is changing? Using very small time windows for the analysis will separate the direct sound and the very early/early reflections, and indicate longer attack duration with early reflections than without. Often one state that up to 80ms adds clarity for music, but that cannot be the case if the signal is very short. Often 20 ms is suggested for the integration time. We have analysed both for 10 ms and 20 ms, as very early reflection often arrives within such time limits. Some researchers use 7 ms as the limit for "stage reflections" that is included in the direct sound, (even if they are not really part of the direct sound).

Meyer[8] states*:".....the perceived point of tone entrance lies about 10 dB below the final sound level, or the masking threshold (in the presence of pre-existing noise), and this is relatively independent of the speed of the attack. For very soft tones the point of attack can move as close as 7 dB to the final sound pressure level, i.e., it is sensed even later. For very loud tones, the tone entrance is already perceived at a sound pressure level of 15 dB below the final value".*

For the actual design of a hall, one should of course also pay attention to the direction of the reflection, and the fact that a single, distinct reflection gives audible coloration (comb filter with a distance between the dips (or CBTB, Comb Between Teeth Bandwidth) that is in the order of the critical band, which means delays in the region 5-25 ms, see Halmrast[3].

4.1 Measuring attack from recorded music. MIR and Spectral Flux

Measuring using the parameter Attack Time in common Music Information Retrieval/MIR- programs (like MIR Toolbox[9] and the new Mining Suite[10], and also parameters like Intensity (in Praat etc.) often includes some kind of low pass filtering ("long window"), giving that the attack is somewhat smoothed also in the actual analysis, so some of these methods are not quite useful for our task. (A new version of MIR Toolbox will incorporate improved measurements of attack time).

Spectral flux is a measure of how quickly the power spectrum of a signal is changing, comparing the power spectrum for one frame against the power spectrum from the previous frame. It is usually calculated as the *2-norm* (also known as the Euclidean distance) between the spectra. The spectral flux can be used to determine the timbre of an audio signal, or onset detection. There are numerous variants of Spectral Flux, and they all give different results and present the results in different ways. One version of Spectral Flux is incorporated in MIR Toolbox, and other versions can be found as plugins for Sonic Visualiser etc. Figure 4 shows the overall measurements of spectral flux from the recordings of the whole selection of music, for each of the acoustical settings. We see that the shortest reverberation time (*5.Zetlitz,* jazz-club setting), gives the highest Spectral Flux.

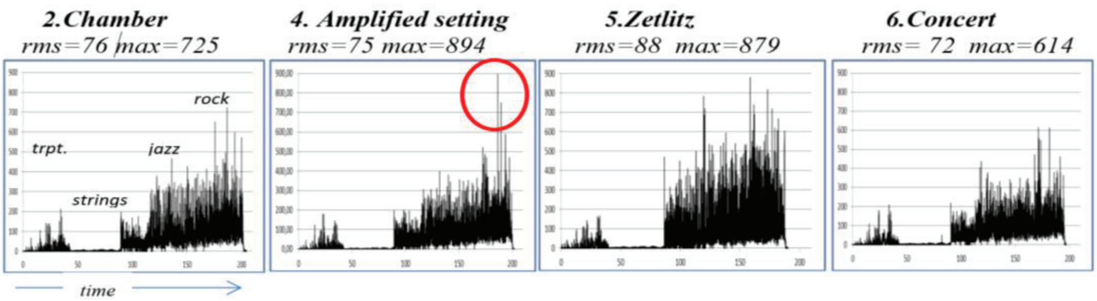

Figure 4 –Spectral Flux for same music in different acoustic settings in Stavanger Concert Hall
(The red circle indicates an accidental strong drum stroke)

4.2 Measuring attack from Impulse Responses

In electronics, **Rise Time** is the time taken by a signal (step function) to change from a specified low value to a specified high value. These values may be expressed as ratios or as percentages or dB values with respect to a given reference value. In analogue and digital electronics, the percentages are commonly the 10% and 90% of the output step height, however, other values are commonly used. (Examples of "other values" are -5 /-3 dB mentioned in part 2). We shall see that these parameters often are too "general", so we need to examine the attack more in detail. The method we found most convenient was to integrate the squared impulse response, which also might be called a Cumulative Step Response.

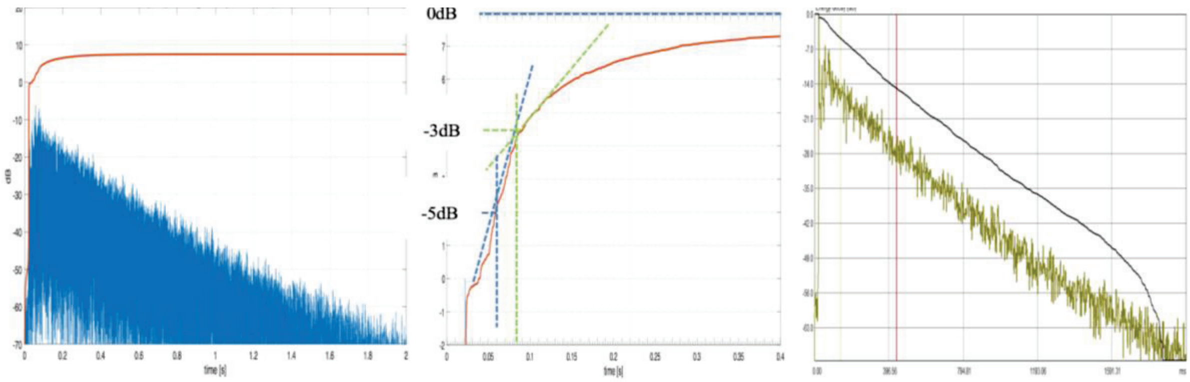

Figure 5 – *Left:* Imp.Resp. and Int.Imp.Resp. *Middle:* Variation of Steepness during attack phase. *Right:* Imp.Resp. and Schroeder curve.

Figure 5 shows measurements in a shoebox hall with reasonable exponential decay, (the University Aula, Oslo, empty). To left we see the squared impulse response (up to 2s, in blue) and the integral of this (red) in the left pane. The pane in the middle shows a zoom in of this Integrated Impulse Response (up to 0.4s) for. To the right is shown the common energy decay and the Schroeder curve.

The reverberation time (T30 and T20) for this hall is app. 2.2 s (empty, mid freq.). According to Jordan (in Part 2), Steepness should then be 0.13/RT= 0.13/2.2=0.059 dB/ms. From the middle pane in the figure above, we see that the steepness is changing during the attack, but we find a typical value around the -5 dB point of 0.087 dB/ms, and 0.033 dB/ms around the -3 dB point. The mean value of these might actually correspond quite well. From the same figure, we find that Rise Time (up to -5 dB) is 38 ms. For the build-up unto -3 dB, we get a Rise Time of app. 60 ms. The calculated rise time, TR according to Jordan (up to -5 dB), should be 0.05 x 2.2 = 0.110 s= 110 ms. As a conclusion, both Steepness and Rise Time give measured values that deviate from the equations for exponential decay (and build-up). The hall is a moderately small regular shoebox, so this hall, if any, should be assumed to have exponential decay. One reason why even this hall differs from the equations might be that it actually has some (nice) early reflections. Keeping in mind that the measurements highly depends on where on the build-up curve we analyse these parameters, we should not relay too much on either Rise Time or Steepness before we have more measurements from different halls. For now, we should inspect the shape/curvature of the Integrated, Cumulative Squared Impulse Responses itself in order to find the interesting issues of attack.

5 ROOM ACOUSTIC MODEL

A very simple, large hall was modelled in Odeon, with sidewalls and rear wall behind audience as reflective, highly diffusing/scattering. (See Halmrast[14] for details). Dimensions: L x W x H = 46 x 31 x 20 m. Receiver: 30 m distance, 1m off centre, height 2 m. Three different settings of a "box" around the source, open only towards the hall, were analysed, called; *Transparent*, *Reflecting* and *Absorbing*. Especially the two last ones will be discussed here. Figure 6 shows both the impulse responses and the Integrated Imp.Resp. up to 320 ms. (PS! For the first part of the Imp. Resp., both curves are identical, so the red curve is covered by the black one).

Comparing the common acoustic parameters for *Refl.Box* and *AbsorbBox,* the close reflections give an increase in C50 and C80. Spectral centroid for the Impulse Responses is also increased from 7165 Hz to 7504 Hz due to the close reflections. Adding the close reflections changes EDT more than RT. (For this simple simulation, it seemed like the close reflections gave an increase in EDT for 500 Hz and below, but a decrease for 1 kHz and above. This should be investigated further, together with close examination of the EDT algorithm in use, as the first reflection(s) actually might be stronger than the direct sound, and make confusions in choosing the exact time of arrival of the direct sound). From analyses of Spectral Flux, we clearly see that the (changes in) Spectral Flux is larger for the black curves/Refl.Box.

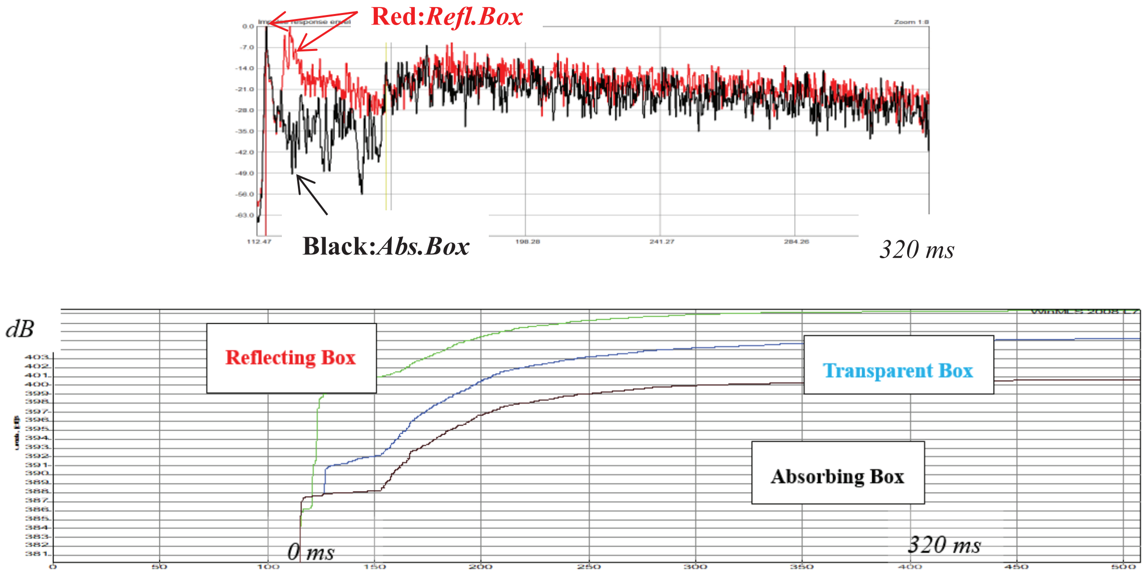

Figure 6 – Upper pane: Impulse response with/without early reflections (Odeon)
Lowe pane: Integrated Impulse Response. *Red*= with early reflections, *Black*=without early reflections:
(*Blue*= with transparent box, not discussed)

5.1 Note Length and Musical Instruments own attack time/build-up

Figure 7 shows a short musical phrase that was played by different instruments, "dry" and convolved with the measured impulse response from the most reverberant setting in Stavanger Concert Hall (*6.Concert*). Figure 7 shows a comparison of the attacks for an instrument with very short sounds; a xylophone, compared with a "slow reacting" and long sustaining instrument; a bowed violin. We see that for the convolved curves, the attack is preserved as rather short for the xylophone, but prolonged for the violin. We also see that for the violin, the decay (and sustain) of one note masks the entrance of the next. Listening to these examples, each note is heard separately for the xylophone, and the first attack is rather well preserved, but the violin has a got an added build-up for the first note, and the second and especially the third note is almost not perceived as a new attack, but is masked by the first notes. (Total length is 1.5 s. Division is 5 dB).

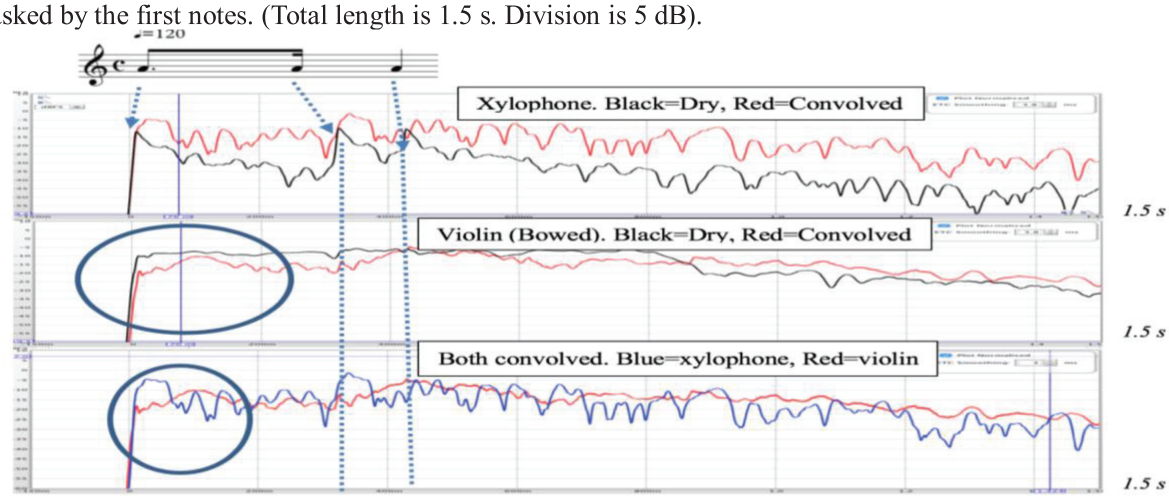

Figure 7 – Analysis of xylophone and violin playing the same music. Dry and convolved with long RT

Figure 8 shows Energy Time Curve (ETC) of the first part of the phrase, (up to 60 ms) for xylophone. *Black*=Dry recording, *Green*=Convolved/Odeon/Refl.Box and *Blue*=Convolved/Odeon/Abs.Box. The leftmost pane is for very short ETC-smoothing (0.2 ms), the middle pane is for 5 ms, and the pane on the right is for 10 ms ETC-smoothing. (Division is 2 dB).

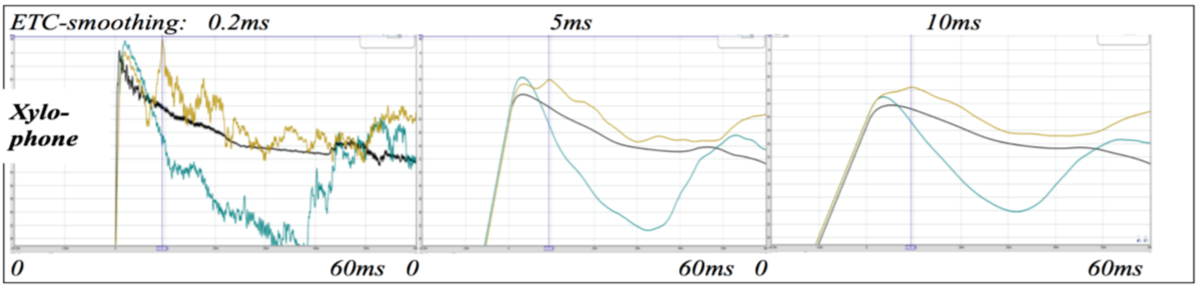

Figure 8 – ETC (Energy Time Curve) of the same xylophone for different smoothing: 0.2 ms, 5 ms and 10 ms, *Black*=Dry recording, *Green*=Convolved/Odeon/Refl.Box and *Blue*=Convolved/Odeon/Abs.Box

Figure 8 clearly shows the importance of the decisions we have to make when analysing small differences in short attacks. If we assume that our ear has an integration time of 10 ms (or more), the setting with close reflections, *Refl.Box*, will be perceived with the "clearest" attack.

For the bowed violin in figure 9 it is problematic to see if close reflections give any influence, because the build-up of a violin tone itself is so slow. The following figure shows the same 60ms, but now for the "slow", bowed violin convolved with *Refl.Box* (Black) and with *Abs.Box* (red), and we see that the influence on the attack is much smaller than for the xylophone, and that the issue of integration time is not that important for the "slow" violin.

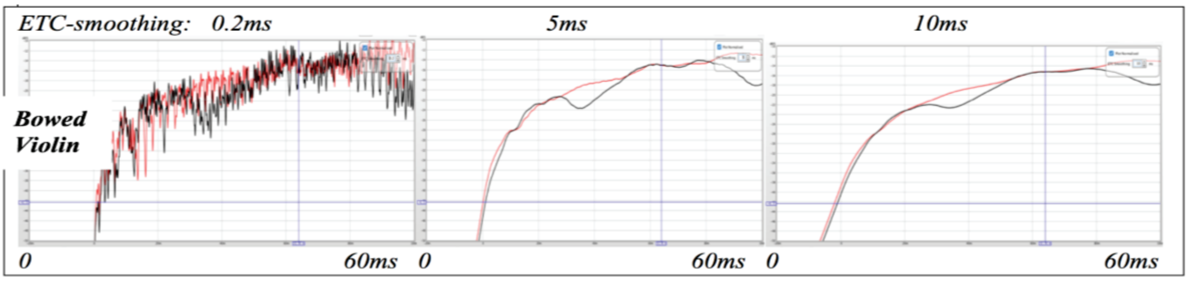

Figure 9 – Energy Time Curve of the same violin (arco) for different smoothing: 0.2 ms, 5 ms and 10 ms *Refl.Box* (Black) and with *Abs.Box* (red

6 MEASUREMENTS IN A CHURCH

Figure 10 shows the attack (Integrated Impulse Response) for sender position *Without*(aisle) and *With* close reflections (pulpit) in a medium sized church. (see Halmrast[14] for details).

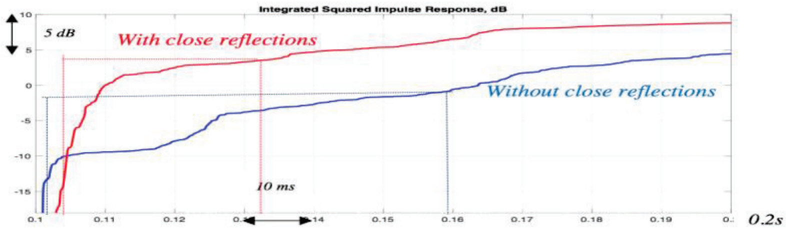

Figure 10 – Integrated Impulse Responses with/without close reflections in a church.

We see that the overall attack is faster with the close reflections. If we should want to measure the Steepness, we would need to closely define which part of the curve is interesting (especially for the blue curve). Quick estimations of Rise Time (to – 5dB) gives: $TR_{WithCloseReflections} = 30ms$, and $TR_{WithoutCloseReflections} = 58\ ms$. Schroeder´s "rule of thumb" for exponential decay in Part 1 gives: $2.4s/40 = 60\ ms$ so, for this quick test, the agreement is nice for the measurement without close reflections, and the close reflection practically halves this attack time. However, until we have more analyses and simulations, we should inspect the shape of the attack curve in detail and compare with the typical note length, and not rely too much on parameters like Steepness and Rise Time.

7 CONCLUSION

Reverberation “smoothens/prolongs” the attack. For rooms with an exponential decay, the build-up of the attack can be determined from the decay. However, most interesting halls do not have exponential decay, especially in the early part, and we need to investigate the attack more in detail.

Integrated, Squared Impulse Response (Cumulative Step Response) is a good way of investigating attack. Parameters like Rise Time and Steepness can be derived from this, but for many interesting situations with early reflections, the curvature of the attack is non-uniform and we should inspect the actual shape of the curve rather than trust these parameters. It is shown from computer simulations and measurements in a church that **early reflections** in might help preserving time for halls with long reverberation times.

The effect reverberation (and early reflections) have on attack is highly dependent on the type of signal:

- **Extremely short, bright signals** can be so short that they do not “build up” due to the reverberation.
- **Instruments with long internal build-up/onset** (like bowed strings) get a nice development from the smoothed attack due to long reverberation time in the hall.
- **For most instruments in between these groups,** (especially piano with its special “resonance” phase) there is a problem of “smoothing” due to prolonged attack from the reverberation.

This can be reduced by introducing early reflections. For the design of halls, however, we must also remember that distinct early reflection might give comb filter coloration, and take the direction and delay times of the early reflections into consideration (See Halmrast[3,14]). Attack is highly important for today´s listeners, who are used to listening to recordings where any wanted amount of direct sound is mixed with a (too?) long, diffuse reverberation.

REFERENCES

1. Schroeder, M. R. *‘Complementarity of Sound Buildup and Decay’*. JASA 40, 549 (1966)
2. Jordan, V. L. *‘Acoustical Design of Concert Halls and Theatres’.* Applied Science Publishers, London (1980) p.11 and 206-211. (and J. Audio Eng. Soc. 13, 98-103 (1965))
3. Halmrast, T *‘Orchestral Timbre: Comb-filter coloration from reflections”.* Journ. Sound and Vibration, 232(1),53-69, (2000)
4. Halmrast, T ‘*Analysis of Music Performed in Different Acoustic Settings in Stavanger Concert Hall’.* Int. Congress on Sound and Vibration, ICSV24, London (2017), paper 398
5. Ritmo, Centre for Interdisciplinary Studies in Rhythm, Time and Motion. https://www.hf.uio.no/ritmo/
6. Hajda, J. M. *‘The Effect of Dynamic Acoustical Features on Musical Timbre’* in *‘Analysis, Synthesis, And Perception Of Musical Sounds:The Sound Of Music’* ed. J.Beauchamp. Ch.7, p.254
7. Vos, J. and Rasch, R. (1981): *´The perceptual onset of musical notes´,* Percept. Psychophys. 29, S. 323
8. Meyer, J. *‘Acoustics and the Performance of Music’* Springer, p.12, (2009)
9. MIR Toolbox. https://www.jyu.fi/hytk/fi/laitokset/mutku/en/research/materials/mirtoolbox
10. Mining Suite. https://www.hf.uio.no/imv/english/people/aca/temporary/oliviel/
12. Halmrast, T. *‘Acoustics in Between: Perception of Sound in Rooms Beyond Standard Criteria’.* Psychomusicology: Music, Mind, and Brain, Am. Psychological Association 2015 Vol25, No3, 256–271
13. Halmrast, T *‘Attack the Attack’* IoA proceedings, Hamburg 2017, Vol.40, p 335-345
14. Halmrast, T. (2019) *‘Sam Philips´ Slap Back Echo, Luckily in Mono”.* Journ. Art of Record Production http://urn.kb.se/resolve?urn=urn:nbn:se:kmh:diva-3124

PROCEEDINGS of ISMA 2019
International Symposium on Music Acoustics

13 - 17 September 2019 in Detmold, Germany

High resolution 3D radiation measurements on the bassoon

Timo GROTHE and Malte KOB

Hochschule für Musik Detmold, Germany, grothe@hfm-detmold.de

Abstract

Musical wind instruments with tone-holes have complex radiation patterns. Since openings act as sound sources, depending on their relative distance and phase soundwave superposition can lead to boosts or cancellations at different observation points. These phenomena are particularly prominent in the bassoon, as a multitude of differently sized tone-holes are distributed irregularly across a long, bent corpus. To extend our knowledge on pitch-related directivity patterns of such complex instruments the bassoon was chosen as a test case measurement object for a high resolution radiation measurement in 3D, using a repeatable, artificial excitation and a 2 axis turntable. We compare the radiation patterns of four different tonehole configurations, and discuss implications for simultaneous measurements with a microphone array.

Keywords: Sound, Music, Acoustics

1 INTRODUCTION

The bassoon has a long bent corpus with many toneholes of different size and opening direction distributed across it. Like in other large wind instruments, the position of the player holding the instrument has important influence on the radiation. Being a sound source of large geometrical irregularity, the bassoon/player combination is assumed here to be a good test case for a complex musical instrument radiator.

Tonmeisters, who record the bassoon sound for music production, experience an imbalanced sound, especially when placing spot microphones in the vicinity of the instrument. Besides obvious sound disturbances like keywork noise and level variations due to the varying position of the first open tone hole with respect to the microphone, also the timbre appears imbalanced between notes [5].

The purpose of this work is to study how the radiation pattern of the bassoon without player changes due to variations in the fingering.

After the pioneering works of Jürgen Meyer [6], who was the first to unravel the directions of the bassoon's main radiation lobes with 3 dB dynamics (Fig. 5), very few systematic attempts to measure the radiation of the bassoon have been reported - to the knowledge of the authors.

Among these are the works of Pollow *et al.*, who recorded the bassoon (among a broad variety of musical instruments) in anechoic conditions with a spherical array of 32 microphones in an truncated icosahedric arrangement of 4.2 m diameter [8, 9]. The data of these measurements is now publicly available [11]. In a similar fashion, Paetynen and Lokki [7] recorded the bassoon (among other instruments) using an array of 22 microphones in pentagonic arrangement at 6 height levels. The angular resolution of the microphone arrays in these studies is near to 36 and 72 degrees, respectively.

In contrast to these studies, Grothe and Kob employed an artificial player for continuous blowing of the bassoon and derived 2D directivity pattern from continuous measurements with the turntable method. In the horizontal and a vertical plane polar pattern of the bassoon radiation without player are rendered in 1 degree resolution [4].

Using a repeated capture measurement scheme with a musician playing notes and a rotated microphone arc, Bodon measured the 3D directivity of the bassoon (among other instruments) in 5 degree resolution [2]. Most recently, Ackermann *et al.* analyzed variations in bassoon radiation patterns using spherical harmonic (SH) representations of the data recorded by Pollow *et al.* [9, 11]. With this interpolation technique, 3D radiation pattern of 1 1 degree resolution were produced, at SH order 4 [1].

As a complement to these earlier studies, the purpose of this paper is to present a 3D directivity data set of the bassoon without player, with a high spatial resolution of 5 degrees in the measurement.

2 MATERIALS AND METHODS

For a repeated measurement scheme in acoustical radiation experiments, a precise positioning system and a stable excitation of the measurement object is vital. For the excitation, an impulsive sound source has been used. It provides sufficient excitation level for radiation measurements from a few Hz to about 1.5 kHz (Fig. 1).

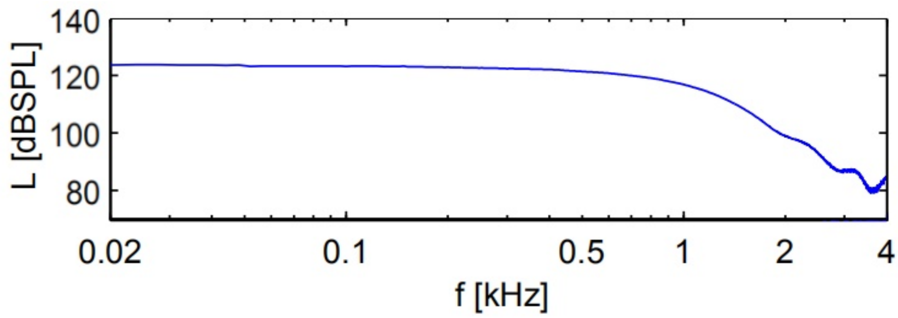

Figure 1. Frequency response of the excitation mechanism

Experimental setup Bassoon and excitation mechanism were mounted on a frame of metal tubing with 16-20 mm diameter. This frame was mounted on a 2 axis turntable (ELF, fouraudio, Herzogenrath, Germany) such that the bassoon's longitudinal axis matched the vertical rotation axis of the turntable (y in Fig. 2). A measurement microphone (Type 4190, Brüel and Kjær, Naerum, Denmark) was positioned in the horizontal plane, in negative x-direction in a distance D=2 m (Fig. 2). The setup was placed in an anechoic chamber with a cutoff frequency of about 200 Hz.

During a measurement series, the turntable was rotated clockwise

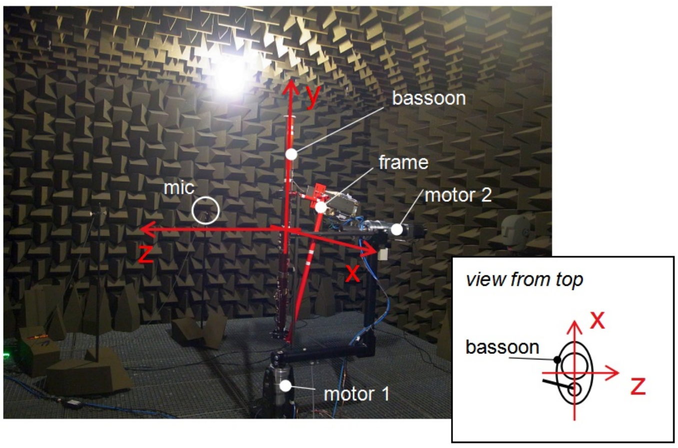

Figure 2. Setup and coordinate system for the bassoon radiation measurement with a 2 axis turntable.

- about the vertical axis (motor 1), by angle H (perpendicular to the horizontal plane);
- about the pivoted horizontal axis (motor 2), by angle V (perpendicular to a vertical plane).

Figure 2 shows the initial state of the setup ($H = V = 0$). For this setup, the microphone position $\vec{m}$ in a bassoon centered coordinate system $(x|y|z)$ as a function of turntable rotation angles H and V writes

$$\vec{m} = (-\cos(V)\cos(H)D, \sin(V) - \cos(H)D, \sin(H)D)^T. \quad (1)$$

Signal processing Aiming at comparable results, the postprocessing followed the procedures described in the earlier studies [2], and [10]:
The position dependent levels $L(H,V,f^n_{0,nom})$ shown in the following are calculated from the absolute values of the fft-coefficients at $f^n_{0,nom}$. The latter are the fft-lines closest to the frequencies of the harmonic series $n\,f_0$, where n is the ordinal number of the harmonics and and f_0 is the fundamental pitch of the respective fingering. Pitches are referenced to equally tempered tuning at A4 = 440 Hz. For the signal processing, an open toolbox[1] for MATLAB® [3] has been used.
To generate frequency dependent balloon plots from the spectral level data, the position of the microphone $\vec{m}(V,H)$ was converted to azimuth and elevation angle with respect to the bassoon centered coordinate system (Fig. 2), and the level of the corresponding measurement is displayed as radius.

Repeatability The combination of excitation mechanism and 2-axis turntable shows a good repeatability. A full rotation series in 5 ° resolution in both angles H and V, with 3 repetitions in each position took about 28 h. The average difference between the first ((V|H) = (0 °|0 °)) and the last ((V|H) = (360 °|360 °)) measurement is < 1 dB between 150 Hz and 1.5 kHz, maximum difference < 1.5 dB.

Studied fingerings In total, four fingerings, namely B♭1, E♭3, E♭3$_{aux}$, and F3 were studied. The fingerings B♭1 (f_0=58.3 Hz) and F3 (f_0=174.6 Hz) mark the extremes of all holes being closed, and no keys pressed, respectively (Fig. 3: top, and bottom). The fingering E♭3 (f_0=155.6 Hz) is a so-called fork fingering. It is identical as for the neighboring note E3 (f_0=164.8 Hz), except the next tone-hole is closed[2] (Fig. 3, upper mid). The fingerings E♭3 and E♭3$_{aux}$ (f_0=155.6 Hz) differ only in one hole additionally opened (approx. at x =1.75 m (Fig. 3, lower mid)). This very common auxiliary fingering for E♭3 is known among bassoonists not only to stabilize the tone production and slightly flatten the pitch, but also to produce a significant change in timbre. For the fingering F3 (f_0=174.6 Hz), by lifting the fork, three closely spaced finger holes in the region $0.52m < x < 0.6m$ are open (Fig. 3: bottom), instead of only one as in E♭3.

3 RESULTS

The observed complex radiation patterns of the bassoon are the result of a superposition of single point sources that contribute with individual phase and amplitude to the measured sound pressure level at the microphone position. For the relation of wavelength and open tone-hole distances the following basic acoustic relations apply: For very low frequencies the sound radiation of a wind instrument with multiple sound sources can be described as omnidirectional when the overall size of the instrument is small, e.g. $1/4$, compared to the wavelength λ. In this case, the radiation of all instruments' openings is more or less in phase. For the bassoon this is never the case since the lowest fundamental produced at B♭1 is 58 Hz, and with a waveguide length of 2.5 m the associated frequency for $\lambda/4$ would be 34 Hz. However, for the lowest fundamental the radiation pattern is mostly omnidirectional (see pattern marked with + in Fig. 4) because only one opening, the passive end, radiates sound. For other tones, the fundamentals and all partials of the contributing sound sources are therefore not in phase, and superpose with amplitudes and phases that are individual for each fingering. The effect of the fingering is shown in Fig. 4. The fundamental E♭3 (155.6 Hz) is realised with two different

[1] http://www.ita-toolbox.org/index.php

[2] downstream of the active tone-hole at approximately x =0.6 m

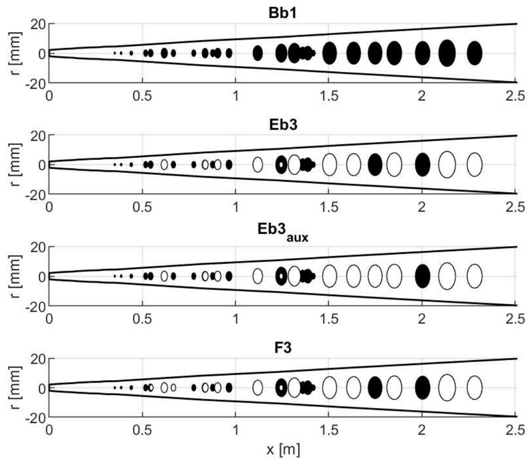

Figure 3. Tonehole-pattern of the studied fingerings

fingerings (○: normal fingering, ×: auxiliary fingering). The tone-hole openings only differ in the fifth hole from the passive far end of the bassoon bore which is open in case of the auxiliary fingering (Fig. 3). The effect on radiation is shown in the radiation analysis of the 2^{nd} partial near 300 Hz (Fig. 3 (a), left) and of the 5^{th} partial near 700 Hz (Fig. 3 (b), right). Whereas the overall shape of the polar pattern is similar, at 700 Hz the details exhibit differences of up to 3 dB for the side-lobes which – when played in temporal proximity – would produce a perceivable timbre change.

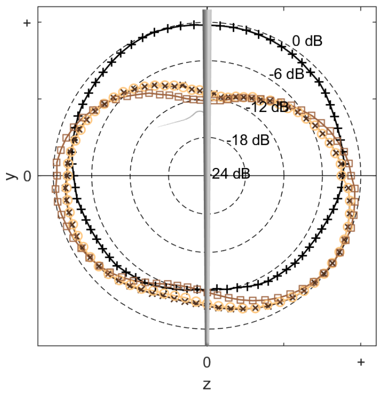

(a) $n\,f_0 \approx 300$ Hz

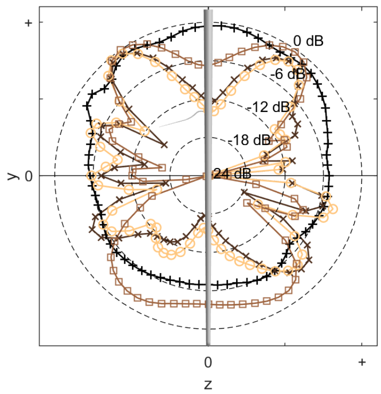

(b) $n\,f_0 \approx 700$ Hz

Figure 4. Single-partial radiation pattern in the frontal plane. Comparison of 4 different bassoon fingerings
+: B♭1 ($f_0 = 58.3$ Hz (a): n=6, (b): n = 12; Fig. 3 top);
×: E♭3,($f_0 = 155.6$ Hz (a): n=2, (b): n = 5; Fig. 3 upper mid)
○: E♭3$_{aux}$ ($f_0 = 155.6$ Hz (a): n=2, (b): n = 5); Fig. 3 lower mid)
□: F3 ($f_0 = 174.6$ Hz, (a): n=2, (b): n = 4; Fig. 3 bottom)

Even small musical differences in melody such as a diatonic interval from E♭3 to F3 can produce large level differences of more than 12 dB as shown in the comparison of the patterns with circle markers (E♭3) and square markers (F3), respectively. Not only the location but also the number of lobes vary strongly around the instrument. As shown in Fig. 3, the only difference between F3 and the regular fingering of E♭3 are two more open toneholes (5^{th} and 7^{th} from the bocal).
These results, produced with a technical broadband excitation mechanism, are in good agreement with an earlier study of the authors on a bassoon blown with an artificial mouth [4]. The measured data can be compared to a model of the radiation characteristics of the bassoon with spherical harmonics (SH) of order 4, generated with data from a database of anechoic microphone array measurements [11]. This comparison is shown in Fig. 6 (b) vs. (c) and Fig. 7.

4 DISCUSSION

Whereas measurements from our study match well with earlier investigations [6, 4, 2], they do not resemble order 4 SH-based interpolations of directivity pattern recently published [1, 11]. Reasons for this is the low resolution of their microphone array (approximately 36° degree [8]) with respect to the complexity of the sound source.

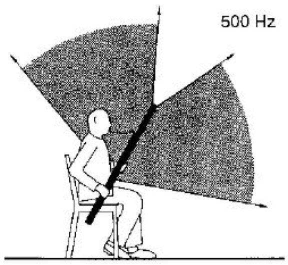

Figure 5. Directivity plot of the Bassoon (Meyer 1972) [6], reprinted with kind permission of the author.

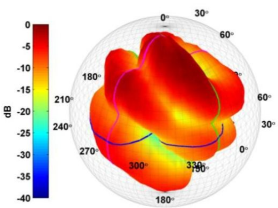

(a) 5° repeated measurements with musician (Bodon 2016) [2]

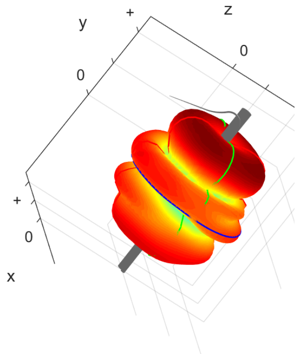

(b) 5° repeated measurements without musician (this study)

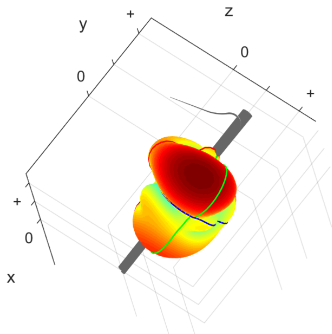

(c) 4^{th} order SH-based interpolation 32 ch. spherical array measurement with musician [1, 8, 11]

Figure 6. Bassoon directivies in 5°-resolution near 600 Hz
(a): 4^{th} harmonic frequency of D3 $f_0 = 146.8$ Hz.
(b),(c) : 4^{th} harmonic frequency E♭3, $f_0 = 155.6$ Hz.
Figure (a) is shown here for comparison, reprinted from [2] with kind permission of the author.

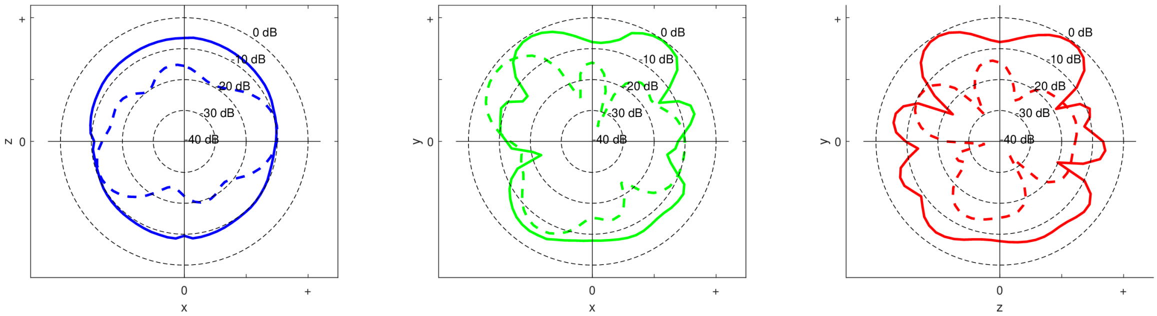

(a) horizontal plane (b) median plane (c) frontal plane

Figure 7. Polar plots of the bassoon directivity pattern in 5° resolution.
solid line: measured (this study); dashed line: 4^{th} order SH-based interpolation of a 32 ch. spherical array measurement [1, 8, 11].

The validity of single-center SH-based interpolations computed from measurement data with low spatial resolution depends critically upon the question if the object under study can be considered as a single, centered source.
In contrast to the approach of calculating a virtual center for a given array measurement [10], it might be interesting for muscial auralization purposes to model multi-pole radiation of one instrument as a superposition of low-SH-order-sources, i.e. to decompose 3D data into multiple sources with known positions. The data from this study is well suited for such attempts, and might also serve as benchmark to estimate the complexity of the source in terms of SH-order and design a suitable microphone array. However, for the case of the bassoon, we conclude from our measurement data that at 5° resolution spatial aliasing occurs already from 1 kHz.
If a high spatial resolution in a musical instrument radiation measurement is required, repeated capture measurements with technical excitation have many advantages over array measurements.

Future work should include a listening test with auralizations of variable SH-order basing on even higher resolution measurement data to investigate the necessity of precise radiation models of musical instruments with respect to sound perception.

ACKNOWLEDGEMENTS

The authors thank David Ackermann and Alexis Baskind for very helpful discussions, Nathan Flipo and Rainer Günther for assistance in the measurements, Michael Makarski and Rainer Thaden for supporting the measurement automation, and Uwe Meier for the possibility to use the anechoic chamber of TH Ostwestfalen-Lippe.

REFERENCES

[1] D. Ackermann, F. Brinkmann, and S. Weinzierl. Musical instruments as sound sources with time- variant directivity. In *Proceedings of the German Conference on Acoustics (DAGA 2019), Rostock; German Acoustical Society (DEGA)*, 2019.

[2] J. Bodon. Development, evaluation, and validation of a high- resolution directivity measurement system for played musical instruments. Master's thesis, Brigham Young University, 2016.

[3] P. Dietrich, B. Masiero, M. Müller-Trapet, M. Pollow, and R. Scharrer. Matlab toolbox for the comprehension of acoustic measurement and signal processing. In *Proceedings of the German Conference on Acoustics (DAGA 2010), Berlin; German Acoustical Society (DEGA)*, 2010.

[4] T. Grothe and M. Kob. Investigation of bassoon directivity. In *Proceedings of the Stockholm Music Acoustics Conference 2013, SMAC 2013, Stockholm, Sweden*, 2013.

[5] W. Hyronimus and T. Grothe. Untersuchung der Richtungsabhängigkeit der Klangfarbe des Fagotts im Anwendungskontext der Musikübertragung (examination of the directional dependence of the timbre of the bassoon with regards to applications in sound recording). In *Proceedings of the German Conference on Acoustics (DAGA 2019), Rostock; German Acoustical Society (DEGA)*, 2019.

[6] J. Meyer. *Akustik und musikalische Aufführungspraxis*. Edition Bochinsky, 1972.

[7] J. Pätynen and T. Lokki. Directivities of symphony orchestra instruments. *Acta Acustica united with Acustica*, 96(1):138–167, 2010.

[8] M. Pollow. Measuring directivities of musical instruments for auralization. In *Proceedings of the German Conference on Acoustics (NAG-DAGA 2009), Rotterdam; German Acoustical Society (DEGA)*, 2009.

[9] M. Pollow, G. Behler, and F. Schultz. Musical instrument recordings for building a directivity database. In *Proceedings of the German Conference on Acoustics (DAGA 2010), Berlin; German Acoustical Society (DEGA)*, 2010.

[10] N. R. Shabtai, G. Behler, M. Vorländer, and S. Weinzierl. Generation and analysis of an acoustic radiation pattern database for forty-one musical instruments. *The Journal of the Acoustical Society of America*, 141(2):1246–1256, 2017.

[11] S. Weinzierl, M. Vorländer, G. Behler, F. Brinkmann, H. von Coler, E. Detzner, J. Krämer, A. Lindau, M. Pollow, F. Schulz, et al. A database of anechoic microphone array measurements of musical instruments, 2017.

PROCEEDINGS of ISMA 2019
International Symposium on Music Acoustics

13 - 17 September 2019 in Detmold, Germany

Study of the effect of acoustic sound bridges on wind instruments: Perceptual study with a panel of trumpet players

Jean-François PETIOT

LS2N, UMR CNRS 6004, Ecole Centrale de Nantes, France, Jean-Francois.Petiot@ec-nantes.fr

Abstract

The study of the quality of a musical instrument, as perceived by the musician, is a complex problem. Many subtle phenomena are involved and several devices, or materials, are proposed to musicians, with a noticeable commercial success for some of them. We are interested in a particular device: sound bridges for wind instruments (made of two plates, clipped at a joint of a wind instrument with a rubber band). The objective of the work is to study if audible differences, due to the presence of the sound bridges, can be highlighted during trumpet playing. An ABX test was carried out with a panel of 5 skilled trumpet players with various status (from amateur to professional) and various use degrees of the bridges in their practice (from always to not-user). After a training phase, musicians were blinded and asked to answer to several repetitions of an ABX test in free playing conditions. Results were analyzed with the binomial distribution and the Signal Detection Theory (SDT). In addition, several repetitions of different notes were blind recorded with and without the bridges. A spectral analysis was carried out to test whether or not a significant effect of the acoustic bridges can be highlighted.

Keywords: sound quality, blind test, ABX test

1 INTRODUCTION

The high degree of performance required to professional musicians leads them to continuously try to improve the quality of their instrument, together with a relative ease of playing. Different materials [1], mouthpieces [1w], additional devices [2w] are proposed to help them to improve the tonal quality of their instrument. Several years ago, acoustic bridges [2w] were developed for wind instruments. They are made of two plates, clipped with a rubber band. According to the maker, these bridges must be placed at a joint of a wind instrument. "*They acoustically connect the sections of your wind instrument, combining the benefits of both. The result is an unequaled improvement of your sound quality: purer overtones, accurate tuning, clear response, smooth intervals, extended dynamics, surround projection" [2w].* From a scientific point of view, the functioning of such bridges is very intriguing but few documented. It seems that they modify the wall vibrations at the connection between different parts of the instrument, but explanations are rather laconic and unclear. Despite their uncontestable commercial success, there are very few scientific studies on the effect of these sound bridges on the acoustical qualities of musical instruments. The only work that deserves to be cited concerns a spectral analysis of the effect of bridges on the sound of a piccolo flute, played by a musician [3w]. The authors present a spectral analysis of steady state piccolo sounds, and compare the spectra. They claim that difference observed between the spectra are due to the presence of the bridges, and that the spectral centroid of the instrument increases with the presence of the bridges. But the conclusions presented in [3w] are worthless for at least two reasons:

- The player is aware of the condition played (with or without the bridges) for the recording of the sounds. On the contrary, the player should be blindfolded, ignoring which condition he/she plays (with or without the bridges). This is imperative to prevent the player adjusting his/her playing with respect to the experimental condition,
- No statistical analysis is provided on the magnitude of the differences observed between the spectra w.r.t. the experimental error (repeatability error). This analysis is also imperative, a perfect repeatability of a real musician in the playing of a note being totally impossible.

In view of the multiple discussions present on the Internet about these bridges, and their adoption by many skilled musicians (and also their students), we decided to start an impartial study on the effect of these bridges. We are of course aware that things may become quickly very complex when one tackles the problem of the subtle interactions between a musician and his/her instrument. Before any study, we suspect that a main effect, the *placebo* effect, is certainly very important in the perception of musicians. We are not studying this effect in this paper: we concentrate on stable effects that can be measured, justified with physical measurements, and highlighted with a scientific experimental protocol. For this reason, this study uses a statistical approach with blindfolded musicians.

The objective of this paper is to determine whether a significant effect of the presence of the bridges can be highlighted during Bb trumpet playing. Section 2 presents the material and methods used for the test. Section 3 presents the results of the tests and conclusions are drawn in section 4. In the reminder of the paper, the acoustic sound bridges are simply called "the bridges".

2 MATERIAL AND METHODS

2.1 Acoustic sound bridges for the trumpet

A picture of the sound bridges for a trumpet is presented figure 1 (left). The bridges consist of two curved metallic plates, clipped between the mouthpiece and the receiver with a rubber band [2w]. The bridges were set on the trumpet as recommended on the website. Two acoustic sound bridges were used: a 33mm red brass, and a 33mm gold (provided by one of the musicians of our panel).

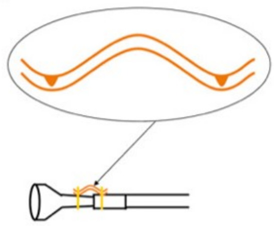

Figure 1. (left): Assembly of the bridges on the mouthpiece of the trumpet. (right): Trumpet player performing an ABX blind test of the bridges in free playing conditions

2.2 Recordings with a musician

Using the same mouthpiece (Yamaha 15C4), and the same trumpet (Yamaha, model *6335*), P = 9 repetitions of the same note (Bb4) were recorded with the same musician. The musician was blindfolded for all the recordings. All the recordings (sampling frequency 192 000Hz, 16 bits) were made in the same room (recording studio) with an *APEX 191* microphone. The microphone was placed in the axis of the bell (distance = 10 cm) and connected to the preamplifier and a *Digigram* Vx pocket V2 soundcard. The position of the tuning slide was the same for all the recordings. In order to limit as much as possible the variability inherent to the musician, he was asked to play the note in a given dynamic (mezzo forte), without vibrato and with an as stable as possible way. The duration of each note was about 3 seconds, two series of 9 notes being recorded, one with the bridges, and one without the bridges.

The sounds were next windowed to suppress the transient part of the signal, and standardized with their RMS pressure. With the remaining part of the signal (considered as the permanent regime), a spectral analysis was made (FFT) to extract the amplitude of the different harmonics. For each experimental condition (with or without the bridges), an average spectrum was computed by averaging the magnitude of the spectra for the 9 repetitions, as well as the average amplitudes of the 10 first harmonics and their standard deviation. To compare the differences between the amplitude peaks, a permutation test was used to test the difference between the average values for the 10 first harmonics [2].

2.3 Participants to the perceptual test

Five musicians participated to the perceptual test. They were all regular trumpet players, since more than 10 years. All of them knew the existence of these bridges, some of them having their own. The main characteristics of the participants of the test concerning their trumpet playing are given in table 2. Musician M3 used the gold bridges for the test, whereas the other musicians used the red brass.

2.4 ABX test

2.4.1 Procedure

The ABX test is a common test in the audio engineering community. It is used in studies of auditory perception and discrimination [3] mainly to determine if an audible difference exists between two stimuli A and B. After a listening of the two stimuli A and B, a stimulus “X” (randomly chosen between A or B) is presented to the participant. The task of the listener is to identify whether stimulus X is A (X = A), or B (X = B). To increase the confidence in the decision, several repetitions of the ABX presentations to the same participant are required. In each round of tests, a minimum of 10 listening trials is generally required, whereas the maximum number of repetitions does not generally exceed 30, to not fatigue the listener. The ABX test relies on the short-term memory of the participant, and to conscious differences.

In our test, the objective is to determine if the differences in the playing of the trumpet with or without the bridges are perceptible by the player. The two stimuli A and B correspond respectively to the presence of the bridges on the trumpet mouthpiece (A) and the absence of the bridges (B). The experiment made was simple-blinded (the experimenter, who set the bridges on the trumpet, was aware of the condition X presented to the participant (we assume a double-blinded test was not necessary, given that the experimenter stayed salient during the experiment – the time for preparing the condition A or B was the same whatever the condition). The following stages were defined for the progress of the test:

- **Welcome**: the participant is informed about the objective of the test and basic explanations on an ABX task are provided,
- **Training phase** (30mn): the participant is invited to play freely his/her own trumpet and mouthpiece with or without the bridges. Feedbacks of the participant about the possible effect of the bridges are recorded by the experimenter,
- **ABX test** (40mn) (Cf. figure 1 right): the participant is blindfolded during all the stage. N = 20 successive repetitions of the ABX presentations are proposed to the participant. The bridges are set to the instrument by the experimenter. Each presentation includes the following stages:
  - Presentation of the condition A = with the bridges. The participant is informed, and asked to play freely the trumpet,
  - Presentation of the condition B = without the bridges. The participant is informed, and asked to play freely the trumpet,
  - Presentation of the condition X (with a random assignment of A or B to X). The participant is asked to play freely the trumpet, and to make a decision, A, or B. No time limit is imposed for the decision. The experimenters paid particular attention to the fact that the participant did not touch the mouthpiece (and of course the bridges) during the free playing phase.
- **Debriefing** (10mn): Blindfold is removed. Discussion with the participant about the test, and feedbacks are recorded by the experimenter.

At the end of the test, the confusion matrix of each participant is built (table 1). It summarizes the results of the N = 20 ABX presentations.

Table 1. Confusion matrix of an ABX test

Stimulus/response	Response “A”	Response “B”
X = A (with bridges)	True positive (HA)	Omission (FB)
X = B (without bridges)	False alarm (FA)	True Negative (HB)

Several performance indexes can be computed from the confusion matrix. The percentage of correct responses, *p(C)*, is given by:

$$p(C) = \frac{HA + HB}{HA + HB + FA + FB} \quad (1)$$

The sensitivity *Se* represents the subjects’ ability to detect the presence of the bridges, while the specificity *Sp* represents the subjects’ ability to detect its absence.

$$Se = \frac{HA}{HA + FB} \quad (2)$$

$$Sp = \frac{HB}{HB + FA} \quad (3)$$

2.4.2 Statistical analysis

2.4.1.1 Binomial distribution

The first way to analyze the results of an ABX test is to use a simple application of the binomial distribution to determine a probability to obtain such results by chance. The principle is to consider that the response of the participant is random (A or B, with probability = 0.5) when no difference is detected. It corresponds to a Bernoulli trial (random experiment with exactly to possible outcomes; success and failure). The discrete probability distribution of the number of successes in a sequence of N trials corresponds to the binomial distribution. Under the assumptions of random guesses of the participant along the test, a p-value can be calculated with the number of successes, the number of trials, and the binomial distribution. This p-value corresponds to the probability of randomly getting a number of successes at least higher than the one obtained, in the same conditions. A 5% threshold is generally considered for the p-value. In summary, the outcomes of the test are as follows:

- If p-value ≥ 5%: the test is not significant (the probability to obtain such results by chance is too important). Conclusion: there is no significant perceptual difference between A and B. It is important to mention here that this does not signify that there is no difference between A and B. It only signify that the differences can be so weak that they cannot be highlighted with the ABX test carried out,
- If p-value < 5%: the test is significant. There is a significant perceptual difference between A and B

Some assumptions are needed to employ the binomial distribution

- the distribution of the correct answer X = A and X = B is random throughout the test
- the N trials must be N independent experiments. This assumptions is debatable, the same participant is doing the experiment, subjected to learning effect or fatigue
- when the participant is unable to identify the correct answer, the response is random. This assumption

is also highly debatable: possible response biases of participants can occur (the participant can e.g. always respond A when he/she is unsure).

For these reasons, a more robust analysis of ABX tests can be done with signal detection theory [3]. It allows the distinction between sensitivity (the ability of an observer to reflect a stimulus–response correspondence defined by the experimenter) from response bias (the tendency to favor one response (A or B) over the other).

2.4.1.2 Signal detection theory

The results of confusion matrices can be represented with a common plot in signal detection theory, the ROC plot (Receiver Operating Characteristic) [4]. This graphical plot represents the sensitivity *Se* (true positive rate) according to (1-specificity) (1-*Sp*), i.e. the false positive rate. Each confusion matrix is represented by a point in the ROC space. A perfect detection is represented by the (0, 1) point, and a random detection is located along the diagonal line ($p(C) = 0.5$ – line of no discrimination). The relevance of the discrimination can be assessed on this plot by the distance of the point above the diagonal: the greater this distance, the more relevant the discrimination. To qualify the performance in the detection relatively to random choices, an independence test using the Binomial Distribution is proposed [5]. From the Binomial Distribution, with a specific number of trials, and an observed number of correct identifications, a 95% confidence threshold can be calculated for the sensitivity (lower bound) and for (1- specificity) (upper bound). These limits are indicators helping to estimate the musicians' reliability.

In addition to ROC curves, it is possible to calculate an index, *d'*, that allows the separation of sensitivity (ability to discriminate between A and B) from bias (conservative or liberal response, favoring A or B when the participant is unsure) [3]. The principle is to consider that the detection between two stimuli A and B is presented along some sensory continuum. The decision between A and B is represented by two distributions, supposed normal. From the confusion matrix of an ABX experiment, the hit rate and false detection are used to estimate the relative location of these two distributions. Two classical measurements are computed to characterize the detection: the sensitivity index, *d'*, that measures the distance between the means of the two distributions A and B in standard deviation units, and the bias, *c*, that represents the tendency to favor one response (A or B) over the other.

In our experiment, we assume that the decision strategy of the participant is similar to a yes/no experiment (yes: bridges are present; no: bridges are absent – we do not consider the independent-observations or the difference decision strategies that are relevant for true ABX tests [6]). The sensitivity index *d'* and bias *c* are given by:

$$d' = z(HA) - z(FA) = z(HB) - z(FB) \tag{4}$$

$$c = \frac{z(HA) + z(FA)}{-2} = \frac{z(HB) + z(FB)}{2} \tag{5}$$

Where z represents the z-score ($z(x) = \phi^{-1}(x)$: inverse normal cumulative distribution function).

A value of 0 for *d'* indicates an inability to distinguish signals from noise (A from B), whereas larger (positive) values indicate a correspondingly greater ability to distinguish between A and B.

SDT states that *d'* is unaffected by response bias (i.e., is a pure measure of sensitivity) if two assumptions are met regarding the decision variable: (1) The signal and noise distributions are both normal, and (2) the signal and noise distributions have the same standard deviation. We consider that these assumptions are valid.

A standard deviation σ can be calculated for *d'*, given by [3] [7]:

$$\sigma^2(d') = \left(\frac{HA(1-HA)}{(\frac{N}{2}).(\varphi(HA))^2} \right) + \left(\frac{FA(1-FA)}{(\frac{N}{2}).(\varphi(FA))^2} \right) \quad (6)$$

Where φ is the probability density function of the standard normal distribution

From the standard deviation σ, a 95% confidence interval CI can be computed for *d'* with $CI = \pm 1{,}96.\sigma$.

3 RESULTS

3.1 Binomial distribution

The analysis of the results of the ABX test with the binomial distribution is given in table 2. For all the musicians, the percentage of correct responses is always lower than 70% (14/20). The results are not significant at the 5% level (p-values greater than 5%). The p-value being greater than 5%, we cannot reject the assumption that the participants were merely guessing. Therefore, we can conclude that the effect of the presence of the bridges on the perception of trumpet player is not significant at the 5% level. Nevertheless, two musicians, M1 and M2, obtained high ratio of correct answer (70%), even if not significant. Investigations should be carried out to confirm whether these relatively high ratios of correct answer are stable or not, with slightly different conditions of the test.

Table 2. Results of the ABX test (Ratio of correct answer and p-value w.r.t. the binomial distribution) for the five musicians M1 to M5.

Name	Years of practice	Main practice	Level	Degree of familiarization	% Correct answer p(C)	p-value (P(X>s))
M1	>10	Brass band	Adv. amateur	Occasional user	70% (14/20)	5.8% (n.s.)
M2	> 30	Brass/big band symphonic orchestra	Professional	Non user	70% (14/20)	5.8% (n.s.)
M3	> 40	Symphonic orchestra	Professional	Daily user	40% (8/20)	87% (n.s.)
M4	> 10	Brass band/big band	Amateur	Occasional user	40% (8/20)	87% (n.s.)
M5	> 45	Big band/jazz combos	Adv. amateur	Non user	60% (12/20)	25% (n.s.)

It is important to mention that there is no correlation between the performance of the participants to the test and their habit of use of the bridges, or their overall level: the daily user of bridges (M3) got the lowest ratio, whereas one non-user (M2) obtained the highest score.

3.2 ROC (receiver-operating characteristics) analysis

The locations of the five musicians in the ROC space are given in figure 2.

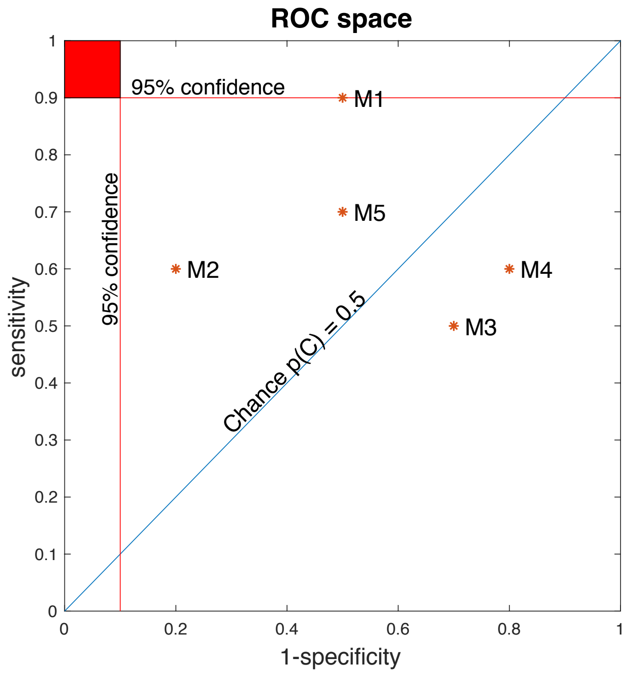

Figure 2. Locations of the five musicians in the ROC space

Musician M1, M2 and M5 are slightly above chance for the detection of the bridges. Musician M1 obtained the best sensitivity (Se = 0.9) but the false alarm rate (1-specificity) is important (0.5). This is because he favored the response “A” in the ABX test. Musician M2 obtained a low false alarm rate (0.2) but he is not very sensitive in the detection (Se = 0.6). Musician M3 and M4 are slightly under the chance line, due to too many reverse decisions in the ABX test. A musician with a perfect detection of the bridges should locate in the upper left corner of the ROC space (coordinates (0,1)). To be significant at the 95% level, the musician should locate in the red square in the upper left corner. As a conclusion, the detection of the bridges is not significant for none of the musicians.

3.3 Signal detection theory

The analysis of the test with the SDT gives the results presented in table 3. They confirm the previous results: even if the values of *d’* are greater than 1 for some musicians (M1, M2), the confidence intervals include the value “0” and do not allow one’s to conclude to a significant detection of the bridges.

Table 3. Results of the ABX test according to sensitivity index *d'* and bias *c*

Name	Sensitivity index *d'* and 95% Confidence interval	Bias *c*	Conclusion
M1	1.28 ± 1.31	0.64	Average sensitivity. Important bias (in favor of the "A" response). Confidence interval include "0": detection not significant
M2	1.09 ± 1.18	-0.29	Average sensitivity. Bias in favor of the "B" response Confidence interval include "0": detection not significant
M3	-0.52 ± 1.12	0.26	Low sensitivity (d' negative). Bias in favor of the "A" response Confidence interval include "0": detection not significant
M4	-0.58 ± 1.18	0,55	Low sensitivity (d' negative). Bias in favor of the "A" response Confidence interval include "0": detection not significant
M5	0.52 ± 1.12	0.26	Average sensitivity. Bias in favor of the "A" response Confidence interval include "0": detection not significant

3.4 Spectral analysis

The average spectra for the two conditions (with and without bridges) for the note Bb4 of the trumpet are given in figure 3 (left). No noticeable difference can be highlighted between the average spectra: the variations are weak and probably due to the variability of the musician.

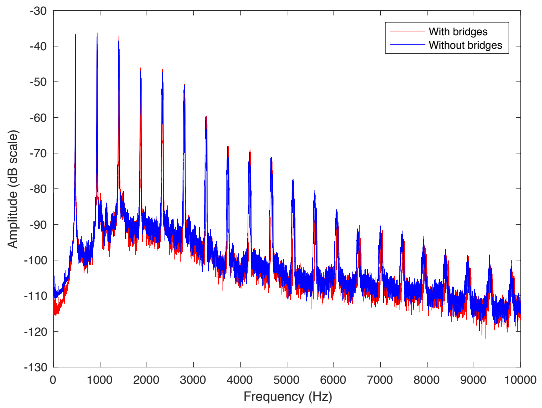

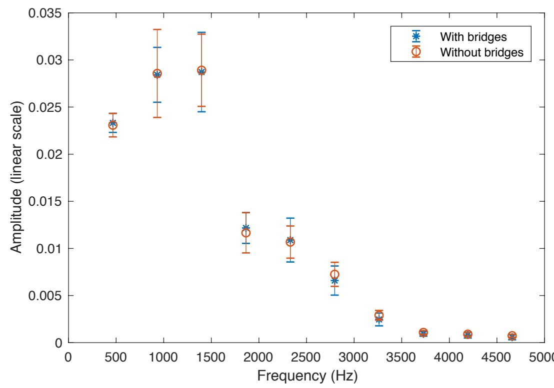

Figure 3. (left): Average spectra with and without the bridges of the note Bb4 – (right): Average amplitude and standard deviation of the 10 first harmonics of the note Bb4

To study statistically the difference between the spectra, the average amplitude of the ten first harmonics, with their standard deviation, are given in figure 3 (right). A permutation test, presented in table 5, confirms that none of the difference between the average values of the amplitudes of the harmonics is significant.

Table 5. p-value of the permutation test for the differences between the average values of the harmonics amplitude

Harmonics n°	1	2	3	4	5	6	7	8	9	10
p-value	0.67	0.94	0.92	0.60	0.83	0.38	0.17	0.20	0.51	0.20

4 CONCLUSIONS

The main conclusion of this work is that with the ABX test carried out, the experimental conditions (free playing on his/her own trumpet) and the panel of 5 musicians, there is no significant effect of the presence of the bridges on the perception of the trumpet players. Similarly, the spectral analysis of sound in permanent regime did not allow the highlighting of significant difference between the sounds, with or without the bridges.

If there is an effect of these bridges on the acoustics of the trumpet, and on the perception of the musician, it is weak, very difficult to highlight. It is important to mention here that the ABX test carried out does not prove that there is no effect of the bridges: these perceptual tests can only prove differences between stimuli, not prove that there is no difference. Other tests, with different experimental conditions, could be organized to try to highlight in a scientific way the effect of the bridges. Nevertheless, for at least two musicians (M1 and M2), the results of the ABX tests are relatively close to significance. This should ask questions about the cues used by the musicians to make their decision. On this subject, things are unclear: one of them reported an easiness in the playing of the high range with the bridges, while the other reported a brighter sound. This refers to the scientific explanations on the functioning of the bridges, which are flimsy for the moment, from an acoustical point of view. The explanations presented on the Internet are not scientifically valid, and no clear explanation on the physical principles used by the bridges is provided. This could be the topic of another paper.

ACKNOWLEDGEMENTS

Acknowledgments to Camille Berlizot and Marie Thibeaud of the specialization “Science and Music” of Ecole Centrale Nantes who led the perceptual tests. The author would also warmly thank the trumpet players (Emilie Boudou, Florent Buisson, Jean-Marie Cousinié, Eric Mussotte) who took part in the perceptual tests with great care and patience. Thank to Dominique Brisson from the music shop *DB Musique Service* (44400 Rezé, France) for lending different acoustic bridges.

This research was financed by public founds and is totally independent of any commercial company.

REFERENCES

[1] Smith R. The effect of material in brass instruments: a review. Proceedings of the Institute of Acoustics. Vol. 8, Part 1, pp 91-96, 1986.

[2] Good, Phillip. Permutation tests. A practical guide to resampling methods for testing hypotheses. Springer series in Statistics, 2000.

[3] Macmillan, N.A; Creelman, C.D. Detection Theory: A User’s Guide. Second edition. LEA Publishers, Mahwah, New Jersey, Erlbaum, 2005.

[4] Mahony M.; Hautus, M.J. The signal detection theory ROC curve. Some applications in food sensory science. Journal of Sensory Studies 23, 2008, 614-621.

[5] Boley, J; Lester, M. Statistical Analysis of ABX Results Using Signal Detection Theory. Convention paper Audio Engineering Society, 127th Convention, 2009.

[6] Hautus, M. J.; Meng, X. Decision strategies in the ABX (matching-to-sample) psychophysical task. Perception & Psychophysics, 2002, 64, 89-106.

[7] Miller, J.O. The sampling distribution of d’. Perception &Psychophysics, 1996, 58,65-72.

[1w] https://www.syos.co/fr. Internet page of the SYOS company. Customization of saxophone mouthpieces. Last visited June 19, 2019.

[2w] https://www.lefreque.com. Web site of a seller of acoustic bridges. Last visited June 19, 2019.

[3w] https://www.lefreque.com/how-to-use/spectral-analysis: Research conducted by the Department of Applied Physics and the Centre for Physical Technology (Acoustics, Materials and Astrophysics) from the Polytechnic University of Valencia (Spain) of Valencia, (Spain). Last visited June 19, 2019.

PROCEEDINGS of ISMA 2019
International Symposium on Music Acoustics

13 - 17 September 2019 in Detmold, Germany

How the directivity of bundengan affects its musical performance

Indraswari KUSUMANINGTYAS[1]; Raymond CHRISTIANTO[2]; Gea O.F. PARIKESIT[2], Rosie H. COOK[3], Muhammad S. ABDULLOH[4], Luqmanul CHAKIM[4], Mulyani MOELYA[5], Nicole A. TSE[6], Margaret J. KARTOMI[7], G.R. Lono L. SIMATUPANG[8]

(1) Dept. Mechanical & Industrial Eng., Universitas Gadjah Mada, Yogyakarta, Indonesia, i.kusumaningtyas@ugm.ac.id
(2) Dept. Nuclear Eng. & Eng. Physics, Universitas Gadjah Mada, Yogyakarta, Indonesia
(3) Conservation Center, Cheng Shiu University, Kaohsiung City, Taiwan
(4) Woohoo Art-Space, Rowopeni, Kalianget, Wonosobo, Indonesia
(5) SMPN 2 Selomerto, Kalierang, Selomerto, Wonosobo, Indonesia
(6) Grimwade Centre for Cultural Materials Conservation, University of Melbourne, Carlton, VIC, Australia
(7) Music Archive of Monash University, Clayton, VIC, Australia
(8) Performing Arts and Visual Arts Studies, Universitas Gadjah Mada, Yogyakarta, Indonesia

Abstract

Bundengan is a traditional musical instrument from Indonesia that has a half-dome structure, and uses clipped strings and long, thin bamboo plates to generate metal-like and drum-like sounds, respectively. The physics of the clipped strings have been unraveled, but the interaction between the strings and the half-dome resonator has been largely unknown. In this work, we investigate this interaction, particularly by measuring the directivity of the bundengan as the string vibrations are amplified by the resonator. We performed two sets of measurements, where a number of bundengans were played by traditional and contemporary artists, respectively. This quantitative data complement our interviews with, and qualitative observations on, the artists to provide a comprehensive insight on how the directivity affects the musical performance of the bundengan. Our results show that the directivity patterns of different bundengans are generally similar, although the detailed characteristics have variances. This is mainly due to the traditional, unstandardized, manufacturing method of the bundengans by different craftsmen. The interaction of the string and the resonator creates a directivity pattern that is unique from the vibrating string displacement or the resonator shape. These findings allow bundengan makers and players to make improvements to enhance the instrument's musical performance.

Keywords: Bundengan, Directivity, Performance.

1 i.kusumaningtyas@ugm.ac.id

PROCEEDINGS of ISMA 2019
International Symposium on Music Acoustics

13 - 17 September 2019 in Detmold, Germany

Feasibility study of computational environment for assisting musical instrument manufacturing

Guilherme ORELLI PAIVA[1]; Rodolfo THOMAZELLI[2]; Guilherme NISHINO FONTEBASSO[3]; Lucas EGIDIO[4]

(1) Turbonius R&D, Brazil, pitupaiva@gmail.com

(2) Turbonius R&D, Brazil, rodolfo.thomazelli@gmail.com

(3) School of Mechanical Engineering, University of Campinas, Brazil, guilhermenishifonte@gmail.com

(4) School of Mechanical Engineering, University of Campinas, Brazil, lucasegidio1@gmail.com

Abstract

The musical instruments manufacturing requires several project demands related to the instrument structural capacity and to the desired aesthetic and sound attributes. Although technologies to support these projects have been available for at least two decades, most of what has been done is the empirical reproduction of consolidated models, which hinders innovations since it is often based on trial and error methods. Computational tools, therefore, are useful because they may provide a certain prediction level of the instrument structural behavior and its sound, leading to time and costs reduction in the instrument project. In this context, the Urutau project is emerging as a computational enviroment for assisting musical instrument manufacturers. This work presents a preliminary architecture of the Urutau enviroment as well as an objective validation study of its simulation tools. Initially, a simplified monochord is built and its corresponding CAD model is obtained. A finite element modal analysis is then performed and results are compared with experimental data. A physical modelling based on a modal approach is applied to generate a set of monochord synthesized sounds which are compared objectively to captured real sounds.

Keywords: Sound synthesis, virtual prototyping, physical modelling

PROCEEDINGS of ISMA 2019
International Symposium on Music Acoustics

13 - 17 September 2019 in Detmold, Germany

Damping of waves at the walls of a conical tube

Cornelis J. NEDERVEEN[1]; Timo GROTHE[2]; and Johannes BAUMGART[3]

(1) Acacialaan 20, 2641AC Pijnacker, The Netherlands
(2) Hochschule für Musik Detmold Neustadt 22, 32756 Detmold, Germany
(3) Dresden, Germany

Abstract

Resonators of reed wind instruments are tubular ducts with one open and one closed end. The ratio of pressure response to flow excitation at the closed end is the input impedance. Resonance frequencies of the duct are near to peaks in the impedance spectrum. Damping due to visco-thermal effects at the walls influences the frequency and the magnitude of the impedance-spectrum peaks, which influence intonation, playing behaviour and timbre. For cylindrical instruments theory to account for wall losses is available and experimentally confirmed. The wave equation in a conical tube while accounting for dissipative effects at the walls appears to be complicated. Four approximative solutions are compared: (1) Nederveen (1969) presented an approximate analytical solution while neglecting some higher order terms. (2) a transmission line method mimicking the conical pipe as a series of short conical (or cylindrical) pipes, (3) directly solving the equation with a Runge-Kutta procedure, (4) applying a finite difference method. For a "simplified bassoon" (a perfect cone of 3000 mm length, input diameter 4.2 mm, output diameter 46.9 mm) the four methods give different results. Measurements are planned, but the narrow tube entrance and smoothness requirements make a high accuracy difficult. Suggestions are welcome.

1 cjnederv@xs4all
2 grothe@hfm-detmold.de
3 research@johannes-baumgart.eu

PROCEEDINGS of ISMA 2019
International Symposium on Music Acoustics

13 - 17 September 2019 in Detmold, Germany

Non-linearities of the mechano-electrical tonegenerator of the Hammond organ *†

Malte Münster[(1)], Florian Pfeifle[(2)]

[(1)]Institute for Systematic Musicology; University of Hamburg, Germany, malte.muenster@uni-hamburg.de 1

[(2)]Institute for of Systematic Musicology; University of Hamburg, Germany, florian.pfeifle@uni-hamburg.de 2

Abstract

The Hammond Organ with its electro-magnetic generator is still a standard instrument in the western music world. The organ still fulfils musicians' demand for a distinctive sonic identity with intuitive control of some arbitrary parameters. Bequeathed a heritage of some hundreds of thousands of tonewheel organs to the world, most of them still in service since the original manufacturer went out of business. The worldwide organ scene remains a vibrant community. A description of the tone production mechanism is presented based on measurements of a pre-war Model A. The survey includes high-speed camera measurement and tracking of the generator as well as oscilloscope recordings of single pickups. Some properties emerge due to the interaction of the mechanical motion of interaction with the magnetic B-H-field. A FEM model of the geometry shows accordance with the proposed effects. A FDM-model is written and a more complex physical model having a special regard on the geometry and electronic parts of the sound production mechanism.

Keywords: Sound, Music, Acoustics

1 INTRODUCTION

Following the publication of the Wurlitzer and the Rhodes E-Pianos at ISMA 2014, we have a closer look at the unique Hammond Organ with electro-magnetic sound production. It is one of the remaining standard musical instruments in the western world of Jazz-, Rock-, Funk-, Soul-, Gospel-, Reggae-Music and related genres. This can be attributed to its specific mechanical-electromagnetic tone production, key mechanism, wiring, lead dress and amplification/speaker-system. The Hammond Organ still fulfils the musicians' demand for assertiveness and a distinctive sonic identity in some ways, never reached by any other electronic-, sampler-keyboard. Even newer physical-, or PCM-based models struggle with an adequate reproduction. Every decade since the original manufacturer went out of business in 1986, experienced a revival of the original instrument, bequeathed a heritage of some hundreds of thousands of tonewheel organs to the world, most of them are still in service at home, in studios and on stage. Original spare parts and professional service are still available.

In this survey, a description of the outstanding tone production mechanism is presented based on measurements taken on a Hammond Model A built in 1938. The measurements include high-speed camera measurement and tracking of the tonewheel generator. In the case of the Hammond Organ, characteristic sound properties emerge due to the interaction of the mechanical motion of up to 91 small ferromagnetic, toothed wheels interacting with the magnetic H-field of their respective pick-up. Non-linear crosstalk effects like leakage between wheels, changing the complexion of harmonics are descried. The measurements are compared to a FEM model of the respective geometry showing accordance with the proposed effects. A simplified FDM-model is written along with a physical model having a special regard to the geometry and electronic parts of the sound production mechanism.

2 STATE OF RESEARCH

Besides a deeply involved community organised in organ clubs, blogs and forums around the world, few scientific research is done since pre-war era.

*malte.muenster@uni-hamburg.de
†florian.pfeifle@uni-hamburg.de

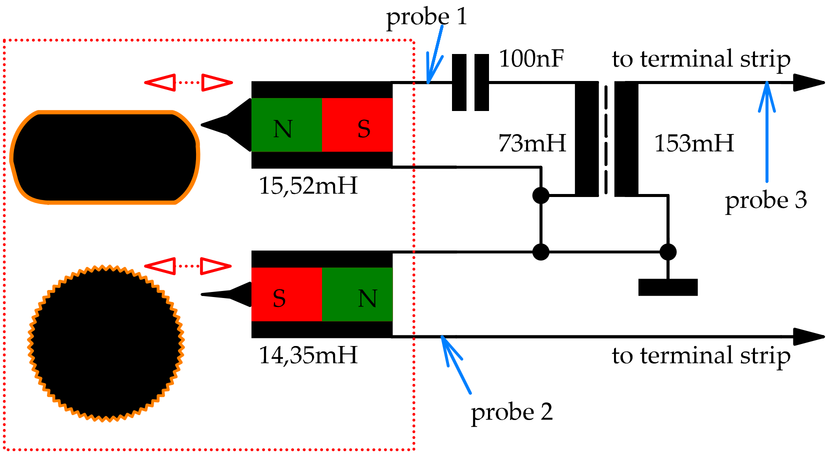

Figure 1. Probe position and some data of a pair of tonewheel 9 of G#0 and 57 of G#4 with pickup and filter attached.

A waveguide filter model of the Hammond organ vibrato/chorus has been build by Werner, Dunkel and Germain. The LC ladder-filter is modeled by using the Wave Digital Filter formalism to introduce their approach to resolving multiple nonadaptable linear elements at the root of a WDF tree. [21]

Werner and Abel describe audio effects emulating the response characteristics of the organ to process audio signals. [22] Savage refined the effects processor. He focused on emulating induced crosstalk between tonewheels. Filtering adds a frequency-dependent tremolo effect to the sound. [19].

Moro, McPherson and Sandler studied the key mechanism. A ninefold lamellar switch toggles the dialed harmonics by pressing a key. The inconsistancy of the switch-mechanism is ultimately responsible for generating the transient by adding a "chiff"-noise to the sound. This can be influenced by key velocity to a certain extend. [17]

A complete model of the tone-production is proposed by Pekonen, Pihlajamäki and Välimäki. An additive computational sythesis of the simplified tone-generator is discussed. A model of the obligatory rotating Leslie-speaker by time-varying specrtal delay filters is also shown. [18]

3 HISTORY OF ELECTRONIC INSTRUMENTS WITH ROTATING DISCS

The most simplest way to produce a low frequency signal is to chop direct current. According to a principle proposed by Karl Ochs, the Rangertone Organ has been introduced by Richard H. Ranger in 1931. 24 rotating electrical choppers with different numbers of teeth matching semitones of two octaves were mounted on a common drive shaft. With additional assemblies running at rotating velocities in a ratio of 1:4:16, enough sounds are provided to build an instrument of six octaves ambit. [16]

The first attempts using profiled iron discs in front of magnet coils for musical purposes were done due to the lack of electron tubes in the late 19th century. A common device was the magneto or ring generator to find in hand-cranked telephones generating a ringing voltage to call the operator. By use of this method, the Dynamophone or Telharmonium has been build by Thaddeus Cahill. In 1906 he played concerts over the telephone network by reason of the lack of loudspeakers. In consideration of the required power, the instruments weight became tremendous around 200t. It consists of 12 multi-tone-generators providing siunsoidal voltage swings. Using an organ-like register table, different harmonics can be mixed by adding the 2nd, 3rd, 4th, 5th, 6th, 8th, 10th, 12th and, or 16th harmonics with the fundamental. Intensities were controlled by damping resistors for each harmonic. [10] [2]

Charles–Emile Hugoniot experimented with Gramme machines, using rotating toroidal inductors and multiple, adjustable pick-ups per unit. [13] [10]

The tone-generator of the Magneton by Wilhem Lenk and Rudolf Stelzhammer makes use of discs with different profiles to provide a greater range of sound colours. The Instrument has two manuals and one pedal-manual. The compass is five octaves. By using a frequency controlled motor regulator the instrument is able to be transposed. [8]

A synthesis of sounds of 100 harmonics is proposed by Harvey Fletcher. The fundamental can be chosen between $50Hz$ and $100Hz$. The highest harmonic varies therefore between $5kHz$ and $15kHz$. [12]

Electrostatic field charged pick-up rotors are developed by Leslie E.A. Bourn, for the Compton Electrone and Melotrone-Organs. Earlier experiments are done by Wien, Pose und Klein. [10] [6]

A by far larger prevalence is reached by photo-optical methods with rotating discs. The Superpiano and Welte Lichtton-Orgel are the predecessors of a wide range of phonetic instruments and theatre organs. [8] [7]

4 THE HAMMOND ORGAN

Laurens Hammond modernised, miniaturised and stabilised Cahills mechanism in his Organ and made it ready to start mass production in 1935 with big success. [1] The organ uses one profiled disc per note. They are cut to produce a sine wave-form. A lot of different sounds are possible by mixing the fundamental with overtones. The overall tuning is the equal temperament. With higher order harmonics, the overtones differ more and more from the harmonic series. The equal temperament increasingly deviates. For this reason just 8 harmonics are realised, omitting the 7'. Therefore the number of tone-wheels can be reduced. The ambit of 7 octaves is produced by 91 tone-wheels with a diameter of ca. $4cm$ each. [10]

By pressing a key the respective inductive pick-up, lengthways pointing to the edge of the tone-wheels, a switch of nine lamellar contacts is closed nearly simultaneously forming the transient[17]. Two fundamentals and seven harmonics can be mixed by nine drawbars for each manual and three for the bass-manual. A LC-filter is attached in parallel to most pick-ups. Depending on the model, the upper most octave omits these, resulting in a rich, typical squealing sound typical for the instrument. Moreover later models use harmonic foldback: the notes of the highest octave or fifth of the 3'-register and higher harmonics and the 16' sub-fundamental, depending on the model, are taken from the lower octave. [11] [20]

5 STRUCTURE OF HAMMOND ORGAN'S TONE PRODUCTION

As indicated earlier, the tone production of the Hammond organ consists of differently shaped rotating disks influencing the H-field over a magnetic pickup. By their rotation frequency and their specific shape they are able to produce differently pitched tones. According to the user's manual, the wheels have different numbers of teeth, ranging from 2 to 192. By rotating in front of a magnetic pickup they are changing their distance to the magnetic pickup and thereby influencing and changing the magnetic flux amplified by the following preamplifier. In addition to this, every tonewheel has a differently shaped pickup that influences the magnetic field in front of the pickup thereby shaping the strength of the disks influence.

In an idealised version of the instrument the shapes and the positions of the disks are approximately analytical and can be approximated using simple sinusoidal formalism. But as our measurements have shown, the position of the tonewheels in front of the magnetic pickup can vary considerably during several cycles and the distance of the disks perimeter can vary within one period.

Comparable to the pickups of the fender Rhodes, the magnetic pickups are pointy shaped thus influencing the strength of the magnetic field in front of the pickups and thereby minimizing the cross-talk between adjacent rotating disks.

A number of different pickup shapes as well as disk shapes are illustrated in Figure 2 and Figure 1.

Table 1. Number of teeth on number of discs for the measured Hammond organ.

Number of teeth	2	4	8	16	32	64	128	192
Number of discs	12	12	12	12	12	12	12	7
Notes	C0-B0	C1-B1	C2-B2	C3-B3	C4-B4	C5-B5	C6-B6	C7-F#7

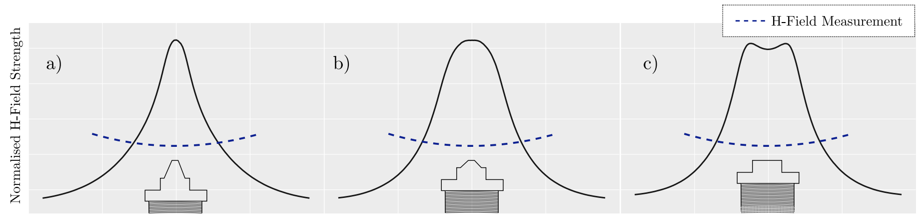

Figure 2. Magnetic field for different pickup shapes.

6 METHODS

To characterise the properties of the different components belonging to the Hammond's tone production, several measurements are performed using a high-speed camera as well as oscilloscope measurements.

6.1 Camera tracking

To qualitatively assess the motion of the tonewheels, a high-speed camera is used to record a set of two tone generation disks, one lower and one higher disks of different pairs of tonewheels. To achieve this, a *Vision Research Phantom V711* high-speed camera is used. The motion of the discs are tracked and the resulting trajectories exported, analysed and evaluated using standard signal processing software. To indicate the period of one disc revolution it is marked with a black marker at one point on its outer circumference.

An image section of a measurement is depicted in Figure 4a).

The voltage produced by the motion of the rotating disc in front of the magnetic pickup are measured with two probes at 3 points in front of the filter circuit and behind it. They are measured using a standard high resolution digital oscilloscope with measurement probes as indicated in Figure 1

6.2 Measurement Results

As is shown in Figure 4a) the tracked motion of the tonewheels are periodic with the basic revolution as well as others motions overshadowing the fundamental rotation. Due to its imperfect fixation and material defects, the measured tonewheels wobble along the x as well as the y-axis. This leads to a pronounced amplitude modulation effect in the resulting voltage as is shown in the next section. As is shown in Figure 3 the voltage induced after the pickup is approximately sine-like and has strong amplitude fluctuation due to the non-linearities in the motion of the tonewheels.

7 Intermediate Summary

The motion of the tonewheels as well as unspecified effects due magnetisation and self-magnetisation of the rotating disk, the pickup rod as well as the copper winding around the metallic core of the pickup,

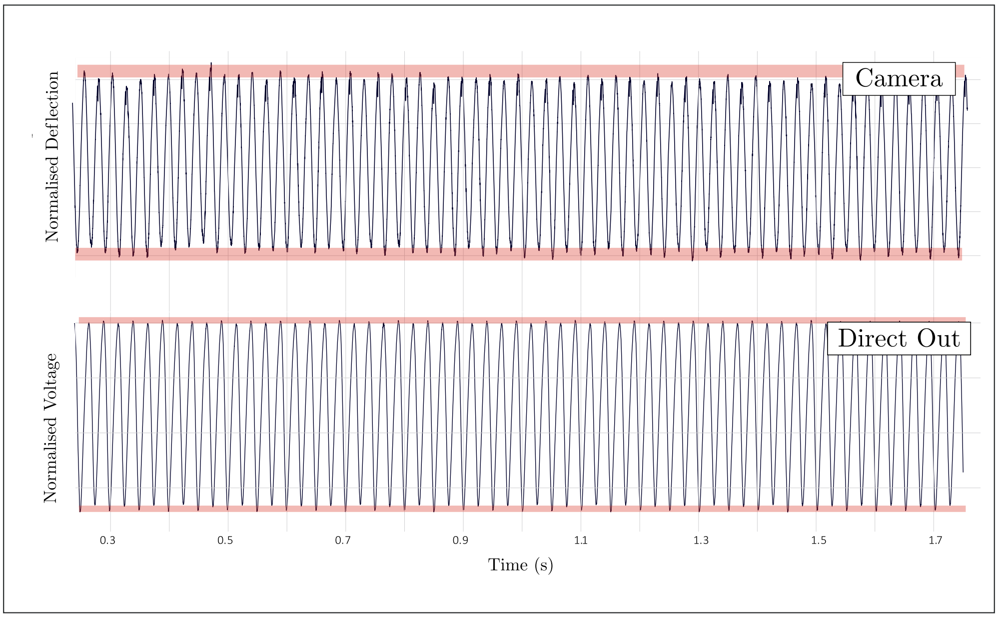

Figure 3. The upper plot shows the camera tracking of the varying distance between pickup and rotating tonewheel. The lower timeseries is the voltage recorded at position "Probe 2" as indicated above. The red bar indicates the amplitude modulation due to nonlinear effects in the motion of the tonewheel.

8 FEM-MODEL OF THE TONEWHEEL

The model is a time-depended 2D simulation of the tone-generator comprising an iron rotor and a magnetic coil forming the stator. The core of the rotating disc with 16 teeth consists of steel with iron powder coating on the edge covering the teeth. The generator rotates with a rotational velocity of $1961.25rpm$ to optain a freuquency of $523Hz$ respective the note C. The original wheel runs at $20000rpm$ to provide a C due to another diameter as measured. The model is solved in the time domain from $t = 0$ s to $t = 1$ s.

The tip of the stator consists of soft iron, which is a non-linear ferromagnetic material which saturates at high magnetic flux density. This material is preferential to provide suitable speed in change of magnetisation.It is implemented as an interpolation function of the B-H curve of the material. The center of the stator is a permanent magnet made of an AlNiCo-alloy, creating a strong magnetic field. The winding is wound around the magnet behind the tip. The copper coil winding is not part of the geometry. The edge of the rotor is covered with iron powder coating.The geometry is represented in Figure 4.

The conducting part of the stator, respectively the pick-up is modeled using Maxwell's formulation of Ampère's. Due to simulating the system under no-load condition (without the tuned bandpass filter) the Lorentz term is omitted in the PDE:

$$\sigma \frac{\partial A}{\partial t} + \nabla \times \left(\frac{1}{\mu} \nabla \times A \right) = 0 \tag{1}$$

For the non-conducting or insulating parts of the generator the magnetic flux conservation equation for the scalar magnetic potential is deployed:

$$-\nabla \left(\mu \nabla V_m - B_r \right) = 0 \tag{2}$$

Rotation is modeled using the ready-made physics interface for rotating machinery in Comsol 5.4. The rotor

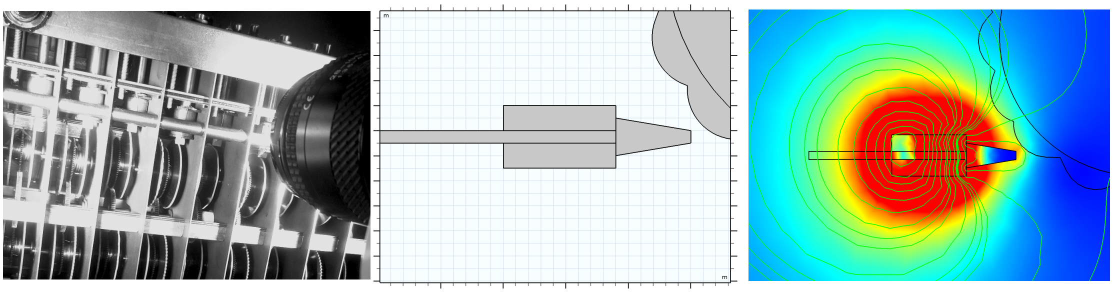

Figure 4. a) A typical setting of a high speed camera recording setup showing the Hammond's tone generator from the bottom. The rotating discs as well as the pickups are visible. b) Geometry of the fem arrangement of pickup and tonewheel. c) Magnetic flux density distribution $|B|$ ($Tesla$), and the field lines of the B field ($Weber$)

and an air-gap are modeled as rotating relative to the coordinate system of the pick-up.

The model solves for magnetic scalar potential V_m in nonconductive regions and for the magnetic vector potential A. The scalar formulation is solved by suitable transformations to the magnetic flux definitions in all domains depending on rotational velocity features, while the vector formulation is solved by Ampére's Law features. The electric scalar potential V and the magnetic vector potential A are given by the equalities: $B = \nabla \times A$ and $E = \nabla V - \frac{\partial A}{\partial t}$.

Rotation is modeled as follows: The center part of the geometry, containing the rotor and part of the air, rotates relative to the coordinate system of the stator.

The output voltage is calculated as the line integral of the E-field of the winding. It is obtained by taking the average z-component of the E-field for each winding crosssection, multiplyed by the axis-length of the stator, and taking the sum over all winding cross sections. Here L is the length of the inductor, $Trns$ the number of windings an A the surface of the winding crossection.[23]

$$V_i = Trns \sum \frac{L}{A} \int E_2 dA$$

The generated voltage in the coil winding is a sinusoidal signal. At a rotation speed of $1961.25 rpm$ the voltage has an amplitude peak of 40mV. The signal is slighly toothe. It us caused by the non-linearities of the unsteady magnetisation/demagnetisation-times and change in magnetic flux in the rotor and stator of the generator, as explained. See Figure2. They can be enforced by more cornered geometries as found in tonewheels of the lowest registers or magnetic disturbance through neighbouring tonewheels in conjunction with bandpass filters designed to reduce noise which is an unavoidable part of the sound.

9 SIMPLIFIED PHYSICAL MODEL

Comparable to the model developed in [55], the tone production of the Hammond organ can be approximated by using a periodic oscillator influencing a magnetic field having a specific distibution depending on the pickup's tip geometry. In this way, it is possible to approximate the tone production of the Hammond organ's tonewheel to a high degree of accuracy. The model developed here is based on the model from the same publication which is inspired by a model derived in [53].

The numerical model presented in present section is based on measured properties presented before, see section 6, qualitative observations on the FEM model and using measured material properties of the Hammond's tonewheel and the pickup.

Using the measurements as a ground-truth for the model leads to several assumptions that simplifies a model of

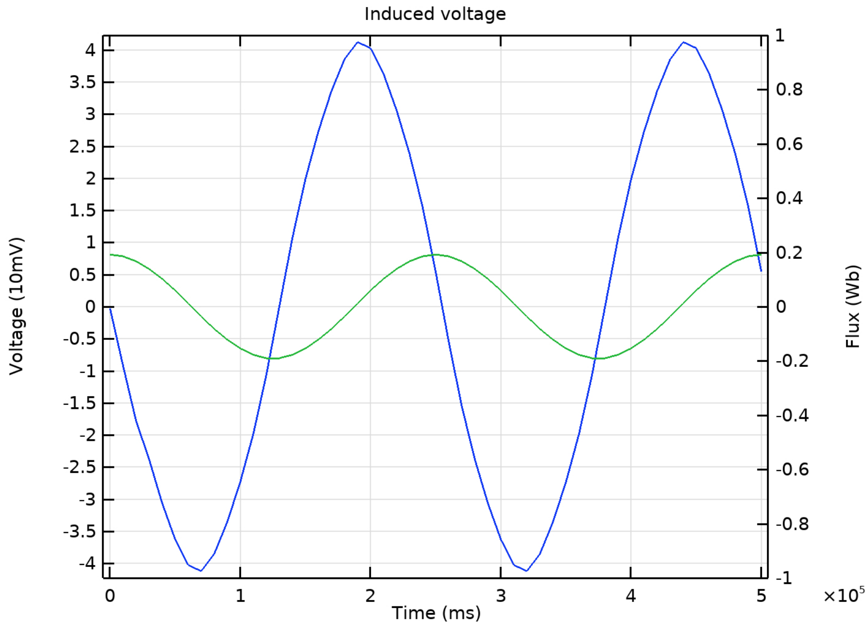

Figure 5. Voltage output swing versus change in magnetic flux in the coil

the tone production. Regardless of the introduced simplifications both models are able to capture the vibratory motion and the acoustic properties of both instruments to a high degree while minimizing computational as well as modeling complexity.

A model of both pickup systems including all physical parameters would have to take time-varying electromagnetic effects into account using Maxwell's equations for electromagnetism to describe the respective pickup mechanism in complete form. But, due to the small changes in the magnetic as well as electric fields the proposed simplifications lead to models that are able to approximate the vibratory as well as the sonic characteristics of the instruments very accurately.

9.1 Tonewheel exciter model

As shown in Figure 1 the tonewheel rotates in front of the electromagnetic pickup. As the FEM simulations, given in figure 4, show, only a small radial part of the disk is influenced by the magnetic field. Therefore, the exciter of the Hammond is modeled as an oscillating mass-point in the normal direction of the magnetic field distribution.

Using Newton's second law, the temporal evolution of a SHO can be written as a second order ordinary differential equation

$$x_{tt} = -\kappa \cdot x \tag{3}$$

with $\kappa = \frac{k}{m}$ the stiffness/springiness of the system, m the mass of the harmonic oscillator, x the deflection and the subscript by t on the left hand side indicating a second derivative in respect to time.

9.1.1 Finite difference approximation

The exciter model of the tonewheel and the magnetic pickup are discretised applying standard finite difference approximations using a symplectic Euler scheme for iteration in time. The discretisation method and the scheme are published in more detail in [48]; [47]. Applying standard FD approximations for the given problem using the operator notation given in [55] and iterating the scheme in time by using mentioned method leads to the equations

$$\begin{aligned} \delta_t v_{sho} &= -\kappa_{sho} \cdot x_{sho} - \gamma \delta t x_{sho} - F_{int} \\ \delta_t x_{sho} &= v \end{aligned} \tag{4}$$

for the SHO.

9.2 Pickup model

The electromagnetic effects of the organ's pickup system can be reduced from Maxwell's equations for transient electromagnetic effects to a more tractable formulation know as Faraday's law of induction. As shown above, the pickup consists of a magnetized steel tip and a coil wrapped permanent magnet; leaving reciprocal magnetic effects of the induced current in the coil out of our consideration, the voltage induced over the pickup is equivalent to the change of the magnetic flux in the field produced by the magnet

$$\varepsilon = -\frac{\partial \Psi_\mathbf{B}}{\partial t} \tag{5}$$

with ε the electromotive force and Ψ_B the magnetic flux due to the change in the magnetic field given by

$$\Psi_\mathbf{B} = \int \vec{B} \cdot d\vec{S} \tag{6}$$

with B the magnetic field strength integrated over surface S. Using these equalities, the induced voltage directly depends on the change of magnetic field strength which depends solely on the position of the tonewheel disturbing the field as shown in Figure 2.

The following derivation of the magnetic field distribution uses the unphysical assumption that there exist magnetic monopoles which produce a distributed magnetic field. This assumption proposes an equivalence between the efficient causes of electric fields and magnetic fields and can be used as a mathematical modeling tool, see: [53, pp. 174 ff]. As is shown in [40] this approach yields good approximations of notional magnetic induction fields produced by guitar pickups. Consisting of a plainer geometry, the tip of a guitar pickup bar magnet can be simplified to a circular, magnetically charged disc with a certain cross-section, which reduces the problem to a position-dependent integration of the field over the pickup. Due to the specific pickup geometry of the Hammond organ, a different approach is taken here to calculate the induction field strength above the tip of the magnet.

As depicted in Figure 6 our derivation makes use of several simplifying assumptions facilitating the computation.

The disc rotates in an approximate periodic motion in one horizontal plane in front of the pickup. A radial part of the disc oscillates on the trajectory of an ideal circle with the center at its fixation point. Using definition I and II, the calculation of the magnetic induction field depending on the position of the disc tip can be formulated as an integral over the lumped mass point as a centralisation of the part of the disc influencing the magnetic field.

Comparable to an electric point charge we define a magnetic point charge which produces a magnetic field given by

$$\mathbf{B} = B_0 \frac{r_{21}}{|r_{21}|^3} \tag{7}$$

with r_{21} the relative positions of the point charge and a test charge in the surrounding field. Because the magnetic flux changes only due to changes in the z direction we can reduce equation 7 to

$$\mathbf{B}_z = B_0 \frac{\Delta z}{|r_{21}|^3} \tag{8}$$

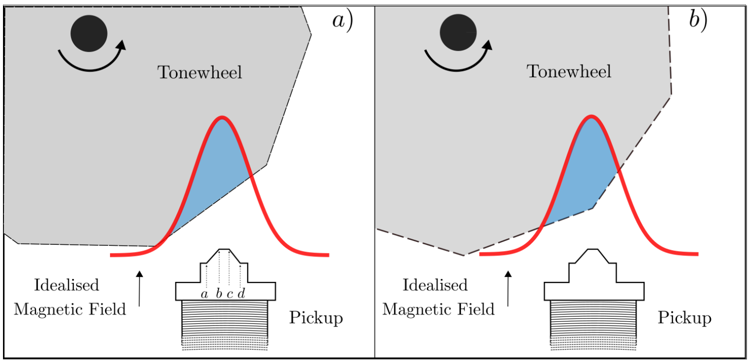

Figure 6. Simplified geometry of the pickup system and the rotating disc. The blue area indicating the influence of the magnetic field on the disc.

The magnetic field for position $(x^{'},z^{'})$ in front of the of steel tip can thus be written as a three-part integral

$$\begin{aligned}\mathbf{B}_z(x^{'},z^{'}) = |\mathbf{B}_{disc}| \quad &\cdot \quad \left[\int_a^b \frac{\sigma(z^{'}-z(x))x}{[(x^{'}-x)^2+(z^{'}-z(x))^2]^{3/2}}dx\right. \\ &+ \int_b^c \frac{\sigma(z^{'}-z_k)x}{[(x^{'}-x)^2+(z^{'}-z_k)^2]^{3/2}}dx \\ &+ \left.\int_c^d \frac{\sigma(z^{'}-z(x))x}{[(x^{'}-x)^2+(z^{'}-z(x))^2]^{3/2}}dx\right] \end{aligned} \tag{9}$$

with σ the constant magnetic charge density.
Integrating this formula for all points on a trajectory given by the position of the Hammond's tonewheel

$$\begin{aligned} z^{'} &= \mathrm{r} - \sqrt{\mathrm{r}^2-(x^{'})^2} \\ x^{'} &= \hat{\mathrm{x}} \cdot sin(2\pi f_{disc} t) \end{aligned} \tag{10}$$

with f_{disc} the fundamental frequency of the disc, leads to a magnetic potential function characterising the magnitude of relative magnetic field change.
An idealised form of the magnetic field in front of the Hammond's pickup is depicted in Figure 6**a** and 6**b**, it is comparable to the measurements results published in [40].

9.3 Modeling results

Simulation results of a model of one Hammond organ tonewheel-pickup system including measured non-linear motion of the wheel as well as the distribution of the magnetic field distribution are given on the accompanying website which can be found under `www.digitalguitarworkshop.de/ISMA2019.html`.

10 CONCLUSIONS

In this treatise a fundamental consideration of the tone production mechanisms of the Hammond organ was presented. We showed that the characteristic timbre of the instruments is due to the specific setup and geometry of the pickup systems. A simplified modeling approach for the instruments was proposed showing good accordance with the measured sounds. The model is able to run in real-time on a not-so-recent personal computer and can be parametrised for different geometries as well as different pickup designs.

This work serves as a starting point for further research regarding the electro-mechanical and acoustic properties of this family of instruments. Learning about the fundamental mechanism of this and similar instruments can help to elucidate the fact why the sound of this iconic semi-acoustic instruments is still held in such high regards among listeners and musicians.

ACKNOWLEDGEMENTS

Thanks to keyboard artist Michael Petermann for allowing us to work on his Hammond Model A, build in 1938.

CONFLICT OF INTEREST

The authors declare that they have no conflict of interest.

REFERENCES

[1] William Bagally:*The Hammond Organ.* In: Wireless World Vol. XLI. , pp.134, Iliffe & Sons Ltd., London(1937).

[2] Ray Stannard Baker:*New music for an old world - Dr.Thaddeus Cahills Dynamophone, an extraordinary electrical invention for producing scientifically perfect music*, In: Mc Clure s Magazine Vol. 27,p.201, The S.S.McClure Co., London(1906).

[3] J. Barrett: *The Hammond Electric Organ.* In: Nature Volume 139, p.1043–1044, London(1937).

[4] William. L. Barrow:*The multitone.*In: Journal of the Acoustical Society of America 10, p.275-279, (1938).

[5] Douglas E. Bush:*The Organ Enzyclopedia.* p.52, pp.122, Routledge, New York(2006).

[6] Leslie E.A. Bourne: US patent: US2579358A. (1951). Retrieved from https://patents.google.com/patent/US2579358

[7] Karl Heinz Dettke:*Kinoorgeln und Kinomusik in Deutschland.* J.P. Metzler, Weimar(1995).

[8] Peter Donhauser:*Elektrische Klangmaschinen.*p.16,51,145,223,pp. 241, Böhlau(2007).

[9] W. Ross Dunkel, Maximilian Rest, Kurt James Werner, Michael Jørgen Olsen, Julius O. Smith III:*The Fender Bassman 5F6-A Family of Preamplifier Circuits - A Wave Digital Filter Case Study.* In: Proceedings of the 19th International Conference on Digital Audio Effects (DAFx-16),Brno (2016).

[10] Werner Meyer-Eppler: *Elektrische Klangerzeugung.*, p. 108-114, Ferd. Duemmlers Verlag, Bonn (1949).

[11] *The Hammond Organ Manual for the Service Engineer.* Ed.: Joe Luca 2016, Hammond Organ Co., Chicago (1978). https://archive.org/details/HSM4952016

[12] Harvey Fletcher:*The pitch, loudness and quality of musical tones. A demonstration lecture introducing the new tone synthesizer.* In: American Journal of Physics 14, p.215-225, (1946).

[13] Charles–Emile Hugoniot: French patent FR22866 (E) 1921-09-05, (1919). Retrieved from https://patents.google.com/patent/DE345923C/

[14] Stevens Irwin:*Dictionary of Hammond-Organ Stops*, Read Books, London(2013).

[15] Earle L. Kent:*A New Electronic Musical Instrument.* In:The Journal of the Acoustical Society of America 11, p.352 (1940). https://doi.org/10.1121/1.1916046

[16] Benjamin F. Miessner:*Electronic Music and Instruments.* In:Proceedings of the institute of Radio Engineers November 1936 Volume 24, New York(1936).

[17] Giulio Moro, Andrew P. McPherson, and Mark B. Sandler: *Dynamic temporal behaviour of the keyboard action on the Hammond organ and its perceptual significance.* In: The Journal of the Acoustical Society of America 142, 2808, (2017).

[18] Jussi Pekonen, Tapani Pihlajamäki, Vesa Vlälimäki: *Computationally efficient Hammond Organ Synthesis.*In: Proceedings of the 14th International Conference on Digital Audio Effects (DAFx-11), Paris(2011).

[19] Evan Savage: *Hammond Organ Effects Synthesis.* MUMT 618, McGill University, Montreal, QC (2018).

[20] Mark Vail: *The Hammond Organ.* Backbeat Books, San Francisco(2002).

[21] Kurt James Werner, W. R. Dunkel, F. G. Germain: *A Computational model of the Hammond Organ Vibrato/Chorus Using Wave Digital Filters.*, in P. Rajmic, F. Rund, J. Schimmel (Eds.), Proceedings of the 19th International Conference on Digital Audio Effects, pp. 271–278, (2016).

[22] Kurt James Werner, Jonathan S. Abel:*Modal Processor Effects Inspired by Hammond Tonewheel Organs.* In: Applied Science 2016, 6(7), 185, (2016).

[23] o.N. ,"AC/DC Module User's Guide", Stockholm 2018, S. 212ff.

[24] Martin Martinez, "Finite element modeling of the magnetic field of guitar pick ups", Regendsburg 2003.

[25] T.Furukawa, H. Tanaka, "Dynamic Electromagnetic Analysis of Guitar Pickup Aided by COMSOL Multiphysics", Tokyo 2012.

[26] A. Kovetz, "The Principles of Electromagnetic Theory", Cambridge University Press, 1990.

[27] Jianming Jin, "The Finite Element Method in Electromagnetics", 2nd ed., Wiley-IEEE Press, May 2002.

[28] R.K. Wangsness, "Electromagnetic Fields, 2nd ed.", John Wiley, 1986.

[29] D.K. Cheng, "Field and Wave Electromagnetics, 2nd ed.", Addison-Wesley, 1991.

[30] . O.C. Zienkiewicz, C. Emson, and P. Bettess, "A Novel Boundary Infinite Element," International Journal for Numerical Methods in Engineering, vol. 19, no. 3, pp. 393–404, 1983.

[31] Fanny Littmark, "Permanent Magnet", Stockholm 2013

[32] o.N., "Das elektroakustische Klavier", VDI-Verlag, Berlin 1936.

[33] Peter Donhauser, "Elektrische Klangmaschinen: die Pionierzeit in Deutschland und Österreich", Böhlau Verlag, Wien 2007.

[34] Werner Meyer-Eppler, "Elektrische Klangerzeugung: elektronische Musik und synthesische Sprache", Bonn, 1949

[35] Oskar Vierling,"Das elektroakustische Klavier", Berlin 1936

[36] Oskar Vierling, "Elektrisches Musikinstrument Electric musical instrument", DE1932V0030615, 1937.

[37] Benjamin F. Miessner, "Method and apparatus for the production of music", US Patent 1,929,027, 1931.

[38] A. R. Duchossoir , "Gibson Electrics - The Classic Years", Milwaukee 2006.

[39] David K. Cheng. *Field and wave electromagnetics*. The Addison-Wesley series in electrical engineering. Addison-Wesley, Reading, Mass, 1989.

[40] Nicholas G. Horton and Thomas R. Moore. Modeling the magnetic pickup of an electric guitar. *American Journal of Physics*, 77(2):144, 2009.

[41] Jian-Ming Jin. *The finite element method in electromagnetics*. John Wiley & Sons Inc, Hoboken. New Jersey, third edition edition, 2014.

[42] Attay Kovetz. *The principles of electromagnetic theory*. Cambridge University Press, Cambridge [England] ; New York, 1990.

[43] Karl Küpfmuller, Wolfgang Mathis, and Albrecht Reibiger. *Theoretische Elektrotechnik*. Springer-Lehrbuch. Springer Berlin Heidelberg, Berlin, Heidelberg, 2013.

[44] Martin Martinez Villar. *Finite element modelling of the magnetic field of guitar pickups with ANSYS*. Master, University of Applied Sciences, Regensburg, July 2003.

[45] Malte Muenster and Florian Pfeifle. Non-Linear Behaviour in Sound Production of the Rhodes Piano. In *Proceedings of the International Symposium of Musical Acoustics (ISMA) 2014*, pages 247–252, Le Mans, France., 2014.

[46] Malte Muenster, Florian Pfeifle, Till Weinrich, and Martin Keil. Nonlinearities and self-organization in the sound production of the Rhodes piano. *The Journal of the Acoustical Society of America*, 136(4):2164–2164, 2014.

[47] Florian Pfeifle. Multisymplectic Pseudo-Spectral Finite Difference Methods for Physical Models of Musical Instruments. In Rolf Bader, editor, *Sound - Perception - Performance*, volume 1 of *Current Research in Systematic Musicology*, pages 351–365. Springer International Publishing, 2013.

[48] Florian Pfeifle and Rolf Bader. Real-Time Finite-Difference Method Physical Modeling of Musical Instruments Using Field-Programmable Gate Array Hardware. *J. Audio Eng. Soc*, 63(12):1001–1016, 2016.

[49] Roald K. Wangsness. *Electromagnetic fields*. Wiley, New York, 2nd ed edition, 1986.

[50] O. C. Zienkiewicz, C. Emson, and P. Bettess. A novel boundary infinite element. *International Journal for Numerical Methods in Engineering*, 19(3):393–404, March 1983.

[51] Stefan D. Bilbao. *Numerical sound synthesis: finite difference schemes and simulation in musical acoustics*. Wiley, Chichester, 2009.

[52] Charles Jordan. *Calculus of finite differences*. Chelsea Publ. Co, New York, 1 edition, 1950.

[53] John D. Jackson *Classical Electrodynamics* John Wiley & sons, Inc., 3rd edition, 1998

[54] John C. Strikwerda. *Finite Difference Schemes and Partial Differential Equations, Second Edition*. Society for Industrial and Applied Mathematics, Philadelphia, USA, 2nd ed edition, 2004.

[55] Florian Pfeifle and Malte Münster, Tone Production of the Wurlitzer and Rhodes E-Pianos. In Albrecht Schneider, editor, *Studies in Musical Acoustics and Psychoacoustics*, volume 4 of *Current Research in Systematic Musicology*, pages 75–107. Springer International Publishing, 2017.

PROCEEDINGS of ISMA 2019
International Symposium on Music Acoustics

13 - 17 September 2019 in Detmold, Germany

Physical principle of pitch bent by cross-fingering

Seiji ADACHI[†]

Fraunhofer Institute for Building Physics, Germany,

Abstract

Cross-fingering is a technique of playing woodwind instruments in which one or more tone holes are closed below the first open hole. It usually yields a pitch lower than that played with normal fingering. However, pitch is raised in exceptional cases. Pitch flattening has been traditionally understood using the lattice tone hole theory. On the other hand, pitch sharpening has been scarcely explained except for pointing out the possibility for the open hole to act as a register hole. This paper proposes understanding these pitch bending phenomena in a unified manner with a model of two coupled mechanical oscillators. Bores upstream and downstream of the open hole interact with each other by sharing the air in the open hole oscillating as a lumped mass. This mechanism is known in physics as avoided crossing or frequency repulsion. With an extended model having three degrees of freedom, pitch bending of the recorder played with cross-fingering in the second register can also be explained.

Keywords: woodwind instruments, resonance frequencies, avoided crossing

1 INTRODUCTION

Systematic research on passive acoustic resonance of the woodwind instruments aiming at their tone hole design dates back in the 1960s [1, 2]. In the following decades, where digital computers were dramatically developed, the theories and models obtained in the research were applied to practical design of the instruments while they were developed and refined on their own [3, 4, 5, 6]. From the engineering point of view, it can be said that passive acoustics of the woodwind instruments has attained perfection today. It is possible to design the instruments in a satisfactory manner with the aid of computer analysis based on the theories.

However, it is not always sufficient from the physical point of view to understand the mechanism by which the resonance characteristics of the instrument appear. The acoustics of cross-fingering is one such topic. Pitch flattening due to cross-fingering has been traditionally understood using the lattice tone hole theory [7]. On the other hand, pitch sharpening has been scarcely explained except for pointing out the possibility for the open hole to act as a register hole [8]. Recently, Yoshikawa and Kajiwara [9, 10] shed a new light on this problem by examining pitch bending in a shakuhachi played with cross-fingering experimentally in detail. Adachi [11] proposed a minimal model with which both pitch flattening and sharpening due to cross-fingering can be understood in a unified manner. This paper attempts to explain the pitch bending mechanism based on this model as plainly as possible.

Table 1 lists a few examples of cross-fingerings on the alt recorder. The first three examples are at the first register and the last four are at the second register. The pitch is lowered in the first five examples, whereas it is raised in the last two. The general tendency is that the pitch is lowered at the lower register. The pitch tends to rise at the higher register and when more holes are closed. Note that the pitch sharpening also occurs at the first register, for example, when two more downstream open tone holes of fingering C♯5 are closed, although this fingering is not used in a normal performance.

2 RESONANCE CHARACTERISTICS OF A ONE-HOLE FLUTE

Pitch bending with cross-fingering is due to the interaction between the two parts of the instrument bore upstream and downstream of the open hole. To overview this interaction, a simplified flute having only one open tone hole is considered first. Figure 1 (a) shows the model of this flute. The section from the input (left) end to the open hole is called upper bore and that from the hole to the output (right) end is called lower bore. The

[†]seiji.adachi@ibp.fraunhofer.de

Table 1. A few examples of cross-fingerings on the alt recorder. The symbols denote ●: open, ○: close and ◑: ‘pinched’ (half open).

Normal fingering			Cross-fingering	
C5:	● ●●● ○○○○	pitch lowered $\longrightarrow$	B4:	● ●●● ○●●○
D5:	● ●●○ ○○○○	pitch lowered $\longrightarrow$	C♯5:	● ●●○ ●●○○
E5:	● ●○○ ○○○○	pitch lowered $\longrightarrow$	E♭5:	● ●○● ●○○○
C6:	◑ ●●● ○○○○	pitch lowered $\longrightarrow$	B5:	◑ ●●● ○●○○
D6:	◑ ●●○ ○○○○	pitch lowered $\longrightarrow$	C♯6:	◑ ●●○ ●○○○
D6:	◑ ●●○ ○○○○	**pitch raised** $\longrightarrow$	E6:	◑ ●●○ ●●○○
D6:	◑ ●●○ ○○○○	**pitch raised** $\longrightarrow$	D♯6:	◑ ●●○ ●●●○

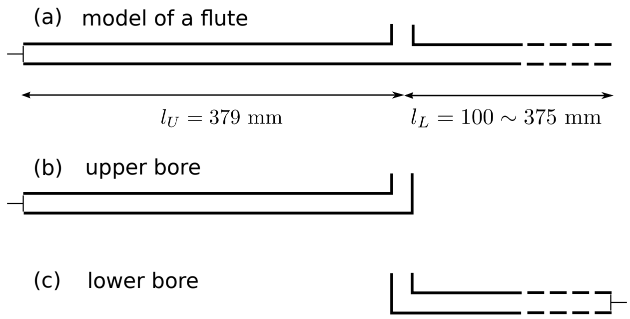

Figure 1. (a) A simplified flute having one open tone hole. (b) The upper part and (c) the lower part of the instrument bore.

upper bore length l_U is fixed to 379 mm, while the lower bore length l_L is increased from 100 to 250 mm with a 25 mm step. The bore radius is assumed to be 9.5 mm, the tone hole radius to be 9.5 mm and its acoustical length h_e to be 22 mm.

The resonance characteristics of the flute are represented by the input admittance, which is the ratio of the volume velocity to the sound pressure at the input (left) end when the flute is excited by a piston as shown in Figure 1 (a). The blue thick curves in Figure 2 show the input admittance calculated using the transmission-line matrix model [12] and the tone hole theory [6]. The flute resonates at the frequencies where the admittance takes maxima and can be played near one of these frequencies. These plots are essentially the same as Figure A6.3 in [2]. To help understanding the admittance of the flute, two additional admittances of the upper and lower bores are plotted with the green and red thin curves, respectively. The upper bore admittance can be conceptually measured in the setup illustrated in Figure 1 (b). The bore is closed just after the open hole so that only the air column in the upper bore vibrates while that in the lower bore (not shown in the figure) stays still. Likewise, the lower bore admittance can be obtained as shown in Figure 1 (c). The lower bore closed just before the open hole is excited from the output end in this case.

Resonances of the upper bore (peaks in the green thin curves) occur at 433, 867, 1303 and 1742 Hz. These of course remain the same even if the lower bore length l_L is changed. The first resonance of the lower bore (the lowest peak in the red thin curves) gradually shifts its frequency from 1363 to 622 Hz as l_L extends from 100 to 250 mm. If the lower bore frequency is far from one of the upper bore frequencies, the flute resonates approximately at the same frequency as that of the upper bore. On the other hand, if the lower bore frequency approaches one of the upper bore frequencies, for example, at the second register near 860 Hz for the case of $l_L = 175$ mm, two resonance frequencies of the flute appear; one is shifted upward and the other is shifted

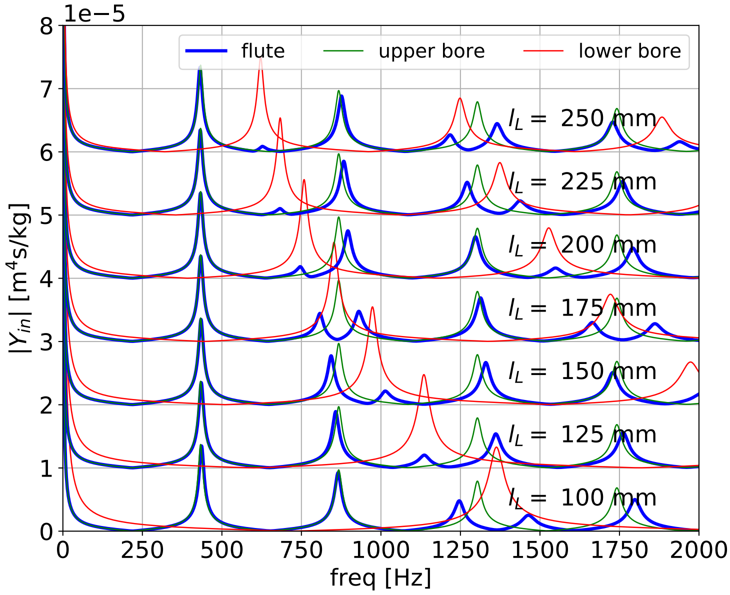

Figure 2. The input admittance spectra of the simplified flute with one open tone hole are plotted in blue thick curves as the lower bore length l_L is increased from 100 to 250 mm while the upper bore length l_U is fixed to 379 mm. The two additional input admittances of the upper and lower bores are also plotted in green and red thin lines to help understanding how the resonance of this flute is generated. The plots are shifted vertically for better visibility.

downward from the resonance frequencies of the upper and lower bores. These flute resonance frequencies are formed as if they repel each other even though the frequencies of the upper and lower bores intersect each other. This phenomenon is called avoided-crossing [13, 14]. The avoid crossing happens not only at the second register but also at the third (when $l_\mathrm{L} = 100\,\mathrm{mm}$ and $225\,\mathrm{mm}$) and fourth (when $l_\mathrm{L} = 175\,\mathrm{mm}$) registers.

The second resonance frequency f_2 of the flute is apparently lower than the upper bore resonance frequency for $l_\mathrm{L} = 150$ and 175 mm. If the flute makes sound at this frequency, the played pitch noticeably becomes lower than the pitch played when l_L is short. On the other hand, the third resonance frequency f_3 is higher than the upper bore resonance frequency for $l_\mathrm{L} = 175$ and 200 mm. Sounding at this frequency results in pitch sharpening.

The second and third resonance modes of the flute can be easily discriminated if their standing-wave pressure patterns are compared. For $l_\mathrm{L} = 150$, 175 and 200 mm, these (and that of the first mode) are drawn in Figure 3. In the second mode, pressure on both sides of the open hole at $x = 379$ mm vibrates in phase. In the third mode, a pressure node appears near the open hole. On both sides of the node, pressure vibrates in anti-phase.

3 MECHANICAL MODEL OF A ONE-HOLE FLUTE

To explain why pitch is bent by cross-fingering, the mechanical model shown in Figure 4 is presented. In this model, the air in the open hole is regarded as mass M vibrating up and down. Two mechanical oscillators, each of which is composed of a spring and a mass, are assigned to the resonances of the upper and lower bores. Masses of the oscillators have the same amount of m. The spring constant of the upper bore is fixed to k, whereas that of the lower bore is varied, with which the lower bore resonance frequency ω_L can be adjusted. As the three masses are linked through lubricating oil at the junction, the two oscillators interact with each other by sharing M.

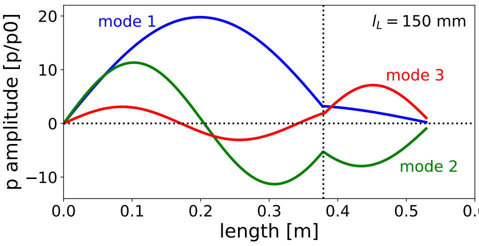

(a) $l_{\mathrm{L}} = 150$ mm

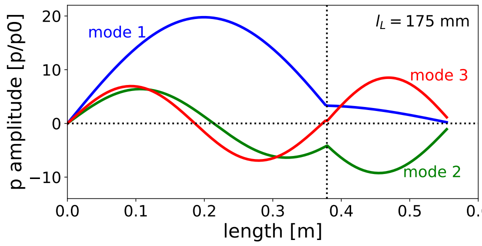

(b) $l_{\mathrm{L}} = 175$ mm

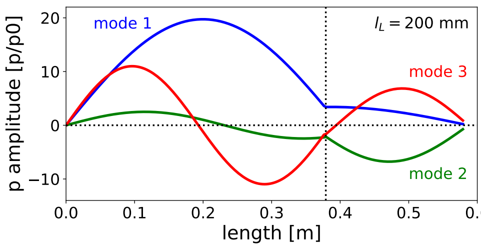

(c) $l_{\mathrm{L}} = 200$ mm

Figure 3. Standing-wave pressure patterns of the lowest three modes.

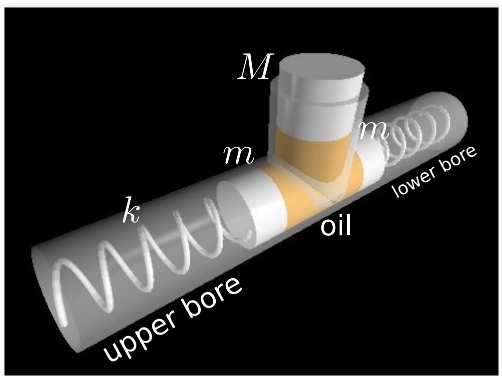

Figure 4. Mechanical model of the one-hole flute.

If the lower bore resonance frequency ω_{L} is much higher than the upper bore resonance frequency ω_{L}, the two bores do not interact. When the upper bore vibrates, mass M vibrates together. However, the lower bore does not vibrate. The vibration frequency in this case is $\omega_{\mathrm{U}} = \sqrt{k/(m+M)}$. This situation correspond to normal fingering. If an actual flute is played with normal fingering, the lower bore or the downstream section of the instrument has a few open tone holes aligned at short intervals. The resonance frequency of this section is much higher than that of the upper bore where the tone holes are closed.

If the lower bore resonance frequency ω_{L} is comparable to the upper bore resonance frequency ω_{U}, the mechanical model has two vibration modes shown in Figure 5. In case (a), the upper and lower bores vibrate symmetrically. Mass M vibrates at twice the acceleration of mass m, so the vibration frequency becomes $\omega_{-} = \sqrt{k/(m+2M)}$, which is lower than $\omega_{\mathrm{U}} \approx \omega_{\mathrm{L}}$. This vibration mode therefore corresponds to the pitch flattening in cross-fingering. In case (b), the upper and lower bore vibrate anti-symmetrically. Mass M does not vibrate. The frequency is then $\omega_{+} = \sqrt{k/m}$, which is higher than $\omega_{\mathrm{U}} \approx \omega_{\mathrm{L}}$. This vibration mode causes pitch

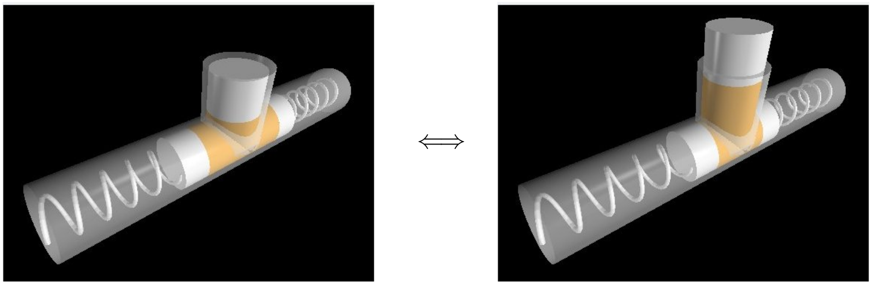

(a) mode ω_-

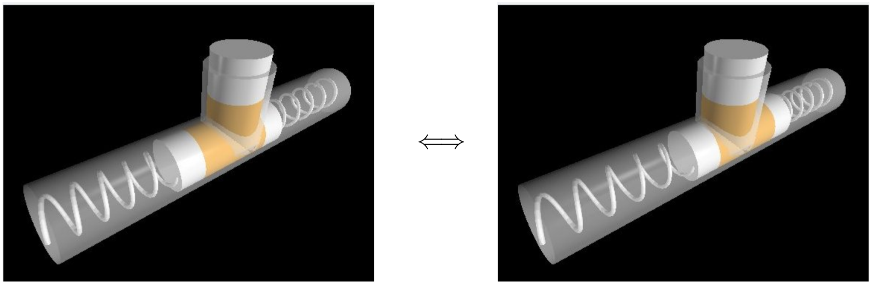

(b) mode ω_+

Figure 5. Two vibration modes when $\omega_{\mathrm{U}} \approx \omega_{\mathrm{L}}$.

sharpening.

As it looks possible to explain the pitch bending due to cross-fingering with this mechanical model, let us write down the equation of motion and calculate $\omega_\pm$ in the general case of $\omega_{\mathrm{U}} \neq \omega_{\mathrm{L}}$. The ratio $r = \omega_{\mathrm{L}}/\omega_{\mathrm{U}}$ is defined here. Let the displacements of the upper and lower masses m and of the open hole mass M be $x_{\mathrm{U}}(t)$, $x_{\mathrm{L}}(t)$ and $x(t)$, respectively. Positive $x_{\mathrm{U}}(t)$ and $x_{\mathrm{L}}(t)$ are defined towards the direction where the springs are stretched. Positive $x(t)$ is defined upward. By disregarding oil inertia, the equation of motion becomes

$$m\ddot{x}_{\mathrm{U}} = -kx_{\mathrm{U}} - Sp, \quad m\ddot{x}_{\mathrm{L}} = -r^2 kx_{\mathrm{L}} - Sp, \quad M\ddot{x} = Sp, \tag{1}$$

where S is the cross-sectional area of the bore and $p(t)$ pressure in the junction. If the oil is an incompressible fluid, $x(t) = x_{\mathrm{U}}(t) + x_{\mathrm{L}}(t)$ is held. The $x(t)$ or $p(t)$ can therefore be eliminated from the equation of motion. When x_{U} and x_{L} vibrate at the same frequency ω, the equation of motion results in

$$\begin{bmatrix} 1 & \alpha \\ \alpha & 1 \end{bmatrix}^{-1} \begin{bmatrix} 1 & 0 \\ 0 & r^2 \end{bmatrix} \begin{bmatrix} x_{\mathrm{U}} \\ x_{\mathrm{L}} \end{bmatrix} = \frac{\omega^2}{\omega_{\mathrm{U}}^2} \begin{bmatrix} x_{\mathrm{U}} \\ x_{\mathrm{L}} \end{bmatrix} \tag{2}$$

with $\omega_{\mathrm{U}} = \sqrt{k/(m+M)}$ and $\alpha = M/(m+M)$. Solving this equation, we have two eigenfrequencies:

$$\omega_\pm^2 = \frac{\omega_U^2 + \omega_L^2 \pm \sqrt{(\omega_U^2 - \omega_L^2)^2 + 4\alpha^2 \omega_U^2 \omega_L^2}}{2(1-\alpha^2)}. \tag{3}$$

The $\omega_\pm$ are plotted as functions of $\omega_{\mathrm{L}} = r\omega_{\mathrm{U}}$ in Figure 6. When $r = \omega_{\mathrm{L}}/\omega_{\mathrm{U}}$ is large, ω_- approaches ω_{U} and ω_+ approaches ω_{L}. If $r \approx 1$ or ω_{L} approaches ω_{U}, two curves of $\omega_\pm$ avoid crossing.

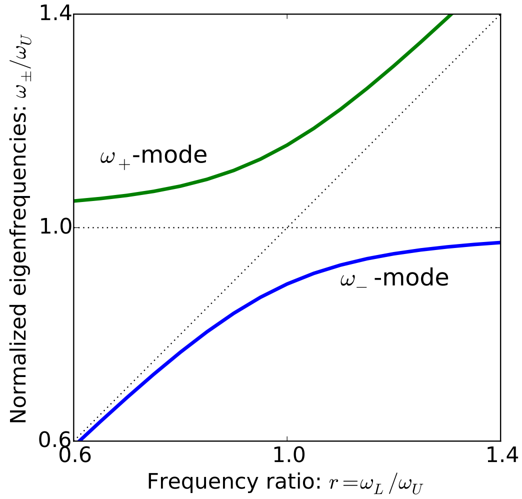

Figure 6. The two eigenfrequencies $\omega_\pm$ of the mechanical model are plotted as functions of $\omega_L = r\omega_U$, where $\alpha = 0.2$ is assumed. The dotted lines represent ω_U, ω_L. These cross each other at $r = 1$, whereas the flute resonance frequencies $\omega_\pm$ are changed as if they avoid crossing.

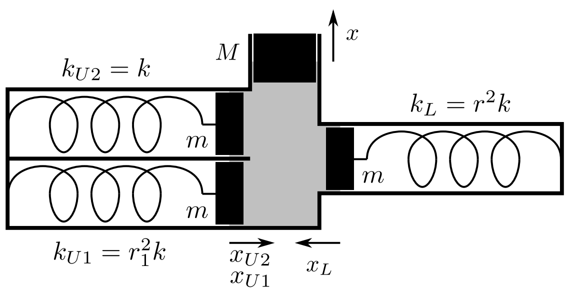

Figure 7. Mechanical model for explaining resonance frequencies of the recorder played with cross-fingering. The upper bore has two fixed resonance frequencies ω_{U1} and ω_{U2}, where $r_1 = \omega_{U1}/\omega_{U2} \approx 0.5$ is a model parameter. The lower bore has a resonance frequency ω_L varying with ratio $r = \omega_L/\omega_{U2}$.

4 MECHANICAL MODEL OF A RECORDER

The basic mechanism of pitch bending due to cross-fingering has been clarified so far. In this section, actual pitches at the second register on the alt recorder played with cross-fingering are explained. For this purpose, a mechanical model with three degrees of freedom as shown in Figure 7 is employed.

The upper bore is assumed to have only the lowest two resonance frequencies ω_{U1} and ω_{U2}. These are almost harmonically related and a model parameter $r_1 \equiv \omega_{U1}/\omega_{U2} \approx 0.5$ is introduced. The lower bore has just one resonance frequency ω_L as before. The ratio of this frequency to ω_{U2} is written as $r = \omega_L/\omega_{U2}$. Displacements of the three mechanical oscillators are denoted by x_{U1}, x_{U2} and x_L. In the same way as in the last section, the eigenvalue equation of this mechanical model becomes

$$\begin{bmatrix} 1 & \alpha & \alpha \\ \alpha & 1 & \alpha \\ \alpha & \alpha & 1 \end{bmatrix}^{-1} \begin{bmatrix} r_1^2 & 0 & 0 \\ 0 & 1 & 0 \\ 0 & 0 & r^2 \end{bmatrix} \begin{bmatrix} x_{U1} \\ x_{U2} \\ x_L \end{bmatrix} = \frac{\omega^2}{\omega_{U2}^2} \begin{bmatrix} x_{U1} \\ x_{U2} \\ x_L \end{bmatrix}. \tag{4}$$

By solving this equation, three eigenfrequencies can be obtained. These are plotted as functions of the lower

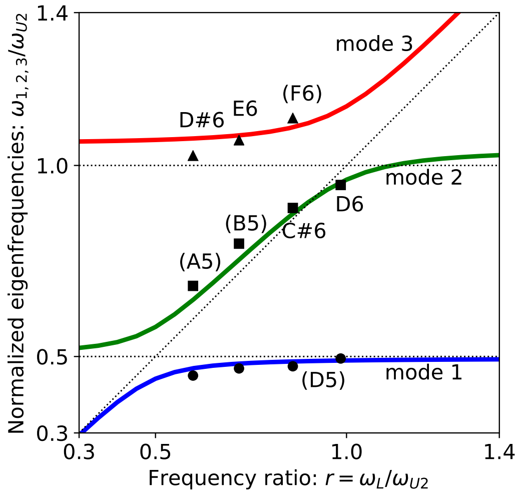

Figure 8. Three eigenfrequencies of the recorder's mechanical model as functions of the lower bore resonance frequency or the ratio $r = \omega_{\mathrm{L}}/\omega_{\mathrm{U2}}$. The model parameters are $\alpha = 0.25$ and $r_1 = 0.5$. Sound frequencies played on an actual alt recorder are also plotted with circle, square and triangle markers together with corresponding note names.

bore resonance frequency or $r = \omega_{\mathrm{L}}/\omega_{\mathrm{U2}}$ in Figure 8. The lower bore resonance frequency ω_{L} depicted by the dotted line inclined at 45 degrees intersects the two upper bore frequencies ω_{U1} and ω_{U2} shown with the horizontal dotted lines. In contrast, the eigenfrequencies of the recorder ω_1, ω_2 and ω_3 avoid crossing twice at $r = 0.5$, and 1. This is because the lower bore interacts with the upper bore twice near the first and second resonance frequencies.

An alt recorder was played with fingerings D6, C♯6, E6, and D♯6 in Table 1. The output sound was recorded and analyzed. The played frequencies are compared with the eigenfrequency curves in Figure 8. By changing the blowing pressure for each fingering, two or three pitches could be played. For example, if the recorder was played with normal D6 fingering and with normal blowing pressure, the pitch of D6 was gained as indicated by the square marker. This is identified as sounding in the second mode. If the blowing pressure was lowered, a pitch close to D5 was obtained as shown in the circle marker. This is sounding in the first mode. It was not possible to excite the third mode with fingering D6 even if the blowing pressure was increased. With cross-fingering of C♯6, the first and second resonance modes could be excited. The C♯6 sound results from the normal effect or pitch flattening due to cross-fingering. By just blowing harder, F6 in the third mode could not be played. However, F6 could be gained after playing E6 with fingering E6 by increasing the blowing pressure and at the same time by gradually changing the fingering to C♯6. The E6 sound that is one whole tone higher than the normal fingering was identified as the excitation in the third mode of the recorder. Furthermore, when fingering was changed to D♯6, the D♯6 sound that is a half tone higher was played. If the flute is blown softer in these fingerings, soundings in the first and second modes were also generated.

5 CONCLUSIONS

The resonance frequencies of the mechanical model and the frequencies actual played on the recorder were in good agreement. The usual pitch flattening and anomalous pitch sharpening due to cross-fingering on the recorder could thus be explained in a unified way with the model of three mechanical oscillators, two of which are associated with the upper bore resonances and one of which is with the lower bore resonance. The central mechanism is avoided crossing where the mechanical oscillators in the upper and lower bores are coupled by sharing the mass of the open tone hole.

REFERENCES

[1] Benade, A. H. On the mathematical theory of woodwind finger holes, J. Acoust. Soc. Am., **32**, 1960, pp 1591–1608.

[2] Nederveen, C. J. Acoustical aspects of woodwind instruments, Northern Illinois Univ. Press, DeKalb (USA), Revised Ed., 1998.

[3] Keefe, D. H. Theory of the single woodwind tone hole, J. Acoust. Soc. Am., **72**, 1982, pp 676–687.

[4] Keefe, D. H. Experiments on the single woodwind tone hole, J. Acoust. Soc. Am., **72**, 1982, pp 688–699.

[5] Keefe, D. H. Woodwind air column models, J. Acoust. Soc. Am., **88**, 1990, pp 35–51.

[6] Lefebvre, A.; Scavone, G.P. Characterization of woodwind instrument toneholes with the finite element method, J. Acoust. Soc. Am., **131**(4), 2012, pp 3153–3163.

[7] Benade, A. H. Fundamentals of Musical Acoustics, Chapter 21.4D, Oxford Univ. Press, New York (USA), 1976.

[8] Wolfe, J.; Smith, J. Cutoff frequencies and cross fingerings in baroque, classical and modern flutes, J. Acoust. Soc. Am., **114**(4), 2003, pp 2263–2272.

[9] Yoshikawa, S.; Kajiwara, K. Acoustics of cross fingerings in the shakuhachi, Proc. of Forum Acusticum, Kraków September 7–12, 2014.

[10] Yoshikawa, S.; Kajiwara, K. Cross fingerings and associated intonation anomaly in the shakuhachi, Acoust. Sci. & Tech., **36**(4), 2015, pp 314–325.

[11] Adachi, S. Resonance modes of a flute with one open tone hole, Acoust. Sci. Tech., **38**(1), 2017 pp 14–22.

[12] Caussé, R.; Kergomard, J.; Lurton, X. Input impedance of brass musical instruments — Comparison between experiment and numerical models, J. Acoust. Soc. Am., **75**(1), 1984, pp 241–254.

[13] Lockhart, A. B.: Skinner, A.; Newman, W.; Steinwachs, D. B.; Hilbert, S. A. An experimental demonstration of avoided crossings with masses on springs, Am. J. Phys., **86**, 2018, pp 526–530.

[14] Newman, W.; Skinner, A.; Hilbert, S. A. An acoustic demonstration of an avoided crossing, Am. J. Phys., **85**, 2017 pp 844-849.

PROCEEDINGS of ISMA 2019
International Symposium on Music Acoustics

13 - 17 September 2019 in Detmold, Germany

A parametric study of finger motions when playing the clavichord : towards characterization of expressive control.

Jean-Théo JIOLAT, Jean-Loïc LE CARROU, Christophe d'ALESSANDRO

[1]Sorbonne Université, CNRS, Institut Jean le Rond d'Alembert, Équipe LAM, France,
{jean-theo.jiolat,jean-loic.le_carrou,christophe.dalessandro}@sorbonne-universite.fr

Abstract

The clavichord is considered to be the most demanding keyboard instrument in terms of finger control. This is because of its direct mechanisms: the key works as a lever. When the finger presses the key, the tangent (metal blade) on the key's extremity goes up and strike the string. And as long as the finger remains pressed on the key, the tangent remains in contact with the string, leading to string's tone variation. The loudness of the sound is proportional to the velocity of the key's displacement. Then there is a duality between loudness and pitch accuracy. This is the paradox of the clavichord. The objective of the study is to analyze experimentally the vibro-acoustical consequences of the instrument with respect to the gestural strategies of the finger. To proceed, an experimented player performs in different configurations two main gestures: the pushed and pulled gesture. A robotic finger is used to simulate different trajectories in terms of downward displacement and velocity. The study shows that the pushed and pulled gestures have opposed influences on the fundamental frequency and on the sound level. The robotic finger demonstrates that a rise in sound level without a rise in fundamental frequency is possible.

Keywords: Clavichord, gesture, robotic finger

1 INTRODUCTION

1.1 The clavichord's paradox

The clavichord is the earliest stringed keyboard instruments, dating back to the XVth century [1]. Its sound level is low compared to other stringed instruments, and it is the only keyboard instrument allowing for some pitch control. When a key is pressed, the corresponding pair of strings is impacted by a small metal blade (the tangent) placed at the end of the key. As long as the key is pressed, the tangent remains in contact with the strings. The tangent is at the same time the nut (i.e. one extremity) of the string and the string exciter (the string is then excited at a vibration node). It has been showed experimentally that the sound level of the clavichord is proportional to the tangent velocity at impact [7]. So the faster the key is pressed, the louder the sound becomes. However, when a key is pressed with a high velocity, the key's displacement tends to be higher. The tangent raises the string, then increases its tension, and thereby increases the vibration fundamental frequency. As a result, playing louder ends up in raising the pitch, if the key is pressed in a simple vertical motion. To control independently loudness and intonation would require a paradoxical gesture: at the tangent-string contact, the tangent should have enough velocity, but should not raise the string. In other words, the key should transfer all the tangent momentum to the string, but without raising it, or losing contact. This dependence between loudness and pitch accuracy is coined "the clavichord's paradox"[4, 5]. It is difficult, at least for human players, to achieve exactly such a motion. However compromises between tangent impact velocity and string displacement are possible.

1.2 Historical clavichord techniques

The clavichord is considered as the most demanding among keyboards instruments in terms of finger control. This is because every nuance of pressure of the finger on the key is likely to change loudness and intonation. In addition both finger velocity and displacement must be controlled because of the clavichord's paradox. To

Figure 1. Photo from above of the Hubert clavichord.

deal with these constraints, specific performance practice have been elaborated. Because of these constraints, the clavichord has always been highly praised as a pedagogical instrument. Several texts describing clavichord performance around Johann Sebastian Bach's circle, "Every Players first Grammatica" to quote J.G. Walther (1732) (see [12], page 169), mention a specific technique called "Schnellen" [11], which can be translated in French by "tire" [5] and in English by "pulled" (see for instance, J.J. Quantz, 1752, C.P.E. Bach 1752, Forkel 1802). In this technique, the finger tip is drawn back quickly after contact with the key, in a sliding motion.

1.3 Measurement and simulation of fingers motions

In a preceding work [4], the effect of vertical finger motion ("pushing motion") and sliding finger motion ("pulling") on loudness and pitch of clavichord tones have been studied. It has been shown that the pulling gesture is a better compromise for dealing with the clavichord's paradox: loudness and pitch are controlled more independently with pulled than with pushed motions. The aim of the present work is to study the clavichord's paradox with the help of new measurement techniques and robotic simulation: 1/ to measure accurately finger trajectories and their consequences on vibration and sound patterns (Section 2); 2/ to reproduce these trajectories using a robotic finger, in order to study the limits of the clavichord's paradox, and then the "optimal" trajectories, decoupling key velocity at impact and string displacement (Section 3).

2 MEASUREMENTS OF FINGER AND VIBRATORY MOTIONS

2.1 Experimental setup

The instrument under study has been built by C. d'Alessandro and C. Besnainou, and completed in 2007 (at The Paris Workshop, led by M. Ducornet, in Montreuil). It is based on a kit designed by E. Dancet and M. Ducornet after XVIIIth century unfretted clavichord models by G. Hubert. The instrument is not an exact copy of an historical model. It has been built especially for acoustic investigations, but it has occasionally been played in concert. The instrument has 51 keys, from C to d3, with double strings in brass. Its dimensions are 1267 mm x 358 mm x 112 mm. It is tuned at A=415 Hz, in a Kirnberger II temperament. Vibrating string lengths C = 1097mm, c = 926mm, c1 = 509mm, c2 = 262mm, c3 = 122mm.

The objective is to measure the vibration of the excited string resulting from the motion of the musician's finger. In preceding works, measurements were performed with the help of an accelerometer near the tangent, a string-tangent contact signal and a measurement microphone. It appeared necessary to measure directly the finger motion and the string motion, using non-invasive measurement devices. Finger motions are filmed by a high-speed camera (Phantom Miro M 120) with a 2000 frame per second rate. Several marks are placed on the finger. Trajectories of these marks are estimated thanks to image processing.

String vibrations are measured with the help of calibrated opto-switch sensors [8]. These sensors are optical forks, positioned around the string. The string motion in one direction is measured with accuracy and without contact. Only the vertical displacement of the string is considered here (although the horizontal displacement can also be significant). The string chosen for our measurements is the G2 string (length is 70 cm, fundamental frequency 185 Hz). The sensor is placed at 2 cm from the extremity of the string, near the bridge in order to be within its measurement range. Sound pressure is measured with the help of an omnidirectional DPA 4006-TL microphone placed at 30 cm above the soundboard. A set of 8 trajectories are recorded, using index and middle fingers, pulled and pushed motions for long and short notes.

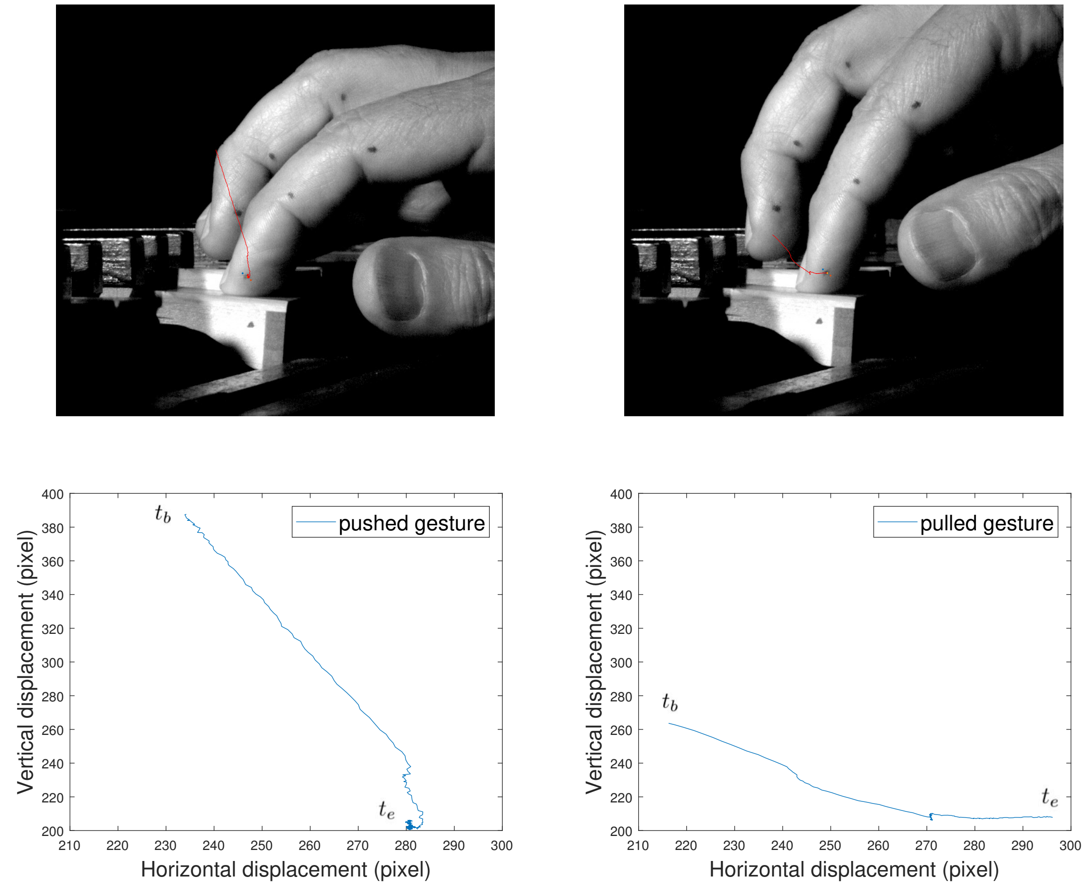

Figure 2. (Top) Images of the pushed (left-hand side) and the pulled gesture (right-hand side) performed by the index finger. (Bottom) Trajectories of the pushed (left-hand side) and the pulled gesture (right-hand side) performed by the index finger (with t_b the beginning time and t_e the ending time).

2.2 Results

In figure 2, we used the videos to extract the trajectories representative of the two distinct motions : the pushed and pulled gestures. The pushed motion refers to a vertical trajectory, the finger going mostly downward. The pulled motion corresponds to a vertical and horizontal trajectory, the finger sliding on the key and going downward at the same time. Figure 2 displays a selection of extracted trajectories. Note that the key depression is shallower in the second case.

Example of string vibration pattern are displayed in figure 3 and 4 for the pushed and pulled gestures by the index finger. As the sensor is placed near the bridge, the vibratory motion is of small amplitude, about 0.2 mm.

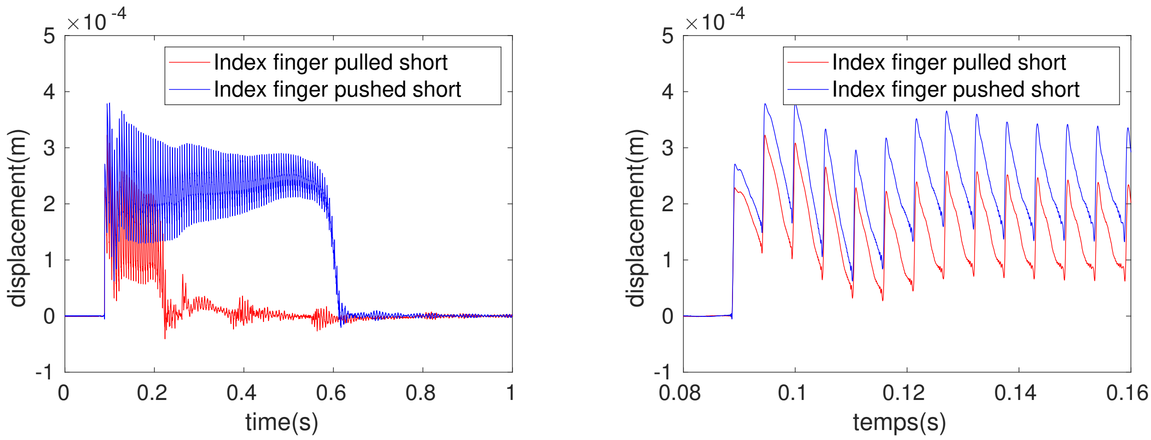

Figure 3. Vibratory signal of the G2 string excited by means of the two different trajectories done by the index finger with a short length (left-hand side), with a zoom at the beginning of the signals (right-hand side).

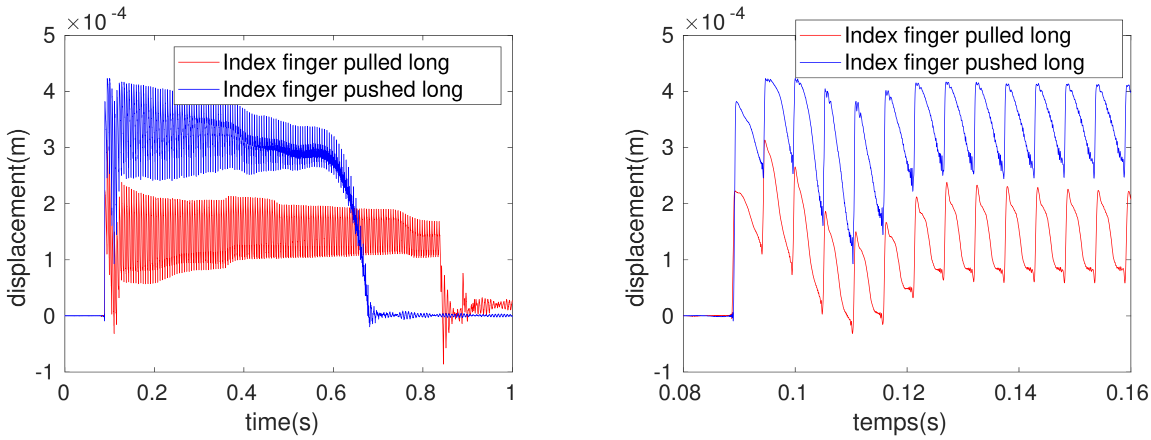

Figure 4. Vibratory signal of the G2 string excited by means of the two different trajectories done by the index finger with a long length (left-hand side), with a zoom at the beginning of the signals (right-hand side).

The string height is also small at this position, about 0.2-0.3 mm. It is much larger at the tangent position. The string is much more elevated in the case of the pushed gesture than the pulled one (see figure 3 and 4). Because of this difference in string height, the string tension and then the sound fundamental frequency is higher for the pulled motion. Note that the vibration amplitude is also larger in the case of the pushed gesture, resulting in a louder tone. Fundamental frequency is measured on the sound and vibration signals using the Yin algorithm [6] implemented in Matlab. Fundamental frequency with respect to time (G2 string) is displayed in figure 5. As predicted, the fundamental frequency is higher for the pushed gesture compared to the pulled gesture. The difference between the pushed and the pulled gesture is more than 4 cents for some conditions. Such a difference is perceptually noticeable. Fundamental frequency gives information about the way the musician deals with the contact between the tangent and the string with respect to time. In figure 5, one can observe that the fundamental frequency for the pushed gesture decreases with respect to time, whereas that of the pulled gesture remains around the same fundamental frequency although with some little hills. This shows that the key control differs for both gestures. These variations of finger depth after the string-tangent contact are certainly perceived in terms of quality of touch.

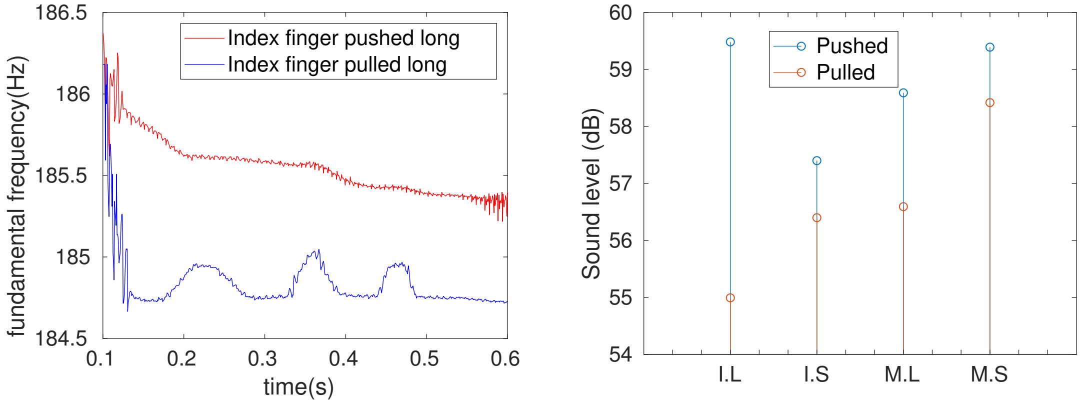

Figure 5. Fundamental frequency of the signals in the case of the pushed and pulled gesture done by the middle finger and the index finger (left-hand side). Sound level of the different exciting configurations (right-hand side) (I : Index finger, M : Middle finger, S : Short, L : Long).

Figure 6. Measurement devices: (left-hand side) optical forks for string displacement. (right-hand side) DRoPiCrobotic finger for key trajectory control.

The sound level in dB for the different microphone signals are displayed in figure 5 (integration time 250 ms). Pushed gestures produce higher sound levels than pulled gestures. This has already been observed on the signal amplitude in figure 3 and 4.

In summary, different gestures, corresponding to different finger trajectories, are producing different vibratory patterns of the string, and then different sounds. In the small set of recordings available, the pushed motions always produce a larger string displacement : the string is always raised higher, and the amplitude of vibration is larger. A larger amplitude of vibration results in a louder sound. A higher string height results in a higher fundamental frequency. For the same reasons, the finger motion in the case of pulled gestures gives lower fundamental frequencies and also weaker sounds. Note that in previous studies it has been shown that pulled motions, to some extent, allows for independent loudness and pitch control, a result that cannot be observed here, because no sample have similar loudness. These measurements are the first direct measurements of string height, and are in good agreement with the theory developed in [7].

3 ROBOTIC SIMULATION OF FINGERS MOTIONS

3.1 Experimental setup: the robotic finger

Measurements of finger motion show the dependence between string height, sound radiated and fundamental frequency. As predicted by the clavichord's paradox, it seems difficult to control simultaneously the key (then tangent, then string) velocity and displacement. The pulled motion provides a better control and a better management of the clavichord's paradox, because the finger trajectory is more complex: pressure on the string can be released after the tangent-string impact.

It is interesting to study the clavichord's paradox with the help of controlled and reproducible key trajectories. For this purpous, a robotic finger is used. The DROPIC robot [9] has been initially developed for simulation of finger trajectories in plucking gesture of harps [3, 2]. It has been applied to keyboard instruments in studies of the plectra effects for the harpsichord. [10]. The robotic finger has two degrees of freedom. It can reproduce any trajectory in a plane parallel to the axis of the key. Note that the key itself has only one degree of freedom. The effort for depressing a key is relatively weak, less than 2 N.

For a given starting trajectory, two parameters are considered and modified: downward displacement (resulting in string height) and its maximal velocity (corresponding to loudness). The A2 string (length is 59.1 cm, fundamental frequency 205Hz) is studied. The initial position of the robotic finger above the key is set before modifying either the velocity or the displacement. A joint measure of the string vibration by means of calibrated opto-switch sensors is performed. Three different velocities with the same displacement, and three different downward displacements with the same velocity have been programmed. The displacement of the key corresponding to a referent trajectory performed by the robotic finger is displayed in figure 8. The trajectory has a typical shape with a notch followed by a plateau. It is possible to adjust independently the depth of the notch and the height of the plateau, that correspond roughly to the key velocity at contact and to the string height.

3.2 Trajectories simulation and sound results

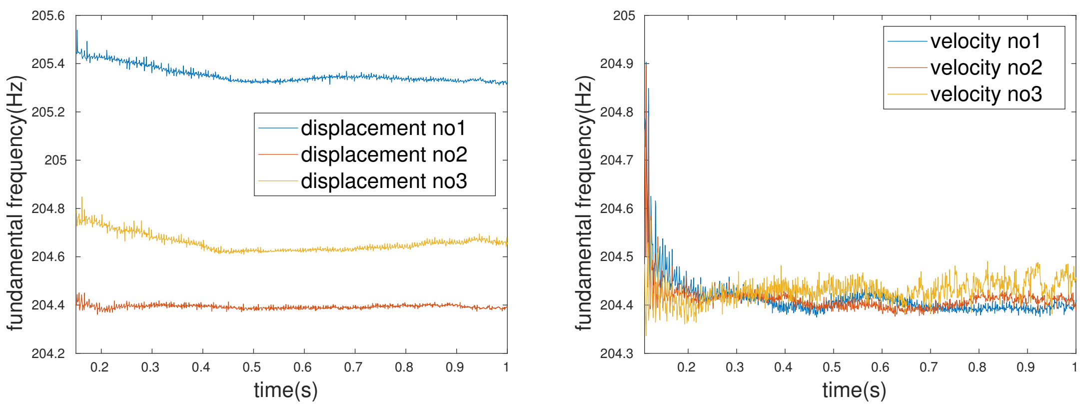

Figure 7. Tracking of the fundamental frequencies of the signals in the case where we modify the displacement of the key (left-hand side) and in the case where we modify its velocity (right-hand side).

Systematic variations of displacement and velocity are performed. Note that in this second experiment, the note studied is A2 instead of G2 studied in Section 2. These two notes are close enough to be compared. In figure 8, the key velocity is varying but the key depth is constant. The key depth is about 5-6 mm in this case. The resulting average string elevation is 0.1 mm.

Figure 7 displays the fundamental frequency of the different signals measured when the key is played with

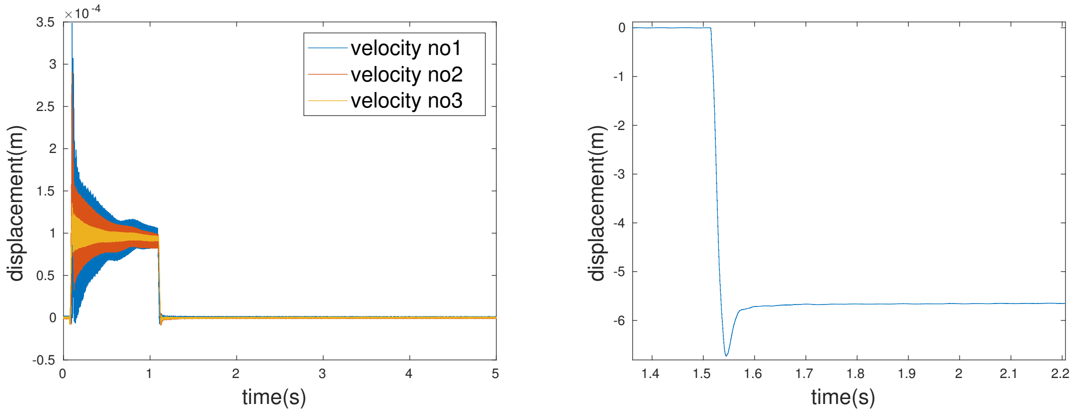

Figure 8. Temporal signals of the A2 string produced by the different velocities of the key (left-hand side). Displacement of the key in the case of the referent trajectory performed by the robotic finger (right-hand side).

the robotic finger. The resulting fundamental frequency does not change, while the amplitude of the signal increases. This shows that the trajectory of the finger is well repeated by the robot no matter the change in velocity. Moreover, it demonstrates that the clavichord's paradox can be managed with appropriate trajectories. These results also confirm that the displacement of the key is directly linked to the string's fundamental frequency. Conversely, changing the displacement of the key but maintaining the same velocity produces changes in fundamental frequency. However, fundamental frequency is very stable in the case of the robotic finger compared to a musician's finger (compare figures 7 and 5).

These results demonstrate that a robotic control is able to manage the clavichord's paradox. Whether human and robotic control are comparable is questionable. In the present experiment, the robotic finger has no haptic or sound feedback: the trajectories are optimized directly, without any perceptual loop. On the contrary, human control relies much on audio and haptic feedback. The musicians tend to control the contact between the tangent and the string after the excitation by modifying the key position according to the perceived effect of their initial motion. This variation in time of the key position is probably an essential feature of the specific style of a musical performance. Another difference between the robotic finger and human finger is their mechanical and dynamical properties. Human fingers have a much limited range of velocity and acceleration than the robot. Oscillations of the key-string-finger system that are observed in human control [7] seem negligible in the case of the robotic finger (see the displacement of the key in figure 8).

4 CONCLUSIONS

This work presents two experiments addressing the clavichord's paradox, i.e. simultaneous control of velocity and displacement of the string and tangent when playing the instrument. In a first part, new measurements using a new methodology is used. Two types of finger trajectories have been used for performing two different motions : the pushed and the pulled gesture. This experiment confirms the dependence of displacement and velocity, and the possibility to modulate this dependence with appropriate gestures. In the second experiment, a robotic finger is used to further optimize the key trajectory, by modifying in terms of velocity and downward displacement a referent trajectory. In this case it seems possible to manage the clavichord's paradox, and to control independently velocity and displacement, i.e. intonation and loudness of the instrument. Whether a musician would be able to effectively perform this type of movement remains an open question.

ACKNOWLEDGEMENTS

The authors thank Sebastien Guy and Laurent Quartier for their help during the measurements.

REFERENCES

[1] B. Brauchli. *The clavichord*. Cambridge University Press, 1998.

[2] D. Chadefaux, J.-L. Le Carrou, and B. Fabre. A model of harp plucking. *The Journal of the Acoustical Society of America*, 133(4):2444–2455, 2013.

[3] D. Chadefaux, J.-L. Le Carrou, M.-A. Vitrani, S. Billout, and L. Quartier. Harp plucking robotic finger. In *Intelligent Robots and Systems (IROS), 2012 IEEE/RSJ International Conference on*, pages 4886–4891. IEEE, 2012.

[4] C. D'Alessandro. Le paradoxe du clavicorde. In *Congrès Français d'Acoustique (CFA 2016)*, pages 2263–2269. Société Française d'Acoustique, 2016.

[5] C. D'Alessandro. Le paradoxe du clavicorde et la technique de Bach au clavier. *Revue musicale OICRM*, 6(1):87–112, 2019.

[6] A. De Cheveigné and H. Kawahara. Yin, a fundamental frequency estimator for speech and music. *The Journal of the Acoustical Society of America*, 111(4):1917–1930, 2002.

[7] C. d'Alessandro. On the dynamics of the clavichord: From tangent motion to sound a. *The Journal of the Acoustical Society of America*, 128(4):2173–2181, 2010.

[8] J.-L. Le Carrou, D. Chadefaux, L. Seydoux, and B. Fabre. A low-cost high-precision measurement method of string motion. *Journal of Sound and Vibration*, 333(17):3881–3888, 2014.

[9] J.-L. Le Carrou, D. Chadefaux, M.-A. Vitrani, S. Billout, and L. Quartier. Dropic: A tool for the study of string instruments in playing conditions. In *Acoustics 2012*, 2012.

[10] A. Paté, J.-L. Le Carrou, A. Givois, and A. Roy. Influence of plectrum shape and jack velocity on the sound of the harpsichord: an experimental study. *The Journal of the Acoustical Society of America*, 141(3):1523–1534, 2017.

[11] M. Van Delft. Schnellen. a quintessential articulation technique in eighteenth-century keyboard playing. *The Keyboard in Baroque Europe*, Christopher Hogwood (dir.)(1):187–197, 2003.

[12] J. G. Walther. *Musicalisches Lexicon oder Musicalische Bibliothec*. Wolfgang Deer, 1732.

PROCEEDINGS of ISMA 2019
International Symposium on Music Acoustics

13 - 17 September 2019 in Detmold, Germany

Factors affecting transients in rapid articulation on a bass crumhorn

Alan WOOLLEY; Murray CAMPBELL; Simon CARLYLE.

(1) University of Edinburgh, United Kingdom, awoolley@staffmail.ed.ac.uk
(2) University of Edinburgh, United Kingdom
(3) University of Edinburgh, United Kingdom

Abstract

The generation of a pitched note on a reed instrument involves a nonlinear acoustic coupling between the mechanical reed and the air column of the instrument. Once a stable regime of oscillation has been achieved the reed vibrates at the playing frequency, which is much lower than the reed natural frequency. On windcapped instruments like the crumhorn a change in the playing frequency is initiated by opening or closing toneholes. This modifies the acoustic resonances frequencies of the air column, and the pressure feedback to the reed causes its vibration frequency to change. Factors affecting the transients during rapid pitch changes on a bass crumhorn have been investigated using high speed video recording of reed motion, laser-based position tracking of the reed tip vibration, and measurements of pressure upstream and downstream of the reed.

Keywords: Woodwind, Double-reed, Transients.

1 INTRODUCTION

The crumhorn is a double reed windcap instrument dating back to the renaissance. Although the acoustics of single reed woodwind instruments has been very intensively studied there has been relatively little work on double reed instruments. The thesis of André Almeida [1] was a major step in filling this gap, and a paper by Almedia et al. [2] reported an investigation of modern double reeds using an artificial blowing machine and high speed photography. The work described here is part of a study taking a similar approach to the behaviour of renaissance and baroque double reed woodwinds. We chose to start with the bass crumhorn for a number of reasons. The windcap completely encloses the reed, so that unlike on the modern oboe or bassoon the player's lips are not in contact with the reed. The crumhorn has the further advantage that the bore is cylindrical along the majority of its length, apart from a very short flare at the end, thus eliminating the complications of tapered bores and bells. A final reason for choosing the bass crumhorn was that this unusual instrument has already been studied in experiments on period doubling [3].

This project seeks to examine the transient behaviour of the reed during rapid pitch changes. The normal windcap was replaced by a cylindrical Perspex cap, pressurised by an air pump and fitted with a window through which the reed opening could be videoed. Three different playing regimes were examined. First the reed motion was studied for continuous stable playing over a range of different blowing pressures and fingering patterns. Then the effect of a rapid change in the air column resonances caused by the opening or closing of one of the two metal keys on the instrument was investigated. Finally the action of the player in starting or stopping the note by 'tonguing' at the entrance to the windcap slot was simulated by constricting the air supply tube.

2 EQUIPMENT

The equipment used in this project included a multistage centrifugal air pump which supplied pressure to the transparent windcap. Pressure sensors in the windcap and the reed staple, and sensors measuring displacement of the reed tip and the instrument keys, supplied signals to an Iotech Wavebook 516E data acquisition system. The maximum data collection rate was 10^6 samples per second with 16 bit resolution. All recordings were taken at 10k samples per second per channel. The software used was Waveview v. 7.15.19.

The movement of the reed was recorded with a Baumer OADM 12U6430/S35A laser sensor. This has an operating range of 16-26mm with a distance resolution of 0.005mm and a response time of <0.9ms. Tests confirmed that worked through the Perspex tube used for the windcap and also in close proximity to the bright lights necessary for the high speed camera. A similar sensor was used to record the movement of the keys.

A Sensortechnics HCXM050D6V pressure sensor was used to measure the windcap pressure. This has a calibrated pressure limit of 5kpa although experiments confirmed that it remains linear slightly outside this limit. A G.R.A.S. 46BG high pressure microphone was used to measure the acoustic pressure downstream of the reed, through a short side tube on the reed staple. This microphone has a calibrated output of 0.27 V/Pa. Sound recordings used an AKG CE391B microphone. This was sampled at 10 kHz by the data acquisition system and was also fed to a Tascam DR100 mk2 digital recorder, allowing for recording sound files at higher sample rates.

High speed video recordings were made with a Photron SA1.1 camera operating at 4000 frames per second. The lens was a Nikon Macro Nikkor 24-85mm f2.8-4 with 2.2 times teleconvertor and 4cm extension tube. Software: Photron Fastcam Viewer v. 3670. The camera was triggered in synchronism with the data acquisition system. The lighting of the reed was provided by small led spotlights that were selected for being flicker free. They are also cool running, and using multiple lights gives the even and adjustable field crucial for clear imaging of reed motion. High speed video recordings will be shown during the presentation, but have not yet been quantitatively analysed.

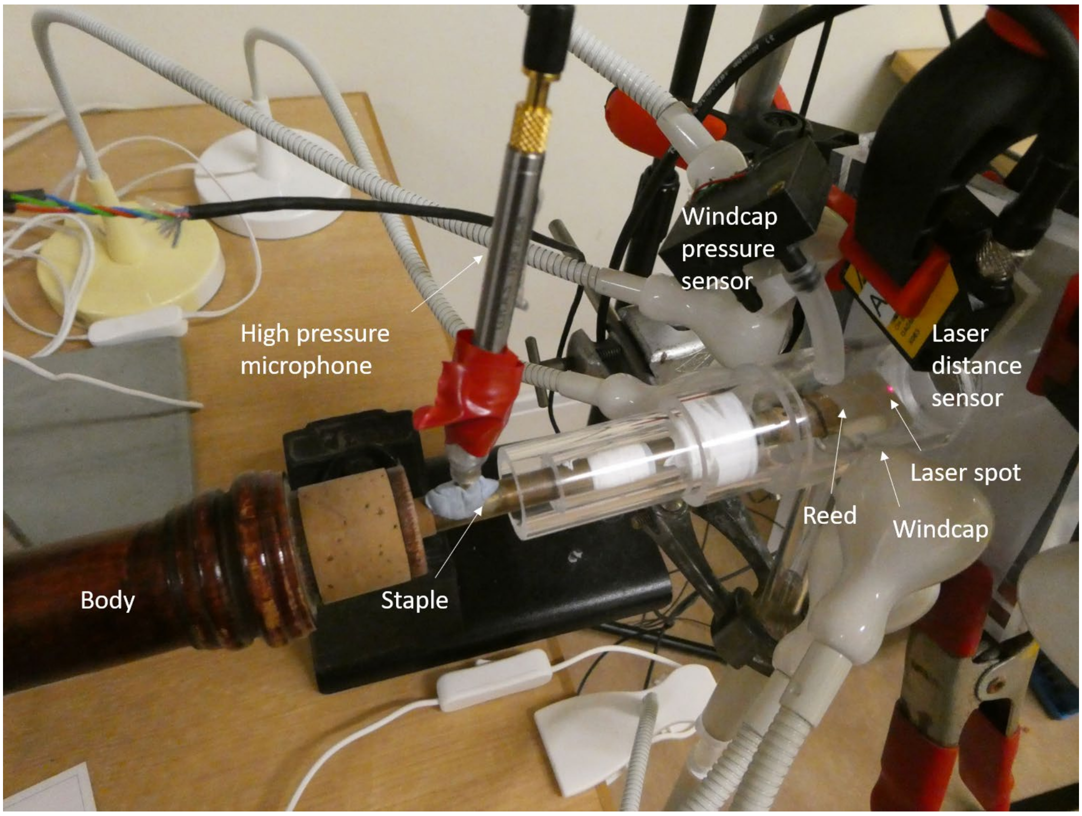

Figure 1. Instrumented transparent windcap.

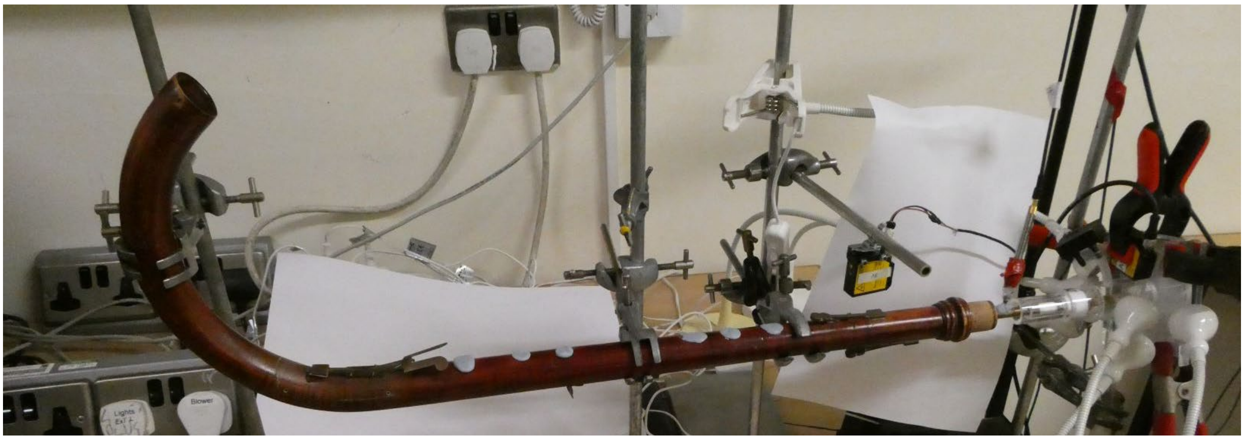

Figure 2. The mounting arrangement of the bass crumhorn, with six tone holes closed by BluTak. The laser displacement sensor is positioned above the upper key

3 EXPERIMENTAL WORK

3.1 Constant sounding

The first set of readings were taken with the crumhorn playing a stable note, first at the nominal pitch and then at reduced pressure. The instrument has six open tone holes, which can be covered by the fingers. It also has two holes, one above the open set and one below, which are covered by pads and opened by depressing keys. For the measurement shown in Fig. 3, the lowest three finger holes were closed with BluTak. Fig. 3 shows the results of the crumhorn with the pressure adjusted to play at c^3 130.8Hz.

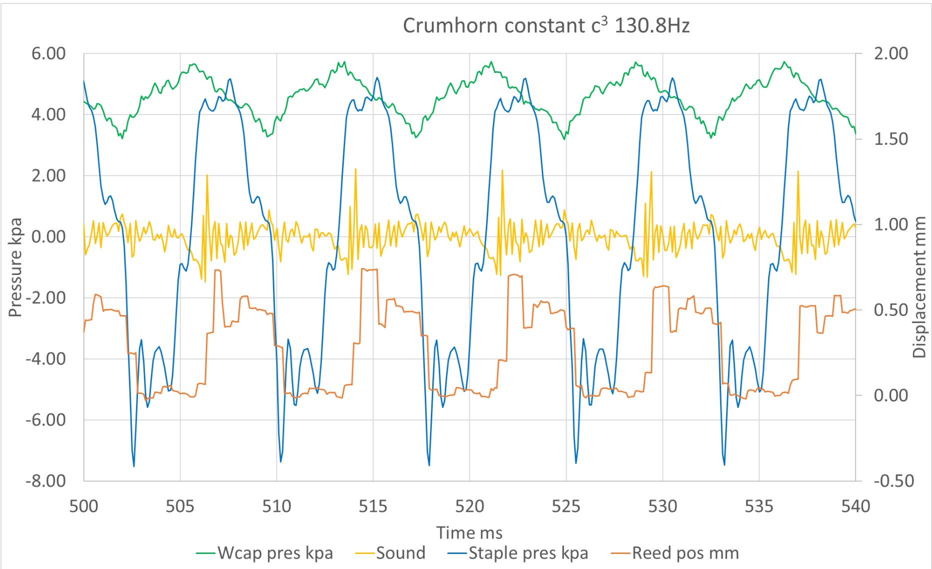

Figure 3. Steady note. Green: windcap pressure. Blue: pressure in reed staple. Yellow: radiated pressure. Red: displacement of reed tip.

The green line shows the pressure in the windcap measured in kPa; it is always positive and with a mean of 4.62kPa. The blue line is the pressure in the staple, alternating between positive and negative relative to atmospheric pressure with a mean of zero kPa. The red line is the position of the reed with zero representing fully closed. It was necessary to position the laser beam approximately 0.3mm from the edge of the reed. This shows the reed giving a distinct bounce on opening and also shows that when fully closed, the section of the reed between the front edge and the staple also bounces. The microphone was placed approximately 10 cm from the open end of the crumhorn and approximately 50 cm from the reed. There is therefore a delay of approximately 1.6 ms between a pressure change at the reed and the resultant change at the microphone.

3.2 Key opening

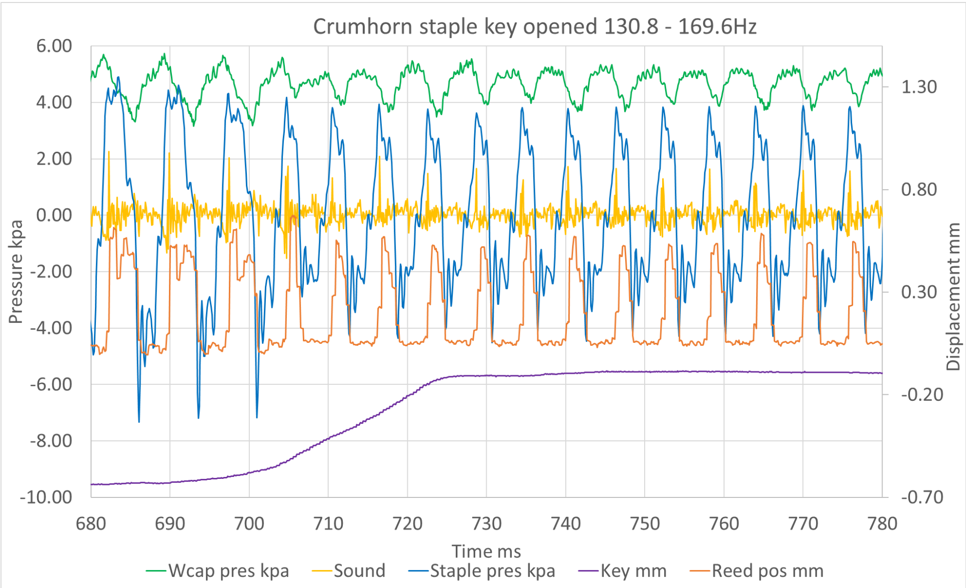

Figure 4. Opening of a key. Green: windcap pressure. Blue: pressure in reed staple. Yellow: radiated pressure. Red: displacement of reed tip. Magenta: displacement of key.

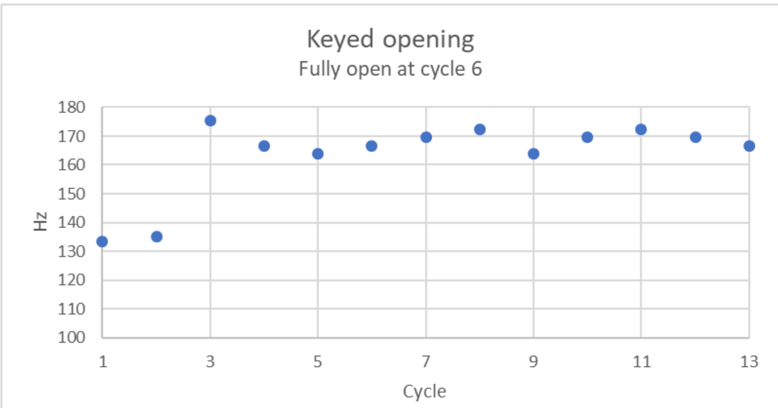

Figure 5. Frequency change during 13 cycles of vibration in Figure 4.

The downward staple pressure spike in Fig. 4 coincides with the closing of the reed. Cycles in Fig. 5 are measured from this point, starting at 686.1 ms; ‘frequency’ is the inverse of the cycle period.

The key starts to open at 690 ms and is completely open at 725 ms. The peak pressure in the staple starts reducing within one cycle and is stabilised at the higher frequency within two cycles. At 130.8 Hz the reed is open for approximately half of the cycle. At 169.6 Hz the reed is open for a significantly smaller proportion of the cycle and does not exhibit the characteristic bounce observed at the initial lower frequency.

3.3 Key closing

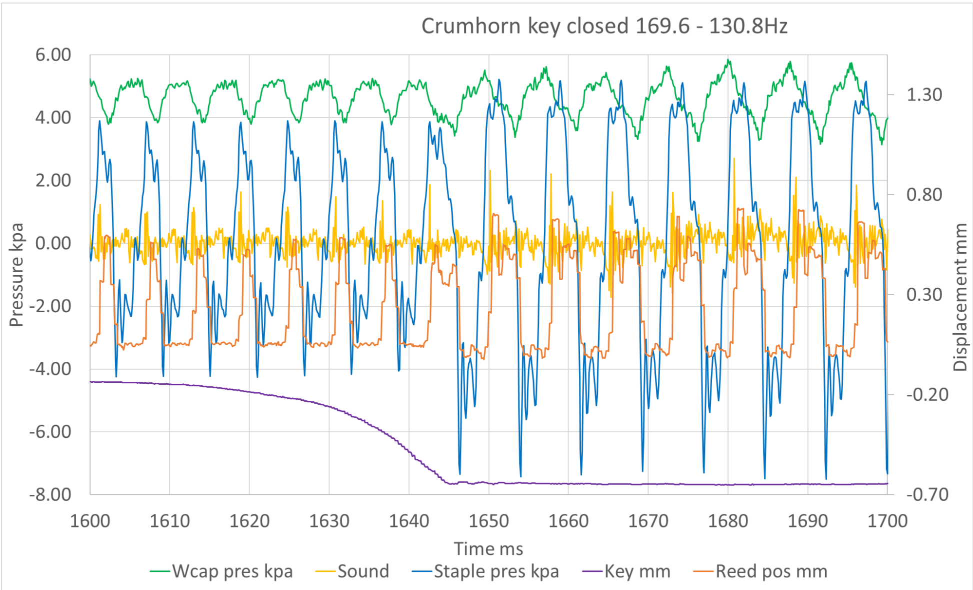

Figure 6. Closing of a key. Green: windcap pressure. Blue: pressure in reed staple. Yellow: radiated pressure. Red: displacement of reed tip. Magenta: displacement of key.

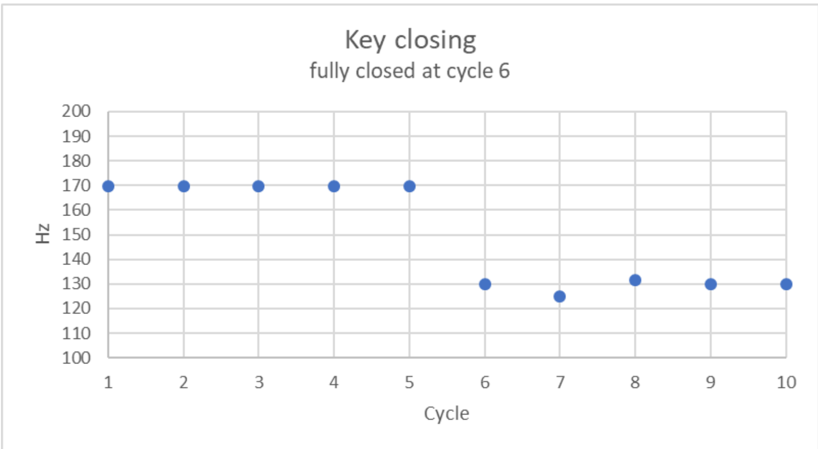

Figure 7. Frequency change during 13 cycles of vibration in Figure 6.

Cycle 1 is defined as 1609.2 ms to 1615.1 ms. The valve is fully closed at the end of cycle 6. As in the key opening case, the transition occurs almost completely within one cycle.

3.4 Simulated tongued start

In order to simulate the effect of tonguing, that is blocking the air inlet into the windcap with the tongue in order to cut off the wind supply quickly, a short length of flexible tube was incorporated into the supply tube from the air supply. This could be manually squeezed in order to cut off the air supply as quickly as possible**.**

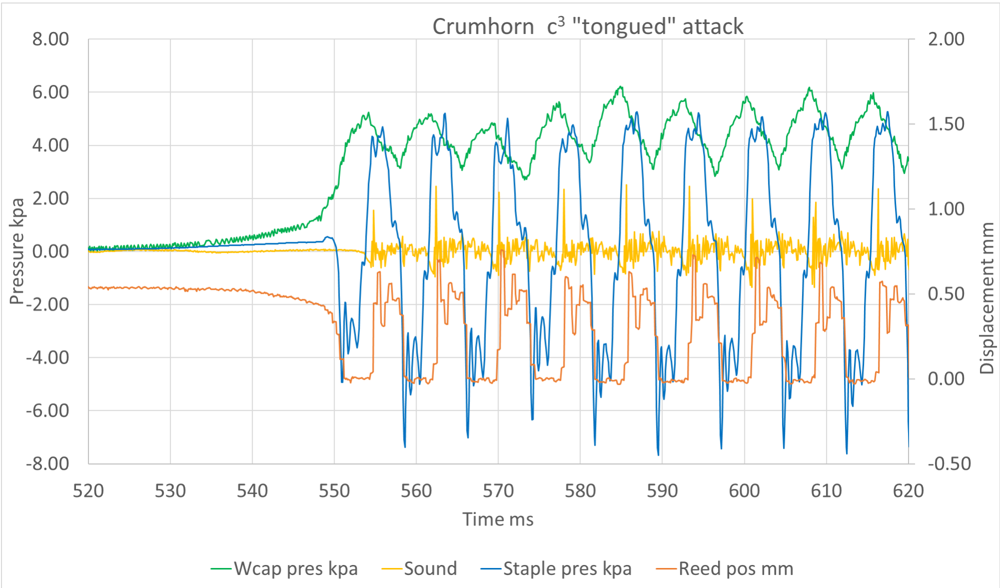

Figure 8. Simulated tongued start. Green: windcap pressure. Blue: pressure in reed staple. Yellow: radiated pressure. Red: displacement of reed tip. Magenta: displacement of key.

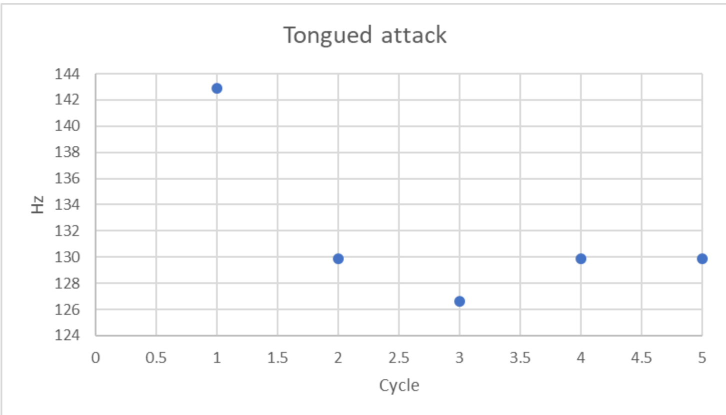

Figure 9. Frequency change during 4 cycles of vibration in Figure 6.

The pressure starts to rise at 530 ms, and the first downward spike in staple pressure occurs at 551.6 ms. The steady oscillation is almost completely established after one cycle.

3.5 Simulated tongued stop

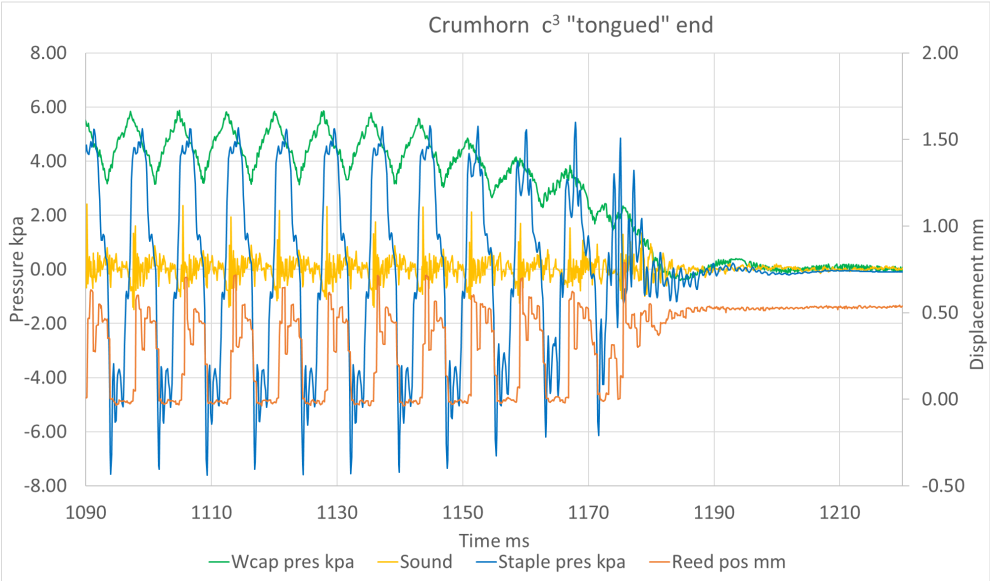

Figure 10. Simulated tongued stop. Green: windcap pressure. Blue: pressure in reed staple. Yellow: radiated pressure. Red: displacement of reed tip. Magenta: displacement of key.

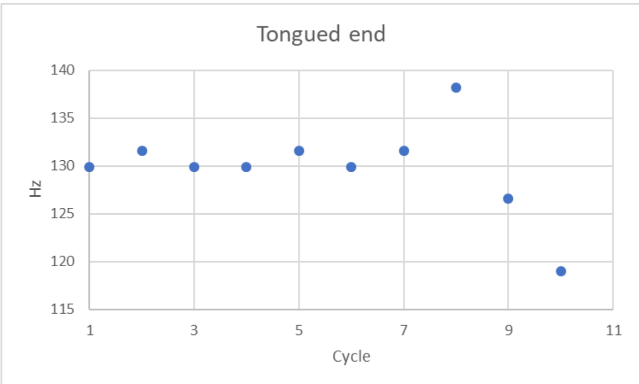

Figure 11. Frequency change during 10 cycles in Fig. 10.

Cycle 1 is defined as 1101.7ms to 1109.3ms. The inlet is closed at 1140 ms, but the air in the wind cap has to exhaust through the reed. The windcap pressure falls to zero at 1180 ms, the main part of the closing transient lasting around four cycles of the steady vibration. There is a small amplitude sinusoidal fluctuation in the tail of the windcap pressure with a period of approximately 20 ms.

4 CONCLUSIONS

The experiments described above have examined the transients during normal playing behaviour of the bass crumhorn. When a key is pressed or released, the reed responds to the change in air column geometry by changing its vibration state, and the new state is almost completely stabilised after one cycle of the new vibration. When a note is initiated by rapidly raising the blowing pressure above its threshold value, the starting transient lasts approximately one cycle, although small fluctuations are observed over the following few cycles. When the note is ended by rapidly closing the entry of the air flow, the fluctuations in pressure in the windcap die away over several cycles as the air is exhausted through the reed aperture. The final transient is therefore considerably longer than the starting transient.

Experiments have also been carried out for values of windcap pressure above the playing threshold but well below the values used in normal playing. Considerably longer transients are then encountered, including temporary excitation of period multiplying states. These phenomena require further investigation, and comparison with physical modelling of the instrument.

5 REFERENCES

[1] Almeida, A. The Physics of Double-reed Wind Instruments and its Application to Sound Synthesis. PhD Thesis, Univ. Pierre et Marie Curie, Paris, 2006.

[2] Almeida, A; Vergez, C; Caussé, R. Experimental investigation of reed instrument functioning through image analysis of reed opening. Acta Acustica united with Acustica, 93(4), 2007, pp 645-658.

[3] Gibiat, V; Castellengo, M. Period doubling occurrences in wind instrument musical performance. Acta Acustica united with Acustica, 86, 2000, pp 746-754.

PROCEEDINGS of ISMA 2019
International Symposium on Music Acoustics

13 - 17 September 2019 in Detmold, Germany

Music practice rooms: Ambitions, limitations and practical acoustic design

Claudiu POP[1]; Riduan OSMAN[2]; Julia KNIGHT[3]

(1) The University of Sydney, School of Architecture, Design and Planning, Australia, claudiu.pop@sydney.edu.au

(2) Northrop Consulting Engineers, Australia, ROsman@northrop.com.au

(3) Sydney, Australia, juliaknightaudio@gmail.com

Abstract

The acoustic design of music practice rooms is a well-researched and investigated topic. This study reviews critically the acoustic parameters generally accepted as desirable for these rooms and provides insight from a practitioner's perspective. A series of music practice rooms are discussed and a holistic discussion is provided on the design challenges and successes as part of a multidisciplinary team of acousticians, architects, building services and structural engineers.

Keywords: Music, Acoustics

1 REHERSAL ROOM ACOUSTIC DESIGN CONSIDERATIONS

1.1 Parameters

A number of considerations of music rehearsal rooms are common among research and design advice. These include but are not limited to; room size, room dimensions and symmetry, sound isolation, reverberation time, early reflections, diffusivity, room modes, as well as coordinated design for environmental factors such as lighting, ventilation and temperature control.

1.2 Sizing

There is a range of rehearsal room sizing recommendations from recent research. Drotleff et al investigate rehearsal room case studies and recommend a minimum of 1.4m2 per musician with minimum distance parameters to each wall in a space that is 70% as high as its width (14). While the Finish code of conduct specifies volumes per instrument type such as wind instruments at ≥20 m 3 /person, grand pianos require ≥80 m 3 /person and other instruments ≥10 m 3 /person for the purpose of education (13).

1.3 User requirements for music practice rooms

The music practice room probably receives the greatest level of usage of all the specially built music spaces. Music practice rooms vary in size, and accommodate diverse groups ranging from a solo instrumentalist to small music ensembles. In the past noise control and isolation have been the main concerns in their design. As music students can spend up to 40 hours per week in music practice and rehearsal rooms, these rooms are very important in the daily activity of a music school or department (18). Good room acoustics in a music practice room enable a music teacher to more effectively teach subtle concepts such as intonation, articulation, balance, dynamics and tone production while a poor acoustical environment can adversely affect the development of basic musical skills of a music student (22).

Although many acousticians may have a musical background, they may not be acquainted with the problems of teaching music, which requires a different acoustical situation from that of the auditorium or concert hall. Another issue confronting the acoustician and architect in the design of music practice rooms is the lack of understanding of the problems of teaching young musicians. The job of solving the acoustical problems has been complicated, in part, by the lack of communication between the musician-teacher and those involved in building

1 claudiu.pop@sydney.edu.au

2 ROsman@northrop.com.au

3 juliaknightaudio@gmail.com

construction. This has been complicated further by the failure of music teachers to separate acoustical problems from the general problems created by the inexperience of young performers. For example, in teaching situations involving balance, intonation, articulation, dynamic control, and tone-colour control, the teacher may it difficult to determine whether the disappointing result is due to inexperience or a poor acoustical environment (27).

1.4 Music practice rooms design issues

As recently as 2015, in the British Government guide [Building Bulletin 93] for the design of rooms for music teaching in schools only specified the desired room reverberation times and general mention of sound diffusion in the music rooms. Most of the focus of the acoustical issues is still the background noise from external (e.g. vehicular traffic) and internal (e.g. building services) sources and sound isolation between the adjacent music rooms. This indicates that not much has transferred from research work in small room acoustics to the design and construction of them since the days of Sabine (31) and Knudsen (16).

In this paper the acoustical issues in the design of small music practice rooms addressed are:

- Room Modes and Standing Waves
- Room Reverberation Times
- Room Diffusivity and Flutter Echoes
- Room Noise Isolation and Background Noise are mentioned but not covered in any detail.

1.5 Room modes and standing waves

As early as 1896, Rayleigh had recognised and shown that the air enclosed in a rectangular room has an infinite number of normal modes of vibration. The frequencies ‘f’ at which these modes occur are given by the following equation: [Beranek,1986] [Everest, 1991].

$$f = 0.5c\ ((p/L)^2+(q/W)^2+(r/H)^2)^{0.5} \tag{1}$$

Where c is the speed of sound (344m/s),
L is the length of the room in metres,
W is the width of the room in metres,
H is the height of the room in metres,
p, q, and r are the integers 0, 1, 2, 3 etc.

With the rapid growth of radio broadcast industry in the first half of the twentieth century, interest in small room acoustics, particularly small rectangular announcers’ studios and music studios, revealed the negative impact of room modes. As a consequence of this, Gurin & Nixon (12) proposed a height, width and length ratio of 2:3:5 for radio broadcast studios so as to minimize the objectionable grouping of resonant frequencies in the space.
In 1965, Sepmeyer (33) suggested that to minimise the room modal effect (an improvement on Gurin & Nixon, (12)), the following room proportions as the best starting point:

Table 1. Room proportions (12)

	Height	Width	Length
A	1.00	1.14	1.39
B	1.00	1.28	1.54
C	1.00	1.60	2.33

(The room proportions A, B, and C are ratios relative to the room height. If in the case of room Type B, the height of the room is 3.0 metres, the width should be 3.42 metres and the length should be 4.17 metres.) A summary of studies relating to room modes done by other researches in this field is summarised below in Table 2.

Table 2. Recommended room dimension ratios for small rooms

Name of Ratio	Ratio of Room Dimensions	Normalised for Equal Volume	Relative Floor Area	Normalised Equal Height	Relative Floor Area
Harmonic	1:02:03	1:02:03	6.00	1:02:03	6.00
V.O.Knudsen	1.6:3:4	1.09:2.04:2.71	5.53	1:1.88:2.5	4.69
European	3:05:08	1.11:1.84:2.95	5.43	1:1.67:2.67	4.44
J.E.Volkmann	1:1.6:2.5	1.14:1.83:2.86	5.24	1:1.6:2.5	4.00
Golden Ratio	1:1.25:1.6	1.44:1.80:2.31	4.16	1:1.25:1.6	2.00
Golden Section	(5½-1):2: (5½+1)	1.12:1.82:2.94	5.35	1:1.63:2.63	4.25
P.E.Sabine	2:03:05	1.17:1.75:2.92	5.13	1:1.5:2.5	3.75
Sepmeyer 1	1:1.14:1.39	1.56:1.78:2.17	3.85	1:1.14:1.39	1.58
Sepmeyer 2	1:1.28:1.54	1.45:1.86:2.23	4.14	1:1.28:1.54	1.97
Sepmeyer 3	1:1.6:2.33	1.17:1.88:2.73	5.12	1:1.6:2.33	3.73
Louden	1:1.4:1.9	1.31:1.83:2.49	4.55	1:1.4:1.9	2.66
BBC Prototype	3.25:4.9:6.7	1.25:1.88:2.57	4.82	1:1.51:2.06	3.11

Adapted from: (12, 20, 29, 37, 10).

Bonello (4) noted that at low frequencies, in small rectangular rooms, the room modes (eigentones) spacing can be very large and usually greater than half octave apart and he asserted that this caused 'peaks and valleys' in the room response which is undesirable. To minimise the effects of the 'peak and valleys' Bonello proposed the criteria for the acceptability of room modes distribution pattern based on his prescribed spread of the room modes (eigentones). Bonello's first criterion for room acceptability is to plot the eigentones over each one-third octave band and examine the resulting plot to check that each one-third octave has at least the same number or more modes than the preceding one-third octave. This provides an even spread and gradual increase in room modes as the frequency increases. Bonello's second criterion is to examine the modal frequencies to make sure that there are no coincident modes (11). A check of the above combinations in Table 1 using the 'Bonello Criteria' shows that the Knudsen, European, Volkmann, Golden Section and Sabine marginally failed the first criterion, but all the combinations passed the second criterion. The second criterion is probably the more significant of the two.

1.6 Music practice room reverberation times

The Reverberation time (RT) is probably the most widely used parameter in room acoustics, and is usually measured using the Schroeder integrated impulse response technique (32), and linear regression between -5 and -35 dB (or -25 dB when the dynamic range is insufficient) (28). Studies by Lamberty (18) on room reverberation noted that 59% of music students preferred a 'live' room while 11% preferred a 'dead' room and 30% preferred something midway. By the process of elimination, it was found that when the students were thinking of a 'dead' room they were thinking of a room with a reverberation time of 0.4 to 0.5 second and a live room having a reverberation time of 0.8 to 0.9 seconds. Over 85% of the students found domestic bedrooms far too dead to practise in and the majority felt that a bathroom would be impossible to practice in. The overall preferred reverberation time was in the region of 0.7 seconds. Most students agree that the ideal room would have variable acoustics, which would enable them to practice in different conditions, including difficult ones: e.g., in dead conditions (which the students believed to be better to practice in) for a certain period, and then live conditions which are far more pleasurable and more rewarding for them. Most students agreed that a room of 15m2 would be acceptable.

In their study in determining the optimum reverberation times and minimum acceptable size for music teaching studios and practice rooms, Lane et al (19) concluded that for small practice rooms a reasonable design for the reverberation time would be between 0.4 to 0.5 seconds. A slight rise to 0.6 or 0.7 sec at 100 Hz is acceptable. For the teaching studios with a volume of approximately 60 m3, a reverberation time of 0.5 to 0.6 seconds with a rise to approximately 0.8 seconds at 100 Hz is satisfactory. As a relative comparison with larger spaces, Kuttruff (15) considers an RT of 1.8 to 2.1 sec. a sensible target for concert halls and an RT of 1.4 to 1.6 sec as appropriate for recital halls (for solo and chamber music performances). Table 1.2 below shows the typical dimensions and the recommended mid-frequency (Tmf) reverberation times for the various music rooms normally found in educational facilities.

Table 3. Recommended reverberation times for small practice rooms

Music Activity Space	Area m2	Height m	Volume m3	AS2107 2016	DfES 2002	BB93 2015	OCPS 2003	ANSI S 12.60
Music theory classroom	50-70	2.4-3.0	120-210	0.5-0.6	0.4-0.8	<1.0	N/A	<0.6
Ensemble /music studio	16-50	2.4-3.0	38-150	0.7-0.9	0.5-1.0	0.6-1.2	0.5-0.7	<0.6
Recital rooms	50-100	3.0-4.0	150-400	1.1-1.3	1.0-1.5	1.0-1.5	N/A	N/A
Teaching/practice room	6.0-10	2.4-3.0	14-30	0.7-0.9	0.3-0.6	<0.8	<0.5	<0.6
Studio Control room	8.0-20	2.4-3.0	19-60	0.3-0.7	0.3-0.5	<0.5	<0.6	N/A

In their White Paper on Acoustic Criteria and specification, the British Broadcasting Corporation (37) stated that "the reverberation time is the only objective measure of the internal acoustic conditions within a small studio or room that is reasonably well understood, but it is, at best, a poor guide to the subjective acoustic environment. Many proposals for alternative or additional measurements have been made over the years but none can, at present, be interpreted subjectively, at least in small rooms. There is some good evidence that these alternatives are meaningful in concert halls and other large spaces."

1.7 Room noise isolation and background noise

Lamberty (18) noted that when asked about the back-ground noise levels, 86% of the music students found the noise from other students practicing most disturbing, followed by 9% that found traffic noise most disturbing and 4% found other noises disturbing. This emphasizes the importance of the isolation between music rooms and the need for proper zoning of music rooms and facilities.

As musical instruments can produce as much sound power in small rooms as in large auditoriums, they can be uncomfortably loud in small spaces. This is a common problem in small music rooms with insufficient acoustic absorption, and can give rise to sound levels which could, in the long term, lead to hearing damage. Many professional orchestra musicians have noise-induced hearing loss due to extended exposure to high noise levels both from their own instruments and, to a lesser extent, from others instruments nearby. For reduced sound intensity, sound absorbing materials or membrane absorbers are normally used extensively in music buildings (9, 39). Small practice rooms also require a good deal of installed sound-absorbing material for the sake of reverberation control, and in particular instances, elimination of flutter echo paths between parallel walls (21).

AS2107 (2016) recommends an ambient sound level of 30dBLAeq for music studios, 35dBLAeq for drama studios and 40dBLAeq for music practice rooms. DfES (9) recommends the indoor ambient noise level by for all school music facilities is 30dBLAeq,30mins, and for some uses noise limits below 30 dB LAeq may be required. Table 1.4 above shows a summary of recommended maximum levels.

Table 4. Summary of recommended maximum levels

Music Activity Space	Cav.(6)	AS2107 2016	ANSI 2002	DfES 2002	BB93 2015	OCPS 2003
Recording Studio	20dBA	25dBA	N/A	S/A	30dBA	NC 15-25
Recital Hall	25dBA	S/A	N/A	25dBA	30dBA	N/A
Rehearsal Room	35dBA	35dBA	35dBA	30dBA	35dBA	35dBA
Music Classroom	35dBA	40dBA	35dBA	30dBA	35dBA	N/A
Ensemble Practice	38dBA	45dBA	35dBA	30dBA	30dBA	35dBA
Individual Practice	42dBA	45dBA	35dBA	30dBA	35dBA	35dBA
Music Listening	42dBA	35dBA	35dBA	30dBA	35dBA	N/A

S/A = Special Advice N/A = Not Available NC = Noise Criteria
(from AS2107-2016, 6, 1, 9, 10, 23)

1.8 Room diffusivity and flutter echoes

Brown (1964) stated that although diffusion is an issue, but for practical reasons it is not always possible to alternate types of treatment evenly over all surfaces. In such cases the following prescriptions should be observed for broadcast studios.

a. Some of each type of absorption should be applied normal to each of the three planes (longitudinal, transverse and vertical of each room).

b. Untreated areas should not face each other.

Brown (5) did not specifically comment on potential problems with parallel walls and flutter echoes but this was addressed in later work by others. (38, 9). There have been various ways 'traditionally accepted' ways of dealing with problems of parallel walls and flutter echoes such 'item b' above described by Brown (5) and treating the walls with absorptive fabric wrapped panels, or absorptive materials directly applied on the walls. Flutter echoes can also be reduced and room diffusivity increased with the use of the quadratic residue diffusers proposed by Schroeder (32), and later commercially developed by D'Antonio (8). Unlike absorptive wall panels or finishes, the quadratic residue diffusers can minimise flutter echoes and improve room diffusivity without significantly reducing the room reverberation times.

1.9 Music room requirements for various musical instruments

Various types of musical instruments have differing requirements from a small music practice room. Issues to be taken into consideration are the potential sound power that can be generated by the instrument, the frequency range of the instrument and the type of instrument itself (wind, string, percussion etc.). This would determine the sound insulation requirements between music rooms and the type of internal acoustic treatment.

Research conducted on subjective listener assessments of the sounds of various instruments in practice rooms indicates the following are the preferred mid-frequency reverberation times for the various types of instruments for rooms between 20 and 100 cubic metres (24, 25).

Table 5. Preferred reverberation time per musical instrument type

Instrument Type	Preferred RT
Percussion Instruments	0.3 - 0.5 secs
Bowed String Instruments (violin, cello)	0.6 – 0.9 secs
Wind Instruments (trumpet, flute)	0.4 – 0.7 secs

The lower range of the reverberation time is recommended for room volume of about 10m3 and the higher range for room volumes of about 100m3.

Other factors such a loudness, signal to noise ratio, clarity, balance (interaural level difference) and music genre has a slight influence the ideal reverberation times (25) but this is beyond the scope of this paper.

1.10 Start with the room shape and size

Although rooms with non-parallel walls, floors and ceilings are preferred for music rooms, to maximize the utilisation of the available space the rooms in music teaching facilities are normally rectangular in size with floors and ceilings perpendicular to the walls. Where rectangular rooms with parallel walls, floors and ceilings are adopted, care should be taken to determine the ratios of the room length, width and height.

Computer modelling by the author shows that based on a 3 metre room height and the musical instruments tuned to the noted in a tempered scale, the BBC prototype ratios provided the room dimensions for the optimum predicted performance, taking into consideration the Bonello criteria and Room Mode frequencies (at standard speed of sound of 344m/s).

For rooms with non-parallel straight walls and ceilings, it is recommended that the optimised dimensions be applied to the room dimensions in the middle of the room (i.e. averaged room length, width and height). Curved walls are not recommended for small practice rooms to avoid focusing and other undesirable effects.

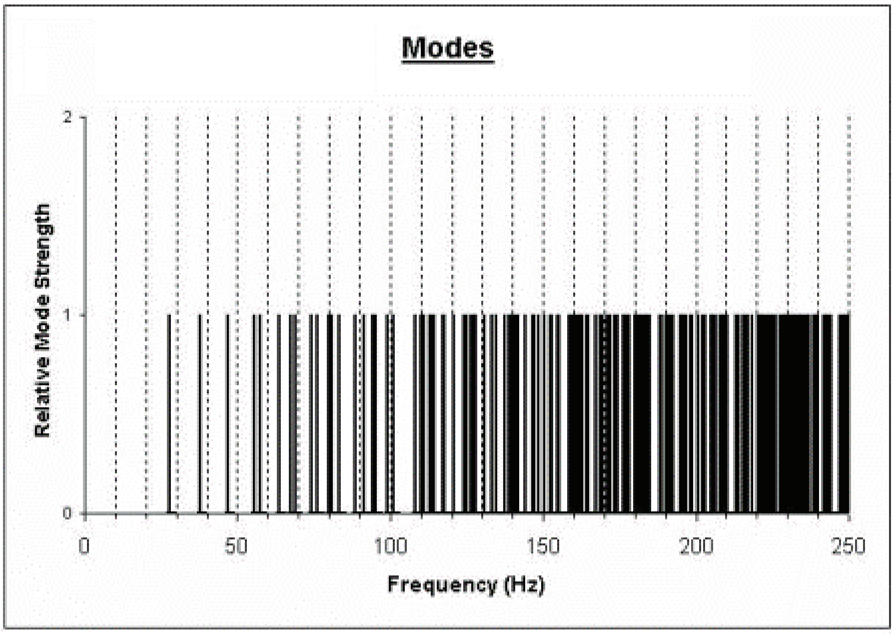

Figure 1. Room modes for a 6.58m X 4.52m X 3.0 high (BBC Prototype ratios) room.

2 CASE STUDIES AND PRACTICAL DESIGN

Two case studies are briefly presented, an existing large rehearsal space upgrade and a new design.

2.1 Existing rehearsal space upgrade

The existing studio is able to accommodate a full symphonic orchestra and is currently the main rehearsal space of a prestigious orchestra. It is intended to be the daily practice venue of the company and is used by both instrument players and opera singers.

The volume of the studio is approximately 2400 m3 and it has existing curtains, diffusion and some absorbers. The scope of the acoustic consultancy was to optimise the space to be more suitable in terms of reverberation and diffusion, as well as sound levels.

Figure 2. Acoustic measurements in an unoccupied rehearsal space

The measured reverberation time is long at 1.98s, and whilst this is good for performance venues, it is not ideal for rehearsal studios.

A detailed acoustic 3D model has been developed for the rehearsal room, with a view to auralize the space for the orchestra with the levels of reverberation they are satisfied with.

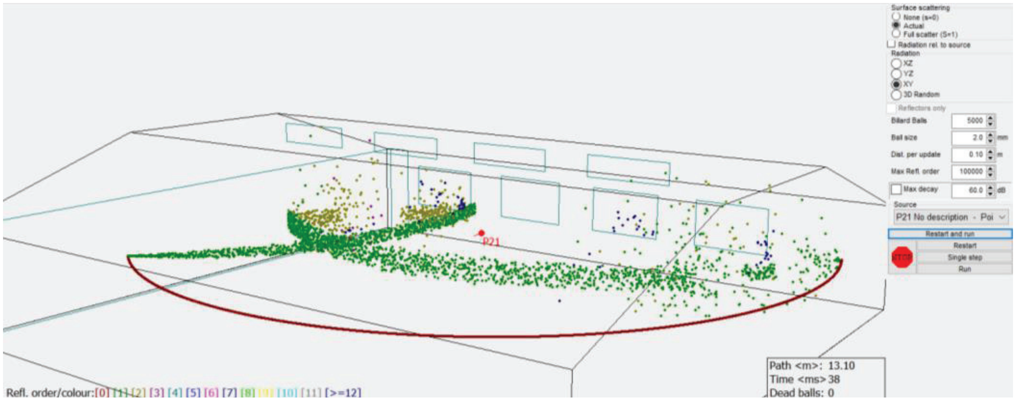

Figure 6. Optimizing acoustic parameters

A close collaboration with the orchestra players was considered essential, and incorporating the details and their experience into the design was paramount. The space is a difficult room to play in - the biggest issues being difficulty hearing other sections, resulting in poor ensemble and balance, and high noise levels. This is evident in rehearsals for both opera and ballet repertoire, and as a result conductors often have to spend considerable time trying to remedy the shortcomings of the room, at the expense of working on finer artistic and musical details.

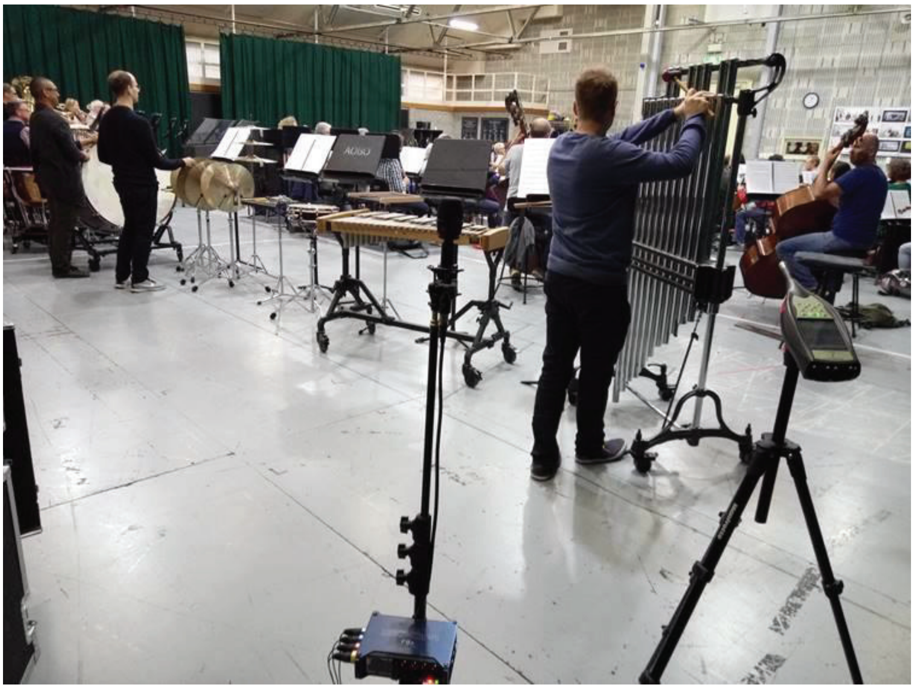

Figure 7. Measurements during rehearsals

2.2 New rehearsal space design

When designing a new rehearsal space, opportunities and challenges are different from the upgrade of an existing studio.

Figure 8. New rehearsal studio design (Courtesy of Visionata Architects and Norrebro Design)

When designing a new rehearsal space, opportunities and challenges are different from the upgrade of an existing studio. Whilst design for acoustic excellence in terms of the objective parameters is possible with a good team of acousticians, the detail work in terms of coordination with the orchestra, chorus, opera singers, but perhaps most importantly the design team is paramount.

In terms of coordination with the end users, we found that sound files from auralization are a great asset in terms of acoustic outcomes. This is important when orchestra and opera singers share a space, as high sound level fatigue is a stress factor for the players, whilst the singers often prefer a more reverberant field.

Perhaps the most important factor in the successful design of a new rehearsal space is the coordination with the design team. All team members must be involved early in the design process, but the collaboration between the architect and the acoustician is where the journey must begin. The careful selection of the location of the materials to diffuse and control the sound field is of great importance. The synergy between the two disciplines must be seamless and collaborative. The acoustician needs to understand the constraints the architect is facing, whilst the architect must be able to design with acoustics in mind to achieve his visual strategy.

The structural limitations of the building, if existing, can impose great constraints on the design of a rehearsal space. Ideally the height of the orchestra spaces should be approximately 9-10m, with more headroom required with the addition of solo singers and Chorus. Sometimes the ambitions of the players and singers, the acousticians and the design team must conform to the limitations of an existing building. For practical acoustic design, the team must always coordinate with the services engineers and work together. In addition to sound levels from mechanical services suitable for rehearsal, the mechanical services treatment in terms if cross talk via the ducting system needs to be addressed to maintain the sound insulation requirements between different practice rooms.

3 CONCLUSIONS

To design for a holistic music rehearsal room experience, it is critical to coordinate and collaborate with all consultants involved in the design. It is important that all of the musician's requirements are met besides acoustic excellence, including temperature control, lighting, aesthetics, and ergonomics of room layout.

REFERENCES

[1] ANSI S12.60-2002 (2002), "American National Standard Acoustical Performance Criteria, Design Requirements, and Guidelines for Schools"

[2] Blankenship J., Fitzgerald R.B. & Lane R.N. (1955), 'Comparison of Objective and Subjective Observations on Music Rooms' J. Acoust. Soc. Am., Vol.27, p774 – 780.

[3] Benade, A.H. (1985), "From Instrument to Ear in a Room: Direct or via Recording" J.Audio Eng. Soc., Vol.33 Issue4 p218-23

[4] Bonello O.J. (1981), "A New Criterion for the Distribution of Room Normal Modes" J.Audio Eng. Soc., Vol.29, p579 - 606.

[5] Brown S. (1964), 'Acoustic Design of Broadcasting Studios' J. Sound Vib., Vol.1, p239 - 257.

[6] Cavanaugh, W.J. (1990), "Keeping Things Quiet, Acoustical Design of Music Education Facilities", E.McCue & R.H.Talaske Editors, Acoustical Society of America, p48 - 54.

[7] Cox T.J. & D'Antonio P. , (2004) "Acoustic Absorbers and Diffusers. Theory, Design and Application" Spon Press, Taylor & Francis Group, London & NY.

[8] D'Antonio P. & Konnert J.H. (1984), "The Reflection Phase Grating Diffuser: Design Theory and Application" J.Audio Eng.Soc., Vol.32 No.4, p228-238.

[9] DfES (Dept. for Education and Skills, United Kingdom) (2002), "Draft Building Bulletin 93 – Acoustic Design of Schools", UK.

[10] DfES (Dept. for Education and Skills, United Kingdom) (2015), "Acoustic Design of Schools: A Design Guide - Building Bulletin 93", The Stationery Office, London.

[11] Everest F.A. (1991), "Acoustics of Small Rooms" Handbook of Sound Engineers, Editor G.M. Ballou, SAMS (Macmillan Computer Publishing), Carmel, Indiana.

[12] Gurin H.M. & Nixon G.M. (1945), 'A Review of Criteria for Broadcast Studio Design' J. Acoust. Soc. Am., Vol.19, p404 – 411.

[13] Heli Koskinen, Esko Toppila & Pekka Olkinuora (2010) Facilities for Music Education and Their Acoustical Design, International Journal of Occupational Safety and Ergonomics, 16:1, 93-104, DOI: 10.1080/10803548.2010.11076831

[14] H. Drotleff, X. Zha, H. Fuchs and X. Zhou, New room acoustic design concept for rehearsal rooms, pp. 483-484.

[15] H. Kuttruff 'Acoustical design of the Chiang Kai Shek Cultural Centre in Taipei' Applied Acoustics Vol.27 Issue 1, 1989, P 27-46

[16] Knudson V.O. (1930), 'Acoustics of Music Rooms' J. Acoust. Soc. Am., Vol.2, p434 – 467.

[17] Laitinen, H. (2005). Factors affecting the use of hearing protection among classical music players. Noise Health, 21-9.

[18] Lamberty, D.C. (1980), "Music Practice Rooms" Journal of Sound and Vibration, Vol.60, No.1, p149-155.

[19] Lane R.N. & Mikeska E.E. (1955), 'Study of Acoustical Requirements of Teaching Studios and Practice Rooms in Music School Buildings' J. Acoust. Soc. Am., Vol.27, p1087 - 1091.

[20] Louden M.M. (1971), 'Dimension-Ratios of Rectangular Rooms with Good Distribution of Eigentones' Acustica, Vol.21, p101 - 104.

[21] Marshall G.L. & Klepper D.L. (1999), “Acoustical Design: Places for Listening” Architectural Acoustics: Principles and Practice, Editors W.J.Cavanaugh & J.A.Wilkes, John Wiley & Sons, New York.

[22] McCue, E. (1990), “Rehearsal Room Acoustics,” Acoustical Design of Music Education Facilities, E.McCue & R.H.Talaske Editors, Acoustical Society of America, New York, p36 - 41.

[23] OCPS (Orange County Public Schools Standards) (2003), “Music Suite Acoustics”, Design Guidelines Manual, Facilities & Environmental Services, Orange County.

[24] Osman R. & Fricke R. (2003), ‘Perceived Acoustic Quality of Small Rooms for Music’ Proceedings of 8th

WESPAC, Melbourne, Australia.

[25] Osman R., Cabrera D. & Fricke R. (2003), ‘Acoustic Design of Small Music Practice Rooms’ Proceedings of 37th Australian and New Zealand Architectural Science Association (ANZAScA) Conference, Sydney, Australia.

[26] Osman R, (2010), ‘Designing small music practice rooms for sound quality’ Proceedings of 20th International Congress on Acoustics, ICA 2010

[27] Patrick N.G. & Boner C.R., 1967, “Acoustics of School-Band Rehearsal Rooms” J. Acoust. Soc. Am. Volume 41, Issue 1, p 215-219

[28] Pelorson, X, Vian, J.P. & Polack, J.D.(1992) “On the variability of room acoustical parameters: Reproducibility and statistical validity”, Applied Acoustis, Vol.37, Issue 3, p. 175-198

[29] Rettinger, M. (1988), “Handbook of Architectural Acoustics and Noise Control” TAB Books Inc., NY.

[30] Rossing, T.D. (1990), “The Science of Sound, 2nd Edition” Addison-Wesley Publishing Co., NY.

[31] Sabine W.C. (1922), ‘Collected Papers on Acoustics’ Reprinted by Dover Publications, Inc., 1964, p3-68.

[32] Schroeder, M.R., Gottlob, D., and Siebrasse, K.F., (1974), “Comparative study of European concert halls: Correlation of subjective preference with geometric and acoustic parameters,” Journal of the Acoustical Society of America, Vol.56, p1195 - 1201.

[33] Sepmeyer L.W. (1965), “Computed Frequency and Angular Distribution of the Normal Modes of Vibration in Rectangular Rooms” J. Acoust. Soc. Am., Vol.37, p413 – 423.

[34] Sinal, Ö. and Yilmazer, S., 2015. A comparative study on indoor sound quality of the practice rooms upon classical singing trainees’ preference. Proceedings of Euronoise 2015.

[35] Towne, M. (1990) Hall of Music, Washington, Acoustical Design of Music Education Facilities, E.McCue & R.H.Talaske Editors, Acoustical Society of America, p174 - 177.

[36] Walker R. (1995), ‘Controlled Image Design: The management of stereophonic image quality’ BBC R&D Re-port RD1995/4, Research & Development Dept, British Broadcasting Corporation, London, UK.

[37] Walker R. (2002), “Acoustic Criteria and Specification” BBC R&D White Paper WHP021, Research & Development Dept, British Broadcasting Corporation, London, UK.

[38] Wenger Corporation (2001), “Planning Guide for Secondary School Music Facilities” (in conjunction with the American Institute of Architects), Wenger Corporation, Minnesota, USA.

[39] Zha X., Fuchs H.V. & Drotleff H. (2000), “Improving the acoustic working conditions for musicians in small spaces” Applied Acoustics, Vol.63, p203 – 221.

PROCEEDINGS of ISMA 2019
International Symposium on Music Acoustics

13 - 17 September 2019 in Detmold, Germany

Acoustical evaluation of differences in Sanshin's tone depending on shapes of *SAO*

Kojiro NISHIMIYA[1]; Mao TOKUDA[1];Yuki YOKOTA[1], Hideo CHO[1]

(1) Aoyama Gakuin University, Japan, nishimiya@me.aoyama.ac.jp

Abstract

Sanshin is an OKINAWA's traditional musical string instrument. Generally, "sound board", "bridge", and "string" are the main factors on the string instrument's tone from the acoustical points of view. Nevertheless, about Sanshin, the players and the craftsman have thought that *Sao* (Neck) has been the most important. Sanshin has many types of *Sao* and there have many arguments of the relationship between "*Sao*" and "Tone (Timbre)". However, the sound mechanism is still not clarified. Therefore, the purpose of this research is to elucidate the sound mechanism of Sanshin which include the influence of *Sao*. We measured the Sanshin's tone using different types of *SAO* with the same body, string, and bridge. As a result, we found the several differences in the tones. Especially the differences were confirmed in the overtone distributions and the attenuation rates. For the understanding of these behaviors, we focused about the change of the thickness of *SAO*, and the mass loading of the head of *SAO*. By the cutting process of one wood-Sanshin, we found that the thickness of *SAO* influences the overtone distributions and the mass loading influences the attenuation at the ringing tone.

Keywords: Sanshin, Okinawa, *Sao*, string instruments, coupled vibrations, eigen frequency, bending stiffness

1 INTRODUCTION

Sanshin is an Okinawa's traditional string musical instruments and it has been always invaluable role for Okinawans. Sanshin is used to play in the various events and ceremonies. Also, Sanshin has a role not only as an instrument but also as a traditional craft. Therefore, it is also required the beauty of the shape. Sanshin has many types of *Sao* (Neck), although "Shamisen", which is the similar instruments as Sanshin in Japan, doesn't have such many types. This is one of the unique characteristics of Sanshin. Furthermore, the players and the craftsman of Sanshin have thought that the *Sao* has been the most important and there have many consideration and research results about *Sao* [1]. Also, there have many arguments of the relationship between "*Sao*" and "Tone (Timbre)". However, the sound mechanism of Sanshin is still not clarified from the acoustical points of view. Although some attempts for the sound analysis of Sanshin have been made [2,3,4], the detailed mechanism is still not clarified and also the different types of *Sao* are not evaluated. Therefore, we aim to elucidate the sound mechanism which include the influence of *Sao*. The different types of *Sao* with the same string, bridge, and body, were evaluated. Also, the influence of the thickness of *Sao* and the weight of top of *Sao* (which is called "*Ten*") by the cutting process using one wood sanshin were evaluated.

2 Characteristics of Sanshin

Sanshin mainly consists of "*Sao* (Neck)", "String", "Body", and "*Koma* (Bridge)". Detailed structure of Sanshin is shown in Figure 1. "*Ten*" is a top of *Sao* and the shape of *Ten* is various with different types of *Sao*, and *Ten* becomes the mass loading to the *Sao* in the vibration condition. A part of *Sao* is called as "*Shin*" and it is inserted in the body. Three strings are fixed by the edge of *Shin* (*Itokake*) and *Itogra*. Currently the strings made by the nylon and Tetron are generally used, although the silk strings were extensively used before.

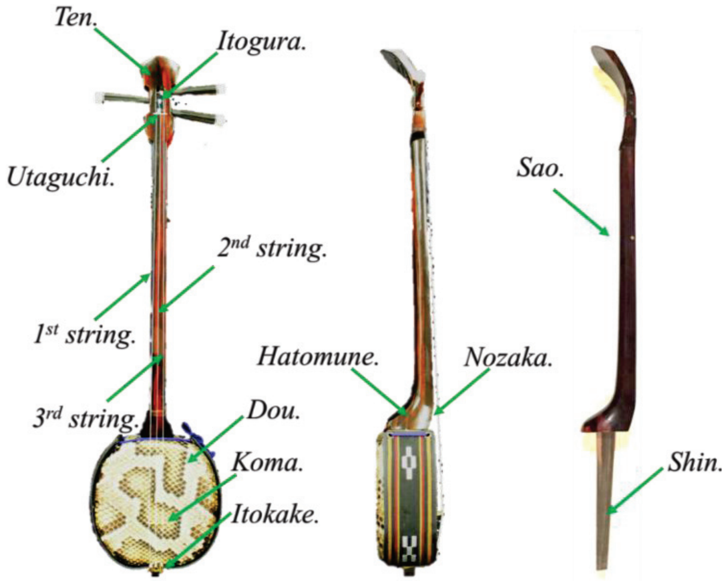

Figure 1. Structure of Sanshin

3 Measurement Method

In the acoustical measurement of the music instruments, the repeatability is most important. Sanshin is played by picking Bachi (pick) and the picking angle and the speed are different with the people and also for each music. The auto picking system was manufactured for the improvement of the repeatability [5]. The structure of the auto picking system is shown in Figure 2. Bach is rotated by the stepping motor and is controlled by the motor driver which is programed by the Raspberry Pi. Then the picking speed is controlled and also the position of Bach is fixed by the frame. The sides of the body of Sanshin is fixed by the pins and also the *Sao* is put on the formed polystyrene for not preventing the vibration of the instrument.

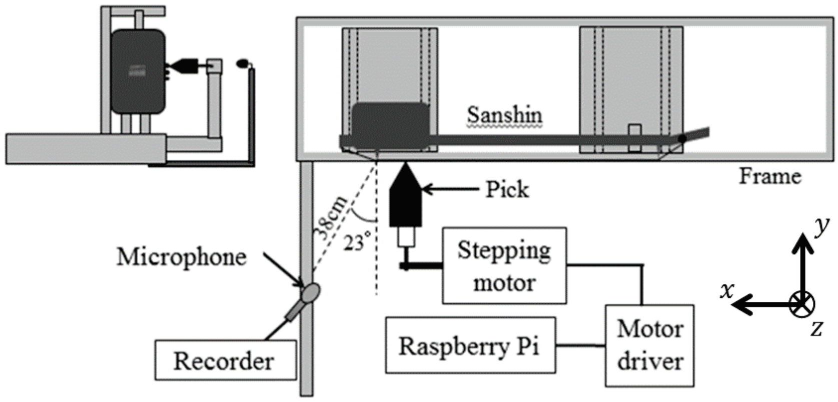

Figure 2. Auto picking system for Sanshin

4 Evaluation with different types of *Sao*

Four types of *Sao* were measured for this research. Figure 3 shows the photo of the *Sao*. The names of types are "*Yunagusuku*", "*Makabe*", "*Febaru*", and "*Kubashundwun*", respectively. The materials of woods are all same "*Kokutan* (ebony)". The same "string", "bridge", "body" and "*Koma*" are used for the measurement and the *Sao* is only changed by each measurement. The microphone is set above 30 cm from the *Koma*. The acquisition waveforms of sound are shown in Figure 4. Horizontal axis is time [s] and vertical axis is amplitude. Is is known that the waveform of Sanshin has double attenuation. They are the attenuation at the attack tone (immediately after the picking) and the attenuation at the ringing tone. The frequency spectra at the both tone were evaluated and the peak amplitude of each overtone was extracted. The overtone distributions are shown in Figure 5. The attack tone is until 0.05s after the picking and the ringing tone is after 0.05s in this analysis. From this result, it was found that the ringing tone have totally different overtone distributions with different *Sao*s, on the other hand, the attack tones have two trends of the overtone distributions. "*Makabe*" and "*Febaru*" are similar distributions and the maximum peak amplitude were 6th overtone, and "*Yunagusuku*" and "*Kubashundwun*" are the similar distributions and the maximum peak amplitude were 7th overtone. The similarity of "*Yunagusuku*" and "*Kubashundwun*" from the geometrical points of view, are the thickness of *Sao*. Comparing to "*Makabe*" and "*Febaru*", the thicknesses are both thicker. Therefore, it has a possibility that the thickness of *Sao* affects to the overtone distributions at the attack tone.

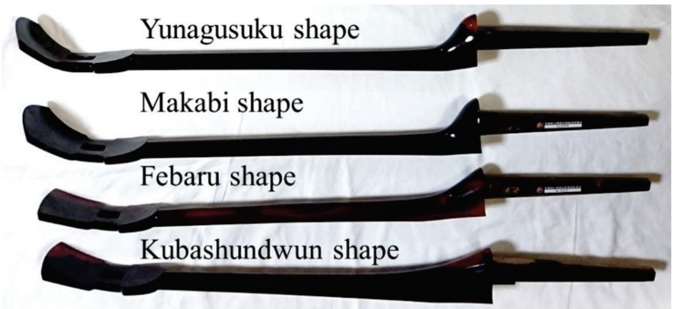

(a) Side View

(b) Top View

Figure 3 Photo of different types of *Sao*

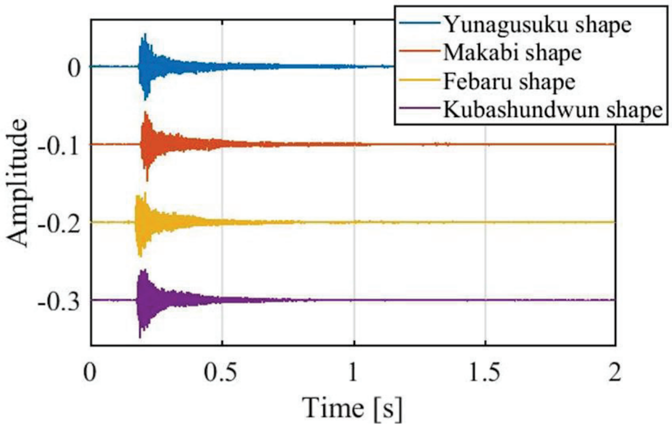

Figure 4 Time waveforms of different types of *Sao*

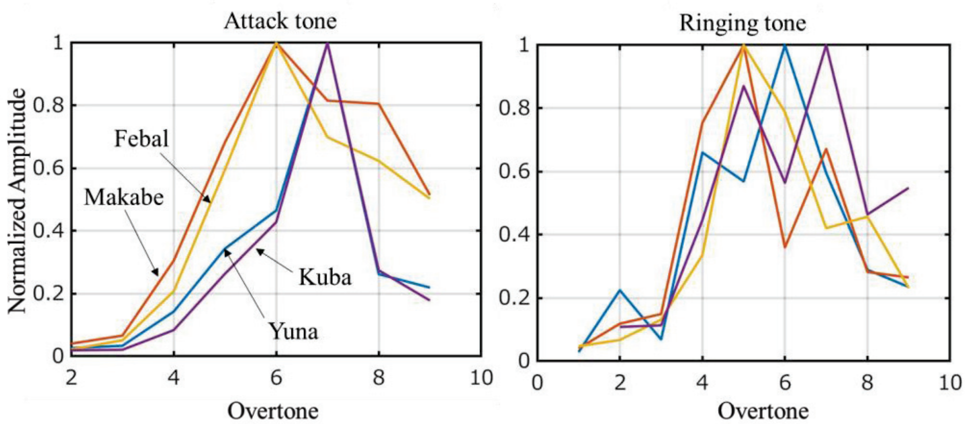

Figure 5 Overtone distributions with different types of *Sao*

5 Wood Sanshin with cutting process

From the results of acoustical evaluation with different *Sao*s, the influences of *Sao* were confirmed. However, it is difficult to conclude the cause of the influence, because there are many different parameters among each *Sao*. We used the same wood materials, but the actual wood parameters should be different due to the gnarl and the anisotropy of the woods, etc. Also, the thickness of *Sao* is different in each position and each type. Therefore, we cannot compare the thickness of *Sao* with different type simply. Therefore, we conducted the acoustical evaluation using one wood Sanshin with cutting process. Wood Sanshin is one of the Sanshin for the practice and the photo is shown in Figure 6. We can simply evaluate the difference of the thickness of *Sao* by cutting process. First, the characteristics of wood Sanshin was compared with the normal Sanshin (*Yunagusuku* type). The results of time waveform and the frequency spectra are shown in Figure 7. The waveform of wood Sanshin looks slightly low attenuation than normal Sanshin, and the frequency spectra are similar from Fig. 7 (b). Also, the comparison of the overtone distribution is shown in Fig. 7(c). Generally, they are similar distributions, although the maximum peak amplitude of normal Sanshin was 5th and it of wood Sanshin was 6th. Also, the higher modes around 12th overtone of normal Sanshin have several amplitudes, however, the modes of wood Sanshin have few amplitudes.

Figure 6 Photo of normal Sanshin and wood Sanshin

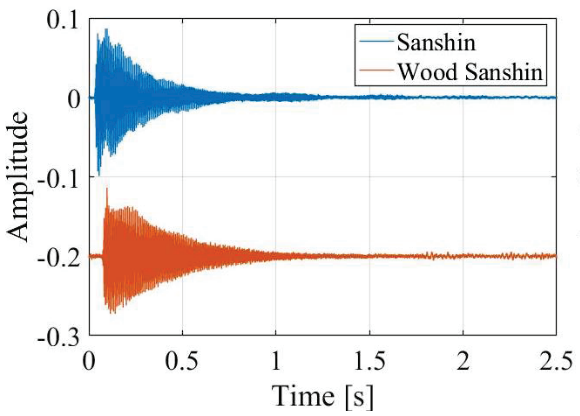

(a) Time Waveform

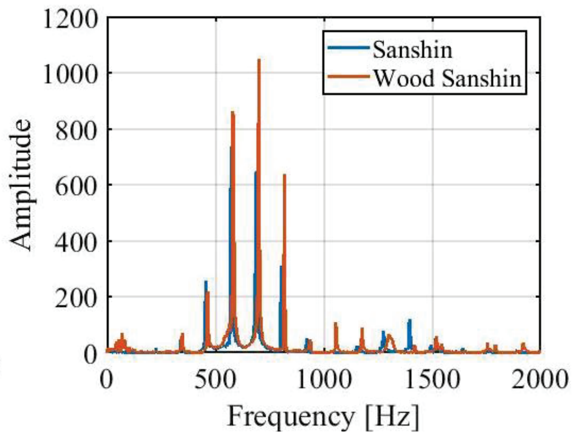

(b) Frequency Spectra

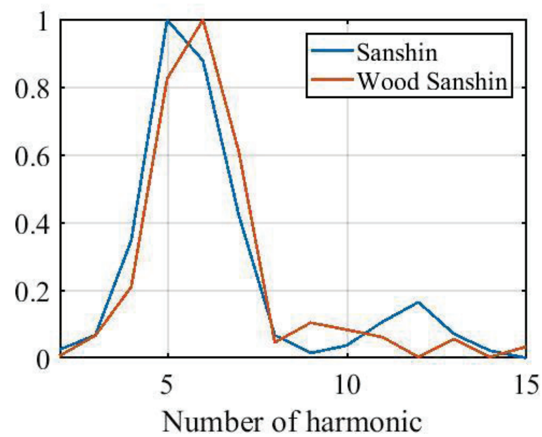

(c) Overtone distributions

Figure 7 Acoustical comparison between normal Sanshin and wood Sanshin

Sao was cut to the thickness direction as shown in Figure 8. Original thickness of *Sao* was 23 mm and 10 mm was cut. For the comparison of the eigen frequencies of *Sao* before and after cutting process, the hitting test was conducted. The acceleration pickup was attached at the "*Utaguchi*" and the center of *Sao* was hit by the impact hammer. The results are shown in Figure 9 (a). Horizontal axis is frequency [Hz] and vertical axis is the amplitude. The eigen frequencies of thinner *Sao* by cutting process were generally lower than the original *Sao*. The acoustical evaluation before and after the cutting process was also conducted. Time waveforms of the sound and the overtone distributions are shown in Figure 9 (b) and (c). The time waveforms were similar amplitude and attenuation ratio, however, the overtone distributions were slightly different. The maximum peak amplitude of the original wood Sanshin was 6th overtone, although the maximum peak amplitude of the thinner *Sao* was 5th overtone.

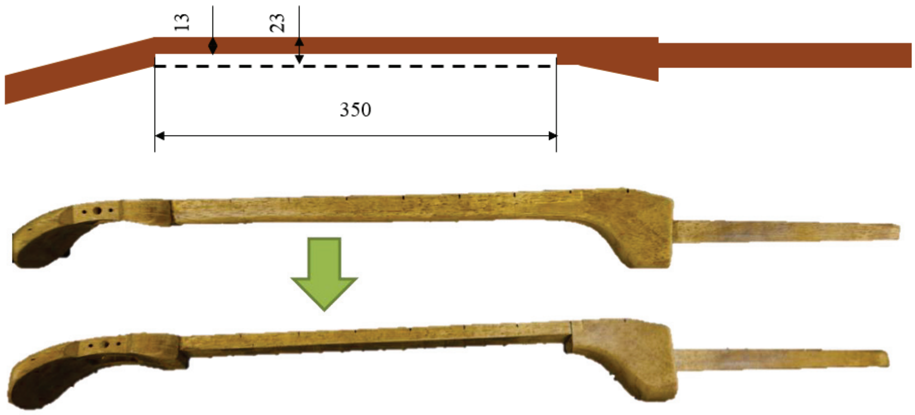

Figure 8 Cutting process of wood Sanshin for the reduction of thickness of *Sao*

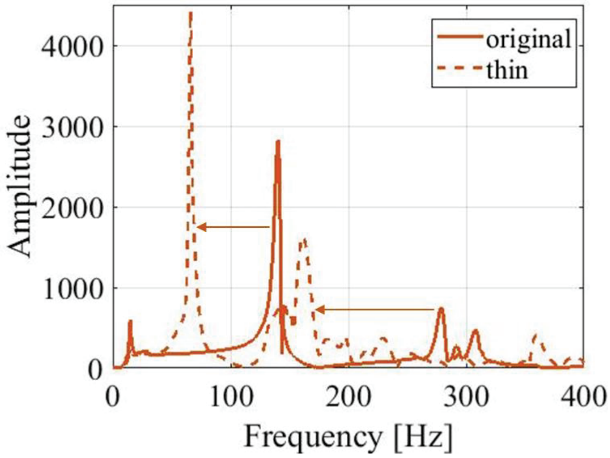

(a) Frequency spectrum of vibration of *Sao*

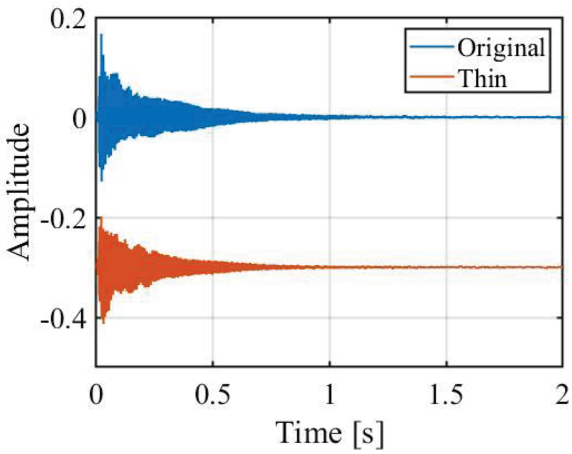

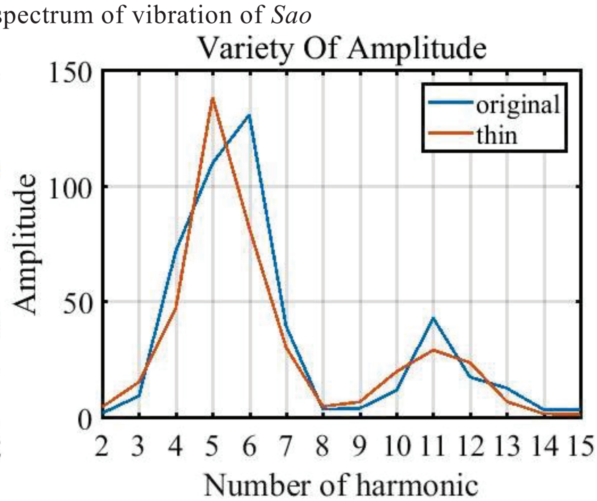

(b) Time waveform of sound (c) Overtone distributions of sound

Figure 9 Acoustical comparison before and after the cutting process of the thickness

The change of the overtone distributions was generated by the difference of the thickness of *Sao*. In other words, the change was generated by the change of "eigen frequency" and "bending stiffness" of *Sao*. In order to understand the dominant factor of the change between "eigen frequency" and "bending stiffness", we conducted the additional test. The clay was added on *Sao* as a mass loading as shown in Figure 10. When the mass loading is added on a material, it is considered that the eigen frequencies decrease but the bending stiffness does not change. The results of eigen frequency by the hitting test is shown in Figure 11 (a). The eigen frequency of original *Sao*, thinner *Sao*, and thinner *Sao* with mass loading are shown. The eigen frequency of *Sao* with mass loading decreased from *Sao* without mass loading. The results of the acoustical test acquired by the microphone is shown in Figure 11 (b). The overtone of maximum peak amplitude of thinner *Sao* decreased from the original *Sao*, but the overtone distribution of the thinner *Sao* with mass loading did not change from the thinner *Sao* without mass loading at all. This means that the change of the overtone distributions due to the decrease of the thickness of *Sao* was generated by the "bending stiffness" rather than "eigen frequency".

Figure 10 additional mass loading to *Sao* by clay

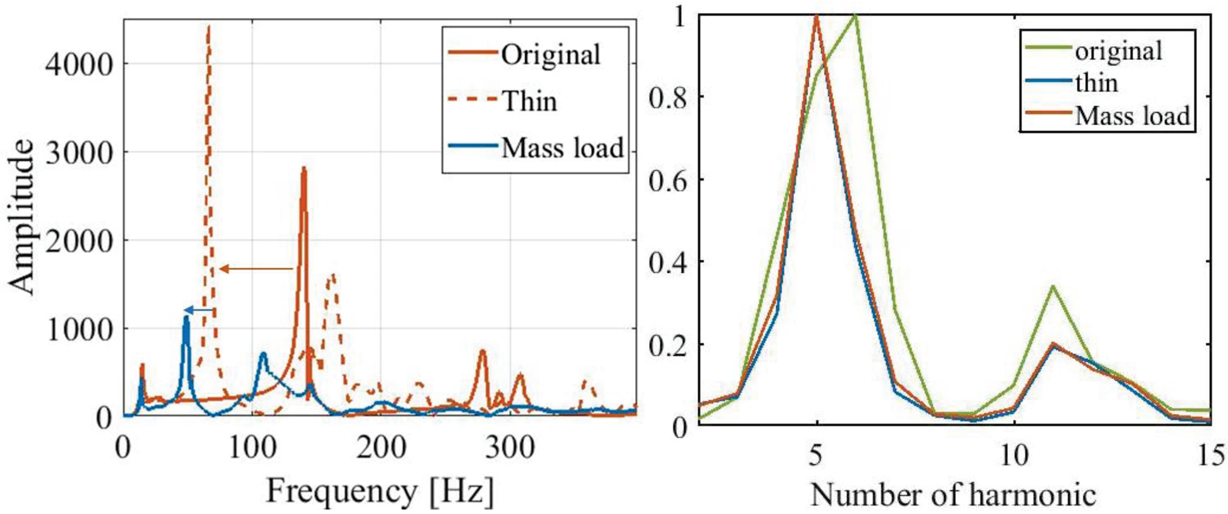

(a) Frequency Spectra (b) Overtone distributions

Figure 11 Acoustical comparison among original *Sao*, thinner *Sao* and thinner *Sao* with mass loading

Finally, the influence of the "*Ten* (top of *Sao*)" was evaluated. The shape and the weight of "*Ten*" differ substantially among the types of *Sao*. Therefore, it is considered that "*Ten*" becomes the mass loading to *Sao*. The weight of *Ten* decreased by the cutting process as shown in Figure 12, and the eigen frequency and the acoustical evaluation were conducted. Figure 13 and Figure 14 show the results of the eigen frequency by the hitting test and the acoustical evaluation by the microphone, respectively. The eigen frequency of *Sao* with the cutting *Ten* increased because of the less mass loading. From the results of time waveforms in Figure 14 (a), the waveform of the *Sao* with cutting *Ten* attenuated soon after the picking. The envelope of the time waveforms with logarithmic scale is shown in Figure 14 (b). The attenuation of the waveform of *Sao* with cutting *Ten* was larger than that of *Sao* without cutting *Ten*. It has a possibility that the large attenuation is caused by the decrease of the inertia due to the less mass loading. The overtone distributions at the ringing tone had large difference with the different types of *Sao* in the section 4, therefore, the existence of *Ten* could affect to the attenuation, especially at the ringing tone. Also, this difference of the attenuation could affect to the overtone distributions at the ringing tone.

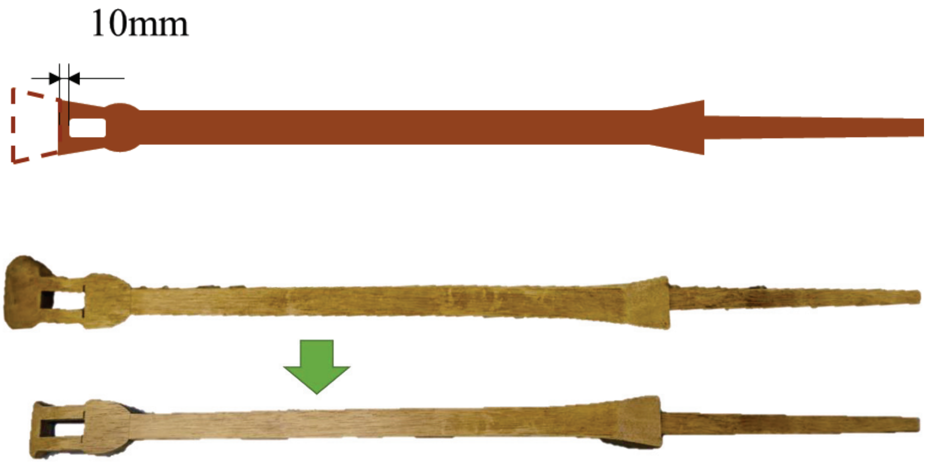

Figure 12 Cutting process of wood Sanshin for the reduction of weight of *Ten*

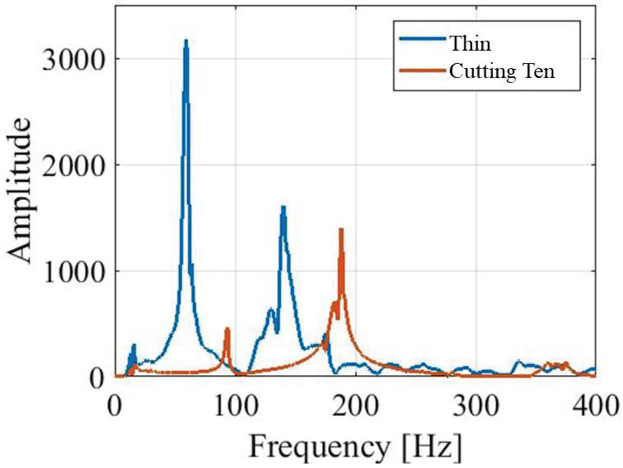

Figure 13 Frequency spectrum of thinner *Sao* and thinner *Sao* with cutting *Ten*

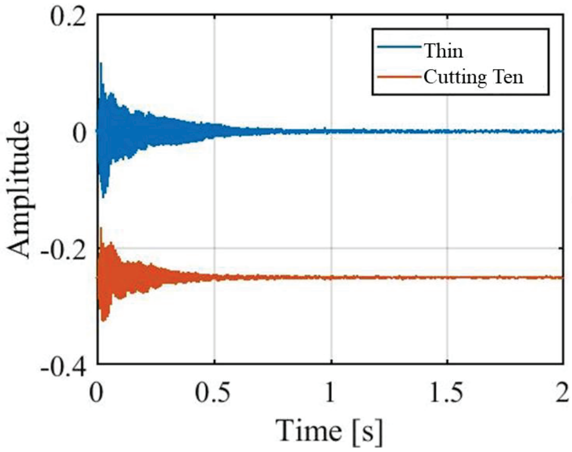

(a) Time waveforms

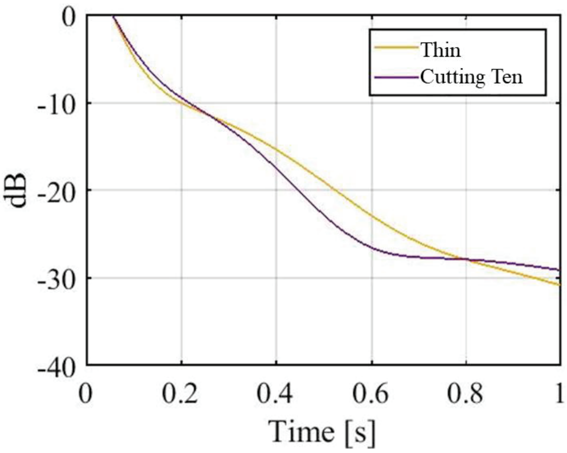

(b) At*Ten*uation rate

Figure 14 Acoustical Comparison between thinner *Sao* and thinner *Sao* with cutting *Ten*

6 CONCLUSIONS

Acoustical evaluation of Sanshin in order to understand the influence of *Sao* were conducted. Using same "string", "body", and "*Koma* (bridge)", the different types of *Sao* were characterized. Dividing attack tone and ringing tone, it was found the differences in the overtone distributions among each *Sao*. In the attack tone, the overtone distributions had a trend which was depending on the thickness of *Sao*, on the other hand, in the ringing tone, the overtone distributions were substantially different with different types of *Sao*. For more detailed analysis, the acoustical evaluation with wood Sanshin by the cutting process was conducted. The thickness of

Sao and the weight of *Ten* were changed by the cutting process. As a result, we found two considerations. First, the change of the bending stiffness due to the decrease of the thickness could affect to the overtone distributions. Second, the change of the inertia due to the change of the mass loading at *Ten* could affect to the attenuation and also it could affect to the overtone distributions.

These results are still not enough as a quantitative evaluation, and so further measurements and analysis are going to be conducted in the future. Especially the coupled vibration among "string", "body", "bridge" and "*Sao*" will be analyzed.

ACKNOWLEDGEMENTS

This work was partially supported by Aoyama Gakuin University-Supported Program "Promotion for Ongoing Research Program".

REFERENCES

[1] Mitukuni MATAYOSHI. Investigation into the length of the "pole" of Okinawa Sanshin documented in Okinawa no Sanshin [in Japanese/only English abstract]. Journal of Industry and Information Science, Vol. 6 (No. 1), 2009, pp47-62.

[2] Ken SONOHARA. An Approach to Sound Color of Sanshin I: A Trial of an Original Sound of "Morishima keejyo"s Sanshin [in Japanese/only English abstract], Bull. Mus., Okinawa Pref. Mus. Art Mus., No. 6, 2013, pp 69-85.

[3] Tomohide, AWAKUNI, Tsuyoshi YAMASHIRO, Minoru TOGUCHI. Overall evaluation concerned with timbre Sanshin (1). Bulletin of the Faculty of Engineering, University of the Rykyus, Vol. 61, 2001, pp91-95.

[4] Yoshimitsu TAKASAWA, Matsuo NAKASONE. 三線（沖縄三味線）の発音機構について（第一報）[in Japanese], Proceedings of Acoustical Society of Japan, 1997, pp 639-640.

[5] Kojiro NISHIMIYA, Mao TOKUDA, Yuki YOKOTA, Hideo CHO. Acoustic Measurement of "Sanshin" using Auto-Picking System [in Japanese], Musical Acoustics, Acoustical Society of Japan, Vol. 36, No. 1, 2017. pp1-7.

PROCEEDINGS of ISMA 2019
International Symposium on Music Acoustics

13 - 17 September 2019 in Detmold, Germany

The khaen as a miniature pipe organ

James COTTINGHAM[1]

(1) Coe College, United States, jcotting@coe.edu

Abstract

The khaen is a Southeast Asian mouth organ consisting of a number of free-reed pipes (commonly sixteen) mounted in a wooden wind chamber. From one point of view, it is possible to think of this instrument as an extremely small pipe organ: one with one rank of sixteen free-reed pipes. There have been a number of studies of the khaen in recent decades, often focusing on the coupling between a single reed and the pipe in which it is mounted. Yet music for the khaen, both traditional music and new music by current composers and players, almost always involves multiple notes sounding simultaneously. This paper summarizes some investigations involving the instrument as a whole, sometimes observing similarities and differences between the khaen and the pipe organ. A significant difference is the wind supply, which in the khaen is continually reversing direction. This certainly affects the musical playing style of the instrument, but may have other acoustical complications. Another area recently explored experimentally involves possible musical consequences of mode locking between pipes.

Keywords: Free reed, mode locking

1 INTRODUCTION

Mouth-blown instruments using a free reed coupled to a pipe resonator have a long history in China, Japan, and throughout Southeast Asia. The khaen is an instrument of the Lao people in Northeastern Thailand and Laos. The most common type of khaen employs sixteen open pipes, each with an effective length determined by the placement of tuning slots cut in the pipe. For an effective length L, the reed is located at approximately L/4. Unlike the free reeds found in Western instruments such as the reed organ, accordion, and harmonica, the reeds of the khaen are not only coupled to pipe resonators, but are approximately symmetric, so that the same reed can operate on both vacuum and pressure (inhaling and exhaling). Figure 1 shows a khaen along with a typical reed. Details on the khaen and other Asian free reed instruments are found in the book and article by Miller [1, 2].

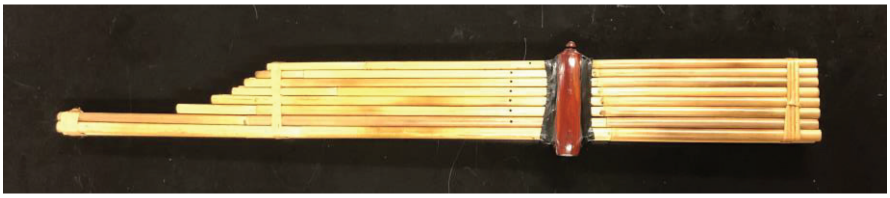

Figure 1. One of the khaen used in this study, along with a photo of a reed from a similar instrument.

The free reeds used in the khaen are cut from a single piece of thin metal, typically brass or a bronze alloy, and set into a bamboo pipe. In this single note per pipe instruments, a finger hole is drilled at a point that destroys the pipe resonance and prevents the reed from sounding unless the hole is closed. Wind is provided by blowing either in or out through the mouthpiece which forms the opening of the air chamber that surrounds the reeds. The instrument is held upright with the air chamber supported by the hands, with fingers and thumb of both hands are available to close the holes and sound notes. It is typical in playing the instruments that several notes are sounded simultaneously, some of them serving as drones.

[1] jcotting@coe.edu

The frequency of reed vibration is determined by both the reed and the pipe. The tuning slots (usually two per pipe for the khaen) are cut into the back of the pipe, determining the effective acoustical length. The vibrating frequency of the blown reed can within certain limits be pulled to match the pipe resonance so that fine tuning of pitch is done by means of the position of the tuning slots. In the khaen, reed length only approximately corresponds to sounding frequency, with pipe length apparently used as the prime means for tuning. [3] A characteristic shared by the Asian free reed mouth organs with other free reed instruments is that the sounding frequency drops as blowing pressure is increased. Data on this has been reported elsewhere [3,4]. The pitch change encountered in practice does not generally seem to cause musical problems.

2 SUMMARY OF PREVIOUS RESULTS

2.1 Playing frequency

Figure 2 shows the general relationship between frequency and pipe length for a khaen pipe. The pipe length was gradually shortened by cutting lengths from the original pipe. As can be seen in the graph, the sounding frequencies follow closely the fundamental pipe frequency, always remaining slightly above it. At the shortest pipe length in this example, the reed did not sound at normal blowing pressure (0.8 kPa), but could be made to sound at +1.7 kPa. At this same length, underblowing (0.3 kPa) caused the reed-pipe to sound at a frequency very close to the reed frequency. The results presented in Figure 4 show that the sounding frequency of the reed-pipe combination is higher than the natural resonance frequencies of either the reed or the pipe taken alone.

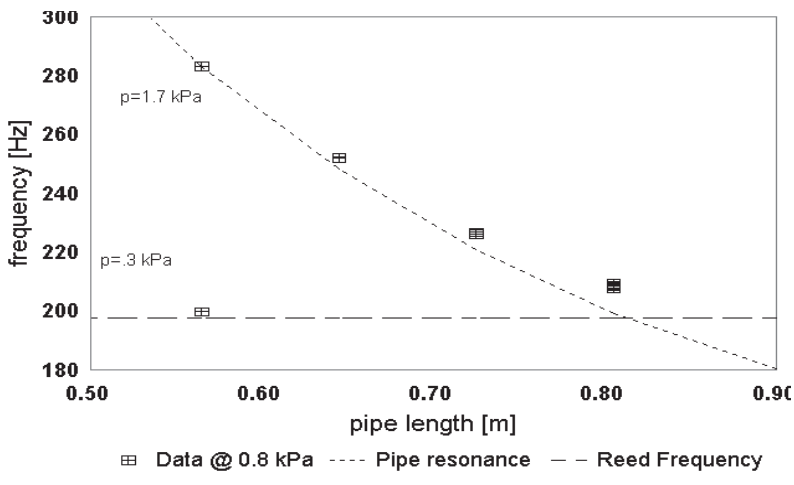

Figure 2. Sounding frequency of a khaen pipe as a function of fundamental pipe frequency at 0.8 kPa, with exceptions as noted for in the case of the shortest pipe.

2.2 Calculation of impedance curves and sounding frequencies

The sounding frequency measurements shown above suggest that the reeds in the khaen behave as "blown-open" reeds in which the playing frequency is above both the natural frequency of the reed and the first peak of the measured impedance curve. Detailed calculations of input impedance curves have been made for the khaen and other similar instruments using a method of transmission matrices [5]. These calculations take into account the position of the reed along the pipe, tuning slots, finger holes, and non-uniform cross sections. The details of these input impedance calculations are in good agreement with the measured impedances of the same instruments. Treating the reed as a damped, driven harmonic oscillator, the sounding frequencies of these reed-pipes can be predicted using a pipe-reed phase relation between the reed vibration and the phase of the complex impedance as formulated in the paper by Fletcher [6]. A sample result is illustrated below in Figure 3 and Figure 4.

The impedance curves calculated by the methods in this paper agree well with experimental results, even in smaller features and at higher frequencies. The agreement between calculated and experimental values is good, even for cases in which the sounding frequencies are not close to the pipe frequencies.

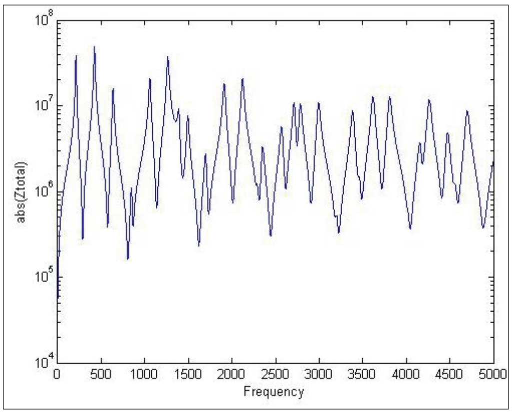

Figure 3. Magnitude of the calculated input impedance for a khaen pipe.

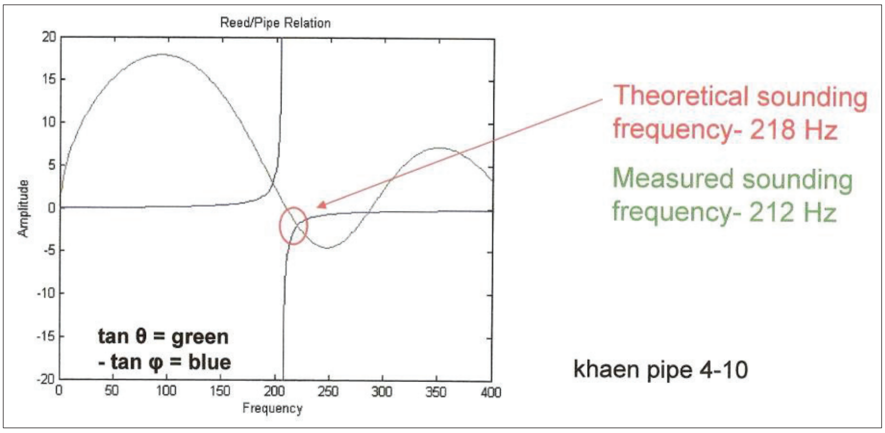

Figure 4. Determining the sounding frequency of the khaen pipe of Figure 3.

As shown in the above example, the methods used to obtain the sounding frequencies for the free-reed pipes of the khaen were quite successful. Similar calculations were also made for other Asian free reed instruments with pipes of more varied cross sections than the khaen pipes. There are some features of the khaen that have not been explored until recently. The acoustical effects of the end sections (the sections of the pipes extending beyond the tuning slots) have not been previously studied in any detail. The following section of this paper includes some results on this topic from simulations.

Another area of study is that of interactions between pipes. Music for the khaen almost always involves the sounding of several pipes simultaneously, yet most acoustical research thus far has been on the properties of a single pipe. One phenomenon that had been suggested for investigation is that of mode locking or synchronization, for which some preliminary results are presented in Section 4 of this paper.

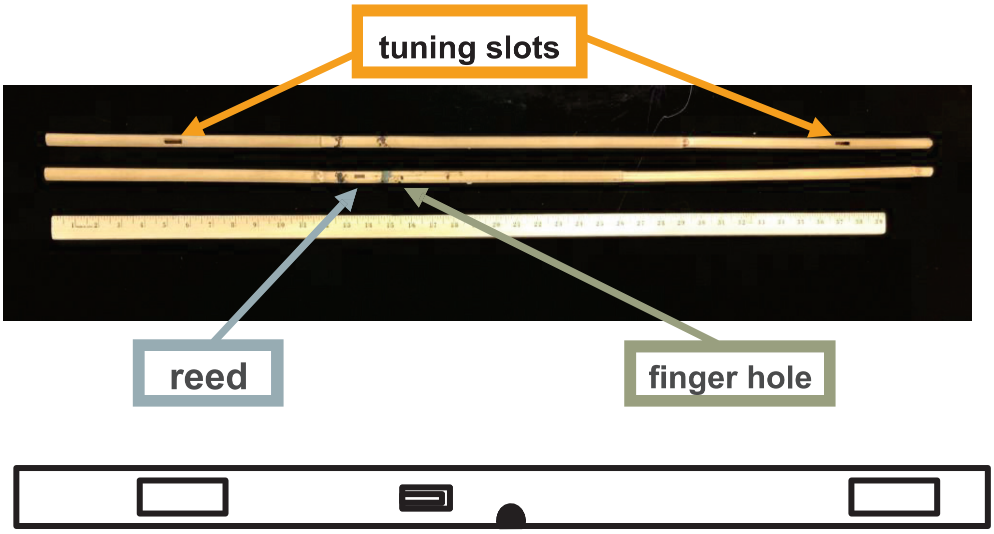

Figure 5. Above: Two views of the khaen pipe for which the calculated impedance is shown in Figure 6. Below: A diagram of a similar pipe showing the tuning slots, reed and finger hole.

3 KHAEN PIPE SIMULATIONS

A project has recently begun with the object of modeling the khaen using the finite element and multiphysics COMSOL® software. Some preliminary results are shown in the following figures. Figure 6 shows a calculated input impedance curve obtained by locating an oscillating pressure source at the reed position of the pipe. The impedance curve shows the expected maxima at the resonances of the open pipe with length determined by the tuning slots. The amplitude of the fourth harmonic is reduced, as expected, due to the location of the pressure source near a node of that mode.

In addition, there are a number of modes of the complete pipe indicated by the very narrow peaks that appear in the impedance curve. Some of these correspond to modes of one of the two end sections, while others involve both an end section along with the main pipe section.

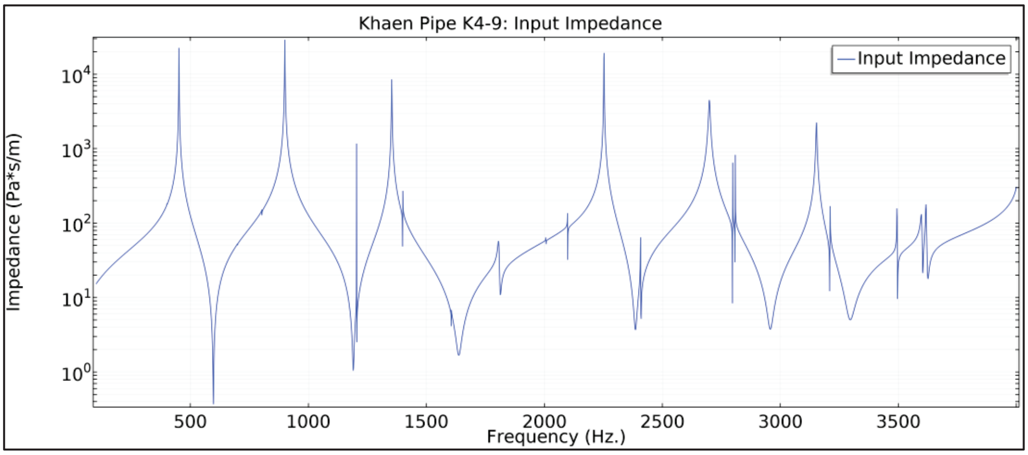

Figure 6. A COMSOL® generated impedance curve for khaen pipe K4-9.

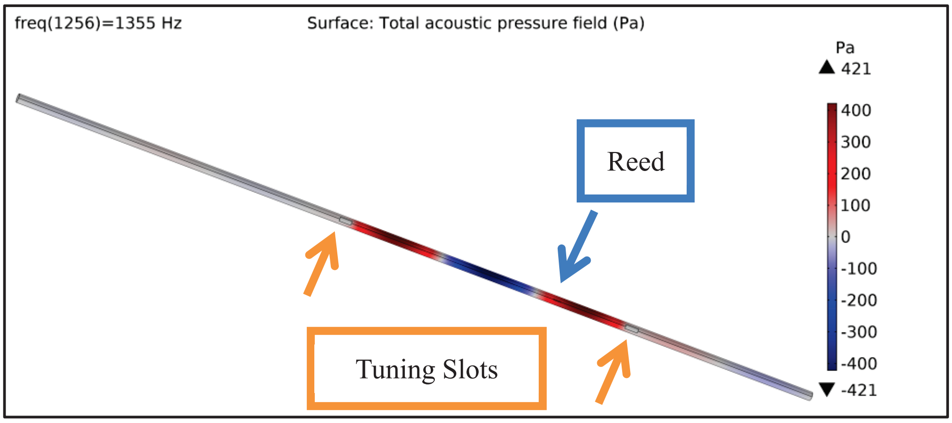

Figure 7. Mode 3 of the main pipe section (1355 Hz), locations of the reed and the tuning slots marked.

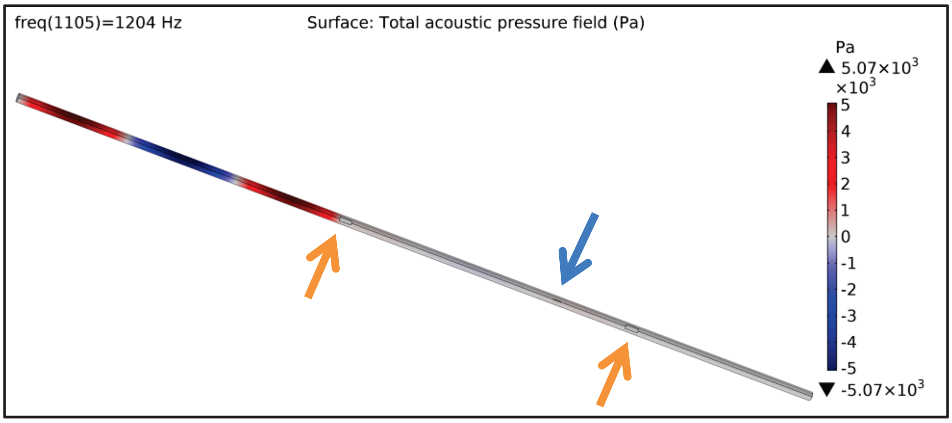

Figure 8. A mode of the upper end section (1205 Hz).

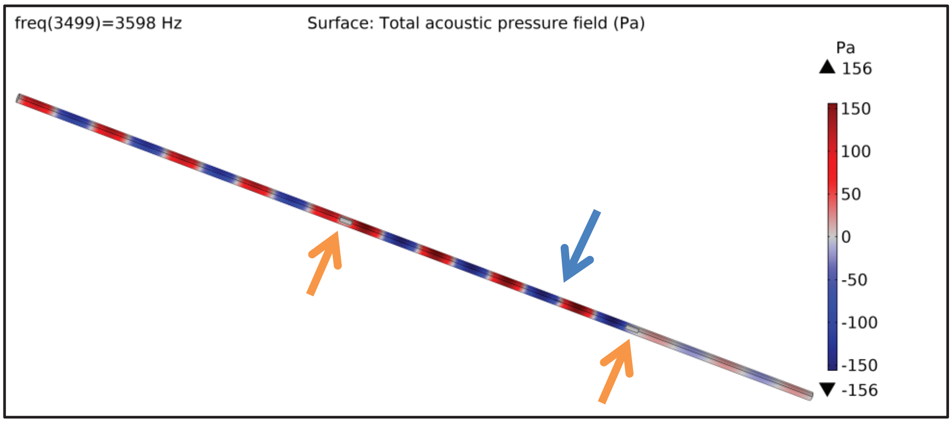

Figure 9. A mode (3598 Hz) involving both the main pipe section and the upper end section.

4 PIPE SYNCHRONIZATION

The phenomenon of frequency locking or synchronization in organ pipes has long been observed and has recently been the subject of acoustical investigations [6,7]. As part of an ongoing investigation, frequency synchronization has been studied in the khaen among pipes of the same nominal pitch and pipes with pitches in close harmonic relation (e.g., a perfect fifth). An example of this is illustrated below for the C_4 and C_5 pipes indicated in the diagram of Figure 10.

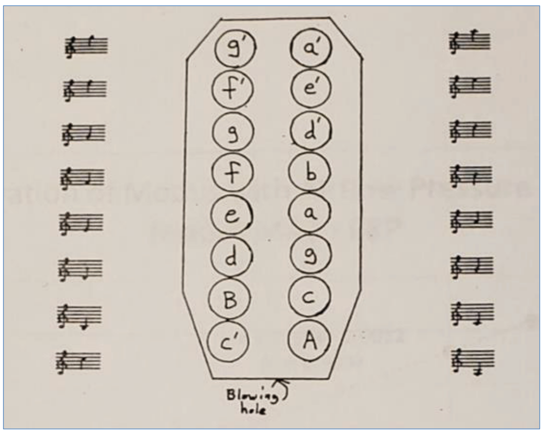

Figure 10. Pitch relationships for the sixteen-pipe khaen (from Miller [1]).

Two khaen pipes in a khaen, nominally at pitches C_4 and C_5, with sounding frequencies when played alone of 251.95 Hz and 503.91 Hz, are sounded simultaneously. At low pressure (0.4 kPa), observation of the frequency range around 500 Hz, which includes the second harmonic of the C_4 pipe and the fundamental of the C_5 pipe shows two frequencies (503.5 Hz and 505.9 Hz) with an average frequency and audible beats. As the pressure is gradually increased to 0.9 kPa, the two pipe modes synchronize into one frequency with no beats. This is illustrated in the four sections of Figure 11.

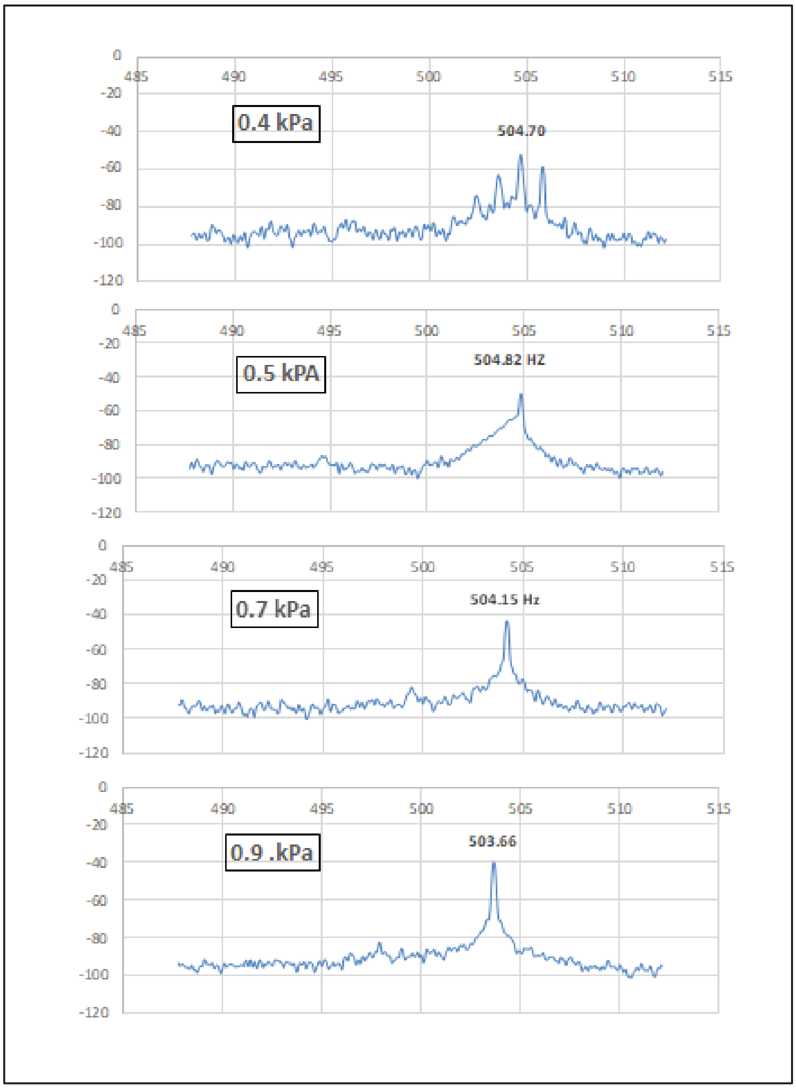

Figure 11. Two slightly mistuned octave khaen pipes sounding simultaneously synchronize as the blowing pressure is increased

5 SUMMARY

Both the simulations using COMSOL® and the experimental studies of pipe synchronization are ongoing investigations. It is anticipated that the modeling will eventually result in a more complex rendering of the complete instrument, including reed-pipe interaction and sound radiation. The frequency synchronization studies are being extended to cases involving multiple harmonically related notes.

ACKNOWLEDGEMENTS

Many of the results in Section 3 and Section 4 were obtained with the assistance of Will Martin and Kali Nash. Partial financial support for this research has been provided by United States National Science Foundation Grant NSF-REU1358968

REFERENCES

[1] Miller, T.E. Traditional Music of the Lao: Kaen Playing and Mawlum Singing in Northeast Thailand. Greenwood Press, 1985.

[2] Miller, T.E. Free-Reed Instruments in Asia: A Preliminary Classification. Music East and West: Essays in Honor of Walter Kaufmann Pedragon, New York, 1981.

[3] Fetzer, C.A.; Cottingham, J.P. Acoustics of the khaen: The Laotian free-reed mouth organs. Journal of the Acoustical Society of America, Vol. 101, 1997 p. 3143.

[4] James P. Cottingham, The Asian free reed mouth organs, Proceedings of the International Symposium on Musical Acoustics, Perugia, Italy, 10-14 September 2001.

[5] Cottingham, J.P.; Dieckman, E.A. Measured and calculated sounding frequencies of pipes coupled with free reeds. Proceedings of Meetings on Acoustics, Vol. 4, 2008, 035003, https://doi.org/10.1121/1.3167422

[6] Fletcher, N.H. Excitation in woodwind and brass instruments, Acustica Vol. 43, 1979.

[7] Abel, M.; Bergweiler, S.; Gerhard-Multhaupt, R. Synchronization of organ pipes: experimental observations and modeling. Journal of the Acoustical Society of America, Vol. 119, 2006, pp. 2467-2475.

PROCEEDINGS of ISMA 2019
International Symposium on Music Acoustics

13 - 17 September 2019 in Detmold, Germany

The air jet development in organ pipe tone attack caused by voicing adjustments

Zdenek OTCENASEK[1]; Pavel DLASK[2]; Jan OTCENASEK[3]

(1) (2) (3) Academy of Performing Arts in Prague, Czech Republic, zdenek.otcenasek@hamu.cz

Abstract

The contribution presents the results of a research on differences in development of air jet flux in labium of an organ pipe caused by different voicing adjustments. Air jets of tone starting transients were observed by laser PIV on a single rectangular open pipe with transparent walls in varied combinations of the upper lip height and the flue slit area. The visualizations of the air jet velocity vectors are presented in slides issued gradually in time and they are linked to the sound pressure and to the descriptions of sound quality obtained in listening test.

Keywords: Organ pipe, Air jet, Voicing

1 INTRODUCTION

The development of sound onset of an organ pipe is of importance to its sound character and has been subject of extensive interest both in research as well as in the practice of organ voicing, building and restauration (see e.g. 1, 2, 3, 4, 5, 6 for an overview of such works). As of recently, new acoustic and optical methods became available (see e.g. 15) enabling for an improved observation of the associated phenomena e.g. (7, 8, 9, 10). The present study therefore focused on documenting and interpreting the tone-onset development a jet flow of air in the labium in relation to modification of select voicing adjustments.

Since the air-jet is very sensitive to changes in the surrounding boundary (Kelvin-Helmholtz instability), an amplification of small disturbances in air-jet surface occurs also in the context of sound onset (5). Based on the measured data, it is hypothesised that small increments of sound pressure or velocity at the jet boundary cause deflections in the path of the jet and the sound pressure fluctuations in the labium which observably influence the jet routing after a time-delay determined by the path to the end of pipe and back, and moreover alter the labial sound pressure even further.

To measure the effect of different voicing parameters on the air-jet, an experimental transparent pipe and windchest was constructed, allowing for variance of windchest air pressure upper lip height (cut-up) and flue slit area (breadth) was used and documented by means Particle Image Velocimetry method PIV see e.g. (11). The presented visualizations of onset air-jet velocity vectors are also accompanied by synchronised time courses of recorded sound pressure and sound quality descriptors obtained in a listening test.

Under standard conditions, tracing the air jet in transient events using PIV is limited to use of a high speed camera and an illumination with double pulse laser at high sampling frequency. It has been observed in previous experimental measurements that the tone onsets of pipes with stable windchest pressure and valve opening are largely repeatable. A simpler, low frequency laser and the method of gradual shifts of snapshot time frames against a trigger reference on repeated onset sounding can therefore be possibly used for the observations, and was used in this study.

2 EXPERIMENT and METHOD

An experimental wooden open principal pipe (f0 ≈ 207 Hz, inner length 718 mm and rectangle area 55 x 45 mm) with an all Plexiglas (polymer of methyl acrylate) walls and adjustable position of wooden kernel (see Figure 2) was used in the study (since PIV laser visualizations of labium air jets require a pipe with transparent upper lip and at least two side walls).

2.1 Sound and jet recordings

Voicing parameters on experimental pipe were gradually adjusted in a 10 to 26 mm range for the cut-up *height* (1 mm increments), in a 0,4 to 3,25 mm range for its *breadth* (0,15 mm increments) and in a 392,3 to 980,7 Pa range for *air pressure* (98,07 Pa increments); the ranges deviate around an optimal best-sound setting (best voicing positions: 18 mm; 1,35 mm; 588.42 Pa). Only a selection of the obtained variants is however presented in this study (e.g. with air pressure 588.42 Pa).

The air system was controlled using an electromagnetic valve (pressure instability was <1%). The sound was recorded in anechoic room (Neumann KU100 dummy head at 1 m distance 20^{o} in front to labium, A/D 24 bit, sample rate192 kHz, calibrated on 0 dB SPL, temperature 22°C, humidity 41%). The sound records and PIV tracking were triggered by an electric signal on the valve opening.

Windchest air was seeded with glycerin micro particles generated by Safex FOG 2010 Plus instrument. The particles were illuminated using a double pulse laser with 15 Hz double-pulse frequency (with 6.10^{-6} s interval between the double pulses). Single PIV double pulse snapshots were captured intervals shifted consecutively stepwise relative to a trigger (signal of a valve opening; shifting step 5.10^{-4} s) on repeated sounding of the tone. On a single voicing setting, the results were also compared to results of continual PIV measurement with laser with 2 kHz frequency (the laser was unavailable for other observations). The differences in the development of jet positions in time (and also of the sound pressure amplitudes) were considered as negligible (the timings in between tone soundings changed at maximum 5.10^{-4} s). The high speed camera (Phantom SpeedSense 9060) was set to capture a side view of the labial space (33 x 53 mm), the PIV interrogation area was 8 x 8 pixel (≈ 0,33 x 0,33 mm).

The subjective verbal descriptions of the tone onset were collected in a listening test. Binaurally recorded tones of 300 ms length were standardized with 75 ms fade outs and were used as stimuli. The tests were performed on a PC in the listening test editor software (LiTeD; © the authors institute). The stimuli were presented using Sennheiser HE60 headphones (calibrated on KU100) and were evaluated by ten experienced subjects (organ voicers and sound engineers). Frequent verbal descriptors utilized by most respondents were used to describe the tone transient and are presented together with the recorded graph of sound pressure development (see Figures 1, 4, 5).

3 RESULTS

The voicing adjustments result not only in changes to the character of jet oscillation but also to the character of jet oscillation development. Due to page count limit, only three representative voicing adjustments are documented herein: the best voicing position (18 mm and 1,35 mm), lowered cut-up (15 mm and 12 mm), broader and thicker slit (2,00 mm 0,9 mm) are presented, all displaying a typical variance in an air particle velocity and upper labium arrival time of the jet. The associated jet developments are documented in Figures 1, 3, 5, where slides with particle velocity vectors are ordered in *triads of columns* top-down left-right for each time interval from valve opening (the time is shown in the header of each column triad). The shapes of jet and vortexes are distinguishable from the surroundings as grey contrast areas. The shades of grey correspond to lengths of velocity vectors (darker area represents higher velocity; scale shadings are constant through columns). The velocity vector arrows can also be discerned at higher magnifications of the document. The kern (with visible slit gap) and upper lip tip outlines are depicted in red. The numbers between columns quote the approximate phase angle of the in-out movements of the jet (relative to in-out times of a regularly oscillating jet; 90^{o} represents a maximum jet protrusion). The particle velocity, measured immediately above the slit in a particular time after a valve opening (e.g. for a 36,5 ms time, the velocity is shown as $v_{36,5}$ = 1,0 ms^{-1}), is presented in Figure 1, 4, 5 under the slides (at the bottom) together with verbal descriptions from the listening test. A sound pressure graph is also included in Figures 1, 4, 5, below the first *triads of columns*. The lines in the graph mark out the triple time-sections, where the snapshots were made for each slide in the column.

The slides show the type of first outburst from the slit is associated with changes and deviations to the jet route through a two possible feedback mechanisms. The acceleration and deceleration of air particles in specific areas of the labia (which can be identified in slides or between adjoining slides as change in grey intensity or as progression of the length of velocity vector arrows) is associated with a temporal and local changes of the air density and pressure at a given location. The manner of a first release of particles from the slit therefore likely predetermines, through acoustic feedback, the succeeding jet route and causes a jet declination. At low thickness of the slit (here 0,9) or high pressures (not presented) interruption of the stream of the jet can be observed: e.g. see slide 3 in column 1 in Figure 1 (at 0,0375 s), where the velocity of particles is decreased amidst an active jet. A feedback repeating increase in outward protrusion of the jet can then be observed (with the reflection propagation delay) when such pressure discontinuity occurs.

In the observations, a first feedback can be seen as associated with a *back wall reflection*. It can be observed gradual changes of velocities above the slit (positive sound pressure) correspond to changes in outward oriented velocity vectors after reflection, with successive extended deflection of the jet. The pressure behind the jet also decreases during its outward deflection. Then after the conclusion of the *back wall reflection event* the velocity vectors are oriented inward. This is accompanied by a larger jet deflection to the inside. On our experimental pipe, the periodicity of the jet out – in movement was shorter than the PIV step 5.10^{-4} s and the effect is under sampled in slides; the changes in jet routing can, however, still be followed across the slides in the columns.

Next feedback is associated with a reflection from an *open end of pipe*. The feedback is characterized by an inversion of phase of the pressure radiated through the pipe after reflection. The open end reflects the initial sound pressure as the negative, the reflected sound velocity vectors are oriented inwards, and also the jet deviates to the inside. The inward and outward jet deflections we can be repeatedly observed in all Figures 1, 4, 5.

4 CONCLSION

The differences between the settings of used voicing parameters were observed as associated with stabilisation of the length of the jet oscillation and irregularity of jet movements. Both are observed as connected to aspects of a first outburst and to the velocity of air particles in the jet on the route to the upper lip. Smaller air pressure in windchest or the broader slit area is associated with lower speed of air-jet particles and with a more continuous first outburst. The pressure changes (sound pressure) in the labium produced by such outburst are also continuous. This is theorised to be associated to regularity of time-delayed pressure changes reflected from the pipe end and back wall (which periodically change the jet direction).

REFERENCES

[1] Adelung, W. Einführung in den Orgelbau. Breitkopf & Härtel, 1972.

[2] Benade, A. H. Fundamentals of musical acoustics. Oxford University Press, 1976.

[3] Lottermoser, W. Orgeln, Kirchen und Akustik. Das Musikinstrument, 1983.

[4] Campbell, D. M. – Greated, C. The musician’s guide to acoustics. Oxford University Press, 1987.

[5] Fabre, B. Flute-Like Instruments. In Acoustics of Musical Instruments. New York, NY: Springer, 2016

[6] Angster, J. – Angster, J. – Miklos, A. Akustische Messungen und Untersuchungen an Orgelpfeifen. Acta Organologica. 1997, 25, s. 151–176.

[7] Miklos, A. – Angster, J. Properties of the Sound of Flue Organ Pipes. Acustica united with Acta Acustica. 2000, 86, s. 611–622.

[8] Paal, G. et al. A combined LDA and flow-visualization study on flue organ pipes. Experiments in Fluids. 2006, 40, 6, s. 825–835.

[9] Perre, van der, Greet. 2011. Experimental Study of Organ Pipe Behavior Using Optical Measurement Techniques. PhD thesis. Brussel: Vrije Universiteit.

[10] Yoshikawa, Shigeru – Tashiro, Hiromi – Sakamoto, Yumiko. 2012. „Experimental Examination of Vortex-sound Generation in an Organ Pipe: A Proposal of Jet Vortex-layer Formation Model“. Journal of Sound and Vibration 331 (11), s. 2558–2577.

[11] Raffel, M., at al. 2007. Particle Image Velocimetry, 2rd ed., New York: Springer 2007

15 0,90 60 (from 0,0365 s to 0,0495 s) **15 0,90 60** (from 0,064 s to 0,077 s)

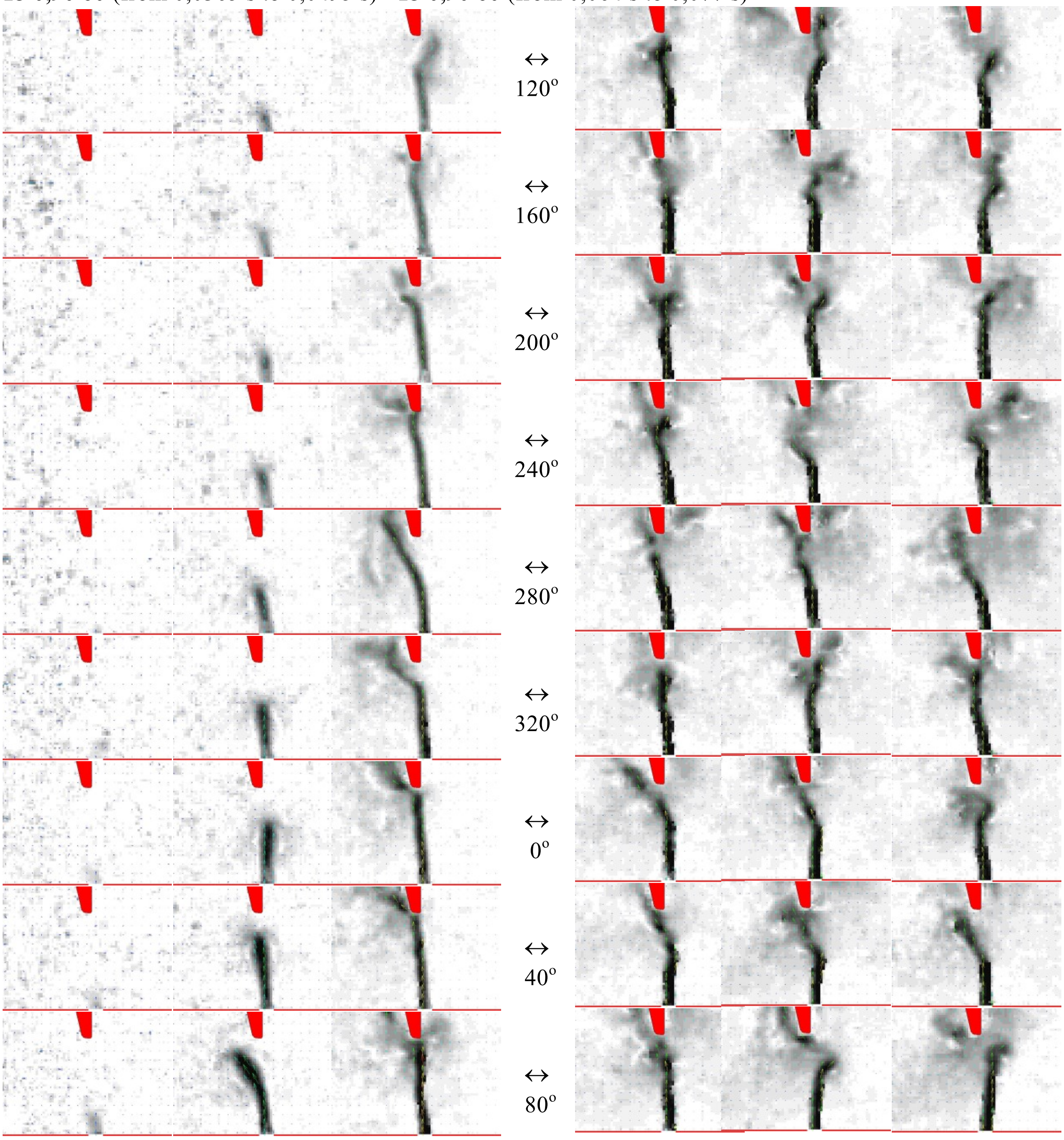

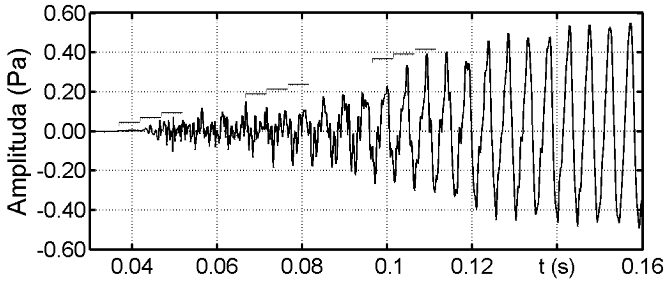

Velocity (m/s) in jet from a time (ms) after valve opening:

$v_{36,5}$ 1,0; $v_{40,5}$ 2,5; v_{45} 8,5; $v_{49,5}$ 17; $v_{>60}$ 19,7;

Verbal description of perceived sound quality:

strong; slow; fizzy; rustle; hard; sharp; bright; diapason; expressive; concrete; distinct;

15 0,90 60 (from 0,0915 s to 0,1045 s)

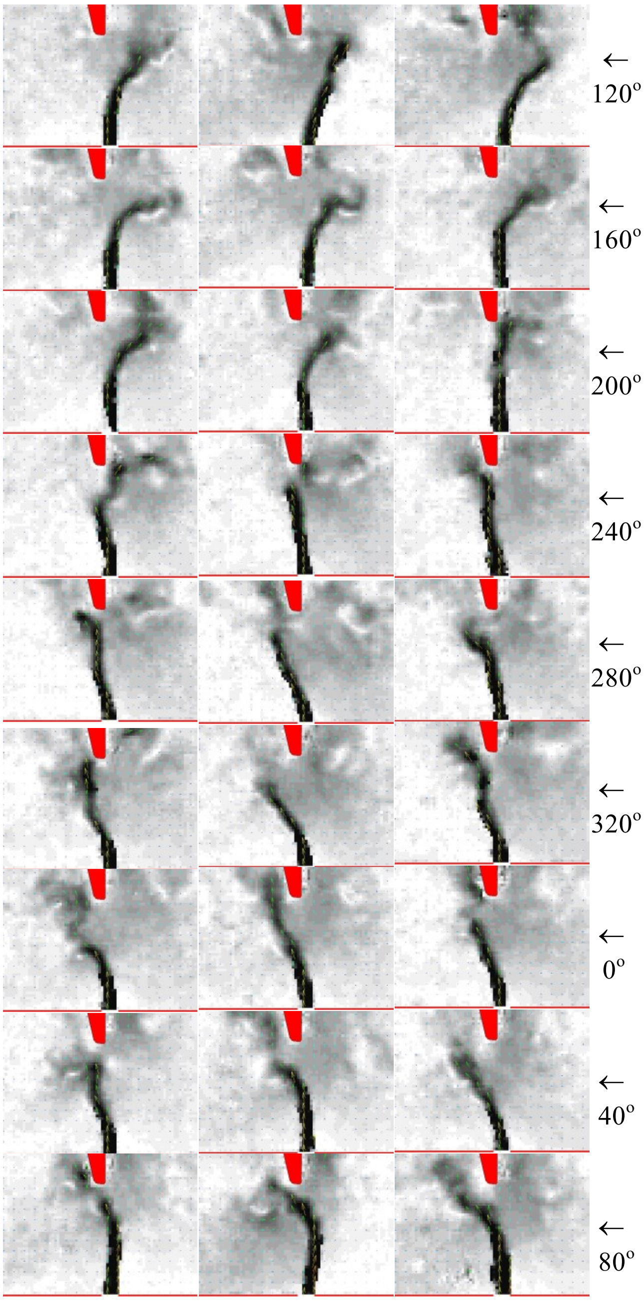

Figure 1. (*Top*) The 3x3x9 slides with velocity vectors of labial air jet for the 15-0,90 voicing adjustment in the times shown above (from first slide in column 1 to last in column 3). (*Previous page bottom Left*) The lines in the sound pressure time development mark the timing of slides presented in separate columns; (*Right*) jet particle velocity and verbal descriptions of perception of the tone attack.

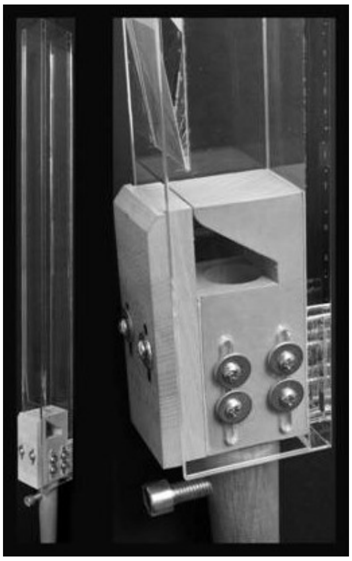

Figure 2. The adjustable experimental pipe with transparent walls

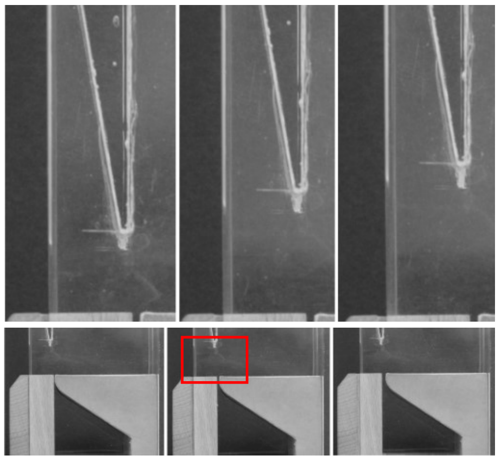

Figure 3. The adjustment range of upper lip height and flue slit area. Optimum voicing adjustment (cut-up height 18 mm, slit breadth 1,35 mm) is shown in the middle. The PIV area used in presented slides is marked by red rectangle.

12 2,00 (from 0,033 s to 0,046 s)

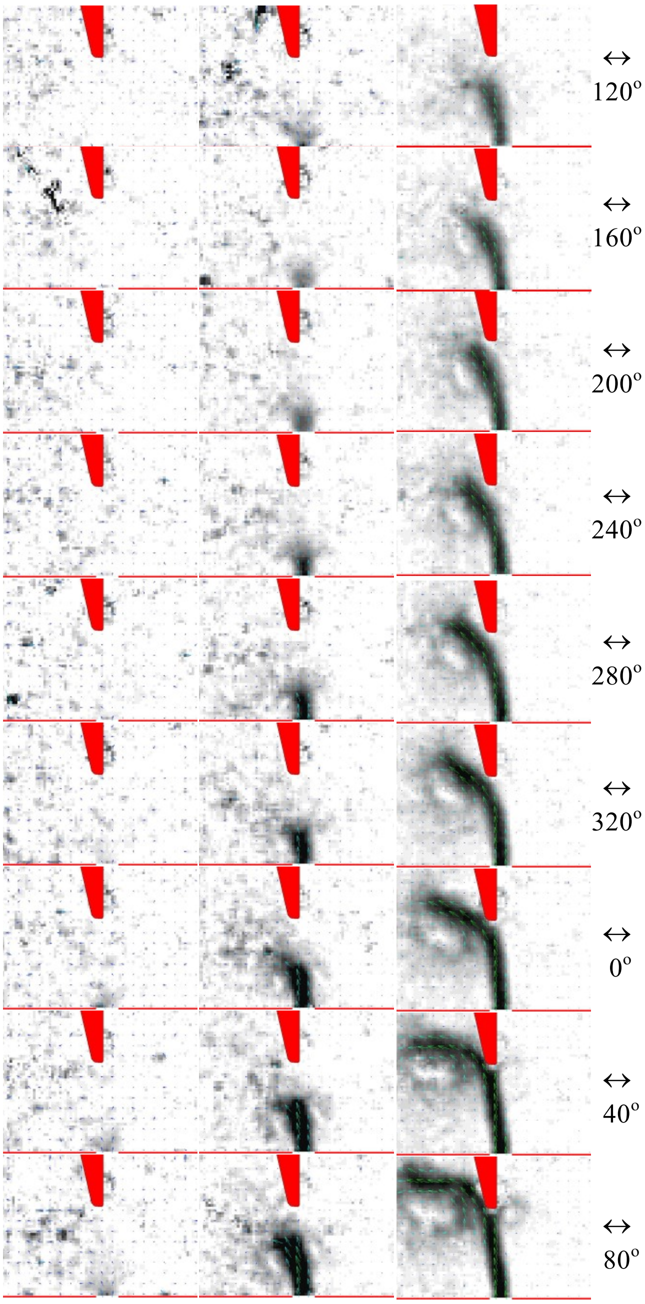

12 2,00 (from 0,0605 s to 0,0735 s)

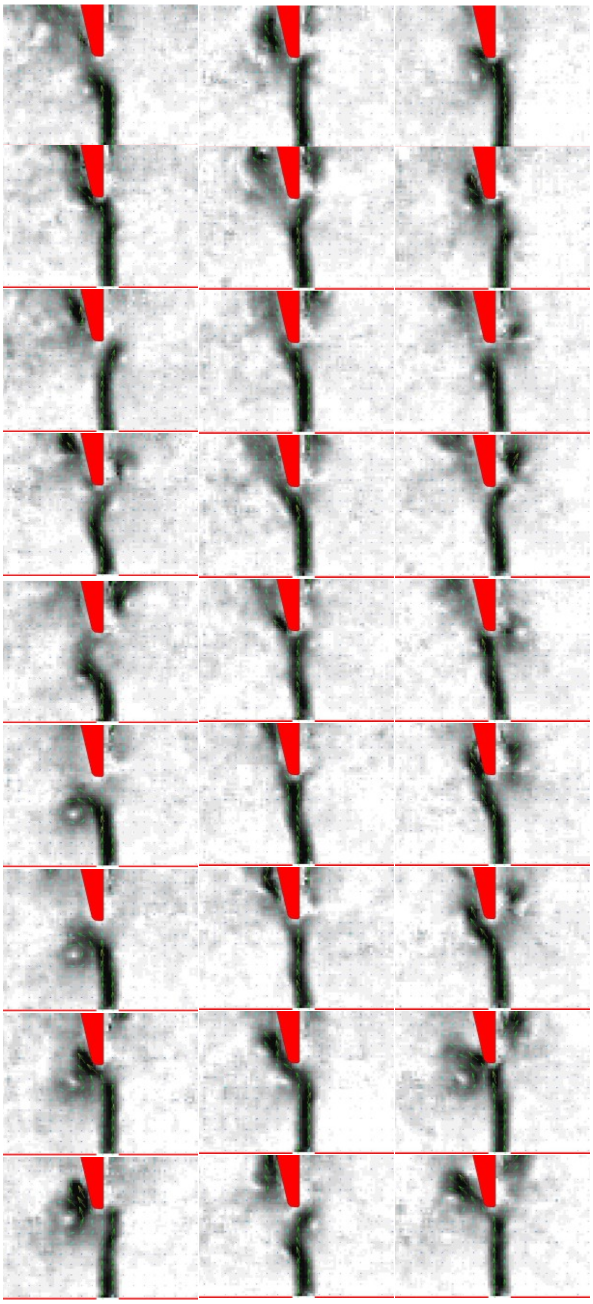

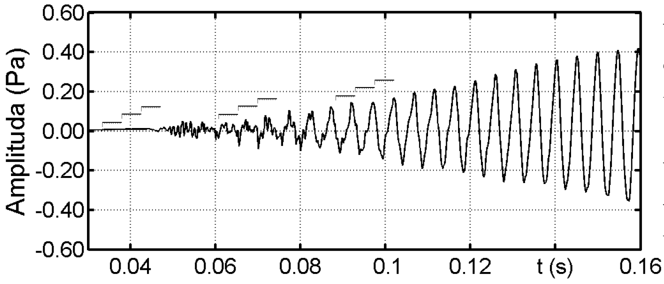

Velocity (m/s) in jet from a time (ms) after valve opening:

v_{33} 0,7; v_{37} 3,7; $v_{41,5}$ 9,2; v_{46} 12,5; $v_{>50}$ 13,5;

Verbal description of perceived sound quality:

weak; slow; rounded; smooth; dark; obtuse; rustle; under-excited; fluty;

12 2,00 60 (from 0,088 s to 0,101 s) **18 1,35** (from 0,0325 s to 0,0455 s)

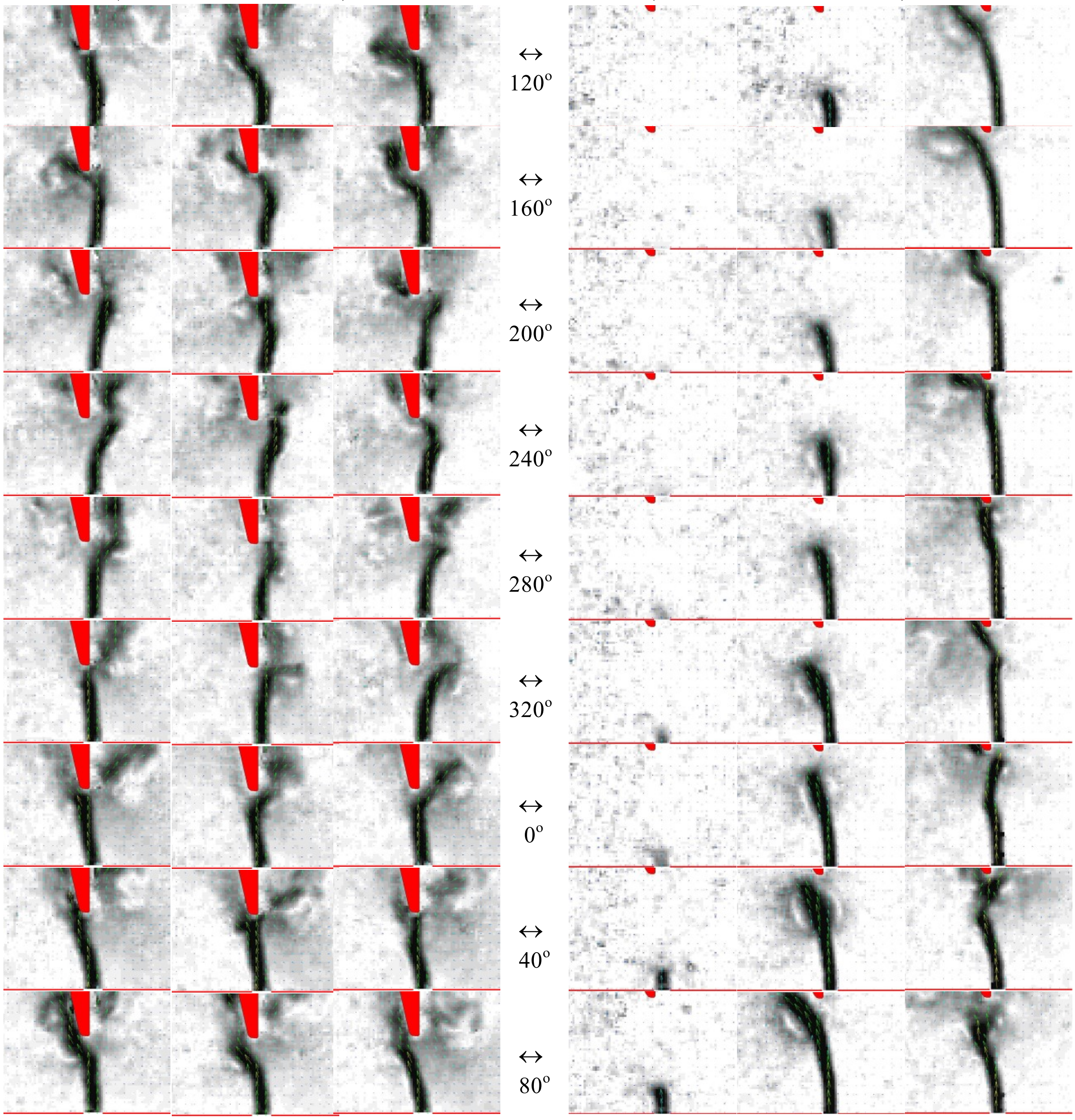

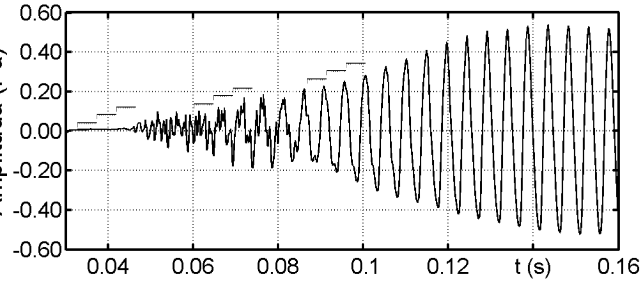

Figure 4. (*Top*) The 3x3x9 slides with velocity vectors of labial air jet for the 12-2,00 voicing adjustment in the times shown above (from first slide in column 1 to last in column 3). (*Previous page bottom Left*) The lines in the sound pressure time development mark the timing of slides presented in separate columns; (*Right*) the jet particle velocity and the verbal descriptions of perception of the tone attack.

18 1,35 (from 0,06 s to 0,073 s) **18 1,35** (from 0,0875 s to 0,1005 s)

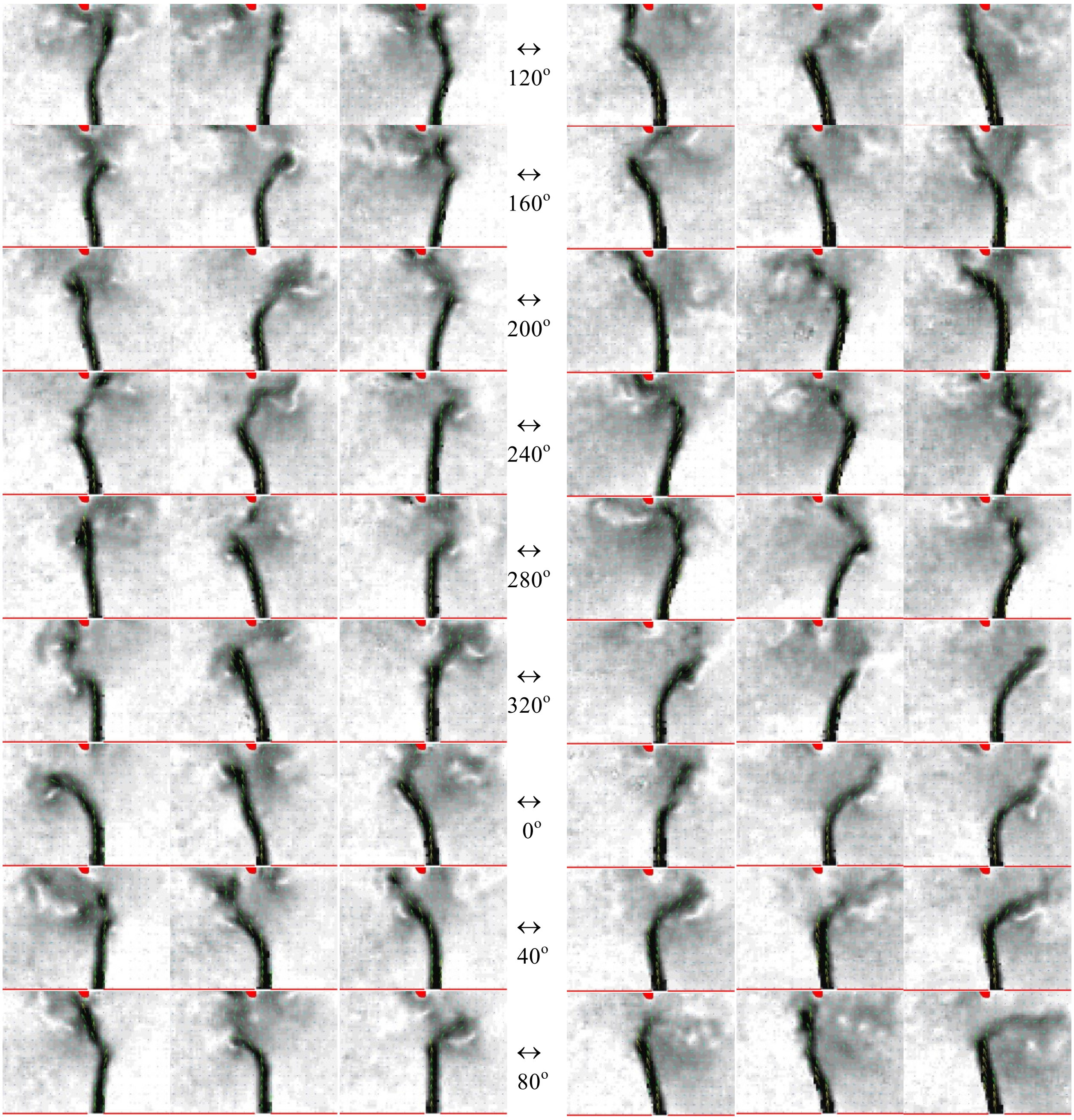

Velocity (m/s) in jet from a time (ms) after valve opening:

$v_{32,5}$ 1,2; $v_{36,5}$ 4,9; v_{41} 913; $v_{45,5}$ 14,5; $v_{>50}$ 16,5;

Verbal description of perceived sound quality:

quick; rounded; dark; mellow; obtuse;
veiled; full; clean; copula like;

Figure 5. (*Top*) The 3x3x9 slides with velocity vectors of labial air jet for the 18-1,35 voicing adjustment (from first slide in column 1 to last in column 3, times shown above); (*Left*) the jet particle velocity and the verbal descriptions of the tone attack perception.

(*Previous page bottom Right*) The lines in the sound pressure time development mark the timing of slides presented in separate columns.

PROCEEDINGS of ISMA 2019
International Symposium on Music Acoustics

13 - 17 September 2019 in Detmold, Germany

Distortion of acoustic shockwaves by U-shaped tube portions *

Sébastien OLLIVIER(1), Thomas LECHAT(2), Didier DRAGNA(2), Arnaud GLUCK(2)

(1)Université de Lyon - Univ. Lyon 1 - LMFA UMR CNRS 5509, France
(2)Université de Lyon - Ecole Centrale de Lyon - LMFA UMR CNRS 5509, France

Abstract
Nonlinear propagation models for wave propagation in the resonator of brass instruments are generally based on a one-dimensional description. This description is made under the hypothesis that sound wave propagation does not depend on bends, and is the same for straight or curved resonators. However, brass instruments resonators are not straight, and the effects of bends have to be considered. Modal approaches have shown that the pressure field has no symmetry in curved ducts, both in linear and weakly nonlinear propagation. The present study addresses the question of the behavior of shockwaves in U-shaped tubes with geometries close to some parts of brass instruments resonators, For this purpose, both experiments and numerical simulations in time domain have been performed. The experiments are based on “Schlieren” optical measurements requiring a square section of the U-shaped portion of the duct. The corresponding numerical simulations have been performed by solving the 2D Euler equations in curvilinear coordinates using a finite-difference time-domain approach. Results reveal the dynamics of shock propagation: an initial plane shockwave is strongly distorted by bends, secondary shocks are generated, multiple reflections generate oscillations in the waveform, nonlinear interaction of shocks can occur.
Keywords: shockwaves, nonlinear propagation, brass instruments

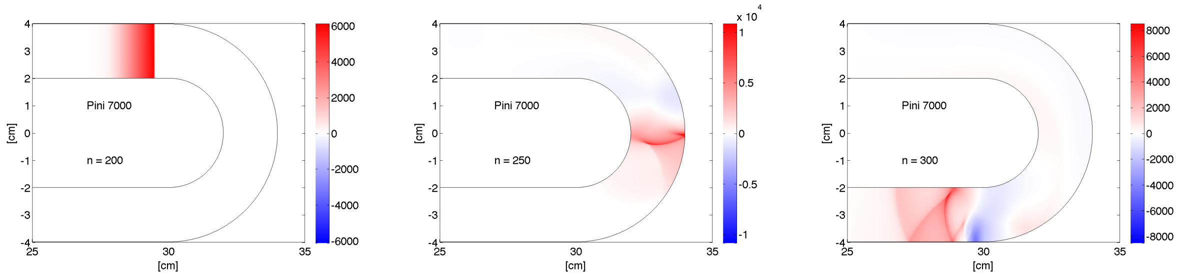

Figure 1. Example of propagation of a shockwave in a 2 cm × 2 cm cross section waveguide with a 30 mm radius bend. Result of a 2D numerical simulation of the propagation of an initial short duration pressure pulse. Simulation method: FDTD solution of Euler’s equations in curvilinear coordinates. Color scale: pressure in Pascals.

ACKNOWLEDGEMENTS
This work is supported by RSF-17-72-10277 and by the Labex CeLyA of Université de Lyon, operated by the French National Research Agency (ANR-10-LABX-0060/ANR-16-IDEX-0005).

*sebastien.ollivier@univ-lyon1.fr

PROCEEDINGS of ISMA 2019
International Symposium on Music Acoustics

13 - 17 September 2019 in Detmold, Germany

Numerical study on the function of the register hole of the clarinet

Kin'ya TAKAHASHI[(1)], Kana GOYA[(1)], Saya GOYA[(1)], Genki TSUTSUMI[(1)], Taizo KOBAYASHI[(2)]

[(1)]Kyushu Institute of Technology, Japan, takahasi@mse.kyutech.ac.jp
[(2)]Kyushu University, Japan, tkoba@cc.kyushu-u.ac.jp

Abstract
The function of the register hole of the clarinet can be basically explained from the common property of two delay systems (J. Phys. Soc. Jpn, Vol.83, 124003 (2014)). Namely, if the strength of a short time delay is sufficiently small but non-negligible, the third harmonic is well sustained over a wide range of the short delay time. This fact indicates that the register hole with a small radius raises the pitch of the first register notes in a wide range more than an octave to the second register notes by a twelfth (19 semitones). However, the reflection function has many delay peaks even when only the register hole is opened. That is, the clarinet should be characterized as a multi-delay system. In this paper, we focus on the effect of a very short time delay, which characterizes the reflection from the discontinuity in the mouthpiece. We numerically found that the function of register hole survives even for such a three delay system including the reflection from the mouthpiece.

Keywords: Clarinet, Resister hole, Delayed Model

1 INTRODUCTION

It is well known that wind instruments are modelized by differential and difference equations with time delay [1, 2, 3, 4]. Actually, the time delay is involved in the model as a convolution of the reflection function and the past data of the acoustic pressure $p(t)$ in the mouthpiece and of the volume flow $u(t)$ injected into it [1]. The open end reflection makes a negative peak with a delay time t_o, which is given as $t_o = 2l_p/c_0$, where l_p and c_0 are pipe length and the speed of sound, respectively. If adding a bell to the open end, the peak becomes broad. The tone hole reflection also makes a negative peak with a delay time $t_t = 2l_t/c_0$, where l_t is the distance of the tone hole from the mouthpiece tip [1, 5]. Therefore, the clarinet with some tone holes opened is characterized as a multi-delay system.

The function of the register hole (key) of the clarinet is a long standing problem in the field of musical acoustics [4]. The register hole with a small radius of 1.5mm is used to play in the second register. Namely, it raises the pitch of most first-register notes by a twelfth (19 semitones), i.e., generating third harmonics, when opened: for the B-flat clarinet, each note from D3 (147.5 Hz) to D4♯ (312.5 Hz) in the first register changes to a corresponding note from A4 (442Hz) to A5♯ (936.6 Hz) in the second register. The register hole is placed nearly at a distance of 0.16m from the tip of the mouthpiece for the B Flat clarinet. Since the portion of the reed valve, i.e., sound generator, is separated from the pipe in dynamical models as shown in Figure 1, the effective length between the register hole and the entrance of the pipe is estimated as $l_r \approx 0.14$m by using an acoustic tube model [6, 7, 8].

In the previous study [8], to consider the function of the register hole, we introduced a simple model formed by a closed pipe with only a tone hole (register hole), which is driven by a sound generator attached to the closed end (see Figure 2). Let us introduce the notion of the effective length of the pipe l_o. That is, l_o is adjusted to generate the pitch of a given note in the first register as $l_o = c_0/4f$, where f is the frequency of the note. When $c_0 = 340$ m/s at a temperature of 288 K, l_o is estimated as 0.576 and 0.272 m for the notes D3 and D4♯, respectively. Namely, the register hole works in the range $(1.9 \le l_o/l_r \le 4.1)$. The pipe with the register hole, whose length l_o is changed depending on a given note, is analogous to a two-delay system.

In the previous study [8], we explained the function of the register hole from the common properties of two-delay systems [9, 10]. Let us consider a pipe with a small tone hole, which makes a short time delay with weak intensity(see Figure 2(a)). When the register hole (tone hole) is placed at 1/3 length of the pipe from the closed end (top picture of Figure 2(a)), the third-harmonic mode satisfies the boundary condition of this pipe: antinodes exists at the tone hole and the open end. Even in the cases that the tone hole is placed at the middle of the pipe (middle picture) and at the quarter (bottom picture), the third-harmonic mode can still be excited in the pipe, while the antinode shifts from the tone hole to the left and right, respectively. This is because if the tone hole is sufficiently small, it does not strictly require that one of the antinodes exists on it, but it still stimulates the excitation of the third-harmonic mode rather than the other harmonic modes. This fact is a common property of two-delay systems and explains the function of the register hole [8, 9, 10].

Let us consider the case of pipes with a large tone hole, i.e., the short time delay with high intensity (Figure 2(b)). If the tone hole is placed at 1/3 length of the pipe (top picture), the third-harmonic mode satisfies the boundary condition of this pipe. However, the large tone hole requires that oscillation modes satisfy the boundary condition caused by it: one of the antinodes is placed on it. In the cases shown by the middle and bottom pictures, there is no resonance mode that simultaneously satisfies both boundary conditions of the tone hole and the open end, because they make mismatched boundary conditions for harmonic modes. However, higher harmonic modes, which nearly satisfy both boundary conditions at the tone hole and at the open end, will be accepted reluctantly. This fact is explained by a common property of two-delay systems [8, 9, 10].

Thus, the above discussion indicates that the register hole should be sufficiently small but non-negligible. In the previous work [8], we focused on the theoretical analysis of the common properties of two-delay system by using a general two-delay system and discussed only one example of the clarinet model with a simplified reflection function. In this paper, we treat models including more realistic reflection functions and discuss the problem of how the change of the reflection function affects the function of register hole. Especially, we consider the effect of the mouthpiece reflection with a very short delay, which is caused by the mouthpiece discontinuity and plays an important role in reproducing the complicated mode-transitions observed in the experiment [6, 7, 11].

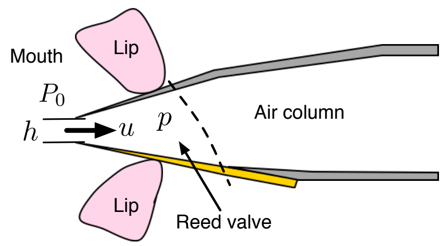

Figure 1. Cross section of the operating portion of the clarinet.

2 MODEL SYSTEMS

2.1 Delayed difference model of the clarinet

In this section, we introduce a delay difference model of the clarinet [2, 3, 8]. The operation of the clarinet is characterized with four dynamical values in Figure 1: the acoustic pressure in the mouthpiece p, the volume flow through the reed slit u, the height of the reed slit h and the blowing pressure in the mouth P_0.

By using the reflection function $r(t)$ [1, 8], the relationship between p and u is given by

$$p = Z_0 u + p_{inc}, \tag{1}$$

where p_{inc} is defined by

$$p_{inc}(t) = \int_0^\infty r(\tau)[p(t-\tau) + Z_0 u(t-\tau)]d\tau, \tag{2}$$

and Z_0 denotes the characteristic impedance defined by $Z_0 = \rho c_0 / S_c$, where ρ, c_0 and S_c are the air density,

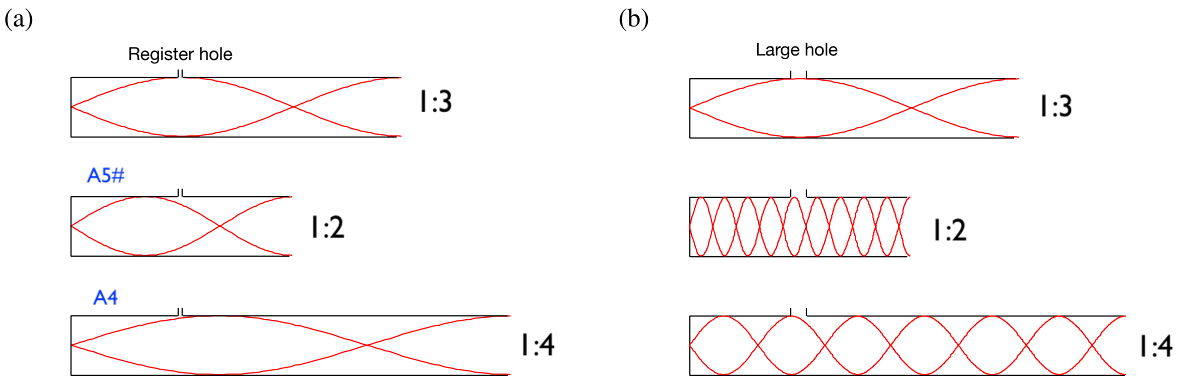

Figure 2. Function of the register hole. (a) Pipes with a small tone hole (register hole). (b) Pipes with a large tone hole.

the speed of sound and the area of the cross section at the entrance, respectively. The cross section S_c can be written as $S_c = \pi r_d^2$, where r_d is the effective radius of the pipe entrance.
Under quasi-static approximation [3, 8], the volume flow passing through the reed slit is obtained with Bernoulli's principle. Since the flow velocity in the mouth is negligibly small, Bernoulli's principle gives

$$P_0 = p + \frac{1}{2}\rho v^2, \tag{3}$$

where v is the flow velocity passing through the reed slit. The volume flow is given as $u = whv$, where w is the width of the reed slit.
The reed is driven by the pressure difference between the mouth and mouthpiece. Since the eigenfrequency of the reed is much larger than the acoustic frequency, the reed displacement $h - h_0$ is almost proportional to the pressure difference $p - P_0$,

$$k(h - h_0) = p - P_0 \equiv -\Delta p, \tag{4}$$

where h_0 is the height of the reed at rest and k is the effective stiffness of the reed. When the reed is closed, i.e., $h = 0$, the pressure is at $p = p_M$, which is obtained from

$$kh_0 = P_0 - p_M \equiv \Delta p_M. \tag{5}$$

From Eqs.(3), (4) and (5), the volume flow passing through the reed slit, $u = whv$, is given by [3, 8]

$$u = \begin{cases} u_0\left(1 - \frac{\Delta p}{\Delta p_M}\right)\sqrt{\frac{\Delta p}{\Delta p_M}} & (\Delta p < \Delta p_M) \\ 0 & (\Delta p \geq \Delta p_M), \end{cases} \tag{6}$$

where u_0 is defined by

$$u_0 = wh_0\sqrt{\frac{2kh_0}{\rho}}. \tag{7}$$

For the case of $\Delta p \geq \Delta p_M$, the reed is closed and no flow enters the mouthpiece, i.e., $u = 0$.
Combining eq.(6) with eq.(1), one can obtain the pressure $p(t)$ and the volume flow $u(t)$ at the present time t, if p_{inc} is calculated from the past values of p and u by eq.(2). To calculate the time evolution of p and u,

we consider the values of p and u at discrete times $t_n = n\Delta t$, namely $p_n = p(t_n)$ and $u_n = u(t_n)$, where Δt is a small time interval, which is taken as $\Delta t = 5\times 10^{-6}$s in this paper. Then, p_{inc} at $t = t_n$ is given as

$$p_{inc,n} = \sum_{i=1}^{\infty} r_i(p_{n-i} + Z_0 u_{n-i})\Delta t, \tag{8}$$

and from eq.(6) and eq.(1) with $p_{inc,n}$, p_n and u_n are obtained; thus, $p_{inc,n+1}$ is obtained and the process is repeated over and over. This process is written as a delayed difference equation.

2.2 Reflection functions

In this paper, we use a simplified reflection function with three peaks [8],

$$r(t) = -\tilde{\alpha}_o f_r(t-t_o, \Delta t_o) - \tilde{\alpha}_r f_r(t-t_r, \Delta t_r) - \tilde{\alpha}_m f_r(t-t_m, \Delta t_m), \tag{9}$$

where the function $f_r(t-t', \Delta t)$ represents a reflection peak and is defined by

$$f_r(t-t', \Delta t) = \frac{1}{\Delta t}\exp\Big(-\frac{1}{\Delta t}(t-t')\Big)H(t-t'), \tag{10}$$

where $H(t)$ is the Heaviside function and Δt determines the width of the peak owing to dispersive reflection. When the direct current resistance of the pipe is ignored, the average pressure in the mouthpiece is equal to the pressure of the atmosphere; thus, the reflection function satisfies the following condition [1]:

$$\int_0^{\infty} r(t)dt = -1, \tag{11}$$

which is reduced into

$$\tilde{\alpha}_r + \tilde{\alpha}_o + \tilde{\alpha}_m = 1. \tag{12}$$

In eq.(9), the peaks at $t = t_o$, t_r and t_m indicate the reflections from the open end, register hole and mouthpiece discontinuity, whose heights are given as $\alpha_o = \tilde{\alpha}_o/\Delta t_o$, $\alpha_r = \tilde{\alpha}_r/\Delta t_r$ and $\alpha_m = \tilde{\alpha}_m/\Delta t_m$, respectively.

In this paper, we calculate three models with different reflection functions. The settings of Δt_o and α_m/α_o for the three models are shown in Table1. But, t_r and Δt_r of the register hole reflection as well as t_m and Δt_m of the mouthpiece reflection are common parameters for the three models as shown in Table2.

The Models 1 and 2 ignoring the mouthpiece reflection are characterized as two-delay systems, though the Model 3 including the mouthpiece reflection is regarded as a three-delay system. The height α_m and width Δt_m of mouthpiece reflection are determined by the reflection function of the mouthpiece model in our previous studies [6, 7]. The peak width of the open end reflection Δt_o is wider for the Models 2 and 3 than the Model 1. The peak width Δt_o of the Model 1 is almost the same as that of the cylindrical pipe without a bell [6, 7]. For the reflection function of the clarinet with a bell, the Models 2 and 3 with a wide peak width Δt_o seem to be more realistic. To consider the function of the register hole, α_r and t_o are set up as follows: α_r is fixed in the range $(0.001 \le \alpha_r/\alpha_o \le 1)$ while t_o is fixed in the range $(t_r \le t_o \le 5.5t_r)$ depending on the effective length of the pipe determined by a given note. Note that the ratio t_o/t_r is in the range $1.9 \le t_o/t_r \le 4.1$ for the real clarinets. Figure 3 shows the reflection functions for the Models 1, 2 and 3 at $\alpha_r/\alpha_o = 0.1$ and $t_o/t_r = 4$.

Table 1. Parameters of the models

Model	Δt_o[s]	α_m/α_o
Model 1	0.4×10^{-4}	0
Model 2	0.8×10^{-4}	0
Model 3	0.8×10^{-4}	1

Table 2. Common parameters of the reflection functions

t_r[s]	Δ_r[s]	t_m[s]	Δt_m[s]
8.25×10^{-4}	0.4×10^{-4}	1.25×10^{-4}	0.8×10^{-5}

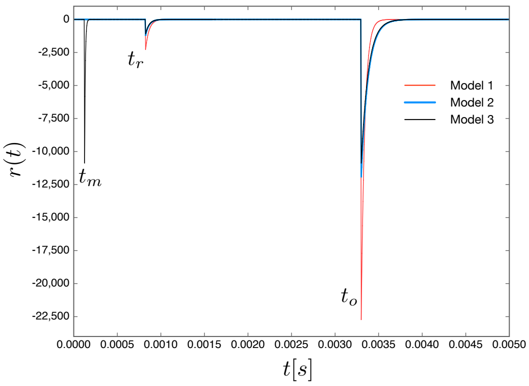

Figure 3. Reflection functions of the clarinet models at $\alpha_r/\alpha_o = 0.1$ and $t_o/t_r = 4$.

3 NUMERICAL CALCULATION

3.1 Setup of numerical calculations

We assume that the first excited mode in the range of the control parameter is the most dominant mode among possibly excited modes for the system, first, third, fifth modes and so on. Thus, we take the blowing pressure P_0 as a control and find the first excited mode, when P_0 is increased from 0 to 10kPa at a rate of 10Pa/s. Other parameter values are shown in Table 3.

Table 3. Parameter values

parameter	value
r_d	7.5×10^{-3}m
ρ	$1.2\text{kg}/\text{m}^3$
c_0	340m/s
w	1.4×10^{-2}m
h_0	6×10^{-4}m
k	12486993.75Pa/m

3.2 Numerical results

Before checking numerical results, let us remember the common properties of two-delay systems. Namely, in a neighborhood of $t_o/t_r = (2m+1)/(2n+1) \geq 1$, i.e., relevant condition, $(2m+1)$th mode is well sustained. However at $t_o/t_r = (2m)/(2n+1)$ or $(2m+1)/(2n)$, i.e., irrelevant condition, $2m$ or $(2m+1)$th mode is prohibited owing to the boundary condition and odd higher modes, which nearly satisfy the boundary conditions, are observed in its neighborhood. When the peak widths are sufficiently large, higher modes disappear and odd lower modes dominate: for example, the first, third and fifth modes appear in wide neighborhoods of $t_o/t_r = 1$, 3 and 5, respectively.

Figure 4 show pressure waves $p(t)$ at $\alpha_r/\alpha_o = 0$ and 0.1 for the Model 2 with $t_o/t_r = 4$ and $P_0 = 3000$Pa. At $\alpha_r/\alpha_o = 0$, the system is regarded as the single-delay system and a wave of the first mode is observed, while, at $\alpha_r/\alpha_o = 0.1$, a wave of the third mode is excited even though the condition $t_o/t_r = 4$ is irrelevant. This means that adding a delay with small intensity at $t = t_r$ stimulates the third mode and it works like a register hole.

Figure 5 shows phase diagrams of the excited modes in the parameter space of t_o/t_r and α_r/α_o for the Models

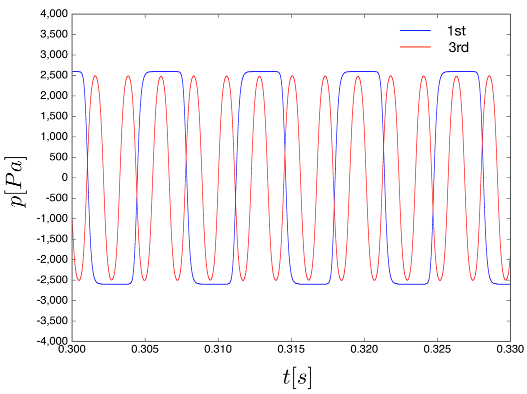

Figure 4. Pressure wave forms of the first harmonic mode at $\alpha_r/\alpha_o = 0$ and of the third harmonic mode at $\alpha_r/\alpha_o = 0.1$ for the Model 2 with $t_o/t_r = 4$ and $P_0 = 3000$Pa.

1, 2 and 3. For the Model 1, at $\alpha_r/\alpha_o = 1$, modes equal to and more than the fifth mode are observed in a neighborhood of the irrelevant condition $t_o/t_r = 2$ and the modes more than the fifth mode are excited near the irrelevant condition $t_o/t_r = 4$, which is explained by the common properties of two-delay systems [8, 9, 10]. With decreasing α_r/α_o, the higher modes near the irrelevant conditions gradually disappear, and at $\alpha_r/\alpha_o = 0.1$, the first, third and fifth modes occupy the ranges $(1.0 \leq t_o/t_r \leq 2.1)$, $(2.1 \leq t_o/t_r \leq 4.2)$ and $(4.2 \leq t_o/t_r \leq 5.5)$, respectively. With decreasing α_r/α_o further, the ranges of the third and fifth modes go to right and at $\alpha_r/\alpha_o = 0.01$ the first mode occupies the whole range. The function of the register is almost achieved at $\alpha_r/\alpha_o = 0.1$, where third modes appear in the range $(2.1 \leq t_o/t_r \leq 4.2)$.

For the Model 2, the areas of the higher modes around the irrelevant conditions shrink. Actually, at $\alpha_r/\alpha_o = 1$, there exists the area of the fifth mode in the left side of $t_o/t_r = 2$, which disappears below $\alpha_r/\alpha_o = 0.7$, while, in the right side, the higher modes appear only at $\alpha_r/\alpha_o = 1$. No higher mode appears around the irrelevant condition $t_o/t_r = 4$. Thus, the peak of the open end reflection with a wider width reduces the higher modes around the irrelevant conditions. At $\alpha_r/\alpha_o = 0.1$, third modes appear in the range $(2.4 \leq t_o/t_r \leq 4.7)$, which is not convenient for archiving the function of the register hole, because the first mode overcomes the third mode in the range $(t_o/t_r < 2.4)$.

For the Model 3, the areas of the higher modes around the irrelevant conditions are enhanced by the mouthpiece reflection. Actually, at $\alpha_r/\alpha_o = 1$, modes equal to and more than the fifth mode are observed in a neighborhood of the irrelevant condition $t_o/t_r = 2$, though no higher mode appears near the irrelevant condition $t_o/t_r = 4$. At $\alpha_r/\alpha_o = 0.1$, third modes appear in the range $(2.2 \leq t_o/t_r \leq 4.3)$. Thus, the mouthpiece reflection moves the area of the third mode to the left and the Model 3 is better than the Model 2 to archive the function of the register hole. As a result, the Model 3 at $\alpha_r/\alpha_o = 0.1$, which is the most realistic model among the three models, almost reproduces the function of the register hole. However, the register hole of the clarinet works in the range $(1.9 \leq t_o/t_r \leq 4.1)$, while for the Model 3, the first mode appears as a first excited oscillation in the range $(1.9 \leq t_o/t_r \leq 2.2)$. In general, the third mode is potentially excited even in this region and may be excited if one properly controls the attack, e.g., adjusting the embouchure. Anyhow, our result gives the answer to the questions why the diameter of the register hole is smaller than those of the other tone holes but not extremely small and why such a small register hole works in the wide range of the register.

4 CONCLUSIONS

In this paper, we investigated the function of the register hole with the models with two and three delays, and found that the basic function of the register hole is explained by the common properties of two-delay systems.

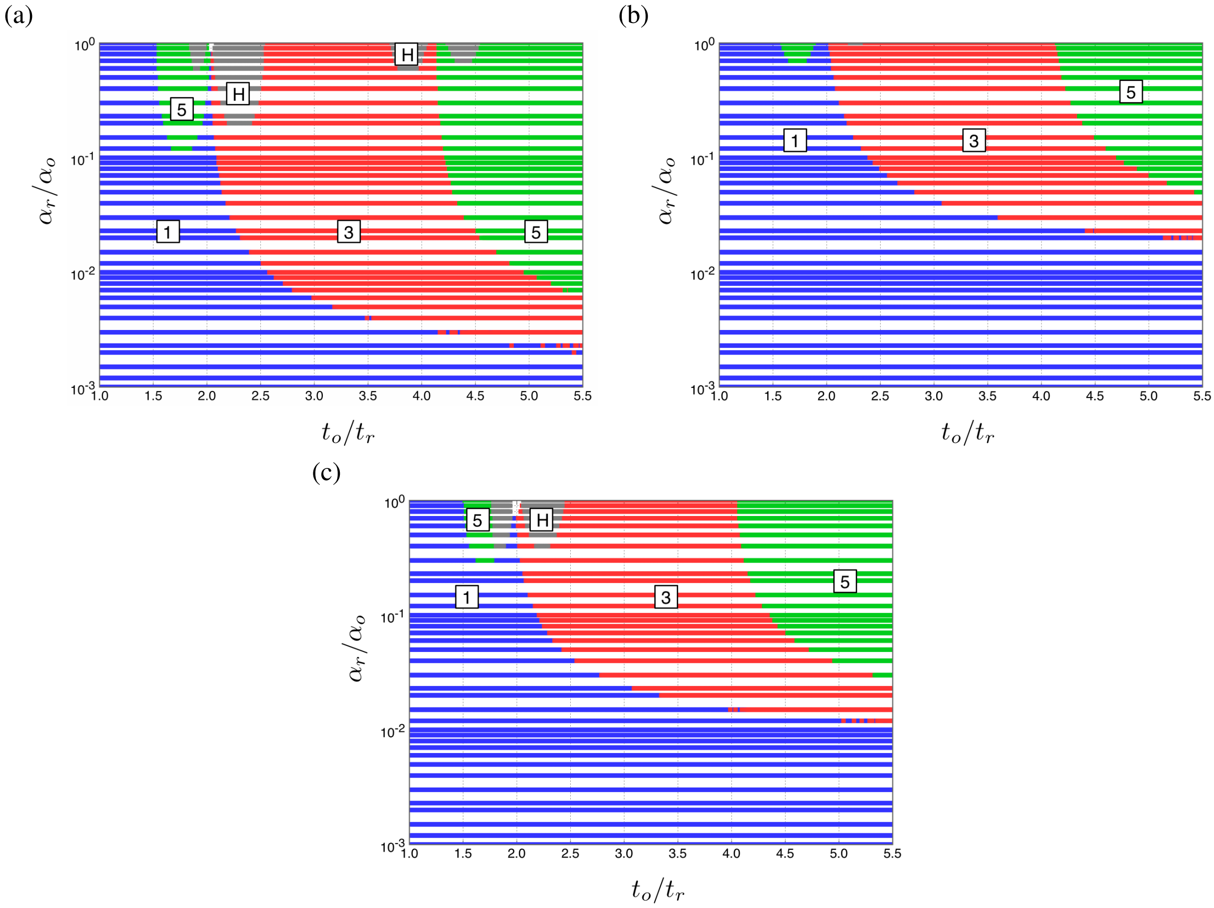

Figure 5. Phase diagrams of the first excited models in the parameter space of t_o/t_r and α_r/α_o. In the regions labeled '1', '3' and '5', first, third and fifth modes are observed, respectively, though modes equal to and more than seventh mode are excited in the regions labeled 'H'. (a) Model 1. (b) Model 2. (c) Model 3.

For the two-delay models, if the strength of the reflection from the register hole is sufficiently small but non-negligible, i.e., $\alpha_r/\alpha_o \approx 0.1$, the third mode is well sustained in the range $(2 \lesssim t_o/t_r \lesssim 4)$. This fact explains the setting of the position and radius of the register hole: the register hole is placed nearly at a quarter of the pipe length from the mouthpiece tip and its radius is about 1.5mm, which is much smaller than those of the other tone holes $(2.5-6.0\text{mm})$. The register hole with a large radius should induce higher modes around the irrelevant conditions $t_o/t_r = 2$ and 4.

The reflection caused by the bell is mimicked by the peak with a wide width, which reduces higher modes near $t_o/t_r = 2$ and 4, but shifts the range of the third mode at $\alpha_r/\alpha_o \approx 0.1$ to a positive direction, which is inconvenient for the register hole. The effect of the mouthpiece reflection with a very short delay is interesting. It induces higher modes around $t_o/t_2 = 2$ when α_r/α_o is large enough, but it shifts the range of the third mode at $\alpha_r/\alpha_o \approx 0.1$ to a negative direction and enhances the function of the register hole.

For the real clarinet, the register hole works in the range $(1.9 \leq t_o/t_r \leq 4.1)$, while for the Model 3 including the mouthpiece reflection, third modes appear in the range $(2.2 \leq t_o/t_r \leq 4.3)$. In general, the third mode is potentially excited even when the first mode dominates and it is expected that the third mode can be excited if properly controlling the attack, e.g., adjusting the embouchure [8]. For the real clarinet, the reflection function is much complicated owing to many opened and closed tone holes and should be characterized as a multiple-delay model [1, 5]. Nevertheless, the two-delay model and three-delay model including the mouthpiece reflection seem to well capture the underlying mechanism of the register hole. We postpone the study of the function of the register hole in terms of multiple-delay model with a real bore for future works.

ACKNOWLEDGEMENTS

The present work was supported by Grant-in-Aid for Scientific Research (C) Nos. 16K05477 and 19K03655 from the Japan Society for the Promotion of Science (JSPS), "Joint Usage/Research Center for Interdisciplinary Large-Scale Information Infrastructures" and "High Performance Computing Infrastructure" in Japan (Project IDs: jh180007-MDH and jh190010-MDH), and Kawai foundation for sound technology & music.

REFERENCES

[1] Schumacher R. T. Ab initio calculations of the oscillations of a clarinet, Acustica, Vol 48, 1981, pp.71-85.

[2] McIntyre M. E.; Schumacher R. T; Woodhouse J. On the oscillations of musical instruments, Journal of the Acoustical Society of America, Vol 74, 1983, pp.1325-1345.

[3] Hirschberg A.; Kergomard J.; Weinreich G. Mechanics of Musical Instruments, Springer-Verlag, Vienna(Austria) 1995.

[4] Fletcher N. H.; Rossing T. D. The Physics of Musical Instruments, Springer-Verlag, New York (USA), 2nd edition, 1998.

[5] Keefe D. Journal of the Acoustical Society of America, Vol 88, 1990 pp.35-51.

[6] Tachibana T.; Takahashi K. Sounding mechanism of a cylindrical pipe fitted with a clarinet mouthpiece, Progress of Theoretical Physics, Vol 104, 2000, pp.265-288.

[7] Takahashi K.; Kodama H.; Nakajima A.; Tachibana T. Numerical study on multi-stable oscillations of woodwind single-reed instruments, Acta Acustica united with Acustica, Vol 95, 2009, pp.1123-1139.

[8] Takahashi K.; Goya K.; Goya S. Mode selection rules for two-delay systems: dynamical explanation for the function of the register hole on the clarinet, Journal of the Physical Society of Japan, Vol 83, 2014, 124002.

[9] Ikeda K.; Mizuno M. Frustrated instabilities in nonlinear optical resonators, Physical Review Letters, Vol 53, 1984, pp.1340-1343.

[10] Mizuno M.; Ikeda K. An unstable mode selection rule: frustrated optical instability due to competing boundary conditions, Physica D, Vol 36, 1989, pp.327-342.

[11] Idogawa T.; Kobata T.; Komuro K.; Iwaki M. Nonlinear vibrations in the air column of a clarinet artificially blown, Journal of the Acoustical Society of America, Vol 98, 1993, pp.540-551.

PROCEEDINGS of ISMA 2019
International Symposium on Music Acoustics

13 - 17 September 2019 in Detmold, Germany

Numerical study on unsteady fluid flow and acoustic field in the clarinet mouthpiece with the compressible LES

Toshiaki KOIWAYA(1), Sho IWAGAMI(1), Taizo KOBAYASHI(2), Kin'ya TAKAHASHI(1),

(1)Kyushu Institute of Technology, Japan, koiwaya@chaos.mse.kyutech.ac.jp
(2)Kyushu University, Japan, tkoba@cc.kyushu-u.ac.jp

Abstract
The sound generation in the clarinet mouthpiece is still an unsolved problem from the viewpoint of aeroacoustic and has been studied theoretically, experimentally and numerically by many authors. Numerical simulations on the unsteady flow in the clarinet mouthpiece using LBM have been reported by several authors. In this paper, we numerically study unsteady fluid flow and acoustic field in the clarinet mouthpiece with compressible LES. We adopt 2D and 3D models and the 3D model has numerical grids more than one hundred and 50 million to reproduce detail behavior of air-jet motion, vortices and acoustic filed. In our models, the reed is fixed and a uniform flow is injected from the reed slit to study the behavior in the attack transient. The 2D and 3D models behave in different ways. For the 2D model, the injected jet is rolled up making long-lived rotors in the mouthpiece, while for the 3D model it is destabilized in a certain distance is broken into a lamp of turbulence. We also study the station that an alternating current is injected from the slit to reproduce the acoustic resonance.
Keywords: Clarinet, Mouthpiece, Numerical study

1 INTRODUCTION

Elucidation of the sounding mechanism of single reed instruments is one of the important subjects in the field of musical acoustics [1, 2, 3, 4, 5]. Single reed instruments are modelized by differential and difference equations with time delay, which well reproduce the pressure oscillation in the mouthpiece and the volume flow injected through the vibrating reed valve and capture the mechanism of bifurcation, which triggers oscillation with change of a control parameter, e.g., blowing pressure [2, 3, 4, 6, 7].

In delay equation models, it is always assumed that the volume flow U injected through the reed slit changes to the acoustic pressure p, more precisely aerodynamic sound, in the mouthpiece like $p = Z_0 U$, where Z_0 is the characteristic impedance of the mouthpiece[1, 2, 3, 4, 6, 7]. However, no one clearly answers questions of how and where the volume flow changes to the aerodynamic sound and how the assumption $p = Z_0 U$ holds true. In order to answer these questions, one needs an analysis based on the theory of aeroacoustics[8].

The numerical simulation by using compressible fluid solvers is one of the important tools to attack this problem. Actually, compressible fluid schemes simultaneously reproduce the fluid and acoustic fields and can be used for the analysis of the interaction between them[9]. Silva and Scavone succeeded to calculate fluid-structure interactions in single-reed mouthpiece with the Lattice Boltzmann Method (LBM)[10]. However, the mechanism of the transition process from an injected jet to an aerodynamic sound in the clarinet mouthpiece is still an open question.

In this paper, as the first step to attacking this problem, we construct 2D and 3D models of a clarinet mouthpiece and calculate the models by using compressible Large Eddy Simulation (LES) with two manners of driving the mouthpiece: the mouthpiece is driven by a constant flow and by a flow with periodically oscillating velocity. The latter method mimics the flow injected through a vibrating reed valve. The 3D model has a huge mesh with nearly 160 million cells and is calculated with a parallel computation technique by using a supercomputer.

2 SETUP OF NUMERICAL CALCULATIONS

2.1 3D model of clarinet mouthpiece

Figure 1 shows the cross-section of a clarinet mouthpiece (YAMAHA 4C), from which we measure dimensions of the clarinet mouthpiece. First, we construct a 2D model adding reed and square-shaped outer side area ($250 \times 250\text{mm}^2$) to the cross-section of the mouthpiece (see Figure 2). The distance between the mouthpiece tip and the reed, i.e., tip opening, is fixed at 1mm throughout this paper.

For convenience of constructing a 3D model, we add a uniform width of 12mm to the 2D cross-sections of the clarinet mouthpiece and reed and connecting a cube ($250 \times 250 \times 250\text{mm}^3$) as an outside volume to the open end of the mouthpiece (see Figure 3). To make a numerical mesh, the geometry of the 3D model is constructed by using FreeCAD and is converted to a mesh by using Snappy-HexMesh in OpenFOAM utility. As shown in Table 1, the minimum mesh size around the mouth opening is 0.1mm and the number of the cell is nearly 160 million, although the number of the cell is nearly 1.8 million for the 2D model.

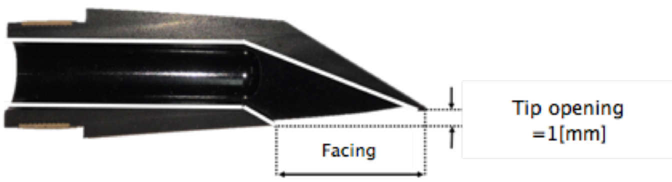

Figure 1. Cross section of clarinet mouthpiece.

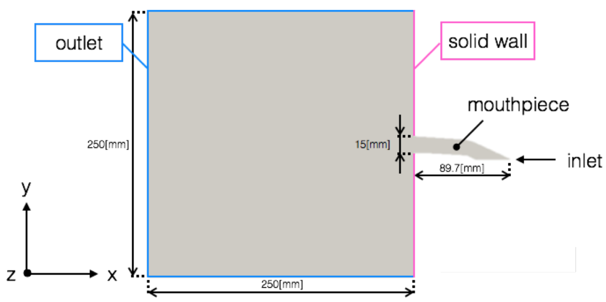

Figure 2. 2D model and boundary conditions.

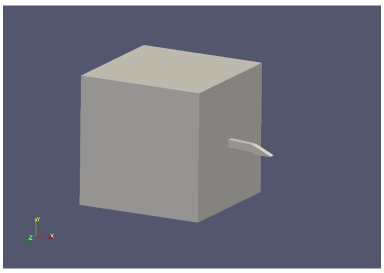

Figure 3. 3D model.

2.2 Numerical Method

To reproduce the transition process from the fluid flow to the aerodynamic sound, one needs a numerical scheme of compressible fluid, which reproduces the fluid and acoustic fields simultaneously. For this purpose, we use the compressible Large Eddy Simulation (LES) with the one-equation sub-grid-scale (SGS) model: RhoPimpleFoam, an unsteady solver of compressible laminar and turbulent flow in OpenFOAM Ver.5.0. Numerical simulations are performed with parallel computing technique by a supercomputer, ITO subsystem A of Kyushu University.

As shown in Table 1, the equilibrium pressure and temperature are set as $p = 100$ kPa and $T = 300$ K, respectively. The time step is set at $\Delta t = 5.0 \times 10^{-8}$ and the simulation is continued up to $t = 0.01$s. To save the amount of the output data for the 3D model, we pick up the data on the central cross-section, which corresponds to the 2D model, by using Function Object of OpenFOAM. We also detect the pressure data at the center of the open end of the mouthpiece.

The 2D and 3D mouthpiece models are driven by two ways. In the first way, the flow velocity at the tip opening takes a constant value of 15 m/s in the steady state (see Table 1). More precisely, the flow velocity is gradually increased and reaches 15 m/s at t = 0.0002s. In the second way, the instrument is driven by the flow, whose velocity periodically changes as

$$v_{in} = 15(1 - \cos \omega t), \tag{1}$$

where ω is the angular frequency of the Helmholtz resonance, which can be estimated from the simulation in the first way as shown later. The flow with periodically changed velocity mimics the flow injected through the vibrating reed, and the simulation in the second way resembles the situation that the mouthpiece is played in the normal way.

Table 1. Numerical parameters

parameter	value
Flow velocity [m/s]	15
Pressure at rest [kPa]	100
Temperature at rest [K]	300
Time step [s]	5×10^{-8}
Calculation time [s]	0.01
Numerical grids (2D)	1801208
Numerical grids (3D)	157417412
Minimum mesh size [mm]	0.1

3 NUMERICAL RESULTS

3.1 Results for the case that the 2D and 3D mouthpiece are driven by a constant flow.

In this subsection, we consider results for the case that the 2D and 3D mouthpiece are driven by a constant flow. Figure. 4 (a) and (b) show the spatial distributions of velocity and pressure at $t = 0.01$s for the 2D model, respectively. Figure 5 (a) and (b) show the spatial distributions of velocity and pressure at $t = 0.01$s for the 3D model, respectively.

As shown in Figure 4 (a), for the 2D model, the jet injected from the tip opening first goes along the bottom reed, but suddenly bends up, touches the aslope ceiling of the mouthpiece and forms an anti-clockwise rotor, which induces a clockwise rotor in the left side. As shown in Figure 5 (a), for the 3D model, the jet behaves in a similar way to that for the 2D model. However, the anti-clockwise rotor becomes weak breaking up into a lump of turbulence and the clockwise rotor disappears. This comes from the fact that vortex tubes are more robust for 2D systems than 3D systems owing to the two-dimensional inverse energy cascade[9].

The pressure distribution in Figure 4 (b) indicates that there is no clear resonance oscillation in the mouthpiece, although the pressure takes negative values in the areas of vortices. On the other hand, the pressure distribution in Figure 5 (b) forms a resonance field in the mouthpiece.

Fig.6 (a) and (b) show the time evolution of the pressure fluctuations for the 2D and 3D models, respectively. For both cases, damped oscillations are observed, but the pressure oscillation for the 2D model attenuates more rapidly. This is owing to the fact that the reflectance at an open end for a 2D pipe becomes smaller than that for a 3D pipe, especially in high frequency range (see Appendix of Ref.[9]). This fact also indicates that the resonance field for a 3D pipe is more stronger than that for a 2D pipe. Anyway, for the 2D model, the oscillation amplitude becomes very small at $t = 0.01$s and the resonance oscillation almost disappears. From the periods of the damped oscillations, we can estimate the resonance frequencies of the 2D and 3D mouthpiece: 949.4 Hz for the 2D model and 1041.7 Hz for the 3D model.

(a) (b)

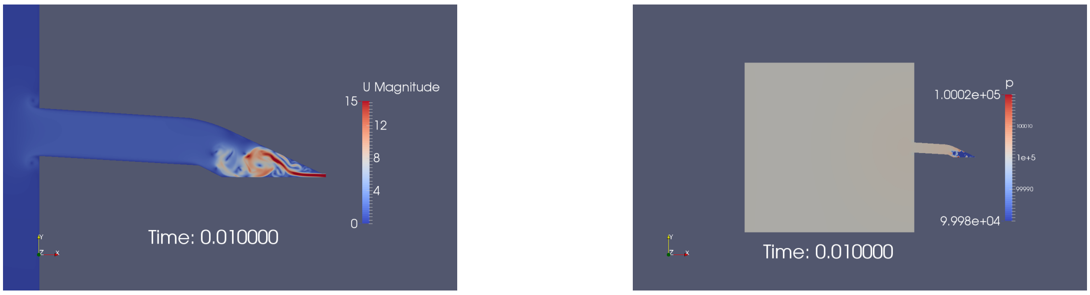

Figure 4. Spatial distributions of velocity and pressure at $t = 0.01$s for the 2D model driven by a constant flow. (a) Velocity. (b) Pressure.

(a) (b)

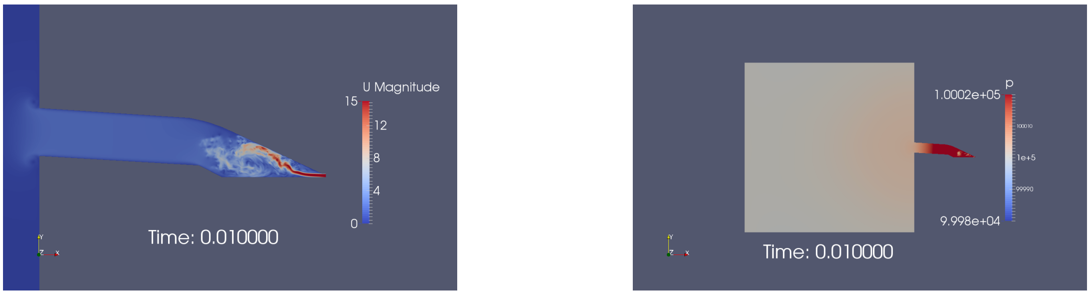

Figure 5. Spatial distributions of velocity and pressure at $t = 0.01$s on the center cross section of the 3D model driven by a constant flow. (a) Velocity. (b) Pressure.

(a) (b)

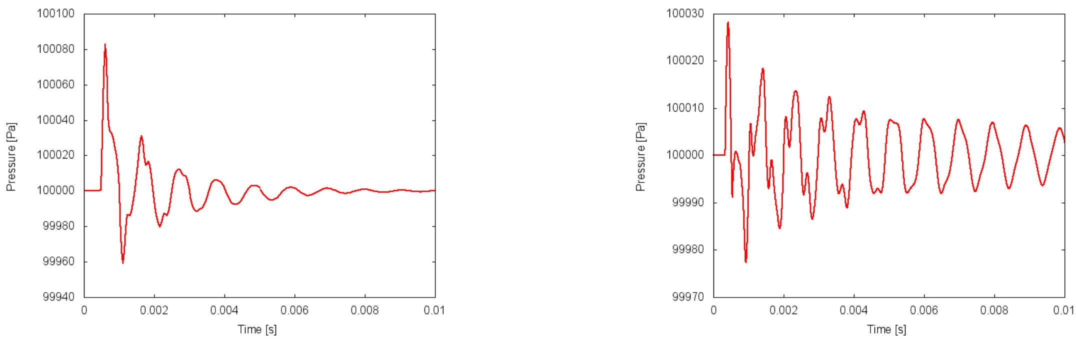

Figure 6. Time evolution of the pressure when a constant flow is injected. (a) 2D model. (b) 3D model.

3.2 Results for the case that the 2D and 3D mouthpiece are driven by an oscillating flow.

Let us consider results for the case that the 2D and 3D mouthpiece are driven by an oscillating flow. The driving angular frequencies are 949.4 Hz and 1041.7 Hz for the 2D and 3D models, respectively.

Figure. 7 (a) and (b) show the spatial distributions of velocity and pressure at $t = 0.01$s for the 2D model, respectively. Figure 8 (a) and (b) show show the spatial distributions of velocity and pressure at $t = 0.01$s for the 3D model, respectively.

As shown in Figure 7 (a) and Figure 8 (a), the jet generated by the oscillating flow at the tip opening behaves in a different manner from the jet with a constant velocity. For the 2D model, the jet, from the beginning, goes along the sloped ceiling of the mouthpiece, but after going a short way it changes to a rolled up eddy. For the 3D model, the jet also goes a rather long way along the sloped ceiling and breaks up into a lump of turbulence. Comparing with the case of the constant flow injection, fluid velocity, i.e, jet, eddies and turbulence, exists in a rather small area. This fact indicates that a strong acoustic resonance filed affects the fluid motion.

As shown in Figure 7 (b) and Figure 8 (b), strong pressure oscillations in resonance are observed for both 2D and 3D models. Fig.9 (a) and (b) show the time evolution of the pressure fluctuations for the 2D and 3D models, respectively. Resonance oscillations are observed for both cases. For the 2D model, the oscillation rapidly grows and reaches the steady oscillation with the amplitude of nearly 500Pa at $t = 0.01$s. For the 3D model, the oscillation grows rather slowly and does not reach the steady state at $t = 0.01$s, yet. The amplitude of the 3D model at $t = 0.01$s is nearly 650Pa, which is larger than that of the steady state for the 2D model. This means that the resonance for the 3D model is stronger than that for the 2D model.

(a) (b)

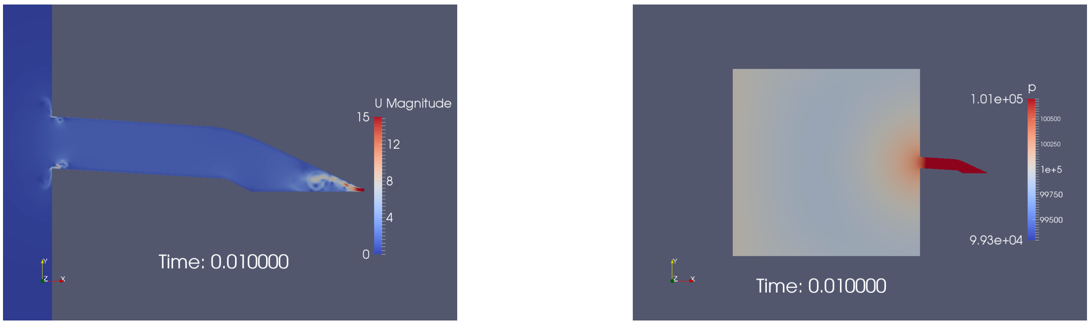

Figure 7. Spatial distributions of velocity and pressure at $t = 0.01$s for the 2D model driven by a periodically oscillating flow. (a) Velocity. (b) Pressure.

(a) (b)

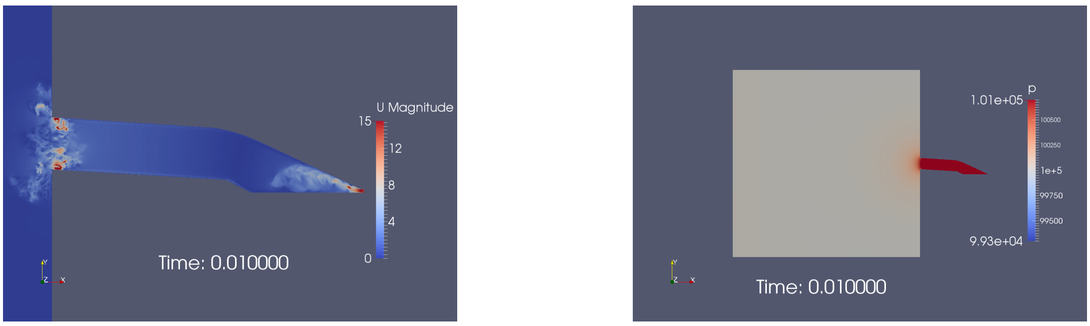

Figure 8. Spatial distributions of velocity and pressure at $t = 0.01$s on the center cross section of the 3D model driven by a periodically oscillating flow. (a) Velocity. (b) Pressure.

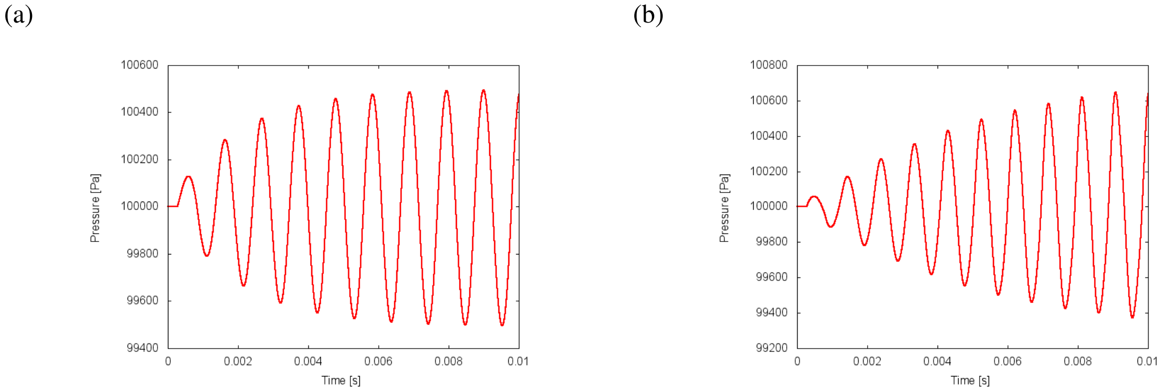

Figure 9. Time evolution of the pressure when a periodically oscillating flow is injected. (a) 2D model. (b) 3D model.

4 CONCLUSIONS

In this paper, as the first step to exploring the mechanism of the transition from an injected jet to an aerodynamic sound in the clarinet mouthpiece, we calculated the 2D and 3D models of the clarinet mouthpiece. As a result, we found the differences in the fluid motions and acoustic oscillations between the 2D and 3D models and the changes of the fluid motions and acoustic oscillations depending on the input boundary conditions, the constant flow driving and the oscillating flow driving.

Due to the weakness of the acoustic reflectance at the open end and the robustness of vortex tube for 2D systems, the weak acoustic resonance is observed and clear rolled up eddies are created compared with the 3D model. Thus, the calculation of the 3D model is necessary for our purpose.

When the mouthpiece is driven by the constant flow, the damped oscillations are observed. On the other hand, when the mouthpiece is driven by the flow with oscillating velocity, the acoustic resonance oscillations are excited in the mouthpiece. In this sense, the flow with oscillating velocity well mimics the flow injected through the vibrating reed and our model may become a minimal model for the study of the mechanism of the transition from an injected jet to an aerodynamic sound in the clarinet mouthpiece. For future work, we are planning to develop a moving reed model as a more realistic model.

ACKNOWLEDGEMENTS

The present work was supported by Grant-in-Aid for Scientific Research (C) Nos. 16K05477 and 19K03655 from the Japan Society for the Promotion of Science (JSPS), "Joint Usage/Research Center for Interdisciplinary Large-Scale Information Infrastructures" and "High Performance Computing Infrastructure" in Japan (Project IDs: jh180007-MDH and jh190010-MDH), and Kawai foundation for sound technology & music.

REFERENCES

[1] N. H. Fletcher and T. D. Rossing, The Physics of Musical Instruments, 2nd ed. (Springer-Verlag, New York, 1998).

[2] A. Hirschberg, J. Kergomard, G. Weinreich (eds.), Mechanics of Musical Instruments (Springer-Verlag, Vienna and New York, 1995).

[3] R. T. Schumacher: "Abinitio cal culations of the oscillations of a clarinet", Acustica 48, 71–85 (1981).

[4] M. E. McIntyre, R. T. Schumacher, J. Woodhouse: "On the oscillations of musical instruments", J. Acoust. Soc. Am. 74, 1325–1345 (1983).

[5] T. Idogawa, T. Kobata, K. Komuro, M. Iwaki: "Nonlinear vibrations in the air column of a clarinet artificially blown", J. Acoust. Soc. Am. 98, 540–551 (1993).

[6] T. Tachibana, K. Takahashi: "Sounding mechanism of a cylindrical pipe fitted with a clarinet mouthpiece", Prog. Theor. Phys. 104, 265–288 (2000).

[7] K. Takahashi, H. Kodama, A. Nakajima, T. Tachibana: "Numerical study on multi-stable oscillations of woodwind single-reed instruments", Acta Acustica united with Acustica, 95, 1123-1139 (2009).

[8] M. J. Lighthill, "On sound generated aerodynamically", Proc. R. Soc. London Ser. A 211, 564-587 (1952).

[9] M. Miyamoto, Y. Ito, T. Iwasaki, T. Akamura, K. Takahashi, T. Takami, T. Kobayashi, A. Nishida, and M. Aoyagi, "Numerical study on acoustic oscillations of 2D and 3D flue organ pipe like instruments with compressible LES", Acta Acustica united with Acustica, 99, 154-171 (2013).

[10] A. Ricardo da Silva and G. P. Scavone, "Numerical simulations of fluid-structure interactions in single-reed mouthpiece" J. Acoust. Soc. Am. 122, 1798-1809 (2007).

PROCEEDINGS of ISMA 2019
International Symposium on Music Acoustics

13 - 17 September 2019 in Detmold, Germany

Computational aeroacoustic modeling of single-reed mouthpiece using Palabos

Song WANG *, Gary SCAVONE †

Computational Acoustic Modeling Laboratory (CAML),
Centre for Interdisciplinary Research in Music Media and Technology (CIRMMT),
Schulich School of Music, McGill University, Canada

Abstract

The sound generation behavior of a single-reed instrument can be determined from its aeroacoustic characteristics. Computational aeroacoustics (CAA) modeling offers a mean to analyze the aeroacoustics behavior of such a system. The lattice Boltzmann method (LBM) models fluid on a mesoscopic level and has certain advantages over traditional Navier-Stokes approaches in solving CAA problems. In this study, we present results from an aeroacoustic analysis of a 2D single-reed mouthpiece system using an open-source, parallelized lattice Boltzmann solver called Palabos. A variety of functionalities and components are investigated, including the parallelization, the moving boundary, and the non-reflecting boundary condition, which demonstrates the versatility of Palabos. Different mouthpiece geometries are tested with both static and moving reeds. The nonlinear characteristics of the mouthpiece-reed system derived from this study are then compared with the theoretical quasi-static flow model.

Keywords: Computational aeroacoustics, Single-reed mouthpiece, Lattice Boltzmann method

1 INTRODUCTION

Wind instruments can generally be decomposed into two components, the sound resonator, and the sound generator. For a single-reed instrument, the sound generator corresponds to its nonlinear mouthpiece-reed system that largely determines the dynamics of the whole instrument. The mouthpiece-reed system is generally analyzed in terms of a nonlinear relationship between the volume flow rate and the pressure difference across the reed channel.

The flow through the reed channel was initially assumed to be frictionless, incompressible, and quasi-stationary so that the mouthpiece-reed system can be modeled based on the Bernoulli equation [1]. Hirschberg et al. (1990) [2] improved the model by introducing viscous effects while keeping the incompressible and quasi-static approximation. The reed channel of the mouthpiece is modeled as a two-dimensional Borda tube. The flow separation at the reed channel entrance is taken into account by introducing the vena contracta coefficient ($0.5 < \alpha \leq 0.611$). For a larger Reynolds number and a longer channel, the flow will reattach in the reed channel, and the flow after the reattachment point is approximated by the Poiseuille flow. Van Zon et al. (1990) [3] further extended this model by replacing the Bernoulli flow by the boundary layer flow to represent the flow in between the separation point at the entrance and the reattach point in the reed channel. The Van Zon model is validated by measurements with a static reed [3]. However, the quasi-stationary approximation fails in dynamic flow even though the estimated Strouhal number is much smaller than one [3]. Discrepancies of the vena contracta coefficient are also found when comparing the theoretical value to both the measurement [4, 5] and the numerical simulation results [6, 7].

In this paper, the dynamic behavior of the single-reed mouthpiece-reed system is studied using Palabos [8], an open-source computational fluid dynamics solver based on the lattice Boltzmann method (LBM). In contrast with traditional Navier-Stokes (NS) solvers, LBM is a mesoscopic method based on the discretization of the Boltzmann equation and has been proven to perform well in solving aeroacoustic problems [9, 10, 11]. In order to model the mouthpiece-reed system of a single-reed instrument, different algorithms are used including the

*song.wang5@mail.mcgill.ca
†gary.scavone@mcgill.ca

multi-block technique for parallelization, the non-reflecting boundary condition [12], and the immersed boundary method (IBM) for building the off-grid boundary and the moving boundary [13].

This paper is organized as follows: Section 2 presents the basic LBM scheme and different algorithms used in the simulation. The details of the simulation setup are described as well. The numerical results of the static reed case and their comparison with the theoretical solution are discussed in Section 3. A preliminary moving reed test is also presented. Finally, a conclusion is given in Section 4.

2 NUMERICAL PROCEDURE

2.1 Lattice Boltzmann method

The lattice Boltzmann method (LBM) is a numerical method based on the lattice Boltzmann equation (LBE) that is obtained by discretizing the Boltzmann equation in physical space, velocity space and time, given as

$$f_i(\boldsymbol{x}+\boldsymbol{e}_i\Delta t, t+\Delta t) = f_i(\boldsymbol{x},t)+\Omega_i(\boldsymbol{x},t), \tag{1}$$

where f_i is the distribution function, $\{e_i\}$ is the discrete velocity set, Δt is the time step that usually equals 1, and $\Omega(\boldsymbol{x},t)$ is the collision operator. The D2Q9 model is used in this paper, which discretizes the velocity space into nine directions for a two-dimensional space. The lattice sound speed is defined as $c_s = 1/\sqrt{3}$, the weight coefficients $\{w_i\}$ are set as

$$w_i = \begin{cases} \frac{4}{9}, & i=0, \\ \frac{1}{9}, & i=2,4,6,8, \\ \frac{1}{36}, & i=1,3,5,7, \end{cases} \tag{2}$$

and $\boldsymbol{e}_i$ is given as

$$\boldsymbol{e}_i = \begin{cases} (0,0), & i=0, \\ (\cos\frac{(i+2)\pi}{4}, \sin\frac{(i+2)\pi}{4}), & i=2,4,6,8, \\ \sqrt{2}(\cos\frac{(i+2)\pi}{4}, \sin\frac{(i+2)\pi}{4}), & i=1,3,5,7. \end{cases} \tag{3}$$

One of the most widely used collision operators is known as Bhatnagar-Gross-Krook (BGK),

$$\Omega_i(\boldsymbol{x},t) = -\frac{1}{\tau}(f_i - f_i^{\mathrm{eq}})\Delta t, \tag{4}$$

where τ is the relaxation time related to the kinematic viscosity $\nu = c_s^2(\tau - \frac{\Delta t}{2})$, and f_i^{eq} is the equilibrium distribution function given by

$$f_i^{\mathrm{eq}}(\boldsymbol{x},t) = w_i\rho\left(1+\frac{\boldsymbol{u}\cdot\boldsymbol{e}_i}{c_s^2}+\frac{(\boldsymbol{u}\cdot\boldsymbol{e}_i)^2}{2c_s^4}-\frac{\boldsymbol{u}\cdot\boldsymbol{u}}{2c_s^2}\right) \tag{5}$$

The macroscopic density and velocity are found as $\rho = \sum_i f_i$ and $\boldsymbol{u} = \sum_i \boldsymbol{e}_i f_i/\rho$, respectively. Based on the isothermal condition, the pressure p can be determined by $p = \rho c_s^2$.

Despite the simplicity of the original BGK scheme, it can be unstable for high Mach number and high Reynolds number flow. Spurious waves due to the numerical error might also disturb the acoustic field. In order to achieve a better solution, the recursive regularized BGK (rrBGK) LBM is applied in this paper. The rrBGK was first introduced to increase the stability and accuracy by Malaspinas [14] for isothermal and weakly compressible flow, based on the original regularized BGK proposed by Latt and Chopard [15]. Coreixas et al. [16] further generalized it for thermal and fully compressible flow. The rrBGK starts by expressing the distribution function f as the sum of the equilibrium distribution f^{eq} and the non-equilibrium part f^{neq} based on the Chapman-Enskog expansion

$$f = f^{\mathrm{eq}} + f^{\mathrm{neq}}. \tag{6}$$

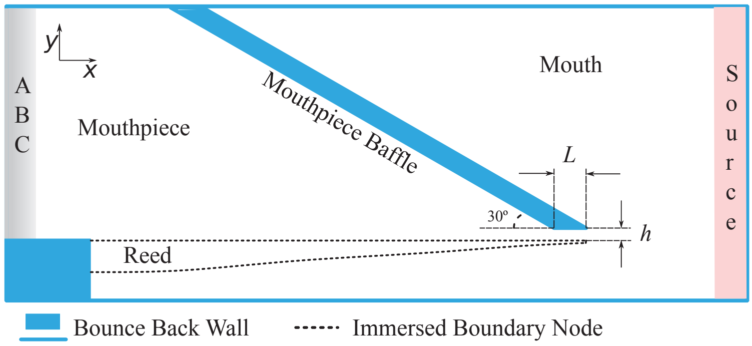

Figure 1. The schematic view of the computational domain

Then, both f^{eq} and f^{neq} can be expressed in terms of Hermite polynomials whose coefficients can be calculated recursively. Further details of the algorithms can be found in the paper by Malaspinas [14].

2.2 Simulation setup

A simplified two-dimensional mouthpiece is set up in the fluid domain as shown in Figure 1. The size of the domain is 5×2 cm^2 with the spatial grid size of $\Delta x = 8 \times 10^{-5}$m. The time step is set as $\Delta t = 1.35 \times 10^{-7}$s. The lattice relaxation time is $\tau = 0.5098$, corresponding to the physical kinematic viscosity of $\nu = 1.55 \times 10^{-4}\mathrm{m}^2/\mathrm{s}$, which is an order of magnitude larger than the air kinematic viscosity.

The absorbing boundary condition (ABC) proposed by Kam et al. [12] is applied at the exit of the mouthpiece (left side of Figure 1) to get rid of the acoustic feedback. The same algorithm is used at the inlet with a non-zero flow and pressure target, working as the pressure source [17]. The immersed boundary method [13] is implemented in Palabos for modeling the reed, which allows the off-lattice boundary and the moving boundary conditions. The one-dimensional distributed model [18] is used for modeling the reed as well as the reed-mouthpiece interaction. Different from previous LBM simulations [6, 7], the reed thickness is introduced into the model. For the fixed walls of the mouthpiece, the bounce-back scheme is used for a no-slip flow condition.

In Palabos, the parallelization is performed with the message-passing interface (MPI). By using the multi-block technique, the computational domain is divided into multi-blocks and are assigned to different processors. As well, the one-side communication technique is used for distributing the reed information to different processors. All the simulations were run on the Compute Canada CPU cluster (Intel E5-2683 v4 Broadwell @ 2.1GHz) with 32 processors.

For this study, we intended to apply the grid refinement technique to improve the simulation efficiency. With such a scheme, the finest grid could be deployed around the reed channel to help better capture the flow properties. However, the problem becomes complex due to the interaction between the off-lattice boundary and the moving boundary across regions of different resolution. So, even though the grid refinement has already been implemented [19] in Palabos and tested in other aeroacoustic simulations [10], its application in our wind instrument model is left for a future investigation.

3 RESULTS

3.1 Static Reed Results

In the static reed case, two different mouthpiece profiles with different channel lengths ($L/h = 1$ and $L/h = 4$) are studied, where L stands for the reed channel length and $h = 1.3$ mm represents the channel height. The simulation lasts for 500,000 iterations in total. The mouth pressure starts from 0 Pa and linearly increases to

11 kPa within 200,000 iterations, and holds for 50,000 iterations. It then decreases back to zero within the next 200,000 iterations and holds there until the end of the simulation. The mouth pressure p_{mouth} is measured by averaging a rectangular field in between the top and bottom domain boundaries, starting from the tip of the mouthpiece to the left of pressure source buffer. The flow volume rate U_{jet} is calculated by multiplying the cross-section area by the averaged flow velocity measured across the end of the reed channel. The pressure p_{jet} is measured by taking the average of the pressure over the cross-section area at the end of the reed channel. The pressure difference is defined as $\Delta p = p_{mouth} - p_{jet}$.

Simulation results and the comparison with the theoretical results [3] are shown in Figure 2 and Figure 3. Four different plots are shown to better explain the results, including the Δp - U_{jet} plot, the Δp - α plot, the pressure/flow history plot, and the Re - α plot. The Re - α plot only includes the first half of the simulation, i.e., 250,000 iterations.

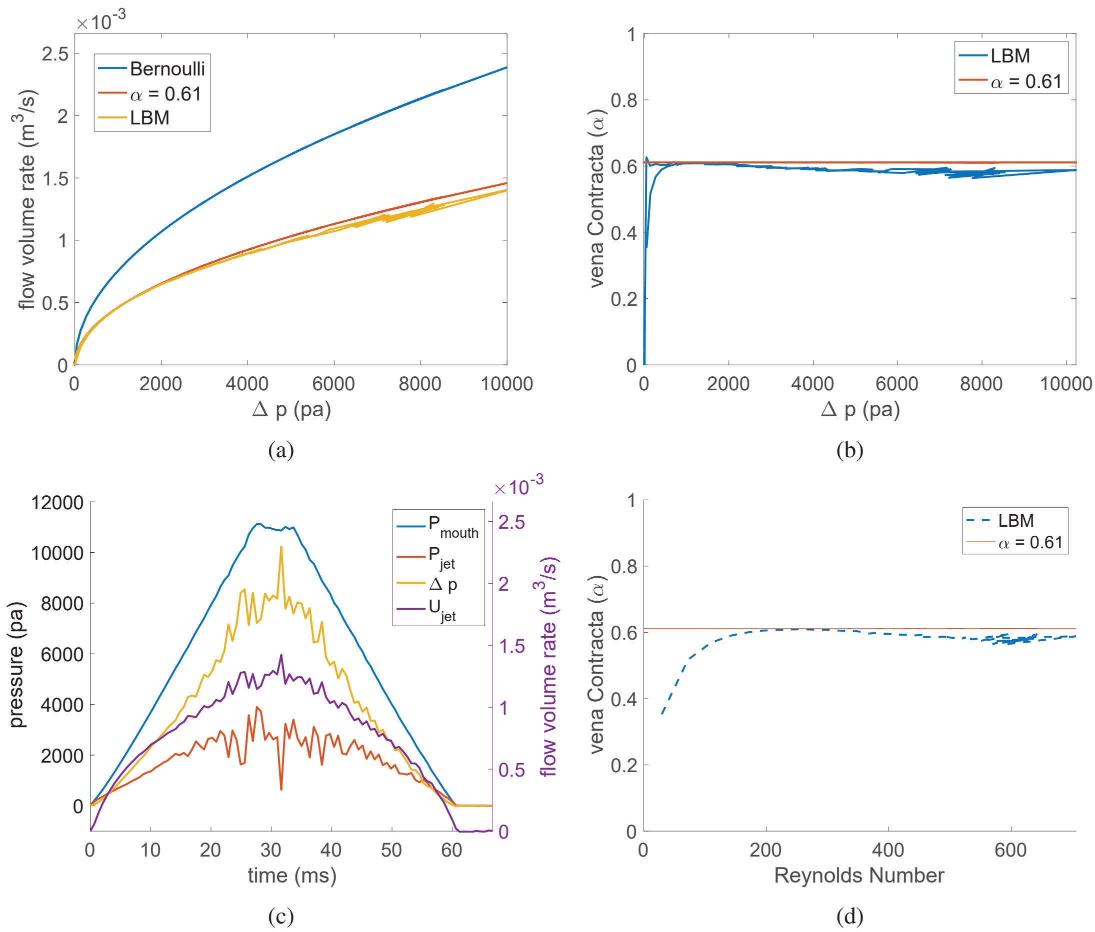

Figure 2. The LBM simulation results for the mouthpiece with $L/h = 1$.

For the short reed channel mouthpiece ($L/h = 1$), the simulation result matches the theoretical estimation very well and the calculated vena contracta coefficient α falls into the theoretical range $(0.5, 0.611]$ as proposed by Hirschberg et al. 1990 [2]. However, for the long reed channel mouthpiece ($L/h = 4$), instead of being comparable with the van Zon model for long reed channel, the LBM flow is more similar to the short reed channel flow with a slightly lower α. Similar results were also observed by Shi et al. [6], who attributed them to the large viscosity used in LBM. In order to test this explanation, the mouthpiece with a more realistic kinematic

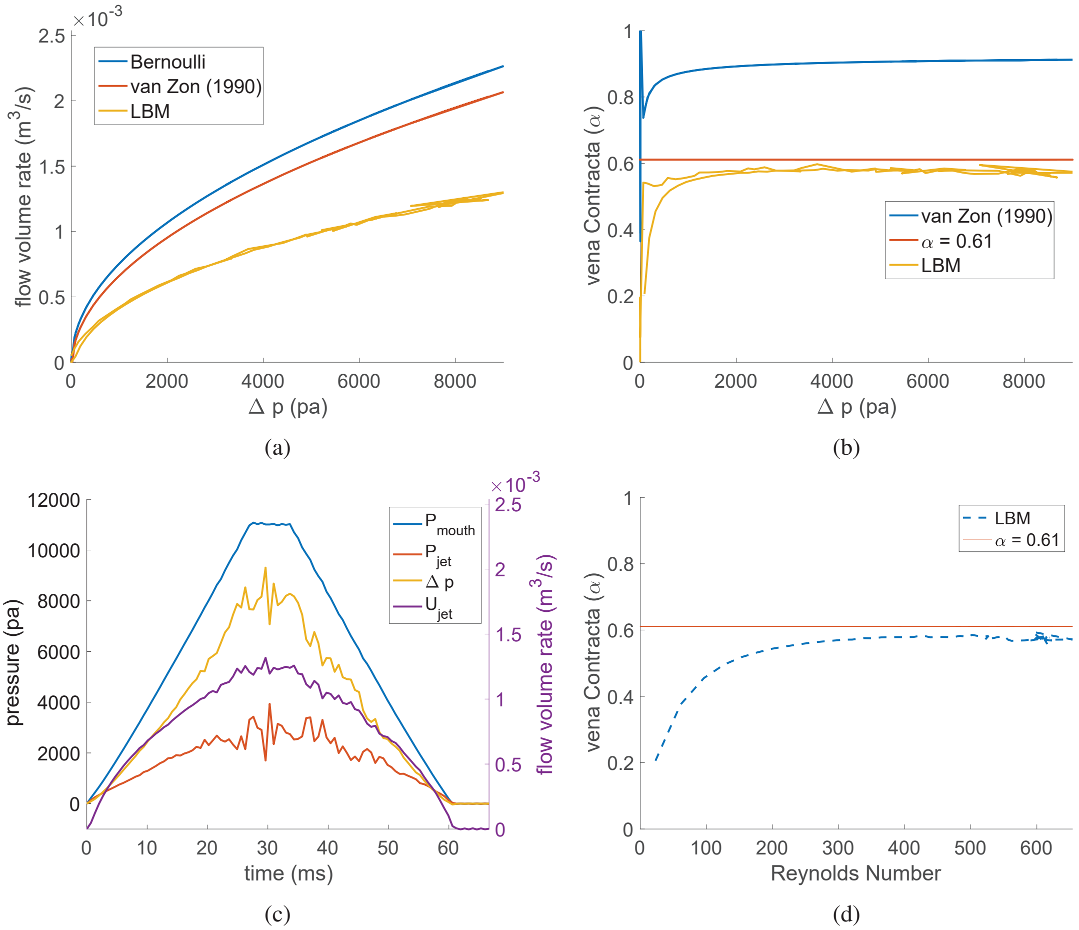

Figure 3. The LBM simulation results for the mouthpiece with $L/h = 4$.

viscosity ($\nu = 4.75 \times 10^{-5}\mathrm{m}^2/\mathrm{s}$) flow is simulated with finer grids ($\Delta x = 4.25 \times 10^{-5}\mathrm{m}$). As shown in Figure 4, decreasing the viscosity does help increase the flow rate a little bit. However, the flow becomes more turbulent as the Reynolds number increases.

3.2 Moving Reed Results

In this section, a simulation with a moving reed is presented. The pressure difference between the top and bottom of each immersed boundary node of the reed is taken as the external force that drives the reed to move. The velocity of each node is then used in the immersed boundary method. The target pressure of the source buffer is set as 8kPa. The mouth pressure, the jet volume flow rate, and the jet pressure are measured at the same position as discussed in the previous section. In addition, the mouthpiece pressure at the downstream of the mouthpiece, near the absorbing boundary layer, is also measured. All the results, together with the tip displacement, are shown in Figure 5. In this preliminary simulation setup, the system does not achieve a steady-state regime but instead decays over time. The volume flow rate appears to be noisy, which might be due to the low grid resolution. For example, when the reed tends to close, there could be only one grid point for calculating the volume flow rate, which is insufficient. Despite this, the result shows the ability of the framework to simulate the fully coupled fluid-structure interaction problem.

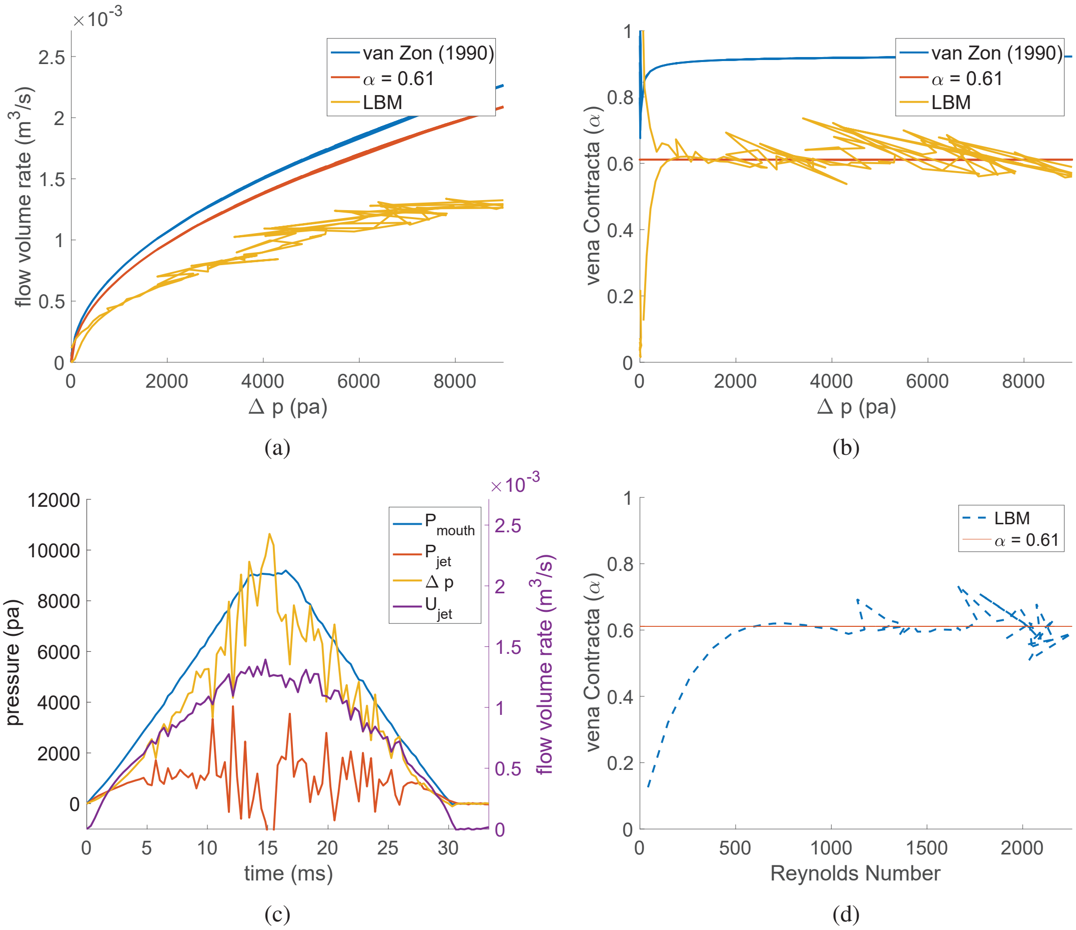

Figure 4. The LBM simulation results for the mouthpiece with $L/h = 4$ with the kinematic viscosity of $\nu = 4.75 \times 10^{-5} \mathrm{m}^2/\mathrm{s}$.

4 CONCLUSIONS

In this paper, a single-reed mouthpiece reed system is modeled within Palabos. Different functionalities have been tested. For the static reed simulation, the results of the short reed channel show a good agreement with the theoretical model. However, for a longer reed channel mouthpiece, a large discrepancy is found between the LBM simulation and the van Zon model. Though it is partially due to the high kinematic viscosity used in the simulation, it might also be caused by the relative larger numerical dissipation of the MRT or the rrBGK scheme that helps maintain the stability. In addition, as shown in the pressure/flow history plots and the Re - α plots, the flow starts to get turbulent as the pressure goes higher. Such turbulent behavior that happens in the simulation might be another reason for the discrepancy. However, considering the Reynolds number is still much smaller than 4000, further experiments is need to judge if this behavior is a physical turbulence or the numerical noise.

For the moving reed simulation, a preliminary result is presented, which shows the ability of the framework in solving the fully coupled fluid-structure interaction problem. However, the low-resolution and first-order IBM might be insufficient for complicated cases, such as the flow that involves the collision of the reed with the mouthpiece. In such case, a high-order of IBM and grid refinement should be implemented. In addition, impedance acoustic boundary condition is also needed to study the fluid-acoustic-solid interaction in

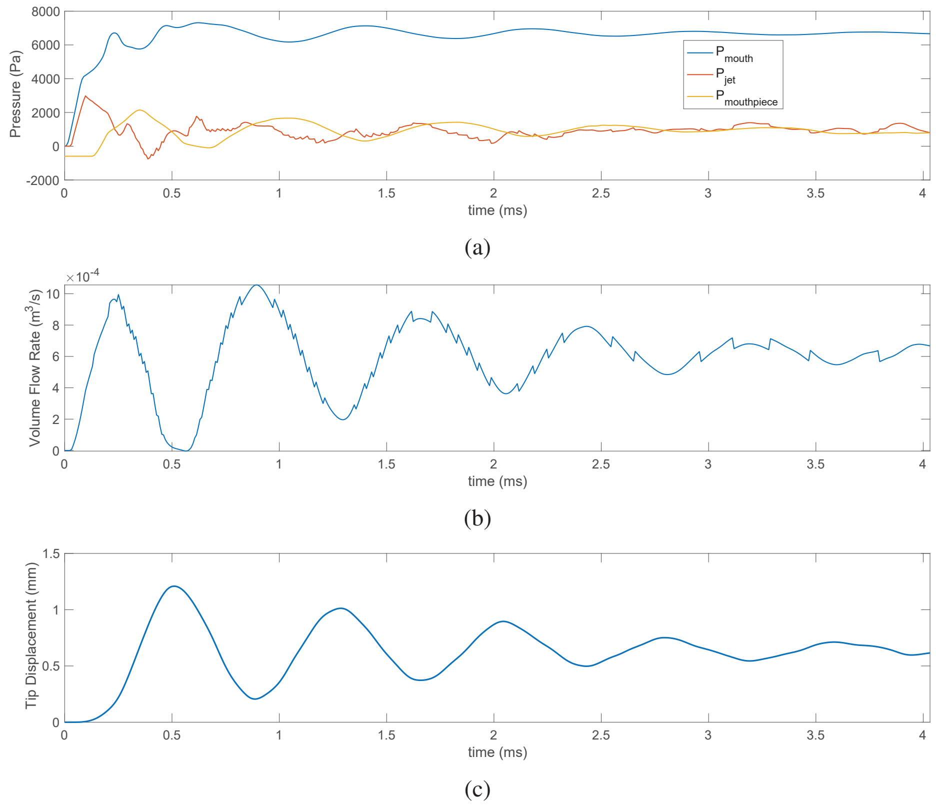

Figure 5. The moving reed simulation result.

the mouthpiece-reed system.

ACKNOWLEDGEMENTS

The authors wish to acknowledge the support from Natural Sciences and Engineering Research Council of Canada, and the Centre for Interdisciplinary Research in Music Media and Technology at McGill University. The authors also acknowledge the compute resources provided by Compute Canada.

REFERENCES

[1] John Backus. Small-Vibration Theory of the Clarinet. *The Journal of the Acoustical Society of America*, 35(3):305–313, 1963.

[2] A. Hirschberg, R. W. A. Van de Laar, J. P. Marrou-Maurieres, A. P. J. Wijnands, H. J. Dane, S. G. Kruijswijk, and A. J. M. Houtsma. A quasi-stationary model of air flow in the reed channel of single-reed woodwind instruments. *Acta Acustica united with Acustica*, 70(2):146–154, 1990.

[3] J. Van Zon, A. Hirschberg, J. Gilbert, and A. P. J. Wijnands. Flow through the reed channel of a single reed music instrument. *Le Journal de Physique Colloques*, 51(C2):C2–821, 1990.

[4] Jean-Pierre Dalmont, Joël Gilbert, and Sébastien Ollivier. Nonlinear characteristics of single-reed instru-

ments: Quasistatic volume flow and reed opening measurements. *The Journal of the Acoustical Society of America*, 114(4):2253–2262, 2003.

[5] Valerio Lorenzoni and Daniele Ragni. Experimental investigation of the flow inside a saxophone mouthpiece by particle image velocimetry. *The Journal of the Acoustical Society of America*, 131(1):715–721, 2012.

[6] Yong Shi, Andrey R. da Silva, and Gary P. Scavone. LBM SIMULATION OF THE QUASI-STATIC FLOW IN A CLARINET. In *Proceedings of the Third Vienna Talk on Music Acoustics*, 2015.

[7] Andrey Ricardo da Silva, Gary P. Scavone, and Maarten van Walstijn. Numerical simulations of fluid-structure interactions in single-reed mouthpieces. *The Journal of the Acoustical Society of America*, 122(3):1798–1809, September 2007.

[8] Palabos. http://www.palabos.org/.

[9] Guillaume A. Brès, David Freed, Michael Wessels, Swen Noelting, and Franck Pérot. Flow and noise predictions for the tandem cylinder aeroacoustic benchmark. *Physics of Fluids*, 24(3):036101, March 2012.

[10] Federico Brogi, Orestis Malaspinas, Bastien Chopard, and Costanza Bonadonna. Hermite regularization of the lattice Boltzmann method for open source computational aeroacoustics. *The Journal of the Acoustical Society of America*, 142(4):2332–2345, 2017.

[11] Yu Hou, David Angland, Alois Sengissen, and Aline Scotto. Lattice-Boltzmann and Navier-Stokes Simulations of the Partially Dressed, Cavity-Closed Nose Landing Gear Benchmark Case. In *25th AIAA/CEAS Aeroacoustics Conference*, page 2555, 2019.

[12] E. W. S. Kam, R. M. C. So, and R. C. K. Leung. Lattice Boltzmann method simulation of aeroacoustics and nonreflecting boundary conditions. *AIAA journal*, 45(7):1703, 2007.

[13] Takaji Inamuro. Lattice Boltzmann methods for moving boundary flows. *Fluid Dynamics Research*, 44(2):024001, 2012.

[14] Orestis Malaspinas. Increasing stability and accuracy of the lattice Boltzmann scheme: Recursivity and regularization. *arXiv preprint arXiv:1505.06900*, 2015.

[15] Jonas Latt and Bastien Chopard. Lattice Boltzmann method with regularized pre-collision distribution functions. *Mathematics and Computers in Simulation*, 72(2-6):165–168, 2006.

[16] Christophe Coreixas, Gauthier Wissocq, Guillaume Puigt, Jean-François Boussuge, and Pierre Sagaut. Recursive regularization step for high-order lattice Boltzmann methods. *Physical Review E*, 96(3):033306, September 2017.

[17] A. R. da Silva, G. P. Scavone, and A. Lefebvre. Sound reflection at the open end of axisymmetric ducts issuing a subsonic mean flow: A numerical study. *Journal of Sound and Vibration*, 327(3):507–528, November 2009.

[18] Federico Avanzini and Maarten Van Walstijn. Modelling the mechanical response of the reed-mouthpiece-lip system of a clarinet. Part I. A one-dimensional distributed model. *Acta Acustica united with Acustica*, 90(3):537–547, 2004.

[19] Daniel Lagrava, Orestis Malaspinas, Jonas Latt, and Bastien Chopard. Advances in multi-domain lattice Boltzmann grid refinement. *Journal of Computational Physics*, 231(14):4808–4822, 2012.

PROCEEDINGS of ISMA 2019
International Symposium on Music Acoustics

13 - 17 September 2019 in Detmold, Germany

Design, construction, and material of an ancient Indian string instrument

Anurag GUPTA[(1)], Chaitali DANGARIKAR[(1)]

[(1)]Department of Mechanical Engineering, IIT Kanpur, UP 208016, India, ag@iitk.ac.in

Abstract

Ekatantrī vīṇā is a one-stringed fretless tubular zither from ancient India whose descriptions and representations are variously found in musicological texts and sculptures, respectively, between 11th and 15th century AD. The present work is a first of its kind attempt to study one of these sources to understand the precise structural and material nature of the *vīṇā*. In particular, we use a Sanskrit text where *ekatantrī vīṇā* is unambiguously described, and prepare accurate computed aided models of various parts of the *vīṇā* as well as describe their assembly. Our work is motivated, on one hand, from an aim to establish historicity of certain unique design features of the present day Indian stringed instruments and, on the other hand, to initiate a systematic study towards reconstruction of ancient Indian instruments. Our investigations also provide grounds for further study in acoustics, mechanics, and materials, all in the context of ancient Indian science.

Keywords: Ancient Indian zithers, Reconstruction, *Ekatantrī vīṇā*

1 INTRODUCTION

Ekatantrī[1] *vīṇā*[2] is an ancient Indian, one-stringed, fretless, tubular zither with a rounded gourd resonator attached to one end of a long hollowed wooden tube. At the other end, a large wooden peg is inserted which, in turn, supports a bulky, doubly curved, bridge engraved with a thin metallic plate. The playing string, made of animal gut, clamped towards the gourd side of the tube, and wrapped around the wooden peg at the other, vibrates while facing a unilateral constraint in the motion due to the finitely curved bridge. A bamboo thread is suitably inserted between the metal plate and the string such that the latter makes a grazing contact over the former. The *vīṇā* is played being held in a slanting position while placing the gourd over the left shoulder and tactfully positioning the bridge on the right heel. The string is plucked with fingers of the right hand, close to the bridge, whereas the variations in pitch are obtained by sliding a little wooden rod, held in the left hand, along the string. The above description, summarized from the early 13th c. text *Saṅgīta-ratnākara* (hereafter SR) [1], is qualitatively consistent with the *vīṇā* in the hands of the 12th c. *Sarasvatī* (Figure 1) where, even with a broken tube (in the central region), all the essential structural features, and the mannerism of playing, are unambiguously discernible. The simple structure of the instrument notwithstanding, it is an extremely difficult instrument to play requiring advanced techniques to produce a rich array of notes all from a single string.

Our aim is to prepare precise structural drawings, and study the material nature, of the *vīṇā* parts, leading to their assembly and a complete computer aided digital reconstruction of *ekatantrī vīṇā*. Our work, which uses SR as the primary source text, provides all the technical details for an actual reconstruction of the instrument (see also [2]); it can be, in fact, immediately used for 3D printing of a visual replica of the *vīṇā*. Our findings can be also used to establish the historicity of various design features in the present-day Indian stringed instruments; e.g. the doubly curved bridge in *tānpurā*, *sitār*, *rudra vīṇā*, etc., the thread between the string and the bridge in *tānpurā*, the metallic plate in *Sarasvatī vīṇā*, among several others. Besides formal reconstruction and historical benchmarking, there can be several other implications of our work. Our discussions, for instance, provide information on the workmanship, material culture, and musical traditions followed in 13th c. India and, at the same time, are potent in initiating a further study in acoustics, mechanics, design, and materials, all in the context of ancient Indian science and craftsmanship.

[1]The italicized words in this article are in Sanskrit. They are written using the International Alphabet of Sanskrit Transliteration (IAST) scheme.
[2]The word *vīṇā* has been used in ancient Indian parlance for all kind of string instruments.

Detmold HOCHSCHULE FÜR MUSIK ISMA 2019 DEGA

Figure 1. *Sarasvatī* holding *ekatantrī vīṇā* from Gorakhpur, Uttar Pradesh, 12th c.; presently at Lucknow State Museum.

The earliest Indian *vīṇā* were of the bow-shaped harp-type with a hollow belly covered with stretched leather and furthered by a curved, and hollowed, wooden arm [3]. The strings, stretched from arm to the belly, could vary in number; e.g. both *citrā* and *parivādinī vīṇā* had seven strings but *vipañchī* had nine. The strings were plucked either with fingers (*citrā*) or with a plectrum (*vipañchī*). These harp-like *vīṇā* find widespread mention in the earliest Indian literature from Vedic, Epic, Buddhist, and Jain periods [3, 4, 5]; both *citrā* and *vipañchī* are also mentioned as important *vīṇā* in the *Nāṭyaśāstra*. They appear in the reliefs at *Sāncī*, *Bhāja*, *Bharhut* (all around 2nd c. BCE), *Amrāvatī* (1st c.), *Nāgārjunakonda* (2nd-4th c.), and in the famous Samudragupta coins (4th c.). Certain lute-like *vīṇā* also appear at *Amrāvatī*, *Nāgārjunakonda*, *Pawāyā* (Gupta period), and *Ajantā* (4th-6th c.), although there is no clear description of such instruments in the ancient literature [3, 4, 5]. Another widely mentioned *vīṇā* is a 21 stringed, dulcimer-like, board zither *mattakokilā* (the main *vīṇā* of *Nāṭyaśāstra*), with a structure similar to the modern day *svaramaṇḍala*.

The earliest tubular zithers with gourd resonators are noticed at *Ajantā* and *Bādāmī* (7th c.) [4]. They gradually acquire a dominant presence both in plastic art and literature, including several extant musicological texts. Almost until the turn of the millennium, the tubular zithers were fretless, had a cut or covered resonator (mostly made out of bottle gourd), were both with and without the thread (inserted between the bridge and the string), and sometimes had a broad curved bridge [4]. Noticeable among the early tubular zithers was a simple, single stringed, instrument with a cut gourd on one end to be pressed against the chest while playing (yielding the human body as the resonator); such a design survives today in *tuila* [5]. The evolution of fretless tubular zithers culminated in the development of *ekatantrī vīṇā*, which was not only larger (in appearance) than its predecessors, but also had well developed parts, most of which survive in several Indian string instruments. The importance of *ekatantrī vīṇā*, and its role in the development of subsequent instrument forms, cannot simply be overstated (SR 6.53-54).[3]

2 THE STRUCTURE OF THE *VĪṆĀ*

2.1 Metrology

The musicological text of our interest use three classical length scales for various measurements: *aṅgula*, *vitasti*, and *hasta*. One *aṅgula* is usually understood as the breadth of the middlemost joint of the middle finger of a medium-sized man or equal to the thickness of six husk-less barley grains put together width-wise one after another; moreover, twelve *aṅgula* make a *vitasti*, and twenty-four make a *hasta* [6]. One *aṅgula* is approximately equal to three-quarter of an inch or 1.905 cm [6]. We take it to be 2 cm. Consequently, *vitasti* becomes 24 cm and *hasta* becomes 48 cm. Our design can be easily rescaled for any change in measurements for an *aṅgula*.

2.2 Parts of the *vīṇā*

(a) **Tubular fingerboard**. The fingerboard of the *ekatantrī* is made out of a single piece of wood through which air columns, of various arrangements, are bored in the longitudinal direction; see Figure 2. The wood should be from *khadira* (Acacia Catechu) tree, straight, free from knots and bends, smooth, polished, well rounded, and well-seasoned (SR 6.29). The length and the circumference of the tube should be 144 cm and 24 cm, respectively (SR 6.29-30). The longitudinal air column can be either (i) a single cylindrical cavity (diameter 3 cm), (ii) two cylindrical cavities chambers, meeting to form a single hole (diameter 3 cm) at the bottom but two holes each of diameter 1.8 cm at the upper end, or (iii) three chambers meeting to form a single hole (diameter 3 cm) at the bottom but three holes each of diameter 1.5 cm at the upper end (SR 6.31-32), see Figure 2. The entire fingerboard therefore serves as a resonator. The bottom hole is jammed by inserting a wooden peg, over which a bulky bridge is placed.

(b) **Wooden peg**. The peg, made of strong wood, when inserted into the fingerboard, provides it both structural stability and strength. Most importantly, it acts as a sound post transmitting the string vibrations via the bridge, which it carries on itself, to the tubular fingerboard. The peg is a 16 cm long cylinder and has a circumference of 6 cm in one half and 3 cm in the other (SR 6.37); see Figure 3. The latter half is completely inserted inside the fingerboard while the former is elevated like a tortoise back to prevent the bridge from falling down (SR 6.38).

(c) **Bridge**. The bridge of the *ekatantrī* is carved out of a rectangular block of *khadira* wood (SR 6.32). The

[3]The number refers to the verse in our primary source text.

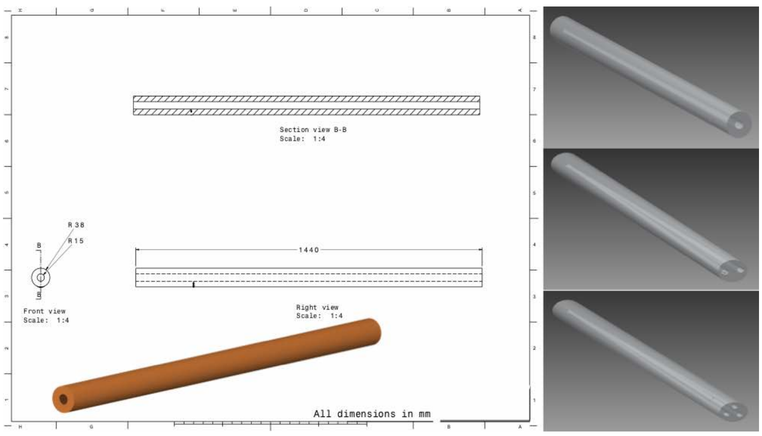

Figure 2. The tubular fingerboard with three possible arrangements for the longitudinal bore.

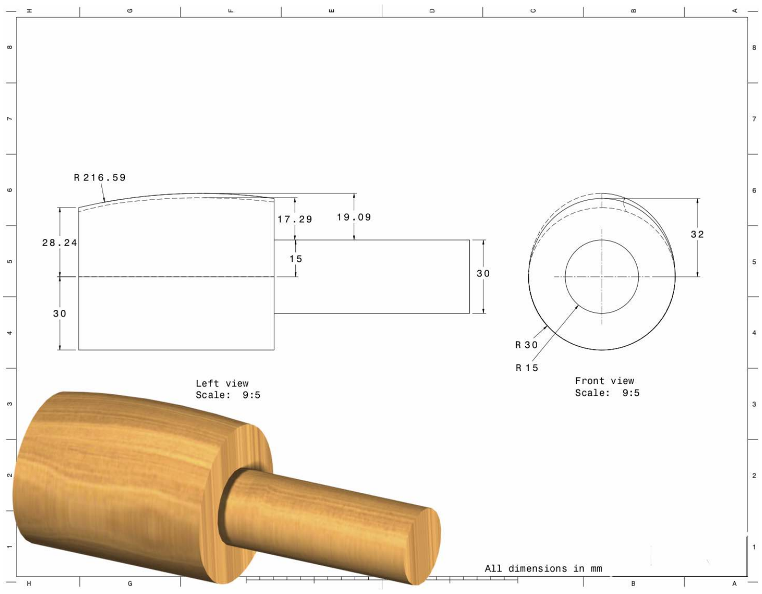

Figure 3. The wooden peg, the narrow part of which is to be inserted into the tubular fingerboard.

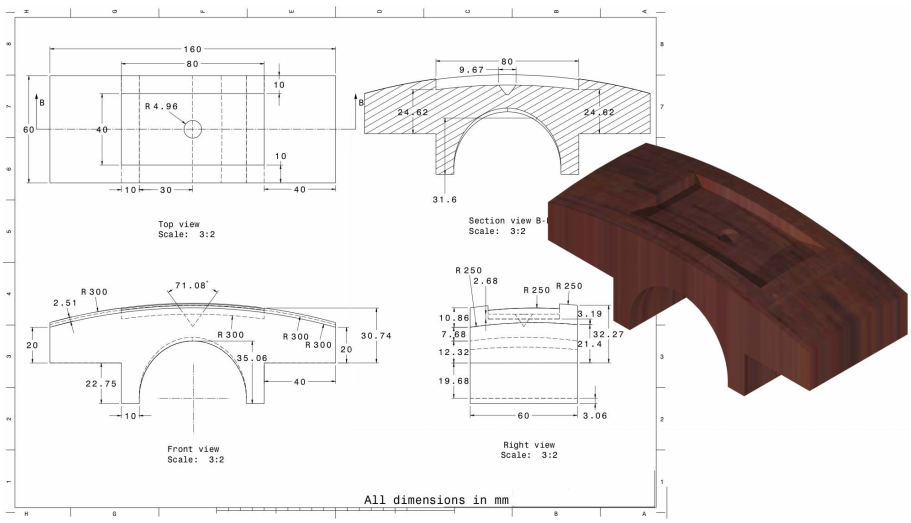

Figure 4. The bridge with a groove for placing the metal plate.

two footed bridge has an intricate shape which ensures that it sits stably on the peg (without being glued) and supports a rectangular convex plate of metal on top (SR 6.37-38). With a curvature like a tortoise back, it has a length of 16 cm, width of 6 cm, and has sides around 2 cm high (SR 6.33); a detailed dimensioning can be seen in Figure 4. A rectangular groove and a conical pit are provided at the elevated high portion of the bridge to support the metal plate (SR 6.34), see Figure 4.

(d) **Convex plate**. A convex plate, made of brass (SR 6.35) is fitted seamlessly within the groove provided on top of the bridge; the plate should be 4 cm wide and 8 cm long (SR 6.35-36). The seamless placement of the plate is clearly visible in the bridge assembly in Figure 5. The overall curved bridge is a standard feature

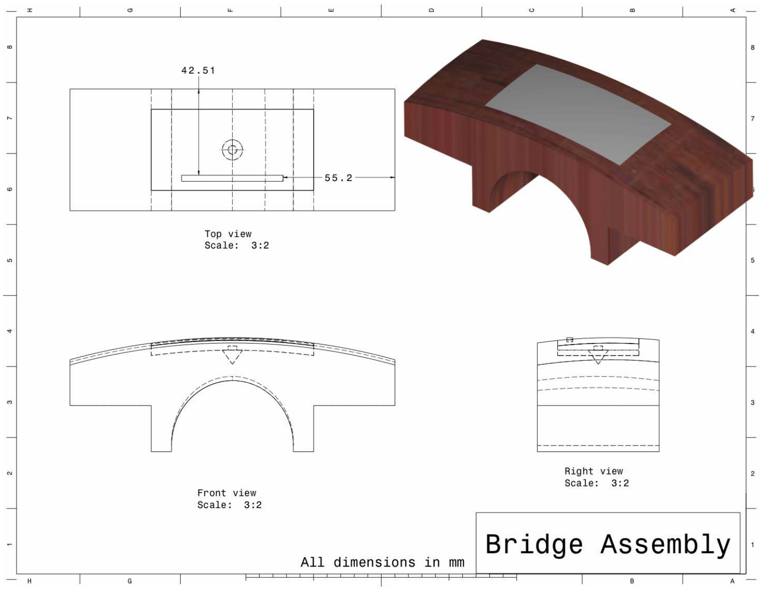

Figure 5. The metal plate (in grey colour) attached to the bridge using a spike.

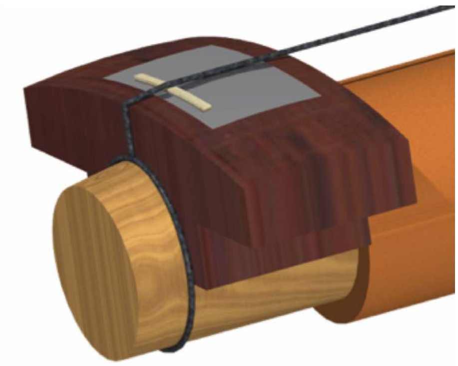

Figure 6. Partial assembly of *vīṇā* parts. The bridge is placed over the peg which is inserted into the finger-board. The bamboo skin (in light brown) is placed below the string (in black) to maintain a grazing contact of the latter over the metal plate

in many modern Indian string instruments (*tānpurā*, *sitār*, *rudra vīṇā*, *Sarasvatī vīṇā*, etc.), where it is used to produce an overtone rich sound with sustained transfer of energy to higher modes of vibration [7, 8]. The metallic plate is however retained only in *Sarasvatī vīṇā*.

(e) **Wooden Spike**. A wooden spike is used to fix the convex metal plate onto the bridge (SR 6.35). On one side it fits into the conical pit located at the centre of the rectangular groove on the bridge and, on the other side, it has a cylindrical protrusion which holds the plate in the required position. The spike can be noticed, upon close observation, in Figure 5.

(f) **Bamboo skin**. A bamboo skin, 4 cm long and 0.3 cm wide (SR 6.49), is placed on the metal plate below the playing string at the point where they come in contact with each other (SR 6.50), see Figure 6. The purpose of the skin is to raise the string just enough to maintain a grazing contact with the plate (SR 6.50). The skin is supposed to enhance the quality of sound and deliver an overtone rich buzzing sound (SR 6.50) [9]. Presently

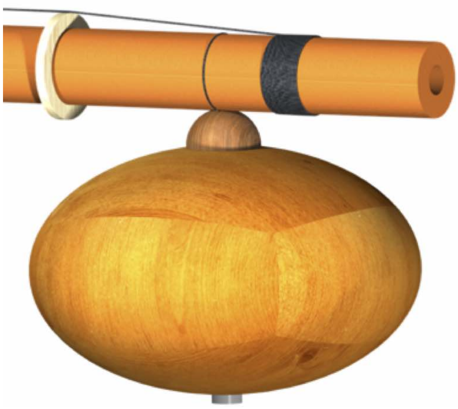

Figure 7. Partial assembly of the *vīṇā* from the resonator side. The top plate, in the form of a coconut shell (brown colour), is visible between the resonator and the fingerboard. The nut (light brown coloured ring) is a mobile sleeve which acts as one end of the vibrating string.

it is found most commonly in *tānpurā*, where it is otherwise made out of a cotton thread.

(g) **Resonator**. The resonator of *ekatantrī* is made out of a bottle gourd and is covered partially with a coconut shell cap (SR 6.42-44). The gourd should be matured, thoroughly ripe, dried, cleaned, and uniform in its circular shape (SR 6.42). It should have a circumference of 120 cm and height of around 24 cm (SR 6.42). On the naval side, a hole of 6 cm diameter is carved (SR 6.43). This hole is to be covered with a coconut shell before being fixed to the fingerboard. At the stem side, a small hole is to be provided to attach a bolt-like device. The basic design is illustrated in Figure 7.

(h) **Top plate**. A hemispherical cap, made out of a clean and polished coconut shell, is used to cover the 6 cm diameter hole on the resonator (SR 6.44). A small hole is to be drilled on top of the shell for fixing it to the fingerboard. The cap can be seen in Figure 7.

(i) **Cotton chord**. A strong triple stranded cotton thread is used to tie the resonator to the fingerboard (SR 6.39-41). The two ends of the cord are first threaded into the eye-like fingerboard holes (which form two ends of an arc like bore in the fingerboard, SR 6.39) to form a tight loop and thereafter inserted into the aligned holes of the gourd and coconut shell before being tied to a bolt-like wooden device at the other end of the resonator. The bolt is to be twisted till the gourd is firmly attached to the fingerboard (SR 6.45-46). This arrangement can be visualized in Figure 8.

(j) **Nut**. Nut is a mobile sleeve made of three-ply braided bamboo skin which is used to change the length of the vibrating string thereby affecting its pitch (SR 6.51). The thickness of the sleeve should be such that the string remains at the same height between the bridge and the nut, see Figures 7.

(l) **Playing string**. The playing string, made of strong, smooth, and solid animal gut, is tied on one end to a loop of a cotton thread, with a hanging noose for bringing minor variations in the string tension (SR 6.47-48). The other end is stretched over the bridge, pressing the bamboo skin and grazing the metal plate, before being firmly tied to the peg, see Figures 8 and 9.

(m) **Plectrum**. A small bamboo chip is used to press upon the playing string from the resonator side while plucking it with the right hand closer to the bridge (SR 6.58).

2.3. The assembled *vīṇā*

To summarize the above, we start by inserting a large wooden peg on one side of the hollowed wooden tube and then placing the bridge and the metal plate assembly over the peg. The metal plate should be firmly placed in the groove on top of the bridge and they together should be stable over the peg. At the other end, a gourd resonator is attached to the tube with the help of a coconut shell cap and a bolt-like arrangement. A stretched

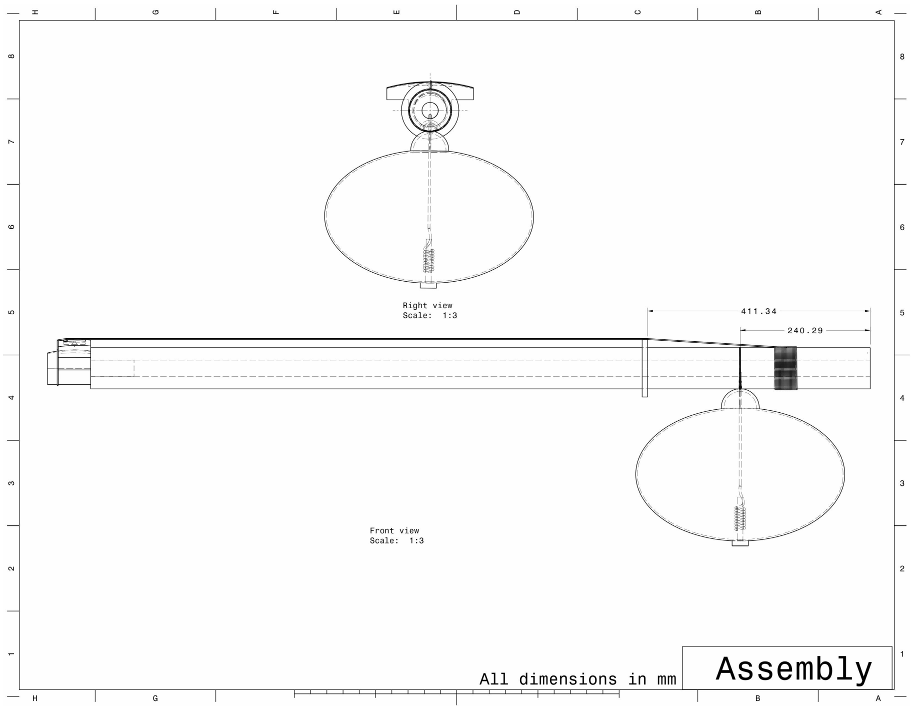

Figure 8. Design of the complete *ekatantrī vīṇā*.

Figure 9. The digital reconstruction of *ekatantrī vīṇā*.

playing string is then finally attached over the fingerboard in a way as pointed above. The final assembly is shown in Figures 8 and 9.

3 CONCLUSIONS

The purpose of this work has been to present a computer-aided reconstruction of an ancient Indian string instrument based on a 13th c. Sanskrit text. Detailed drawings were presented, the material used discussed, and complete assembly of various parts were given. It should be emphasized that this is first of its kind of study in the context of Indian musical instruments. This can possibly lead to a more systematic study of acoustics, mechanics, and materials in the context of ancient Indian science. It also provides a way towards actual reconstruction of ancient Indian musical instruments.

ACKNOWLEDGEMENTS

We gratefully acknowledge the assistance from Mr. Gaurav Agrawal in preparing the CAD drawings using the CATIA software.

REFERENCES

[1] Śārṅgadeva. *Saṅgīta-ratnākara* vol. III (in Sanskrit), S. S. Sastri (ed.), Adyar, Madras, 1986. Verses 6.29-6.53 on pp. 324-328.

[2] Sharma, P.; Bhat, S. in Seminar on Instrument makers, Sangeet Research Academy, Calcutta, 1993, pp. 1-12.

[3] Coomaraswamy, A. The parts of a *vīṇā*, Journal of the American Oriental Society, 50, 1930, pp. 244-253.

[4] Tarlekar, G. H. Fretted *vīṇā* in Indian sculpture, The Journal of the Music Academy Madras, 36, 1965, pp. 170-175.

[5] Deva, B. C. Musical Instruments of India, Firma KLM Calcutta, 1978.

[6] Srinivasan, S. Mensuration in Ancient India, Ajanta, Delhi, 1979, Ch. 2.

[7] Raman, C. V. On some Indian stringed instruments, Proceedings of the Indian Association for the Cultivation of Science, 7, 1921, pp. 29-33.

[8] Burridge, R.; Kappraff, J.; Morshedi, C. The sitar string, a vibrating string with a one-sided inelastic constraint, SIAM Journal on Applied Mathematics, 42, 1982, pp. 1231-1251.

[9] Pisharody, R.; Gupta, A. Experimental investigations of *tānpurā* acoustics, Acta Acustica united with Acustica, 104, 2018, pp. 542-545.

PROCEEDINGS of ISMA 2019
International Symposium on Music Acoustics

13 - 17 September 2019 in Detmold, Germany

Vibration characteristics of oud soundboard

Sinan INANLI[1]; Ercan ALTINSOY[2]

(1) TU Dresden, Germany, inanli@gmail.com

(2) TU Dresden, Germany, ercan.altinsoy@tu-dresden.de

Abstract

Oud is a plucked musical instrument played in many countries. It has a short neck, fretless keyboard and lute-like body. There are three sound holes on the soundboard arranged in triangular position. Its soundboard has a thickness varying between 1.5-2.0 mm and seven fan braces are placed on the inner side parallel to each other and perpendicular to the string alignment to withstand the force created by the string tension. Walnut, mahogany, maple, rosewood family and wenge are some of the most common hard woods used in the body of the instrument whereas spruce and cedar are the tone woods used to construct the soundboard. This historical musical instrument involves many structural parts effecting its acoustics and sound quality. This study aims at investigating the vibration characteristics of an oud soundboard for free-free and fixed (at its edges and no back cavity) boundary conditions. Also, as a final step, soundboard-air cavity coupled modes were measured by assembling the soundboard and body together. Frequency response function (FRF) measurements were carried out by experimental modal analysis technique to reveal the dynamic behavior (mode frequencies, mode shapes and damping coefficients) of the soundboard which has a conventional strutting configuration.

Keywords: Oud, Soundboard, Modal Test

[1] inanli@gmail.com

[2] ercan.altinsoy@tu-dresden.de

PROCEEDINGS of ISMA 2019
International Symposium on Music Acoustics

13 - 17 September 2019 in Detmold, Germany

Numerical Simulation of Aerodynamics Sound in an Ocarina Model

Hiroaki OKADA(1), Sho IWAGAMI(2), Taizo KOBAYASHI(3), Kinya TAKAHASHI(4)

(1)Kyushu Inst. Tech, Japan
(2)Kyushu Inst. Tech, Japan
(3)Kyushu Univ, Japan, tkoba@cc.kyushu-u.ac.jp
(4)Kyushu Inst. Tech, Japan, takahasi@mse.kyutech.ac.jp

Abstract

The body of an ocarina is regarded as a Helmholtz resonator. Thus, we can expect differences in sounding mechanism between ocarinas and other air-jet instruments with a resonance pipe. Furthermore, ocarinas are driven by cross blowing like transverse flutes so that the driving mechanism with an air-jet should be different from that for vertical flues like a recorder. In this paper, we numerically explore the sounding mechanism of an ocarina from the viewpoint of aeroacoustics with compressible fluid simulation. We adopt compressible LES as a numerical scheme of compressible fluid, which simultaneously reproduces fluid and acoustic fields and with which we can investigate the interaction between the fluid and acoustic fields near the mouth opening. Our 3D model has numerical grids more than one hundred and 50 million to reproduce detail behavior of air-jet motion, vortices and acoustic filed near the mouth opening. We numerically observed an acoustic oscillation with the Helmholtz resonance frequency in the body together with the detail structure of fluid field.

Keywords: Sound, Music, Acoustics

1 INTRODUCTION

The sounding mechanism of air-jet instruments has been studied in the field of musical acoustics for many years [1, 2, 3]. The numerical simulation based on the theory of aeroacoustics is one of the important tools to attack this problem [4, 5, 6, 7, 8]. The main difficulty in the numerical study of air-jet instruments comes from the mutual interaction between the fluid field and the acoustic field, which is hardly reproduced by the hybrid method of the fluid solver and acoustic solver, although it is commonly used for the analysis of aerodynamic noise in the case that the feedback from the acoustic field to the fluid field is negligible [1, 5]. For the analysis of air-jet instruments, the feedback from the acoustic oscillation in the resonator to the jet motion is key to understanding the sounding mechanism.

There are two types of air-jet instruments, which are different in the function of the resonator. The group of the flute, recorder, flue organ pipe and so on has a pipe as a resonator and the pitch is determined by the resonance of the air column. On the other hand, the body of the ocarina is regarded as the Helmholtz resonator and the pitch is determined by the Helmholtz resonance. Furthermore, the ocarina is driven by cross blowing like transverse flutes so that the driving mechanism with an air-jet should be different from that for those vertical flues like a recorder, which have been numericaly studied by several authors[4, 5, 6, 7, 8].

Nearly ten years ago, the author's group numerically studied the 2D and 3D models of an ocarina with compressible LES[9]. Then, the 3D model with a mesh of nearly 1.3 million cells was calculated up to 0.005s; thus, an oscillation in an attack transient was roughly reproduced and the behavior of the jet motion and that of the acoustic oscillation were not analyzed in detail. In this study, to explore the sounding mechanism of ocarinas from the viewpoint of aeroacoustics, we construct a 3D model of an ocarina with a finer mesh of nearly 160 million cells and calculate the 3D model with parallel computation technique by using a supercomputer.

The structure of this paper is as follows. In section 2, we roughly explain the sounding mechanisms of the edge tone and air-jet instruments and introduce the 3D model of the ocarina. In Section 3 we explain the numerical method and shows the numerical results: spatial distributions of velocity and pressure, and pressure oscillation at an observation point with its power spectrum. Then, we discuss the characteristic properties of the ocarina with a Helmholtz resonator. Section 4 is a conclusion.

2 THREE DIMENSIONAL OCARINA

2.1 Frequency of Edge tone

The sound source of air-jet instruments is an aerodynamic sound called the edge tone, which is generated by an air jet impinging on a sharp edge [1, 10]. The edge tone has been a long standing problem in the fields of aeroacoustics and musical acoustics, but its detail mechanism is not fully understood yet. In 1937, Brown introduced the semi-empirical equation, which gives the relation between the jet velocity V[m/s] and the oscillation frequency f[Hz] [11],

$$f = 0.466j(100V - 40)(1/(100l) - 0.07), \tag{1}$$

where l[m] is the distance between the nozzle and the edge, j is a parameter taken as $j = 1.0$, 2.3, 3.8 and 5.4, where $j = 1$ corresponds to the fundamental mode of hydrodynamic oscillation, and others corresponds to the overtones, which appear through hysteretic transitions with increasing the jet velocity. The frequency f of the fundamental mode is proportional to the jet velocity V. However, when the jet velocity V exceeds a certain threshold value, a transition to the next mode occurs. The transitions with increasing and decreasing the jet velocity are hysteretic, namely the threshold value of the downward transition is smaller than that of the upward transition. The fundamental mode is normally used for the air-jet instruments.

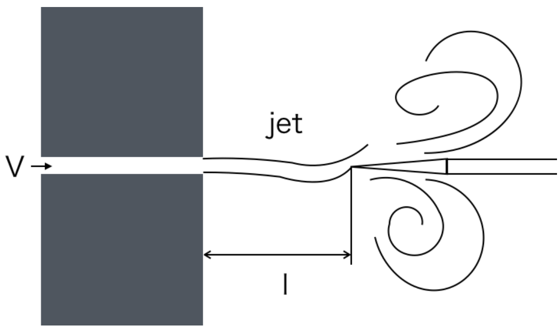

Figure 1. Edge tone.

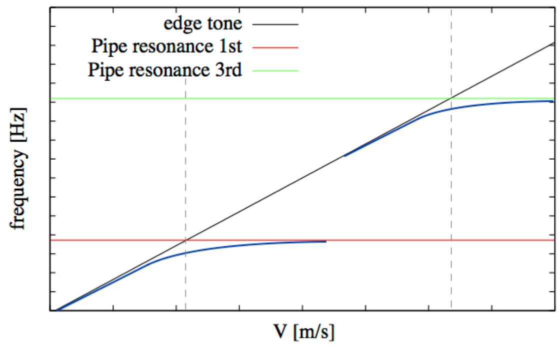

Figure 2. Relationship between jet velocity and oscillation frequency.

2.2 Sounding mechanism of air-jet instruments

Due to the interaction between the acoustic oscillation in the resonator and the jet motion, the characteristic frequencies of air-jet instruments do not obey Brown's equation (1)[1, 12]. As shown in Fig.2, with increasing the jet velocity, the frequency of sound oscillation first follows that of the edge tone. However, just before it reaches the first resonance frequency of the pipe, the frequency locking starts so that the frequency of sound converges to the first resonance frequency. Furthermore, a little before the edge tone frequency reaches the second resonance frequency, the frequency of an overtone appears and converges to the second resonance frequency. Finally, the second mode dominates the first mode in magnitude. For the ocarina with a Helmholtz resonator, there is no overtone or the resonance frequencies of the cavity, i.e., overtones are much higher than the Helmholtz resonance frequency. Then, the transition to an overtone substantially disappears.

2.3 Dimensions of the 3D model and the frequency of Helmholtz resonance

Figure 3 (a) shows the inner volume of the 3D model of Night Pla Ocarina soprano C (Otsuka Musical Instrument), whose lowest note is A5, and Figure 3 (b) shows its cross section, called Central cross section. The length of the Helmholtz resonator is 86mm and the area of the mouth opening is $6 \times 5\text{mm}^2$. The resonance

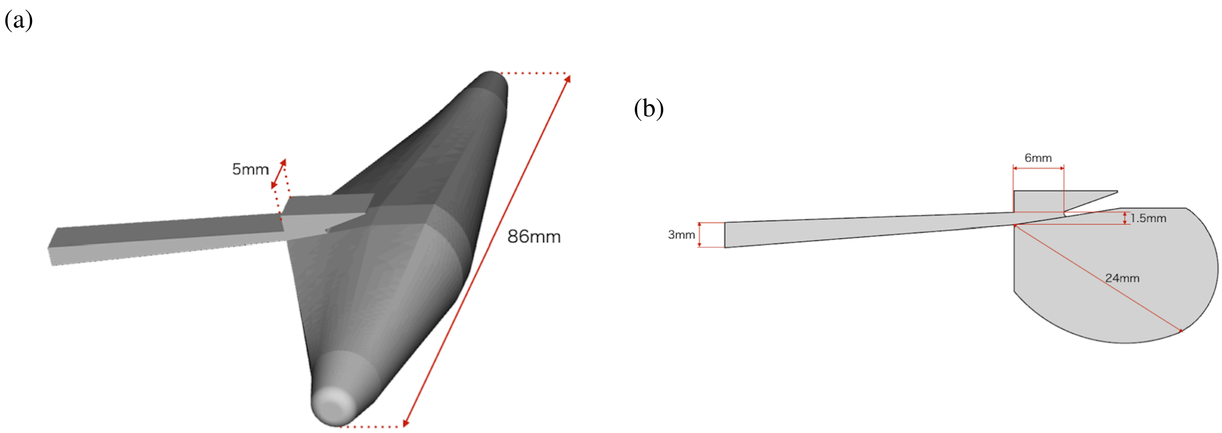

Figure 3. Inner volume of the 3D ocarina model. (a) Dimensions of the inner volume. (b) Cross section of the inner volume (Central cross section).

frequency is estimated by the theory of the Helmholtz resonance, which is caused by the elastic properties of air volume. The resonator frequency depends on the volume of the body and the geometry of the neck[1],

$$f_0 = \frac{c}{2\pi}\sqrt{\frac{S}{VL}}, \tag{2}$$

where L, S and V are the effective length of the neck, its cross-section and the volume of the cavity. Taking the end correction into account, the neck length is estimated as $L \simeq d + 2 \times 8\alpha/3\pi$, where α is the effective radius of the opening obtained from $S = \pi\alpha^2$. For our model, the parameters are given by $V = 9.425 \times 10^{-6}\text{m}^3$, $S = 3.0 \times 10^{-5}\text{m}^2$, $\alpha = 3.09 \times 10^{-3}\text{m}$, $d = 1.5^{-3}\text{m}$ and $c = 340\text{m/s}$. Then, the resonance frequency of the model is estimated as

$$f_0 = 1175\text{Hz}, \tag{3}$$

although this value is quite higher than the lowest note $A5$ (880Hz). We need to check the frequency of the model with numerical calculation.

3 OSCILLATION IN THE 3D OCARINA MODEL

3.1 Numerical method

In this paper, to reproduce fluid motion and acoustic oscillation, the compressible Large Eddy Simulation (LES) with the one-equation sub-grid-scale (SGS) model was used[5, 13, 14, 15]. Actually, we adopted RhoPimple-Foam, an unsteady solver of compressible laminar and turbulent flow in OpenFOAM Ver.5.0.

The numerical mesh of the ocarina model is shown in Figure 4 and the mesh parameters are shown in Table 1. A rectangular parallelepiped $500 \times 500 \times 400\text{mm}^3$, which works as an outside area, is put on the mouth opening. The geometry of the 3D model is constructed by using FreeCAD and is converted to a mesh by using SnappyHexMesh in OpenFOAM utility. The minimum mesh size around the mouth opening is 0.1mm and the number of the cell is nearly 160 million.

To calculate fluid motion for such a huge mesh model, parallel computing by using a supercomputer is necessary. Actually, we used ITO subsystem A of Kyushu University. To make the videos of spatial distributions of pressure and velocity, we pick up the data on the Central cross section (see Figure 3 (b)) by using Function Object of OpenFOAM. We also observe the fluid velocity and vorticity near the edge and detect the sound pressure at the right end tip of the resonator, where the acoustic field dominates and fluid field is negligibly small. Thus, the resonance frequency and amplitude of the sound oscillation are calculated from the data at the end tip.

The equilibrium pressure and temperature are set as $p = 100$ kPa and $T = 300$ K, respectively. To reproduce the oscillations of the ocarina, the sound wave and the fluid motion must be calculated simultaneously. The speed of sound $c \approx 340$ m/s is greater by a degree of magnitude than the fluid velocity, which is estimated as several tens m/s at the highest. To capture sound waves accurately, the time step is set at $\Delta t = 1.0 \times 10^{-7}$ s and the simulation is carried out up to $t = 0.02$s.

In Figure 4 (a) and (b), the arrow shows the inlet, whose the area of the cross-section is 3×5mm. The flow velocity at the inlet is gradually increased and reaches 10 m/s at $t = 0.0002$s. Since the ratio of the height of the inlet to that of the flue exit is 2, the average jet velocity at the flue exit becomes 20 m/s in the steady state. For the top wall and side walls of the rectangular volume over the instrument, i.e., the outside, the transparent boundary condition is adopted and other walls are solid walls.

Table 1. Numerical parameters of 3D ocarina model.

Caluculation time	Δt	p at rest	T at rest	Number of cells	Minimum mesh size
0.02 sec	1×10^{-7} sec	100 kPa	300 K	159680000	0.1[mm]

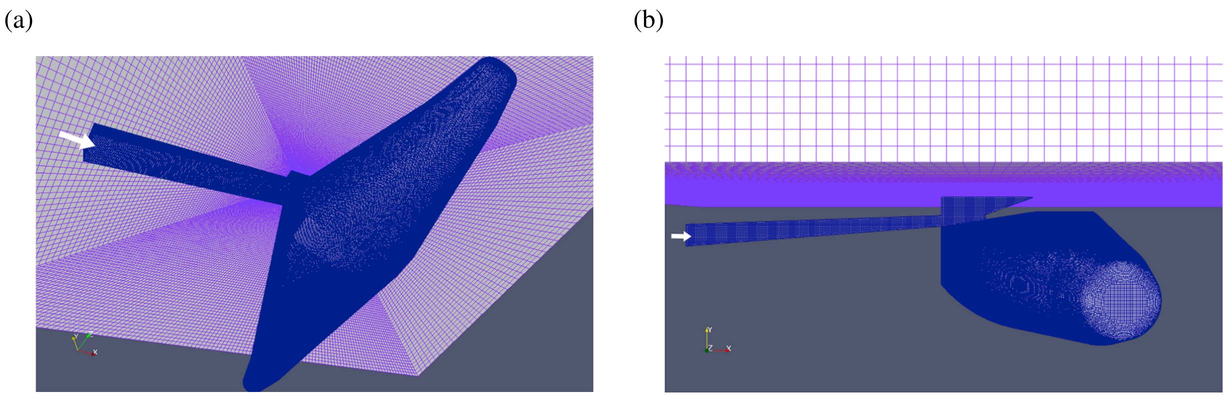

Figure 4. Numerical mesh of the ocarina model. The arrow indicates the inlet. (a) Bottom view. (b) Side view.

3.2 Spatial distributions of velocity and pressure

Figure 5 (a) and (b) show the spatial distributions of fluid velocity and the pressure on the Central cross-sectional at $t = 0.02$. As shown in Figure 5 (a), the jet oscillation is well sustained in the steady state. A part of the jet flow is injected into the resonator body and is spread over some area being broken into smaller scale vortices. Another part of the jet flow goes outside and is also broken into smaller scale vortices. As shown in Figure 5 (b), a nearly spherical pressure wave is emitted from the mouth opening. Therefore, our numerical simulation seems to well reproduce the jet motion and acoustic oscillation for the ocarina.

3.3 Frequency of pressure oscillation

Figure 6 (a) and (b) show the oscillation of pressure in the resonator, which is detected at the end tip of the resonator and the Fourier spectrum of the pressure oscillation, respectively. The amplitude of the pressure oscillation is nearly 300Pa and the waveform approaches a sinusoidal wave in time evolution. From the Fourier spectrum, the resonance peak exists at $f = 850 \pm 50$ Hz. Thus, the lowest note A5 (880Hz) is in its error range ($800 < f < 900$), although the theoretical estimation given by Eq.(3), 1175Hz, is much higher than it.

(a) (b)

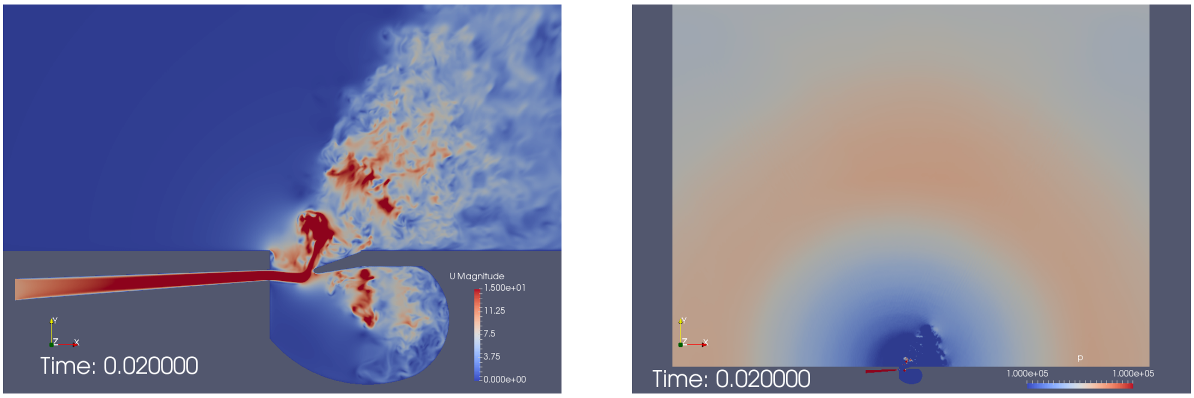

Figure 5. Spatial distributions of velocity and pressure at $t = 0.02$s on the Central cross section. (a) Velocity. (b) Pressure.

The overtone peaks are quite smaller than the main resonance peak, which is the characterisic of the Helmholtz resonator.

(a) (b)

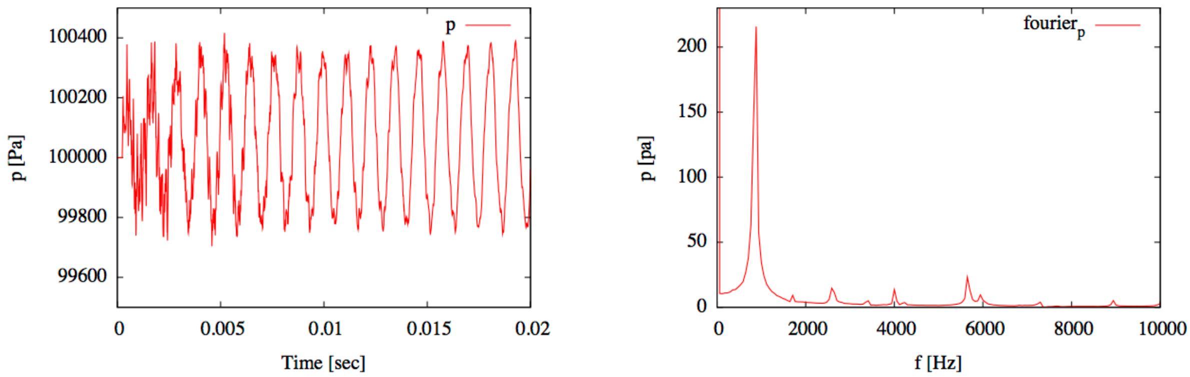

Figure 6. Pressure at the observation point. (a) Pressure oscillation. (b) Fourier decomposition.

4 CONCLUTION

We numerically studied the 3D model of the ocarina with compressible LES. The acoustic oscillation of the ocarina is well reproduced by the numerical simulation. The acoustic oscillation numerically reproduced well captures the properties of the Helmholtz resonance which are regarded as the characteristics of ocarinas. Namely, the peaks of the overtones are much smaller than the peak of the Helmholtz resonance. In this paper, we treated the 3D model with a large number of cells, nearly 160 million, and demonstrated that such a huge 3D model is well handled with parallel computing technique. In future work, we will check the change of the resonance frequency with the jet velocity. Furthermore, we are planning to create a 3D model with tone holes and to reproduce the change of the pitch depending on the change of fingering.

ACKNOWLEDGEMENTS

The present work was supported by Grant-in-Aid for Scientific Research (C) Nos. 16K05477 and 19K03655 from the Japan Society for the Promotion of Science (JSPS), "Joint Usage/Research Center for Interdisciplinary Large-Scale Information Infrastructures" and "High Performance Computing Infrastructure" in Japan (Project IDs: jh180007-MDH and jh190010-MDH), and Kawai foundation for sound technology & music.

REFERENCES

[1] N. H. Fletcher and T. D. Rossing, *The Physics of Musical Instruments*, 2nd Edition, (Springer-Verlag, New York 1998).

[2] A. Hirschberg, "Aero-acoustics of wind instruments"in *Mechanics of Musical Instruments*, Eds. A.Hirschberg, J.Kergomard and G.Weinreich. (Springer-Verlag, Vienna and New York 1995), pp.291-369.

[3] B. Fabre, J. Gilbert, A. Hirschberg and X. Pelorson, " Aeroacoustics of musical instruments " , Annu. Rev. Fluid Mech. **44** 1-25 (2011).

[4] H. Kühnelt, " Simulating the sound generation in utes and ue pipes with the lattice-bolzmann-method, " Proceeding of ISMA, pages 251-254 (2004).

[5] M. Miyamoto, Y. Ito, T. Iwasaki, T. Akamura, K. Takahashi, T. Takami, T. Kobayashi, A. Nishida, and M. Aoyagi, " Numerical study on acoustic oscillations of 2D and 3D flue organ pipe like instruments with compressible LES " , Acta Acustica united with Acustica, **99**, 154-171 (2013).

[6] N. Giordano, " Direct numerical simulation of a recorder " , J. Acoust. Soc. Am. **133** 1111-1118 (2013).

[7] N. Giordano, " Simulation studies of a recorder in three dimensions " , J. Acoust. Soc. Am. **135** 906-916 (2014).

[8] H. Yokoyama, A. Miki, H. Onitsuka and A. Iida, "Direct numerical simulation of fluid-acoustic interactions in a recorder with tone holes " , J. Acoust. Soc. Am. **138** 858-873 (2015).

[9] T. Kobayashi, T. Takami, K. Takahashi, R. Mibu, and M. Aoyagi, " Sound Generation by a Turbulent Flow in Musical Instruments - Multiphysics Simulation Approach –," in Procedings of HPCAsia07, 91-96 (2007).

[10] M. J. Lighthill, "On sound generated aerodynamically," Proc. R. Soc. London Ser. A 211, 564-587 (1952).

[11] G.B. Brown " The vortex motion causing edge tones " , Proc. Phys. Soc., London XLIX 493-507 (1937).

[12] J. W. Coltman, " Jet driven mechanisms in edge tones and organ pipes " , J. Acoust. Soc. Am. **60** 725-733 (1976).

[13] C. Wagner, T. Hüttl, and P. Sagaut, ed. " Large-Eddy Simulation for Acoustics, " (Cambridge, 2007).

[14] C. Seror, P. Sagaut, C. bailly, and D. Juvé, " On the radiated noise computed by large-eddy simulation, " Physics of Fluids, 13(2), 476-487, (2001).

[15] B. J. Boersma, "Large eddy simulatoin of the sound eld of a round turbulent jet," Theoret. Comput. Fluid Dynamics 19, 161-170 (2005).

PROCEEDINGS of ISMA 2019
International Symposium on Music Acoustics

13 - 17 September 2019 in Detmold, Germany

Measurement and modeling of a resonator guitar

Mark Rau(1)*, Julius O. Smith III(1)

(1)Center for Computer Research in Music and Acoustics, Stanford University, USA

Abstract

Resonator guitars are acoustic instruments which have one or more spun metal cones embedded in the top plate, with strings driving the cone directly through a bridge. They were originally designed to be louder than traditional acoustic guitars and are often played with a metal slide. The vibrational characteristics of resonator guitars having a single inverted-cone are studied as the basis for a synthesis model. The small-signal input admittance is obtained using an impact hammer and laser Doppler vibrometer. As well, sinusoidal sweeps are made using a modal shaker at various driving amplitude levels. The shaker measurements show that some of the modes exhibit nonlinear characteristics. These measurements are used to design body resonator filters with time-varying resonant modes for a digital waveguide model of the resonator guitar.

Keywords: Guitar, Measurement, Modeling

1 INTRODUCTION

During the early twentieth century, the playing levels of American bands were increasing due to the use of brass instruments and percussion. Conventional stringed instruments were not loud enough to compete, leading to the invention of “resophonic” or “resonator” instruments. Resonator instruments have similar construction to their traditional counterparts, with the addition of one or more spun metal cones replacing the majority of the top plates. With the introduction of electronically amplified musical instruments, the need for louder acoustic instruments was reduced, but by this time, resophonic instruments had already become part of the canon of American music such as blues and traditional music. While there are resophonic versions of many instruments such as banjos, mandolins, and ukuleles, by far the most popular variant is that of the guitar.

There are three main styles of resonator cone instruments: the single-cone “biscuit”, single inverted cone, and tricone designs [1]. The biscuit design uses a large cone having an approximately 24 cm diameter, mounted flush with the instrument’s top plate, with the bridge mounted at the peak of the cone. The inverted cone design uses a similar cone, but with it being inverted, and a small protrusion where the bridge is mounted. Tricone resonators use three smaller cones, typically of the biscuit style, with the bridge mounted to a metal structure connecting the peaks of each cone.

In addition to the different cone styles, there are two different neck setups commonly found on resonator guitars. Some resonator guitars have a standard round neck and can be played with a slide or with fingers to stop the notes. This style of guitar is played in the same manner as a standard guitar and is favored by blues musicians. The other category of resonator guitars have a thick square neck and are played on the musician’s lap. The strings are roughly 1 cm above the fretboard so it is only possible to play with a slide. Square neck resonator guitars are most often played by traditional and bluegrass musicians.

There is not much literature on resophonic instruments, with only brief mentions of them, but they have interesting properties which warrant further investigation [2]. In this study, a square neck inverted cone style resonator guitar is measured. Driving point admittance measurements are made using a hammer strike method to study the small signal response of the instrument. Resonator cones are made of very thin aluminum, typically less than 0.5 mm which is quite thin as compared to the standard top plate thickness of roughly 3 mm for traditional acoustic guitars. The cone of the guitar measured is 0.35 mm thick. Since the cones are thin, it is more likely that the instrument will exhibit nonlinear characteristics when played in normal conditions. To measure potential nonlinearities of the instrument, a modal shaker was used to drive the instrument with various amplitude sinusoidal sweeps.

*mrau@ccrma.stanford.edu

Mode fitting is performed on the small and large signal admittance measurements to be used as a body filter for a waveguide string synthesis model [3, 4, 5, 6, 7]. A modal architecture is used for this body filter so that the frequency, damping, and amplitude of each resonance can be adjusted during the synthesis. Some of the resonances observed with the shaker are shown to exhibit nonlinear weakening spring characteristics, resulting in a lowering of resonance frequency at high amplitude. These nonlinear resonances are approximated as time-varying linear modes using the modal architecture to vary the resonant frequency in relation to the amplitude of the bridge velocity at each mode. Synthesis examples are generated and compared to determine if this nonlinear behavior is audible and worth including in a model where a trade-off between accuracy and computational complexity has to be taken into account.

The outline is as follows. Section §2 describes the measurements of resonator guitar. Then in §3 we describe the modal analysis and how the parameters are obtained. The waveguide synthesis model is described in §4. The results are discussed in §5. Finally, in §6 concluding remarks are provided.

2 MEASUREMENTS

A square neck resonator guitar with a single inverted cone was measured as part of this study. Small signal driving point admittance measurements were made using a hammer strike method while large signal measurements were made with a modal shaker.

2.1 Measurement Setup

The guitar was suspended vertically by its tuning pegs and the bottom end pin was supported lightly with foam to insure the instrument remained mostly stationary. The strings were tuned to a common tuning of GBDGBD having frequencies 98.00, 123.47, 146.82, 196.00, 246.94, and 293.66 Hz. While the body resonances were being measured, all strings were damped using foam. A replacement bridge was manufactured for the instrument, as not to harm the original bridge when the shaker was attached. This bridge caused the low strings to be slightly offset from their normal position. The bridge was used for all measurements, including when the shaker was not used. The measurement setup is shown in Fig. 1.

2.2 Small Signal Measurements

Small signal bridge admittance measurements were taken by striking the bridge perpendicular to the instrument string's lengthwise direction. The miniature force hammer (PCB 086E80) was suspended as a swinging pendulum and dropped remotely. A Polytec PDV-100 laser Doppler vibrometer (LDV) was used to measure the resulting vibrations. The laser was focused as close as possible to the striking location of the hammer to measure the driving point velocity. The measured driving point force and velocity are used to compute the admittance in the frequency domain as $\Gamma(\omega) = V(\omega)/F(\omega)$, where V and F are the velocity and force, and ω is the frequency. Bridge admittance measurements were taken with the force hammer and vibrometer in the direction perpendicular to the top plate of the guitar. Measurements were also taken in the direction parallel to the top of the guitar and normal to the string, and with the hammer striking along this direction and the vibrometer measuring perpendicular to the top plate. These additional measurements allow for a two dimensional model which includes both directions of transverse string vibration to be constructed with coupling between the directions, but for simplicity, only a one dimensional string model was constructed at this time.

2.3 Large Signal Measurements

In order to check if the resonator guitar's modes exhibit nonlinear behavior, the instrument was driven with a signal having greater force. A modal shaker (Modal Shop 2004E) was used to drive the instrument. A force sensor (PCB 208C01) was used to measure the force imparted by the shaker. The LDV was again used to measure the resulting velocity of the instrument's vibrations. Epoxy was used to glue the shaker tip to the bridge of the guitar, ensuring that the shaker would stay attached as the instrument was driven. Twenty-second long

Figure 1. Measurement Setup showing the LDV, force hammer, and shaker. Note, the shaker's force sensor is not shown.

linear sinusoidal sweeps ranging from 50-2000 Hz were played through the shaker at thirteen different amplitude levels. Sine sweep measurements were made increasing from 50-2000 Hz, and decreasing from 2000-50 Hz to check if the resonant behavior included hysteresis.

3 MODAL ANALYSIS

The bridge admittance measurements are used to form efficient digital filters to be used in a waveguide synthesis model. Modal fitting is performed on the admittance measurements to form a parallel bank of second-order filters which simulate the instrument's vibrational characteristics.

3.1 Mode Fitting

Mode fitting was performed on the hammer and sweep bridge admittance measurements to gain insight into the resonant frequencies, damping, and amplitudes. Modes were fit assuming the system has damped harmonic oscillator behavior with an impulse response of the form,

$$h(t) = \sum_{m=1}^{M} \gamma_m e^{2\pi f_m t(i-\zeta_m)}, \tag{1}$$

where γ_m, f_m, and ζ_m are the amplitude, natural frequency, and damping ratios of modes $m = 1,2,...,M$ [8, 9]. The mode fitting was done using a method derived by Jonathan Abel which involves analysis of the eigenstructure of a Hankel matrix of admittance impulse response samples [10]. The M largest singular values of this decomposition can be viewed as the singular values associated with the signal space as opposed to the noise space, and thus M was used as the model order. This mode fitting architecture does not guarantee positive-real modes which are needed to ensure the stability of the filters. However, the measurements were of high enough quality that when properly processed, the fitting yielded positive-real modes. The complex amplitudes were ob-

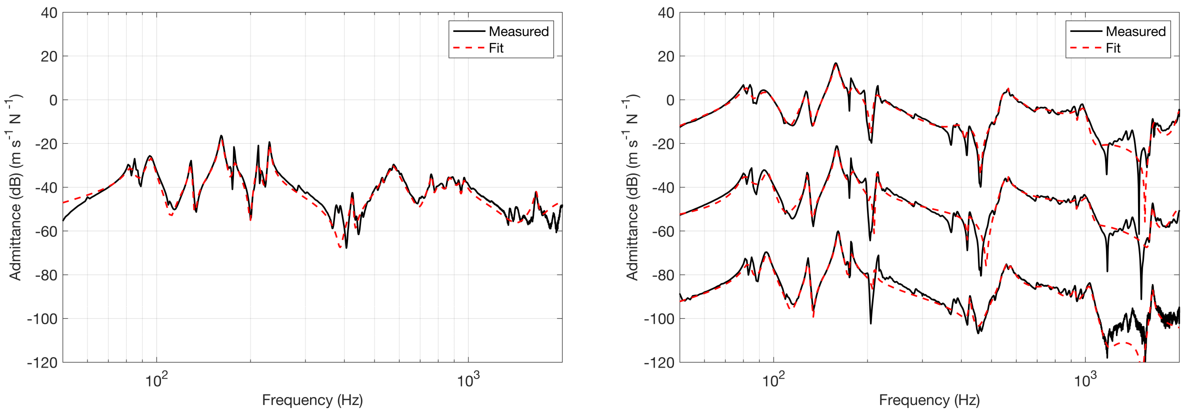

(a) Hammer Taps

(b) Shaker Sweeps

Figure 2. Figure 2a shows the measured and fit admittance from the hammer taps with M = 24 modes. Figure 2b Shows the measured and fit admittance from the shaker sweeps having RMS velocity of 0.000041, 0.0032, and 0.0102 m s^{-1} with M = 14, 16, and 18 modes respectively. The shaker sweeps are offset by -40, 0, and 40 dB for clarity.

tained using least squares to minimize the error between the measured admittance and a basis of the fit modes. Figure 2a shows the measured and fit admittance as measured with the hammer tap method.

3.2 Nonlinear Resonances

Figure 2b shows the measured and fit admittance as measured with the shaker sweep method at three different levels. The sweeps were made at different amplitudes, and since the waveguide model will be constructed to model transverse velocity and force waves, the sweep levels are characterized here by the root mean square (RMS) velocity of the measured velocity during the sweep.

Figure 3 shows a zoomed in version of the low frequency portion of the admittance measured using the shaker for 13 different amplitude levels of the upward frequency trajectory sweeps. Note that for some of the modes, the resonant frequency shifts to a lower frequency at higher amplitudes. This phenomenon is known as a weakening spring if the modes are approximated as a nonlinear spring system such as a Duffing oscillator [11, 12]. The downward frequency trajectory sweeps show similar behavior, and no hysteresis is observed, so only the upward trajectory sweeps are shown.

4 DIGITAL WAVEGUIDE MODEL

To simulate the resonator guitar, we use the digital waveguide architecture where samples stored in delaylines represent the transverse velocity waves of the simulated strings. The left and right travelling velocity waves are represented by $v^+(n)$ and $v^-(n)$, and the force waves are represented by $f^+(n)$ and $f^-(n)$ for each string. The transverse velocity and force at the bridge junction are $v(n) = v^+(n) + v^-(n)$ and $f(n) = f^+(n) + f^-(n)$. To calculate the reflected velocity waves at the bridge, the reflection scattering junction,

$$S_b(z) = \frac{R_B(z) - R_s}{R_B(z) + R_s}, \tag{2}$$

can be calculated from the string characteristic impedance, R_s, and the bridge impedance $R_B(z) = 1/\Gamma(z)$. The string impedance is calculated as, $R_s = \sqrt{T\varepsilon}$, where the tension, T, and the linear mass density, ε, of the string are calculated from manufacturer provided data [13]. The reflection scattering junction is implemented as a

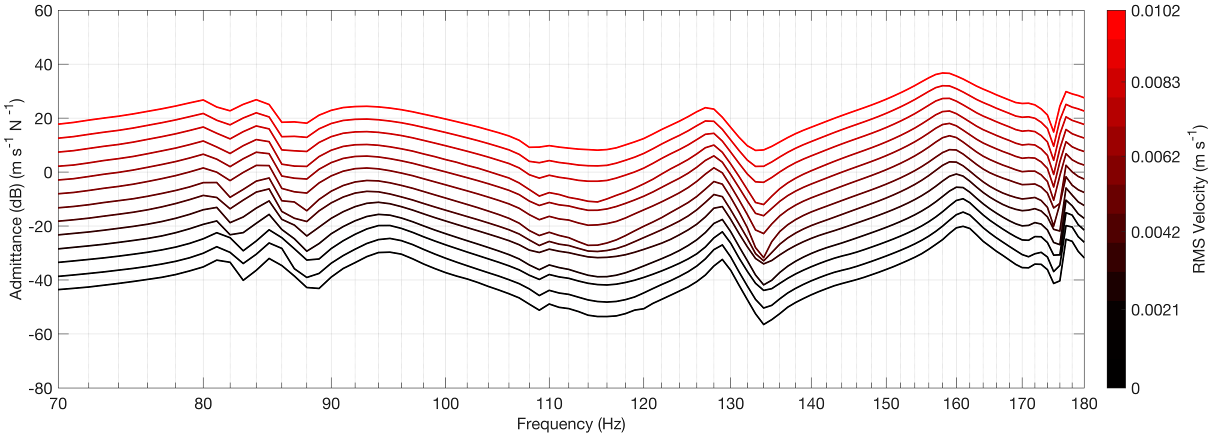

Figure 3. Admittance from the upward frequency trajectory shaker sweep measurements at 13 different levels. The 12 highest levels are offset in increments of 5 dB for clarity.

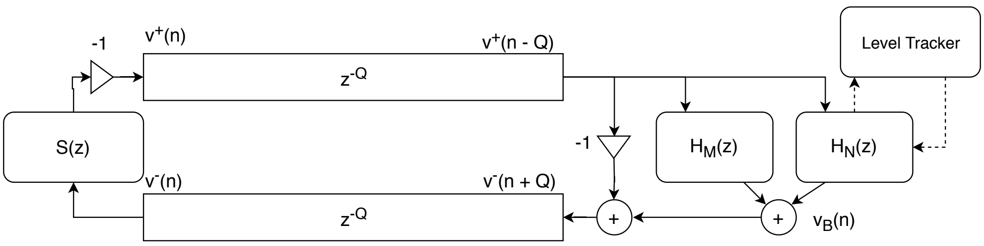

Figure 4. Block diagram of the waveguide synthesis architecture.

parallel bank of second order filters as in [7], and used to calculate the reflected transverse velocity samples at the bridge.

For simplicity, and since the resonance nonlinearity is the focus of this paper, only a 1D string with no string to string coupling is implemented. The neck termination is treated as a simple lossless reflection. The string losses are modeled in a simplified way using a 2nd order FIR lowpass filter, shown as $S(z)$. Two delay lines are used, one for $v^+(n)$ and one for $v^-(n)$. They are each of length $Q = \frac{f_s}{2f_0}$, where f_s is the sample rate and f_0 is the fundamental frequency of the string being simulated. At this time, the instrument radiation is not simulated, and the output is taken as the bridge velocity $v_B(n)$.

A block diagram of the waveguide synthesis is shown in Fig. 4, and the details of the bridge termination filter will be explained in the following two subsections.

4.1 Bridge Termination Filter Architecture

The bridge reflectance filter is constructed as a parallel bank of second order filters which can include linear and nonlinear resonances. The shaker admittance measurements were not as reliable as the hammer taps, so the hammer tap measurement modes are used as the basis for the reflectance filter bank. However, 5 distinct nonlinear resonances were found using the shaker sweep measurements, they are at 83.2, 95.7, 128.8, 161.1, and 177.5 Hz. These are likely not the only nonlinear resonances, but they were found with more confidence than other modes, so only this set will be modeled as nonlinear resonances while the rest are modeled as linear modes. This leaves $M = 19$ linear modes and $P = 5$ nonlinear resonances.

The filter banks are constructed in terms of their center frequency, damping ratio, and complex amplitude to give the two parallel filter banks as:

$$H_m(z) = \gamma_m \frac{1 - z^{-2}}{1 + a_{m,1}z^{-1} + a_{m,2}z^{-2}}, \tag{3}$$

$$H_p(z) = \gamma_p \frac{1 - z^{-2}}{1 + a_{p,1}z^{-1} + a_{p,2}z^{-2}}, \tag{4}$$

where $a_{m,1} = -2r_m \cos(2\pi f_m/f_s)$, and $a_{m,2} = r_m^2$, with $r_m = \exp(-2\pi f_m \zeta_m/f_s)$ being the pole radius, and f_s the sampling rate. The variables indexed with m represent the linear modes with $M = 19$ being used, and the variables indexed with p represent the nonlinear resonances with $P = 5$.

The nonlinear resonances are modeled as time-varying linear modes. As a first approximation, only the center frequency of the modes will be varied. The center frequencies and peak velocity of each of the nonlinear resonances were calculated at each RMS velocity level. To parameterize the nonlinear resonance frequency as a function of the instantaneous velocity, v_p, linear fits were made of the form, $f_p(v_p) = c_m \times v_p + f_m$, where f_p is the calculated nonlinear resonance center frequency, c_m is the slope of the fit, and f_m is the center frequency calculated from the hammer tap measurement. During the shaker measurements, the instrument was mass loaded by the force sensor, decreasing the center frequencies, so the center frequencies from the hammer measurements are used as the base frequencies for the nonlinear resonances. The parameters of the linear fitting are shown in Table 1.

Table 1. Center frequency and slope of the linear fitting to calculate the amplitude dependant nonlinear resonance center frequencies.

Center Frequency, f_m (Hz)	83.2	95.7	128.8	161.2	177.5
Frequency Slope, c_m (m^{-1})	-8.3	-12.6	-21.4	-16.7	-0.6

4.2 Level Tracking

To vary the center frequencies of the nonlinear resonances, an estimate of each mode's component of the bridge velocity, $v_n(n)$ was needed. The level detection is done on the output of each nonlinear resonance's associated filter using a leaky integrator based peak detector. This is implemented using the update equation,

$$\begin{aligned}
&\text{if } |v_p(n)| > \lambda: \\
&\qquad \lambda = \lambda + (1 - e^{\frac{-1}{\tau_a f_s}})(|v_p(n)| - \lambda) \\
&\text{else:} \\
&\qquad \lambda = \lambda + (1 - e^{\frac{-1}{\tau_r f_s}})(|v_p(n)| - \lambda),
\end{aligned} \tag{5}$$

where λ is the level estimate, $v_p(n)$ is the bridge velocity at each mode, τ_a is the time constant when the level detection is increasing, and τ_r is the time constant when it is decreasing. The attack and release time constants were chosen as $\tau_a = 0.1$ ms, and $\tau_1 = 100$ ms, so that transients are detected quickly but the level does not drop directly after the transients [14].

5 RESULTS AND DISCUSSION

String pluck approximations were generated by initializing the delaylines with a triangular string displacement which was used to calculate the transverse velocity at each sample of the delayline. Example plucks are generated using only linear modes and using the hybrid linear-nonlinear model. Audio examples can be found

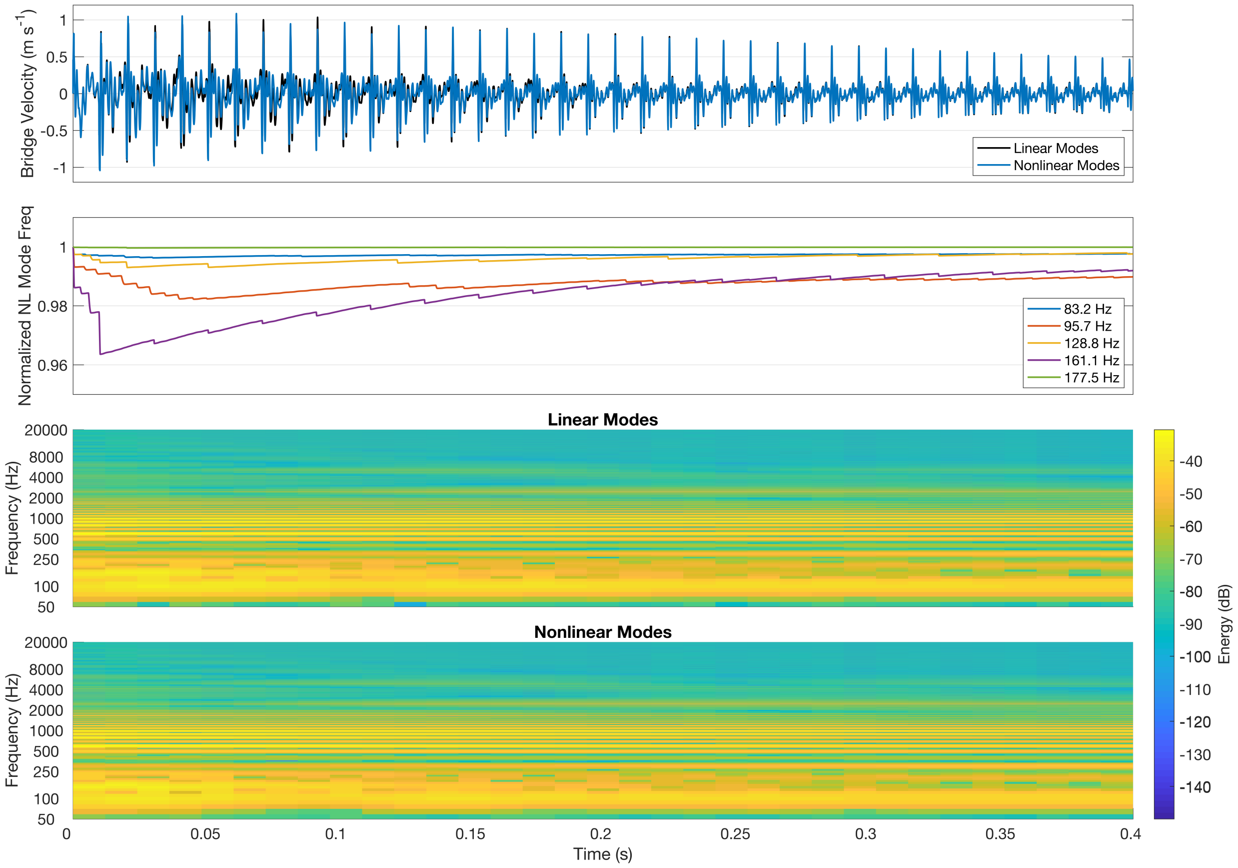

Figure 5. Bridge velocity and normalized frequencies of the nonlinear resonances during a one pluck of the low G string at 98 Hz. Spectrograms are shown, one with only linear modes, and one which included the nonlinear resonances.

online[1]. Figure 5 shows a linear and a nonlinear pluck as well as the normalized frequencies of the nonlinear resonances during the nonlinear pluck. It is clear that the waveforms are quite similar but deviate, especially when the bridge velocity is high.

Informal listening suggests that the linear and and nonlinear models are quite similar, but do have a slight timbre difference, especially during the attack of the plucks. However, this evaluation is informal and a formal listening test would be required to give more conclusive results of the timbre differences.

6 CONCLUSIONS

Measurements of a resonator guitar were made with small and large signal excitations as a basis for modal analysis. The small signal hammer excitation provided high quality measurements to perform modal fitting, while the large signal shaker measurements revealed that some of the instrument's resonances behave nonlinearly. These linear and nonlinear resonance parameters were used to create a digital waveguide model of the resonator guitar.

[1] https://ccrma.stanford.edu/~mrau/ISMA2019/

This study provides preliminary results which suggest that modeling the weakly nonlinear resonances of resonating instruments may be important to properly model the timbre, especially during transients. However, this study is not complete and there is plenty of room for future work. First, the model constructed is only one dimensional and does not include string-string coupling. Expanding on this model would likely aid in the accuracy. As well, the signals used to synthesize the pluck are not physical, as a higher energy pluck will not be an exactly scaled version of a low energy pluck. The model uses the bridge velocity as the output signal, but a more accurate model would include radiation modeling [7].

The nonlinear resonances were approximated as time-varying linear modes, but this assumption should be checked to see how well it perceptually compares to a more complicated model. A more complicated model may also include varying the damping ratios and complex amplitudes of each resonance.

In addition to improvement to the waveguide model, more measurements could be made to improve the modal fitting. More shaker sweeps could be made at other amplitude levels and on different days to confirm the results. As well, other similar instruments could be measured and modeled to see how this approach translates to similar or dissimilar instrument modeling.

REFERENCES

[1] Peter T. Veru, *The National-Dobro Guitar Company: How the resonator guitar survived the age of electric amplification*, The George Washington University, 2009.

[2] Thomas D. Rossing and Andrew Morrison, *The science of string instruments*, Springer, 2010.

[3] Julius O. Smith III, "Efficient synthesis of stringed musical instruments," in *Proc. of the International Computer Music Conference*, 1993, pp. 64–71.

[4] Matti Karjalainen, Vesa Välimäki, and Tero Tolonen, "Plucked-string models: From the Karplus-Strong algorithm to digital waveguides and beyond," *Computer Music Journal*, vol. 22, no. 3, pp. 17–32, 1998.

[5] Julius. O. Smith III, *Physical Audio Signal Processing*, W3K Publishing, 2004, online book: http://-ccrma.stanford.edu/~jos/pasp/.

[6] Esteban Maestre, Gary. P. Scavone, and Julius. O. Smith III, "Digital modeling of bridge driving-point admittances from measurements on violin-family instruments," in *Proc. of the Stockholm Music Acoustics Conference*, 2013, pp. 101–108.

[7] Esteban. Maestre, Gary. P. Scavone, and Julius. O. Smith III, "Digital modeling of string instrument bridge reflectance and body radiativity for sound synthesis by digital waveguides," in *Proc. of the IEEE Workshop on Applications of Signal Processing to Audio and Acoustics*. IEEE, 2015.

[8] Anders Brandt, *Noise and Vibration Analysis: Signal Analysis and Experimental Procedures*, John Wiley & Sons, 2011.

[9] Agilent Technologies, "Fundamentals of modal testing," 2000.

[10] Jonathan S. Abel, "Direct modal filter design," *Personal Communication*, November 2018.

[11] Lev Landau and Evgenii Lifshitz, *Course of theoretical physics: Mechanics*, vol. 1, Elsevier, 2013.

[12] Marco Amabili, *Nonlinear vibrations and stability of shells and plates*, Cambridge University Press, 2008.

[13] D'Addario, "Catalog Supplement/String Tension Specifications: A complete technical reference for fretted instrument string tensions," 2019.

[14] Udo Zölzer, *DAFX: Digital Audio Effects, 2nd Edition*, John Wiley & Sons Ltd, Hamburg, Germany, 2011.

PROCEEDINGS of ISMA 2019
International Symposium on Music Acoustics

13 - 17 September 2019 in Detmold, Germany

Modelling of Gabonese harps *

Antoine Caillon(1), Jean-Loïc Le Carrou(1), Baptiste Chomette(1), Sylvie Le Bomin(2)

(1)Sorbonne Université, CNRS, Institut Jean Le Rond d'Alembert

(2)Muséum National d'Histoire Naturel, CNRS, éco-anthropologie et ethnobiologie

Abstract

Traditional instruments handed down from generation to generation, Gabonese harps have various shapes, often anthropomorphic, that depending on the population and the region concerned. Nevertheless, harps are all composed of eight strings, each wrapped up on one side to a tuning peg fixed on the neck and at the other side linked to a wooden tailpiece. It is often nailed to both ends of the resonance box, under the soundboard made of animal skin. In order to study the evolution of these instruments within the framework of a multidisciplinary project, an acoustic modelling of the instrument is undertaken. The main objective of this modelling is to understand and highlight maker's elements that predominate in their sound. For this purpose, the Udwadia-Kalaba formulation is used to model vibrating systems coupled together by mechanical constraints. In particular, this formulation can take into account geometrical non-linearities of strings induced by their high-amplitude excitation. Model parameters were first extracted from an instrument at our disposal. Then, time-domain simulations were confronted to experimental data. Finally, a parametric study showed that the low string tension and modal behaviour of the tailpiece are of great importance in the characteristic sound of the instrument.

Keywords: Physical Modelling, Gabonese harps, Udwadia-Kalaba formulation

*jean-loic.le_carrou@sorbonne-universite.fr

PROCEEDINGS of ISMA 2019
International Symposium on Music Acoustics
13 - 17 September 2019 in Detmold, Germany

Exploring dependency between instrument design and musician's control

Patricio de la Cuadra[1], Augustin Ernoult[2] and Benoit Fabre[3]

(1) Pontificia Universidad Catolica de Chile
(2) Aix Marseille Univ, CNRS, Centrale Marseille, LMA, UMR 7031, Marseille
(3) LAM Sorbonne Universite France
pcuadra@uc.cl

Abstract

In flute-like instruments the pitch of the notes produced depend on the instrument geometry as well as on the control the musician exerts on it. Thus, a particular flute design requires from the musician a specific strategy to obtain a set of notes “in tune” with a certain cultural intonation agreement. The control parameters available in most flutes include the jet speed and the opening of one end of the flute, normally adjusted by the proximity from the lips to the labium. In this paper we explore the relationship between the design of the instrument and the control exerted by the musician, proposing algorithms to automatically design the bore geometry and position and size of the tone holes for different musicians control strategies.

PROCEEDINGS of ISMA 2019
International Symposium on Music Acoustics

13 - 17 September 2019 in Detmold, Germany

A real-time physical model to simulate player control in woodwind instruments

Vasileios Chatziioannou(1)*, Alex Hofmann(1), Sebastian Schmutzhard(2)

(1)Department of Music Acoustics, University of Music and Performing Arts Vienna, Austria

(2)Acoustics Research Institute, Austrian Academy of Sciences, Vienna, Austria

Abstract

The interaction between woodwind players and their instruments is a key aspect of expressive music performance. Therefore, recent studies have focused on understanding how the actions of the players affect sound generation. Based on experimental results obtained using both human performers and an artificial blowing machine, this paper presents a numerical model that, taking the players' actions into account, may synthesise expressive woodwind instrument sounds. Implemented in C++ the model allows real-time performance on a standard desktop computer, thus enabling the user to modify the model parameters in a live performance scenario. Apart from varying parameters related to the embouchure of the player and the effective length of the resonator (i.e. mimicking modifications that could take place in real playing) this model also allows virtual modifications that would not be possible to realize in the physical world, such as a cone gradually morphing into a cylinder and vice versa. Besides parameters related to the excitation mechanism and the geometry of the instrument, the user is able to modify the properties of the air inside the instrument and the magnitude of the viscothermal losses.

Keywords: Physical Modelling, Woodwinds, Sound Synthesis

1 INTRODUCTION

Using physical modelling techniques, it is possible to numerically reproduce sounds of musical instruments that are directly related to the physical phenomena that take place [1, 10]. Advances in numerical analysis and computer science allow the formulation of efficient physical modelling algorithms that are even suitable for real-time performance. In order for the produced sound to be perceived as realistic by the listener, it is of paramount importance to consider the way the oscillations of the instrument are excited. This player-instrument interaction has attracted a lot of attention in the last decade [2, 11]. Several studies have been conducted in order to analyse the performance of experienced players and understand how this affects the sound generation. Focusing on single-reed woodwind instruments, this work presents a model that attempts to capture the interaction between the player and the instrument that takes place at the excitation mechanism. The formulation of the model is presented in the next section. Section 3 gives some details on the implementation and efficiency of the algorithm, section 4 presents some results obtained with the proposed model and section 5 discusses the findings of this work.

2 PHYSICAL MODELLING OF SINGLE-REED WOODWIND INSTRUMENTS

Wave propagation in an axisymmetric tube of length L and cross-sectional area $S(x)$, x indicating the position along the length of the tube, can be modelled using the following equations for the acoustic pressure p and the particle velocity v

$$\frac{\partial p(x,t)}{\partial x} + \rho \frac{\partial v(x,t)}{\partial t} + z_v * v(x,t) = 0 \tag{1a}$$

$$\frac{\partial \big(S(x)v(x,t)\big)}{\partial x} + \frac{S(x)}{\rho c}\frac{\partial p(x,t)}{\partial t} + S(x)y_\theta * p(x,t) = 0, \tag{1b}$$

*chatziioannou@mdw.ac.at

where $*$ denotes convolution with respect to time, ρ is the air density, c the speed of sound and z_v and y_θ are respectively related to the viscous and thermal losses within the tube (see [9] for more details). The boundary condition at the open end of the tube may be given as

$$p(t,L) = S(L) z_r * v(t,L), \tag{2}$$

z_r being a time-domain radiation impedance. At the excitation end, where the player-instrument interaction takes place, the above wave-propagation model needs to be coupled with a model of the reed oscillation, which takes into account the actions of the player. This is achieved by introducing an additional nonlinear term in the equation of motion of the reed, which, in previous studies, involved only two nonlinear components, namely the Bernoulli flow through the reed channel, and the collision of the reed with the mouthpiece lay [6]. This additional term describes the interaction of the player's tongue with the vibrating reed. Thus the equation of motion of the reed takes the following form

$$m\frac{\mathrm{d}^2 y}{\mathrm{d}t^2} + m\gamma\frac{\mathrm{d}y}{\mathrm{d}t} + ky - k_{\mathrm{tg}}\lfloor y_{\mathrm{tg}} - y\rfloor^{\alpha_{\mathrm{tg}}}\left(1 + r_{\mathrm{tg}}\frac{\mathrm{d}(y_{\mathrm{tg}} - y)}{\mathrm{d}t}\right) + k_{\mathrm{lay}}\lfloor y - y_{\mathrm{lay}}\rfloor^{\alpha_{\mathrm{lay}}}\left(1 + r_{\mathrm{lay}}\frac{\mathrm{d}y}{\mathrm{d}t}\right) = S_{\mathrm{r}} p_{\Delta}, \tag{3}$$

where y is the displacement of the reed from its equilibrium position, γ is the reed damping, α_{tg} and α_{lay} are collision exponents, r_{tg} and r_{lay} contact damping, y_{tg} is the tongue displacement, S_{r} the effective reed surface and p_Δ the pressure difference across the reed. $\lfloor y\rfloor^{\alpha} = \theta(y)y^{\alpha}$, where $\theta(y)$ denotes the Heaviside step function. Casting this in a Hamiltonian formulation and discretising using the finite-difference method, one may arrive at the solution of a nonlinear equation

$$F_{\mathrm{NL}}(y) = 0 \tag{4}$$

at each time step, whence the reed displacement and subsequently pressure and flow at the mouthpiece may be calculated (see [5] for full details). A key feature of this approach is that numerical stability is ensured via the conservation of the system energy. Figure 1 (left) shows the simulation of a clarinet staccato note, along with the error in the conservation of energy, which is of the order of machine precision. The virtual tongue has been used in order to release the reed (start the note) and stop the reed (end the note), in an attempt to replicate signals generated by professional clarinet players ([8]). Figure 1 (right) shows a similar plot for portato articulation; in that case the tongue is used to separate the two notes. The ability of the model to resynthesise sounds produced by an actual instrument has been validated using measurements with real players [4] and an artificial blowing machine [5].

3 IMPLEMENTATION

The numerical model was implemented in C++ within the *Csound Plugin Opcode Framework* [7]. This provides the physical model as an opcode to the sound synthesis environment of Csound. In order to experiment with varying model parameters, a simple graphical user interface has been designed using FLTK Widgets[1], including an oscilloscope that visualises the mouthpiece pressure (see Figure 2). The model runs faster than real time on a standard desktop computer (Intel® Xeon(R) CPU E5-1650; 16Gb RAM). Nevertheless, computational efficiency should still be considered, in case several such models need to run in parallel.

The main drawback in order to assess the efficiency of the model is the need to use an iterative solver for the resulting nonlinear equation (4). In the presented case, this is solved using the Newton-Raphson method. This method has the ability to converge very fast given a starting point close to the root of the nonlinear function F_{NL}. Indeed, even though a maximum number of 8 Newton iterations has been specified in the code, this number is never reached for any case of wind instrument simulation. The slow varying motion of the reed, in comparison to the sampling rate that is used (44100 Hz) ensures that by using the solution at the previous time step as starting point, the nonlinear solver converges to machine precision $\varepsilon \approx 10^{-16}$ usually after 2 iterations.

[1] https://www.fltk.org/doc-2.0/html/index.html

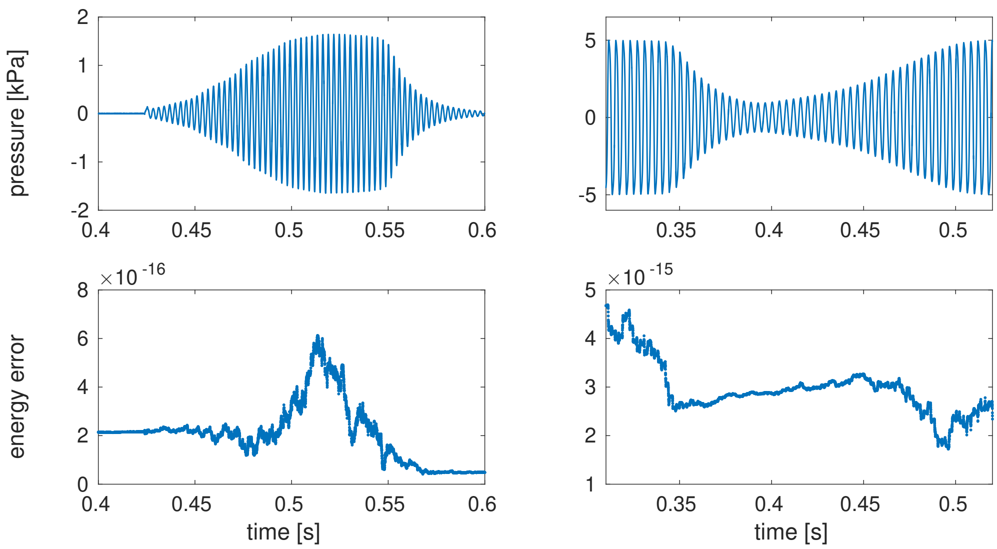

Figure 1. Simulated mouthpiece pressure during staccato (left) and portato (right) articulation. Model parameters are taken from [5]. The bottom plots show the error in the conservation of energy.

However, the fact that an unknown number of iterations is, in principle, required for convergence, introduces an uncertainty to such nonlinear solvers. For specific cases it is possible to pre-calculate the maximum number of iterations required to find the root of a nonlinear function [3]. Alternatively, there are different strategies to ensure computational efficiency. For instance, using a linear approximation of F_{NL} allows a direct solution subject to some loss of accuracy. A simple way to arrive at such an approximation is to perform only one Newton iteration per time step. This effectively acts as a local linearisation of F_{NL}. Given the slow-varying state of the system, in comparison to a high sampling rate, the accuracy loss is kept low. Such a strategy is particularly suited when oversampling is required (e.g. due to numerical dispersion or for perceptual considerations). Performing only one Newton iteration per time step, i.e. using a direct solution for the nonlinear equation, in the case of the examples shown in Figure 1, results to an energy error of 10^{-8} for staccato and 10^{-6} for portato articulation. Since a collision nonlinearity is modelled, which poses a rather strongly nonlinear element, this shows the feasibility of such an approach to increase computational efficiency. Using a higher sampling rate may reduce the approximation error when only one iteration is used, as summarised in Table 1. In practice, a compromise between computational efficiency and numerical accuracy can be made, e.g. enforce two Newton iterations per time step with a sampling rate of 44100 Hz.

Table 1. Order of magnitude of the error in the conservation of energy for different configurations of the number of Newton iterations per time step (Niter) and the chosen sampling rate (fs).

	portato		staccato	
	Niter < 8	Niter = 1	Niter < 8	Niter = 1
fs = 44100 Hz	10^{-15}	10^{-6}	10^{-16}	10^{-8}
fs = 200000 Hz	10^{-15}	10^{-8}	10^{-16}	10^{-10}

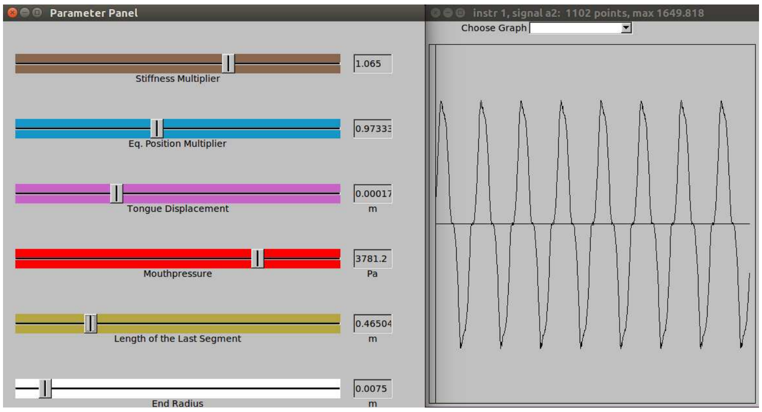

Figure 2. A graphical user interface to tune model parameters during the simulation. On the right a real-time plot of the mouthpiece pressure is generated.

4 NUMERICAL RESULTS

The presented model may be used to generate diverse woodwind sounds, while modulating the physical model parameters. One interesting case, that may be only virtually realised, is to gradually morph the shape of an instrument from a cylinder to a cone. The radiated sound of such a numerical experiment is visualised in Figure 3, in the form of a spectrogram. Besides the bore geometry, all other physical model parameters are kept constant. For the first two seconds of the simulation the bore has a cylindrical shape (with radius $r_{\text{in}} = r_{\text{out}} = 0.0075$ m) and in the next ten seconds the output radius linearly increases up to $r_{\text{out}} = 0.015$ m, while the input radius remains constant.

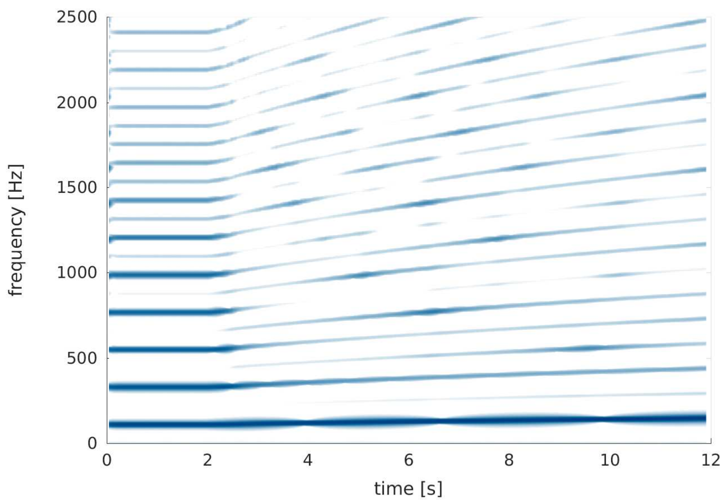

Figure 3. Spectrogram of the radiated sound of a single-reed woodwind instrument, the bore of which gradually morphs from a cylinder into a cone.

It can be observed that the odd harmonics are not present at the beginning of the tone, when the bore is cylindrical. They gradually appear when the instrument takes a conical shape. During that time all harmonics increase with increasing cone angle.

5 CONCLUSIONS

This work presents the formulation of a physical model, that may simulate embouchure control in single-reed woodwind instruments and is suitable for real-time performance. Numerical stability is ensured using an energy-based method. Implemented in C++, the model allows various approaches to control the model parameters during performance. The fact that all parameters have a direct physical interpretation allows an intuitive control over the system, whereas the virtual nature of the instrument gives infinite possibilities in terms of shaping the instrument geometry and varying model parameters related to the sound excitation mechanism.

ACKNOWLEDGEMENTS

This research is supported by the Austrian Science Fund (FWF): P28655-N32.

REFERENCES

[1] S. Bilbao. *Numerical Sound Synthesis*. Wiley & Sons, Chichester, UK, 2009.

[2] V. Chatziioannou and A. Hofmann. Physics-based analysis of articulatory player actions in single-reed woodwind instruments. *Acta Acustica united with Acustica*, 101(2):292–299, 2015.

[3] V. Chatziioannou, S. Schmutzhard, and S. Bilbao. On iterative solutions for numerical collision models. In *Proc. International Conference on Digital Audio Effects (DAFx-17)*, pages 72–79, Edinburgh, 2017.

[4] V. Chatziioannou, S. Schmutzhard, A. Hofmann, and M. Pàmies-Vilà. Inverse modelling of clarinet performance. In *Proc. 26th International Congress on Sound and Vibration (ICSV26)*, Montreal, 2019.

[5] V. Chatziioannou, S. Schmutzhard, M. Pàmies-Vilà, and A. Hofmann. Investigating clarinet articulation using a physical model and an artificial blowing machine. *Acta Acustica united with Acustica*, 2019.

[6] B. Fabre, J. Gilbert, and A. Hirschberg. Modeling of wind instruments. In R. Bader, editor, *Springer Handbook of Systematic Musicology*, pages 121–139. Berlin, Heidelberg, 2018.

[7] V. Lazzarini. The csound plugin opcode framework. In *Proc. 14th Sound and Music Computing Conference*, pages 267–274, 2017.

[8] M. Pàmies-Vilà, A. Hofmann, and V. Chatziioannou. Analysis of tonguing and blowing actions during clarinet performance. *Frontiers in Psychology*, 9:617, 2018.

[9] S. Schmutzhard, V. Chatziioannou, and A. Hofmann. Parameter optimisation of a viscothermal time-domain model for wind instruments. In *Proc. International Symposium on Musical Acoustics (ISMA17)*, pages 27–30, Montreal, 2017.

[10] V. Välimäki, J. Pakarinen, C. Erkut, and M. Karjalainen. Discrete-time modelling of musical instruments. *Reports on progress in physics*, 69(1):1–78, 2006.

[11] J. Wolfe, N. Fletcher, and J. Smith. The interactions between wind instruments and their players. *Acta Acustica united with Acustica*, 101(2):211–223, 2015.

PROCEEDINGS of ISMA 2019
International Symposium on Music Acoustics

13 - 17 September 2019 in Detmold, Germany

[The virtual workshop OpenWInD: Towards an optimal design tool of wind instruments for makers]

Guillaume CASTERA[(1)], Juliette CHABASSIER[(1)], Augustin ERNOULT[(1)], Alexis THIBAULT[(1)], Robin TOURNEMENNE[(1)]

[(1)]Inria team Magique 3D, 200 avenue de la vieille tour, 33400 Talence, France.

Abstract

Our project develops an optimisation software (OpenWind) for wind instrument making. The approach is based on a strong interaction with makers and musicians, aiming at computing quantities and defining interesting criteria that should be optimized, from their point of view. Entry impedance is a well studied acoustical quantity that characterizes the linear response of the pipe. However, makers and musicians mostly rely on sounds produced in a musical framework in order to assess an instrument. These sounds can be modeled as a coupling between the pipe (resonator) and an embouchure (oscillator, as a reed for instance). We will present energy based time domain models and simulations where a reed embouchure is coupled with a linear pipe. State-of-the-art numerical techniques are used for the pipe discretization (finite elements for one-dimension Telegrapher's equations). Realistic radiation impedances are formulated in the time domain and an energy based model is derived along with a stable numerical scheme. Pipe junctions are also accounted for, by the means of extended Kirchhoff conditions that are shown to exhibit an inappropriate energy behavior in the time domain. A reed is coupled with the instrument and an energy-based time discretization is derived. Explicit and efficient algorithms are derived for the computation of the scheme's unknowns. Sounds can be heard while the pressure and flow inside the instrument can be observed during the note evolution.

Keywords: wind instruments, time discretization, finite element method, reed mechanism, radiation impedance

PROCEEDINGS of ISMA 2019
International Symposium on Music Acoustics

13 - 17 September 2019 in Detmold, Germany

Numerical analysis and comparison of brass instruments by continuation *†

Vincent Fréour(1), Hideyuki Masuda(1), Satoshi Usa(1), Eiji Tominaga(1), Yutaka Tohgi (1), Bruno Cochelin(2), Christophe Vergez(2)

(1)YAMAHA Corporation, R&D division, Hamamatsu, Japan
(2)Aix Marseille Univ., CNRS, Centrale Marseille, LMA UMR7031, Marseille, France

Abstract

Brass instrument design has long been relying on empirical know-how, build up over the years by the craftsmen. Some relationships between the air-column geometry, the intonation and some attributes of sound color have been formalized through this process by the makers. However, many properties of the instrument, related to timbre, dynamic range, playability, etc. are still very difficult to correlate to the design. Alongside these issues and important questions for the craftsmen, the knowledge in the acoustics of musical instruments has extensively improved in the last decades, benefiting especially from cutting edge engineering methods for the analysis of dynamic systems. In this presentation, we will detail some applications of stability analysis and continuation (Asymptotic Numerical Method), to physical models of trumpets. This approach aims to clarify differences between instruments on the basis of calculated performance descriptors. On a longer term, our goal is to include these technologies in the development of new instruments, by providing some virtual performance analyzers for the design of brass instruments.

Keywords: brass instruments, physical modelling, continuation

*first.last@music.yamaha.com
†last@lma.cnrs-mrs.fr

ISMA2019/17
Numerical synthesis applied to reed instruments: influence of the control parameter transients on the steady-state oscillation regime

Tom Colinot[a], Philippe Guillemain[b], Jean-Baptiste Doc[c] and Christophe Vergez[b]
[a]LMA Marseille
[b]LMA
[c]LMSSC, CNAM
colinot@lma.cnrs-mrs.fr

Physical models of self-oscillating musical instruments include strongly nonlinear elements and delayed terms, leading to a great variety of produced sounds. For example, the same fingering on a wind instrument can produce oscillating regimes at several different fundamental frequencies as well as quasi-periodic regimes. The emergence of these regimes is conditioned mostly by the value of control parameters, representing the action of the musician, such as blowing pressure or lip force on the reed. As a strongly non-linear delayed system, a wind instrument model may converge to different stable regimes depending on the initial conditions and the transient of the control parameters. For the second point, an example would be the speed with which the blowing pressure reaches its final value. In this work, we show that depending on the way the blowing pressure increases to its final value, the steady regime may be oscillating or non oscillating, or correspond to the first or second register. Such considerations are useful when trying to predict the playability of an instrument using numerical simulations.

Number of words in abstract: 172
Technical area: Music acoustics

Special session: Virtual Prototyping of Musical Instruments
Presentation: Oral presentation preferred

Registration: 339190036 - Colinot Tom - 0 0 not paid

PROCEEDINGS of ISMA 2019
International Symposium on Music Acoustics

13 - 17 September 2019 in Detmold, Germany

Simulation of the nonlinear characteristic of the clarinet exciter and of the side holes *†

Pierre-André TAILLARD(1), Jean-Pierre DALMONT(2)

(1)FHNW, Schola Cantorum Basiliensis, Leonhardsstrasse 6, 4051 Basel, Switzerland

(2)Laboratoire d'Acoustique de l'Université du Maine (UMR CNRS 6613), 72085 Le Mans, France

Abstract

At the last ISMA, a method for measuring the nonlinear characteristic and the static mechanical behaviour of the clarinet exciter (reed + mouthpiece + lip of the player) was presented. Here, we show how this measured behaviour can be integrated in a real time simulation using a waveguide clarinet model, including nonlinear losses at the toneholes. The clear separation of the aeraulic (nonlinear characteristic) and mechanical (static bending of the reed against the mouthpiece lay, like a stiffening spring) aspects allows a straightforward, piecewise simulation of the dynamic behaviour, apparently without any numerical stability problem. Taking nonlinear losses in the toneholes into account has proved crucial for a credible simulation of the instrument, especially in the second regime. The model allows to realistically predict the playing frequency, the ease of playing and the timbre of the instrument. An example is given for the simulation of the effect of the two main objective factors characterizing clarinet reeds: stiffness and opening at rest (without lip pressure). The proposed improvements allow a virtual prototyping of the clarinet exciter and resonator.

Keywords: Wind instruments, clarinet, reed characterization, sound synthesis by physical model, waveguides

1 INTRODUCTION

Interested readers will find an extended description of the methods used in Chapters 4, 5 and 7 as well as in Appendices A and B of [1].

ACKNOWLEDGEMENTS

We thank the engineering school HE-Arc (Neuchâtel, Switzerland) for the facilities granted.

REFERENCES

[1] Taillard, P.-A. Theoretical and experimental study of the role of the reed in clarinet playing. PhD thesis, University of Le Mans, France, 2018.

*taillard@hispeed.ch
†Jean-Pierre.Dalmont@univ-lemans.fr

PROCEEDINGS of ISMA 2019
International Symposium on Music Acoustics

13 - 17 September 2019 in Detmold, Germany

Finite element simulation of radiation impedances with applications for musical instrument design

Péter RUCZ[(1)], Judit ANGSTER[(2)], András MIKLÓS[(2)]

[(1)]Budapest University of Technology and Economics, Hungary, rucz@hit.bme.hu
[(2)]Fraunhofer Institute for Building Physics, Germany

Abstract

Creating a musical instrument often involves designing acoustical resonators. The natural frequency and the quality factor of the resonator are affected by the radiation impedance to a significant extent. Therefore attaining as much a priori knowledge as possible on the radiation characteristics is desirable. On the other hand, for the sake of efficiency, radiation characteristics are most often reduced to a sole frequency dependent radiation impedance function. A finite element approach for the calculation of self and mutual radiation impedances was introduced recently [Rucz, JASA 143(4) 2449–2459], which is suitable for these purposes.

In this contribution, the methodology is applied and extended with different applications in musical instrument design. In particular, the radiation from the mouth regions of organ pipes and recorders are examined. The geometrical parameters having the most significant effect on the radiation characteristics are analyzed and the results are compared to previously published data. As another example, finite element simulations of Helmholtz resonators of a mallet percussion instrument are introduced. In this case, the length correction effect of the sound bars partially covering the opening of the resonators is studied. Finally, the effect of viscous losses on the quality of the natural resonance is investigated.

Keywords: Radiation impedance, finite element method, resonator design

1 INTRODUCTION

Designing the resonator of a musical instrument can involve various challenges, one of them being the characterization of the acoustical radiation from the openings into the exterior sound field. The coupling between the interior and exterior acoustical fields affects the natural frequency and the quality factor of the resonator and also the radiation directivity of the instrument. Therefore the accurate prediction of the radiation characteristics of resonators is desirable for the efficient design of musical instruments. However, the acoustical radiation problem can only be solved analytically in case of very simple geometries, and numerical approximations must be used to handle more complex geometrical arrangements.

Numerical simulations can provide a wealth of information and they allow for handling almost arbitrarily complex geometries. On the other hand, they are computationally involving, which renders their usefulness strictly limited in applications such as real time sound synthesis or parameter optimization. Thus, for the sake of computational efficiency, it is useful to reduce the radiation characteristics into a sole frequency dependent radiation impedance function by post-processing the results of 3D field simulations.

In this paper the finite element method is utilized together with a post-processing technique relying on plane wave decomposition in order to attain the frequency dependent radiation impedance in various geometrical configurations. The extracted radiation impedance function can then be used in a simplified waveguide or concentrated parameter model of the resonator. Such "hybrid" models preserve the accurate representation of the geometry and hence the radiation characteristics, while they enable rapid calculations.

In this contribution two different applications are studied. After introducing the methodology briefly, the mouth impedance of recorders and organ pipes are examined with different geometrical parameters. Then, the design of Helmholtz resonators for a mallet percussion instrument is investigated with taking the effect of the sound bars on the radiation properties into account. Finally, the paper is concluded by a short summary.

2 METHODOLOGY

Simulation of radiation impedances involving complex geometries is performed in this paper based on the finite element method (FEM) following the approach proposed by Rucz [1]. As radiation problems are examined here, infinite computational domains need to be emulated in the FEM. For this purpose the infinite element approach is utilized, i.e., a truncated domain is meshed using standard finite elements and the infinite elements are attached to the truncated boundary. By means of discretization, the Helmholtz equation is transformed into a matrix equation of the form

$$\left(\mathbf{K} + \mathrm{j}\omega\mathbf{C} - \omega^2\mathbf{M}\right)\mathbf{p} = -\mathrm{j}\omega\mathbf{A}\mathbf{v}, \tag{1}$$

where the matrices $\mathbf{K}$, $\mathbf{C}$, and $\mathbf{M}$ are the stiffness, damping, and mass matrices, respectively, $\mathbf{A}$ is the boundary mass matrix, and the vectors $\mathbf{p}$ and $\mathbf{v}$ contain the weights of the pressure and normal particle velocity. The angular frequency is ω and the imaginary unit is denoted by j. With the proper boundary conditions, the solution of (1) is unique and the sound pressure field in the whole domain is represented by the weights $\mathbf{p}$ and the corresponding shape functions.

To be able to utilize the results of the finite element simulation in a simplified waveguide or concentrated parameter model, it is necessary to post-process the simulated field and express "lumped" parameters. In particular, the frequency dependent radiation impedance is of primary interest in case of resonator design. In the following, radiation from a straight tube with an irregular opening (such as a tone hole, or the mouth of a flue instrument) is considered. Far from the opening and under the cut-on frequency of transverse modes of the duct the pressure field is essentially one-dimensional and can be written as the d'Alembert solution

$$p(z) = p^{+}\mathrm{e}^{-\mathrm{j}kz} + p^{-}\mathrm{e}^{+\mathrm{j}kz}. \tag{2}$$

where p^{+} and p^{-} are complex amplitudes, z denotes the distance from the opening along the duct, and $k = \omega/c$ is the wave number with c representing the speed of sound.

The complex amplitudes p^{+} and p^{-} in (2) are found by fitting the two exponential functions to the simulated sound pressure field. This is done by choosing a number of virtual microphone locations along the axis of the tube and solving an overdetermined set of equations. Finally, the frequency dependent reflection coefficient R, and the radiation impedance Z are obtained using the relation

$$\frac{p^{-}}{p^{+}} = R = -|R|\,\mathrm{e}^{-2\mathrm{j}k\Delta L} = \frac{Z - Z_0}{Z + Z_0}, \tag{3}$$

with Z_0 denoting the plane wave impedance. The third expression of (3) contains the frequency dependent length correction (or end correction) ΔL that is the primary quantity examined in this paper. The length correction is directly related to the change of natural frequencies resulting from the opening.

In [1] it was shown that the theory can be extended to treat multiple coupled ducts and Salmon horns as well. Furthermore, it was also found that the resulting error of fitting the decomposition (2) to the pressure field serves as a good indicator of the reliablility of the evaluated impedance. In this paper only the straight duct formulation is used for simulating radiation impedances of different geometries.

3 WINDOW IMPEDANCES OF FLUE INSTRUMENTS

Flue instruments produce sound by means of an oscillating air jet forming at the mouth opening of the resonator. The mouth of a recorder or an organ pipe is a rectangular or nearly rectangular opening on the pipe. The radiation impedance of this opening has a great effect on the natural frequencies of the resonator and hence its accurate prediction is important for a proper resonator design. However, the geometry of the mouth opening is fairly complex, making the estimation of the radiation impedance a non-trivial task.

The window impedance and length correction of flue instruments have already been studied in a number of contributions. Without aiming at completeness a few of these examinations are summarized here briefly. The

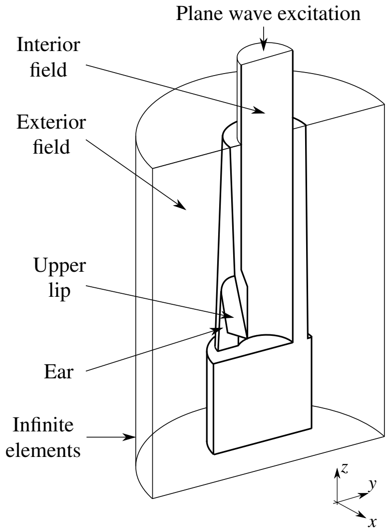

(a) Simulation arrangement

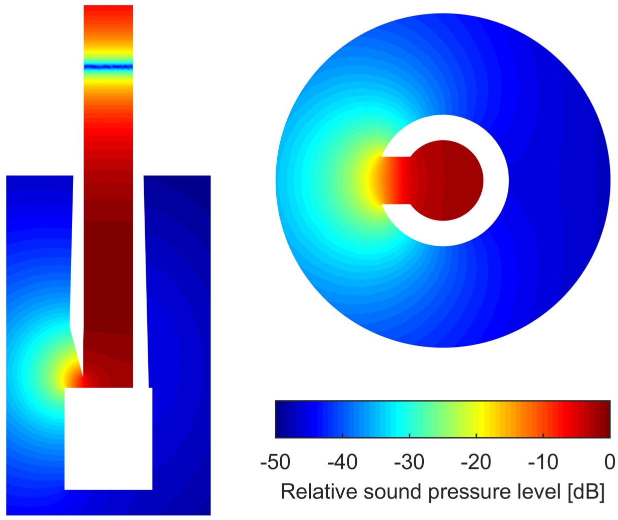

(b) Radiation from the mouth of the alto recorder at $f = 1\,\mathrm{kHz}$

Figure 1. Finite element simulation of the sound radiation from the mouth of a recorder

mouth correction of organ pipes was studied by Ingerslev & Frobenius [2] and an approximate model for the correction was proposed. The window length of different recorders was examined and compared to a theoretical model taking the effect of ears into account by Lyons [3]. Based on somewhat different considerations, the window impedance of a recorder-like instrument was also investigated by Verge *et al.* [4]. In the latter study the length correction of the mouth was assumed to consist of three parts representing the effect of the constriction, the ears, and the radiation into free field, respectively. The model of Verge *et al.* was recently extended by Ernoult & Fabre [5] who simulated the window impedance of recorders using the FEM with simplified geometries. Their model is able to take the effect of the edge angle and ears into account. In this paper geometrically more realistic finite element models are considered and the simulated window length corrections of recorders and organ pipes with different geometries are compared to that of previous studies.

Figure 1(a) shows the arrangement of the finite element simulation, illustrating the geometry of the longitudinal section of the head of a recorder. The main bore is driven by plane wave excitation and radiates into the exterior field through the mouth opening. The upper lip has a sharp edge of angle α at its bottom and it is surrounded by the ears on both sides. The wind channel and the upstream section of the flute head are replaced by a solid cylinder. A cylindrical region of the exterior area is also meshed by finite elements and the infinite elements emulating free field radiation conditions are attached to the outer surface of this cylinder. Similar arrangements were created for simulating the mouth regions of a rectangular and a circular flue organ pipe. The latter pipe does not have ears and the thickness of its walls is much smaller than that of other models. All meshes were generated using the parametric finite element mesh generation tool Gmsh [6]. Figure 1(b) displays the simulated pressure field along the longitudinal section of the bore and the cross section of the mouth of the alto recorder at $f = 1\,\mathrm{kHz}$. The standing waves due to reflections from the mouth are clearly visible inside the bore. The near-field directivity of the opening is also observable both in the horizontal and vertical planes.

Various configurations were simulated using the FEM and the proposed post-processing technique. Figure 2 summarizes the results of the investigation. In Figure 2(a) the window length corrections of different recorders are compared to each other. The dimensions of the recorders were chosen as given in [5]. The frequency dependence of the length correction is not examined in [5], but the low frequency values of the simulated corrections are in good agreement with those of the aforementioned paper. The alto recorder examined by

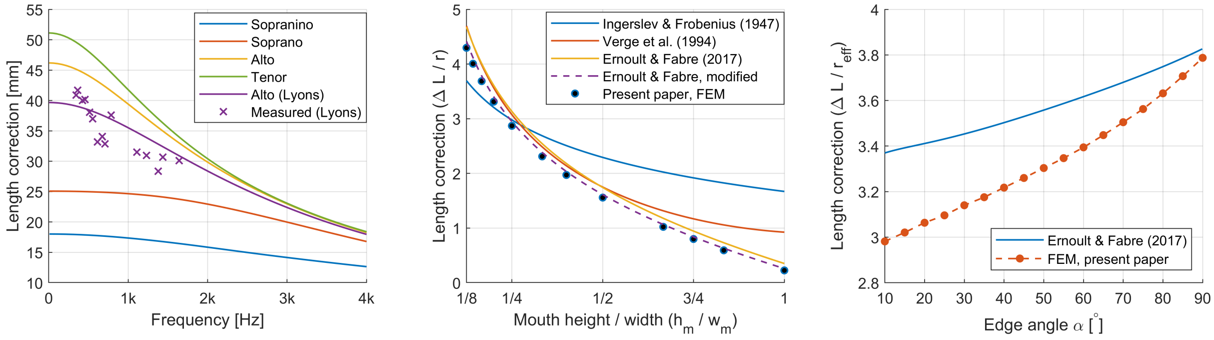

(a) Window corrections of recorders (b) Effect of mouth shape (c) Effect of edge angle

Figure 2. Simulation results of the length corrections of recorders and organ pipes compared to various models

Lyons [3] has a bit different dimensions. The length corrections evaluated from the played frequencies in [3] are also marked on the diagram showing and a fairly good correspondence with the simulation results. It is also observed that the frequency dependence of the correction is significant in the musical range of the instrument.

The low frequency length corrections of a cylindrical thin-walled flue organ pipe with different mouth geometries are shown in Figure 2(b). The simulations were run with changing the height of the mouth opening h_m while keeping the width of the mouth constant as $w_\mathrm{m} = \pi r/2$, with r denoting the inner radius of the pipe. The finite element results are compared to predictions of different models. Ingerslev & Frobenius [2] substitute the mouth opening with an equivalent ellipse having the same area and height to width ratio as the pipe mouth. This approximation shows a good agreement with the simulation results in the region where $h_\mathrm{m}/w_\mathrm{m} \approx 1/4$, a ratio often applied in organ building practice. Farther away from this ratio the deviations between the prediction and simulation become large. The model of Verge *et al.* [4] that estimates the correction as the sum effect of a constriction and radiation into free space gives a good fit to the simulation results if $h_\mathrm{m}/w_\mathrm{m} < 1$. An even better estimation is obtained by the model of Ernoult & Fabre [5] that is based on a function fitted to finite element simulation results. The best agreement is attained if their radiation correction $l_r = 0.695 r_\mathrm{m}$, with $r_\mathrm{m} = \sqrt{h_\mathrm{m} w_\mathrm{m}/\pi}$ denoting the effective radius of the mouth, is replaced by the theoretical value of an unflanged pipe $l_r = 0.613 r_\mathrm{m}$. The re-calculated corrections are shown as “Ernoult & Fabre, modified” in the diagram. The deviations between this model and the simulations are $< 3\%$ in all cases. This modification seems rational, as the thickness of the walls surrounding the mouth is much smaller than that of the recorder models of [5].

In the third study, the effect of the angle of the edge on the low frequency length correction is investigated in case of a rectangular wooden pipe. The pipe has a square cross section with 80 mm width and depth and the height of the mouth is chosen as $h_\mathrm{m} = 20\,\mathrm{mm}$. The walls forming the ears at the side of the pipe mouth have a thickness of 15 mm. The angle of the edge is varied between $10^\circ \leq \alpha \leq 90^\circ$ in 5° steps in the simulations. To our knowledge, the effect of the edge angle is only taken into account in the model of Ernoult & Fabre [5], thus the simulation results are compared to this model in Figure 2(c). Only the low frequency correction is plotted, normalized by the effective radius of the pipe r_eff. While a good agreement is found at large angles $\alpha \approx 90^\circ$ a deviation of $\approx 10\%$ is observed for small angles $\alpha \approx 10^\circ$. The discrepancies may stem from the somewhat different geometrical arrangements used in the two studies or the data fit formula applied in [5].

4 RESONATOR DESIGN OF A MALLET PERCUSSION INSTRUMENT

In this section the design of an Orff instrument is examined. The mallet percussion instrument at hand has thirteen sound bars made of rosewood and arranged in the diatonic scale from C4 (262 Hz) to A5 (880 Hz). The first few longitudinal bending modes of the sound bars are tuned by cutting the typical arch profile into

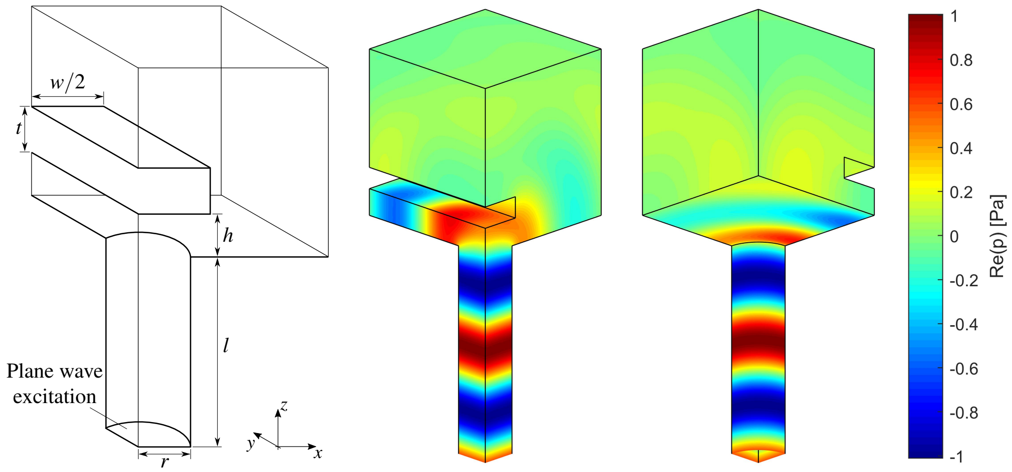

(a) Arrangement and main parameters

(b) Finite element simulation result at $kr = 1.72$

Figure 3. Finite element simulation of the effect of a sound bar partially covering a cylindrical tube

the bar. The sound radiated by the bars is amplified by Helmholtz resonators which are in the focus of the present study. When the resonators are designed, the effect of the sound bars partially covering the opening of the resonator needs to taken into consideration. In case of marimbas with quarter-wavelength tube resonators a practical guideline is to tune the natural frequency of the resonator about 3% sharp [7]. The detuning effect of sound bars is examined in the sequel. First, the effect of a single sound bar is considered, and the length correction due to the sound bar is predicted with varying the geometrical parameters of the arrangement. Then, an assembled instrument is investigated and the measured, simulated, and predicted natural frequencies of the resonators are evaluated and compared to each other.

4.1 The length correction effect of a sound bar

First, a single sound bar partially covering the circular opening of a resonator is studied by the FEM using a model geometry. Figure 3(a) shows the arrangement of the simulation. The cylindrical tube is driven by a plane wave with unit amplitude. The tube radiates into an open half-space, shown by the box-shaped region in the figure. As the length of the sound bars is much greater than the radius of the opening of the resonators, the bar is assumed to be infinitely long along the y axis. The problem has two symmetry planes ($x = 0$ and $y = 0$ in our case), thus, only a quarter of the whole geometry is meshed. On the symmetry surfaces zero normal velocity boundary condition is applied. Infinite elements are attached to the free surfaces of the box-shaped region.

The main parameters that are varied are the width and the thickness of the bar w and t, respectively, and the distance h between the open end of the tube and the sound bar. These lengths are non-dimensionalized by the radius of the tube r. Simulations were performed under the cut-on frequency of the first transverse mode of the tube, i.e. $kr < 1.84$, and the radiation impedance and the length correction were extracted. A typical simulation result showing the asymmetric radiation pattern is displayed in Figure 3(b).

The freqeuncy dependent length correction coefficients $\Delta L/r$ are displayed in Figure 4. The length correction of an open tube in an infinite baffle without sound bar is plotted in each diagram with a dashed line as a reference. The thickness of the bar is found to have only a minor effect on the radiation impedance; and in the diagrams the case $t = 0.6r$ is shown. In the left diagram the effect of the width of bar is visible with $h = r$ kept constant. As seen, the presence of the bar increases the length correction at low freqeuncies in all cases and the effect becomes larger with increasing the width of the bar. Interestingly, until $w < 2r$ the length correction decreases monotonically with the frequency, while for $w > 2r$ the correction increases in the low frequency range and

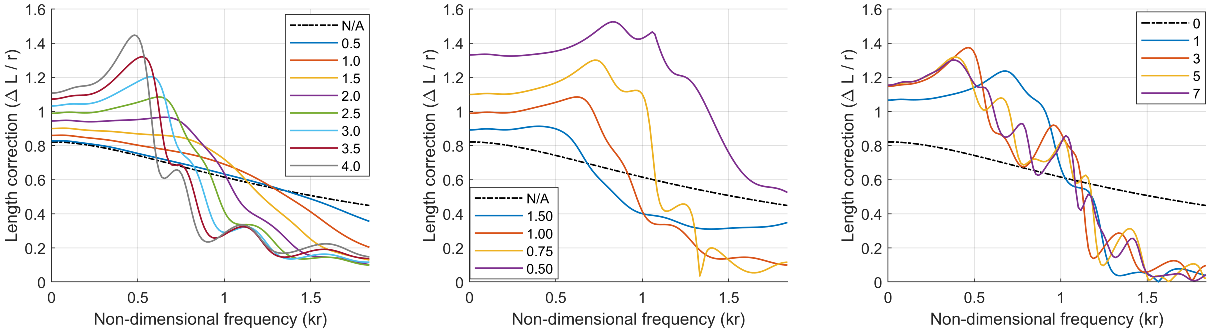

(a) Different widths w/r (b) Different distances h/r (c) Different number of bars n

Figure 4. Length correction effect of sound bars partially covering the open end of a cylindrical tube in different geometrical arrangements. The dash-dotted line shows the reference setup without sound bars.

decays quickly after reaching its maximum. The center digram shows the effect of changing the distance h of the bar from the opening of the tube while keeping the width constant as $w = 2.5r$. As observed, the length correction is very sensitive to the distance, and increases with decreasing the distance h. In case of $h = 0.5r$ the low frequency correction effect is more than 60% greater than that without the bar.

Figure 4(c) shows the length correction effect taking a number of adjacent bars also into account. As the arrangement is symmetric (see Figure 3(a)) the number of sound bars is odd. The diagram shows the case with the parameters chosen as $h/r = 0.8$ and $w/r = 2.5$. The width of the gap between the bars is set as $g/r = 0.56$ which corresponds to the geometry studied in the next section. As seen, the effect of the adjacent bars on the length correction is significant. Adding the neighboring bars increases ΔL in the low frequency range by $\approx 8\%$, while the effect of adding further sound bars is negligible. At higher frequencies the length correction oscillates due to multiple reflections inside the gaps between the bars and the infinite baffle and the bars.

4.2 Examination of assembled resonators

The resonators of the assembled instrument were studied next, using measurements, finite element models, and predictions based on the length correction study presented in the previous section. The natural frequencies of the resonators are determined with and without sound bars and the detuning effect of the bars is quantified and compared with the results of the predictive model. Both in the measurements and simulations the resonators were driven using an external excitation signal. The excitation was provided by a loudspeaker in the measurements and modeled as an ideal point source in the simulations. The sound pressure response at one point inside the resonator was recorded and a transfer function was calculated by dividing the spectrum with that of the reference signal recorded close to the loudspeaker. The natural frequency is found as the maximum location of the transfer function and the quality factor is estimated using the 3 dB-width of the curve.

The natural resonance frequency f_{hr} of a Helmholtz resonator is expressed as

$$f_{\mathrm{hr}} = \frac{c}{2\pi}\sqrt{\frac{S}{V L_{\mathrm{eff}}}} \qquad \text{with} \qquad L_{\mathrm{eff}} = L + \Delta L_{\mathrm{in}} + \Delta L_{\mathrm{out}}, \tag{4}$$

where S is the area of the opening, V is the volume of the cavity, and L_{eff} is the effective length of the neck resulting as the sum of its physical length L, and the inner and outer corrections ΔL_{in} and ΔL_{out}. When no sound bars are present, radiation into a half-space can be assumed with the corrections $\Delta L_{\mathrm{out}} = \Delta L_{\mathrm{in}} = 0.82r$. In case of the examined experimental instrument the physical length of the neck is very small, $L = 3$ mm while the radius of the openings is $r = 12.5$ mm, and hence the effective length is dominated by the length corrections. Thus, the

		Without sound bars					With sound bars					Detuning			
		Meas	FE		Lossy FE		Meas	FE		Lossy FE		Meas	FE	Predicted	
Note	Volume [cm^3]	f [Hz]	f [Hz]	Q [–]	f [Hz]	Q [–]	f [Hz]	f [Hz]	Q [–]	f [Hz]	Q [–]	Δf [%]	Δf [%]	Δf [%]	$\Delta L/r$ [–]
#1	992.88	239	254	71	253	49	228	244	79	244	52	−4.6	−3.6	−4.3	0.99
#4	482.72	332	349	55	348	41	313	335	63	333	45	−5.7	−4.3	−4.9	1.02
#7	262.74	476	483	38	481	31	449	460	44	458	34	−5.7	−4.8	−4.9	1.02
#10	148.96	691	691	22	688	19	606	632	29	630	25	−12.3	−8.4	−8.1	1.17
#13	84.00	920	938	15	933	13	860	873	17	867	15	−6.5	−7.0	−6.0	1.07

Table 1: Comparison of measured and calculated resonance properties of different resonators of a mallet percussion instrument. “Meas”: measurement, “FE”: finite element simulation, “Lossy FE”: FE with viscous losses, “Predicted”: prediction of detuning using the hybrid model.

frequency of natural resonance is sensitive to the length correction and a significant detuning can be expected due to the presence of sound bars. To be able to quantify the importance of viscous losses, the FE model was extended following [8] to account for viscothermal wall effects. The formulation specifies an equivalent wall admittance, which adds a diagonal component to the damping matrix **C** of (1). As the admittance depends on the angle of incidence which is not known a priori, the equation is solved in an iterative manner starting from lossless walls and updating the admittance in each step. Convergence is reached in a few iterations.

Table 1 compares the measurement, simulation, and prediction results for five of the thirteen resonators of the experimental instrument. It is noted that the data represents a raw state of the instrument, i.e., the resonators are not tuned precisely to musical pitch. A good agreement of the simulated and measured results are observed with the greatest deviation of the frequencies being $\approx 6\%$ in case of resonator #4. The geometry of the arrangement is fairly complex as the resonators have irregular shapes and the sound bars cover the openings to different extents. To preserve an equivalent spacing of the bars, the openings of the resonators are not at the center position but are slightly shifted towards the end of the bars. Due to the arch-shaped longitudinal section of the bars, this results in different distances of resonator openings and sound bars. Furthermore, resonators #1 and #13 are the first and last of the instrument and hence their neighboring sound bars are arranged asymmetrically.

The effect of viscothermal losses on the natural frequency is found to be small with the largest difference being $< 1\%$ in case of resonator #13. However, the quality factor is affected by the wall losses to a significant extent in case of the resonators with lower natural frequencies. This result is explained by the radiation losses being lower in the low frequency range. At higher frequencies the radiation losses become dominant and the effect of viscous losses is smaller. The quality factors were also evaluated from the measurements, however, the results exhibited a large amount of scatter and thus the values are not shown in the table. Nevertheless, predicting the expected quality factor of a resonator is useful as, beside the natural frequencies, the quality factors also need to be tuned. Too high quality factors result in an easy detuning from the vibration frequency of the sound bar by the change of the environmental temperature, for example, while a too low quality factors lead to unsatisfactory amplification of the radiated sound.

Finally, the detuning effect of the sound bars was examined. The last column of Table 1 shows the estimated length correction coefficient $\Delta L_{\mathrm{out}}/r$ for the resonators taking the aforementioned geometrical differences of the sound bar arrangement into account. The natural frequencies are in the range $0.05 < kr < 0.25$, thus, a low frequency approximation of the length correction was used. The predictions are based on the parametric finite element study presented in Section 4.1. As seen, the predicted detuning is in very good agreement with the results of the full finite element model and these two models are also in good correspondence with the measurements. The greatest deviation of $\approx 4\%$ is observed in case of resonator #10, while the differences are $< 1\%$ in other cases. One possible cause of the deviations between the measured and modeled resonance properties is the inevitable excitation of wall vibrations in the measurements. While the finite element models assume perfectly rigid walls, the relatively thin plastic walls of the resonators are easily excited by the external loudspeaker. It was already found that the sound bars must be damped when measuring the transfer function of the resonators; however, the inner walls could not be damped without changing the volume of the resonators. Despite the observed discrepancies, it can be assessed that the detuning effect is reproduced well by both the finite element and the hybrid models.

5 CONCLUSIONS

This paper examined two applications of a numerical approach [1] for calculating the radiation impedance of resonators having irregular geometries. In the first study sound radiation from the mouth of flue instruements was examined and the simulation results were compared with measurement data and models published previously. The simulated length correction effect of different recorders agreed well with the measurements and models of [3] and [5]. In case of a cylindrical organ pipe a minor modification of the model presented in [5] lead to a very good agreement with the simulations for all examined geometries. The second study investigated the design of the resonators of a mallet percussion instrument. The detuning effect of a sound bar was found to be significant, and it was also shown that the neighboring sound bars also have a non-negligible detuning effect. Making use of the length corrections determined in a simplified arrangement, the detuning of the resonators of the experimental instrument was predicted accurately. Both applications highlight the usefulness and versatility of the proposed impedance modeling approach.

ACKNOWLEDGEMENTS

P. Rucz acknowledges the support of the Bolyai János research grant provided by the Hungarian Academy of Sciences. Supported by the ÚNKP-18-4 New National Excellence Program of the Ministry of Human Capacities.

REFERENCES

[1] P. Rucz. A finite element approach for the calculation of self and mutual radiation impedances of resonators. *Journal of the Acoustical Society of America*, 143(4):2449–2459, 2018.

[2] F. Ingerslev and W. Frobenius. Some measurements of the end-corrections and acoustic spectra of cylindrical open flue organ pipes. *Transactions of the Danish Academy of Technical Sciences*, 1(3):1–42, 1947.

[3] D. H. Lyons. Resonance frequencies of the recorder (English flute). *Journal of the Acoustical Society of America*, 70(5):1239–1247, 1981.

[4] M. P. Verge, B. Fabre, W. E. A. Mahu, A. Hirschberg, R. R. van Hassel, A. P. J. Wijnands, J. J. de Vries, and C. J. Hogendoorn. Jet formation and jet velocity fluctuations in a flue organ pipe. *Journal of the Acoustical Society of America*, 95(2):1119–1132, 1994.

[5] A. Ernoult and B. Fabre. Window impedance of recorder-like instruments. *Acustica-Acta Acustica*, 103:106–116, 2017.

[6] C. Geuzaine and J.-F. Remacle. Gmsh: a three-dimensional finite element mesh generator with built-in pre- and post-processing facilities. *International Journal for Numerical Methods in Engineering*, 79(11):1309–1331, 2009.

[7] I. Bork. Practical tuning of xylophone bars and resonators. *Applied Acoustics*, 46:103–127, 1995.

[8] A. Lefebvre, G. P. Scavone, and J. Kergomard. External tonehole interactions in woodwind instruments. *Acustica-Acta Acustica*, 99:975–985, 2013.

PROCEEDINGS of ISMA 2019
International Symposium on Music Acoustics

13 - 17 September 2019 in Detmold, Germany

Numerical study of synchronization phenomena of an air-jet instrument using finite-difference lattice boltzmann method

Ryoya Tabata[(1)], Taizo Kobayashi[(2)], Kin'ya Takahashi[(3)]

[(1)]Kyushu Institute of Technology, Japan, tabata@chaos.mse.kyutech.ac.jp
[(2)]RIIT, Kyushu University, Japan, tkoba@cc.kyushu-u.ac.jp
[(3)]Kyushu Institute of Technology, Japan, takahasi@mse.kyutech.ac.jp

Abstract

In this study, we focus on the synchronization between an air-jet instrument and external sound source. We numerically explore the synchronization mechanism using a finite-difference lattice Boltzmann method (FDLBM) as a direct aeroacoustic simulation scheme in two dimensions. We succeed in reproducing the frequency-locking phenomenon between the monopole sound source and air-jet instrument in the stationary state. Numerical simulations are conducted on a GPU cluster to explore the large parameter space. Transient behavior towards the frequency-locking phenomenon was observed, and the results demonstrate that the external sound source strongly affects the air-jet oscillation and the phase relationship of the sound pressure inside the resonator.

Keywords: Air-jet instrument, Synchronization, Aeroacoustic simulation

1 INTRODUCTION

A flue organ pipe is an air-jet instrument whose sound source is an aerodynamic sound generated by an air jet impinging on a wedge-shaped object. A feedback mechanism occurs between the air jet and a resonance tube, owing to the influence of the sound pressure in the resonance tube on the air jet.

When two organ pipes with pitches that are close to each other stand abreast, the frequency-locking phenomenon and oscillation death (quenching) occur, as first mentioned by Lord Rayleigh [1]. To study the synchronization mechanism among flue organ pipes, coupled Van der Pol oscillators [2, 3] are often used. Fischer et al. [2] suggested that the effect of the near-field interaction between the air-jet motion and acoustic field plays an important role in the synchronization mechanism. The synchronization characteristics of Van der Pol model are usually analyzed by relying on synchronization theory [4, 5]. Okada et al. [5] showed that the van der Pol oscillator cannot cause higher-order locking because its infinitesimal phase response curve (iPRC) hardly has any higher Fourier components. To improve the model, it is important to investigate the complex dynamics of the air-jet instrument in the synchronization regime.

A compressible flow simulation has been employed to reproduce the sound vibration of an air-reed instrument [6, 7, 8, 9], and the lattice Boltzmann method (LBM) has been employed as an alternative method to the Navier–Stokes equations owing to its advantage of a simple implementation on many-core accelerators such as GPU [6, 9]. The standard LBM only has second-order accuracy in both the spatial and temporal dimensions, and is not sufficiently accurate for direct aeroacoustic simulations [10]. Furthermore, the LBM is unstable in the high Mach number regime, even with the use of the multiple relaxation time (MRT) model [9]. In contrast, since the finite-difference lattice Boltzmann method (FDLBM) [11] can utilize finite-difference schemes of arbitrary order, it is capable of simulating numerical models stably and efficiently.

In this study, we employ the FDLBM to numerically investigate the synchronization mechanism between an air-jet instrument and external sound source. This paper is structured as follows. In Section 2, we introduce the numerical procedure utilized in this study. In Section 3, the numerical simulation is verified on several benchmark problems. In Section 4, we first discuss the behavior of the air-jet instrument for several air-jet velocities without a sound source. Then, we discuss the synchronization mechanism with a sound source with a varying frequency. Finally, Section 5 provides a discussion of the results and suggestions for future work.

2 NUMERICAL PROCEDURE

2.1 Governing equation and discretization

In this study, we employ the FDLBM model proposed by Tsutahara [11] with the added monopole sound source term proposed by Viggen [12]. The discrete Boltzmann equation (DBE) with a collision term (the third term of the left-hand side) added for numerical stability and the sound source term s_i can be respectively written as

$$\frac{\partial f_i}{\partial t} + \mathbf{c}_i \frac{\partial f_i}{\partial \mathbf{x}} - \frac{A\mathbf{c}_i}{\tau} \frac{\partial (f_i - f_i^{(0)})}{\partial \mathbf{x}} = s_i - \frac{1}{\tau}[f_i - f_i^{(0)}], \tag{1}$$

$$s_i(\vec{x},t) = w_i A_0 \sin(\omega t) exp(\frac{-ln2(\vec{x}-\vec{x}_0)^2}{b^2}). \tag{2}$$

The dispersion-relation-preserving (DRP) scheme [13], or third-order upwind scheme (UTOPIA), is employed for space discretization, and the second-order Runge–Kutta method is employed for time evolution. When using the DRP scheme, artificial selective damping [14] is used to suppress waves with small wavelengths.

Using the D2Q9 model [15], the numerical simulations were performed on the GPU (Tesla P100) cluster of ITO subsystem B (RIIT, Kyushu Univ) using an efficient GPU implementation [16].

2.2 Computational domain and air-jet instrument model

Figure 1 depicts the computational domain of the numerical simulation for reproducing the synchronization between an air-jet instrument and monopole sound source. Figure 2 illustrates the air-jet instrument model employed in this study, with two sampling points displayed in the figure. The characteristic length L is the nozzle width of the air-jet instrument. The non-uniform mesh was constructed by gradually increasing the mesh size of the air-jet region, where the smallest mesh was set as Δy = 0.01 (mm).

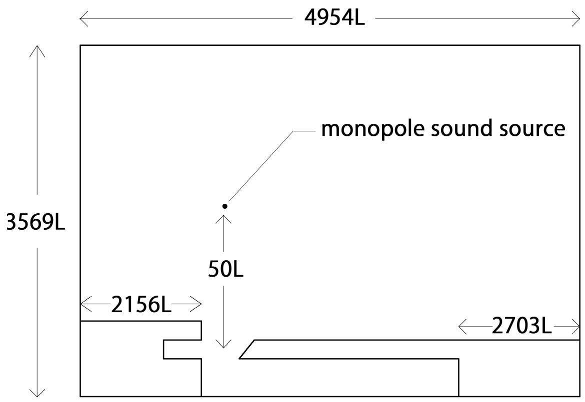

Figure 1. Computational Domain

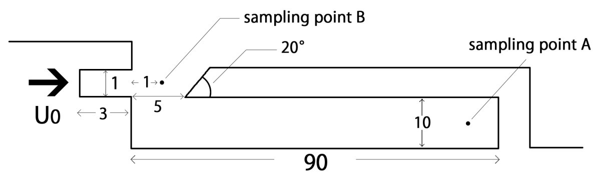

Figure 2. Air-jet instrument model (unit: mm)

2.3 Boundary conditions and initial conditions

An extrapolation method [17] that provides the distribution functions at the boundary by extrapolating using the distribution functions at the adjacent lattice points is employed for the solid boundary. Furthermore, an equilibrium function calculated by zero-order extrapolation of the macroscopic variables is set at the outlet boundary. At the inlet of the air-jet instrument model, the inflow condition is set using a sigmoid function to adjust the flow speed, which reaches the maximum value at t = 0.001 (s).

3 VERIFICATION OF THE NUMERICAL METHOD

3.1 Lid-driven cavity flow

In this subsection, we discuss the accuracy of the numerical method using simulation data provided by Ghia [18] for the 2D lid-driven cavity flow problem. The Reynolds number of the flow is set to 100, with $U_0 = 0.1$. The Zou–He boundary condition [15] is adopted for the LBM calculations. The FDLBM calculations are all performed using a mesh of size 101×101. The following convergence criterion is adopted with ε = 1e-6:

$$\sqrt{\frac{\sum_i \left|\vec{u}\left(\vec{x}_i, t^n\right) - \vec{u}\left(\vec{x}_i, t^{n-1}\right)\right|^2}{\sum_i \left|\vec{u}\left(\vec{x}_i, t^n\right)\right|^2}} < \varepsilon. \tag{3}$$

Figure 3 shows that the FDLBM calculation exhibits a good agreement with Ghia's data. Furthermore, we observe that the LBM calculation gradually approaches Ghia's data as the mesh size increases. This indicates that the FDLBM is capable of calculating the flow more precisely compared with the LBM when the same mesh size is employed.

3.2 2D acoustic pulse propagation

As a typical benchmark problem in computational acoustics, the propagation of a two-dimensional Gaussian pulse simulation is performed. The analytical solution, which can be obtained by solving the linearized Euler equations using the Fourier-Bessel transform [13], is as follows:

$$p'(r,t) = \frac{p_0}{2\alpha} \int_0^{\infty} \exp\left(-\frac{\xi^2}{4\alpha}\right) \cos(c_s \xi t) J_0(\xi r) \xi d\xi, \tag{4}$$

where $J_0(\xi r)$ is the zeroth-order Bessel function of the first kind. The parameters are set as $p_0 = 0.001$ and $\alpha = 10^2/ln2$. Figure 4 demonstrates a good agreement between the analytical solution and the numerical results obtained by the LBM and FDLBM. The good performance of the LBM can be explained by the fact that the LBM achieves a perfect shift solution for the streaming step. Furthermore, we can observe that the FDLBM performs better when utilizing a high-order scheme.

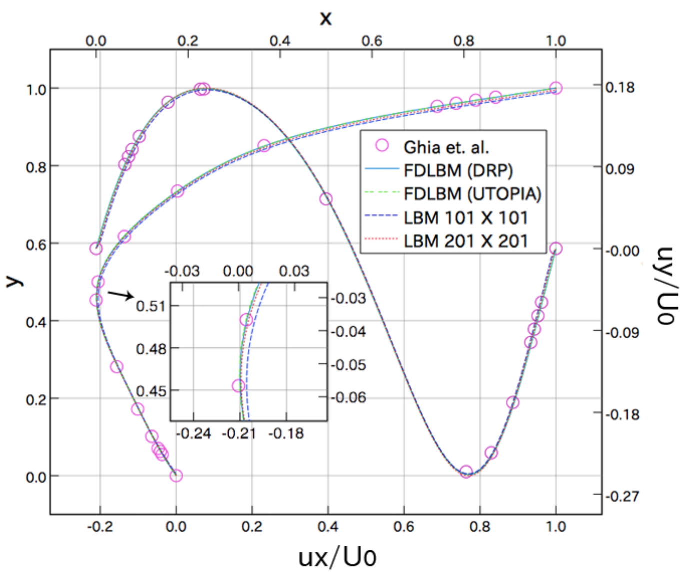

Figure 3. Lid-driven cavity

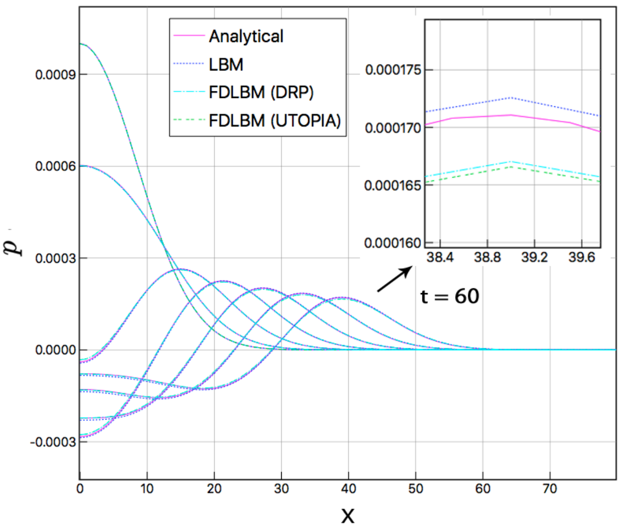

Figure 4. Two-dimensional pulse propagation

4 RESULTS AND DISCUSSIONS

4.1 Simulation without external sound source

In this subsection, we discuss the changes in characteristic frequencies of the sound waves excited in the pipe with an increasing air-jet velocity. Table 1 presents the parameter values adopted in the simulations, which were calculated for up to 0.05 s. For stable calculations, the third-order upwind scheme is adopted for the space discretization. Figure 5 depicts the velocity distributions in the near field of the air-jet instrument model, and Figure 6 shows the pressure fluctuation ($\Delta p = \frac{p-p_0}{p_0}$) distributions in the far field of the calculation domain at time 0.025 s, i.e., the stationary condition, for two inflow velocities (U = 10 m/s, 24 m/s). We can observe that the jet is oscillating and the sound wave is radiating out from the mouth of the air-jet instrument.

Table 1. Parameter values

Parameters	Values
Inflow velocity	U = 6 (m/s) $\sim$ 40 (m/s)
Initial flow density	ρ_0 = 1.184 (kg/m^3)
Coefficient of viscosity	μ = 1.846 × 10^{-5} (Pa · s)
Sound speed	c_s = 346.18 (m/s)
Time step	Δt = 8.3e-9 (s)
Minimum mesh size	Δy = 0.01 (mm)

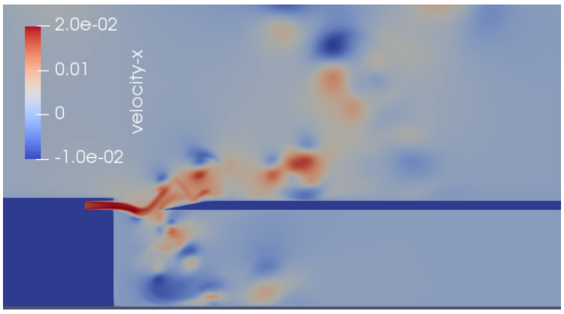

(a) 10 (m/s)

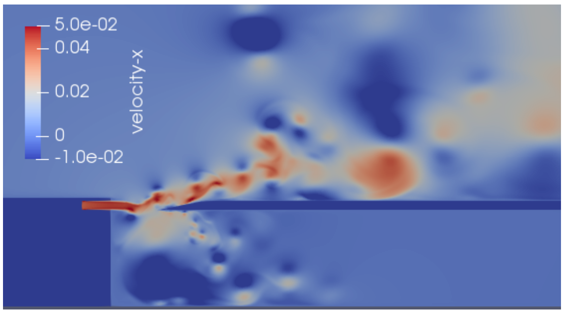

(b) 24 (m/s)

Figure 5. Near field velocity distribution (0.025 s)

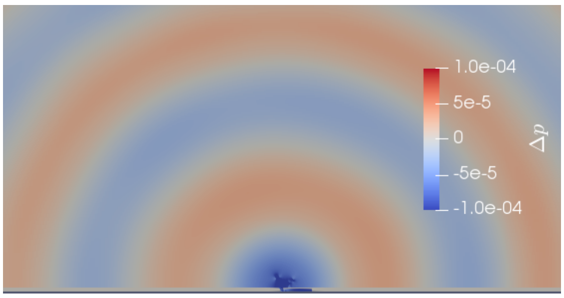

(a) 10 (m/s)

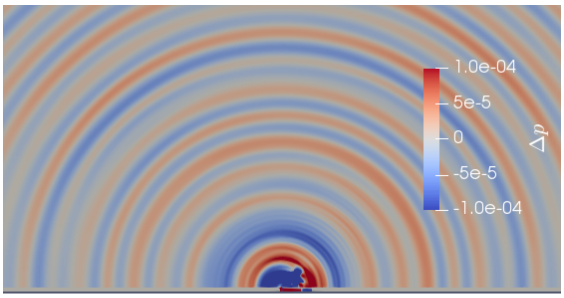

(b) 24 (m/s)

Figure 6. Far field pressure fluctuation distribution (0.025 s)

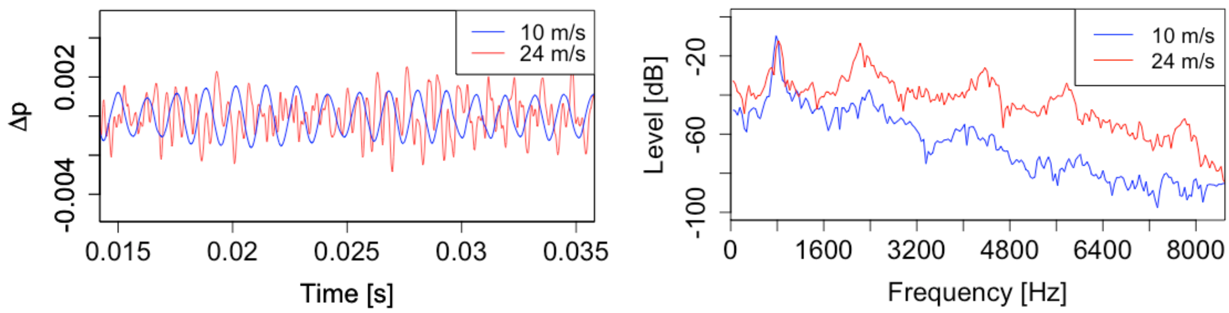

(a) Pressure fluctuations

(b) Power spectra

Figure 7. Pressure fluctuations and power spectra at the pipe end of the instrument

Figure 7a depicts the pressure fluctuations at the pipe end (sampling point A) of the air-jet instrument for the two inflow velocities. A stable oscillation is observed at U =10 m/s, and a slightly unstable oscillation with amplitude modulations is observed at U =24 m/s. Figure 7b depicts the power spectra of the pressure fluctuations. In calculating the spectra, the initial transient oscillation (t < 0.02 s) is omitted. The main peaks of the spectra for U =10 m/s and U = 24 m/s appear at $f = 784$ Hz and $f = 844$ Hz, respectively. The second peak of the spectrum for U = 24 m/s occurs at $f = 2244$ Hz. These results can be explained by the edge tone frequency, the pipe fundamental resonance frequency at $f = 900$ Hz, and the second resonance peak (the third harmonic) at $f = 2755$ Hz, respectively [7]. Brown introduced a semi-empirical equation based on the experimental results, which predicts the frequency of the edge tone [19]:

$$f = 0.466(100U - 40)\left(\frac{1}{100h} - 0.07\right), \tag{5}$$

where U denotes the speed of the air jet and h is the distance between the flue and edge. From Figure 8, it can be observed that our numerical result is in good agreement with the predicted edge tone frequency in some ranges of the jet velocity, and it also reproduces the frequency locking to the fundamental and third harmonic resonances of the pipe.

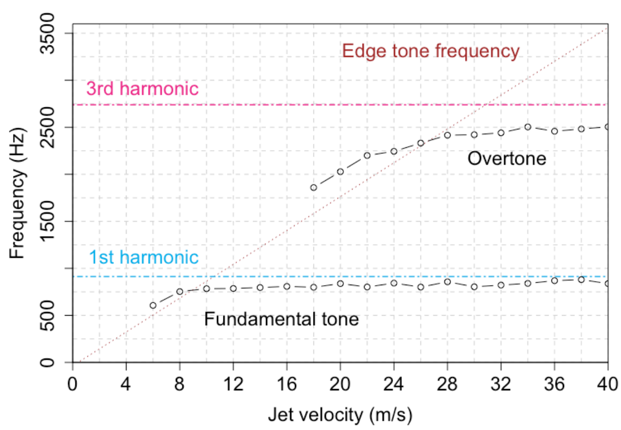

Figure 8. Changes in oscillation frequencies with air jet velocity

4.2 Simulation with an external sound source

In this subsection, we discuss the behavior of the synchronization transition between the air-jet instrument and an external monopole sound source. The inflow velocity of the air-jet instrument is set as $U = 10$ m/s, where the stable oscillation is observed. The sound source strength is set as $A_0 = 3.3 \times 10^{-5}$, which reproduces the same order in pressure fluctuation at the sampling point A as the instrument driven by a jet of 10 m/s.

The frequency of the sound source is set as f =700∼910 Hz with a 2-Hz interval. The sound source is incorporated at t =0.0125 s, where the stable oscillation begins.

Figure 9 depicts the pressure fluctuations at the pipe end (sampling point B) for three cases: the jet driven instrument with a sound source of 796 Hz, that without a sound source, and the case with a sound source but no jet driving. For the case with the sound source, after a short disturbance, we can observe phase locking between the sound source and the pipe end pressure fluctuation. Furthermore, the amplitude of the pressure fluctuation with the sound source becomes greater than that in the case with no sound source in the course of the time evolution.

Figure 10 compares the velocity in the y-direction at the pipe opening (sampling point A) for the cases with and without a sound source. A large velocity fluctuation is observed before the start of the synchronization, as shown in Figure 9. After the synchronization, the amplitude of the velocity fluctuation with the sound source becomes stable, and is greater than that without a sound source.

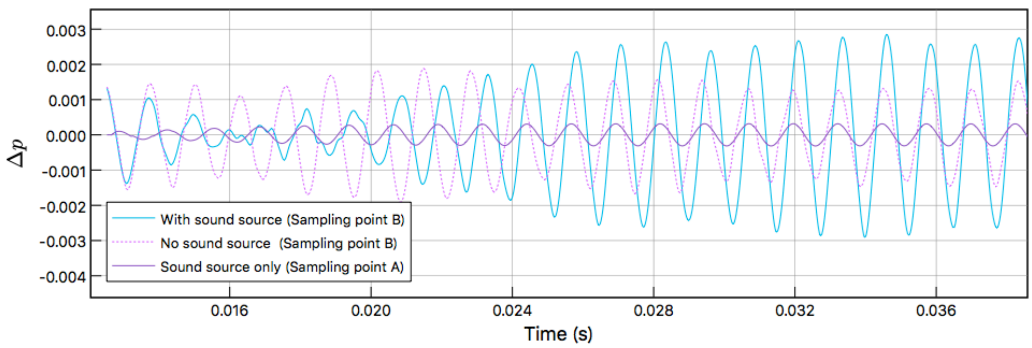

Figure 9. Pressure fluctuations at the pipe end

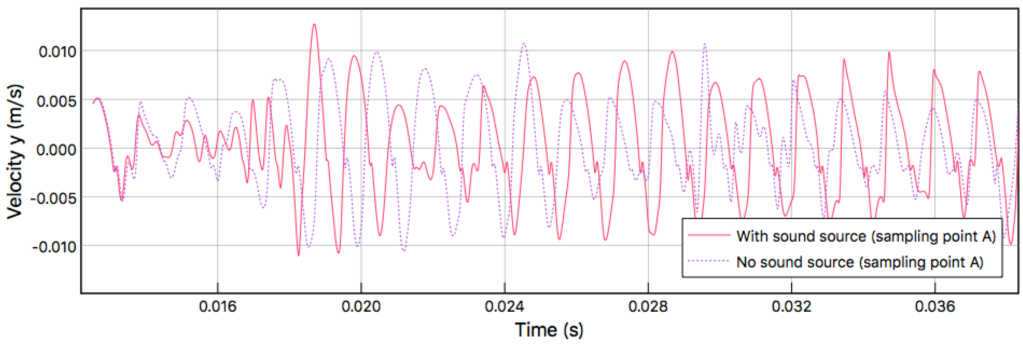

Figure 10. Velocity (y-direction) at the mouth opening of the pipe

Figure 11 illustrates the pressure and velocity distributions for the calculation with the sound source (796 Hz) at 0.054 s. From Figure 11a, the interference between the sound source and the radiated sound from the pipe can be observed. As shown in Figure 11b, a large jet oscillation is observed, which is amplified by the synchronization with the external sound source.

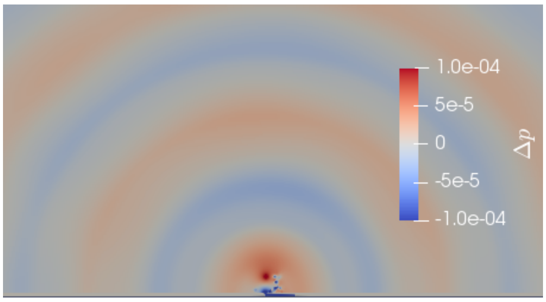

(a) Pressure distribution

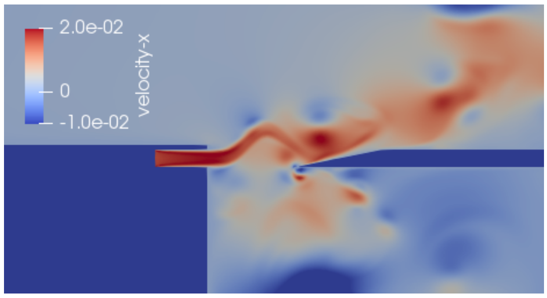

(b) Velocity distribution

Figure 11. Snapshots at $t = 0.054$ (s) of calculation with sound source (796 Hz)

Figure 12 depicts the power spectra of the pressure fluctuations of the pipe end, and Figure 13 illustrates the pressure fluctuation level at the mouth opening in the plane of the frequency f versus the frequency detuning Δf (in Hz). As observed from these figures, the main peak frequency increases as the external sound source frequency increases. However, out of the approximately range of 730 $\sim$ 830 Hz, the synchronization is broken and the main peak is separated into two peaks: the own-mode frequency of the instrument and external sound source frequency.

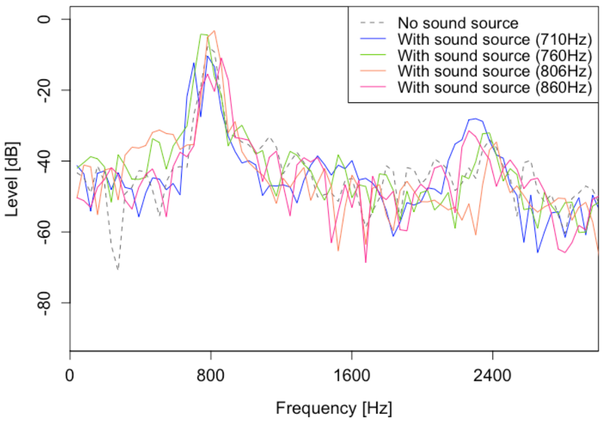

Figure 12. Power spectra at the pipe bottom

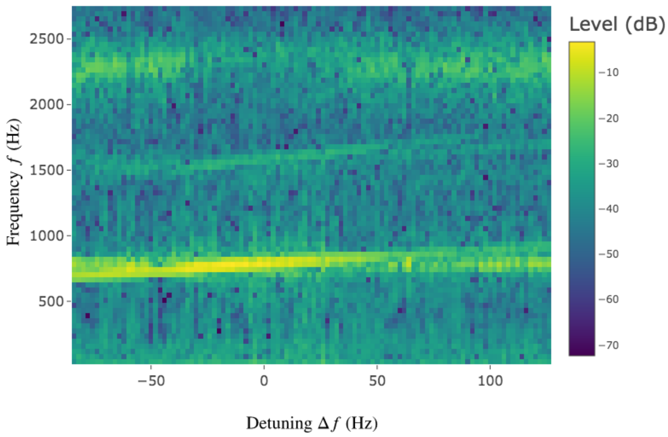

Figure 13. The pressure fluctuation level (in relative dB) in the plane of frequency f versus frequency detuning Δf (in Hz)

5 CONCLUSIONS

In this paper, we have presented the results of numerical simulations of an air-jet instrument using the FDLBM. We found that the FDLBM can reproduce the basic characteristics of the flue instrument and the synchronization between the oscillation mode and an external sound source. Transient behavior towards this synchronization was observed, and it was demonstrated that the external sound source strongly affects the jet oscillation and the phase of the pressure fluctuation. As future work, a three-dimensional simulation should be performed to reproduce more realistic synchronization phenomena between the air-jet instruments.

ACKNOWLEDGEMENTS

This work was supported by JST CREST Grant Number JPMJCR1501, "Joint Usage/Research Center for Interdisciplinary Large-Scale Information Infrastructures" and "High Performance Computing Infrastructure" in Japan (Project IDs: jh190039-ISH and jh190010-MDH). The authors are very grateful to Mr. Sho Iwagami (Kyushu Institute of Technology) for useful discussions.

REFERENCES

[1] J. Rayleigh. *The Theory of Sound*. Vol.2. New York: Dover; 1945. p. 221-222.

[2] Fischer JL, Bader R, Abel M. Aeroacoustical coupling and synchronization of organ pipes. The Journal of the Acoustical Society of America. 2016 Oct;140(4):2344-51.

[3] Sawicki J, Abel M, Schöll E. Synchronization of organ pipes. Eur Phys J B. 2018 Feb 5;91(2):24.

[4] Abel M, Bergweiler S, Gerhard-Multhaupt R. Synchronization of organ pipes: experimental observations and modeling. The Journal of the Acoustical Society of America. 2006 Apr;119(4):2467-75.

[5] Okada M, Kaburagi T. Higher-order frequency locking of an organ pipe: A measurement study based on synchronization theory. The Journal of the Acoustical Society of America. 2018 Mar;143(3):1514-22.

[6] Kühnelt H, Simulating the sound generation in flutes and flue pipes with the Lattice-Boltzmann-Method. Proceedings of ISMA. 2004.

[7] Miyamoto M, Ito Y, Iwasaki T, Akamura T, Takahashi K, Takami T, et al. Numerical Study on Acoustic Oscillations of 2D and 3D Flue Organ Pipe Like Instruments with Compressible LES. Acta Acustica united with Acustica. 2013 Jan 1;99(1):154-71.

[8] Giordano N. Simulation studies of a recorder in three dimensions. The Journal of the Acoustical Society of America. 2014 Jan;135.

[9] Shi Y, da Silva AR, Scavone GP. Numerical Simulation of Whistles Using Lattice Boltzmann Methods. Proceedings of ISMA. 2014.

[10] W. S. Kam E, So RMC, Fu S, Leung R. Finite Difference Lattice Boltzmann Method Applied to Acoustic-Scattering Problems. Aiaa Journal - AIAA J. 2010 Feb;48:354-71.

[11] Tsutahara M. The finite-difference lattice Boltzmann method and its application in computational aero-acoustics. Fluid Dynamics Research. 2012 Aug 1;44(4):045507.

[12] Viggen EM. Acoustic multipole sources for the lattice Boltzmann method. Phys Rev E. 2013 Feb;87(2):023306.

[13] Tam CKW, Webb JC. Dispersion-Relation-Preserving Finite Difference Schemes for Computational Acoustics. Journal of Computational Physics. 1993 Aug;107(2):262-81.

[14] Tam CKW. Computational aeroacoustics - Issues and methods. AIAA Journal. 1995 Oct;33(10):1788-96.

[15] Zou Q, He X. On pressure and velocity boundary conditions for the lattice Boltzmann BGK model. Physics of Fluids. 1997 Jun;9(6):1591-8.

[16] Tabata R, Kobayashi T. Numerical Simulation of a Flue Instrument with Finite-Difference Lattice Boltzmann Method using GPGPU. The International Conference for High Performance Computing, Networking, Storage, and Analysis. 2018.

[17] Hejranfar K, Ezzatneshan E. A high-order compact finite-difference lattice Boltzmann method for simulation of steady and unsteady incompressible flows. International Journal for Numerical Methods in Fluids. 2014 Aug;75(10):713-46.

[18] Ghia U, Ghia KN, Shin CT. High-Re solutions for incompressible flow using the Navier-Stokes equations and a multigrid method. Journal of Computational Physics. 1982 Dec;48(3):387-411.

[19] Brown GB. The vortex motion causing edge tones. Proceedings of the Physical Society. 1937 Sep 1;49(5):493-507.

PROCEEDINGS of ISMA 2019
International Symposium on Music Acoustics

13 - 17 September 2019 in Detmold, Germany

From the bifurcation diagrams to the ease of playing of reed musical instruments. A theoretical illustration of the Bouasse-Benade prescription? *†‡

Joel GILBERT(1), Sylvain MAUGEAIS(2), Christophe VERGEZ(3)

(1)Laboratoire d'Acoustique de l'Universite du Mans, UMR 6613 CNRS, France, Joel.Gilbert@univ-lemans.fr

(2)Laboratoire Manceau de Mathématiques - Le Mans Université, France, Sylvain.Maugeais@univ-lemans.fr

(3)Aix Marseille Univ, CNRS, Centrale Marseille, LMA, UMR 7031, France, vergez@lma.cnrs-mrs.fr

Abstract

Reed musical instruments can be described in terms of conceptually separate linear and nonlinear mechanisms: a localized nonlinear element (the valve effect due to the reed) excites a linear, passive acoustical multimode element (the musical instrument usually represented in the frequency domain by its input impedance). The linear element in turn influences the operation of the nonlinear element. The reed musical instruments are self-sustained oscillators. They generate an oscillating acoustical pressure (the note played) from a static over-pressure in the player's mouth (the blowing pressure).

A reed instrument having N acoustical modes can be described as a 2N dimensional autonomous nonlinear dynamical system. A reed-like instrument having two quasi-harmonic resonances, represented by a 4 dimensional dynamical system, is studied using the continuation and bifurcation software AUTO. Bifurcation diagrams are explored with respect to the blowing pressure, with focus on amplitude and frequency evolutions along the different solution branches. Some of the results are interpreted in terms of the ease of playing of the reed instrument. They can be interpreted as a theoretical illustration of the Bouasse-Benade prescription.

Keywords: Acoustics, reed instruments, bifurcation diagrams, resonance inharmonicity, ease of playing

1 INTRODUCTION

A quest for the grail of wind instruments musical acoustics is to try to understand keys of intonation and ease of playing. From the physic's modelisation point of view, we try to understand keys of what is controlling the playing frequency (for intonation) and the minimum mouth pressure to get oscillations (for ease of playing). A state of art can be found in the recent books dealing with acoustics of musical instruments: [Benade 1990], [Campbell and Greated 1987], [Fletcher and Rossing 1998], [Chaigne and Kergomard 2016]).

Often it has been pointed out how brass instruments generally have a flaring bore so designed that impedance peaks are well aligned in order to reach as close as possible an harmonic series. If this alignment is clearly important for intonation, it is important too to get stable periodic oscillations easy to play. The necessity of an alignment in an harmonic series is called here the 'Bouasse-Benade prescription' because of what Benade wrote in his famous book [Benade 1990], or in [Benade and Gans 1968]: "The usefulness of the harmonically related air column resonances in fostering stable oscillations sustained by a reed-valve was first pointed out by the french physicist Henri Bouasse in his book Instruments à vent". As a counter-example a horn was designed to provide an air column whose resonance frequencies (frequencies of maximum input impedance) were chosen to avoid all possible integer relations between them, this horn has been called 'tacet horn' in [Benade and Gans 1968]. This reed instrument has been made so that the conditions for oscillation would then be most unfavorable.

To try to illustrate the 'Bouasse-Benade prescription', we want to study the influence of the inharmonicity on the playing frequency and on the minimum mouth pressure to get oscillations. And to do so, we will use the

*Joel.Gilbert@univ-lemans.fr

†Sylvain.Maugeais@univ-lemans.fr

‡vergez@lma.cnrs-mrs.fr [Please note: It is optional to provide the email address(es) of the author(s). Please make sure that your co-authors concur with the mention of their email address in this paper.]

bifurcation diagram representation, the control parameter being the mouthp ressure. The bifurcation diagrams are nice results to begin to answer this quest of the grail.

The wind instruments, and particularly the brass, exhibit many resonances, which makes very difficult to demonstrate the Bouasse-Benade prescription. A way to overtake that is to work on the easiest of the complicated resonators: a resonator having two quasi-harmonic resonance frequencies F_{res1} and F_{res2} where the deviation to harmonicity, the inharmonicity parameter Inh, is defined by $F_{res2} = 2F_{res1}(1+Inh)$. And to facilitate the theoretical investigations, we have chosen a low frequency model of inward striking reed instruments, the reed being assimilated to its stiffness only and being undamped. Note that if the resonances are exactly harmonic ($Inh = 0$) this theoretical problem can be analysed analytically, and two bifurcation diagrams have already been obtained (Figure 8 and 10 of [Dalmont et al 2000]).

In section 2 of this paper we present briefly the theoretical backgrounds, and particularly the equations of the elementary model of wind instruments. Then section 2 documents the procedure used to calculate bifurcation diagrams by using a continuation method, after having reformulated the two coupled equations of the model in a set of four coupled first order ODE equations. The influence of the inharmonicity on the bifurcation diagrams is shown and discussed in section 3. The bifurcation diagrams are analysed in the light of the threshold of periodic oscillations (to do a link with the ease of playing of the musicians, and with the Bouasse-Benade prescription), and the effect of the inharmonicity on the playing frequency is discussed too.

2 THEORETICAL BACKGROUNDS

2.1 Acoustical model

The model presented here and used in the present publication is labelled as elementary because a number of major simplifications are made in deriving it (see for example [Hirschberg et al 1995], [Fabre et al 2018]). The vibrating reeds or lips are modeled as a linear one degree of freedom oscillator. The upstream resonances of the player's windway are neglected, as is the nonlinear propagation of sound in the air column of the instrument. Wall vibrations are also ignored. Despite these simplifications, the elementary model is capable of reproducing many of the important aspects of performance by human players on realistic reed and brass instruments. The model is based on a set of three coupled equations, which have to be solved simultaneously to predict the nature of the sound radiated by the instrument. These three constituent equations of the model are presented hereafter.

Besides the control parameters defining the embouchure of the player, including the reed or lips parameters and the mouth pressure p_m, and the input impedance of the wind instrument, there are three variables in the set of the coming three equations as a function of the time t: the reed or lip opening height $h(t)$, the pressure in the mouthpiece of the instrument $p(t)$, and the entering volume flow into the instrument $u(t)$.

In order to describe the vibrating reeds or lips, the first of the three constituent equations of the elementary model is:

$$\frac{d^2h(t)}{dt^2} + \frac{\omega_r}{Q_r}\frac{dh(t)}{dt} + \omega_r^2(h(t) - h_o) = -\frac{p_m - p(t)}{\mu}. \quad (1)$$

In this equation, which describes the reeds or lips as a one degree of freedom (1DOF) mechanical oscillator, the symbols ω_r, Q_r, h_o and μ represent the angular reed resonance frequency, the quality factor of the reed resonance, the value of the reed or lip opening height at rest, and the effective mass per unit area of the reeed or lips respectively. These quantities are parameters of the model, which are either constant (in a stable note) or changing slowly in a prescribed way (in a music performance). Note that if μ is positive, an increase of the pressure difference $(p_m - p(t))$ will imply a closing of the reed or lips aperture. It is called the 'inward striking' model and is used mainly for reed instruments. If μ is negative, an increase of the pressure difference will imply an opening of the reed or lips aperture. It is called the 'outward striking' model and is used mainly for brass (lip reed) instruments.

The second constituent equation describes the relationship between pressure and flow in the reed lip channel:

$$u(t) = wh^{+}(t)\sqrt{\frac{2}{\rho}|p_m - p(t)|}sign(p_m - p(t)) \tag{2}$$

where the square root originates from the Bernoulli equation, and the positive part of the reed or lips aperture $h^{+} = max(h, 0)$ models the closed reed or lips.

The third and last constituent equation describes the relationship between flow and pressure in the instrument mouthpiece. It is written in the frequency domain using the input impedance $Z(\omega)$ of the wind instrument:

$$p(\omega) = Z(\omega)u(\omega). \tag{3}$$

Other than the difference of sign of μ between 'inward striking' reed instruments model and 'outward striking' brass instruments model, there is another difference between these two subfamilies of wind instruments. The control parameter ω_r of vibrating lips is varying a lot, over four octaves, to get the entire tessiture of a given brass instrument. At the opposite the ω_r associated to reeds is more fixed (slightly varying because of the lower lip of the clarinet or saxophone player) and most of the time very large compared to the playing frequencies. This last fact justifies a low frequency approximation of the elementary model: the ω_r is assumed infinite and the reed undampted. In other words, the reed is reduced to its stiffness only and the set of three equations becomes a set of two equations as follows:

$$\begin{cases} u(t) = w[h_o - \frac{p_m - p(t)}{\mu\omega_r^2}]\sqrt{\frac{2}{\rho}(p_m - p(t))} \\ p(\omega) = Z(\omega)u(\omega). \end{cases} \tag{4}$$

When the mouth pressure is too high, the reed can be blocked against the lay of the mouthpiece. Then the 'closure pressure' defined by $p_M = \mu\omega_r^2.h_o$ is the minimal mouth pressure for which the reed remains closed in the static regime (h becomes equal to 0). By using this closure pressure, a dimensionless mouth pressure γ can be defined: $\gamma = p_m/p_M$ (note that most of the time the dimensionless mouth pressure is called abusively mouth pressure).

It is this elementary low frequency model for reed instruments which is used in the present paper. In the following, the nonlinear equation of the model is approximated by its third order Taylor series around the equilibrium position defined by $h_{eq} = h_o - \frac{p_m}{\mu\omega_r^2}$, $u_{eq} = wh_{eq}\sqrt{\frac{2}{\rho}p_m}$ and $p_{eq} = 0$:

$$u(t) = u_{eq} + A_1 p(t) + A_2 p(t)^2 + A_3 p(t)^3. \tag{5}$$

If we assume a non-beating reed which is typically obtained for a dimensionless mouth pressure γ lower than 0.5, the above third order approximation of the flow rates is appropriate.

The above elementary model based on the set of two equations has to be solved to predict the nature of the sound radiated by the instrument.

2.2 Continuation method

A nice way to have an overview of the dynamics over small and large amplitudes is to use the bifurcation diagram representation. A very few of them can be obtained analytically (see the previous subsection). It is possible to obtain bifurcation diagrams numerically for a large range of situations by using continuation methods, such as implemented in AUTO software [Doedel et al 1997] or MANLAB software [Karkar et al 2013]

for example. In order to use AUTO technique in the following section, the elementary model has to be mathematically reformulated in a set of coupled first order ODE equations.
To do so, we have mainly to introduce the derivative of the lips or reed position as a new variable and to reformulate the input impedance equation (Eqn. 3) by a sum of individual acoustical resonance modes in the frequency domain, and then to translate them in the time domain. There are two ways to manage that: sum of real modes (see for example [Debut et al 2004]), sum of complex modes (see for example [Silva et al 2014]). These two ways of approximating the input impedance in the frequency domain lead to two different sets of first order equations $\frac{dX}{dt} = F(X)$. In the present paper we use the 'real mode' representation of the input impedance Z.

The modal-fitted input impedance with N resonance modes, is written as follows:

$$Z(\omega) = \sum_{n=1}^{N} Z_n \frac{jq_n\omega\omega_n}{\omega_n^2 + jq_n\omega\omega_n - \omega^2}. \tag{6}$$

where the n^{th} resonance is defined by three real constants, the amplitude Z_n, the dimensionless damping coefficient q_n and the angular frequency ω_n.
Each term of Eqn. 6 can be written in the time domain as follows:

$$\frac{d^2 p_n}{dt^2} + q_n\omega_n \frac{dp_n}{dt} + \omega_n^2 p_n(t) = Z_n q_n \omega_n \frac{du}{dt}, \tag{7}$$

such that the acoustical pressure is $p(t) = \sum_{n=1}^{N} p_n(t)$.
Taking into account the other equation of the elementary model, the derivative of the volume flow nonlinear equation (Eqn. 4), the previous set of N second order ODE (Eqn. 7) can be rewritten by using the following expression of $\frac{du}{dt}$:

$$\frac{du}{dt} = w\frac{1}{\mu\omega_r^2}\frac{d(\sum_{n=1}^{N} p_n)}{dt}\sqrt{\frac{2}{\rho}(p_m - \sum_{n=1}^{N} p_n(t))}$$
$$+ w[h_o - \frac{p_m - \sum_{n=1}^{N} p_n(t)}{\mu\omega_r^2}](-1/2)\frac{d(\sum_{n=1}^{N} p_n)}{dt}\frac{1}{\sqrt{\frac{2}{\rho}(p_m - \sum_{n=1}^{N} p_n(t))}}. \tag{8}$$

If the third order Taylor series approximation is used (Eqn. 5), then in place of Eqn. 8 we get:

$$\frac{du}{dt} = [A_1 + 2A_2(\sum_{n=1}^{N} p_n) + 3A_3(\sum_{n=1}^{N} p_n)^2]\frac{d(\sum_{n=1}^{N} p_n)}{dt}.$$

Then the equations can be put into a state-space representation $\frac{dX}{dt} = F(X)$, where F is a nonlinear vector function, and X the state vector having $2N$ real components defined as follows:

$$X = \left[p_1; ...; p_N; \frac{dp_1}{dt}; ...; \frac{dp_N}{dt}\right]'. \tag{9}$$

In practice, because our paper is dedicated to a two quasi harmonically resonances instrument, the state space representation is based on the state vector of 4 real components $X = \left[p_1; p_2; \frac{dp_1}{dt}; \frac{dp_2}{dt}\right]$.
Bifurcation diagrams for different values of inharmonicity are presented and discussed in the coming Section. It is assumed the following configuration of relative amplitudes between Z_1 and Z_2 of the two resonances: Z_1 slightly higher than Z_2.

3 BIFURCATION DIAGRAMS

3.1 Exactly harmonic resonances

The results shown in Figure 1 for the case $Inh = 0$ are qualitatively consistent with the one published in [Dalmont et al 2000] (see in particular its Figure 8). Note that the continuation method gives an additional information: the stability nature of the periodic oscillations. The bifurcation diagram shows two branches coming from the equilibrium position:

- the first branch is originating from the linear threshold $p_m = p_{thr1}$, associated to the first resonance F_{res1}, according to an inverse Hopf bifurcation. This fundamental regime is a 'standard Helmholtz motion' according to [Dalmont et al 2000]. Because it is an inverse bifurcation case, the branch is unstable and then becomes stable at the limit point at $p_m = p_{subthr}$.

- the second branch is originating from the linear threshold $p_m = p_{thr2}$, associated to the second resonance F_{res2}, according to a direct Hopf bifurcation. Note that p_{thr2} is bigger than p_{thr1}, because Z_1 is larger than Z_2. This branch which would correspond to the second regime (the octave) is not observable in practice, because the periodic solutions are unstable.

There is a third branch wich is originating from the unstable octave branch, thanks to a period doubling bifurcation. This branch which would correspond to an other fundamental regime (the 'inverted Helmholtz motion' according to [Dalmont et al 2000]) is unstable. The associated lower curve shows the frequency of the periodic oscillations corresponding to the stable branche of the bifurcation diagram. In particular the frequency of the fundamental regime (green curve) is locked at the value $F_{res1} = F_{res2}/2$ whatever p_m is.

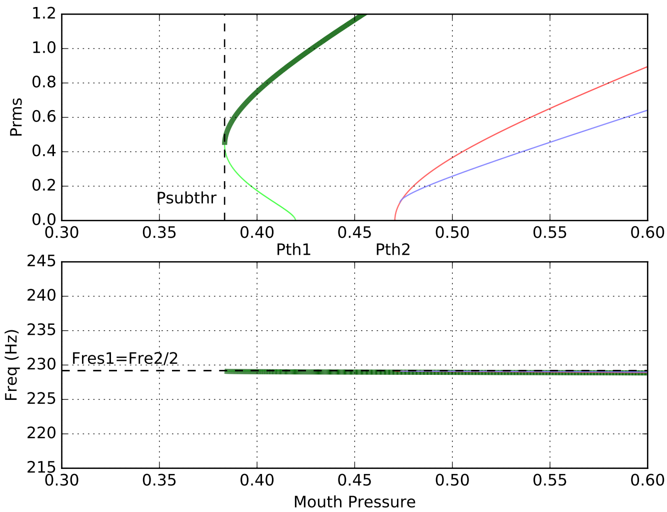

Figure 1. Bifurcation diagram for an air column with two exactly harmonic resonances ($Inh = 0$) as a function of the control parameter p_m. Thick lines describe stable solutions, thin lines unstable solutions. Upper graph: RMS value of oscillating pressure $p(t)$. Lower graph: frequency of oscillation.

3.2 Quasi-harmonic resonances

Let's go to the case $Inh = 0.02$ (Figure 2). The bifurcation diagram is quite close to the one with $Inh = 0$. We would like to point out two things. First, at the threshold $p_m = p_{thr1}$ the Hopf bifurcation has become direct as it can be predicted theoretically ([Grand et al 1997]). Second, again there are periodic oscillations for mouth pressures p_m values below $p_m = p_{thr1}$ (though the bifurcation is direct) until a new value $p_m = p_{subthr}$ which is a bit larger than the one of the case $Inh = 0$. Note that the frequency of the fundamental regime (green curve) is not locked at the value F_{res1} anymore but is partially pull out toward the value $F_{res2}/2$, which is intuitively sensible. If the inharmonicity was negative, we would have the same kind of results, the frequency being pull out toward $F_{res2}/2$ lower than F_{res1}.

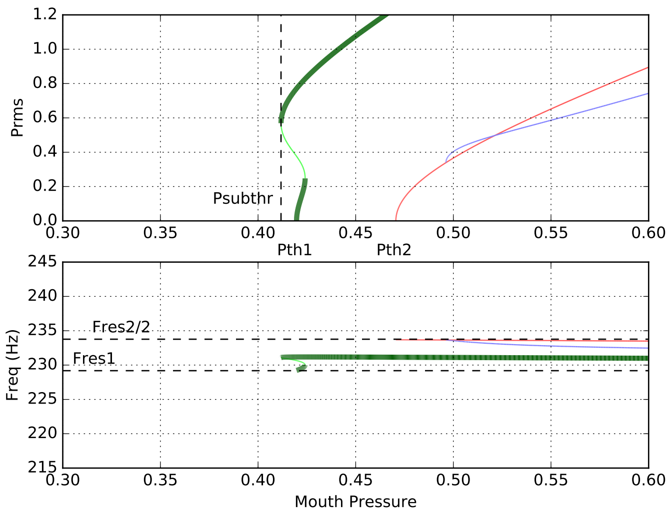

Figure 2. Bifurcation diagram for an air column with two quasi-harmonic resonances ($Inh = 0.02$) as a function of the control parameter p_m. Thick lines describe stable solutions, thin lines unstable solutions. Upper graph: RMS value of oscillating pressure $p(t)$. Lower graph: frequency of oscillation.

Let's go to the case $Inh = 0.04$ (Figure 3). Now the branch coming from the threshold $p_m = p_{thr1}$, corresponding to the fundamental regime, looks like a classical branch associated to the direct Hopf bifurcation, there is no p_{subthr} anymore. $p_m = p_{thr1}$ is now the the threshold of oscillation. In fact, when the inharmonicity is increasing, the dynamics of the system behaves more and more like the dynamics of the one acoustical resonance system. The frequency of the fundamental regime comes from the threshold value $F_{thr1} = F_{res1}$ at the direct Hopf bifurcation point, and then is partially pull out toward the value $F_{res2}/2$.

The above discussion illustrates important things because of the inverse Hopf bifurcation:
- on one hand, there is a minimum value $p_m = p_{subthr}$ lower than p_{thr1} where we can have periodic oscillations. This particular value p_{subthr} is a kind of quantitative caracterisation of the ease of playing. It has been shown that the lowest value of p_{subthr} is obtained when the two resonances are perfectly harmonic ($Inh = 0$). It suggests the reed instrument is the easiest to play when $Inh = 0$. In a way this is a theoretical illustration of the Bouasse-Benade prescription ([Bouasse 1929], [Benade 1990]).
- on the other hand, the stable periodic oscillations which appear for p_m slightly larger than p_{subthr} can have fundamental frequencies significantly different from $F_{thr1} = F_{res1}$ because of the effect of the presence of the second resonance which controls partially the intonation of the fundamental regime. This study illustrates the limit of the linear stability analysis approach to predict the behavior of the small amplitude periodic oscillations. Note that it is the case too when $Z_2 > Z_1$ (see Figure 10 of [Dalmont et al 2000]).

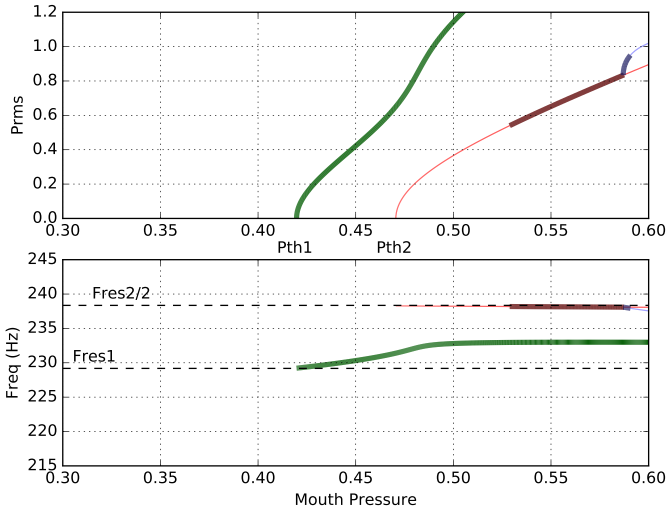

Figure 3. Bifurcation diagram for an air column with two quasi-harmonic resonances ($Inh = 0.04$) as a function of the control parameter p_m. Thick lines describe stable solutions, thin lines unstable solutions. Upper graph: RMS value of oscillating pressure $p(t)$. Lower graph: frequency of oscillation.

4 CONCLUSIONS AND PERSPECTIVES

Bifurcation diagrams of a basic reed instrument having two quasi-harmonic resonances have been calculated by using a continuation method. The dynamical behaviour has been described as a function of the inharmonicity between the two acoustical resonancies, from perfect harmonicity to an inharmonicity equal to 0.04. The Hopf bifurcations, direct or inverse, are observed, the stability of the branches analysed, and their implication on the playing frequency discussed. Some of the mouth pressure thresholds results are interpreted in terms of the ease of playing of the reed instrument. Because of an inverse Hopf bifurcation (perfect harmonicity) or of a double fold after a direct Hopf bifurcation (moderate inharmonicity), there may be a minimum value $p_m = p_{subthr}$ lower than p_{thr1} where periodic stable oscillations can be observed. This particular value p_{subthr} is a kind of quantitative caracterisation of the ease of playing. It has been shown that the lowest value of p_{subthr} is obtained when the two resonances are perfectly harmonic. It suggests the reed instrument is the easiest to play when the resonances are harmonic. In a way this is a theoretical illustration of the Bouasse-Benade prescription ([Bouasse 1929], [Benade 1990]).

Obviously the results given in the present manuscript are depending on a physical model of reed or brass instruments based on approximations which sometimes can be perceived as basic or even crude. For example the non linear equation describing the entering volume fow has been approximated by its third order Taylor series expansion. Preliminary bifurcations diagrams have been successfully obtained by using the exact non linear equation too. The present study which is a preliminary one, offers many possibilities of complementary works which are in progress: same study with the assumption Z_1 slightly lower than Z_2, dynamics of the reed taken into account, more than two resonances in order to study the brass instruments.

ACKNOWLEDGEMENTS

Authors acknowledge their colleagues Murray Campbell and Jean-Pierre Dalmont for fruitfull scientific discussions.

REFERENCES

[Benade and Gans 1968] A.H. Benade and D.J. Gans, Sound production in wind instruments, Annals of the New York Academy of Science 155, 247-263, 1968.

[Benade 1990] A. H. Benade, *Fundamentals of musical acoustics*, 2nd ed., Dover, 1990.

[Bouasse 1929] H. Bouasse, *Instruments à vent tomes I et II)*, Paris: Delagrave, 1929; repr. Librairie Scientifique et Technique Albert Blanchard, Paris, 1986.

[Campbell and Greated 1987] M. Campbell and C. Greated, *The Musician's Guide to Acoustics*. Oxford University Press 1989.

[Chaigne and Kergomard 2016] A. Chaigne and J. Kergomard, *Acoustics of Musical Instruments*, Springer, 2016.

[Dalmont et al 2000] J-P. Dalmont, J. Gilbert and J. Kergomard, Reed instruments, from small to large amplitude periodic oscillations and the Helmholtz motion analogy, Acustica 86, 671-684, 2000.

[Debut et al 2004] V. Debut and J. Kergomard, Analysis of the self-sustained oscillations of a clarinet as a Van der Pol oscillator, International Congress on Acoustics, Kyoto, 2004.

[Doedel et al 1997] E.J. Doedel, A.R. Champneys, T.F. Fairgrieve, Yu.A. Kuznetsov, B. Sandstede and X.J. Wang, "auto97: Continuation and bifurcation software for ordinary differential equations (with HomCont), User's Guide", Concordia Univ., 1997.

[Fabre et al 2018] B. Fabre, J. Gilbert and A. Hirschberg, *Modeling of Wind Instruments*. Chapter 7 of Springer Handbook of SystematicMusicology, Springer-Verlag, 2018.

[Fletcher and Rossing 1998] N.H. Fletcher and T.D. Rossing, *The Physics of Musical Instruments*, 2nd ed. Springer, 1998.

[Grand et al 1997] N. Grand, J. Gilbert and F. Laloë, Oscillation threshold of woodwind instruments. Acustica 83, 137-151, 1997.

[Hirschberg et al 1995] A. Hirschberg, J. Kergomard, and G. Weinreich, *Mechanics of musical instruments*. Springer-Verlag, Wien, Austria, 1995.

[Karkar et al 2013] S. Karkar, B. Cochelin and C. Vergez, A high-order, purely frequency based harmonic balance formulation for continuation of periodic solutions: The case of non-polynomial nonlinearities, J. Sound Vib. 332, 968-977, 2013.

[Silva et al 2014] F. Silva, C. Vergez, P. Guillemain, J. Kergomard and V. Debut, MoReeSC : a framework for the simulation and analysis of sound production in reed and brass instruments, Acta Acustica united with Acustica, 100, 126–138, 2014.

PROCEEDINGS of ISMA 2019
International Symposium on Music Acoustics

13 - 17 September 2019 in Detmold, Germany

Design of a mechanical player system for fatigue-life evaluation of woodwind reeds

Connor KEMP *, Song WANG, Gary SCAVONE †

Computational Acoustic Modelling Laboratory
Centre for Interdisciplinary Research in Music Media and Technology
Schulich School of Music, McGill University, Canada

Abstract

Research into synthetic replacements for woodwind reeds requires the consideration of several factors. To-date, comparisons between synthetic and natural cane reeds have mostly been limited to evaluations of their initial properties in an "unplayed" state. One important mechanical aspect of reed-life and durability is fatigue behaviour. Fatigue is primarily concerned with the degradation of mechanical stiffness over the lifespan of a reed and is important for understanding changing vibrational behaviour, for comparing differences between cane and synthetic materials, and for evaluating the return on investment for (relatively) expensive synthetic reeds. In this work an artificial player system is developed as the initial phase of a study to evaluate the long-term mechanical behaviour of cane and synthetic alto saxophone reeds. The artificial player will be used to "play" reeds on the system with control over playing time, input pressure and playing frequency. Using this setup, reeds can then be compared via several control parameters, including stiffness, mouthpiece pressure and mouthpiece spectral components during the course of the fatigue study, thus evaluating mechanical degradation rates between cane and synthetic reeds. Results will aid in understanding the importance of playing time and frequency on reed lifespan, fatigue-life differences between cane and synthetic reeds and the average return on investment (ROI) for synthetic reeds.

Keywords: Fatigue, reeds, artificial player

1 INTRODUCTION

Alternative materials to traditional Arundo donax L (cane) used for woodwind reeds are of interest for their reduced variability, reduced sensitivity to environmental conditions and their improved durability. The use of these alternative reeds is also of interest to those studying the performance of woodwind instruments for many of the same advantages mentioned above. For the musician (i.e., the consumer), a more unclear aspect of alternative reeds is the return on investment in terms of durability. Polymeric, composite and other alternative reeds all share a commonality with regards to monetary cost; they are all more expensive than their cane counterpart. Some companies sell their alternative reeds for several hundred dollars and thus it is important for the musician to understand the tangible benefits to such an investment in terms of reed longevity. Previous testing on the degradation of cane reeds has been limited to the isolated effects of moisture cycling [1], some of the chemical changes that occur in played reeds [2] and general measures of radiated sound spectra from a number of synthetic and cane reeds over a five day playing test [3]. The motivation for the present study concerns reed fatigue and the effects of playing on a real instrument with well-controlled and repeatable conditions, as reed fatigue-life and pertinent playing parameters is not well understood. For manufacturers, the degradation of mechanical stiffness and corresponding changes in radiated sound spectra are of particular interest.

The testing of reed longevity is complicated by several factors, including the need for a constant air supply, control over the input 'mouth' pressure, control over an applied lip force and the ability to reliably measure experimental parameters such as reed tip displacement and radiated sound pressure. This manuscript presents findings from an ongoing study investigating alto saxophone reed longevity in terms of fatigue life. Presently, the primary focus is on the experimental testing apparatus (artificial player) including the design of a well-controlled lip force system and an artificial 'mouthbox' through which an air supply system is coupled to a

*connor.kemp@mail.mcgill.ca
†gary.scavone@mcgill.ca

saxophone. Consideration is given to the types of measurements that need to be made for defining the fatigue life of alternative and cane reeds and to system modularity of the artificial player for use with other instruments and experimental tests.

2 EXPERIMENTAL DESIGN

This section provides an overview of the artificial player system design process, manufactured components and system calibrations that were required prior to the testing of reeds. Some details of the mouthbox design are provided to illustrate the design process of such a component when reed fatigue was the primary investigative objective.

2.1 Overall design

The artificial player system developed for fatigue testing here consists of a piston pump (air supply rated at 200 Watts, 13500 LPH flowrate, 47.9 kPa (6.96 psi) maximum gauge pressure), a pressure accumulator (pressure vessel), pressure regulator (manual pressure control), mouthbox assembly (artificial mouth and lip and mouthpiece coupling component) and finally the instrument (alto saxophone). These components are given in order of their placement in the artificial player air supply loop. Details of the mouthbox assembly components are provided in subsequent sections.

2.2 Mouthbox design

It was necessary to outline the main design requirements of the mouthbox component to ensure that investigative objectives (fatigue and aeroacoustic testing) would be fulfilled. The positioning of the mouthpiece in the mouthbox was important in order to provide sufficient space to obtain measures of reed fatigue at the reed tip. The overall volume of the mouthbox was designed with previous measures (between 27.14 and 45.79 cm^3) of average vocal tract volume in mind [4, 5]. This volume ($\approx$30 cm^3) needed to be increased approximately 15% to facilitate a modular mouthpiece coupling device. This device and the overall mouthbox design are shown in Figure 1. An overview of the experimental setup is provided in Figure 2 depicting the entire system in an acoustically isolated listening booth.

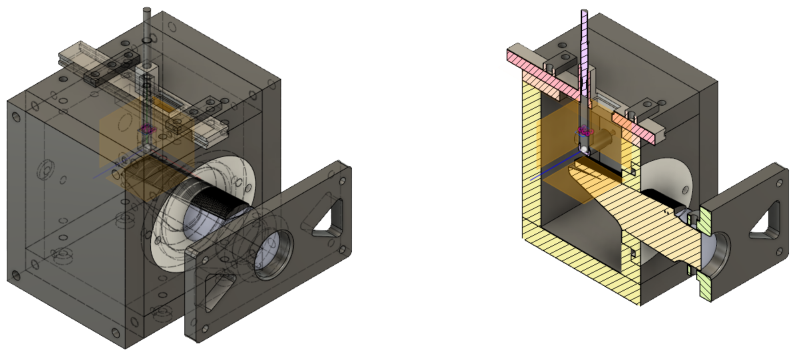

Figure 1. Left: Mouthbox assembly including the mouthpiece, mouthpiece retainer, lip-bar, lip positioning slider and mouthpiece coupling adaptor. Right: The mouthpiece assembly viewed as a cross-section depicting the internal orientation of the lip positioning relative to the mouthpiece.

The mouthpiece coupling adaptor provides flexibility for use of the mouthbox with soprano, alto and tenor saxophones. This modular component also provides sufficient space for the attachment of mouthpiece pressure

Figure 2. The artificial player system setup as will be used for reed fatigue testing in an isolated booth. All major components of the system can be viewed here, apart from the air supply pump that is to the left of the pressure vessel.

transducers and a hotwire probe for mouthpiece baffle flow measurements.

The artificial lip, here termed the “lip-bar", is oriented vertically with respect to the mouthbox and applies a compressive force on the reed. In this configuration, the mouthpiece is attached to the instrument rotated 180° relative to a normal playing condition to expose the reed tip for fatigue related measurements. The lip-bar was designed to allow for manual manipulation of applied lip force in this vertical direction and for control over the horizontal positioning with respect to the mouthpiece (i.e., to modify the vibrating reed tip length). A ≈5mm thick ethylene propylene diene monomer (EPDM) rubber material covers the lip-bar to act as a lip replacement material. Although other materials have been used such as synthetic polyester and polyurethane foam [6, 7], for a fatigue testing scenario, it is important to minimize the effects of creep and stress-relaxation in the lip material. Stress-relaxation in the lip would result in a reduction in applied lip force with time, changing the initial conditions of the experiment. To ensure that fatigue parameters are only reed dependent, EPDM rubber was used as it does not creep significantly with time (i.e., time independent elastic response).

The sliding component of the lip-bar also contains a small plexiglass window positioned directly above the reed tip. This window allows for laser doppler vibrometer (LDV) measurements to be taken while the system is in operation to quantify reed tip displacement. The LDV measures point velocity directly and thus a calibration was required to extract displacement data from the measured signal. Details of this calibration are given in a subsequent section (3).

Previous artificial mouth setups have included a similar artificial lip setup [8] or shaker-style systems linked to the lip [7, 6] in order to investigate the effects of tonguing articulation on several parameters, such as reed displacement, blowing pressure and radiated pressure. The mouthbox design presented above considered aspects of these previous works during iterative design and development, including a controllable lip force component [6], the consideration of lip materials and measurement instruments for reed displacement (i.e, strain gauges) [7]. As fatigue is the primary experimental interest of the present study, this had a significant influence on mouthbox design choices due to a number of complications that would be less critical to previous studies. These complications include air supply temperature fluctuations due to the long-term nature of fatigue experiments and artificial reed bending stiffness changes due to strain gauge placement. Air supply cooling was addressed via pump cooling using passive (heat sinks) and active (forced air) methods. Additional cooling was provided through passive heat dissipation methods in the pressure accumulator component of the supply loop. Strain gauges were not used directly on the reed tip to prevent the gauge and affixing epoxy from influencing long-term stiffness degradation. Another complication of the length of fatigue experiments is the need for humidified air in the case of cane reed testing. An ultrasonic humidification unit could not be added to the air supply stream as back-pressure would prevent the humidified air from mixing with the pressurized supply. Pump longevity concerns prevented the addition of humidified air to the intake side of non-pressurized ambient air. It was therefore decided to use saturated salt solutions (i.e., high purity potassium sulphate) providing passive levels of elevated relative humidity (≈97% between 28 and 38 °C) for the testing of cane reeds [9]. The design of a system to couple this solution to the mouthbox is still in development.

2.3 Fatigue and control parameters

In order to properly compare the fatigue life of alternative and cane reeds it is necessary to calibrate several systems of input parameters such that the initial conditions of each test are the same. This is required to ensure that comparisons between reeds are made using a fair test. Fatigue testing in an engineering sense typically considers the amplitude and rate (frequency) of a cyclic applied stress, and it is important to use this definition as guidance for measuring control parameters [10]. Reeds are mounted on the mouthpiece such that dynamic bending is the primary deformation regime, and in terms of cyclic applied stress reed tip displacement can be used as the stress amplitude component of fatigue life. In order to make fatigue tests comparable between reeds, the present study was designed such that the amplitude of initial reed tip displacement (in bending) was to be used as a control parameter. This displacement can be significant [11] with bending modes generating displacement amplitudes between 150-200% of reed tip thickness. Equal tip displacement is also dependent on the horizontal positioning of the lip mechanism as this controls the effective length of the unsupported vibrating beam (the last ≈5 mm of the reed tip) and this is recorded for each test. It was also desirable to note and record the applied lip force as this parameter required tuning in order to achieve steady-state conditions with the player system, including notes of different frequency and reeds of different strength. Mouthbox and mouthpiece pressure signals were also recorded using two Endevco miniature pressure transducers (mouthbox: 8510B-1 and mouthpiece: 8507C-1) and an Endevco Model 136 DC amplifier.

3 MEASUREMENTS AND CALIBRATIONS

Several mouthbox assembly components required calibration before any real fatigue measurements could be made. This section presents a number of these calibrations with respect to the corresponding mouthbox components.

3.1 LDV reed displacement

A required parameter of reed fatigue characterization is the proper measurements of reed tip displacement. Although a confocal displacement sensor is present in the lab, it cannot fit inside the mouth box. Thus, an LDV was chosen, as its beam can be projected through a plexiglass plate. The LDV was calibrated for displacement measurements for two reasons mentioned here. The LDV exhibits a larger focused "spot" size than the optical sensor reducing its sensitivity to noise. Also, the working distance of the focused beam is substantially larger than the optical sensor and thus it was more suited to mouthbox measurements. LDV measurements were recorded using a Polytec PDV-100 instrument and recorded using a National Instruments USB-4431 signal acquisition board (recorded in MATLAB). For calibration purposes, both velocity and displacement signals were measured simultaneously on a vibrating alto saxophone reed (Légère signature series, 3.25-strength). The displacement signal was measured using a STIL Chromatic Confocal Sensor for non-contact measurements at a sampling rate of 10 kHz. Clamped reed excitation was achieved using a B&K Type 5961 handheld exciter (and stinger) attached to an Agilent 33220A function generator to maintain control over excitation frequency. Measurements of both velocity and displacement were made on opposite sides of the reed and focused ≈5 mm from the tip. A sheet of 4.76 mm (3/16 inch) plexiglass was placed between the incident LDV beam and the reed to simulate the conditions of the mouthbox configuration. Figure 3 presents a sample time-domain signal comparing LDV and optical displacement results.

Overall the integrated LDV signal corresponds well to the independently measured displacement signal.

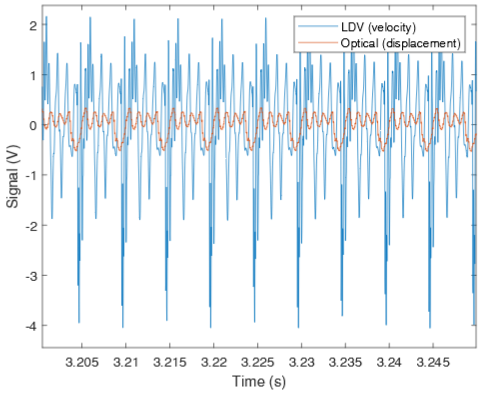

(a) Velocity and displacement signals.

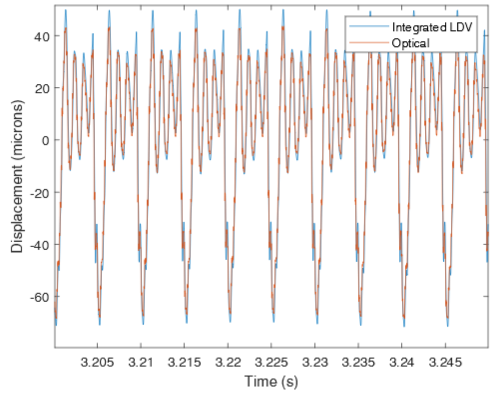

(b) Integrated LDV signal with reed displacement in microns.

Figure 3. Comparison of integrated LDV reed displacement results with those obtained via the optical sensor Note that data was acquired with a reed excitation frequency of 200 Hz and a peak-to-peak amplitude of 5V.

Comparisons between LDV measures with and without the plexiglass plate indicate that the plate does not introduce significant noise related errors to the signal. The LDV signal was conditioned using a lowpass filter with a cutoff within 10% of the reed excitation frequency. The integrated LDV signal was then mapped to known displacement values (in microns, µm) from the optical displacement sensor whereby future measurements using the mouthbox assembly could be made using only the LDV.

3.2 Lip-bar strain gauge calibration

The lip-bar was calibrated using a compression testing configuration by mounting the bar on the mouthbox sliding mechanism and clamping it to a rigid testing fixture (a large steel drill press table). The testing fixture was assumed to exhibit compliance several orders of magnitude lower than the 3D-printed lip-bar and therefore compressive strain during testing originated only in the lip-bar (with no error due to fixture compliance). The measurements were performed over a range of 0 to 3.5 N, similar to previous studies considering applied lip force versus playing frequency [6]. The configuration of the lip-bar and the corresponding calibration data is provided in Figure 4.

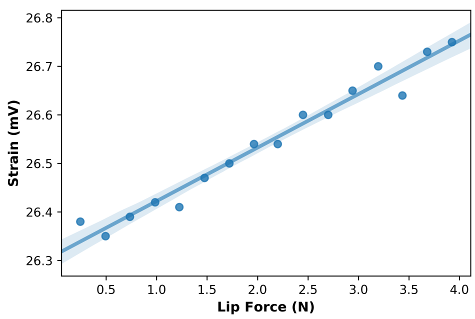

(a) Strain gauge output voltage in response to increasing compressive (vertical) load.

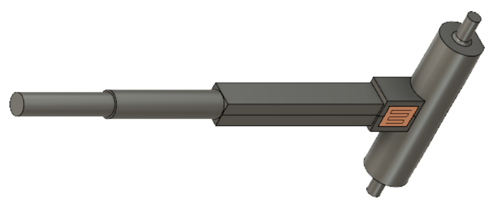

(b) Lip-bar with attached strain gauge.

Figure 4. Overview of the lip-bar and strain gauge calibration results for lip-force with 95% confidence shown.

3.3 Piston-pump pressure pulsation

A piston pump supplies air to the artificial player system and offers a number of advantages over compressed air and blower systems, primarily reduced operational noise, improved pressure head (back-pressure tolerance), airstream temperature uniformity and ease of operation. There is a noted pulsing in the air supply stream generated by the pump due to a 60 Hz pump-rate. These pulses were minimized through the use of the pressure accumulator that produces a volume of air at a static pressure and mitigates the influence of dynamic pressure components to the output. Mouthbox pressure measurements taken with and without the included pressure accumulator confirm this.

3.4 Sample measurements: Pressure, force and displacement

Initial measurements taken on the artificial player system are shown in Figure 5 for an alto saxophone played at ≈330 Hz (alto C#$_5$, concert E). For the Légère reed (strength 3.25) and lip material used, initial reed vibration begins at an input blowing pressure of approximately 2 kPa, although only 'squeaking' is produced at this level.

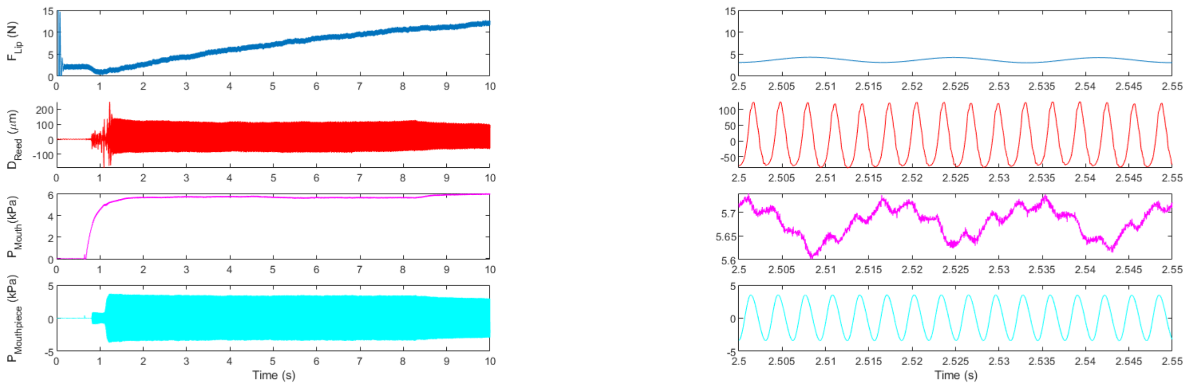

(a) Sample measurement of the four control parameters including the initiation of playing on the artificial player system.

(b) The same four control parameter measurements depicting reed displacment over a 50 ms duration.

Figure 5. An example of initial measurements taken using the artificial player system. These four signals represent the control parameters of interest for fatigue testing.

As blowing pressure increases above 5 kPa, reed oscillations reach a steady-state regime with a peak-to-peak displacement amplitude of 200 μm (a similar amplitude to that measured for a clarinet [11]) and an initial applied lip force of 2 N (compressive). In terms of reed fatigue, displacement amplitudes measured here represent ≈66% of the reed-tip thickness when a symmetrical strain amplitude configuration is considered (i.e., positive and negative direction). Through the cross-section of the tip, reed fatigue contains both compressive and tensile loading senses distributed perpendicularly to the neutral axis of the reed (for this setup considered a cantilever beam). For each cycle of reed vibration at the playing frequency these compressive and tensile strains at the outer tip surfaces represent the maximum and minimum strain amplitudes in a typical fatigue regime. For further long-term tests on reed fatigue life, the displacement amplitude of reed vibration (peak-to-peak) will define the maximum and minimum strain values, and the playing frequency the cyclic loading rate.

4 DISCUSSION

The current state of an artificial player system for the investigation of reed fatigue has been outlined above. The system design is modular and can be used with various sizes of saxophone or clarinet mouthpieces. Though primarily designed for fatigue studies, it can also be used for mouthpiece flow measurements. Many of the constraints that influenced the final mouthbox design were outlined in the context of fatigue experimentation. Calibration of fatigue control parameters was presented and included the use of LDV measurements for reed displacement and strain gauge voltage for applied lip-force.

Some initial fatigue-life control parameter measurements on the artificial player system (Légère signature alto reed, strength 3.25) have been presented in terms of changing mouthbox and mouthpiece pressure, lip-force and reed displacement. It was found that applied lip force increases with a decaying rate during initial playing measurements and this may be the result of viscoelastic effects in the reed-lip assembly and/or thermal drift in the strain gauge. The lip-bar and reed may exhibit a slowly increasing stiffness response with exposure to cyclic strain during an initial phase (during the first few minutes of playing) where viscous forces are not given sufficient time for relaxation, resulting in a temporarily increased effective stiffness. The time frame over which this process occurs will be investigated as the artificial player system is developed further as the influence of this effect on reed-tip displacement is important for quantifying fatigue-life.

There are a number of challenges associated with the evaluation of cane reeds that must be addressed before fair fatigue-life comparisons can be made to alternative reeds. Primarily, the injection of humidified air into the artificial player system requires careful consideration of pressure, air temperature and humidification source. The pressurized air delivered by the pump must be kept at constant temperature over the duration of the fatigue experiment (between 4 and 24 hours) such that fluctuations in temperature are minimized. Otherwise, measured pressure results may be difficult to compare between samples, and humidity levels may drift as the moisture capacity of air changes.

5 ONGOING AND FUTURE WORK

The design of an artificial player system for the fatigue testing of alternate (synthetic) and cane reeds has been considered in the context of control parameter measurements, measurement techniques, calibrations and initial system measurements. Some of the practical problems associated with fatigue experiments lasting over 12 hours have been discussed including air supply temperature, air supply humidity (for cane reeds) and lip-bar (and material) viscoelastic and creep effects. Continuing work on this project will include the design of a humidity chamber for attachment to the mouthbox assembly such that elevated levels of relative humidity (˜98%) could be maintained for the testing of cane reeds in a moist state. Complete simulation of playing conditions for cane reeds is challenging as the reed-tip is nearly saturated during playing, however very high values of relative humidity have been shown to swell and saturate the pores of natural Arundo donax L material [12] providing similar moisture conditions to playing. The results of fatigue testing will include the comparison of synthetic and cane reed performance using the control parameters mentioned (tip displacement, input blowing pressure, mouthpiece pressure) and a number of other measurements that manufacturers are interested in (namely radiated sound pressure level and spectral components). These results will be used to evaluate the ROI of synthetic reeds, average reed lifespan for a given playing frequency, decay rates of reed stiffness and changes in timbre more generally (via saxophone radiated sound measurements).

ACKNOWLEDGEMENTS

The authors would like to acknowledge Légère Reeds Ltd. for their help with experimental design, fatigue control decisions and the supply of reeds for testing. Financial aid from an NSERC Engage Industrial grant is also acknowledged, as well as CIRMMT for travel funding.

REFERENCES

[1] Hikaru Akahoshi and Eiichi Obataya. Effects of wet–dry cycling on the mechanical properties of arundo donax l. used for the vibrating reed in woodwind instruments. *Wood Science and Technology*, 49(6):1171–1183, November 2015. ISSN 0043-7719, 1432-5225. doi: 10.1007/s00226-015-0760-6. URL https:

//link.springer.com/article/10.1007/s00226-015-0760-6.

[2] Donald Jay Casadonte. *The clarinet reed: an introduction to its biology, chemistry, and physics*. PhD thesis, The Ohio State University, 1995. URL http://rave.ohiolink.edu/etdc/view?acc_num=osu1487929230741742.

[3] Aaron Mulder. *A Comparison of Cane and Synthetic Reeds for Student Musicians*. Master of Music Education, VanderCook College of Music, 2015. URL https://www.researchgate.net/publication/299457478_A_Comparison_of_Cane_and_Synthetic_Reeds_for_Student_Musicians.

[4] Brad H. Story, Ingo R. Titze, and Eric A. Hoffman. Vocal tract area functions from magnetic resonance imaging. *The Journal of the Acoustical Society of America*, 100(1):537–554, July 1996. ISSN 0001-4966. doi: 10.1121/1.415960. URL https://asa.scitation.org/doi/10.1121/1.415960.

[5] Baptiste Bergeot, André Almeida, Bruno Gazengel, Christophe Vergez, and Didier Ferrand. Response of an artificially blown clarinet to different blowing pressure profiles. *The Journal of the Acoustical Society of America*, 135(1):479–490, January 2014. ISSN 0001-4966. doi: 10.1121/1.4835755. URL https://asa.scitation.org/doi/10.1121/1.4835755.

[6] Weicong Li, André Almeida, John Smith, and Joe Wolfe. The effect of blowing pressure, lip force and tonguing on transients: A study using a clarinet-playing machine. *The Journal of the Acoustical Society of America*, 140(2):1089–1100, August 2016. ISSN 0001-4966. doi: 10.1121/1.4960594. URL https://asa.scitation.org/doi/abs/10.1121/1.4960594.

[7] Vasileios Chatziioannou, Alex Hofmann, and Montserrat Pàmies-Vilà. An artificial blowing machine to investigate single-reed woodwind instruments under controlled articulation conditions. *Proceedings of Meetings on Acoustics*, 31(1):035003, December 2017. doi: 10.1121/2.0000794. URL https://asa.scitation.org/doi/10.1121/2.0000794.

[8] Jean-Pierre Dalmont, Joël Gilbert, and Sébastien Ollivier. Nonlinear characteristics of single-reed instruments: Quasistatic volume flow and reed opening measurements. *The Journal of the Acoustical Society of America*, 114(4):2253–2262, October 2003. ISSN 0001-4966. doi: 10.1121/1.1603235. URL https://asa.scitation.org/doi/10.1121/1.1603235.

[9] Arnold Wexler and Saburo Hasegawa. Relative Humidity-Temperature Relationships of Some Saturated Salt Solutions in the Temperature Range 0 to 50c. *Journal of Research of the National Bureau of Standards*, 53 (1):19–26, July 1954. URL https://nvlpubs.nist.gov/nistpubs/jres/53/jresv53n1p19_a1b.pdf.

[10] Yung-Li Lee and Darryl Taylor. 4 - Stress-Based Fatigue Analysis and Design. In Yung-Li Lee, Jwo Pan, Richard B. Hathaway, and Mark E. Barkey, editors, *Fatigue Testing and Analysis*, pages 103–180. Butterworth-Heinemann, Burlington, January 2005. ISBN 978-0-7506-7719-6. doi: 10.1016/B978-075067719-6/50005-1. URL http://www.sciencedirect.com/science/article/pii/B9780750677196500051.

[11] P. Picart, J. Leval, F. Piquet, J. P. Boileau, T. Guimezanes, and J. P. Dalmont. Study of the Mechanical Behaviour of a Clarinet Reed Under Forced and Auto-oscillations With Digital Fresnel Holography. *Strain*, 46(1):89–100, 2010. ISSN 1475-1305. doi: 10.1111/j.1475-1305.2008.00593.x. URL http://onlinelibrary.wiley.com/doi/10.1111/j.1475-1305.2008.00593.x/abstract.

[12] Connor Kemp. *Characterisation of woodwind instrument reed (Arundo donax L) degradation and mechanical behaviour*. PhD thesis, McGill University, Montreal, 2019.

PROCEEDINGS of ISMA 2019
International Symposium on Music Acoustics

13 - 17 September 2019 in Detmold, Germany

The player-reed interaction during note transitions in the clarinet

Montserrat PÀMIES-VILÀ[(1)]*, Alex HOFMANN[(1)], Vasileios CHATZIIOANNOU[(1)]

[(1)]Department of Music Acoustics, University of Music and Performing Arts Vienna, Austria

Abstract

When playing woodwind instruments, most of the player's control over the instrument takes place inside the player's mouth. Blowing pressure, tonguing strategies, embouchure and vocal tract configuration are modified during playing to perform expressively. Aiming at analysing the player's actions at the note transitions, an experiment with eleven clarinet players was carried out. The mouth pressure, the mouthpiece pressure and the reed oscillation were recorded in order to track blowing and tonguing actions and to identify vocal tract adjustments. The paper shows that the players adapt tonguing and blowing actions according to the dynamics and to the articulation style (legato, staccato). Similar patterns in the blowing technique are observed among most of the players, and some particular effects are described. The attack and the release transients are found to vary with blowing pressure. Moreover the release transients depend on the tonguing technique used to play articulation.

Keywords: Clarinet acoustics, Articulation, Performance analysis

1 INTRODUCTION

Single-reed woodwinds are the wind instruments in which the vibration of a single reed coupled to the resonance of an air column in a tube is responsible for the sound production; this includes the clarinet and saxophone families. The bore is the primary (linear) resonator of the instrument, where an air volume oscillates and radiates sound [6]. The tube's geometry determines the acoustic impedance of the instrument, thus allowing certain tones at the extended register, achieved when actuating a register key and/or by overblowing. The excitation mechanism (reed and mouthpiece) is a highly nonlinear element controlling the air flow into the instrument. The reed deflects against the mouthpiece, influenced by both the upstream (the player's respiratory system) and downstream (the resonator) air columns. The lower lip of the player (position and force) determines the vibrating length and the equilibrium position of the reed. Pressure-flow control at the player's mouth together with standing waves in the resonator lead to sustained oscillations of the reed [6].

In the view of this general description, one can discern several actions of the player's control over the instrument. Globally there are two locations where the sound can be modified: at the bore and at the mouthpiece. At the bore, the fingers control the pitch of the played tones, through tone holes and a set of keys [8]. Intonation issues and extended techniques (multiphonics, key slaps, rattles and other effects) might require particular finger manipulations [14]. At the mouthpiece, where most of the player's control in a wind instrument takes part, the blowing action, the embouchure (lips and jaws), the tongue-reed interaction and the vocal tract configuration combine efforts to create and modify sounds (Figure 1-left).

The first woodwind models and experimental setups considered only a part of this player-instrument interaction, namely the blowing action and the lip force. With this simplified player-control representation, reasonably accurate physical models and artificial-blowing setups were generated. Generally, the reed-mouthpiece behaviour is described in terms of mouth-to-mouthpiece pressure difference, reed opening and volume flow [5], with the lip force determining the equilibrium position of the reed oscillation. Recently, there have been two parallel lines of study to analyse the player-instrument interaction in single-reed woodwinds: determining the effect of the player's vocal tract on the produced sound [e.g. 15, 4, 13] and analysing the player's articulatory actions in different playing techniques [e.g. 1, 9, 12]. The latter is motivated by a need to characterise the transient phenomena that arise at the attack and release of tones, and has led to the first physical models of single-reed woodwinds with tongue-reed interaction [3].

In the current paper, we present some examples of the player-reed interaction taking place in the clarinettists'

*pamies-vila@mdw.ac.at

mouth that have been found after analysing the playing technique of 11 clarinet players. In a previous study, an exercise combining articulation techniques was analysed [12], and the relationship between blowing and tonguing techniques and the characteristics of transients was established. Motivated by the fact that a music exercise might provide less realistic music experience than a real clarinet piece, in the present analysis, some excerpts from a clarinet concerto are explored, in search for articulatory patterns leading to a significant modification at the transients between tones.

2 METHODOLOGY

2.1 Experimental setup

To analyse the player-instrument interaction in the mouth of clarinet players, an experimental setup is prepared. A Maxton NA-1 mouthpiece is mounted on a German B♭ clarinet (Thomann GCL-416 Synthetic Line) and equipped with sensors as follows (Figure 1). The mouth and the mouthpiece acoustic pressures are measured with two pressure transducers (Endevco 8507C-2; with Endevco model 136 amplifier). One transducer is attached to the side of the mouthpiece next to the reed, so that it reaches the player's mouth during playing. Another pressure transducer is inserted through a drilled hole into the mouthpiece.

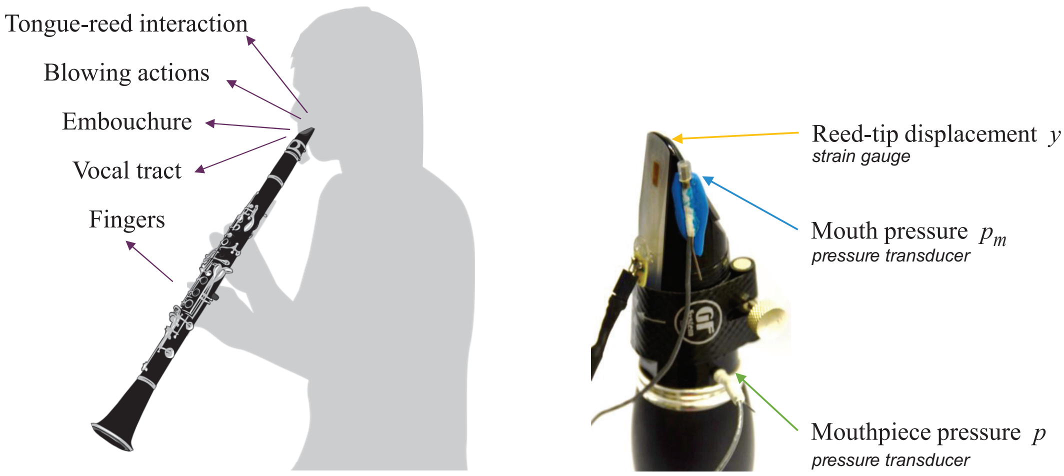

Figure 1. Left: Scheme of the main components of the player's control over the clarinet. Right: Experimental equipment on a German B♭-clarinet mouthpiece: pressure transducers for mouth and mouthpiece pressure measurements and strain-gauge on a synthetic reed to track the reed-tip displacement.

The tongue-reed interaction is tracked with a stain gauge on a reed (strength 2.5, German cut, by Légère) [7]. This sensor measures the deformation at the surface of the synthetic reed: when the reed vibrates, this sensor gives a voltage proportional to the tip-reed opening [11]. When the tongue contacts the reed, the sensor detects a lack of oscillation, thus giving the instances of tongue-reed contact and tongue-reed release with an accuracy of a few periods. Finally, the external sound is recorded with a microphone (d:vote 4099U, by DPA) mounted on the instrument. All signals are simultaneously recorded at 50000 Hz using a digital acquisition platform (NI 9220, by National Instruments).

2.2 Experimental design

Eleven clarinet players were invited to the music acoustics laboratory of the University of Music and Performing Arts Vienna and were asked to play articulation-related exercises and some music excerpts. Among the clarinettists there were 9 advanced students from the University and 2 professional players. For the current study, three excerpts showing a variety of articulation and dynamics were selected from the Clarinet Concerto n. 2 by Carl Maria von Weber (see an excerpt in Figure 2), a common clarinet solo part that was known by all participants.

Figure 2. Two measures from an excerpt selected from the Clarinet Concerto n. 2 by Carl Maria von Weber (Op. 74).

All participants performed on the same sensor-equipped clarinet. They were given about 10 minutes to familiarise themselves with the setup before the actual recording began. At the beginning of the recording of the excerpts, the players were given a tempo indication through a metronome-click at 108 bpm. The metronome was then turned off, in order to achieve more realistic concerto-playing conditions. Many players maintained the given tempo during performance (players 1, 5, 7, 9 and 10). Players 2, 3, 4 and 11 performed faster (about 120 bpm) and players 6 (102 bpm) and 8 (98 bpm) performed slower.

At the beginning of every experimental session, the participants were informed about the experimental procedure. Following the experimental protocol approved by the Ethics Committee of the University, the participants allowed anonymous usage of their data and gave written consent of their voluntary participation in the experiment, for which they received a nominal fee. Every session lasted for about 40 minutes to one hour. At the end of the session, the participants filled an anonymous form in which they were asked about their playing technique and music practice habits, as well as about their impressions during the experiment.

2.3 Signal conditioning and parameter extraction

The strain-gauge signal is calibrated to obtain the reed-tip displacement y during oscillation (see botom of Figure 3), as detailed in [11]. The displacement values given during tongue-reed contact are for indicative purposes only, since the deformation of the reed in presence of the tongue does not follow the same calibration curve. The mouth and mouthpiece pressure measurements are calibrated according to the manufacturer. These pressure transducers can measure both DC and AC values. In the mouthpiece, only an AC value is present (mouthpiece pressure p, in green in Figure 3), because the tube is open to the surrounding air. In the mouth, both DC and AC values are measured: the DC being related to the blowing actions (blowing pressure $\hat{p}_{\mathrm{b}}$; dashed line on top of Figure 3) and the AC to the resonance in the vocal tract (dynamic mouth pressure p_{m}; pale-blue in Figure 3). To obtain the blowing pressure $\hat{p}_{\mathrm{b}}$ (DC), a moving-average filter is used to low-pass filter the measured signal (using 6.8 ms time-windows). Then, the dynamic mouth pressure p_{m} (AC) is obtained by subtracting the blowing pressure $\hat{p}_{\mathrm{b}}$ from the measured signal.

The tongue-reed interaction is analysed in terms of the instances of tongue-reed contact and tongue-reed release, and the duration of the tongue-reed contact. To detect the instances of tongue-reed contact and release, the low-pass filtered strain-gauge signal is computed (solid line in the bottom of Figure 3). The tongue-reed contact instant is established as the maximum of its derivative (vertical solid lines in Figure 3), i.e. the instant when the reed displacement moves the fastest while closing against the mouthpiece lay. The tongue-reed release instant is found at the first zero crossing of the derivative after a minimum, i.e. the instant when the reed is back to the equilibrium position (vertical dashed lines in Figure 3). The tongue-reed contact duration T_{c} is obtained as the difference between these two instances.

The interaction between the player's mouth resonance (vocal tract resonance) and the reed can be assessed in terms of an energy comparison between the dynamic mouth pressure and the mouthpiece pressure, as in [13], for example by comparing the root-mean-square (RMS) of both signals. The vocal tract is able to drive the reed vibration [15, 4] when the energy of the vocal tract oscillation is comparable to the energy at the mouthpiece.

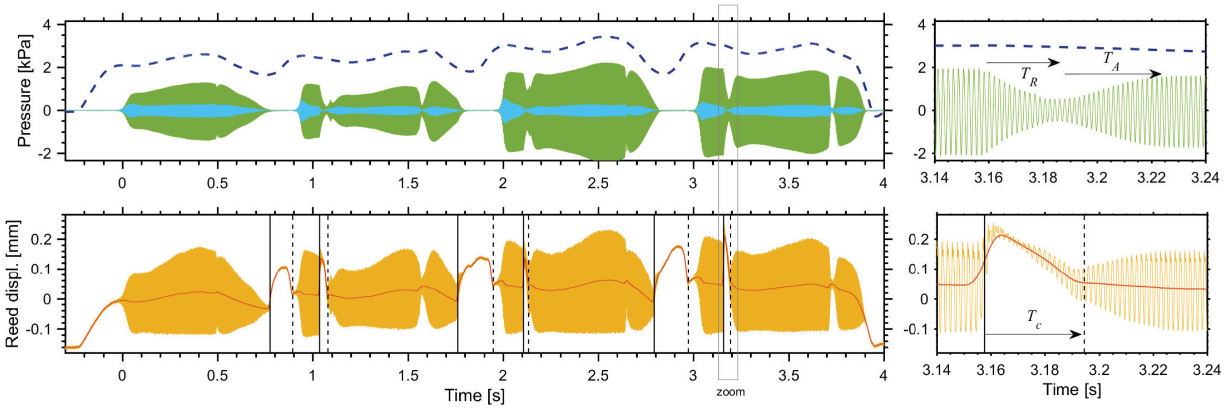

Figure 3. Signals measured for two measures of the performed Clarinet Concerto (music in Figure 2): blowing pressure, mouthpiece pressure, dynamic mouth pressure, reed displacement and low-pass-filtered reed displacement. Vertical lines indicate the tongue-reed contact (solid: instant of contact, dashed: instant of release). In the zoomed-in view (n. 2 in Figure 2), T_A and T_R indicate the duration of the attack and release transients and T_c indicates the tongue-reed-contact duration. Player 10.

In some advanced techniques, like playing a pitch bending, the mouth-pressure RMS might be much higher than the mouthpiece-pressure RMS [13].

Both the articulation technique and the blowing pressure affect the duration of the transients of the tones and the spectral content at the transients [12]. The transients are located at the part of a signal where the oscillations increase in amplitude (attack transient) or decrease in amplitude (release transient). The mouthpiece pressure is often considered to determine the duration of these transients (as indicated with T_A and T_R in Figure 3); also the external sound or the reed oscillation can also be used for that purpose. The duration of the transients is obtained by considering the instances where the envelope of the signal is at 5% and at 95% of its maximum at the attack transient and the analogous values for the release transient.

3 RESULTS

The players use blowing and tonguing strategies to regulate the dynamics of the music (piano, forte...), to obtain articulation techniques (legato, portato, staccato, accents...), and to start and stop tones. In [12] the authors analysed the same participants when playing a given exercise and observed the coordination of blowing pressure and tongue actions to stop the tones. When looking into the Concerto played for this study, some of the previous observations are consistent and new effects are found, because of the wider pitch range of the concerto compared to the exercise, and the broader variety of rhythm, tempo and dynamics.

3.1 Common blowing and tonguing strategies

Most of the players use a similar blowing-pressure pattern during playing. The blowing pressure is used to obtain the dynamics (piano, forte) written in the music and to regulate the dynamics within a passage. An example is shown on the top of Figure 4, where nine players are compared (two players are omitted in this comparison because they performed significantly slower). All players use a progressively increasing blowing pressure up until $t = 2.5$ s. The signals are synchronised so that $t = 0$ s corresponds to the beginning of the first attack transient (measured at the reed displacement). At this instant, the threshold of oscillation of the reed can be obtained: the blowing pressure values at $t = 0$ s (dashed lines at the top plots) show consistency among players (2-2.5 kPa); the small variability is introduced by each player's different embouchure settings, changing the effective reed stiffness.

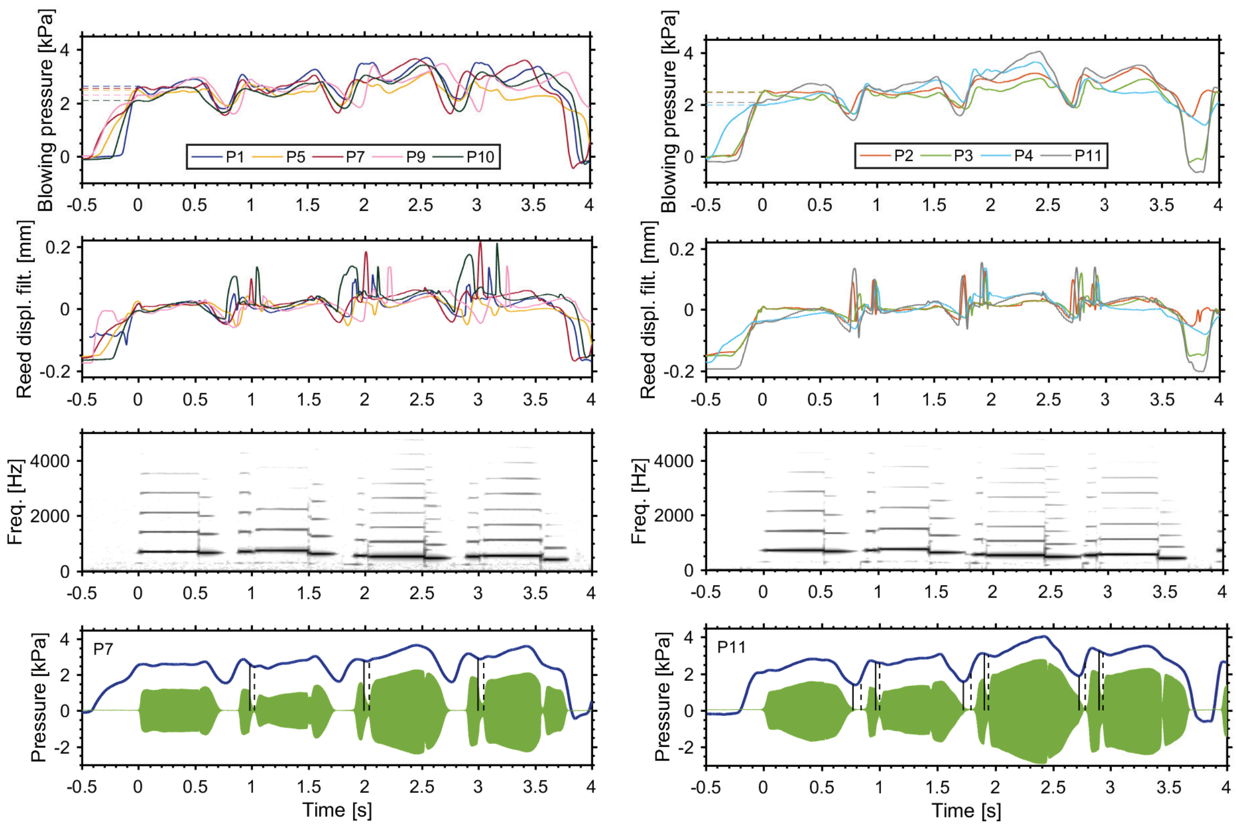

Figure 4. Blowing pressure and low-pass-filtered reed displacement compared among players (music in Figure 2). Right and left plots group the players with similar tempo. On the top plot, dashed lines indicate the blowing pressure at the beginning of the first attack transient. On the reed-displacement signal, the spikes show the tongue-reed contact. Mouthpiece-pressure spectrograms are plotted for player 7 (left) and player 11 (right). At the bottom, blowing pressure (blue) and mouthpiece pressure (green) with indication of tongue-reed contact (solid: instant of contact, dashed: instant of release) are plotted for these two players.

In Figure 4, the reed low-pass-filtered displacement (i.e. the reed averaged motion due to the changes in blowing pressure and tongue-reed contact) is plotted in comparison among players. In this signal, the spikes correspond to tongue-to-reed contact, when the reed rapidly closes against the mouthpiece. As observed before $t = 0$ s, most of the players did not use a tongue contact before the first tone onset (except for player 9). When playing legato ($t = 0.5$, 2.5 and 3.5 s) the players do not provide any tongue-reed contact.

Players combine blowing and tonguing strategies to stop and initialise tones [12]. Although there is no written pause in the music, players sometimes stop the sound with a decrease in the blowing pressure (as at $t = 0.7$ s in Figure 3 and 4). However, if the articulation must be fast (as in the staccato tones, at $t = 1$, 2 and 3 s), the reed vibration must be stopped with a tongue contact. For the selected passage, the 3 staccato-articulated tones (see * in Figure 2) are usually performed with 6 tongue strikes, right before and after every tone, as it appears very clear on the right of Figure 4. On the left, however, there is more variability in the tonguing technique, as some players only tongue at the end of the staccato tone but not at the beginning.

At the bottom of Figure 4, two players are compared. For this particular passage, no difference is found in the attack transient regarding whether they use the tongue before the staccato tone (player 11) or not (player 7).

The attack transients are similar in length (about $T_A = 30$ ms) and in spectral content in both cases. Player 11 uses the tongue to prepare the staccato tones, but this tongue-reed contact happens when the previous tone has already decayed (i.e. it is not used to stop the previous tone).

3.2 Other observations

It has been observed that many patterns can be identified in the performing style of all of the participants, however some particular effects are present in a few of them.

An exception of the observed blowing-tonguing coordination to play staccato tones is found in player 6. As shown in Figure 5, this player maintains a high blowing pressure during the whole passage, and stops the tones with a tongue contact. This results in a faster release transient previous to the tonguing ($T_R = 50$ ms), compared to players 7 and 11 (about $T_R = 100$ ms). Moreover as the previous tone is sustained, all the harmonics are present until the tongue-contact happens, and they decay simultaneously at the release transient (at $t = 1$, 2.1 and 3.2 s in Figure 5-right). Instead, in players 7 and 11 the harmonics decay progressively from high to low pitch (at $t = 0.7$, 1.7 and 2.7 s in Figure 4). Also when the blowing pressure is maintained high (player 6), the attack transient of the staccato tone raises faster in amplitude ($T_A = 25$ ms) and in harmonic content, than in the cases when it raises to create the next tone (players 7 and 11).

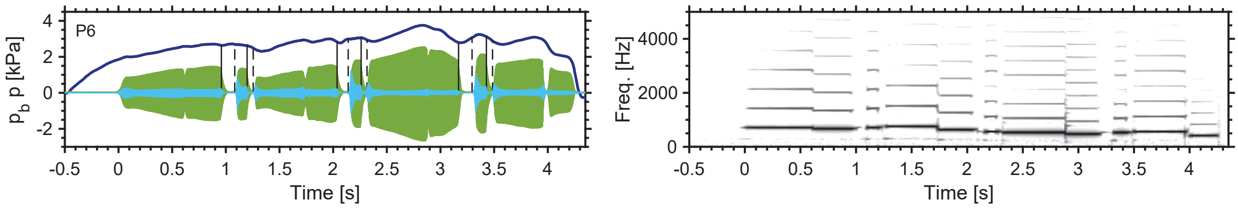

Figure 5. Left: Blowing pressure (blue), mouthpiece pressure (green) and dynamic mouth pressure (pale-blue) with indication of tongue-reed contact (solid: instant of contact, dashed: instant of release). Right: Mouthpiece-pressure spectrogram. Player 6.

Player 5 (orange in Figure 4-left) shows a blowing-pressure pattern similar to other players. However, the reed signal does not show spikes at the staccato articulation. This is because, for this particular clarinettist, the tongue-reed interaction happens much lower on the reed vibrating area than for the other participants, working in collaboration with the damping introduced by the lower lip (according to the description given by the player). Because the blowing pressure for Player 5 is similar with other players, the attack and release transients are also comparable.

A peculiar effect happens at the last note transition of the example passage (n. 2 in Figure 2). This note transition is written to be played in legato articulation, thus players show no tongue-reed contact ($t = 3.6$ s in Figure 3 and 4). However, the mouthpiece pressure presents a release and attack transient that would be assessed as portato articulation (with tongue) rather than legato articulation. The reason for this effect is that the note transition happens between two notes at different registers. Players might achieve a softer transition by adjusting their vocal tract, as observed in the saxophone [13]. In Figure 5, there is a significant increase in the resonance of the oral cavity at the end of the first tone (see pale-blue signal at $t = 3.9$ s); suggesting that the player might support the note transition with vocal tract tuning.

4 FINAL REMARKS

An experimental setup to analyse blowing and tonguing techniques during clarinet performance has been used to determine their effect on the note transitions when playing a Clarinet Concerto. An excerpt from the Clarinet Concerto n. 2 by Carl Maria von Weber has been used to illustrate such effects. The results are in accordance to the observations made when considering a predefined exercise [12]. As rhythm, dynamics and articulation vary during performance, players use a combination of blowing and tonguing techniques to perform expressively.

In the view of the presented observations, we can conclude that a tongue strike on the reed previous to a staccato tone does not seem to have an effect on the attack transient of the tone to be played, if the blowing pressure has been released. As suggested in [12], the attack transients are mainly affected by the blowing pressure. However, a tongue-reed contact before the staccato tones does have a prominent effect on the release transient of the previous tone if the blowing pressure is maintained high. Also a slight effect on the attack transient of the following tone has been observed: the attack transients are shorter when the blowing pressure is maintained at a high level during playing.

A similar methodology, based on mouth and mouthpiece pressure and reed bending measurements, has been used to study articulation in other woodwinds instruments [8, 10]. And it has also been used to provide reference signals to implement inverse modelling of clarinet sounds including tongue articulation [2]. Both the music acoustics and the music education fields could benefit from such a methodology to observe and describe the phenomena taking place during articulation in clarinet and saxophone performance.

ACKNOWLEDGEMENTS

The authors would like to acknowledge the clarinet players for their participation. This research was supported by the Austrian Science Fund (FWF): P28655-N32.

REFERENCES

[1] V. Chatziioannou and A. Hofmann. Physics-based analysis of articulatory player actions in single-reed woodwind instruments. *Acta Acustica united with Acustica*, 101(2):292–299, 2015.

[2] V. Chatziioannou, S. Schmutzhard, A. Hofmann, and M. Pàmies-Vilà. Inverse modelling of clarinet performance. In *Proc. Int. Congress on Sound and Vibration*, Montreal, Canada, 2019.

[3] V. Chatziioannou, S. Schmutzhard, M. Pàmies-Vilà, and A. Hofmann. Investigating clarinet articulation using a physical model and an artificial blowing machine. *Acta Acustica united with Acustica*, 2019.

[4] J.-M. Chen, J. Smith, and J. Wolfe. Saxophonists tune vocal tract resonances in advanced performance techniques. *J. Acoust. Soc. Am.*, 129(1):415–426, 2011.

[5] J.-P. Dalmont, J. Gilbert, and S. Ollivier. Nonlinear characteristics of single-reed instruments: Quasistatic volume flow and reed opening measurements. *J. Acoust. Soc. Am.*, 114(4):2253–2262, 2003.

[6] N. H. Fletcher. Air flow and sound generation in musical wind instruments. *Annual Review of Fluid Mechanics*, 11(1):123–146, 1979.

[7] A. Hofmann, V. Chatziioannou, M. Weilguni, W. Goebl, and W. Kausel. Measurement setup for articulatory transient differences in woodwind performance. In *Proc. Meetings on Acoustics*, Montreal, Canada, 2013.

[8] A. Hofmann and W. Goebl. Finger forces in clarinet playing. *Frontiers in psychology*, 7:1140, 2016.

[9] W. Li, A. Almeida, J. Smith, and J. Wolfe. How clarinettists articulate: The effect of blowing pressure and tonguing on initial and final transients. *J. Acoust. Soc. Am.*, 139(2):825–838, 2016.

[10] P. Mallinger, M. Pàmies-Vilà, V. Chatziioannou, and A. Hofmann. Analysis of reed vibration and mouthpiece pressure in contemporary bass clarinet playing techniques. In *Proc. Int. Symp. Musical Acoustics*, Detmold, Germany, 2019.

[11] M. Pàmies-Vilà, A. Hofmann, and V. Chatziioannou. Strain to displacement calibration of single-reeds using a high-speed camera. In *Proc. Int. Symp. Musical Acoustics*, pages 5–8, Montreal, Canada, 2017.

[12] M. Pàmies-Vilà, A. Hofmann, and V. Chatziioannou. Analysis of tonguing and blowing actions during clarinet performance. *Frontiers in Psychology*, 9:617, 2018.

[13] M. Pàmies-Vilà, G. Scavone, A. Hofmann, and V. Chatziioannou. Investigating vocal tract modifications during saxophone performance. In *Proc. of Meetings on Acoustics*, volume 31, page 035002, 2017.

[14] P. Rehfeldt. *New directions for clarinet*, volume 4. Rev. ed., reissued. Scarecrow Press, 2003.

[15] G. P. Scavone, A. Lefebvre, and A. R. da Silva. Measurement of vocal-tract influence during saxophone performance. *J. Acoust. Soc. Am.*, 123(4):2391–2400, 2008.

PROCEEDINGS of ISMA 2019
International Symposium on Music Acoustics

13 - 17 September 2019 in Detmold, Germany

Clarinet tonguing: the mechanism for transient production

André ALMEIDA[1]; Weicong LI[1]; Lauren INWOOD[1]; John SMITH[1]; Joe WOLFE[1]

[1] School of Physics, UNSW Sydney, Australia

Abstract

Players coordinate tongue release and variation in blowing pressure to produce a range of desired initial transients, *e.g.* for accents and *sforzando*, players use higher pressures at release to give higher rise rates in the exponential stage. The mechanisms were studied with high-speed video and acoustic measurements on human and artificial players of clarinets and simpler models. The initial mechanical energy of the reed due to deformation and release by the tongue is quickly lost in damping by the lip. The varying aperture as the reed moves towards equilibrium produces proportional variations in flow and pressure via a mechanism resembling the water hammer in hydraulics. Superposition of this signal with returning reflections from the bore give complicated wave shapes with variable harmonic content. When the reed gain more than compensates losses, a stage of nearly exponential increase follows until the last few oscillations before saturation. Maximal exponential decay rates (in tongue-stopped *staccato* notes) agree with losses measured in the bore impedance spectrum. Including estimates of the negative reed resistance explains semi-quantitatively the rise rates for initial transients. Different rates for higher harmonics contribute to different wave shapes and spectral envelopes, which are illustrated and modelled here.

Keywords: Clarinet, Transients, Tonguing

1 INTRODUCTION

The initial transients of wind instrument notes have a rapidly varying waveform amplitude. Further, their frequency components—harmonic, nearly harmonic, inharmonic and broadband—grow at different rates, which gives the transient a complicated, time-varying spectrum. So it is not surprising that wind instrument transients are associated with highly salient dimensions of timbre and are important in distinguishing instruments [1,2].

Initial and final transients and other aspects of articulation are judged by musicians to be important in expressive and tasteful performance and are consequently much discussed by teachers. To start a single note or phrase on a clarinet, pedagogues typically advise that the tongue tip should touch and quickly release the reed, as though pronouncing 'te' or some similar syllable.

A tongued initial transient has three stages. In the first stage, which lasts ~several ms, the tongue and the consequent reed motion vary the aperture, admitting varying flow and thus varying the mouthpiece pressure. This provides the initial amplitude for a second stage, lasting ~10 ms. This stage has approximately exponential growth, and usually begins roughly when the first reflected wave returns from the bore. Stages 1 and 2 are seen in Fig 2. In the third stage, seen in Figs 3 and 5-7, the sound pressure amplitude in the mouthpiece becomes comparable with the blowing pressure. In this stage, the non-linear pressure-flow relation has effects including a fall in the rate of increase of the amplitude of the fundamental and mode-locking of partials. These lead to an exactly harmonic spectrum, with amplitude clipping producing a rapid increase rate for some harmonics.

The blowing pressure usually increases during the attack. The blowing pressure, lip forces and reed and mouthpiece properties together determine a gain for the reed. This competes with losses in the bore and mouth and (smaller) losses to radiation; this competition determines the exponential rise rates for the spectral components, which have typical values of hundreds to thousands of $\mathrm{dB.s^{-1}}$.

The combinations of different shapes and characteristic times of stage-1 reed motion with different periods of standing waves in the bore lead to a wide variety of different initial waveforms and spectra and therefore, with different exponential rise rates for each component, to a very wide range of different possible transients. The control parameters mentioned above are under the musician's control, and thus can contribute to a player's range of expressive articulations.

The steady part of a clarinet note has been well studied [*e.g.* 3-6]. Studies of transients between successive notes

[1] a.almeida@unsw.edu.au, weicongli@outlook.com, Lauren.Inwood2@det.nsw.edu.au, john.smith@unsw.edu.au, j.wolfe@unsw.edu.au

on wind instruments have been reported elsewhere [*e.g*. 7-10].
This paper first reviews our recent work on tonguing and transients, some involving human players [11-13] and some using a simplified clarinet playing system with mechanical tongue and independently controlled parameters [14,15]. It then presents simple models for transients illustrating some of the complications mentioned above and compares these with reanalysis of the measurements.

2 EXPERIMENTS ON PLAYERS

Figure 1 is a schematic for the experimental setup used by Li *et al.* [11] and Inwood *et al*. [12]. Sensors are attached to a Yamaha YCL 250 clarinet with a Yamaha CL-4C mouthpiece and a Légère synthetic clarinet reed (hardness 3). This is a Bb clarinet, and the written pitch is reported, *e.g*., written C5 sounds Bb4.

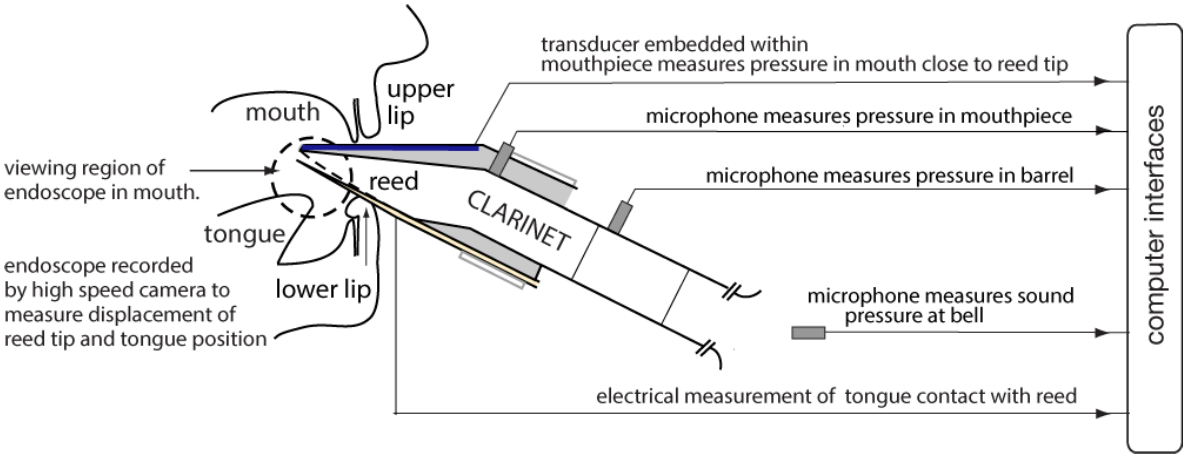

Figure 1 – A schematic of the experimental apparatus for measuring human players.

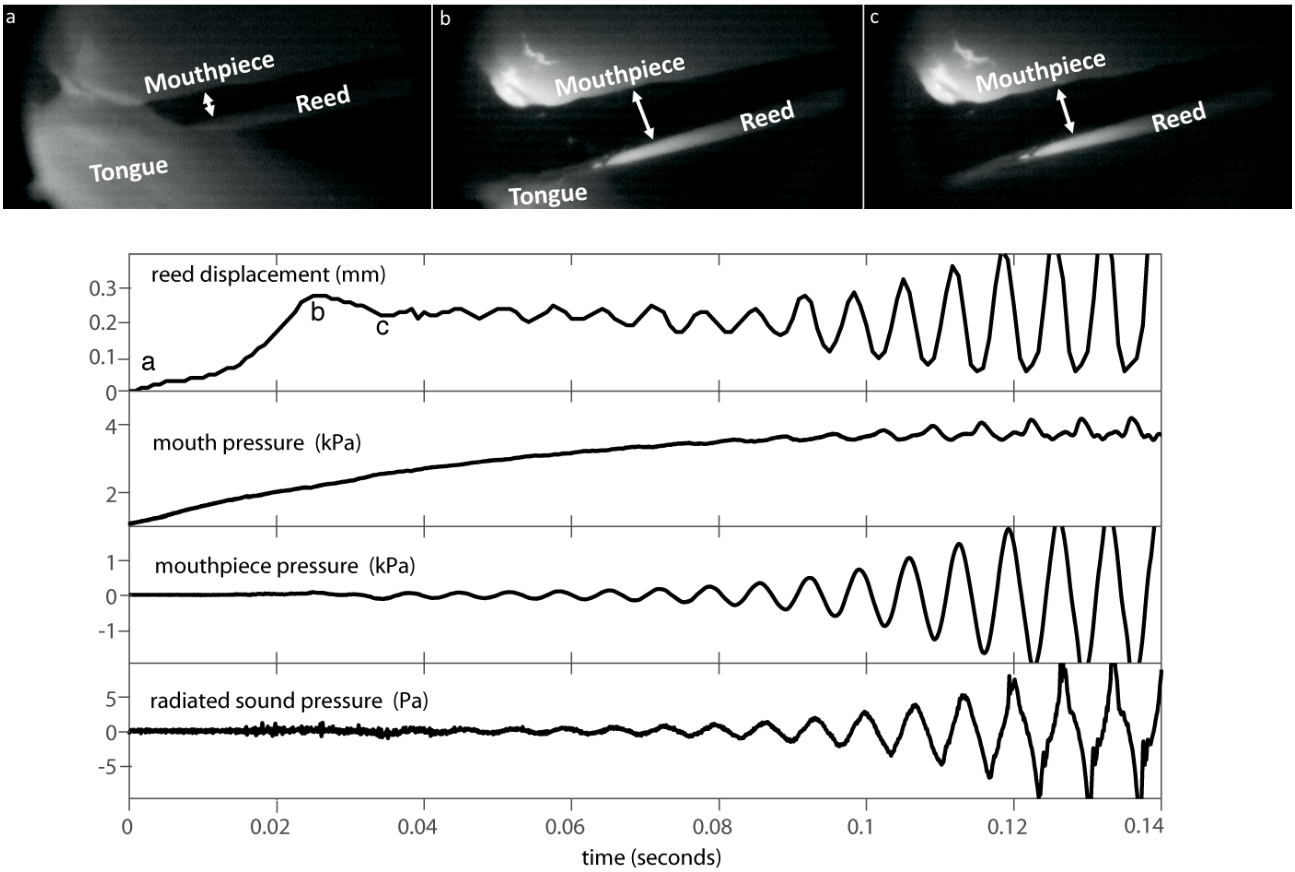

Figure 2 – The images (a, b, c) from the high-speed endoscope video show the labelled points on the graph of reed displacement from its initial position. The lower graphs show pressures in the mouth and mouthpiece and at the bell. An experienced player plays written E3, D3 concert (147 Hz), with normal tonguing. Details in Inwood *et al*. [12].

3 TONGUING: REED MOTION, BLOWING PRESSURE AND SOUND

3.1 Tongue-reed release and the pre-exponential stage

In Fig 2, an experienced player uses normal tonguing for low E on a Bb clarinet, increasing blowing pressure throughout the transient. For about 20 ms, (endoscope images (a) to (b)), the reed follows the wet tongue, which pulls it past its mechanical equilibrium position for this blowing pressure and lip force. The reed leaves the tongue at (b) and its elasticity returns it to equilibrium (c). Overdamped by the lip, the reed loses all the mechanical energy of its initial displacement. Its motion is relatively slow, considering the reed's natural frequency (> 1 kHz). The overdamping also reduces the probability that the reed will squeak. The varying aperture (b–c) at first admits an airflow and produces a mouthpiece pressure change which is, as we discuss later, proportional to the aperture. (This is not visible on the scale of Fig 2, but shown on Fig 5.)

For low notes like this one, the impedance spectrum of the bore has strong peaks at nearly harmonic frequencies, so partials approximating the first, third and fifth harmonics quickly dominate in the mouthpiece. The resonances in the vocal tract are not harmonically related and not tuned for this note [16], so the acoustic component of the mouth pressure is small. The bell radiates high harmonics better than low, giving the more interesting, nearly periodic waveform at right. It also shows inharmonic sound in the early attack.

Sometimes players begin a note without using the tongue; this has been simulated in playing machine studies by Bergeot *et al*. [17]. Interestingly, there is a hysteresis region on the plane of (blowing pressure, lip force) in which regenerative oscillation is not produced spontaneously by simply increasing the blowing pressure. In this hysteresis region, tonguing can initiate a note at lower pressure [11], thus making the start of the note more predictable.

3.2 Reed gain and the exponential stage

Once the reed has approached mechanical equilibrium at (c) in Fig 2, its later motion is driven by the varying air pressure difference across it. Consider a small pulse of low pressure arriving from the bore: it tends to close the reed, reducing the flow from the mouth and thus further lowering the pressure. Conversely, a pulse of high pressure opens the aperture, admits more flow and is thus amplified on reflection. So the reed amplifies pulses coming from the bore (or, in exotic cases, from the mouth [16,18]).

Provided the reed gain exceeds the losses in the bore and mouth, the pulse grows exponentially, until its magnitude approaches the blowing pressure, at which point reed motion and pressure approach saturation. In a simple small-signal model, the reed can be assigned a resistance, R_{reed}, whose negative value is given by the slope of a pressure-flow curve measured on a mechanical system in the absence of resonant loads [19]. R_{reed} is in parallel with the effective resistance R, compliance C and inertance L of the fundamental's bore resonance. (The instrument plays near a peak in the bore's impedance spectrum and this peak can, for this purpose, be empirically modelled as a parallel RLC circuit, where the values are determined from its frequency, magnitude and bandwidth.) For the exponential stage, with $p = p_0 e^{-t/\tau}$, the time constant τ and exponential rise rate r in $\mathrm{dB.s^{-1}}$ are given by

$$\tau = \frac{2R_{bore}R_{reed}C}{R_{bore} + R_{reed}} \quad \text{and} \quad r = -10\log_{10} e \,.\frac{R_{reed} + R_{bore}}{R_{reed}R_{bore}C}$$

This model and the measurements are further explained elsewhere [14]. The empirical circuit model is simplified when the reed is immobilised by the tongue, which can preclude flow between mouth and bore. This situation occurs in the final transient of *staccato* notes, which are therefore briefly discussed next.

3.3 Final transients, *staccato* and losses

At the end of isolated notes or phrases, notes are usually terminated by reducing the blowing pressure until the reed gain falls below the threshold value at which it just compensates the losses in the bore, mouth and radiation. Below this threshold, standing waves decay, as shown in Fig 3a-c, with rates controlled by the blowing pressure and its decrease during the decay. At the end of *staccato* notes, however, the tongue immobilises the reed. Without reed gain, waves in the bore are no longer amplified, and with losses in the mouth disconnected, the exponential decay rate is fixed by the bore: Fig 3d . The exponential decrease rates (~$400\ \mathrm{dB.s^{-1}}$) are consistent with the resistance calculated from the bandwidth of peaks in the measured impedance spectrum of the bore [11,20].

3.4 Comparing different articulations

Figure 3 shows measurements of tongue contact and the pressure in the mouth, mouthpiece and bell for four different articulations. Accented and *sforzando* (and to a lesser extent *staccato*) transients have greater blowing pressure at the instant of tongue release and consequently higher exponential rise rates (~$1300\ \mathrm{dB.s^{-1}}$) than normal articulation. Note that tongue release and blowing pressure are coordinated so that the latter is increasing at the instant of tongue release (as also in Fig 2).

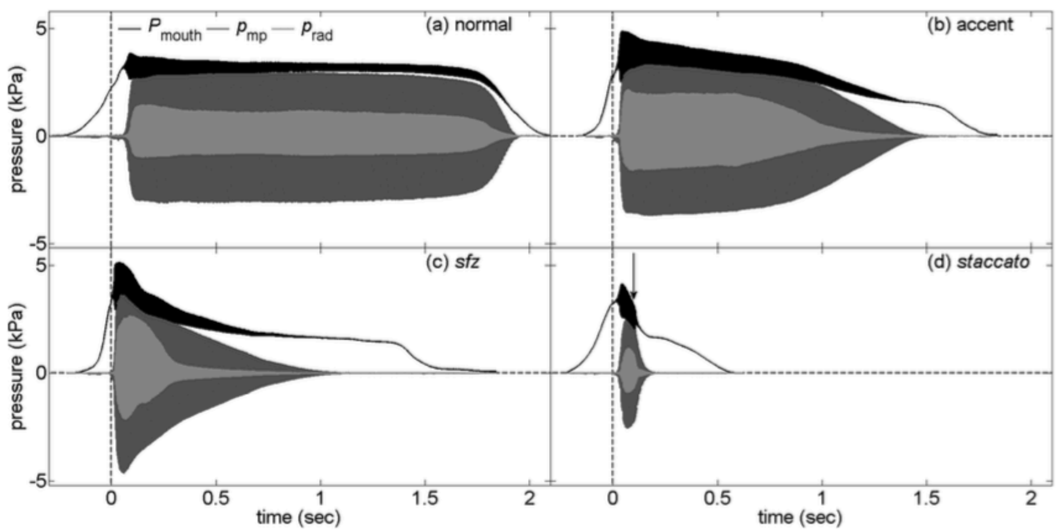

Figure 3 – An expert tongues (written) C5 with four different articulations. Mouth pressure, in black, includes the DC component (the blowing pressure) and the mouth AC signal. Mouthpiece pressure is in mid grey and bell pressure in pale grey. The vertical dotted line shows the instant of tongue release and the arrow (in *staccato*) the instant of tongue contact. From Li *et al*. [11].

3.5 The pre-exponential stage

In the absence of a reflection from the bore, the variation in mouthpiece pressure is simply proportional to the variation in aperture past the reed, because of an effect analogous to the water hammer in hydraulics: an increased aperture admits proportionally more flow from the high pressure source in the mouth and the increase in mouthpiece pressure follows from Newton's second law applied to the pressure pulse in the duct. We demonstrated this experimentally by replacing the clarinet with a tube long enough (L) to make the time for the initial pulse to travel along the tube and return (t_t) longer than the time (t_r) for the reed to reach mechanical equilibrium, thus enabling detailed study [15]. ($t_t = 2L/c = T/2$ where T is a period of the note.)

Depending on tongue motion and reed properties, the reed equilibration time (t_r) may be several to tens of ms so, for practical cases, the initial reed motion effect and the returning waves are in superposition, which is approximately linear for small signals. Some resultant superpositions are illustrated schematically for a simple hypothetical case in Fig 4. Here the aperture has constant acceleration until it reaches equilibrium. The bore is cylindrical. The effect of different ratios $\beta = t_r/t_t$ gives rise to effects that make the pre-exponential amplitude and spectrum complicated functions of the reed motion and t_r.

Figure 4 shows that, when the reed time t_r is shorter than the return time t_t from the bore, the resultant waveform has a clipped shape, and so is expected to have strong higher harmonics, especially odd harmonics. For more realistic cases, with $t_r > t_t$, the shape more closely approximates a triangle wave, suggesting odd harmonics again but with less power in the higher harmonics. The effect of β on the pre-exponential spectrum for a simple system is modelled in more detail by Almeida *et al*. [13].

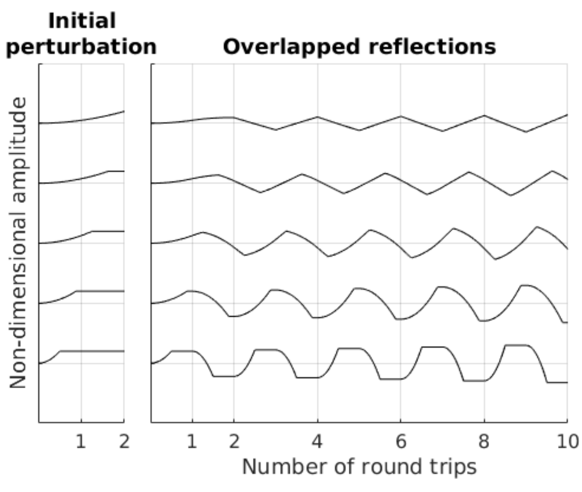

Figure 4 – Reed perturbation effects with the superposition of waves returning from a cylindrical bore. The ratio t_r/t_t varies from 2 (top) to 0.4 (bottom).

In a real clarinet, the impulse response function, and therefore the reflections, are more complicated than a single reflection. For the fingerings for the lowest notes, the bore impedance has several impedance peaks in nearly harmonic ratios (odd number times f_o), so reflections are expected to be nearly periodic. For notes in the second and higher registers, however, there are no or few nearly harmonically related impedance peaks [20], so linear superposition of reflections in the early transient produces strongly non-periodic waves and therefore inharmonic spectra.

4 ANALYSIS OF SPECTRAL EVOLUTION

Transients measured by earlier studies in this lab [11, 14, 15] were analysed using the heterodyne detection technique described by Almeida *et al*. [13]. The microphone recordings were sampled at 50 kHz. A complex exponential with constant frequency equal to that of the partial being analysed multiplies the recording, which is summed over Hann windowed bins of 1024 samples, as an example. If the frequency of the partial is constant within the bandwidth of 50 kHz/1024, then the sum is proportional to the average amplitude of the partial, and the angle of the sum gives the phase difference with respect to the reference signal over the window.

4.1 Analysis of transient measurements on a simple model system

A playing machine with controlled tongue parameters was used to generate reed motion with varying durations on a simplified ‘clarinet’, which was a cylindrical pipe 89 cm in length [14]. Figure 5 shows in the top row the sound pressure measured in the barrel (chosen instead of the mouthpiece for reduced turbulent noise). The second row shows the amplitudes of the first five (nearly harmonic) partials, and the last row the ratio of the amplitude of the third partial to the fundamental (H_3/H_1). As for many human players, the tongue in its initial position pushed the reed towards the mouthpiece, then accelerated away from the mouthpiece with controlled acceleration rates (respectively 23.5, 14.7, 3.2 and 0.9 $\mathrm{mm.s^{-2}}$). The tongue in this case was dry, however, and did not draw the reed past its equilibrium position, so in this case the aperture increased as the tongue accelerated. (Contrast this with Fig 2, where the aperture decreases once the reed breaks free from the wet tongue.) The zoom inset shows the first 10 ms, which is approximately the period of the note. The different acceleration rates produce values of $\beta = t_r/t_t$= 0.3, 0.4. 0.9 and 1.8.

As $\beta = t_r/t_t$ increases (left to right in Fig 5), the relative amplitude of higher partials (for $t \geq 0$) decreases, with qualitative similarity to the calculations in Fig 4. We also see (second row) the nearly exponential growth of the fundamental following the tongue-dominated pre-exponential stage. During this exponential stage, the growth of H_3 and H_5 is slower than that of H_1. This is in part due to visco-thermal losses in the bore that increase in proportion with the square root of frequency. Another reason is frequency-dependent gain: the simple model for reed gain neglects the mass of the reed, which is a more severe approximation at high frequency.

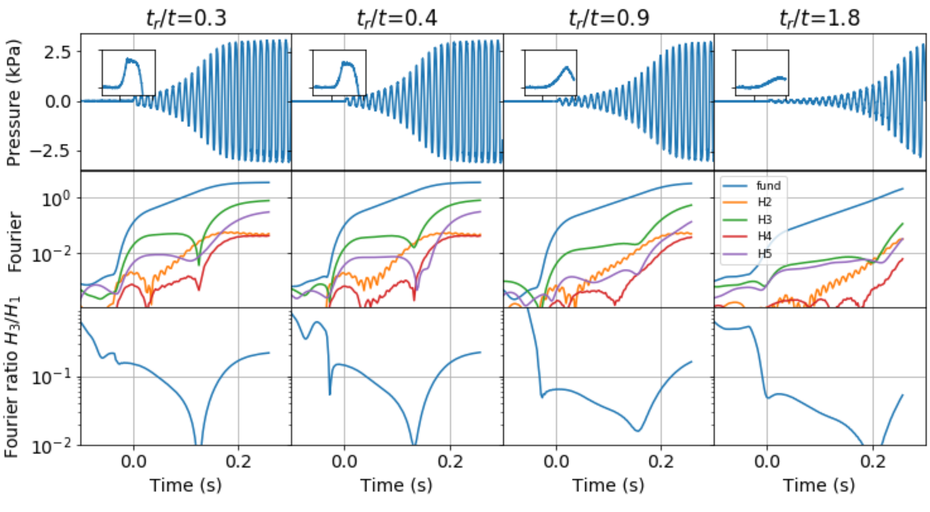

Figure 5 – Barrel pressure and its frequency components in transients on a playing machine.

Saturation occurs over several cycles before the signal reaches its steady or quiescent amplitude. As the amplitude of the sound wave in the bore becomes comparable with the blowing pressure, the reed gain falls below its small-signal value. In this stage, the nonlinearity in the flow-pressure curve for the reed becomes more significant, leading to clipping of the signal, and mode locking of the frequency components begins. The evolution of H_3 and H_5 shows complications in this regime.

The pre-exponential waveform and spectrum are determined by the initial tongue and reed motion, giving rise to the pressure waveform in the insets. This sets the initial magnitudes and phases of the partials, which are not exactly harmonic, and whose relative phases therefore change slowly over time during the linear superposition of the exponential stage [13]. During saturation, however, exactly harmonic H_3 and H_5 are generated by clipping, with phases locked to that of H_1. In the first example of Fig 5, it appears that the H_3 due to the growing linear transient and that due to clipping have a period of destructive interference, before the latter dominates.

4.2 Analysis of transients played by clarinettists

Most notes on the clarinet have the return time (t_t, a half-period) rather shorter than the reed equilibration time. Figure 6 shows the evolution of partials in the note (written) C5, 463 Hz, near the bottom of the clarion register, whose fundamental uses the second resonance of the bore. The figure is a re-analysis of data from Li *et al.* [11]. Notice that the *sforzando* example has a larger pre-exponential amplitude, largely because of the higher blowing pressure at the moment of tongue release. H_1 has a clear exponential stage for both attacks. For *sforzando*, the higher blowing pressure also produces a higher exponential rise rate. The larger pre-exponential amplitude and the larger rise rate together yield a shorter exponential stage for *sforzando*. In neither case is this accompanied by a sustained exponential rise in the other partials: instead, the rapid but smooth rise in some of the partials occurs only during the stage leading to saturation; it is therefore due to non-linear clipping rather than linear gain at the reed. In the *sforzando* attack, it is interesting to observe the strong but brief inharmonic partials at 764 and 1227 Hz (*i.e.* 1.65 and 2.65 times H_1). These are initially strong during the exponential stage, but are suppressed in the saturated steady note, when the third and higher harmonics (both even and odd) dominate the spectrum. Of the two strong inharmonic partials, the first corresponds with the strong third peak in the bore impedance and the latter with the weak fifth peak [20].

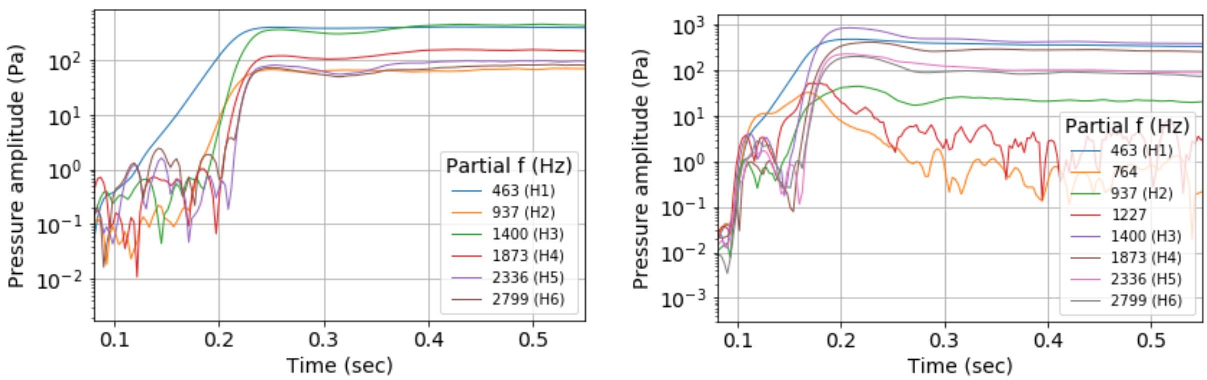

Figure 6 – Evolution of partials as an experienced player plays C5 (463 Hz) with normal articulation (left) and *sforzando* (right). Observe the strong inharmonic partials at 764 and 1227 Hz for *sforzando*.

4.3 From transient to steady note

Figure 3 showed that, after the transient, the mouthpiece pressure is several times larger than the mouthpiece pressure. In this quiescent state, one can use the Wilson [21] method to determine the vocal tract impedance at that frequency: continuity requires that the flow into the bore is minus one times that into the mouthpiece, so the vocal tract and the bore are therefore in series, and the ratio of acoustic pressure in the mouth to that in the mouthpiece pressures is the negative ratio of their impedances ($p_m/p_{mp} = -Z_m/Z_{mp}$), in the quiescent state. However, Figs 3 and 7 also show that p_m/p_{mp} may equal or exceed one during the transient.

In the steady note, players sometimes tune a vocal tract resonance to the note that they are playing to achieve advanced techniques, including pitch bending and altissimo playing [16,18] and the ratio p_m/p_{mp} can identify vocal tract involvement [22]. In normal playing, clarinettists tune the vocal tract resonance not to the note played, but ~100 Hz above, over a range of up to two octaves about C5 [16]. Figure 7 shows, on an expanded scale, accented attacks on the notes C4 (well below the tuning range), G5 (within the range) and C5 (near the lower limit). As expected, the quiescent ratio p_{mp}/p_m is lowest for the note C4 but always >1.

Wilson's impedance ratio argument cannot simply be applied to the rapidly varying amplitudes of currents and pressures during the transient, however, because impedance is inherently a frequency domain parameter. Figs 3 and 7 show that, during the transient, the acoustic pressure in the mouth can be as large as or larger than that in the mouthpiece, in apparent disagreement with the impedance ratio suggested by the steady part of the note.

It is worth observing that, although the mouth sound is unheard by most listeners, it may be perceived by the player and might contribute feedback about the attack, particularly in the clarion or altissimo registers.

The harmonics in Fig 7 show that the second harmonic is substantially weaker than the first and third for the notes C4 and C5, whose impedance spectra have strong peaks at these frequencies, and not at the second harmonic. G5, like other notes in the upper clarion or high range on the clarinet, does not systematically show impedance peaks at odd harmonics and low impedance at even harmonics.

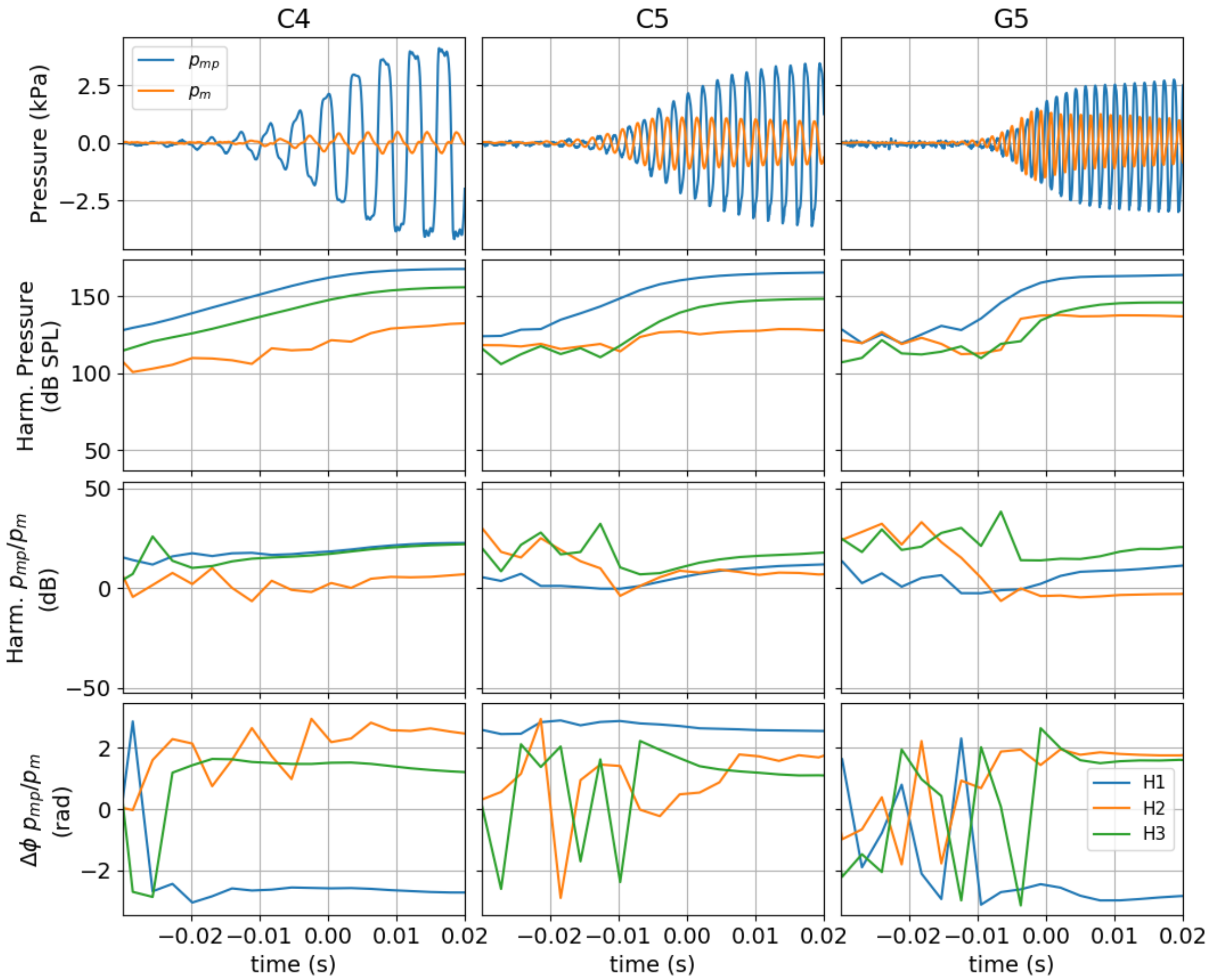

Figure 7 – The middle column shows the accented attack for C5 (Fig 3b) on an expanded time scale. For comparison, left and right columns show accented attacks of C4 and G5 by the same player. Rows show pressure waveforms, harmonics of p_{mp}, amplitude and phase of p_{mp}/p_m. Data from Li *et al* [11].

C4 shows clear exponential phases for H1, H3 and perhaps H2. For the other notes, the late start of the rise in H3 suggests that it comes from nonlinearity rather than reed gain *per se*. Note that H3 is stronger in the mouth than the mouthpiece for G5, whose bore impedance doesn't have a peak at this frequency.
Players achieve a wide range of exponential rise rates for different for different notes (*e.g.* Fig 7) and also for different articulations (*e.g.* Fig 3). Further, the high range for expert players exceeds that for students [11]. Example sound files are available online [23].

5 CONCLUSIONS

- Players coordinate tongue release and variation in blowing pressure to produce desired initial transients, *e.g.* higher pressures at release to give higher exponential rise rates for accents and *sforzando*.
- In a typical attack, the tongue releases the reed, which moves quickly towards mechanical equilibrium, losing its mechanical energy. The resulting variation in the aperture produces a proportional variation in mouthpiece pressure via a mechanism analogous to the water hammer in hydraulics. This stage, which usually ends with the first returning wave from the bore, creates the pre-exponential amplitude and spectrum. Larger blowing pressures and/or more rapid tongue and reed motion produce larger pre-exponential magnitudes.
- The reed release usually occurs when the blowing pressure already exceeds a threshold at which the reed gain compensates for losses. This produces a stage of exponential increase whose rate depends on blowing pressure, embouchure forces, and reed and mouthpiece properties. The partials generated in the preceding stage, which are in general not exactly harmonic, grow in linear superposition at different rates and varying phases. Their amplitude in the mouthpiece may briefly exceed that of the fundamental.
- The tongue can start notes at lower blowing pressures than the threshold measured with rising pressure.

- When the mouthpiece pressure amplitude becomes comparable with the blowing pressure, the reed gain falls below its small-signal value, the exponential rise rate falls, and superposition is no longer linear. Clipping and mode locking produce exactly harmonic partials; these can interact destructively with partials at similar frequency, leading to brief absences of one or more harmonics.
- Players typically coordinate tongue release with increasing blowing pressure to produce a range of different pre-exponential amplitudes and exponential increase rates for different articulation styles. The way in which players control the mouthpiece aperture in the pre-exponential stage influences the spectrum throughout the transient and thus may contribute to their characteristic articulatory styles.

ACKNOWLEDGEMENTS

We warmly thank the Australian Research Council for support, Yamaha for clarinets, Légère for reeds and our volunteer subjects.

REFERENCES

1. Berger KW. Some factors in the recognition of timbre. J Acoust Soc Am. 1963; 36: 1888–1891.
2. Thayer RC. The effect of the attack transient on aural recognition of instrumental timbres. Psychol Music. 1974; 2(1): 39–52.
3. Wilson A, Beavers GS. Operating modes of the clarinet. J Acoust Soc Am. 1973; 56: 653–658.
4. Bak N, Dolmer P. The relation between blowing pressure and blowing frequency in clarinet playing. Acta Acust Acust. 1987; 63:238–241.
5. Dalmont J-P, Frappé C. Oscillation and extinction thresholds of the clarinet: Comparison of analytical results and experiments. J Acoust Soc Am. 2007; 122: 1173–1179.
6. Almeida A, George D, Smith J, Wolfe J. The clarinet: How blowing pressure, lip force, lip position and reed ‘hardness’ affect pitch, sound level, and spectrum. J Acoust Soc Am. 2013; 134:2247–2255.
7. Almeida A, Chow R, Smith J, Wolfe, J. The kinetics and acoustics of fingering and note transitions on the flute. J Acoust Soc Am. 2009; 126:1521–1529.
8. Hofmann A, Goebl W. Production and perception of legato, portato, and staccato articulation in saxophone playing. Frontiers Psych. 2014; 5, 690-
9. Ernoult A, Fabre B. Temporal characterization of experimental recorder attack transients. J Acoust Soc Am. 2017; 141, 383–394.
10. Pamiès-Vilà M, Hofmann A, Chatziioannou, V. Analysis of tonguing and blowing actions during clarinet performance. Front Psychol. 2018; 9: 617.
11. Li W, Almeida A, Smith J, Wolfe J. How clarinettists articulate: The effect of blowing pressure and tonguing on initial and final transients. J Acoust Soc Am. 2016; 139: 825–838
12. Inwood L, Gray J, Li W, Almeida A, Smith J, Wolfe J. Tongue and reed motion producing initial transients in the clarinet. Proc AIP2016; Brisbane, Australia 2016.
13. Almeida A, Li W, Smith J, Wolfe, J. Modelling the spectral evolution of transients in wind instruments. Proc ICSV; Montreal, Canada 2019.
14. Li W, Almeida A, Smith J, Wolfe J. The effect of blowing pressure, lip force and tonguing on transients: A study using a clarinet-playing machine. J Acoust Soc Am. 2016; 140: 1089–1100.
15. Almeida A, Li W, Smith J, Wolfe J. The mechanism for initial transients on the clarinet. J Acoust Soc Am. 2017;142: 3376–3386.
16. Chen JM, Smith J, Wolfe J. Pitch bending and glissandi on the clarinet: roles of the vocal tract and partial tone hole closure. J Acoust Soc Am. 2009; 126: 1511–1520.
17. Bergeot, B, Almeida, A, Gazengel, B, Vergez, C, Ferrand, D. Response of an artificially blown clarinet to different blowing pressure profiles. J Acoust Soc Am. 2014; 135(1): 479–490.
18. Chen JM, Smith J, Wolfe J. Experienced saxophonists learn to tune their vocal tracts. Science 2008: 319: 72
19. Dalmont J-P, Frappé C. Oscillation and extinction thresholds of the clarinet: comparison of analytical results and experiments, Acoust Soc Am. 2017; 122**,** 1173–1179.
20. Dickens P, France R, Smith J, Wolfe J. Clarinet acoustics: Introducing a compendium of impedance and sound spectra. Acoust Aust. 2007; 35(1): 17–24.
21. Wilson TD. The measured upstream impedance for clarinet performance and its role in sound production. Ph.D. thesis, Univ. Washington. 1996. Ch 17.
22. Scavone G, Lefebre A, da Silva AR. Measurement of vocal-tract influence during saxophone performance. J Acoust Soc Am. 2008; 123: 2391–2400.
23. Music Acoustics. Clarinet articulations. 2019. www.phys.unsw.edu.au/jw/clarinet-articulations.html

PROCEEDINGS of ISMA 2019
International Symposium on Music Acoustics

13 - 17 September 2019 in Detmold, Germany

Acoustics of bifacial Indian musical drums with composite membranes

Anurag GUPTA[(1)], Vishal SHARMA[(1)], Shakti S. GUPTA[(1)]

[(1)]Department of Mechanical Engineering, IIT Kanpur, UP 208016, India, ag@iitk.ac.in

Abstract
We are interested in a certain class of bifacial Indian drums which consist of composite circular membranes stretched over an enclosed air cavity on both sides of an axisymmetric wooden shell. There is a large variety of such drums in Indian music which differ from each other in shapes and sizes of the shell and in the nature of the composite membranes. These drums produce sounds with a definite pitch. Whereas the effect of the composite nature of the membrane is well studied in the context of monofacial Indian drum tabla, the acoustical implications of the coupling between two composite membranes through an air cavity remains largely unexplored. The purpose of this work is to present some initial results from our study of this acoustical problem using a finite element method based numerical methodology. We use the developed framework, first to verify some existing results on Japanese wa-daiko, followed by an acoustical study of dholak, an Indian drum with composite membrane on one side, and finally to note the effect of curvature of the shell on modal frequencies.
Keywords: Bifacial drums, Indian drums, Composite membranes

1 INTRODUCTION

The importance of incorporating an enclosed air cavity below the vibrating membrane has been unambiguously demonstrated for monofacial drums such as kettledrum and tabla [1, 2]. The air cavity should arguably play a greater role in the acoustics of bifacial drums where the two membranes are coupled to each other via the enclosed air cavity and the surrounding shell. The most significant examples of such bifacial drums are the snare drums [3], the taiko family of percussion instruments from Japan [4], and the drums such as pakhawaj, mrdangam, dholak, dhol, iddakka, etc. from India [5, 6, 7]. The Indian drums usually have composite membranes (as in tabla) and distinguish themselves in generating sound with a definite pitch. In the following, we will begin by posing a general boundary-value-problem under some simplifying assumptions, followed by a variational principle which will form the basis of a finite element procedure. The developed framework will be verified by recovering some results on Japanese wa-daiko as presented by Suzuki and Hwang [4]. We will then proceed towards an acoustical study of dholak where membrane on one side of the barrel is composite and the two drum heads are unequal in size. We will also discuss the effect of curvature of the barrel shape on modal frequencies.

2 PROBLEM FORMULATION

The vibro-acoustic problem of bifacial Indian musical drums can be described by a system of coupled partial differential equations. These include equations which govern the displacement of the membranes and an acoustic wave equation which governs the internal pressure in the cavity. These equations are supplemented with appropriate set of initial and boundary conditions. In order to simplify the present discussion, we assume the membranes to be two-dimensional elastic continuum which do not resist or transmit bending moment and shear force. The restoring forces arise from the pre-stretching in the plane of the membrane. We neglect the acoustic and structural damping and assume the side walls of the cavity to be perfectly rigid. Moreover, we consider bifacial musical drums with axisymmetric cavity. The cavity is closed by stretched circular composite or homogeneous membranes on both the ends. The cavity is closed in such a manner that the air inside the cavity is confined and the motion of the membranes changes the volume of the air in the cavity. This changes the pressure of the air confined in the cavity. The pressure of the confined air generates a force on the membranes.

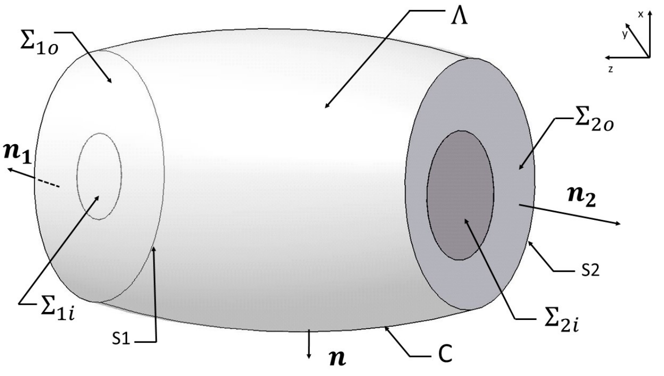

Figure 1. Schematic diagram of the problem domain.

In the following, we will consider a general model, of bifacial drums with composite membranes, as shown in Figure 1. The cavity domain Λ is bounded by surface C of a rigid shell with composite membranes on the two sides. The left side of the cavity has a composite membrane Σ_1 (radius b_1) with a centrally loaded patch (i.e. a patch of added material) Σ_{1i} (radius a_1) and the right side has a composite membrane Σ_2 (radius b_2) with an eccentrically loaded patch Σ_{2i} (radius a_2 and eccentricity d). The composite membrane with a centric loaded patch has a fixed edge S1 whereas the composite membrane with an eccentrically loaded patch has a fixed edge S2. The left side composite membrane is subjected to uniform tension T_1 per unit length such that its transverse motion $\bar{u}_1(x,y,t)$ is governed by

$$\sigma_1(r)\frac{\partial^2 \bar{u}_1}{\partial t^2} - T_1 \Delta \bar{u}_1 = \bar{p}, \tag{1}$$

where $\sigma_1(r)$ is the density per unit area which is piecewise continuous with a constant value σ_{1a} for radius $0 \leq r \leq a_1$ and σ_{1b} for radius $a_1 < r \leq b_1$; the operator Δ represents the Laplacian. The acoustic pressure field $\bar{p}(x,y,z,t)$ is also an unknown variable. At radius $r = a_1$, both the transverse motion (for compatibility) and the normal force (for equilibrium) should be continuous. At $r = b_1$, $\bar{u}_1 = 0$. The right side composite membrane is subjected to a uniform tension T_2 per unit length such that its transverse motion $\bar{u}_2(x,y,t)$ is governed by

$$\sigma_2(r)\frac{\partial^2 \bar{u}_2}{\partial t^2} - T_2 \Delta \bar{u}_2 = \bar{p}, \tag{2}$$

where $\sigma_2(r)$ is the density per unit area which is piecewise continuous with a constant value σ_{2a} for the loaded patch and σ_{2b} for the remaining part. At the boundary of the loaded patch, both the transverse motion and the normal force should be continuous. At $r = b_2$, $\bar{u}_2 = 0$. The acoustic air cavity domain Λ is assumed to be filled with an inviscid fluid (air) with pressure field $\bar{p}(x,y,z,t)$, which is governed by the acoustic wave equation

$$\frac{\partial^2 \bar{p}}{\partial t^2} - c_p^2 \Delta \bar{p} = 0, \tag{3}$$

where c_p is the speed of sound in the medium (air). The boundary condition at the rigid wall surface C is given by $\partial \bar{p}/\partial \mathbf{n} = 0$; at the left side membrane by $\partial \bar{p}/\partial \mathbf{n_1} = -\rho_a \ddot{\bar{u}}_1$, ρ_a is the density of air (1.21 kg/m^3); and at the right side membrane by $\partial \bar{p}/\partial \mathbf{n_2} = -\rho_a \ddot{\bar{u}}_2$.
Substituting the modal solutions

$$\bar{u_1} = u_1(x,y)e^{-i\omega t}, \ \bar{u_2} = u_2(x,y)e^{-i\omega t}, \ \text{and} \ \bar{p} = p(x,y,z)e^{-i\omega t} \tag{4}$$

into Equations (1), (2), and (3), where ω is the modal frequency, we can simplify them as

$$\omega^2\sigma_1(r)u_1 + T_1\Delta u_1 + p = 0 \tag{5}$$

for the composite membrane Σ_1, such that $u_1 = 0$ at edge S1,

$$\omega^2\sigma_2(r)u_2 + T_2\Delta u_2 + p = 0 \tag{6}$$

for the composite membrane Σ_2, such that $u_2 = 0$ at edge S2, and

$$\omega^2 p + c_p^2\Delta p = 0 \tag{7}$$

for the internal pressure field in the cavity Λ, such that $\partial p/\partial \mathbf{n} = 0$ on C, $\partial p/\partial \mathbf{n_1} = \omega^2\rho_a u_1$ on Σ_1 and $\partial p/\partial \mathbf{n_2} = \omega^2\rho_a u_2$ on Σ_2.

The preceding boundary-value-problem can be recast in terms of a variational principle. The solution of the problem, given in terms of smooth functions $u_1(x,y)$, $u_2(x,y)$, and $p(x,y,z)$, extremizes the variational functional $I(u_1,u_2,p) = I_1 + I_2 + I_3$, where

$$I_1 = \int_{\Sigma_1} \frac{1}{2}\Big(T_1\nabla u_1 \cdot \nabla u_1\Big)dA - \omega^2\int_{\Sigma_1} \frac{1}{2}\Big(\sigma_1 u_1^2\Big)dA - \int_{\Sigma_1}\Big(pu_1\Big)dA, \tag{8}$$

$$I_2 = \int_{\Sigma_2} \frac{1}{2}\Big(T_2\nabla u_2 \cdot \nabla u_2\Big)dA - \omega^2\int_{\Sigma_2} \frac{1}{2}\Big(\sigma_2 u_2^2\Big)dA - \int_{\Sigma_2}\Big(pu_2\Big)dA, \text{ and} \tag{9}$$

$$I_3 = \int_{\Lambda} \frac{1}{2\omega^2\rho_a}\Big(\nabla p \cdot \nabla p\Big)dV - \int_{\Lambda} \frac{1}{2\rho_a c_p^2}\Big(p^2\Big)dV, \tag{10}$$

subjected to $\delta u_1 = 0$ on $S1$ and $\delta u_2 = 0$ on $S2$, the three variations δu_1, δu_2, and δp otherwise allowed to vary independently but smoothly over their respective domains; the operator ∇ represents the gradient. This variational principle forms the basis for our finite element procedure for determination of modal frequencies and modeshapes. We choose four-nod quadrilateral elements for discretizing the membranes and the rigid boundary C and eight-nod hexahedral elements for discretizing the acoustic domain, ensuring that the membrane elements match well with acoustics domain elements at the nodes. The basis functions used for the former are $\{1,x,y,xy\}$, whereas the basis functions used for the latter are $\{1,x,y,z,xy,xz,yz,xyz\}$. The integration over domains is evaluated using the standard Gauss quadrature rule for polynomials. The efficacy of our code is tested by using it to verify the existing results for kettledrum and tabla as reported in earlier literature [1, 8, 2], in particular considering non-cylindrical kettle shapes in the former case, see [9] for further details. Besides verifying our framework for monofacial drums, we use it to revisit Japanese bifacial drums, which have homogeneous membranes, as discussed next.

3 WA-DAIKO

We consider the bifacial drum wa-daiko whose geometry is shown in Figure 2(a). It is rotationally symmetric with respect to its central axis. The total length L of the barrel is 0.5 m. The radius R1 of both the membranes is 0.2 m. The maximum radius of the barrel R2 is 0.24 m. The curvature of the drum can be obtained by the three-point circle which passes through the maximum radius point and the two edge points. The other parameters, taken from Suzuki and Hwang [4], are volume density (2000 kg/m^3) and thickness (2 mm) of the membrane. With membrane tensions $T_1 = T_2 = 14$ kN/m, the first two modal frequencies, using our formalism, are 110.42 and 120.01 Hz. These are close to those obtained by Suzuki and Hwang [4] (as 110.5 and 120.0 Hz). The membranes move in phase at 110.42 Hz and in the opposite directions at 120.01 Hz. The corresponding mode shapes are shown in Figure 2(b). Furthermore, keeping tension $T_1 = 14$ kN/m in membrane 1, the modal frequencies for different values of tension in membrane 2 are evaluated and collected in Table 1; these are in agreement with Suzuki and Hwang [4]. Any further increase in tension T_2 beyond 20 kN/m does not affect the value of f_1. At such high tension values, the displacement of membrane 2 becomes very small. The membrane then behaves like a rigid body and stops interacting with membrane 1.

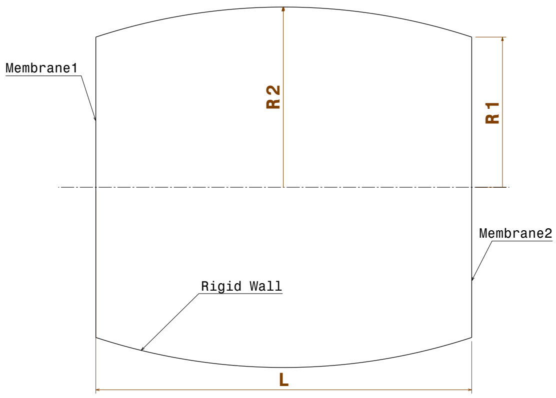

(a)

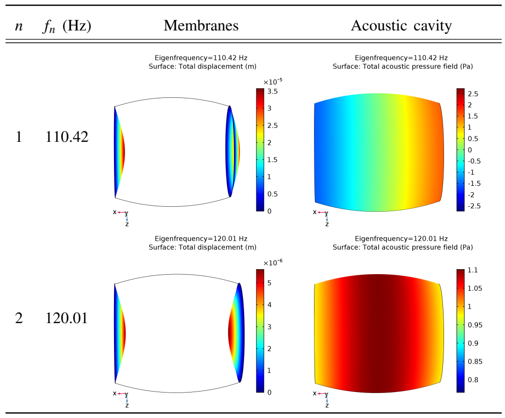

(b)

Figure 2. (a) Geometry of wa-daiko; (b) Mode shapes.

Table 1. Modal frequencies for the first two modes of wa-daiko for different tension values.

T_2(kN/m)	14	15	16	17	18	20
f_1(Hz)	110.42	111.99	112.94	113.51	113.87	114.23
f_2(Hz)	120.01	122.2	124.91	127.88	130.97	137.17

4 DHOLAK

Dholak is a barrel-shaped bifacial drum made of a single piece of wood; it is one of the most widely used drums in north India. The two membrane heads of dholak are different in size, where the smaller head is covered with a homogeneous membrane while the larger head is covered with a composite membrane. The latter has a patch, much like that in tabla, made of a mixture of sand, tar, and clay. However, unlike, tabla, the patch is on the inner side of the membrane and hence not visible on the drum surface. The length of dholak is around 41 cm. The outer diameter of the larger and the smaller drum heads are about 23 and 18 cms, respectively. The thickness of the hollow barrel is around 2 cm. A cross-sectional view of a typical dholak is shown in Figure 3(a). The diameter of dholak at the waist, at mid-length, is around 27.5 cm. The waist forms the base of the two truncated conical shapes which end at the drum heads. The membranes can be tuned separately to different tension values. In the simulations, we have used different tensions in both the membranes. The tensions in the larger and the smaller membranes are taken as $T_1 = 3.5$ kN/m and $T_2 = 3$ kN/m, respectively. The radius of the axisymmetric patch on the larger membrane is taken as 3.8 cm. The density of the homogeneous membrane (and the outer part of the composite membrane) is taken to be 0.18 kg/m^2. The ratio of the central patch density to outer part density is denoted by λ^2. We have fixed all the parameters except the value of λ, which we will vary to obtain different results. In Figure 3(b), we compare frequency ratios of several modes for various values of λ; the values are tabulated in Table 2. The mode shapes for the first twelve modes, corresponding to $\lambda = 1.93$, are given in Table 3 along with the frequency ratios f_n/f_4.

The frequencies f_1 and f_2 correspond to in phase and out of phase membrane motion, respectively, with larger membrane having a larger deflection. The frequencies f_3 and f_6 correspond to in phase and out of phase membrane motion, respectively, with smaller membrane having a larger deflection. All of these modes show a strong coupling between the membrane heads. The frequencies $f_4 = f_5$ correspond to a mode with one nodal diameter on the larger membrane and negligible activity in the other membrane and the air cavity. The frequencies $f_7 = f_8$ correspond to the case when both the membranes have one nodal diameter. The two membranes inter-

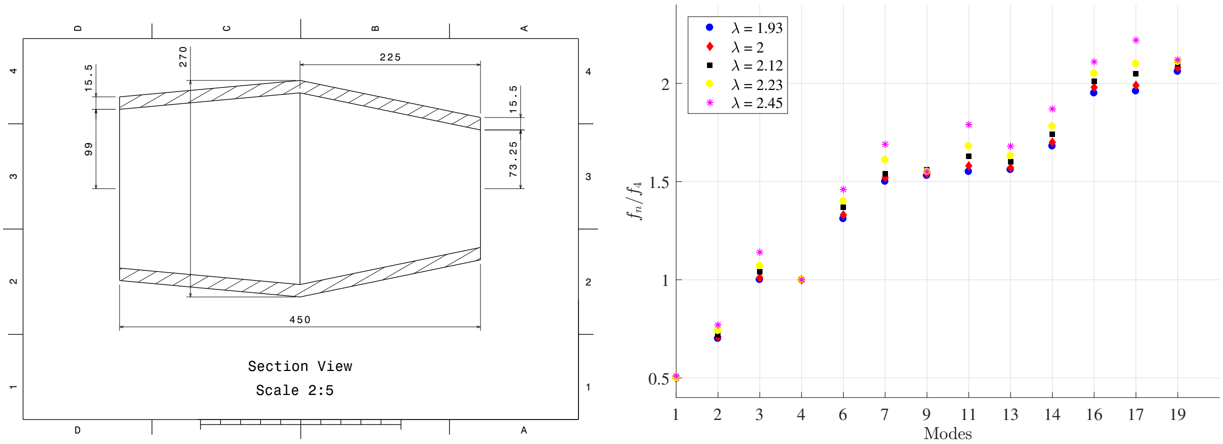

(a) (b)

Figure 3. (a) A sectional view of dholak (all dimensions in mm); (b) Frequency ratios with an increasing value of λ. The missing modes (on the x-axis) are degenerate with respect the preceding mode number.

act strongly even in this case. The frequencies $f_9 = f_{10}$ represent a pair of degenerate modes with two nodal diameters on the larger membrane and negligible vibrations in the other membrane as well in the air cavity. The frequencies $f_{11} = f_{12}$ correspond to the case when there is one nodal diameter in the smaller membrane in addition to small vibrations both in the other membrane and the cavity. Clearly, there are modes in which membranes interact with each other and those in which they do not, the former mostly corresponding to the ones having no nodal diameters on the membranes. If the two drum sizes are equal then there is an increased degeneracy in the spectrum. A change in the value of λ will effect only those modes in which the larger membrane participates. The frequency ratios over a range of λ are presented in Table 2 (graphically in In Figure 3(b)). For $\lambda = 1.93$, we obtain many ratios close to being multiples of 0.25, which is indicative of sound with a definite pitch.

Table 2. Frequency ratios with respect to f_4 for dholak with an increasing value of λ.

n	f_n/f_4 (λ = 1.93)	f_n/f_4 (λ = 2.00)	f_n/f_4 (λ = 2.12)	f_n/f_4 (λ = 2.23)	f_n/f_4 (λ = 2.45)
1	0.50	0.50	0.50	0.50	0.51
2	0.70	0.71	0.72	0.74	0.77
3	1.00	1.01	1.04	1.07	1.14
4 and 5	1.00	1.00	1.00	1.00	1.00
6	1.31	1.33	1.37	1.40	1.46
7 and 8	1.50	1.52	1.54	1.61	1.69
9 and 10	1.53	1.54	1.56	1.55	1.55
11 and 12	1.55	1.58	1.63	1.68	1.79
13	1.56	1.57	1.60	1.63	1.68
14 and 15	1.68	1.70	1.74	1.78	1.87
16	1.95	1.98	2.01	2.05	2.11
17 and 18	1.96	1.99	2.05	2.10	2.22
19 and 20	2.06	2.08	2.10	2.11	2.12

Table 3. Mode shapes and frequency ratios f_n/f_4 for dholak (λ = 1.93, T_1 =3.5 kN/m and T_2 =3 kN/m).

n	f_n/f_4	Membrane	Acoustic cavity
1	0.50	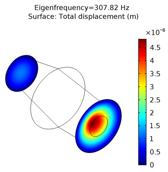	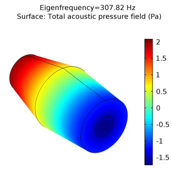
2	0.70	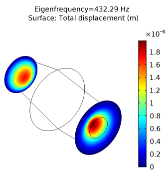	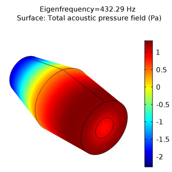
3	1.00	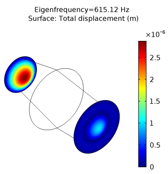	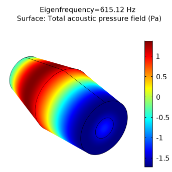
4 and 5	1.00	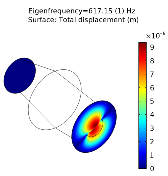	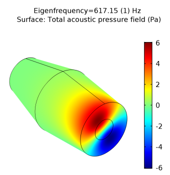
6	1.31	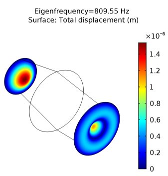	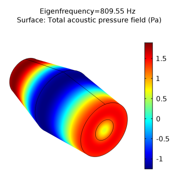
7 and 8	1.50	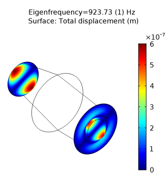	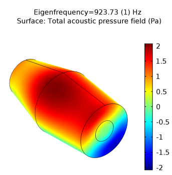
9 and 10	1.53	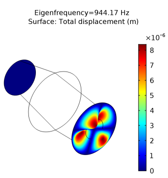	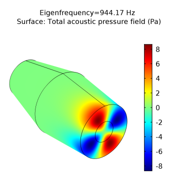
11 and 12	1.55	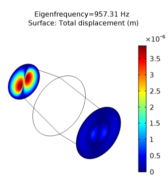	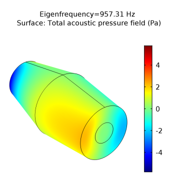

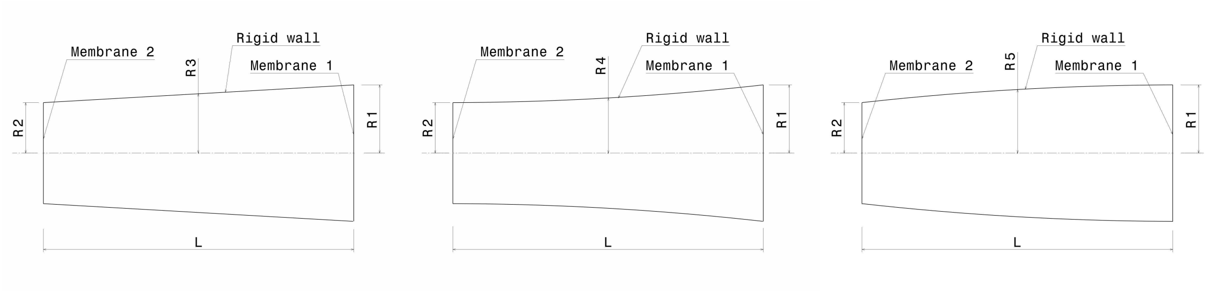

Figure 4. Section of a bifacial drum with varying barrel curvature: (a) truncated conical, (b) concave, and (c) convex shape.

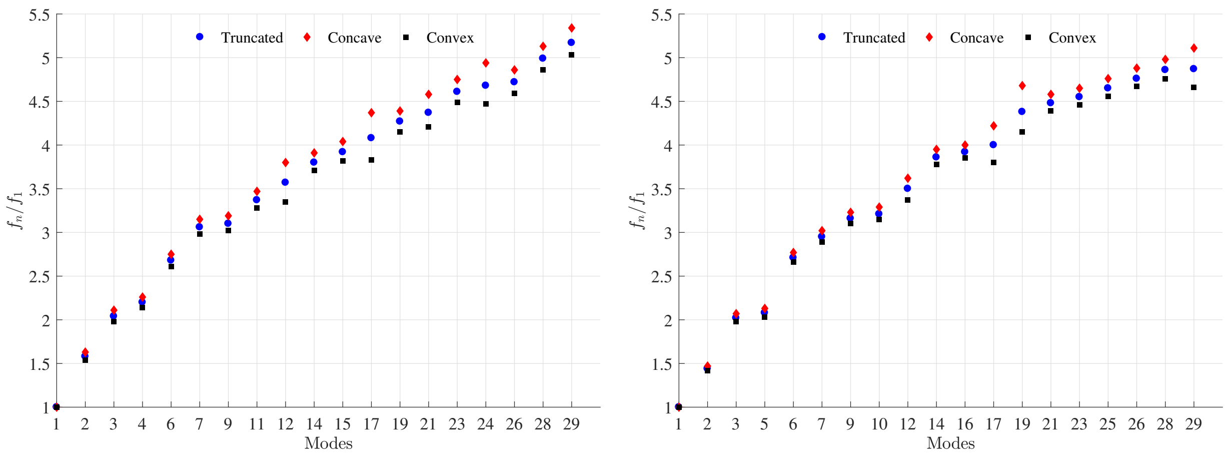

Figure 5. f_n/f_1 ratios for bifacial drums of three different barrel shapes with equal tension ($T_1 = T_2 = 4$ kN/m). (a) Both the membranes are homogeneous; (b) Smaller membrane is homogeneous while the larger one is composite. In both the cases, the missing modes (on the x-axis) are degenerate with respect the preceding mode number.

5 EFFECT OF CURVATURE OF THE BARREL

In this section we will discuss the effect of curvature of the axisymmetric shell which encloses the air cavity. We consider a drum geometry with membrane heads of unequal sizes (as is the case with most of the Indian drums) and a barrel with either conical, concave, or convex shape. Figure 4 shows a section of the three geometries considered in the following. With reference to the figure, R2 = 73.25 mm, R1 = 99 mm, L = 450 mm, R4 = R3 - 6.125 mm, and R5 = R3 + 6.125 mm, where R3 is the radius of the truncated cone at its mid point. The tensions in the larger and the smaller membranes are T_1 and T_2, respectively. We will consider two cases, one where both the membranes are homogeneous and the other where only one membrane is composite.

First, let the two membranes be homogeneous with a density of 0.2451 kg/m^2 and tensions $T_1 = T_2 = 4$ kN/m. The modal frequencies for several modes are compared for the three cases in Figure 5(a). Most of the modes have modeshapes qualitatively similar to those described for dholak, however there are some variations, for instance modes 7 and 8 which here have isolated deformation of the smaller membrane with one nodal diameter; for more details see [9]. Of course, only those frequencies which correspond to the modes where air cavity participates actively are affected by the change in shape of the barrel. The trends are captured in Figure 5(a). Second, we consider the case where the smaller membrane is homogeneous with a density of 0.2451 kg/m^2 but the other membrane is a composite membrane having a centric loaded patch of density twice as that of the outer portion. The outer density of the composite membrane is same as that of smaller membrane. The tension values in both the membranes are identical, $T_1 = T_2 = 4$ kN/m. The modal frequencies for the three drum shapes are compared in Figure 5(b). The composite nature of the membrane lowers the frequencies corresponding to the modes in which the larger membrane participates actively. The degeneracy in the spectrum shifts by a mode, for several modes, when compared to the preceding scenario of homogeneous membranes. Overall, we note that the concave shaped bifacial drums have higher frequency ratios while the convex shaped ones have the lower frequency ratios with respect to the truncated cone shaped drums.

6 CONCLUSIONS

A variational formulation was proposed, and used for a finite element implementation, to study the acoustics of bifacial drums with axisymmetrically curved barrels and composite drumheads. Such drums are found commonly in different cultures across India. The developed method is applied to study a specific Indian drum, dholak, which has a convex shaped barrel and one composite membrane. Modal frequencies were investigated for a range of parametric values and the most optimum solution was identified in the considered range. Further experimental and simulation work, required to discuss a more complete picture of the emergent acoustical phenomena in such bifacial drums, will be discussed in a future study.

REFERENCES

[1] Christian, R. S.; Davis, R. E.; Tubis, A.; Anderson, C. A.; Mills, R. I.; Rossing, T. D. Effect of air loading on timpani membrane vibrations, The Journal of the Acoustical Society of America, 76, 1984, pp. 1336-1345.

[2] Tiwari, S.; Gupta, A. Effects of air loading on the acoustics of an Indian musical drum, The Journal of the Acoustical Society of America, 141, 2017, pp. 2611-2621.

[3] Rossing, T. D.; Bork, I.; Zhao, H.; Fystrom, D. O. Acoustics of snare drums, The Journal of the Acoustical Society of America, 92, 1992, pp. 84-94.

[4] Suzuki, H.; Hwang, Y. F. Coupling between two membranes of a Japanese drum, Acoustical Science and Technology, 29, 2008, pp. 215-220.

[5] Raman, C. V. The Indian musical drums, The Proceedings of the Indian Academy of Sciences, A1, 1934, pp. 179-188.

[6] Jose, K.; Chatterjee, A.; Gupta, A. Acoustics of Idakka: An Indian snare drum with definite pitch, The Journal of the Acoustical Society of America, 143, 2018, pp. 3184-3194.

[7] Deva, B. C. Musical Instruments of India, Firma KLM Calcutta, 1978.

[8] Rhaouti, L.; Chaigne, A.; Joly, P. Time-domain modeling and numerical simulation of a kettledrum, The Journal of the Acoustical Society of America,105, 1999, pp. 3545-3562.

[9] Sharma, V. Vibroacoustics of bifacial Indian musical drums, MS Thesis, IIT Kanpur, 2018.

PROCEEDINGS of ISMA 2019
International Symposium on Music Acoustics

13 - 17 September 2019 in Detmold, Germany

Acoustic measurement of Marimba, Xylophone and Xylorimba

Masanobu MIURA[1]; Nozomiko YASUI[2]

(1) Faculty of Music, Kunitachi College of Music, Japan, miura.masanobu@kunitachi.ac.jp
(2)Graduate School of Science and Engineering, Saitama University, Japan.

Abstract

A set of wooden-keyboard percussion instruments, namely xylophone, marimba and xylorimba are acoustically compared. Since the size of xylophone and marimba has not had a standard size, their size and tone have a variety among them. More concretely, an American company Deagan produced the xylorimba between 1920-1930, which was played by a xylophone player Yoichi Hiraoka, and then conveyed to Japan. The timber of xylophone is felt as to have the features of both marimba and xylophone. The acoustic feature is, however, not measured until now. A professional marimba player cooperated in our experiment. She is asked to play a single note C4 with a consistent hard mallet. The power spectrum of recorded acoustic signal is evaluated in terms of salient peaks on the recorded sound. Although the salient peaks on marimba and xylophone are almost well-known shapse, the one on the xylorimba has a distinct feature, which has 1) consonant peaks to F0, such as 2oct and 3oct+perfect 5th and 2) dissonant peaks to F0, such as 3oct major 2 degree (detuned to +1 and +22 cents). Therefore, the xylorimba is acoustically confirmed as to have both xylophone and marimba's features.

1 INTRODUCTION

Acoustical measurement of musical instruments is the key target of the field of musical acoustics. This study was motivated by a discussion with a professional Marimba player "Ms. Mutsumi TSUZAKI", who is readiing Marimba player in Japan. Her musical instruments "Xylorimba" is originally played by the Marimba player Yoichi Hiraoka, who plays in USA during the 1930-1942. Since his performances were famous not only in US and Japan through radio broadcasting. After Ms. Tsuzaki started to play the Marimba, she felt that the sound or timbre has specific feature, namely it has the timbre both Xylophone and Marimba. The objective measurement of the Xylorimba, has not yet been conducted until now, so that at this time we tried to clarify the difference of the feature of timbre on the Xylorimba.

2 AIMS

At this report we aimed at clarification of the difference of timber among conventional Marimba, Modern-Xylophone, a vintage Xylophone, and Xylorimba. In particular, we measured the frequency component on the played sound to differentiate the four instruments. At this measurement, we focued on the acoustical similarity of the played sound of Xylorimba to either Marimba or Xylophone.

3 ACOUSTIC ANALYSIS

3.1 Measurement conditions

Followings are the list of the details of the measurement.

Instruments to be measured: Marimba, Modern-Xylophone, Vintage-Xylophone, Xylorimba

Task: Single stroke

Note height: C4

Used mallet: Normal mallet with normal hardness

# of trial: Three

[1] miura.masanobu@kunitachi.ac.jp
[2] nyasui@mail.saitama-u.ac.jp.

3.2 Analysis

Firstly, the Marimba player Mustumi Tsuzaki was asked to play an instruments under the conditions denoted in 3.1. The recorded sound's beginning time, at here we use 250 msec from the onset of the waveform, is employed to be analyzed. The FFT (Fast Fourier Transform) was conducted for the beginning 250msec waveform, then its power spectrum is obtained. By observing the peaks in the power spectrum, the peak of the sound is picked up and the frequency is measured. Among the three trials, we observe the frequency on each peak number, then averaged the frequency on each peak, in order to get rid of the differences of frequencies due to trials. The fundamental frequency is obtained as the 1st peak of the analysis. Then, each tone interval between the fundamental frequency (F0) and each peak.

4 RESULTS

Table 1 shows the tone interval from fundamental frequency and peaks on the recoded sound, where the "oct." means 1 octave, and the cents are measured from each interval of the current. If we label as "major 3rd", it is not a precise measurement but somewhat rounded. If the interval's label is apart from 30 cents, the underlines are denoted.

From Table 1, the result of Marimba says the second peak of the sound is 2 octaves, which consists with the literature[1]. Two Xylophones have 2nd peaks lower than the 2 octaves, but they commly have 1 octave with perfect 5th, which meets the result of literature [1]. Interestingly, Xylorimba has the same 2nd peak to Xylophone. Therefore, we can say that the Xylorimba has the Xylophone's feature on 2nd peak. Moreover, Xylorimba has the 2 octave component on the 3rd peaks which corresponds to the 2nd peak of Marimba.

Table 1 Result of measurement.

	Insturment			
Peak Number	Marimba	Modern Xylophone	Vintage Xylophone	Xylorimba
1	(F0)	(F0)	(F0)	(F0)
2	1oct.	<u>1 oct. Perfect 5th</u>	2 oct. Perfect 5th	3 oct. Perfect 5th
3	<u>3oct. Major 3rd</u>	2oct. Minor 7th	<u>2oct. Major 6th</u>	2oct.
4	-	3oct. Perfect 5th	3oct.Major 7th	3 oct. Major 2nd (+0.99cent)
5	-	3oct. Minor 7th	-	3 oct. Major 2nd (+21cent)
6	-	-	-	<u>3oct. Perfect 5th</u>

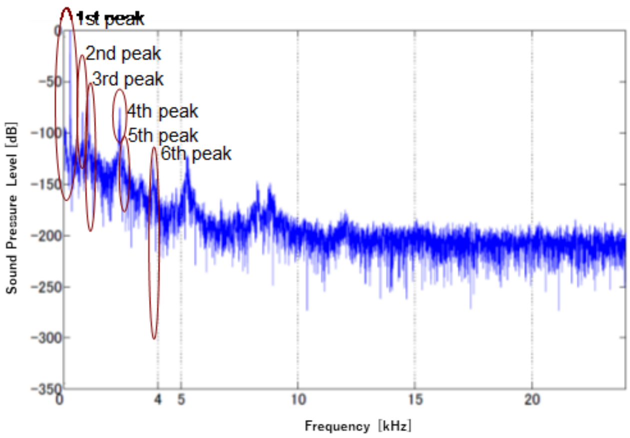

(a) Marimba

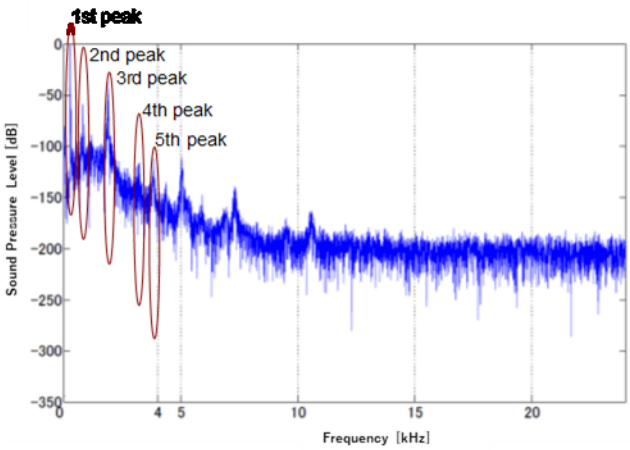

(b) Modern Xylophone

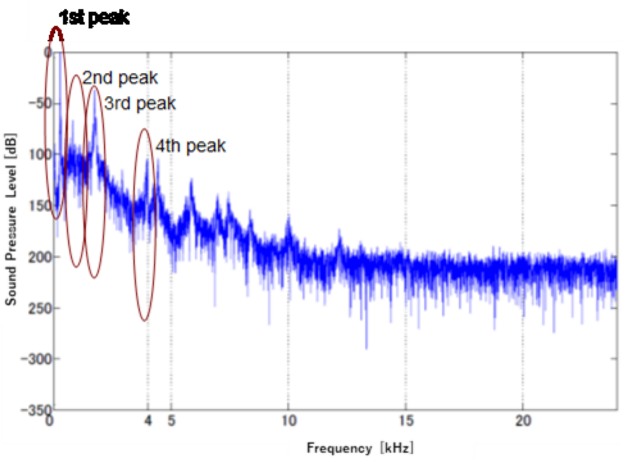

(c) Vintage Xylophone

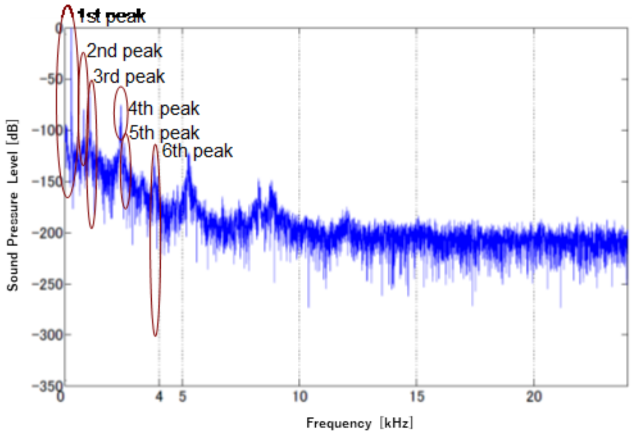

(d) Xylorimba

Figure 1 Result of acoustic measuremts on the four instruments.

5 DISCUSSION

According to the result of Table 1, Marimba has fewer number of peaks compared to the two Xylophones and Xylorimba. Therefore, Marimba is likely to produce purely timbre. On the other hand, the two Xylophones and Xylorimba have more peaks with 7th or 2nd intervals. Therefore, the three has complex sound compared to Marimba.

From here, we discuss the similarity of Xylophone and Xylorimba. In particular we focuses on the 3rd or higher peaks. On the modern Xylophone the 7th intervals are observed, and on the vintage Xlophone it has 6th and 7th, which are expected to produce inharmonic sound[2]. Compared to the modern Xylophone, the vintage Xylophone has fewer peaks, which could be due to deterioration of the instrument. On the Xylorimba, it has perfect 5th components, that elicit Marimba's character, whereas it also has 2nd with out of tune component which elicits inharmonic, or percussive sound, that has different from both Marimba and Xylophone's characters.

6 CONCLUSIONS

At here we aimed at analyzing the acoustic feature of Marimba, Xylophone and Xylorimba. According to the result, the Xylorimba has component of Marimba's (major 3rd and octaves), and Xylophone's (perfect 5th), which is thought to elicit the sound character of both Marimba and Xylophone. Since the number of instruments to measure is quite limited, the obtained results may have biased. In near future we plan to measure another instruments on same category.

REFERENCES

[1] N. Fletcher and T. Rossing, "The Physics of Musical Instruments", Springer, New York, 2008.

[2] R. Plomp, W. J. M. Levelt, "Tonal consonance and critical bandwidth", J. Acoust. Soc. Am., 38, pp.548-560, 1965.

PROCEEDINGS of ISMA 2019
International Symposium on Music Acoustics

13 - 17 September 2019 in Detmold, Germany

Relating tone height and perceived pleasantness in the Didgeridoo and bass trombone

Noam AMIR; Yasmin BACHAR-YAKOBI

Dept. of Comm. Disorders, Tel Aviv University, Israel, noama@tauex.tau.ac.il 1

Abstract

The motivation for this study came from the informal observation that didgeridoo tones seem to sound pleasant only over a span of less than an octave, while brass wind instruments of various types are found to be useful and pleasant over a much wider range. We therefore set out to explore the relationship between tone height and its perceived pleasantness and compare these evaluations both on a set of didgeridoos and on a bass trombone playing identical notes over a range slightly larger than one octave. Twenty listeners compared recordings of short tones from G1 to B2, played both on a bass trombone and a set of tubular didgeridoos, by proficient players. The listeners were asked to rate each note on a sliding scale from “very pleasant” to “very unpleasant”. Results showed that overall, the didgeridoo tones were found to be significantly more pleasant than the trombone tones. Surpisingly, the trombone tones were found to be more pleasant as tone height increased, while no correlation between tone height and pleasantness was found for the didgeridoo..

Keywords: perception, pleasantness, didgeridoo, didjeridu, trombone

PROCEEDINGS of ISMA 2019
International Symposium on Music Acoustics

13 - 17 September 2019 in Detmold, Germany

The Impulse Pattern Formulation (IPF) as a nonlinear model of musical instruments

Simon LINKE[(1,2)], Rolf BADER[(1)], Robert MORES[(2)],

[(1)]Institute of Systematic Musicology, University of Hamburg Germany
[(2)]Hamburg University of Applied Sciences, Germany*

Abstract

The Impulse Pattern Formulation (IPF) is a top-down method which assumes musical instruments to work with impulses which are produced at a generator, travel through the instrument, are reflected at various positions, are exponentially damped and finally trigger or at least interact with succeeding impulses produced by the generator. The underlying recursive equation relates every new system state to previous values and their logarithm. Adding more system components increases the number of reflection points, thus the number of terms in the argument of the logarithmic function increases. Like other nonlinear equations, the IPF can produce stable states but also bifurcation and divergency and fully captures transitions between regular periodicity at nominal pitch, bifurcation scenarios, and noise.

Applying the IPF on musical Instruments, the nonlinear behavior like transients or multiphonics can be described, which would be very complicated or impossible using well-established methods such as modal analysis or finite element models. Furthermore, the IPF is used for sound synthesis which follows the fundamental principles of real musical instruments and, due to the simple mathematical description of the IPF, needs a very limited number of input parameters.

Keywords: Analysis, Modelling, Musical Instruments, Nonlinearities, Synthesis

1 INTRODUCTION

Understanding the fundamental principles of musical instruments has always been a crucial question in Musicology. As musical instruments in general consist of many somehow coupled components, there is a demand for simple model systems. Basic, linear models derived from mechanics or electro-dynamics yield to satisfying results when describing more general phenomenon, but they are lacking experimental evidence when dealing with real instruments. As Fletcher [9] states it is not possible to explain the perfect harmonic spectrum of sustained instruments without taking nonlinearity into account. Further, there are more sophisticated approaches like physical modelling. They offer decent answers even for very detailed questions, but they can be hardly transferred to other problems and usually need lots of calculations.

The Impulse Pattern Formulation (IPF) is a top-down model, which describes systems in the time domain in a strictly nonlinear manner. Due to its very general approach the IPF can be used to observe any arbitrary system which consists of mutually coupled subsystems concerning its stability and is able to reproduce complex transient behavior. Thus, the IPF can be transferred to any arbitrary instrument and further has the potential to be extended to completely different disciplines like neuroscience or network theory.

The following work gives a short overview of the IPF according to [4]. Further, some basic analytical considerations are carried out, to explore mathematical boundaries of the IPF which are necessary to apply the IPF to real systems. Finally, in sections 3 to 5 three different systems are observed to illustrate how the required modeling parameters are chosen and how the results can be interpreted.

*simon.linke@haw-hamburg.de

2 MATHEMATICAL DESCRIPTION

2.1 Derivation

According to Bader [5] musical instruments in general should be considered as self-organized systems. Particularly he assumes every instrument to be driven by impulses. This is reasonable for percussion or plucked string instruments, but it is also plausible for any other instrument, for instance reed and brass instruments: The valve-like behavior of the reed, or the lips of the player leads to distinguished single impulses entering the tube.

Musical instruments are often described as a generator acting on a resonator (e.g. [10]). The IPF is somewhat more general: A musical instrument is a system acting upon itself, consisting of mutually coupled subsystems, possibly even interacting backwards. The system can be analyzed from the perspective of any subsystem, as it sends out impulses while responding to other subsystems. To make this a little bit more ostensive, we choose the simple example of a reed instrument e.g. a saxophone. It consists of two subsystems: a reed and a tube. Taking the point of view on the reed, the reed sends out impulses which are answered by the tube. According to Bader [4, p. 286] the answer is just a callback of the impulses send out by the reed. As the back-traveling impulses have an impact on the reed, the change of the system is caused by the system itself:

$$\frac{\partial \bar{g}}{\partial t} = \frac{1}{\alpha}\bar{g} \tag{1}$$

where α is the strength of the back-traveling impulse. In the chosen example of a reed instrument, this is related to the playing pressure. The system state is represented by $\bar{g}$. Bader [4, p. 286] states that it is connected to the amplitude and the periodicity of a signal. The meaning depends on the system which is observed. In the sections 3, 4 and 5 is meaning of g for three different musical instruments discussed.

According to physics it must be assumed that the impulse needs a certain amount of time to travel through the tube and back to the reed. Furthermore, the impulse would be exponentially damped. Thus, Bader [4, pp. 286-288] deduces the IPF in its most simple form:

$$g_+ = g - ln\left(\frac{g}{\alpha}\right) \tag{2}$$

Where g is the system state for a given time step and g_+ is the system state for the following time step. There is no precise time interval between g and g_+. It is just the time until a new event occurs. Usually, this is just one fundamental period $T = 1/f$. Choosing an initial value g_0, Equation (2) can be iteratively calculated. Observing the limits of the resulting sequence, it can be shown that the IPF can diverge or converge to a limit, depending on α. Furthermore, the IPF can show chaotic behavior like bifurcations. The limits for the IPF depending on α are shown in Figure 1. Bader [4, pp. 294] showed that for a constant control parameter α the IPF usually converge after $n > 300$ iteration steps. Therefore, 2500 iteration steps of Equation (2) were performed. To distinguish between bifurcations and chaotic behavior, the last 500 values g_n were taken into account.

Comparing Figure 1 with the chosen example of a reed instrument, we get a raw impression of the tone production: Low playing pressure, resulting in high values $1/\alpha$, is represented on the right side of the chart. The shown unstable behavior results in noisy sounds. Increasing the playing pressure α results in bifurcations. Here multiple frequencies can be heard at the same time. Further increasing of the pressure leads to stable states resulting in regular periodic motion.

By now, systems consisting of only two subsystems were described. Adding more subsystems results in adding more reflection points. Thus, the send-out impulse will return at additional (later) time steps, with individual strength β_k. Hence, the system state of earlier time points g_{k-} gains influence on the new system state g_+. According to these assumptions, Bader [4, pp. 290-291] describes the IPF in its most general form:

$$g_+ = g - ln\left(\frac{1}{\alpha}\left(g - \sum_{k=1}^{n}\beta_k e^{g-g_{k-}}\right)\right) \tag{3}$$

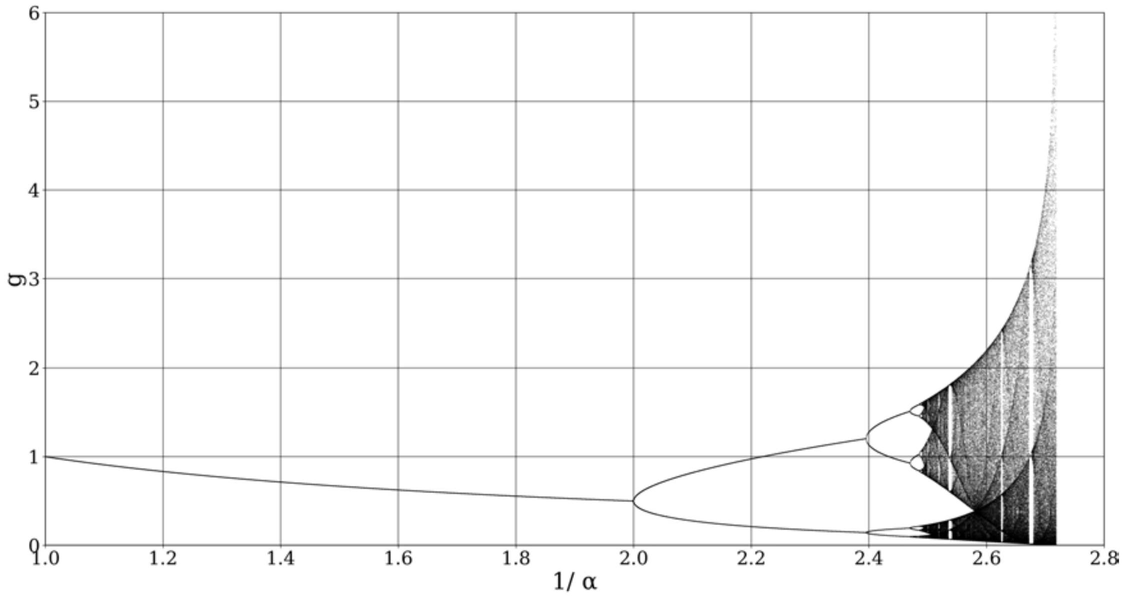

Figure 1. Bifurcation scenario of the IPF with one reflection point

Depending on β_k the IPF can become quite complex. The bifurcation scenario can be similar to the one described in Figure 1. But adding just one single reflection point, can change this significantly. Figure 2 shows the bifurcation scenario for a single reflection point $\beta = 0.164$. Due to the exponential function in Equation (3) two initial values g_{01} and g_{02} must be assumed. When choosing $g_{01} = 0.3$ and $g_{02} = 0$ there is no straight transition from stable, via chaotic to diverging states, directly. It is possible to return from a chaotic stage back to a stable state. Also, stable and chaotic domains can be interrupted by small diverging regions.

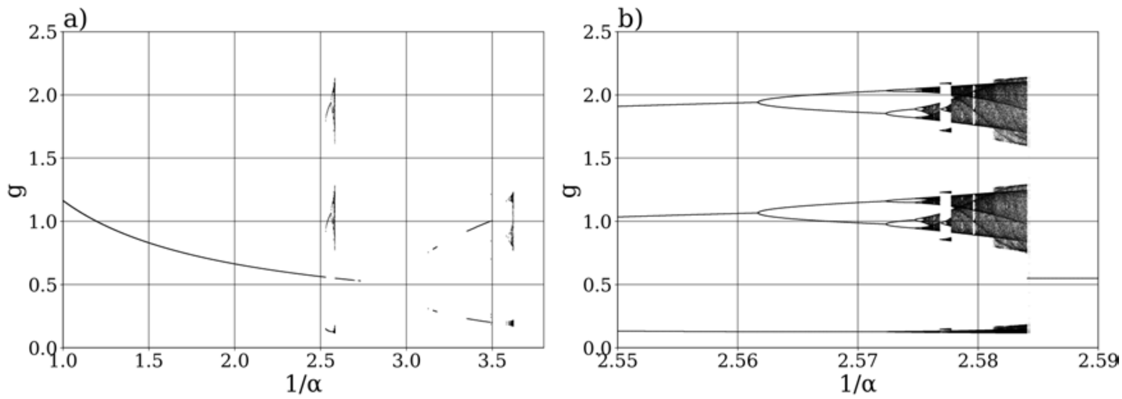

Figure 2. Bifurcation scenario of the IPF with two reflection points in dependence of $1/\alpha$ with $\beta = 0.164$. The right chart **b)** is a zoom of the chaotic region.

2.2 Boundaries and Stability

Referring to Bader [4, pp. 286-288] the parameter α is the input strength of the system. Therefore, only positive values α are physically reasonable. As β_k are the reflection strengths they had to be positive, too. If the conservation of energy is valid, the following restriction can be derived:

$$\alpha \geq \sum_{k=1}^{n} \beta_k \tag{4}$$

According to Bader [4, p. 291], higher orders k will result in smaller β_k, as they represent reflection points farther away from the excitation point. Therefore, reflected impulses return later and weaker. Hence, there is a second condition for the relationship of α and β_k:

$$\alpha > \beta_1 > \beta_2 > \beta_3 > ... > \beta_n \tag{5}$$

Referring to Figure 1, parameter g reaches no values above $1/\alpha \approx 2.7$. In this region g becomes complex and starts to diverge. Consequently, there seems to be a minimum α_{min}, which is the lower boundary for physically reasonable behavior. The only possibility to get complex values g_+ is, if the argument of the logarithm in Equation (3) is negative. Focusing on the simplest case with only one reflection point ($\beta_k = 0\, \forall k$), $g \leq 0$ must be valid. As the IPF is a recursive formula, this can be achieved, once the right-hand side (rhs) of Equation (2) is equal to zero. Thus, the critical value α_{min} must be described as a function in dependence of g:

$$\alpha_{min} = \frac{g}{e^g} \tag{6}$$

To find an expression of α_{min}, which is true for any g, the global maximum of function (6) must be calculated. Determining the first and second derivative results in one single maximum at $g = 1$, which also accords with the previous observation of Figure 1.:

$$\frac{1}{\alpha_{min}} = e \approx 2.7 \tag{7}$$

This approach could be expanded, to determine α_{min} for systems with more than on reflection point. But then, the expression depends on the different reflection strengths β_k and according to Equation (3) to the previous system states g_{k-}. Thus, the equation depends on the initial value g_0 and an analytical solution is no longer possible.

There is a fixed point $f(g_s) = g_s$ of the IPF, where the system state g is constant for all time points:

$$g_- = g = g_+ = g_{2+} = \ldots = g_{n+} = g_s \tag{8}$$

Thus, simplifying Equation (3) leads to a fixed point:

$$\begin{aligned} g_s &= g_s - ln\left(\frac{1}{\alpha}\left(g_s - \sum_{k=1}^{n} \beta_k e^{g_s - g_s}\right)\right) \\ g_s &= \alpha + \sum_{k=1}^{n} \beta_k \end{aligned} \tag{9}$$

A fixed point g_s exists for any combination of α and β_n, but according to Argyris et al. [1, pp.65-66] it is only stable if the absolute value of the first derivative is lower than 1. As the derivative depends again on the previous values g_{k-} and therefore on g_0 an analytic solution could be determined only for systems with one single reflection point ($\beta_k = 0\, \forall k$):

$$\begin{aligned} \left|f'(g_s)\right| = \left|1 - \frac{1}{\alpha}\right| &< 1 \\ \alpha &> 0.5 \end{aligned} \tag{10}$$

The critical point $\alpha_c = 0.5$ is called the first bifurcation point. If $\alpha > \alpha_c$ there exists only one stable fixed point. If α is lower than 0.5 bifurcations occur. Further decreasing of α leads to bifurcation of higher orders. This behavior can be easily verified when looking at Figure 1.

3 THE DIZI-FLUTE

Mirlitons are a special case of wind instruments. Here, one of the holes is equipped with a thin membrane [4, p. 227]. A representative of those instruments is the Dizi, a traditional Chinese transverse flute. It consists of bamboo and in contrast to traditional European transverse flutes there is an additional hole with a mirliton membrane attached, between the blowing hole and the first finger hole [18]. The sound is described to be nasal and buzzing [2], but also to be rough and rich in odd upper partials which result in multi-pitch effects [19].

Bader [4, pp. 227-228] compared two different dizi sounds of the same fundamental pitch. But while one sound was recorded playing the dizi how it is supposed to be, the second sound was recorded with a finger covering the membrane hole, to estimate its influence. He deduces that the membrane adds a noticeable amount of roughness to the sound and even though the overall spectrum stays harmonic each partial gets surrounded by sidebands. The resulting spectrum shown in Figure 3 a) also shows an increasing amount of higher partials.

Such an behavior could be explained by frequency modulation (FM) according to Chowning [6], where a modulating frequency which correspond to the fundamental frequency f_0 extends the spectrum to higher partials and a second significantly lower modulating frequency is responsible for the sidebands of each partials. These two modulation frequencies could be condensed to one modulating frequency fluctuating around f_0. There had already been some approaches to model the dizi using FM (e.g. [2]) but they rather focusing on the transition between to tones, than on the influence of the membrane hole. When modelling the dizi using the IPF the

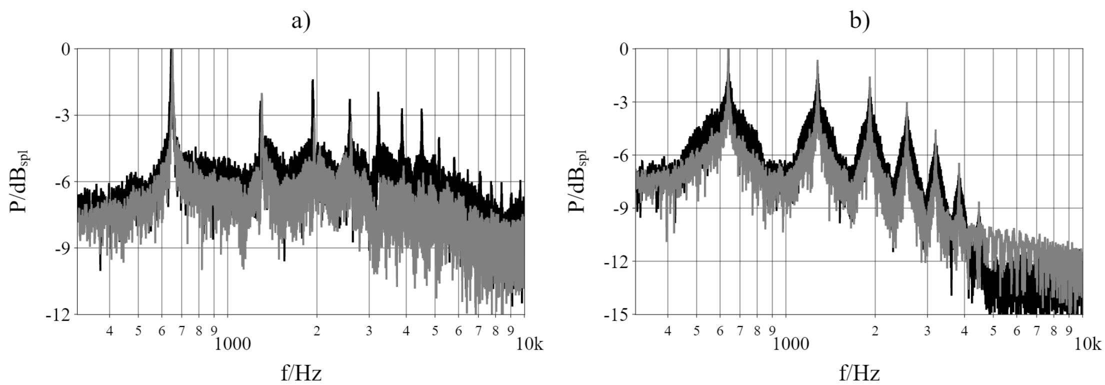

Figure 3. Spectrum of the dizi with (black) and without (gray) a mirliton membrane attached. Where a) corresponds to a measurement and b) to a model using the IPF

necessary number of β_k must be derived from the instrument geometry. If the membrane hole is covered, only one reflection point exists. An impulse entering at the embouchure gets reflected at the first open finger hole (or end of the tube, if all finger holes are closed) and returns to the embouchure. Thus, only α and no β_k is necessary to describe the resulting behavior. Releasing the finger from the membrane hole, adds an additional reflection points and thus β_1.

As α is related to the blowing pressure, it changes during tone production. To obtain a realistic time series of α, the envelope of a recorded dizi sound is chosen. Then a suitable normalization is necessary. The IPF should not diverge but preferably all possible values of α should be utilized. As the membrane hole is closed alpha can be normalized to the interval $[1/e, 1]$ according to Equation (7). If the membrane hole is opened, a suitable value α_{min} in accordance to the chose β_1 must be determined numerically.

With Equation (3) a time series of different g can be calculated using α. Just by observing this time series it is possible to deduce if stable or instable tones are produced. Further, focusing on the transition from instable to stable states, the transient behavior of the dizi can be determined. But for sound production the underlying waveform must be estimated. The spectral content of the waveform is crucial for the produced sound. To stay close to the motivation of the IPF a sharp Gaussian function is chosen. Thus, the resulting sound can be archived, just by creating a train auf those Gaussian pulses. But the length of every pulse must be modulated in respect to the change of g. The resulting period-length T_k could be described as:

$$T_k = \frac{1}{f_0}(1 + (g_k - g_{k-})) \tag{11}$$

where g_k is the current and g_{k-} is the previous system state. If the system is stable every system state corresponds to the fixed point $g_k = g_{k-} = g_S$. Thus, results in a tone with the fundamental frequency f_0. Bifurcations or transient behavior are leading to a frequency simulation similar as described above. According to Bader [4, p. 286] g is also connected to the amplitude. Thus, every Gaussian pulse is weighted by the actual system state g_k. The resulting sound equals the spectral properties of the dizi, but for a more realistic envelope, the resulting signal could be multiplied with the blowing pressure α.

The modelled sounds, as well as the recordings of the dizi, are provided by [12][1]. It is notable, that there is a strong evidence in the change of the sound when adding β_k respectively a mirliton membrane. Still there are some remarkable differences between the model and the recording, as the underlying equation and waveform have been chosen as simple as possible. Looking at the two different spectra in Figure 3 b), it is glaring that adding $\beta_1 = 0.245$ leads to sidebands. Although there is less influence of higher partials, the model in general corresponds to the behavior of a dizi with and without membrane.

4 MULTIPHONICS IN REED INSTRUMENTS

In reed instruments there are several technics to produce sounds with more than on harmonic overtone spectrum [4, p. 226]. One common way to produce these so-called multiphonics is the use of uncommon fingerings [3]. For stable tone production the first open hole determines the length of the tube and thus the fundamental frequency. Up to the first open hole all holes are close and further down all holes are open. When producing multiphonics more complex patterns of open and closed holes are used. Further, the embouchure and the (usually low) blowing pressure must be controlled very carefully [4].

Figure 4 shows a fingering for an multiphonic played on a clarinet, which can be found in multiple collection of multiphonic fingerings (e.g. [16] and [8]). The resulting sound is described to consist of two dominating frequencies which approximately could be notated as the musical interval E_4-G_5 There are three regions of open holes which are likely to reflect the sound wave propagating through the tube. Those can be transferred to the IPF. The first reflection point occurs due to the open register key on the back. It lies closely under the barrel-joint and is represented by α. The press C#-key results in another open hole on the back of the instruments. It lies close to the open hole in the middle of the instruments. So, both could be condensed to one reflection point β_1. The end of the tube is caused by two open holes between the undermost key and the bell and is represented by β_2.

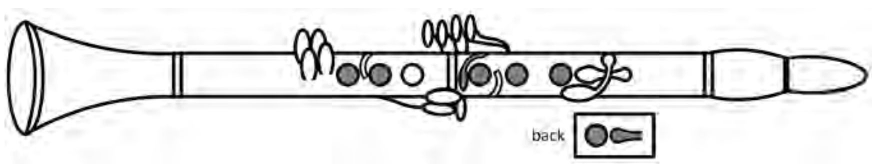

Figure 4. Sketch of a Clarinet: Grey circles correspond to closed holes when producing the investigated multiphonic.

When modeling multiphonics using the IPF, it is plausible that they are related to bifurcating regions. Here, the audible intervals are represented by the ratio of the possible system states g_k/g_{k-}. Thus, it can be examined

[1] https://zenodo.org/record/3258207#.XSSd8Y9CQuU

numerically, which combinations of β_1 and β_2 are able to produce the given interval of 15 semitones for any initial value g_0. As this is possible for many combinations, it is assumed that for reliable production of multiphonics small changes of blowing pressure or embouchure should not change the sound excessively. Therefor the derivative of g_k/g_{k-} in respect to α should be as small as possible. For the given multiphonic this could be achieve choosing $\beta_1 \approx 2.5 \cdot 10^{-3}$ and $\beta_2 \approx 0.35$. Where it is conspicuous that this violates condition (5).

Choosing an appropriate time series for α sounds can be synthesized in as similar manner as already done in section 3. Again, a Gaussian pulse is chosen as a raw approximation auf the fundamental waveform. But this time it must be modulated slightly different, according to the different interpretation of g mentioned above. The length of every period t is changed according to the ratio of the system states:

$$T = \frac{1}{f_0} \frac{g}{\tilde{g}} \tag{12}$$

where g is the actual system state. Choosing $\tilde{g} = g$ results in a signal with oscillates with the fundamental frequency f_0. Now a second signal can be added, where $\tilde{g}$ equals the previous system state g_-. Thus, both signals oscillate with the same frequency f_0 if $g = g_- = g_S$. As soon as bifurcation occurs, two pitches are perceived. Adding additional signals where $\tilde{g}$ equals earlier system states (g_{2-}, g_{3-}, g_{4-}, ...) allows to synthesize bifurcations of higher order.

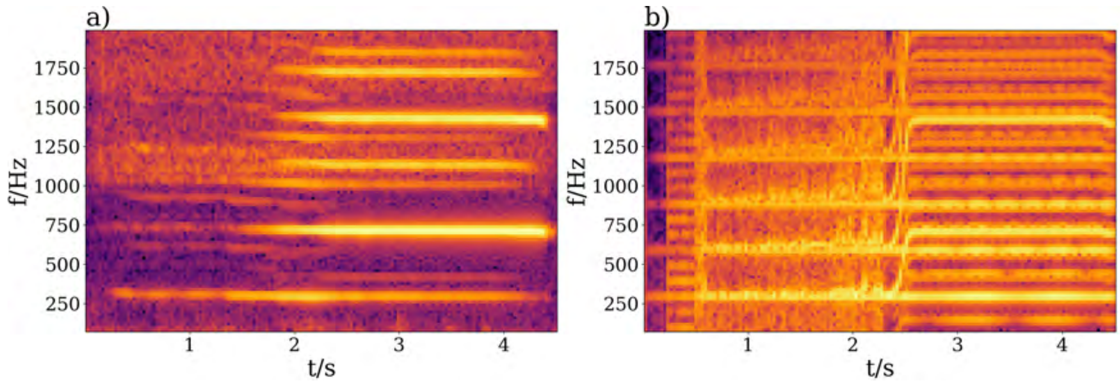

Figure 5. Spectrogram of a) a recorded multiphonic and b) its synthesized version

The multiphonic sound mentioned above was recorded. Slowly adjusting embouchure and blowing pressure allows a transition from a stable sound to a bifurcation. Comparing this sound with a synthesized version (both provided by [12][2]) shows that both presents a sudden transition from one to two pitches and no remarkable pitch glide, even though α was gradually changed. Figure 5 shows the related spectrograms. Looking at the synthesized version b) a pitchglide can be noticed but only during a very short period of time. Further, it is obvious that a Gaussian pulse as the fundamental waveform was not the ideal choice, as there is a strong spectral difference between the model and the recording even for stable tones with one perceived pitch.

5 THE BOWED STRING

The motion of a bowed string has always been a much-discussed question [10]. While bowing, the bow displaces the string due to the stickiness of the rosin. As the restoring force of the string exceeds the static friction of the bow, the string suddenly slips back. Subsequently the bow recaptures the string again, resulting in periodical motion of the string called Helmholtz motion [11]. But such behavior only occurs if the right ratio of bow

[2] https://zenodo.org/record/3258207#.XSSd8Y9CQuU

force F and bow velocity v_b (in respect to the bowing position) is applied. If the bow force is low, the strings slips back to early and gets recaptured by the bow before reaching the equilibrium. Those effects can emerge several times during one period T and result in frequency doubling and scratchy sounds [7, p.58]. Several attempts have been made to find an analytical expression for the necessary minimum bow force (e.g. first time by Raman [15] in 1918 and most prominent by Schelleng [17]). Mores [14] showed, that those expressions change drastically when treating the bow-string interaction as a self-organized system. Further, the transition time from unstable to Helmholtz motion is crucial for quality of bowed string instruments, as Giordano [11] stated. Since the IPF (due to its recursive formulation) is a straightforward model of transient behavior, it seems to be an appropriated solution for investigating this transition. Thus, a dynamical model of the complex transient behavior of a bowed string is obtained, rather than an analytical expression for a quasi-stationary minimum bow force.

The bow-string interaction of a monochord is measured using and a self-organized bowing pendulum as described by [13]. Transition from unstable to Helmholtz motion are achieved by slowly increasing the bow force. When just focusing on bow-string interaction and neglecting all other instrument parts the system can be described by the IPF in its most simple form as given by Equation (2). Then a suitable time series of α is assumed to model the measurement. Thus, an analytical expression for α in respect to bow force and bow velocity could be determined in future research.

As underlying waveform one period of the measured Helmholtz motion is chosen. Again, the amplitude of each period is multiplied with the actual system state g. Another sawtooth signal (with lower amplitude) is added, but every period is phase-shifted proportional to $g - g_-$. Thus, double slips can occur during transients or bifurcations. Two more sawtooth signals are added with phase-shifts proportional to $g - g_{2-}$ and $g - g_{3-}$, to achieve more realistic transients. The amplitudes of added signals are decaying according to the harmonic series. The number of added sawtooth signals as well the decaying of their amplitudes refers to the assumed dampening of the string.

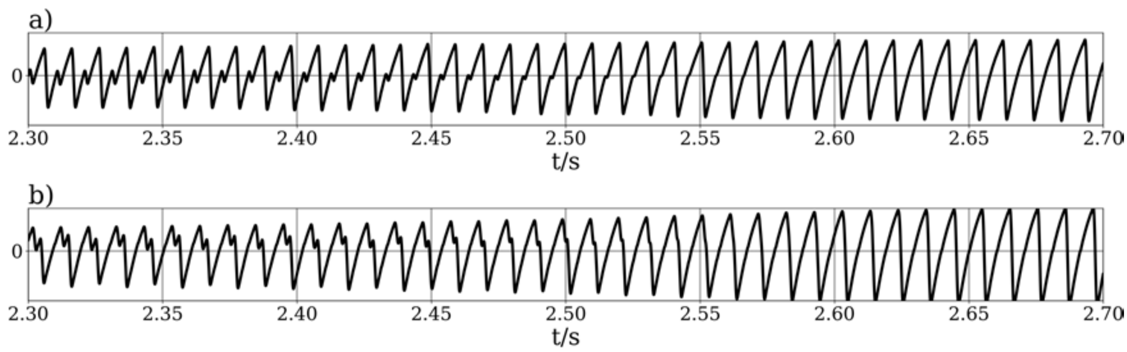

Figure 6. Timeseries of the transition into Helmholtz motion for measured (above) and modeled bow-string interaction (below)

Figure 6 compares the transition into Helmholtz motion of a measured bow-string interaction to the modeled transition. The general behavior is again similar, but the amplitude of the double-slip seems to be too large. They sound very similar too, but it is conspicuous, that when double slips occur, subharmonics are dominating in the synthesized sound, while in the recorded version the upper partials are prominent. This can be perceived when listening to both sounds, as they are provided by [12][3]. This can be avoided if the ratio between amplitude modulation and the introduced phase shift is balanced more carefully.

[3] https://zenodo.org/record/3258207#.XSSd8Y9CQuU

6 CONCLUSIONS

The IPF as introduced in section 2 can model a variety of musical instruments. Only a very limited amount of system parameters (α and β_k) must be deduced when making reliable observations concerning the system stability. For an elaborated investigation of the produced sound, a suitable interpretation of g is crucial. Therefore, some deeper knowledge about the fundamental principles of the observed system is necessary. Three different interpretations of g where given in the sections 3 to 5. In addition, the fundamental spectral content must be chosen very carefully, if the IPF is supposed to be used as a synthesizer.

In future research a deeper comparison between the chosen set of modeling-parameters and measurements of real instruments should be done. Hence, it would be possible to deduce for instance an appropriated set of β_k just from measurements of the instrument geometry or physical input parameter like blowing pressure or bow force could be analytically map to α. Thus, some more profound observations concerning the system stability would be possible.

REFERENCES

[1] J. H. Argyris, G. Faust, M. Haase, and R. Friedrich. *An Exploration of Dynamical Systems and Chaos: Completely Revised and Enlarged Second Edition*. Springer Berlin Heidelberg, Berlin, Heidelberg, 2015.

[2] L. Ayers. Synthesizing trills for the chinese dizi. In *ICMC*, 2003.

[3] J. Backus. Multiphonic tones in the woodwind instruments. *The Journal of the Acoustical Society of America*, 63(2):591–599, 1978.

[4] R. Bader. *Nonlinearities and synchronization in musical acoustics and music psychology*, volume 2 of *Current research in systematic musicology*. Springer, Berlin [et al.], 2013.

[5] R. Bader, editor. *Sound - Perception - Performance*, volume 1 of *Current research in systematic musicology*. Springer, Heidelberg, 2013.

[6] J. M. Chowning. The synthesis of complex audio spectra by means of frequency modulation. *Journal of the Audio Engineering Society*, 21(7):526–534, 1973.

[7] L. Cremer. *Physik der Geige*. Hirzel, Stuttgart, 1981.

[8] G. J. Farmer. *Multiphonic trills and tremolos for clarinet*. PhD thesis, @Eugene, Or., Univ. of Oregon, Diss.,, Ann Arbor, Mich., 1977.

[9] N. H. Fletcher. Mode locking in nonlinearly excited inharmonic musical oscillators. *The Journal of the Acoustical Society of America*, 64(6):1566–1569, 1978.

[10] N. H. Fletcher and T. D. Rossing. *The physics of musical instruments*. Springer, New York, NY, 2. ed., [rpt..] edition, 2010.

[11] N. Giordano. Some observations on the physics of stringed instruments. In R. Bader, editor, *Springer Handbook of Systematic Musicology*, Springer Handbooks, pages 105–119. Springer, Berlin, Heidelberg, 2018.

[12] S. Linke. Sounds, synthesized using impulse pattern formulation, 2019.

[13] R. Mores. Precise cello bowing pendulum. *Proc. of the Third Vienna Talk on Music Acoustics*, 106, 2015.

[14] R. Mores. Complementary empirical data on minimum bow force. *The Journal of the Acoustical Society of America*, 142(2):728–736, 2017.

[15] C. V. Raman. On the mechanical theory of the vibrations of bowed strings and of musical instruments of the violin family, with experimental verification of the results: Part 1. *Indian Assoc. Cultiv. Sci. Bull.*, 15:1–158, 1918.

[16] H. Roche. 27 easy bb clarinet multiphonics, 2018.

[17] J. C. Schelleng. The bowed string and the player. *The Journal of the Acoustical Society of America*, 53(1):26–41, 1973.

[18] A. Thrasher. The transverse flute in traditional chinese music. *Asian Music*, 10(1):92, 1978.

[19] C.-G. Tsai. The timbre space of the chinese membrane flute (dizi): Physical basis and psychoacoustical effects. *The Journal of the Acoustical Society of America*, 116(4):2620, 2004.

PROCEEDINGS of ISMA 2019
International Symposium on Music Acoustics

13 - 17 September 2019 in Detmold, Germany

MAESSTRO: A sound synthesis framework for Computer-Aided Design of piano soundboards

Benjamin Elie(1), Xavier Boutillon(2), Juliette Chabassier(3), Kerem Ege(4), Bernard Laulagnet(4), Benjamin Trevisan(4), Benjamin Cotté(1), Nicolas Chauvat(5)

(1)Ensta-ParisTech, France, name.surname@ensta-paristech.fr

(2)LMS, école polytechnique, France, xavier.boutillon@polytechnique.edu

(3)Inria, France, juliette.chabassier@inria.fr

(4)LVA, INSA Lyon, France, name.surname@insa-lyon.fr

(5)Logilab, France, nicolas.chauvat@logilab.fr

Abstract

The design of pianos is mainly based on empirical knowledge due to the lack of a simple tool that could predict sound changes induced by changes of the geometry and/or the mechanical properties of the soundboard. We present the framework of a program for the Computer-Aided Design of piano soundboards that is intended to bridge that gap by giving piano makers a tool to synthesize tones of virtual pianos. The sound synthesis is solely based on physical models of the instrument in playing situation. The calculation of the sound is split into several modules: computation of the modal basis of the stiffened soundboard, computation of the string dynamics, simulation of the soundboard dynamics excited by the string vibration, and calculation of the sound radiation. Reference tests of sound synthesis of real pianos as well as sound synthesis of modified pianos are used to assess our main objective, namely to reflect faithfully structural modifications in the produced sound, and thus to make this tool helpful for both piano makers and researchers of the musical acoustics community.

Keywords: Piano soundboard, Assistance to musical instrument manufacturing, Sound synthesis

1 INTRODUCTION

When they design stringed musical instruments, manufacturers traditionally use empirical approaches. This usually leads to marginal improvements of existing schemes. One of the main reason explaining the difficulty for a revolution to take place, in musical instrument design, is the lack of a simple tool that might predict sound changes induced by virtual changes of the geometry, and/or the mechanical properties of the instrument.

In the case of the piano, many studies have been made in the past in order to fully comprehend all of the physical phenomena that are involved in the tone production, which is necessary for manufacturers to overstep empirical approaches. For instance, many authors have studied the vibro-acoustic behavior of the piano soundboard, either by experimental characterization [1–5], or by proposing simplified models [6–9] or finite element models [5, 10]. The string behavior, including the hammer-string interaction and the string-bridge coupling, has also been studied by several authors [10–15].

All of the aforementioned studies contributed to a better understanding of the piano functioning and several models are now available to numerically simulate separately the mechanisms of the piano tone production chain, from the hammer activation to the radiated sound. By gathering some of these different numerical methods, a framework of a program for the Computer-Aided Design (CAD) of piano soundboards is presented in this paper. It is solely based on physical models of the instrument in playing situation, and thus provide to piano makers a simple tool to predict the acoustic characteristics of a virtual piano, in regards to its specific geometry and to the mechanical properties of the materials that compose the soundboard and the strings.

This CAD program is made available for any piano maker or academic researcher in the form of a software, called MAESSTRO[1], which present several functionalities to assist the piano maker in the design process. The software architecture is presented in Sec. 2. Case studies are presented in Sec. 3 to highlight the functionalities of MAESSTRO, and analyzes of piano tones synthesized by MAESSTRO are presented in Sec. 4.

2 SOFTWARE ARCHITECTURE

2.1 General principles

The different functionalities of the sound synthesis framework MAESSTRO are the following: i) entering the geometry and the materials of the virtual soundboard thanks to a Graphical User Interface (GUI), ii) feeding MAESSTRO with MIDI files to be synthesized, iii) simulating numerically the physical phenomena involved in the production of piano tones, iv) post-processing the software outputs, and v) creating audio files of synthesized piano tones.

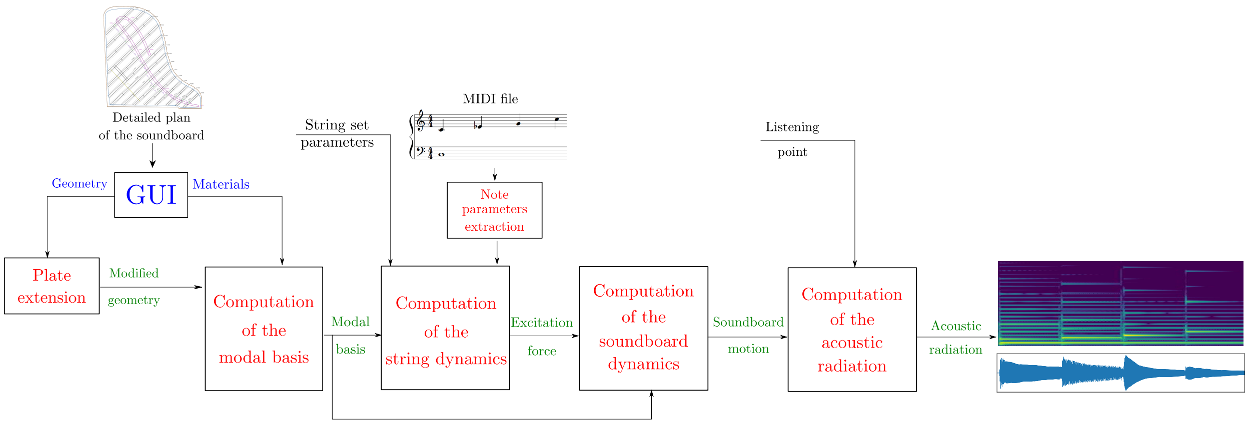

Figure 1. Block-diagram showing the software architecture. The input data provided by the user are represented by a black font color. Blue corresponds to user data entered in the GUI. The software operations and the software outputs are represented by the red and green font colors, respectively.

Fig. 1 represents the global functioning of the software. It consists in a sequence of software operations that yields output synthesized piano tones from inputs specified by the users, including the geometry and the materials of the virtual soundboards, the string set parameters, and the tones to be played. First, the normalized data about the geometry and the materials of the virtual soundboard can be defined with the help of a specifically designed GUI (see Sec. 2.2). Then, the modal basis of the virtual soundboard is computed with a semi-analytical model [9]. To synthesize specific tunes, the user may directly give a MIDI file in which MAESSTRO will extract the tone information, namely the note index, the key activation and release instants, as well as the hammer initial velocity. A non-linear finite-element model of string dynamics [10] is then used to compute the bridge excitation force applied by the struck strings. Using the elements of the modal basis of the virtual soundboard, we can then compute the soundboard dynamics and the acoustic radiation at any listening point specified by the user. The different software operations are detailed in the next sections.

2.2 Computer-Aided-Design of the virtual soundboard

The software needs data about the geometry of the virtual soundboard and about the mechanical properties of its materials, which are gathered into a geometry file in a normalized format (JSON). In order to assist the user to build this geometry file, we specifically designed a Graphical User Interface[2], developed in Typescript+React.

[1] More information available at `https://maesstro.cnrs.fr`
[2] It is available from any web browser at the following url: `https://maesstro.demo.logilab.fr/`

The choice of developing our own GUI has been motivated by the fact that adapting geometry data from standard 3D CAD commercial software to our geometric modeling would have added too much complexity, including naming convention of the soundboard components (panel, bridge, ribs...) to extract the corresponding volumes.

The computation of the soundboard dynamics considers three main classes of structural components of the soundboard geometry, namely the main panel, the bridges and the ribs. The GUI can then be used to define the characteristics that are specific to each class. For instance, this includes the coordinates of the points defining the panel contour, or the evolution of the width and the thickness of the bridge along its median line, and so on.

2.3 Computation of the modal basis

The computation of the modal basis is based on a simplified model of the soundboard geometry that allows us to compute analytically the modal basis of ribbed orthotropic clamped panels with any contour [9]. The general principle is to consider a simply supported rectangular plate with special orthotropy in which the considered panel contour is entirely included. This contour can then be defined inside the so-called *extended plate* with a spring distribution, as shown in Fig. 2.

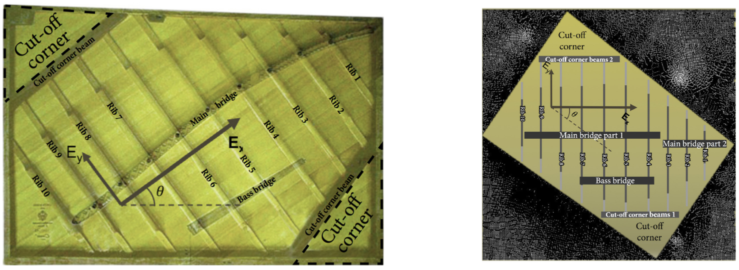

Figure 2. Exemple of modification of the geometry for a Pleyel P131 piano used to compute of the modal basis. Left is the original geometry. Right is the modified geometry. The black region in the right figure is the spring distribution used to define the contour of the analyzed panel in the extended plate geometry. Figure extracted from [9].

2.4 Simulation of the string dynamics

The string dynamics is simulated with a specifically designed module which uses the finite-element code Montjoie [10]. It considers a Timoshenko model to account for the string stiffness, and the geometrically exact model to account for non-linearity due to local geometric deformation of the string. In order to accurately model the string-soundboard coupling, the modal basis of the soundboard should be computed prior to simulate the string displacement.

2.5 Computation of the soundboard dynamics

Once the displacement of the string is simulated, the transverse force applied to the bridge can be computed, as well as the resulting soundboard dynamics. Thus, the soundboard motion for the j^{th} mode, denoted $\phi^j(x,y)$, in the extended plate coordinate system is given by

$$\Phi^j(x,y) = \sum_{n,m} A^j_{n,m} \sin\left[\frac{n\pi x}{L_x}\right] \sin\left[\frac{m\pi y}{L_y}\right], \tag{1}$$

where $A^j_{n,m}$ is the eigenvector associated to the j^{th} mode, and L_x and L_y are the length and width of the extended plate. Then, the motion of the table at time t in response to the transverse force applied by the string i is given by

$$u_i^j(x,y,t) = \sum_j q_i^j(t)\Phi^j(x,y), \tag{2}$$

where $q_i^j(t)$ is the modal coordinate at time t associated to the j^{th} mode.

2.6 Computation of the sound radiation

Finally, considering a point M in a 3D pressure field around the extended plate, defined by its coordinates $\{x_{ac}, y_{ac}, z_{ac}\}$, the radiated sound pressure $p(M,t)$ is computed using the Rayleigh integral and assuming the soundboard is baffled.

3 CASE STUDIES

This section presents the different cases that are used in this paper to show some possibilities of the MAESSTRO software. It consists in building a virtual reference piano, here a Steinway D, which is subject to several modifications to evaluate the acoustic impact of these structural modifications. The chosen modifications include increase of the panel thickness, removal of half the ribs, and removal of all the ribs. This results in 4 cases, namely the reference piano (RP), and the 3 modified pianos (MP1, MP2, and MP3).

The reference piano geometry is a simplified version of the Steinway D. The geometric data has been extracted via the MAESSTRO GUI, as shown in Fig. 3.

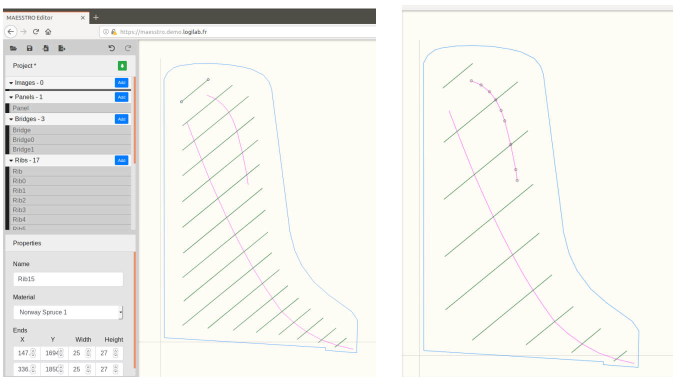

(a) Reference piano (b) Modified piano #2

Figure 3. Screen shot of the GUI after completion of the design of the virtual Steinway D. The panel contour is shown in blue, the median line of the bridges in pink and the median lines of the ribs in green. Left is the reference piano, right is the modified piano 2, labeled as MP2

The first modified piano (labeled as MP1) is similar to the reference piano RP except that the thickness of the soundboard is twice as the one of RP, namely 18 mm, while it is 9 mm for RP. The second modified piano, MP2, is similar to RP but with inter-rib spacing twice as RP (see Fig. 3 (b)). Finally, the third modified piano, MP3, is similar to RP but with no ribs: all ribs have been removed and the bridges are the only superstructures. Qualitatively, in comparison with RP, MP1 is similar to a stiffer piano, whereas MP2 and MP3 are similar to a slightly softer reference piano and to a highly softer piano, respectively.

Although this is unlikely to be representative of what piano manufacturer would try in real life, we chose these caricatural structural modifications of the reference piano in order to emphasize their acoustic impact in the resulting tones. Besides, these gross modifications make the qualitative prediction of the variations in the

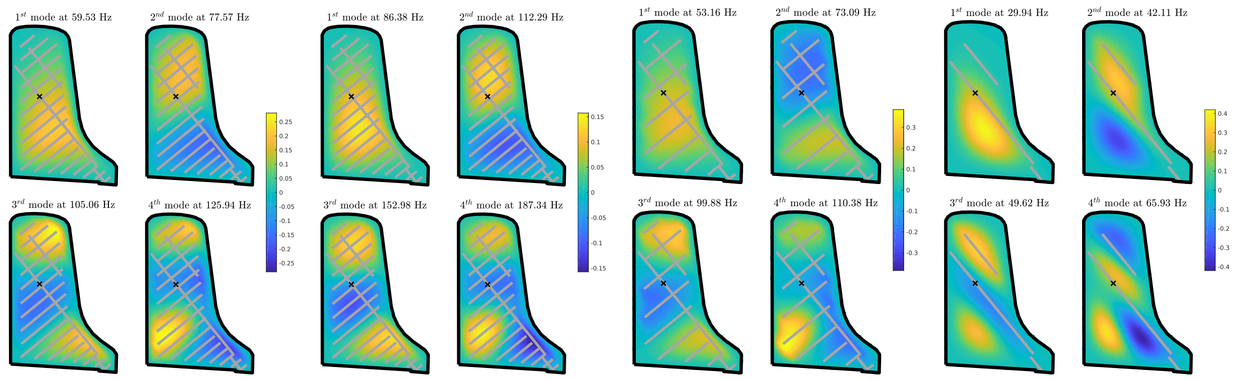

(a) Reference piano (b) Modified piano #1 (c) Modified piano #2 (d) Modified piano #3

Figure 4. First mode shapes of the reference piano and the modified ones computed with the method detailed in Sec. 2.3. The coupling point of the C3 string at the bridge is denoted by the black cross.

mechanical behavior and some acoustic features possible.

For all of the virtual pianos, the strings are assumed to be the same. The parameters of the string set are taken from a technical report [16], which provides all of the required information to compute the dynamics of any string of the virtual reference piano, including string geometry and tension, Young modulus of the string materials, internal damping, and location of the bridge coupling points. It also provides the mechanical parameters of the hammers, namely the mass, the stiffness, and the impact location on the string. For this study, we used the wrapped strings model of [16].

4 RESULTS

For the sake of concision, we present results of a single piano tone that have been synthesized using the four virtual soundboards. The tone is C_3, with a fundamental frequency of 131.11 Hz. The initial velocity is kept at 1 m/s for the four synthesized tones, and the tone is sustained as if the key were not released until the complete note extinction. We present first the computed mechanical properties of the tested soundboards, and then the synthesized tones.

The synthesis has been done on a UNIX machine with 4 CPU processors at 2.3 GHz. The computation times for each module, corresponding to the synthesis of a tone of 7 seconds, are the following: 132 s for the computation of the modal basis, 1007 s for the string dynamics, 70 s for the soundboard dynamics, and 68 s for the acoustic radiation, hence a total of 1277 s.

4.1 Mechanical properties

Fig. 4 shows the first 4 modes associated to the different configurations. Although removing the ribs lowers the mass of the soundboard, its main effect is to lower the global stiffness of the soundboard, hence the fact that the mode frequencies are smaller in the half- and no-ribs configurations. Conversely, a thicker plate, such as for MP1, increases both the mass and the stiffness, but whereas mass increase is proportional to the thickness h, the stiffness increase varies with h^3. As a consequence, the thick plate MP1 has higher modal frequencies than other thinner plates, and consequently, a lower modal density.

Following the mean-value theorem by Skudrzyk [17], for structures with similar mass, the mean-value of the mobility lowers as the stiffness increases. Consequently, MP1 has the lowest mobility while MP3 has the largest.

4.2 Synthetized tones

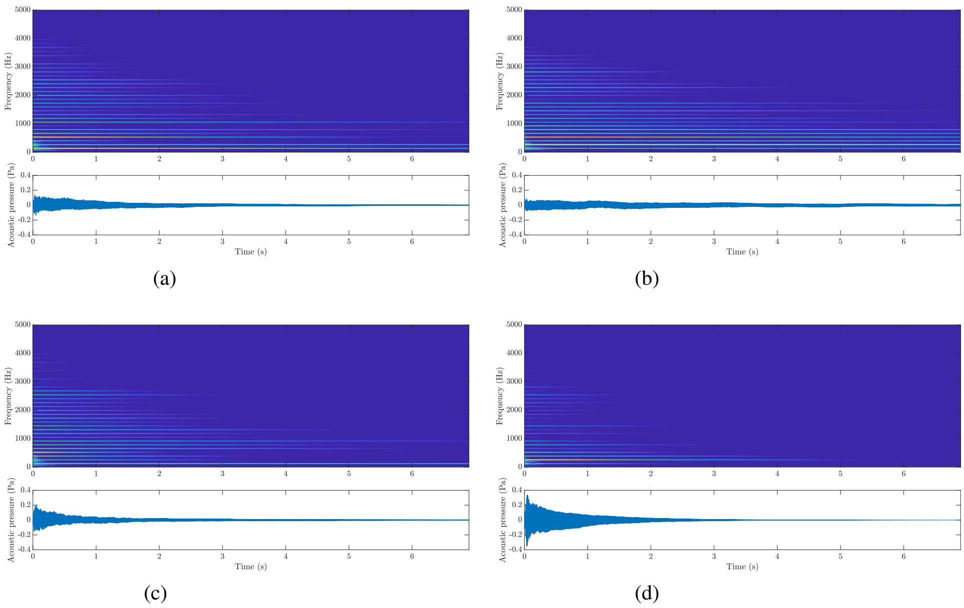

Figure 5. Synthesized tone waveforms and their corresponding narrow-band spectrograms for the 4 different piano configurations.

Fig. 5 displays the narrow-band spectrograms and acoustic pressure waveform of the 4 synthesized C_3 corresponding to the 4 different piano configurations. One can notice salient differences: the synthesized tones from MP2 and MP3 decay much faster than other tones. Interestingly, for MP2 and MP3, individual decays vary significantly from a partial to the next: the second partial of MP3 (at 2 f_0) presents the largest sustain while it is fundamental for MP2. Additionally, although MP3 presents the fastest decay, it also has the highest acoustic pressure level at the beginning of the tone. These observations are in agreement with our expectations, since in addition to the intrinsic dissipative mechanisms in the string, a coupling with a mobile structure adds an additional damping that increases with the structural mobility. Sounds may be heard by clicking on the subplot legends.

Indeed, as stated in Sec. 4.1, MP2 and MP3 have mobility levels higher than RP and MP1, which results in higher additive string damping terms, and consequently in faster decays of the synthesized tones. Also, as the damping mechanism due to the coupling gets large, it may eventually become predominant in comparison with the intrinsic string damping mechanisms. In that case, the total damping term associated with a partial is directly proportional to the mobility at the partial frequency. Consequently, the decay distribution along the different partials present the large variations similar to the mobility curve along the frequency axis.

4.3 Acoustic analysis

We choose to analyze the synthesized tones through its energy decay. This choice is motivated by the fact, as said in Sec. 4.2, that the energy decay is related to the mechanical behavior of the soundboard. The energy decay profile of the acoustic pressure $p(t)$ is computed as the Energy Decay Curves introduced by Schroeder [18] as

$$EDC_{dB}(t) = 10\log_{10}\left(\int_t^{+\infty} p^2(\tau)d\tau\right). \tag{3}$$

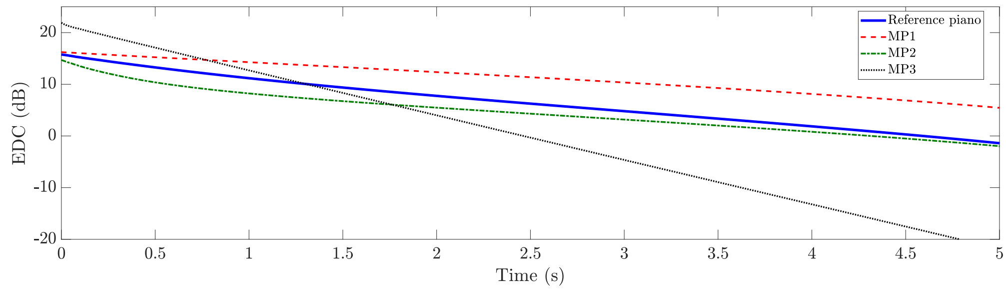

Figure 6. Energy decay curves of the synthesized tones.

Fig. 6 shows the EDC of the synthesized tones. They confirm the qualitative observations made from spectrograms in Sec. 4.2. The global energy decays faster for MP2 and MP3 than for RP and MP1. The decay of MP1 is also slightly slower than RP, which is also in agreement with our expectation since MP1 has a higher stiffness.

5 CONCLUSION

This paper has presented a framework of a program for the Computer-Aided Design of piano soundboards that is intended to help piano makers in the design process by giving them a tool to synthesize tones of virtual pianos. Case studies show the interest of the software in predicting acoustic impacts of structural modifications of a piano soundboard. Indeed, starting from a reference piano, we synthesized tones from three virtual pianos, which are modified versions of the reference piano. Modifications have been chosen to reflect variations of the global stiffness. The impact of these stiffness variations on the soundboard mechanical behavior and on the energy decay profile of the synthesized tone are in agreement with the theory. Stiffer soundboards present higher modal frequencies, which results in a lower modal density and in a lower mobility at the bridge. As a consequence, synthesized tones from stiffer soundboards present slower decays than soft soundboards.

Through a broad utilization of the software, piano makers will be able to virtually test new designs, and thus significantly enhance the pace of the trial and error process. This software might also be a useful tool of communication between piano makers and academic researchers. Thus, we are convinced that significant evolution of the traditional architecture of piano soundboards would emerge in the next future. The resulting synthesized piano sounds may however be still perceived as non-realistic, mainly because of the lack of fine and precise modeling of dissipative phenomena in both the soundboard and the strings, that could be addressed in the future. The coupling between the strings and the plate at the bridge rely on a very simple model (continuity of the vertical velocity) but measurements on real pianos point towards a more complex model allowing rocking and horizontal motion of the bridge. Finally, one major evolution could be the use of composite materials for the soundboards: the software could be used to predict the sound of a piano with soundboard made in specific composite materials, or even be used to find the mechanical properties which yield to the sound desired by the piano maker.

ACKNOWLEDGEMENTS

This work is part to the project MAESSTRO, with the financial support of the French ANR (Agence Nationale de la Recherche). The authors would also like to thank Denis Laxalde, Frank Bessou, and Viet-Hung Nhu from Logilab for the development and implementation of many modules of the software.

References

[1] H. Suzuki, "Vibration and sound radiation of a piano soundboard," *The Journal of the Acoustical Society of America*, vol. 80, no. 6, pp. 1573–1582, 1986.

[2] H. A. Conklin Jr, "Design and tone in the mechanoacoustic piano. part ii. piano structure," *The Journal of the Acoustical Society of America*, vol. 100, no. 2, pp. 695–708, 1996.

[3] N. Giordano, "Mechanical impedance of a piano soundboard," *The Journal of the Acoustical Society of America*, vol. 103, no. 4, pp. 2128–2133, 1998.

[4] K. Ege, X. Boutillon, and M. Rébillat, "Vibroacoustics of the piano soundboard:(non) linearity and modal properties in the low-and mid-frequency ranges," *Journal of Sound and Vibration*, vol. 332, no. 5, pp. 1288–1305, 2013.

[5] A. Chaigne, B. Cotté, and R. Viggiano, "Dynamical properties of piano soundboards," *The Journal of the Acoustical Society of America*, vol. 133, no. 4, pp. 2456–2466, 2013.

[6] N. Giordano, "Simple model of a piano soundboard," *The Journal of the Acoustical Society of America*, vol. 102, no. 2, pp. 1159–1168, 1997.

[7] J. Berthaut, M. Ichchou, and L. Jézéquel, "Piano soundboard: structural behavior, numerical and experimental study in the modal range," *Applied Acoustics*, vol. 64, no. 11, pp. 1113 – 1136, 2003.

[8] X. Boutillon and K. Ege, "Vibroacoustics of the piano soundboard: Reduced models, mobility synthesis, and acoustical radiation regime," *Journal of Sound and Vibration*, vol. 332, no. 18, pp. 4261 – 4279, 2013.

[9] B. Trévisan, K. Ege, and B. Laulagnet, "A modal approach to piano soundboard vibroacoustic behavior," *Journal of the Acoustical Society of America*, vol. 141, pp. 690–709, Feb. 2017.

[10] J. Chabassier, A. Chaigne, and P. Joly, "Modeling and simulation of a grand piano," *The Journal of the Acoustical Society of America*, vol. 134, no. 1, pp. 648–665, 2013.

[11] H. Fletcher, "Normal vibration frequencies of a stiff piano string," *The Journal of the Acoustical Society of America*, vol. 36, no. 1, pp. 203–209, 1964.

[12] G. Weinreich, "Coupled piano strings," *The Journal of the Acoustical Society of America*, vol. 62, no. 6, pp. 1474–1484, 1977.

[13] X. Boutillon, "Model for piano hammers: Experimental determination and digital simulation," *The Journal of the Acoustical Society of America*, vol. 83, no. 2, pp. 746–754, 1988.

[14] H. A. Conklin Jr, "Design and tone in the mechanoacoustic piano. part i. piano hammers and tonal effects," *The Journal of the Acoustical Society of America*, vol. 99, no. 6, pp. 3286–3296, 1996.

[15] H. A. Conklin Jr, "Design and tone in the mechanoacoustic piano. part iii. piano strings and scale design," *The Journal of the Acoustical Society of America*, vol. 100, no. 3, pp. 1286–1298, 1996.

[16] J. Chabassier and M. Duruflé, "Physical parameters for piano modeling," tech. rep., 04 2012.

[17] E. Skudrzyk, "The mean-value method of predicting the dynamic response of complex vibrators," *The Journal of the Acoustical Society of America*, vol. 67, no. 4, pp. 1105–1135, 1980.

[18] M. R. Schroeder, "Integrated-impulse method measuring sound decay without using impulses," *The Journal of the Acoustical Society of America*, vol. 66, no. 2, pp. 497–500, 1979.

PROCEEDINGS of ISMA 2019
International Symposium on Music Acoustics

13 - 17 September 2019 in Detmold, Germany

Navier-Stokes-based modeling of the clarinet

N. Giordano[(1)] and J. W. Thacker[(2)]

[(1)]Auburn University, USA, njg0003@auburn.edu
[(2)]Auburn University, USA, thacker.jared@gmail.com

Abstract
Results are presented from a modeling study of the clarinet in which the air flow through the instrument is calculated using the Navier-Stokes equations. The reed is modeled as an Euler-Bernoulli beam with damping whose motion is driven by the pressure in the mouthpiece. Damping of the reed due to its contact with the lip is studied and shown to be crucial to achieve oscillations in which the reed vibrates at the lowest resonant frequency of the instrument, producing sound at that frequency. This finding is consistent with previous studies in which a clarinet is excited with an artificial blowing machine.

Keywords: Navier-Stokes, Clarinet, Modeling

1 INTRODUCTION

Modeling of musical instruments has yielded many important insights into a variety of different instruments including string instruments (pianos, guitars, and violins), percussion instruments (drums and cymbals), and wind instruments (recorders, trumpets, and clarinets). Physics based modeling strives to apply the fundamental equations of mechanics to understand the vibrations of the instrument and the resulting sound production. This is perhaps most challenging for wind instruments, since these instruments require the application of the Navier-Stokes equations, a set of nonlinear partial differential equations that are notoriously difficult to deal with even numerically. However, available high performance parallel computers are now able to obtain solutions of the Navier-Stokes equations for the air flow through and around wind instruments for fairly realistic instrument geometries. In recent work our group has reported results for the recorder, flute, and trumpet [1,2,3,4]. In this paper we report new results for the clarinet.

2 THE MODEL

Our clarinet model consists of two main components, one that computes a solution of the compressible Navier-Stokes equations for the air velocity and pressure as functions of time, and a second component that calculates the motion of the reed as it is driven by the pressure at its surface as derived from the Navier-Stokes solution. The Navier-Stokes equations are solved using a direct numerical simulation with a predictor-corrector algorithm as described in Ref. 1, while the reed motion is described using the beam model studied by Avanzini and van Walstein [5] including damping internal to the reed and from contact with the lips. Both are explicit, finite-difference-time-domain algorithms; in the future we plan to implement an implicit algorithm for the reed calculation, which should improve the accuracy of that part of the model. The Navier-Stokes calculation uses a nonuniform Cartesian grid with a spacial grid size of 0.1 mm near the reed and in the direction of the reed vibration. The reed moves continuously through this fixed grid according to the immersed boundary method [6], so the resolution for the reed motion is not limited by the Navier-Stokes grid. Other details of the calculation are given in Refs. 1 and 3. The time step for the calculations shown below was 2×10^{-7} s and the total number of grid points was $\sim 1\times 10^{7}$.

The model geometry was a simplified version of a real clarinet, to reduce the required computational time. The resonator was a tube with a square cross-section (5×5 mm) and approximately 7.0 cm long. The reed was 9 mm long with a width of 0.3 mm. The Young's modulus was 150 $\mathrm{N/m^2}$ and density of 150 $\mathrm{kg/m^3}$; both of these are not typical of a real reed, but were chosen to give a resonant frequency and compliance that would yield reasonable oscillations for the chosen resonator dimensions. The fundamental frequency of the instrument was approximately 1.1 kHz, consistent with a closed-open tube.

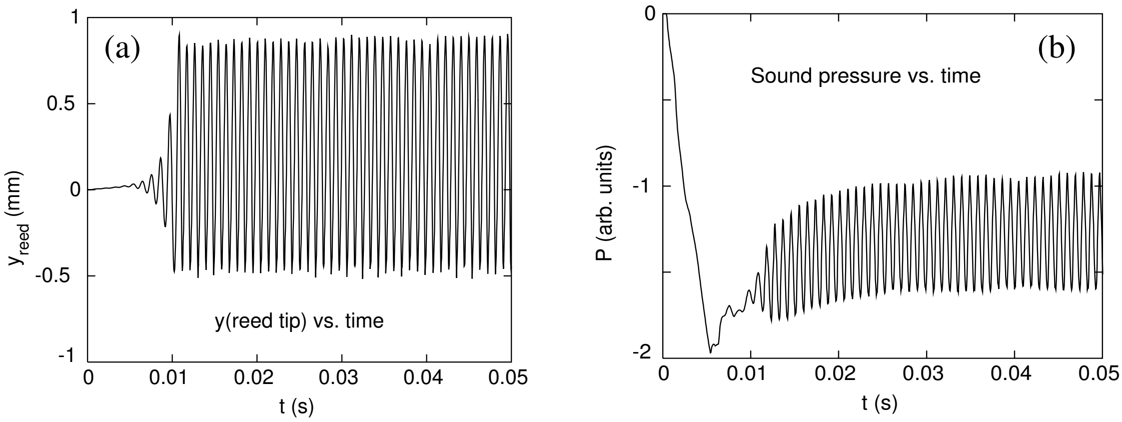

Figure 1. (a) Left: Position of the reed tip as a function of time. $y_{\text{reed}} = 0$ corresponds to an undisplaced reed tip. (b) Right: Sound pressure outside the instrument as a function of time. The air speed in the mouthpiece was 5 m/s and the dimensionless lip-reed damping was $R = 450$ (to be compared with other results below).

Our results are broadly consistent with recent studies of the clarinet using the lattice Boltzmann method to treat the Navier-Stokes equations [7-9], although that work employed a two dimensional model.

3 BASIC REED MOTION AND SOUND PRODUCTION

Figure 1 shows typical results in the parameter regime that produces a steady reed oscillation and an approximately pure tone. Figure 1(a) shows the position of the reed tip as a function of time while Fig. 1(b) gives the sound pressure outside the instrument; this is the sound that would be heard by a listener. In this calculation and in others shown below, the blowing velocity in the mouthpiece was increased linearly from zero to a final value at $t = 5$ ms and then held constant.

After an initial transient period the reed motion reaches a steady oscillation amplitude at about $t = 10$ ms while the sound pressure does not reach steady state until somewhat later, about 30 ms in this example. The lengths of these transient periods depend on how hard the instrument is blown, with larger blowing speeds/pressures giving somewhat shorter transient times.

Figure 2 shows the sound pressure from Fig. 1(b) on an expanded scale. The waveform is approximately sinusoidal at the fundamental frequency of the instrument (about 1100 Hz) although some small contributions from higher frequencies are also evident.

4 EFFECTS OF REED DAMPING

There are several sources of damping that are commonly discussed when describing the dynamics of the reed (see, e.g., [5]). These are damping internal to the reed itself, damping due to contact with the player's lips, and what is sometimes termed "fluid" damping to account for energy loss to the surrounding air. In our model energy loss to the air is accounted for through the interaction of the reed and air, so that effect is included in a rigorous way. We have included damping internal to the reed using a value of the damping parameter suggested in Ref. 5. The lip damping is included in our model using the functional form described in Ref. 5. Since the dimensions of our model instrument and reed are smaller than those of a real clarinet and given the uncertainties in modeling real lips, we have treated this damping as an adjustable parameter we denote as R. A number of experiments with blowing machines (e.g., [10,11]) have reported that if the lip damping is zero or too small,

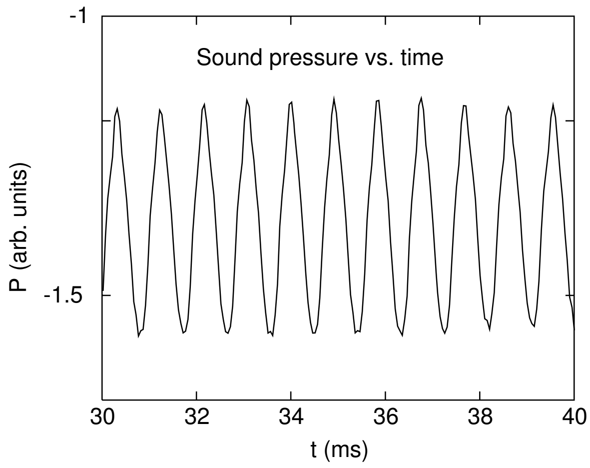

Figure 2. Sound pressure results from Fig. 1(b) on an expanded scale.

the sound produced is a "squeak" rather than a realistic musical tone. Our initial results also suggest that the location of the lip damping, i.e., the place along the reed where the lip contacts the reed, has a noticeable effect on the behavior. For all of the results in this paper the lip contacts about a third of the reed with the center of the contact region about half way along the reed. Here we illustrate the effect of lip damping by repeating the simulation from Figs. 1 and 2 but with different values of the lip damping R strength, and the results are given in Fig. 3. There we show results for the both reed oscillation and the sound pressure. All parameters, including the blowing pressure, were the same as in Figs. 1 and 2, only the damping parameter R was varied. We found that with $R = 0$ (no lip damping) there was no reed oscillation at all (and hence no sound) after a short (less than a few milliseconds) transient period. When R was increased, that is, by *increasing* the damping to a value about half the value in Figs. 1 and 2, a good reed oscillation was found with the expected behavior of the sound waveform.

5 CONCLUSIONS AND FUTURE WORK

This paper describes first results for a "toy" model of the clarinet in which the Navier-Stokes equations are used to compute the air velocity and sound pressure, and the Euler-Bernoulli beam equation is used to describe the dynamics of the reed. Our model of the clarinet differs from a real instrument in several ways; e.g., the dimensions are smaller than those of a real clarinet and the values of several parameters associated with the reed required a corresponding adjustment. Even so, our results indicate that a simulation of a fairly realistic clarinet in three dimensions is now feasible.

ACKNOWLEDGEMENTS

We thank V. Chatziioannou and M. Pàmies-Vilà for several useful discussions. The computations were carried out at the Rosen Center for High Performance Computing at Purdue University and with computational facilities supported by the Office of Information Technology at Auburn University. Work supported by NSF grant PHY1513273.

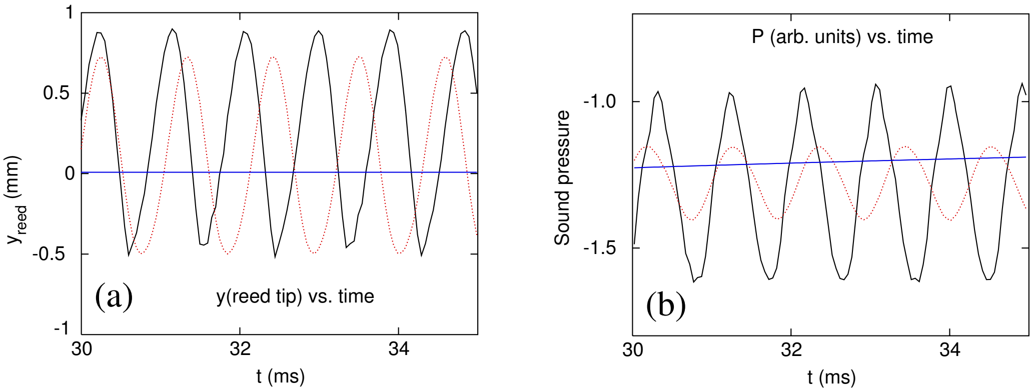

Figure 3. Effect of reed damping. (a) Left: Position of the reed tip as a function of time. (b) Right: Sound pressure as a function of time. Black curves: $R = 450$; Red curves: $R = 250$; Blue curves: $R = 0$. There was no oscillation with $R = 0$.

REFERENCES

[1] Giordano, N. Simulation studies of a recorder in three dimensions. Journal of the Acoustical Society of America, Vol 135, 2014, pp 906-916.

[2] Giordano, N. Computational study of the piccolo: Evidence for chaotic tones. Journal of the Acoustical Society of America, Vol 140, 2016, pp 1887-1893.

[3] Giordano, N. Physical modeling of a conical lip reed instrument. Journal of the Acoustical Society of America, Vol 143, 2018, pp 38-50

[4] Giordano, N. Force on the lips of a trumpet player. Journal of the Acoustical Society of America, Vol 145, 2019, pp 1521-1528.

[5] Avanzini, F.; van Walstijn, M. Modelling the mechanical response of the reed-mouthpiece-lip system of a clarinet. Part 1. A one-dimensional distributed model. Acta Acustica united with Acustica, Vol 90, 2004, pp 537-547.

[6] Mittal, R.; Iaccarino, G. Immersed boundary methods. Annual Reviews of Fluid Mechanics, Vol 37, 2005, pp 239-261.

[7] da Silva, A. R.; Shi, Y.; Scavone, G. Computational analysis of the dynamic flow in single-reed woodwind instruments. Proceedings of Meetings on Acoustics, Vol 19, 2013, pp 1-9.

[8] Shi, Y.; da Silva, A. R.; Scavone, G. LBM simulation of the quasi-static flow in a clarinet. Proceedings of the Third Vienna Talk on Music Acoustics, Vienna, Austria, 2015, pp 35-42.

[9] Yong, Shi. A numerical framework for fluid-acoustics-structure interaction in clarinet-like instruments. Ph.D. thesis, McGill University, Montreal, Canada, USA. 2016.

[10] Wilson, R. A.; Beavers, G. S. Operating modes of the clarinet. Journal of the Acoustical Society of America, Vol 56, 1974, pp 653-658.

[11] Almeida, A.; George, D.; Smith, J.; Wolfe, J. The clarinet: How blowing pressure, lip force, lip position and reed “hardness” affect pitch, sound level, and spectrum. Journal of the Acoustical Society of America, Vol 134, 2013, pp 2247-2255.

PROCEEDINGS of ISMA 2019
International Symposium on Music Acoustics

13 - 17 September 2019 in Detmold, Germany

Experimental and simulative examination of the string-soundboard coupling of an acoustic guitar

Alexander BRAUCHLER[(1)], Pascal ZIEGLER[(1)], Sabina BENATTI CAMARGO[(2)], Peter EBERHARD[(1)]

[(1)]Institute of Engineering and Computational Mechanics, University of Stuttgart, Germany,
[alexander.brauchler, pascal.ziegler, peter.eberhard] @itm.uni-stuttgart.de
[(2)]Sapienza University of Rome, Italy, benatticamargo.1596815@studenti.uniromo1.it

Abstract

The acoustic guitar is a popular string instrument in which the sound results from a coupled mechanical process. The oscillation of the plucked strings is transferred through the bridge to the body which acts as an amplifier to radiate the sound of the guitar. In this contribution, the vibration of a guitar body is examined experimentally and by means of numerical simulation. An experimental setup not only capable of determining eigenmodes and eigenfrequencies but also demonstrating the transient coupling between the strings and the body is presented. This capability is achieved with a plucking mechanism that allows reproducible plucks of a single string and synchronized measurements of multiple plucks at different positions of the guitar body using a scanning laser Doppler vibrometer. Besides the experimental setup, a finite element model of the guitar is developed. The numerical model consists of the body and the neck of the guitar. Furthermore, the struts to reinforce the soundboard and the back of the guitar are included. A comparison between the numerical model and the experimental measurements is conducted.

Keywords: Guitar, Modal Analysis, Finite Elements

1 INTRODUCTION

The acoustic guitar is a popular string instrument in which the sound results from a complex transient process beginning with the oscillation of a plucked string that is then coupled with the guitar body that radiates the sound to the surrounding air. To better understand this transient process, not only measurements shall be carried out, but also a finite element (FE) model shall be created that is able to approximate the vibration of the guitar. In this contribution the guitar body is examined without any influence from forces of the strings with the goal to create an FE model that approximates the eigenfrequencies and eigenmodes of a real guitar. The oscillation of a single string is examined in previous works of the authors [1, 2]. For this reason, an experimental modal analysis is carried out to gather knowledge of the eigenfrequencies and the eigenmodes of the particular examined guitar. This particular examined guitar is then modeled in a high level of detail and the eigenmodes and eigenfrequencies of the model are compared with the ones identified in the experiment.

2 MODAL ANALYSIS OF AN ACOUSTIC GUITAR

The sound of an acoustic guitar results from an interaction between the guitar body and the string through the bridge. In this work the guitar body shall be examined without any influence of the strings as it is necessary to understand the two mechanical systems decoupled to create a coupled model afterwards. For this reason a modal analysis of the guitar body is carried out with the strings unmounted to identify the eigenfrequencies and the eigenmodes as well as the damping and the transmission behavior of the system.

2.1 Experimental setup

The experimental setup contains basically the guitar mounted with rubber bands on a fixture, an electrodynamical shaker and a Polytec PSV-500 scanning laser Doppler vibrometer (LDV). Figure 1 shows the complete experimental setup.

The examined guitar is a rather small traveling guitar equipped with nylon strings and a simple bracing pattern

Figure 1. Experimental setup for the modal analysis.

on the soundboard and the back plate that consists of only three horizontal struts approximatively dividing the soundboard and the back plate in four similarly large parts, respectively. The strings are unmounted during the modal analysis to ensure that coupling effects between strings and body are excluded. As the guitar is a low priced model the soundboard and the back are made of some laminate of which the choice of woods is not known. In the experiment the guitar is held in place by rubber bands which are attached at the head and the strap button. At the head the guitar is fixed with one loop of rubber band while on the strap button three loops of rubber bands are mounted to reduce rotational movement when the guitar is excited eccentrically. The support can be interpreted as a proximate free support because the allowed movement through the rubber bands is expected to be in a very low frequency range that does not interfere with the elastic body modes of the guitar body.

To excite the guitar an electrodynamical shaker is used. The shaker is mounted decoupled from the guitar support and weighted with sand bags to guarantee that there is no significant movement of the shaker support. Since usual frequency sweeps that are carried out with a shaker are rather time consuming in combination with the need of many points to measure, the shaker is used in such a way that it acts like an impulse hammer. Therefore, the shaker is triggered by a function generator with a short trigger signal which leads to a single hammering motion of the shaker. A soft rubber tip is used to not damage the guitar and the shaker is applied on a position close to the lower edge on the left hand side of the soundboard. A shaker position close to the edge is chosen for two reasons. First and foremost, the position should be chosen such that the shaker is not in the way of the laser rays which would prohibit the measurement of certain points. Secondly, close to the edge it is easier to robustly prevent double hits. Behind the tip, a PCB piezoelectric force sensor is adjusted to measure the force input on the guitar body. Before being transmitted to an oscilloscope or the Polytec controller the force signal is preprocessed and amplified by an ICP conditioner.

The oscillation of the guitar body is measured with a scanning LDV. With the scanning LDV it is possible to measure the velocity on a predefined mesh of points on the guitar successively in a convenient way. Generally, an LDV can measure the velocity of a point of a structure owing to a frequency difference between a reference ray and the reflected ray on the structure, which is caused by the Doppler effect. In a scanning LDV, addition-

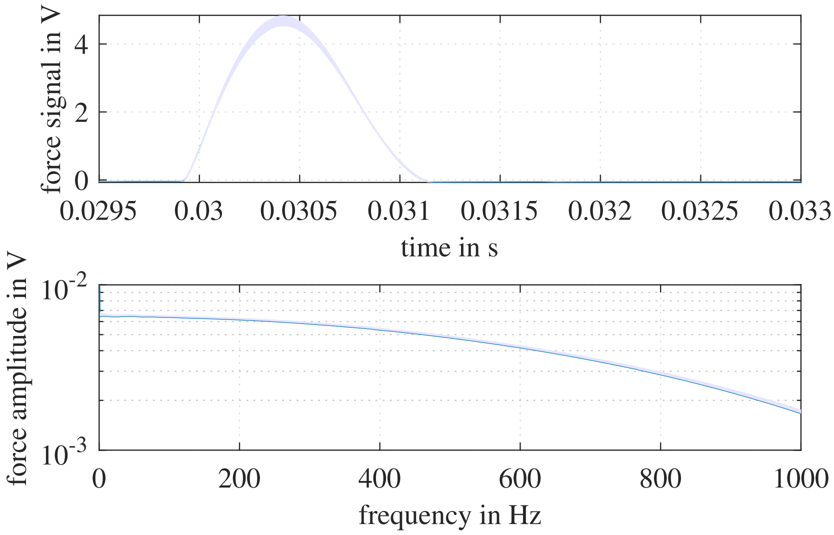

Figure 2. Force signal with confidence interval transient (above) and its Fourier transform (below).

ally, the direction of the laser ray can be controlled via a system of mirrors making it possible to change the measured position quickly and conveniently without changing the position of the LDV itself. The experiment is carried out using a mesh of 73 points distributed over the soundboard. In the current status only the velocity on the soundboard is measured, the neck and the back plate are omitted.

2.2 Modal analysis results

To carry out a modal analysis there is large number of procedures available in the frequency domain as well as in the time domain. An overview over different procedures can be found for example in [3, 4]. For the modal analysis in this work the peak amplitude method combined with an adjusted version of the half-power bandwidth is chosen. This is one of the standard procedures to choose for a modal analysis in the frequency domain and it belongs to the single degree of freedom methods.

The carried out modal analysis identifies not only the eigenfrequencies but also the eigenmodes and the damping. To ensure that the identified data is correct, the transfer function of a reconstructed system is compared with the measured transfer function.

To begin with, the system input, being the force acting from the shaker tip on the guitar body, is displayed in Figure 2. The plot shows the band of forces including 99.73 % of the measured forces on the 73 points in the time domain and in the frequency domain. In the time domain, it is visible that the shaker produces an almost sine shaped impulse and double hits can not be seen. From the plot in the frequency domain one can learn up to which frequency the hammer excites the system with a sufficiently strong impulse such that the measurement is meaningful. From Figure 2 it can be seen that this is at least the case up to 700 Hz.

For the rest of this contribution only the frequency domain will be examined. In the experiment the force action from the shaker tip on the guitar soundboard and the velocity of the guitar body on several points are measured. Due to that, the calculated transfer function

$$Y_{\mathrm{jk}}(\omega) = \frac{V_{\mathrm{jk}}(\omega)}{F_{\mathrm{jk}}(\omega)} \tag{1}$$

is the mobility of the system from an excited point k to a measured point j with the velocity V_{jk} and the force F_{jk}. In a standard peak picking procedure this transfer function is used to identify the eigenfrequencies which

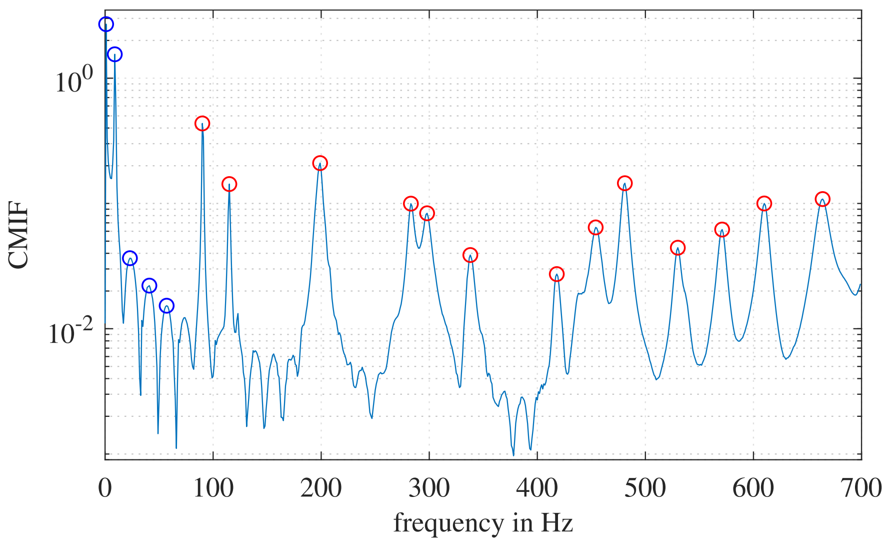

Figure 3. Complex mode indicator function of the measured signals.

are approximately at the peaks of the transfer function if the damping is low enough. An even better approach for finding the eigenfrequencies yields the complex mode indicator function

$$CMIF_1(\omega) = \Sigma_1(\omega), \tag{2}$$

where $\Sigma_1(\omega)$ is the first entry of $\boldsymbol{\Sigma}(\omega)$ which is calculated via a singular value decomposition of the matrix of all transfer functions

$$\boldsymbol{Y}(\omega) = \boldsymbol{U}(\omega)\boldsymbol{\Sigma}(\omega)\boldsymbol{V}(\omega). \tag{3}$$

If the experiment was carried out with different inputs, more CMIFs could be calculated containing even more information about the system [5]. For the conducted measurements the resulting CMIF is displayed in Figure 3. The peaks in the figure are highlighted with circles which indicate the approximate eigenfrequencies. There are several clear peaks in the regarded frequency range. The first two peaks are clearly assigned to the rigid body motion of the guitar allowed by the rubber bands, while the next three peaks come probably from noise in the measurements. The first structural eigenfrequency is then visible around 90 Hz and in total 13 eigenfrequencies are clearly visible in the frequency range up to 700 Hz.

With the given information about the eigenfrequencies, the transfer function is evaluated and reconstructed as a summation of N single degree of freedom systems

$$\tilde{Y}_{\mathrm{jk}}(\omega) = \sum_{r=1}^{N} \frac{{}_{\mathrm{r}}A_{\mathrm{jk}}(\omega)}{\omega_{\mathrm{r}}^2 - \omega^2 + 2i\omega_{\mathrm{r}}\omega\zeta_{\mathrm{r}}}, \tag{4}$$

where N is the number of identified eigenfrequencies, ${}_{\mathrm{r}}A_{\mathrm{jk}}(\omega)$ are the modal constants, ω_{r} are the eigenfrequencies, and ζ_{r} are the modal damping coefficients. The damping coefficients ζ_{r} are calculated with an adjusted version of the half-power bandwidth method as

$$\zeta_{\mathrm{r}} = \frac{b_{\mathrm{r}}}{2\omega_{\mathrm{r}}\sqrt{a^2-1}} \tag{5}$$

with the width b_{r} of the peak in the transfer function at the eigenfrequency ω_{r} at a fraction of the height $1/a$. Using this result the modal constants result to

$${}_{\mathrm{r}}A_{\mathrm{jk}} = 2Y_{\mathrm{j}}(\omega_{\mathrm{r}})\zeta_{\mathrm{r}}. \tag{6}$$

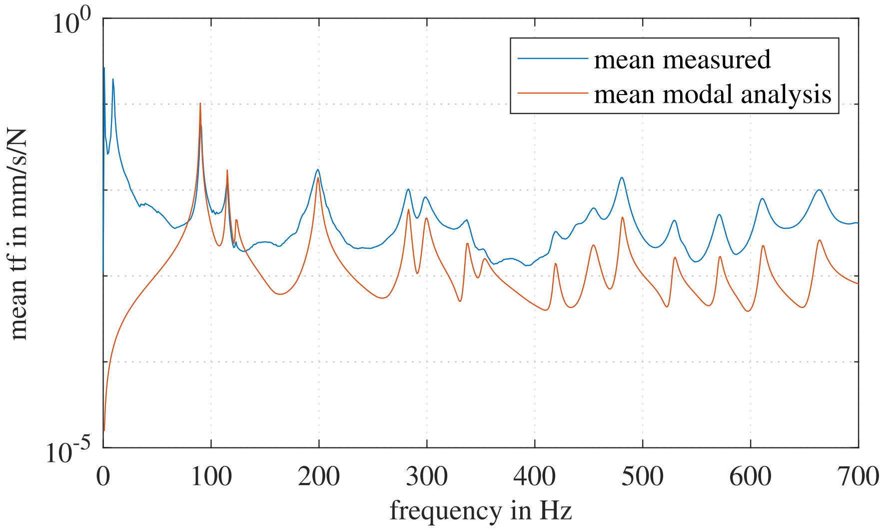

Figure 4. Comparison between mean measured transfer function (mobility) and reconstructed transfer function.

According to the equations above, the transfer function can be reconstructed with the identified eigenfrequencies, modal damping parameters, and modal constants. This resulting reconstructed transfer function is compared against the measured mobility in Figure 4. The results visible in the graph are good. Firstly, the peaks corresponding to the eigenfrequencies are at the same frequencies as they are in the measurement and, secondly, the resulting overall shape of the reconstructed curve is in good accordance with the measured one. Nevertheless there is still room for improvement because not only the identified modal damping parameters seem to be slightly too low, but also the amplitudes of the higher eigenfrequencies are underestimated. This might be solved with different identification methods and a higher frequency resolution [4].

In Figure 5 four identified modes are displayed. Furthermore, the mesh of measured points is visible in these graphs. There are two similar eigenmodes at 115 Hz and 199 Hz, where mostly the lower part of the guitar is moving. These eigenmodes can be explained by an in-phase and an out-of-phase movement of the soundboard and the back plate of the guitar that leads to two eigenmodes. In general, the found modes are in good agreement with the existing literature, see for example [6, 7].

3 NUMERICAL MODEL OF AN ACOUSTIC GUITAR

Besides the experimental study, a numerical finite element model is developed. The model of the guitar is geometrically very similar to the guitar examined in the modal analysis. It contains all parts of the guitar except strings, namely the soundboard and the backboard, both including the bracing pattern of the guitar, the bridge, and furthermore, a detailed model of the neck including the heel and the head of the guitar. Due to that, it should be possible to compare the eigenmodes of the experimental guitar with the ones calculated in the finite element model as a first step of verification.

3.1 Modeling procedure

The modeling of the geometry as well as the meshing and the simulation are carried out using the commercial software `Abaqus`. Figure 6 shows a picture of the whole model on the left which shows the high level of detail in the geometric modeling as well as the mesh used for the simulation. Within the model, two types of elements are used. To create an efficient numerical model, all thin, plate-like parts are modeled with shell elements and volume elements are only used when necessary. Hence, the soundboard, the backplate, and the

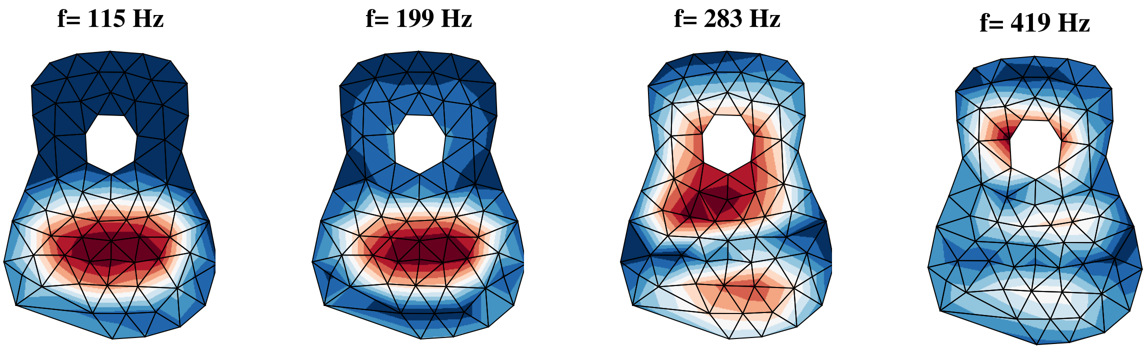

Figure 5. Four modes identified with the modal analysis.

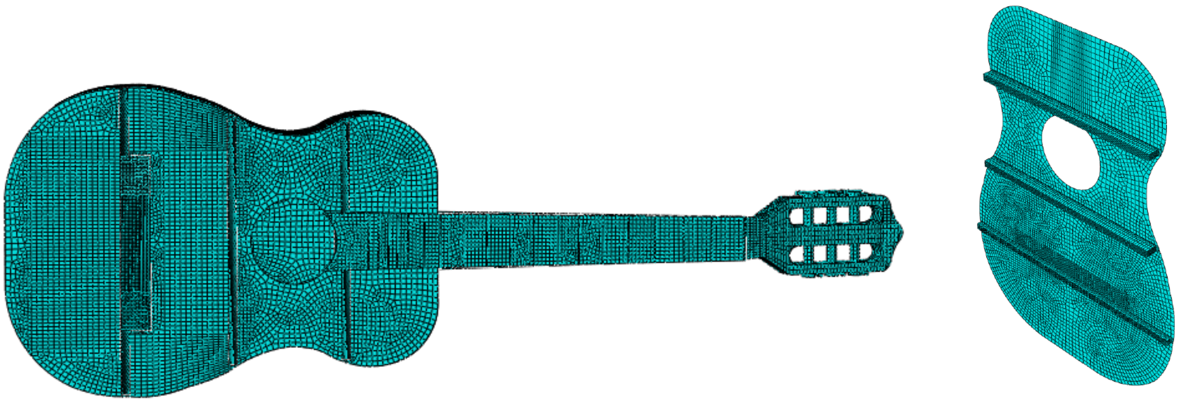

Figure 6. FE Model of the whole guitar (left) and soundboard with bracing (right).

sides are modeled with shell elements of type `S4` while the neck, the head, the fretboard, and the bracing are discretized using volume elements of type `C3D8`.

The shape of the soundboard and the back plate are equal except for the hole in the soundboard and it is modeled using splines between measured points on the experimental guitar. To both, the soundboard and the back plate, three struts are attached, as shown in Figure 6 on the right. The struts in the particular guitar are simple straight rods without any shape variation. They are coupled with the soundboard and the back plate via tie constraints which means that the additional degrees of freedom at the nodes in contact are deleted such that the two parts in contact share these nodes.

In a same level of detail the neck, including the head as well as the heel and the fretboard, is modeled. Only few simplifications are made to make it possible to create a finite element mesh on the complex geometry. In particular, the neck and the heel are modeled conical with trapezoidal cross sections and a rounded lower side instead of the complex curved shape on the real guitar. These details are assumed to be important rather for playability and ergonomic issues but the level of detail should be high enough to get good results for the eigenmodes and eigenfrequencies. For coupling the parts of the neck a different strategy than on the soundboard

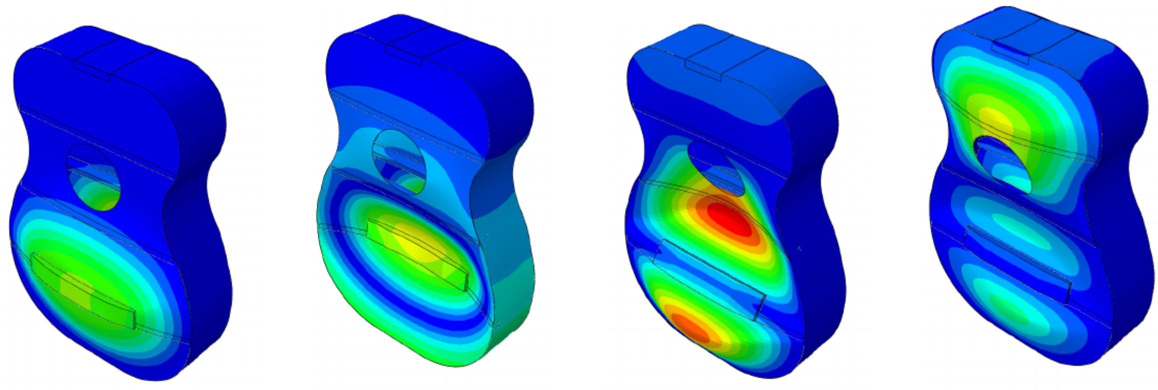

Figure 7. Four modes extracted from the simulated FE model.

and back plate is chosen. Instead of coupling the meshed parts, the neck is created as a single part and meshed afterwards. Only the fretboard is modeled as a separate part and then coupled to the neck via tie constraints. In the end, the complete neck is coupled with the guitar body on the sides and on the soundboard using tie constraints again.

On the contrary to the detailed geometry model, the material model is rather coarse at the current state. A linear elastic, isotropic material is assumed and further, the material is assumed to be equal for all parts of the guitar. This assumption is made because the particular material of the parts is unknown for the experimental guitar and for that reason the material parameters are design parameters at the current state. Hence, the material properties are chosen, such that the first bending eigenmode, occurring at 90 Hz in the experimental modal analysis, appears to be at the same frequency in the finite element model. This results in the Young's modulus $E = 7200\ \mathrm{N/mm^2}$ and the density $\rho = 640\ \mathrm{kg/m^3}$. The Poisson ratio is chosen as $\nu = 0.314$. These values result in a first bending mode, which lies at 90 Hz and additionally, the chosen values are near to the realistic values usually measured for wood.

3.2 Simulation Results

As a first step to verify the ability of the FE model to approximate the behavior of a real guitar, the comparison of eigenmodes and eigenfrequencies is chosen. In Figure 7 four eigenmodes calculated from the model are presented. The modes are chosen such that they fit to the modes extracted from the modal analysis in Figure 5.

For all four modes it can be concluded, that the shapes of the model fit remarkably well to the modes observed in the experiment. However, the two modes on the right hand side are perfectly symmetric in the model while they are not in the experimentally calculated modes. This might occur either due to a not fine enough mesh of measured points in the experiment but it is far more likely to be caused by some non-homogeneous material in the experimental guitar. Furthermore, with the model, it is visible that the two modes, in which the lower part of the soundboard has one antinode, refer to an out-of-phase movement (leftmost picture) and an in-phase movement (second from left picture) of the soundboard and the back plate. This detail cannot be seen in the modal analysis because the oscillation of the back plate is not measured.

Besides the mode-shapes themselves, the frequencies belonging to the mode-shapes are important for the behavior of the system. Figure 8 shows the eigenfrequencies observed in the experiment and the eigenfrequencies calculated from the FE model. Each compared pair of frequencies belongs to a mode shape that matches between experiment and simulation. The material parameters in the FE model are chosen such that the first eigenfrequency matches the one measured in the experiment. Using that procedure, it can be concluded, that all the other frequencies in the model are higher than the ones in the experiment. While some frequencies,

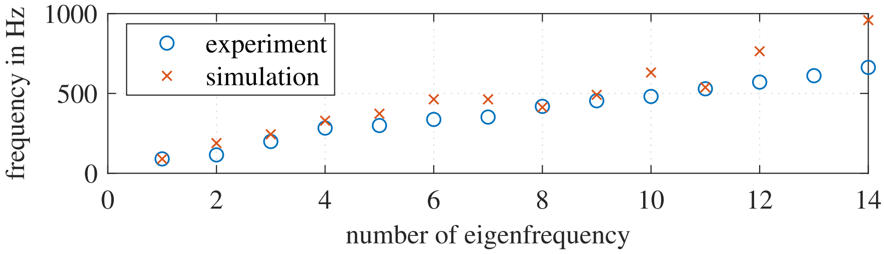

Figure 8. Eigenfrequencies with matching modal shapes compared between experiment and simulation.

like eigenfrequency number 8 and 11, fit quite well, others like eigenfrequency number 12 and 14 are rather far away from the measured value. Furthermore, the eigenfrequencies in the model do not occur in the same order as in the experiment. Hence, the frequency of the eigenmodes belonging to the model in Figure 8 is not monotonically increasing. The different eigenfrequencies might be caused by the assumption of a single material for the whole guitar in the model.

4 CONCLUSIONS

The goal of the authors was, to create an FE model of a guitar which is able to approximate transient behavior of the guitar. In this work the first steps towards this goals are presented. An experimental modal analysis has been carried out which shows good results in comparison to the existing literature referring to the eigenmodes and the transmission behavior of the guitar. The particular guitar examined in the experiment has then been modeled in a high level of detail in the FE software `Abaqus`. Good results regarding the eigenmodes and eigenfrequencies can be seen already in the early stages of the modeling procedure.

REFERENCES

[1] Brauchler A., Ziegler, P.; Eberhard, P. Experimentelle und numerische Untersuchung des Einflusses realistischer Randbedingungen auf Saitenschwingungen, Fortschritte der Akustik - DAGA 2019, Rostock, March 18-21, 2019.

[2] Hanss, M.; Bestle, P.; Eberhard, P. A reproducible excitation mechanism for analyzing electric guitars, PAMM, Vol. 15, 2015, pp. 45-46.

[3] Ewins, D.J. Modal Testing: Theory, Practice and Application, Research Studies Press, Baldock, 2000.

[4] Irretier, H. Experimentelle Modalanalyse, Institute of Mechanics, University of Kassel, Kassel, 2004.

[5] Allemang, R.J.; Brown, D.L. A complete review of the complex mode indicator function (CMIF) with applications. Proceedings of ISMA International Conference on Noise and Vibration Engineering, Katholieke Universiteit Leuven, 2006.

[6] Richardson, B; Jahnson, H.; Joslin, A.; Perry, I. The three-mass model for the classical guitar revisited. Acoustics, Nantes, 2012.

[7] French, R.M. Engineering the guitar: theory and practice. Springer Science and Business Media, New York, 2008.

PROCEEDINGS of ISMA 2019
International Symposium on Music Acoustics

13 - 17 September 2019 in Detmold, Germany

Thai fiddle saw-u modeled as a Helmholtz resonator with circular membrane

Kajornpop TOBOONCHUAY[(1)], Munhum PARK[(2)], Bhanupol KLONGRATOG[(3)]

[(1)]Department of Physics, King Mongkut's Institute of Technology Ladkrabang, Thailand, kajornpop1@hotmail.co.th

[(2)]Institute of Music, Science and Engineering, King Mongkut's Institute of Technology Ladkrabang, Thailand, munhum.pa@kmitl.ac.th

[(3)]Department of Physics, King Mongkut's Institute of Technology Ladkrabang, Thailand, bhanupol.kl@kmitl.ac.th

Abstract

Saw-u is a Thai low-pitched vertical fiddle, of which two strings are bowed to vibrate, via a bridge, a sheet of goatskin or cowhide stretched over a cavity with sound holes. This instrument is similar to Cambodian tro-u, but distinguished from Chinese yehu or Korean haegeum in that animal skin is used for the interface to the bridge (rather than wood in the latter two). In the current study, the unique structure of the instrument body was investigated by establishing a mathematical model where the cavity was assumed to behave as a Helmholtz resonator interacting with a circular membrane. Two coupled equations governing the motions of the membrane and that of the air mass in the sound holes were solved based on simple assumptions. The results showed that the resonance frequencies associated with the circular modes of the membrane were shifted under the influence of the Helmholtz resonator, whereas that of the resonator would remain unchanged. Moreover, it was found that an additional circular mode may be observed near the Helmholtz resonance frequency, which may significantly influence the sound quality by reinforcing the resonance. The application of the current findings to the analysis of similar structures will also be discussed.

Keywords: Saw-u, Thai fiddle, Helmholtz resonator, vibrating membrane, modal analysis

1 INTRODUCTION

Saw-u is a two-stringed, low-pitched fiddle found in Thailand (see Figure 1). When the string is bowed, the vibration is transferred, via a bridge made of a small piece of wood, to the thin animal skin (membrane), stretched over the front cut of a coconut shell (resonator) with sound holes on the other side. The saw-u is similar to Cambodian *tro-u*, but distinguished from Chinese *yehu* and Korean *haegeum* for which thin wooden sheets are used in place of animal skin.

The saw-u has been the subject of some previous studies mostly in Thailand. In the study by Malin and Meesawat (1), the transfer function of the saw-u resonator was measured and used as a filter to synthesize the sound. Punwaratorn (2) compared the sound quality of the two resonators made from alternative materials with that from the conventional (coconut shell). However, the details of the acoustic properties of the saw-u had not been discussed in these studies.

The purpose of this study is to look into the fundamental acoustic properties of the saw-u resonator. The resonator was simplified into a coupled system consisting of a membrane-cavity (or kettledrum-like system) and a Helmholtz resonator. A Newtonian equation of motion was established to analyze the resonance characteristics of the system. Similar models can be found in a few previous studies. For example, Fletcher and Thwaites (3) discussed a number of biological acoustic systems, one of which is the directional ear, consisting of a diaphragm on one side and a port on the other. The frequency and directional response of this system could be analyzed with the equivalent circuit method. Also, Christensen and Vistisen (4) presented a simple system of the guitar in an attempt to study its low frequency response. The model is composed of a plate attached to a spring (acted by the guitar top plate) and an air mass (in the guitar sound hole), both of which are under the influence of the restoring force acted by the air volume in the instrument body. A Newtonian equation of motion was used to analyze the system, and the nature of the coupling frequencies and the frequency response of the system could be accurately predicted. In the two studies mentioned in the previous text, the vibrating diaphragm or plate was

Figure 1. The front, back, and side view of a Thai saw-u.

assumed to be a rigid mass. In the current study, however, the membrane is treated as a vibrating membrane having radial and circular modes.

In section 2, the model for the saw-u resonator is presented, followed by section 3 where the implications of the model are discussed and compared with previous models. Lastly, a summary is given in section 4.

2 A SIMPLE MODEL OF THE SAW-U RESONATOR

2.1 Derivation

The saw-u resonator may be modeled as a combination of three components (see Fig. 2): A circular vibrating membrane of area $S_M = \pi a^2$, areal density σ, and surface tension T, a cavity of volume V_0, and a cylindrical tube with effective length L and cross-sectional area S_H.

Helmholtz resonator is composed of the cavity and the tube. The air in the tube is considered to be a rigid mass or an *air piston* with mass $\rho_0 S_H L$ (ρ_0: equilibrium density of air), whereas the air in the cavity acts as a spring exerting a force $-S_H \Delta P$ to the air piston. The negative sign indicates the direction opposite to the displacement of the piston. $\Delta P(t)$ is the instantaneous pressure deviation from the equilibrium pressure P_0. This model is valid for wavelength λ that satisfies the following: $\lambda \gg V_0^{1/3}$, $\lambda \gg S_H^{1/2}$, and $\lambda \gg L$ (5). Also, the cavity modes and the resistance (elastic resistance and radiation loss) are neglected in the current model.

Without external force, the motion of the air piston resembles a simple mass-spring system. For $\boldsymbol{\xi}(t)$, the instantaneous displacement of the air piston, the equation of motion is represented as $\rho_0 S_H L \ddot{\boldsymbol{\xi}} = -S_H \Delta P$, or

$$\rho_0 L \ddot{\boldsymbol{\xi}} = -\Delta P. \tag{1}$$

Assuming that the pressure inside the cavity is uniform and the membrane displacement is small, it exerts a force $\Delta P \, \mathrm{d}x \mathrm{d}z$ to an infinitesimal element of the membrane surface. When $\boldsymbol{y}(x,z,t)$ represents the instantaneous displacement of the infinitesimal elements (using Cartesian coordinate for convenience) and $\ddot{\boldsymbol{y}}$ the second deriva-

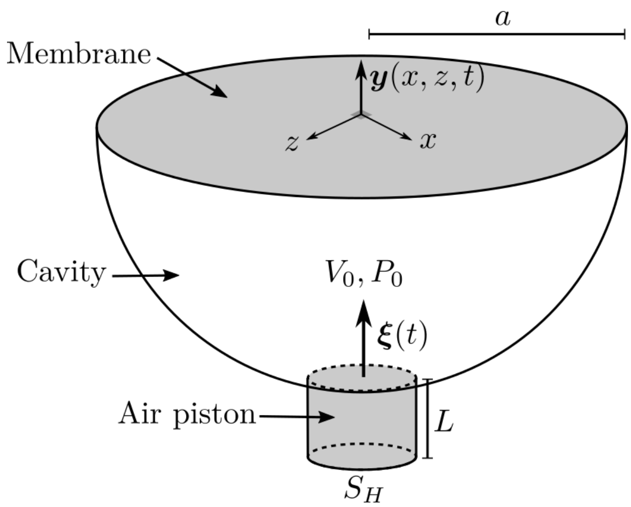

Figure 2. The schematic of the simple model of saw-u resonator for mathematical analysis.

tive in time, the equation of motion for the membrane can be described as $\sigma\ddot{\mathbf{y}}\,\mathrm{d}x\,\mathrm{d}z = T\nabla^2\mathbf{y}\,\mathrm{d}x\,\mathrm{d}z + \Delta P\,\mathrm{d}x\,\mathrm{d}z$, or

$$\sigma\ddot{\mathbf{y}} = T\nabla^2\mathbf{y} + \Delta P. \tag{2}$$

The pressure difference $\Delta P(t)$ results from the volume change $\Delta V(t)$ and can be approximated as

$$\Delta P \approx -\gamma\frac{P_0}{V_0}\Delta V, \tag{3}$$

where γ is the ratio of the heat capacity at constant pressure to that at constant volume of the air in the cavity. Here ΔV is attributed to the volume displacement of the air piston, $S_H\xi$ and that of the membrane, $S_M\langle\mathbf{y}\rangle$, where $\langle\mathbf{y}\rangle$ is the average displacement of the membrane which can be expressed as $\langle\mathbf{y}\rangle = S_M^{-1}\int_{S_M}\mathbf{y}\,\mathrm{d}S_M$. So, ΔV can be expressed as

$$\Delta V = S_M\langle\mathbf{y}\rangle - S_H\boldsymbol{\xi}. \tag{4}$$

Substituting Equations (3) and (4) into (1) and (2) gives

$$\ddot{\boldsymbol{\xi}} + \omega_H^2\boldsymbol{\xi} = \frac{S_M}{S_H}\omega_H^2\langle\mathbf{y}\rangle \tag{5}$$

$$\nabla^2\mathbf{y} - \frac{1}{c_M^2}\ddot{\mathbf{y}} = \frac{S_H}{T}\gamma\frac{P_0}{V_0}\left(\frac{S_M}{S_H}\langle\mathbf{y}\rangle - \boldsymbol{\xi}\right), \tag{6}$$

where $\omega_H^2 = S_H\gamma P_0/\rho_0 L V_0$ is the Helmholtz resonance frequency (assuming a rigid wall instead of a membrane) and $c_M = \sqrt{T/\sigma}$ is the speed of the transverse wave on the membrane.

2.2 Solution

Assuming harmonic solutions for both $\mathbf{y}(r,\theta,t)$ and $\boldsymbol{\xi}(t)$, i.e. $\mathbf{y}(r,\theta,t) = \Psi(r,\theta)e^{i\omega t}$ and $\boldsymbol{\xi}(t) = \Xi e^{i\omega t}$ respectively. Equations (5) and (6) can be rearranged:

$$\Xi = \frac{S_M}{S_H}\frac{\omega_H^2}{\omega_H^2 - \omega^2}\langle\Psi\rangle, \tag{7}$$

$$\nabla^2\Psi + k^2\Psi = \frac{S_H}{T}\gamma\frac{P_0}{V_0}\left(\frac{S_M}{S_H}\langle\Psi\rangle - \Xi\right). \tag{8}$$

Equation (7) indicates that Ξ and $\langle\Psi\rangle$ are in-phase for $\omega < \omega_H$, and out-of-phase for $\omega > \omega_H$.

Finally, combining Equations (7) and (8) gives the decoupled equation of motion for the membrane:

$$\nabla^2\Psi + k^2\Psi = \frac{S_M}{T}\gamma\frac{P_0}{V_0}\left(\frac{\omega^2}{\omega^2 - \omega_H^2}\right)\langle\Psi\rangle. \tag{9}$$

The homogeneous solution to this equation is Bessel function, similar to the solution of a free membrane. However, a particular solution is required for $\Psi(a)$ to be zero. Also, the only affected modes are the axisymmetric ones (modes with only circular nodal lines) because $\langle\Psi\rangle$ becomes zero for the modes with radial nodes and so the equation becomes homogeneous. From now, only the axisymmetric modes will be discussed. Given the boundary condition, the general solution can be represented as $\Psi = A[J_0(kr) - J_0(ka)]$. Equation (9) becomes

$$J_0(ka) = -\frac{S_M a^2}{T}\gamma\frac{P_0}{V_0}\left(\frac{J_2(ka)}{(ka)^2 - \omega_H^2 a^2/c_M^2}\right), \tag{10}$$

which is a conditioning equation for the resonance frequencies of the system.

3 IMPLICATIONS AND COMPARISONS

Equation (10) is similar to the conditioning equation for a membrane over a cavity or a kettledrum mentioned in Kinsler et al. (5), with $(ka)^2$ in the denominator replaced by $(ka)^2 - \omega_H^2 a^2/c_M^2$. The presence of ω_H modifies the resonance frequencies of the membrane modes. Two limiting cases can be evaluated. First, for the case where ω_H approaches zero (when the sound holes are blocked), the system is reduced to a kettledrum. When ω_H approaches infinity (when the sound holes are extremely large or the cavity vanishes), the equation is reduced to $J_0(ka) = 0$, which is the conditioning equation for the free circular membrane vibration. So, the conditioning equation is consistent with the expected behaviors of the system in the limiting cases.

To estimate the resonance frequencies of the system for ω_H in a practical range, the conditioning equation can be rearranged:

$$\omega_H = \left[\frac{S_M}{\sigma}\gamma\frac{P_0}{V_0}\left(\frac{J_2(ka)}{J_0(ka)}\right) + \frac{c_M^2}{a^2}(ka)^2\right]^{1/2}, \tag{11}$$

where the intersections between the left and right sides of the equation indicate the resonance frequencies of the system. Using Equation (11), ω_H can be represented by a horizontal line, which is equivalent to the values in y-axis. In this way, the resonance frequencies of the system (with fixed parameters; S_M, c_M, etc.) can be directly represented by the the right side of the equation as shown by the solid curves in Figure 3. Parameters used in Figure 3, chosen to resemble an actual saw-u, are listed in Table 1. In the specific case of $\omega_H = 308$ Hz, the four resonances, indicated by intersections between the ω_H line and the conditioning curves, are 162, 329, 415 and 638 Hz.

In Figure 3, three axisymmetric modes are shown for free membrane (177, 406 and 637 Hz) and kettledrum (211, 410 and 638 Hz). However, the current model predicts the presence of an additional mode. At low ω_H, the additional resonance (lowest one) is slightly below ω_H, while other resonance frequencies are slightly above the corresponding kettledrum resonance frequencies: The higher the frequency, the smaller the shift. As ω_H rises, the lowest resonance shifts toward the first axisymmetric resonance frequency of a free membrane and the second resonance shifts in parallel with, and slightly above, ω_H. This shifting nature is consistent with the findings in Christensen and Vistisen (4). In addition, this shift can be observed at about 400 and 640 Hz, where the resonance frequencies of free membrane and kettledrum are found. Furthermore, no resonance frequency exists between the free membrane and kettledrum modes.

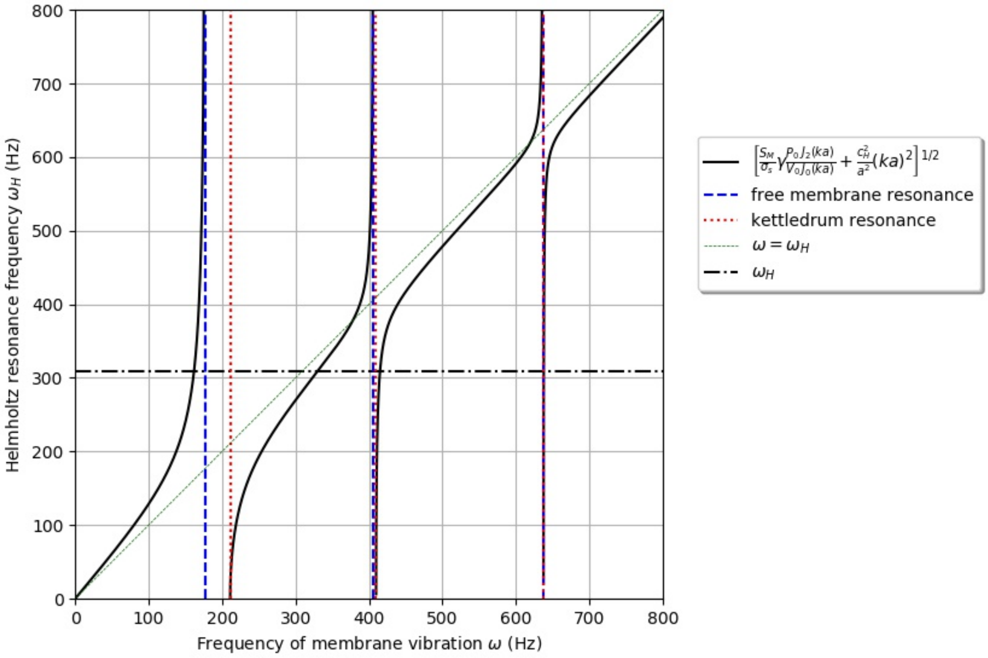

Figure 3. The right side of Equation (11) (black curves). Green thin dotted line indicates $\omega = \omega_H$. Vertical lines are the resonances of the fixed-rimed membrane in vacuum (free membrane; blue dashed lines) and those of the membrane stretched over the closed cavity (kettledrum; red dotted lines). Black dotted-dashed line is ω_H at 308 Hz.

Table 1. Parameters used in Figure 3.

Parameters	symbols	values	units
Membrane radius	a	6.0	cm
Membrane surface area	S_M	113.1	cm^2
Membrane density	σ	1.3	$\mathrm{kg\,m^{-2}}$
Wave speed on membrane	c_M	27.74	$\mathrm{m\,s^{-1}}$
Equilibrium air pressure	P_0	1013.25	hPa
Cavity volume	V_0	1600	cm^3
Helmholtz resonance frequency	$\omega_H/2\pi$	308	Hz

Comparisons are made between the current model and the two previous ones as shown in Table 2. Only the first two resonance frequencies are compared because the previous models can only estimate the lowest two resonance frequencies. All predictions indicate that the lowest resonance frequency is lower than that of the first kettledrum mode and the second is higher than ω_H.

The limitation of the current model is that the frequency range is limited by the assumptions regarding the rigid-body motion of the air piston, as is the case for the model by Christensen and Vistisen. Since the saw-u is a low pitched instrument, however, the model should still be applicable.

Table 2. Comparison of the first two resonance frequencies between different models.

Resonance	Models		
	Current paper	Fletcher and Thwaites	Christensen and Vistisen
Lower	162 Hz	161 Hz	163 Hz
Upper	329 Hz	339 Hz	336 Hz

4 SUMMARY

The saw-u resonator was simplified into a combination of a Helmholtz resonator with circular membrane. By solving a set of Newtonian equations of motion, the conditioning equation for the resonance frequencies of the saw-u resonator was established. The current model suggested that an additional mode of vibration is present along with the kettledrum and free membrane modes. These membrane mode frequencies shift as the Helmholtz resonance frequency varies. The lowest two resonance frequencies were found to agree with those predicted by two previous models. Measurements of a saw-u resonator are to be carried out to verify the findings of the current study.

ACKNOWLEDGMENTS

This study was supported by the King Mongkut's Institute of Technology Ladkrabang research grant (2562-0220004). The first author thanks Science Achievement Scholarship of Thailand (SAST).

REFERENCES

[1] Malin P.; Meesawat K. Acoustic synthesis of saw-aoo using resonator transfer function model. Proceedings of ECTI-CARD 2015. Trang, Thailand, July 8-10, 2015, 606-609.

[2] Punwaratorn M. The use of alternative material fiber glass - a case study of manufacturing processed and quality of saw u resonance box. Institute of Culture and Arts Journal, 16(2), 2016, 18-23.

[3] Fletcher N.H.; Thwaites S. Physical models for the analysis of acoustical systems in biology. Quarterly Reviews of Biophysics, 12(1), 1979, 25-65.

[4] Christensen O.; Vistisen B.B. Simple model for lowfrequency guitar function. The Journal of the Acoustical Society of America, 68(3), 1980, 758-766.

[5] Kinsler L.E.; Frey A.R.; Coppens A.B.; Sanders J.V. Fundamentals of Acoustics. Wiley, NY (USA), 4th edition, 2000.

PROCEEDINGS of ISMA 2019
International Symposium on Music Acoustics

13 - 17 September 2019 in Detmold, Germany

Finite element modelling of Japanese *koto* strings

Kimi COALDRAKE[1]

The University of Adelaide, Australia

Abstract

The development of a high resolution finite element model of the Japanese *koto* has been previously reported. The koto is a plucked zither made of paulownia wood and 1.83m in length. Its 13 strings are made of polyester fibre and supported by 13 moveable bridges approximately 6cm high. A functional representation of each string was included in the high resolution model by using a wave form that entered the koto sounding body at a signal point where the bridge would be located for the standard (*hirajōshi*) tuning. Correlation between spectra generated in the model and spectra of an actual instrument as played provided initial observations of string behavior. This study aims to improve the fidelity of the spectral response by directly coupling the string to the resonating body. A beam model and a truss model with the dimensions of a professional string that is pre-tensioned to yield a close approximation of strings on an actual instrument are studied. Initial results from the string models as compared to notes played on the *koto* used as the basis of the finite element modelling are reported.

Keywords: Finite element modelling, Strings, Koto

1 INTRODUCTION

There are few acoustic studies of the Japanese koto (13-stringed plucked zither) and the study of string behavior has yet to be investigated in any detail. A functional representation of the string was included as part of the development of a high resolution finite element model of the koto using COMSOL Multiphysics®. In that model, the artificial stimulation of the sounding body by means of a wave form at a single point where the moveable bridge would be located for the standard (*hirajōshi*) tuning enabled the comparison of spectra generated in the model and those of an actual instrument. This study aims to improve the fidelity of the spectral response of this finite element model. While it is possible to model string behavior independently of the modelling of the sounding body of the instrument, the main difficulty lies in coupling one to the other in a way that realistically transfers the energy and simulates the physical plucking within the finite element model. Two options are investigated: a truss model and a beam model. This paper focuses on the setting up of the model and how to implement the complexities into Comsol from first principles. The development of these models is ongoing.

The science of plucked strings instruments especially those found in Europe such as guitars are well represented in the literature (1). In recent years, studies of instruments such as the Finnish Kantele (zither) (2) using finite element methods have been undertaken. By comparison, research by Ando (3, 4) remains the principal source of information for the acoustics of the koto while other information on the koto is found as in more general reviews of wooden stringed musical instruments (5) including those of Asia (6). Studies of East Asian plucked string instruments such as *qin* (zither) (7) are now available, but only a small number of finite element studies of Asian instruments have been undertaken (8, 9).

More specific studies of the physical modeling of strings can be found in the context of investigation of the full instrument such as the piano (10). Methods for the real-time synthesis of strings (11) have also been developed. Significantly, while some initial research using finite element modelling of strings have been undertaken (12), few are yet to be fully realized. Of relevance to this study, however, are examples of modeling vibrating strings found in the Comsol Model Library (13).

2 A FINITE ELEMENT MODEL OF KOTO STRINGS

This section discusses the development of the finite element model of Japanese koto strings. It presents an overview of the model of the koto's sounding body used for this study. Other components, namely the strings, the bridges and the pluck are then described. This is done first in terms of traditional materials and practices before

[1] kimi.coaldrake@adelaide.edu.au

discussion of the ways they are the set up in the finite element model of this study. Finally, the constructed string model and its use to investigate string behavior is presented.

2.1 The model of koto's sounding body

The sounding body of the koto is made of paulownia wood and 1.83m in length. Previous work by this author used a high resolution finite element model of the koto (10). The objective of that model was to make it as realistic as possible. This author's hand-crafted professional grade koto and COMSOL® Multiphysics Versions 5.2 to 5.4a were used. The basis of the measurements for the model was 2300 DICOM images of cross-sections of the koto obtained from a high-resolution computer tomography CT scan that were converted to a Simpleware mesh and then imported into Comsol, the so-called CT model (see Figure 1). The physical properties of paulownia were provided by Christopher Waltham from the University of British Columbia (14). It is important to note that no arbitrarily adjusted constants were incorporated. A number of experiments using equipment such as an acoustic camera, a laser scanning vibrometer (LSV) and techniques such as Chladni patterns were part of a multi-faceted validation process. When appropriate, model results were compared to the actual koto including Fourier Transforms of the waveform as played by the author. In this study the strings were removed from the model and frequency input achieved by generating a sound wave (sine or saw tooth) applied at the point where the bridge touches the sounding board.

Figure 1. Geometry of the high resolution finite element model of the koto

This type of high resolution model has a very high number of mesh elements and consequently a very long running time for each simulation. A simplified box model was therefore constructed for this study (see Figure 2 below). It comprises a hollow box with four internal struts and two round sound holes on the base plate. As described in more detail below, a single string was laid down the middle of it across three bridges and attached at each end.

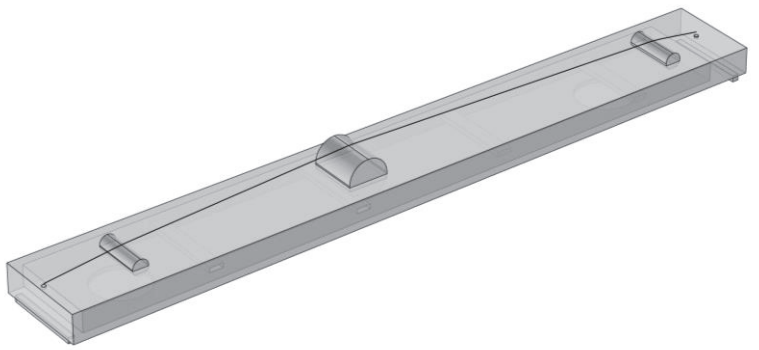

Figure 2. Simplified box model used in this study

2.2 Other components of the box model

In addition to the sounding body, three main components were developed and incorporated into the finite element model for this study. This section discusses these components. It briefly describes historical forms and more recent developments in traditional practice before discussing how the model component was constructed.

2.2.1 The strings

Historically, the thirteen strings of the koto varied in thickness and were made of silk. In the early twentieth century synthetic materials began to be used and the polymer under the trade name Tetron® has been preferred for making strings since the 1950s. All strings are now of equal length, weight and tension. Traditional knots are used to secure the strings at each end and maintain the tension.

The string was constructed for the model by building a four-sectioned Bezier curve whose coordinates touch the end points and the bridges. A cross-section, circular in this case, was then swept along the Bezier curve which acted as a guidepost. Appropriate material, in this case a polymer, was assigned to this new object.

There are two major ways in which string oscillations can be modelled within Comsol: either as a truss or as a beam. Both models are contained within the advanced Structural Mechanics section of Comsol. For this purpose the differences are not great. The truss model is used for modelling slender elements that can only sustain axial forces. It can be used for modelling structures where the edges are straight, but more importantly here, it can be used to model sagging cables such as the deformation of a wire exposed to gravity. The beam model can also be used for modelling slender structural elements, especially those having a significant bending stiffness (15). Both models allow the string to be pre-tensioned as is required here.

The biggest challenge was to couple the string to the sounding body. There are different types of coupling, each with its own characteristics. These include constraints that that allow rotation while others apply constraints in various dimensions. It is assumed for now that no sympathetic coupling of strings occurs, that is, they are considered to be isolated.

The standard (*hirajōshi*) mode based on the pentatonic modal system typical of East Asian zithers is employed in this study. The position of the bridge for each string for an instrument tuned in this way is illustrated in Figure 3. It should be noted that Japanese tuning systems are based on relative pitch and not absolute pitch. The actual position of the bridge may therefore vary, but the relative distance between bridges does not change.

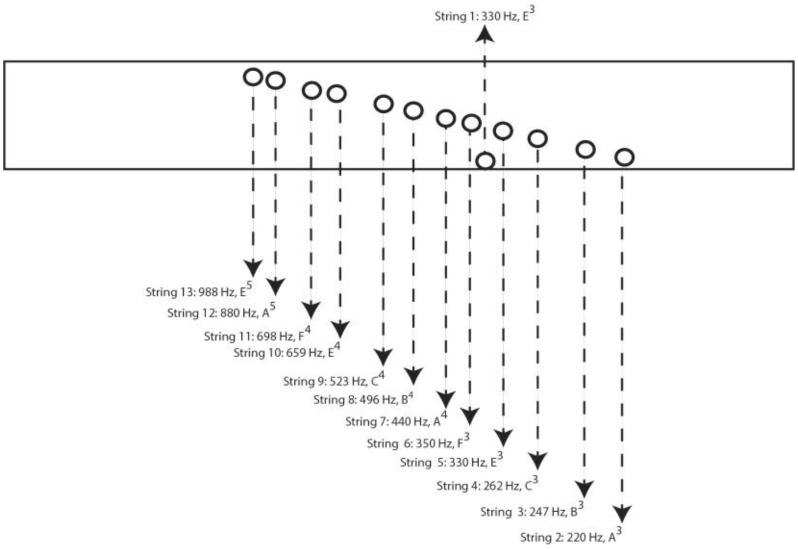

Figure 3. The placement of bridges and frequencies for each string for the standard (*hirajōshi*) mode

2.2.2 The bridges

The koto has both moveable bridges and fixed bridges. There are thirteen moveable bridges. A moveable bridge is placed beneath each string on the top plate and positioned according to the requirements of the tuning for performance. These bridges were historically made of wood or wood with ivory insets in the top segment. In recent times they have been made of ivory or more commonly from plastic. There are three main shapes that are designed to accommodate different positions on the top plate. The standard shape is used for most strings. It is approximately 6cm in height and measures 5cm across the span of the two supporting legs. The bridge supporting the thirteenth string which is closest to the performer typically has an extension on one supporting leg to help prevent it slipping off the edge of the instrument when the highest pitch is played while the second string may require a smaller bridge if a particularly low pitch is required. All bridges have a groove through which the string passes and stabilizes its position on the narrow top. A half cylinder shaped bridge is used in the simplified box model. A realistic model of a bridge, however, has been created using the shape and dimension of the standard bridge for use in future work (see Figure 4).

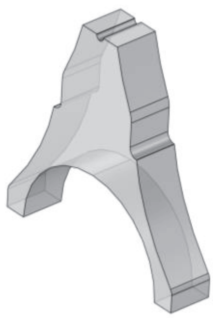

Figure 4. Model of the koto bridge developed for this study

By comparison, there are two fixed bridges located at each end of the koto and secured to the top plate. The strings pass over these bridges and are secured by traditional knots at these locations.

2.2.3 The pluck

Strings are plucked by means of three plectra worn on the player's right hand thumb, index finger and middle finger. The size, shape and materials used in the construction vary among different performance traditions. The two most common are square or rectangular-shaped plectra. The tip of the plectrum historically was made of bamboo, bone or ivory although more recently other materials such as plastic may be used. The tip is glued into a ring typically made of tightly rolled paper that is lacquered or covered with leather. These fit over the end of the finger to just below the player's nail with the plucking edge on the inside of the fingertip.

To model the plucking process, a force, usually a periodic one driven by the exciting frequency, f, is applied across the top face of the instrument in the y-direction. Another equal but opposite force, −f, is applied to the z (downward) direction to give a resultant force at 45 degrees to the top face of the koto.

2.3 Combining the components into the finite element model of the koto strings

The simplified box model was combined with the three other components — a single string was laid down the middle of the box across the three bridges and attached at each end. While the position of the string on the top plate may have an impact on the resonance, this study was concerned with the initial observations with the intention of investigating further details using the knowledge gained for studies using the CT model.

In this study, the koto body in turn required coupling with the surrounding air. The koto was therefore placed along the long axis of a cylinder as shown in Figure 5.

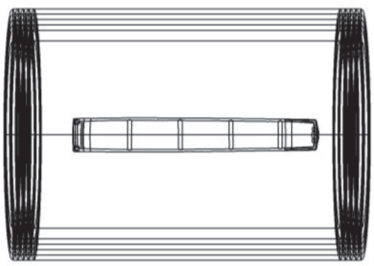

Figure 5. The simplified box model of the koto placed in a cylinder of air

This reduced the degrees of freedom and domain elements of the complex CT model with a proportional reduction in run time. The mesh element size always enclosed a minimum of six elements per wavelength. A sine wave with a frequency of 220 Hz was applied to a point on the string for the studies.

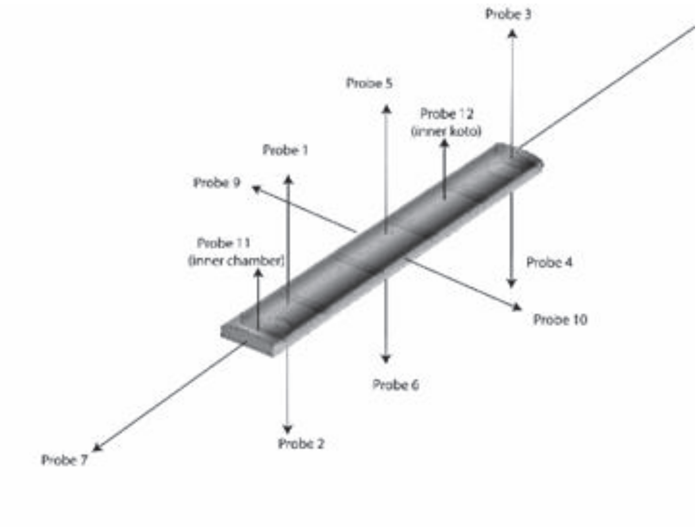

Figure 6. The set of 12 probes distributed around the koto to respond to the total acoustic pressure field

Finally, the response in the surrounding air can be measured through a set of probes distributed around the koto to respond to either the total acoustic pressure field in Pascals or the sound pressure level in decibels (see Figure 6). The advantage of the total acoustic pressure measurement is that the answer is computed as a complex number. Thus, in addition to the magnitude of the signal (at each point as a function of time), the phase angle can thus be readily computed as arctan (imaginary/real) as a useful indicator that each individual peak is indeed resonant and shows the direction of the signal. Solid displacement of the wood elements can be obtained separately.

2.3 Initial results

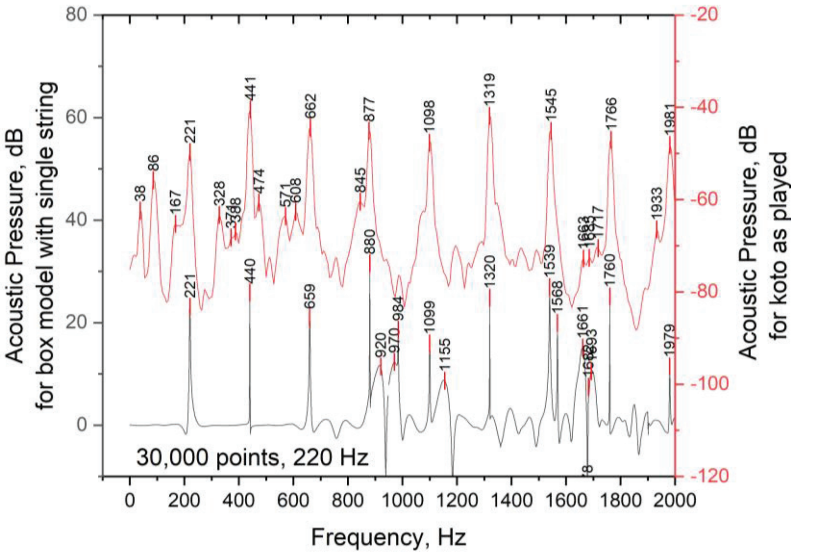

Figure 7. Comparison of the results simple box model of the koto with spectrum of the actual koto as played at 220 Hz

Initial simulations were made. In Figure 7, the lower portion of the graph shows the Fourier Transform of the fluctuating decibel level at Probe 4. The results of the Fourier Transform spectrum of the actual koto as played at 220 Hz are presented above the Probe 4 results. It can be seen that the primary excitation frequency and its harmonics are obtained from the single string box model. The prediction of the intermediate peaks is less successful. This is not surprising since we are not comparing like with like — the box model is an isotropic simplified model of the anisotropic model of the complex geometry of the koto itself. Future work will now attempt to align the two models primarily by using the techniques learned from the simplified box model and applying them to the CT model, then comparing these results with those obtained for the koto as played.

3 CONCLUSIONS

A first step towards creating a finite element model for Japanese plucked stringed instruments and investigati ng string behavior has been undertaken. We have been able to obtain initial results and this will guide ongoing work on modeling the strings of the koto. It is hoped that this work may also contribute to the evaluation of the patterns of sympathetic response across the instrument body for a deeper understanding of the koto's distinctive and tonal coloring.

ACKNOWLEDGEMENTS

This study has drawn on the expertise and goodwill of many people. The author would like to sincerely thank: Chris Waltham from The University of British Columbia for data on the physical properties of paulownia; colleagues at Los Alamos National Laboratory, Adelaide Microscopy and Mechanical Engineering at The University of Adelaide, The Radiology Department of the Royal Adelaide Hospital, The South Australian Wood Carving Academy, HW Technologies and gfai tech GmbH for the acoustic camera and Pan Pacific Technologies for access to equipment and/or technical support; and Shane Underwood from Technics Australia, for technical support for Comsol. Assistance from Synopsys Simpleware and AltaSim Technologies for technical assistance for converting CT DICOM files is also gratefully acknowledged.

REFERENCES

[1] Rossing TD, ed. The Science of String Instruments. Springer, NY (USA), 2010.

[2] Tahvanainen H, Poölkki J, Penttinen H, Välimäki V. Finite Element Model of a Kantele with Improved Sound Radiation. *Proceedings of the Stockholm Music Acoustics Conference, SMAC*, Stockholm, 2013, pp. 193-198.

[3] Ando Y. Acoustics of Sohs ("Koto"s). Proceedings of International Congress of Acoustics, 12; Toronto, Canada 1986. Vol. 3, KI. pp. 5-6.

[4] Ando Y. Gakki no Onkyōgaku (Acoustics of Musical Instruments). Tokyo, Japan: Ongaku No Tomo Sha, 2nd edition, 1996.

[5] Yoshikawa S. Acoustical classification of woods for string instruments. J Acoust Soc Am. 2007, 122, pp. 568-573.

[6] Yoshikawa S. Plucked stringed instruments in Asia. In: Rossing TD, ed. The Science of String Instruments. Springer, NY (USA), 2010. pp. 173-196.

[7] Waltham C, Koster E, and Lan Y. An Acoustical Study of the Qin. J. Acoust Soc Am. 2016, 139 (4), pp. 1592-1600.

[8] Waltham C, Coaldrake K, Koster E, Lan Y. Acoustics of the qin. In Schneider A, ed. Studies in Musical Acoustics and Psychoacoustics. New York, USA: Springer; 2017, pp. 49-74.

[9] Coaldrake K. Construction and validation of a high resolution finite-element model of the Japanese koto. Acoust Soc Am. 2018, 144(2), p. 1891.

[10] Corradi R, Miccoli S, Squicciarini G, Fazioli P. Modal analysis of a grand piano soundboard at successive manufacturing stages, Applied Acoustics, 125 (3), 2017, pp. 113–127.

[11] Lee N. Smith JO. Virtual String Synthesis. In: Rossing TD, ed. The Science of String Instruments. Springer, NY (USA), 2010, pp. 417- 455.

[12] Collins M. Finite Element Analysis of a Vibrating Guitar String and Project Management, Final Project Report, Biomedical Engineering, University of Limerick, 2011.

[13] Vibrating Strings, Comsol v. 5.4 Model Library, COMSOL Multiphysics® v. 5.4. www.comsol.com. COMSOL AB, Stockholm, Sweden, 2018.

[14] Waltham C. Elastic moduli of Paulownia tomentosa. Unpublished Report, University of British Columbia, Canada, 2015.

[15] Vibration Analysis of a Deep Beam, Comsol v. 5.4 Model Library, COMSOL Multiphysics® v. 5.4. www.comsol.com. COMSOL AB, Stockholm, Sweden, 2018.

PROCEEDINGS of ISMA 2019
International Symposium on Music Acoustics

13 - 17 September 2019 in Detmold, Germany

Numerical simulation of the acoustic guitar for virtual prototyping

Henna Tahvanainen, Hideto Matsuda, Ryo Shinoda

Yamaha Corporation, Research and Development Division, Japan *

Abstract

This research presents numerical simulation tools used in the research of acoustic guitars in the industrial context. The focus is on describing a virtual prototyping environment that has been successfully used in product development. The main challenge is achieving an acceptable agreement between simulation and measurement of a random guitar taken in the production line. To this end, detailed geometrical modeling and averaged materials parameters values measured from the production line are used. Simulation and measurement results are compared in terms of mode frequencies, frequency responses, and radiation efficiency.

Keywords: Acoustic guitar, Wave-based modelling

1 INTRODUCTION

According to Music Trades[1] in the US alone about 1.5 million acoustic guitars were sold in 2018. At the same time, it can take months to build an acoustic guitar, depending on the amount of development work and details put into it. Large-scale manufacturers typically maintain a large lineup in order to cater for needs of different players, making the management and building processes more complicated. In addition, introducing model changes in the factory production line can be costly. In order to save time and resources, while maintaining high product quality, virtual prototyping has become a very useful tool for musical instrument manufacturing.

Virtual prototyping requires a numerical simulation model, which essentially means solving by approximation the complicated partial differential equations that govern the vibro-acoustic characteristics of the system. Apart from prototyping, numerical simulation has been applied to sound synthesis [20], study of structure-acoustic phenomena [7, 19], conservation of historical instruments [23], and material property estimation [22], among others. Each application requires a little bit different approach to simulation. For example, for sound synthesis, it is possible to use black-box modelling tools that try to match the timbre of the instrument, and often it is required that the simulation work real-time. On the other hand, for prototyping, the interest is on being able to edit the material properties as well as the geometrical properties directly, and ideally within a reasonable computational time. For this purpose, wave-based modelling methods are often employed.

In the field of scientific computing, the verification and validation process is necessary for credibility and ultimately the usability of the simulation tools [14]. Numerical verification is done with a simple case by comparing the simulation against the analytic solution. As for validation, there are many sources of uncertainty when the simulation data is compared with experimental data. For the case of factory-produced acoustic guitars, when comparing a simulated guitar and a random guitar measured from the production line, the biggest sources of discrepancy are probably the inherit variability of wood and the manufacturing tolerance.

In this paper, a combination of wave-based element methods is adopted for simulating the acoustic guitar body. The structural eigenfrequency analysis of a fairly detailed geometrical model is calculated using finite element method (FEM), and that result is used for forced modal analysis with boundary element method (BEM) in the coupled structure-acoustic domain. Different ways of validating the model with measurements are explored while the manufacturing tolerance and perceptual tolerance for frequency responses of the guitars are considered.

2 BACKGROUND

The guitar can coarsely be divided into two vibrating parts: strings and body. The player sets the strings to vibrate and that vibration drives the guitar body to finally generate an audible sound. It is very common

*henna.tahvanainen@music.yamaha.com

[1]Music Trades, April 2019 issue, p.62

to consider each of them separately for modelling purposes. First proposal for modelling strings for sound synthesis was done by [8] and since then models have developed, especially for sound synthesis purposes [20, 6].

Guitar body models are useful for prototyping purposes, since guitar building is essentially about crafting the guitar body, including bridge, saddle, neck, and nut. One of the first mathematical models of the guitar body was the resonator model of the first two coupled modes [4]. Since the early stages of scientific computing in the 1960's, especially finite and boundary element models for the guitar body started to appear [16]. Finite difference [15] and spectral method [5] have also been used, but FEM has been by far the most popular method. To mention but a few examples from different decades, guitars at different building stages [7] and the effect of bracing [9], bridge design [18], plate thickness [16], and string-fret collisions [2] have been studied with the help of simulations. Simulations have given rise to extended design methods related to, e.g., frequency response optimization [21], material property identification [22], and platforms for designing musical instruments, such as PAFI[2] and Digital Guitar workshop[3]. The coupling between the body and strings has been explored by [25]. A full model has also been considered by [5].

Commonly, simulation validation is done by comparing simulated mode shapes and frequencies, and transfer functions (input admittance, or sound pressure level at a point in space) to the measured ones. Also, directivity patterns and radiation efficiency have been compared [10, 11, 19].

3 METHODS

3.1 Simulation

3.1.1 Geometrical model and material properties

One guitar can have up to about 40 individual parts and about 10 different materials. The materials may also be oriented in different ways, typically requiring about 10 different local coordinate systems in the model. In addition, the line-up of large manufacturers may be extensive. For example, Yamaha maintains more than 10 different guitar models and within each model the materials vary in order to cater for different needs of players. It is important that each guitar model be modelled with respective properties.

For prototyping purposes, the geometrical model of the guitar needs to be easy to edit. To this end, in-context design with envelopes was used in SolidWorks 2016. The geometrical model was constructed from drawings, but it can also be achieved by measuring a physical copy from the production line with, e.g., 3D imaging techniques.

For the model presented in this paper, some simplifications were made: pegs, frets, and strings were omitted. In addition, the top and back plate were modelled flat, not arched. Glue between parts was not considered, instead continuous mesh across the contact surfaces was assumed.

For the simulation, material properties were measured from the wood used in actual production line. Three or more samples were measured and averaged. Wood is an orthotropic material, so three Young moduli, shear moduli, Poisson ratios, and density are needed as input. The material properties were measured by means of experimental modal analysis with beams at free-free boundary conditions. For example, the Young moduli can be approximated from the first bending mode of the sample, and the shear moduli from the first twisting mode. For procedure, the reader is referred to, e.g., [17]. Damping can also be measured, but it is often frequency-dependent. In order to simplify the simulation process, a constant damping ratio of 0.008 was assumed.

3.1.2 Mesh and process

Structural analysis was performed with finite element method (FEM), and the coupling of that structure with air, as well as radiation was calculated using fast multipole boundary element method (FM-BEM) both on commercially available software, Ansys 18.2 and WAON 4.5 (Cybernet), respectively. A review of FM-BEM

[2] http://plateforme-lutherie.com/
[3] http://www.digitalguitarworkshop.de/

methods is given for example in [13]. The process requires two meshes, one for structural analysis in the vacuum and one for the coupled analysis. The meshes are shown in Fig. 1, and for the BEM model, the field point mesh for post-processing is also included.

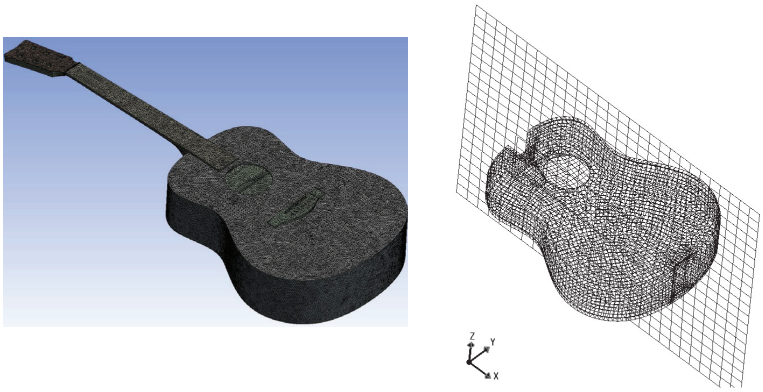

Figure 1. Structural mesh for FEM (left), and the mesh for coupled analysis for BEM with field point mesh included (right).

For the simulated guitar presented in this paper, the structural mesh consisted of solid tetrahedral elements with the maximum size of 4 mm resulting in about 400 000 elements. For the coupled analysis, the structure can be simplified; essentially all structures smaller than the acoustic wavelength can be excluded. In this case, just the enclosed air volume of the guitar was meshed, with tetrahedral elements of a maximum size of 10 mm, resulting in about 5500 elements. The result of eight structural nodal points were averaged and mapped to the each acoustic nodal point. It is recommended to have at least 6 elements per wavelength.

For BEM modelling, there are several algorithms for interior and exterior coupling. In this case, the calculations were performed using the thin panel assumption using the indirect double layer formulation. For examples the reader is referred to [1]. The structure-acoustic simulation took about 30 min for the frequency range of 12-500 Hz with 1-Hz step run with a desktop computer (24 cores, 3 GHz, RAM 256 GB).

Two different excitation methods were used: force of 1 N in the center of the saddle to simulate the impulse hammer excitation, and a point source with amplitude of 2 Pa at a distance of 1 m in order to simulate the acoustic excitation used in the LDV measurements.

3.2 Measurements

In order to understand the material variability in the production line, measurements of eight guitars were performed in an acoustically dry measurement room. Both accelerance (ONOSOKKI PU NP3211) and sound pressure level (microphone ONOSOKKI MI-1234) were recorded with FFT analyzer (ONOSOKKI DS-3000, sampling rate 52100 Hz) by using a miniature impulse hammer (B&K 8203). In addition, one guitar was measured with laser-Doppler vibrometer (LDV) (Polytec PSV-300) in an anechoic room in order to obtain the mode shapes and average top plate velocity for comparison with simulation. It is also possible to reconstruct the radiated sound power and the radiation efficiency of each of the mode shape when the surface velocity is known [24]. The excitation method was random noise through a speaker (Yamaha MSR100). During the measurements of the assembled guitars, the strings were damped, and the guitar was supported from the neck only.

4 COMPARISON OF SIMULATION AND MEASUREMENTS

Firstly, the material property variation in the production line was analyzed. Figure 2 shows the mobility of eight guitars taken from the same production line. The variation of the peak frequencies is limited to a few percent.

This sets a limit for the acceptable difference between simulated and measured mode frequencies.

After careful material measurements and geometrical modelling, an example of the simulated and measured sound pressure level in the near-field of the guitar is shown in Fig. 3. The simulated mode frequencies are within 2 % of their measured values. Some of the simulated mode peaks have a higher Q value than the measured ones, owing to approximating the damping with a constant damping ratio.

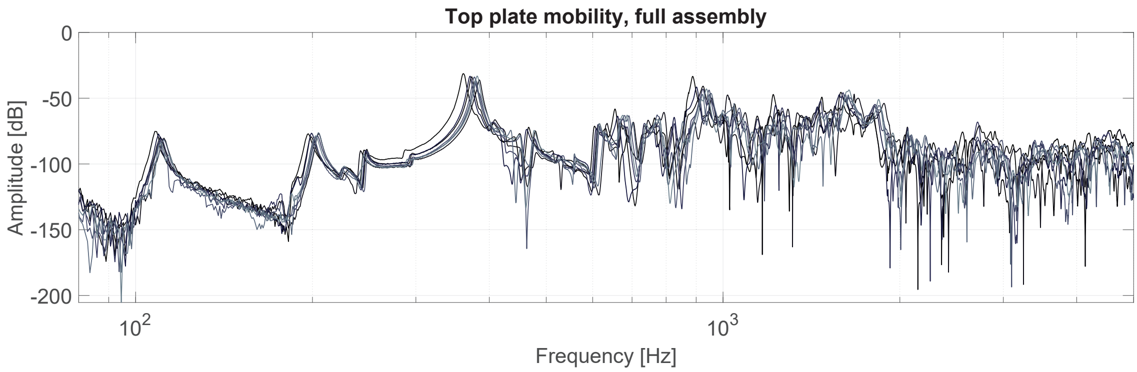

Figure 2. Top plate mobility measured in eight different guitars in the production line.

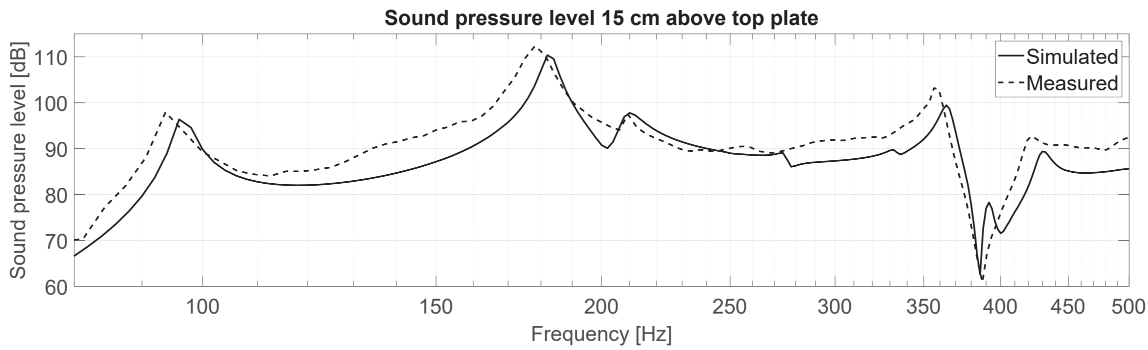

Figure 3. Comparison of simulated and measured sound pressure level at 15 cm above the low bout of an acoustic guitar.

In addition to the frequency response, some of the simulated and measured modes shapes are shown in Fig. 4. The data is real velocity data, and the color scales of the simulated and measured data have been normalised. The mode shape are very similar.

Furthermore, the average velocity of the top plate and radiation efficiency of the mode shapes are compared in Fig. 5. The simulated and experimental average velocity are very similar. The radiation efficiencies, while not matching in all cases, follow similar trends. Again, the simple approximation for damping may be the cause of the differences.

5 DISCUSSION

It can be concluded that even with some geometrical simplifications, and with a simple damping model, the acoustic guitar body can be simulated reasonably accurately. In addition, with the combined FEM-FMBEM approach, the air cavity does not need to be modelled with as much detail as the structural model.

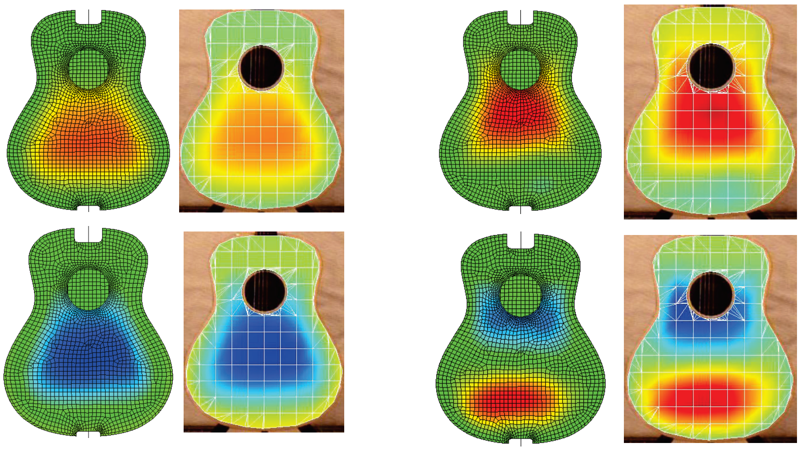

Figure 4. Some of the simulated and measured mode shapes with acoustic excitation.

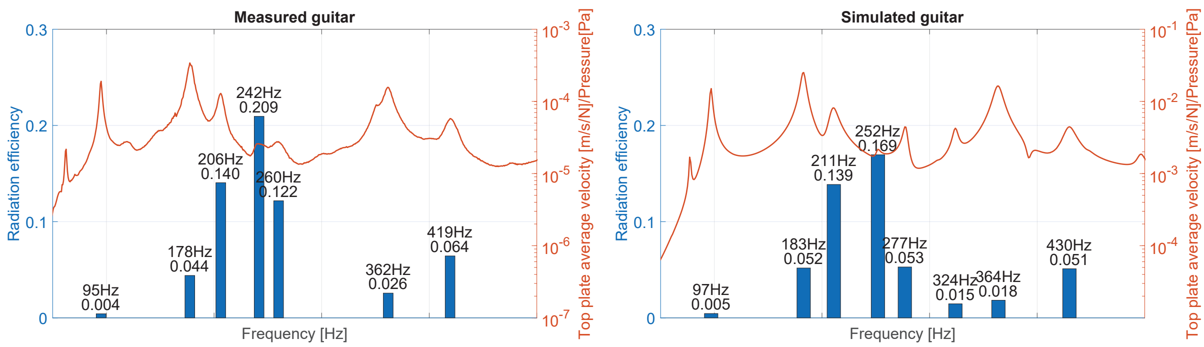

Figure 5. Comparison of simulated and measured average top plate velocity and radiation efficiency of an acoustic guitar with acoustic excitation.

The differences between simulated and measured mode frequencies fall within the variability of the manufactured guitars in the production line when averaged material properties from the production line are used. The measured and simulated mode shapes are also very similar. The more global parameters like average top plate velocity or radiation efficiency of the modes can differ more. Differences can be seen especially in the modal damping and in modes that do not seem to radiate well. This information, together with understanding the origins of the coupled modes, can be used to improve the simulation model.

Perceptually, it seems possible to differentiate between two guitars, if all the mode frequencies are shifted about 2-3 % [25]. However, recent playing and listening tests with actual guitars suggest that even a larger shift might be acceptable when not all modes frequencies are shifted consistently [3]. Furthermore, while studying guitars from the same production line, about 5% reduction in the frequency of the first mode was needed in order the guitar to perceived as more bassy [12]. The frequency response of the current simulated guitar falls within such variation from that of the measured guitar.

After verifying the simulation results, the simulation model can be used in virtual prototyping. The design process for the A-series aiming at louder low-mid frequency range sound with bracing changes is an example of involving virtual prototyping at Yamaha. The numerical simulation serves in a supporting role, meaning that ultimately actual prototypes are built and evaluated.

The feedback loop between simulation and measurement is completed by measuring the prototypes and confirming the simulation result. Consequently, improving the matching between simulation and measurements is an ongoing process at Yamaha. With a large database of measured and simulated guitars, it is possible to spot trends in the mismatch between simulation and measurement, and to improve the simulation model. Generally, a good agreement between simulation and measurements can be reached at much higher frequencies than presented here. The contribution of individual modes can distinguishable up to about 1 kHz, as can be seen in the top plate mobility measurements in Fig. 2.

Examples of further considerations for the simulation include pre-stress from the string tension, although at low frequencies, it does not change the results considerably. Orthotropic damping has also been considered.

6 CONCLUSIONS

A modelling scheme using FEM and FM-BEM was adopted for simulating the acoustic guitar body. By using averaged material properties measured from the wood used in the production line and the detailed geometrical modelling from drawings, it is possible to reach an acceptable agreement between simulated and measured frequency response that falls within the manufacturing variability and the perceivable tolerance of frequency response shifts, when the measured guitar is taken randomly from the production line.

Comparison of the simulated and measured guitars shows that while the mode frequencies and shapes are very similar, average top plate velocity and radiation efficiency of the modes can vary more. One of the reasons is simplified damping properties of wood used in the simulation.

ACKNOWLEDGEMENTS

The authors would like to thank Ryuji Hashimoto and Mirco Pezzoli (Polimi.it) for providing the code to analyse the LDV measurements.

REFERENCES

[1] N. Atalla and F. Sgard. *Finite element and boundary methods in structural acoustics and vibration*. CRC Press, 2015.

[2] S. Bilbao and A. Torin. Numerical modeling and sound synthesis for articulated string/fretboard interactions. *Journal of the Audio Engineering Society*, 63(5):336–347, 2015.

[3] S. Carcagno, R. Bucknall, J. Woodhouse, C. Fritz, and C. J. Plack. Effect of back wood choice on the perceived quality of steel-string acoustic guitars. *The Journal of the Acoustical Society of America*, 144(6):3533–3547, 2018.

[4] O. Christensen and B. B. Vistisen. Simple model for low-frequency guitar function. *The Journal of the Acoustical Society of America*, 68(3):758–766, 1980.

[5] G. Derveaux, A. Chaigne, P. Joly, and E. Bécache. Time-domain simulation of a guitar: Model and method. *The Journal of the Acoustical Society of America*, 114(6):3368–3383, 2003.

[6] M. Ducceschi and S. Bilbao. Linear stiff string vibrations in musical acoustics: assessment and comparison of models. *The Journal of the Acoustical Society of America*, 140(4):2445–2454, 2016.

[7] M. Elejabarrieta, A. Ezcurra, and C. Santamaría. Vibrational behaviour of the guitar soundboard analysed by the finite element method. *Acta Acustica united with Acustica*, 87(1):128–136, 2001.

[8] L. Hiller and P. Ruiz. Synthesizing musical sounds by solving the wave equation for vibrating objects: Part 1. *Journal of the Audio Engineering Society*, 19(6):462–470, 1971.

[9] R. Inta. *The acoustics of the steel string guitar*. PhD thesis, University of New South Wales, Australia, 2007.

[10] J. Lai and M. Burgess. Radiation efficiency of acoustic guitars. *The Journal of the Acoustical Society of America*, 88(3):1222–1227, 1990.

[11] A. Le Pichon, S. Berge, and A. Chaigne. Comparison between experimental and predicted radiation of a guitar. *Acta Acustica united with Acustica*, 84(1):136–145, 1998.

[12] H. Mansour, V. Fréour, C. Saitis, and G. P. Scavone. Post-classification of nominally identical steel-string guitars using bridge admittances. *Acta Acustica united with Acustica*, 101(2):394–407, 2015.

[13] N. Nishimura. Fast multipole accelerated boundary integral equation methods. *Applied mechanics reviews*, 55(4):299–324, 2002.

[14] W. L. Oberkampf and C. J. Roy. *Verification and validation in scientific computing*. Cambridge University Press, 2010.

[15] F. Pfeifle and R. Bader. Real-time finite difference physical models of musical instruments on a field programmable gate array (fpga). In *Proc. of the 15th Int. Conference on Digital Audio Effects (DAFx-12)*, pages 17–21, 2012.

[16] B. Richardson and G. Roberts. The adjustment of mode frequencies in guitars: a study by means of holographic interferometry and finite element analysis. In *SMAC*, volume 83, pages 285–302, 1983.

[17] R. Sproßmann, M. Zauer, and A. Wagenführ. Characterization of acoustic and mechanical properties of common tropical woods used in classical guitars. *Results in physics*, 7:1737–1742, 2017.

[18] J. A. Torres and R. R. Boullosa. Influence of the bridge on the vibrations of the top plate of a classical guitar. *Applied Acoustics*, 70(11-12):1371–1377, 2009.

[19] J. A. Torres and R. R. Boullosa. Radiation efficiency of a guitar top plate linked with edge or corner modes and intercell cancellation. *The Journal of the Acoustical Society of America*, 130(1):546–556, 2011.

[20] V. Välimäki, J. Pakarinen, C. Erkut, and M. Karjalainen. Discrete-time modelling of musical instruments. *Reports on progress in physics*, 69(1):1, 2005.

[21] M. van Boven. Dynamic response optimization of an acoustic guitar. Master's thesis, Delft University of Technology, 2017.

[22] R. Viala, V. Placet, and S. Cogan. Identification of the anisotropic elastic and damping properties of complex shape composite parts using an inverse method based on finite element model updating and 3d velocity fields measurements (femu-3dvf): Application to bio-based composite violin soundboards. *Composites Part A: Applied Science and Manufacturing*, 106:91–103, 2018.

[23] R. Viala, V. Placet, S. Le Conte, S. Vaiedelich, and S. Cogan. Model-based decision support methods applied to the conservation of musical instruments: Application to an antique cello. In *Model Validation and Uncertainty Quantification, Volume 3*, pages 223–227. Springer, 2020.

[24] E. G. Williams. *Fourier acoustics: sound radiation and nearfield acoustical holography*. Elsevier, 1999.

[25] J. Woodhouse, E. Manuel, L. Smith, A. Wheble, and C. Fritz. Perceptual thresholds for acoustical guitar models. *Acta Acustica united with Acustica*, 98(3):475–486, 2012.

PROCEEDINGS of ISMA 2019
International Symposium on Music Acoustics

13 - 17 September 2019 in Detmold, Germany

Creating virtual acoustic replicas of real violins

Esteban Maestre *, Gary Scavone †

Computational Acoustic Modeling Laboratory
Centre for Interdisciplinary Research in Music Media and Technology
Schulich School of Music, McGill University, Canada

Abstract

We provide an overview of a current research project on measuring, modeling, and virtually recreating the sound radiation characteristics of real acoustic violins. Our general approach is based on measuring the directivity of an acoustic violin, and designing a digital filter structure that mimics the observed directivity while allowing interactive operation. The digital filter structure is fed by the electrical signal coming from a silent electric violin as played by a musician. In a hemi-anechoic chamber, we use a microphone array to characterize the frequency-dependent directivity transfer function of a real violin by exciting the bridge with an impact hammer and measuring the acoustic pressure at 4320 points on a sphere surrounding the instrument. From the input force and output pressure signals obtained from the real violin measurements, we use deconvolution to estimate 4320 impulse responses each corresponding to a radiation direction. With such impulse responses, we use State Wave Synthesis to model the observed directivity in time-varying conditions and efficiently render directional wavefronts in a virtual environment. We characterize the silent violin transfer function by exciting the bridge with an impact hammer and measuring the electrical signal at its output, leading to an impulse response that we use to design an inverse filter to recover the force excitation at the bridge.

Keywords: Violin, Radiation, Virtual, Replica, Directivity, Electric Violin, Silent Violin

1 INTRODUCTION

This research project is focused on the accurate characterization of the acoustic properties of traditional musical instruments and the development of digital models capable of efficiently reproducing such properties in interactive contexts. One application of this research is the preservation and virtual reproduction of historically valuable musical instruments, such that they can be played and heard in real time. Our project is motivated in part by the Stradivari *Messiah* violin, considered to be the most treasured masterpiece by this historic Cremonese maker because of its "as-new" condition but which has seldom been played and remains inaccessible, on display at the Ashmolean Museum in Oxford [1, 2]. Our objective is to develop methods for measuring, modeling, and virtually reproducing the acoustic radiation properties of real acoustic violins as a technological means for preserving and reproducing the acoustic properties of valued musical instruments (beyond performance recordings, pictures, or material and geometric data and analysis). This manuscript provides a brief overview of our progress so far.

There have been many reports of violin radiation pattern measurements in the past (a few of these include [3, 4, 5, 6, 7], with a good summary by [8]). In most cases, the measurements and analyses were made to evaluate and/or compare different instruments to one another. In [9], the authors use a frequency-domain approach to estimate directional frequency responses for later use in a sample-based sound synthesis system: glissandi are played on a violin in an anechoic chamber and the sounds are recorded for a discrete set of directions, from which frequency responses are estimated using frame-by-frame deconvolution of the harmonic tones. In our case, we capture a more comprehensive directivity frequency range by exciting the instrument with an impact hammer, and use a time-domain digital filtering method for simulating directivity. In the following, we report our developments on two main tasks: measurement and digital modeling of the acoustic radiation properties of a real violin, and measurement and digital modeling of the transfer function of an electric violin, with which a virtual acoustic replica of the real violin is to be virtually performed.

*esteban@music.mcgill.ca
†gary@music.mcgill.ca

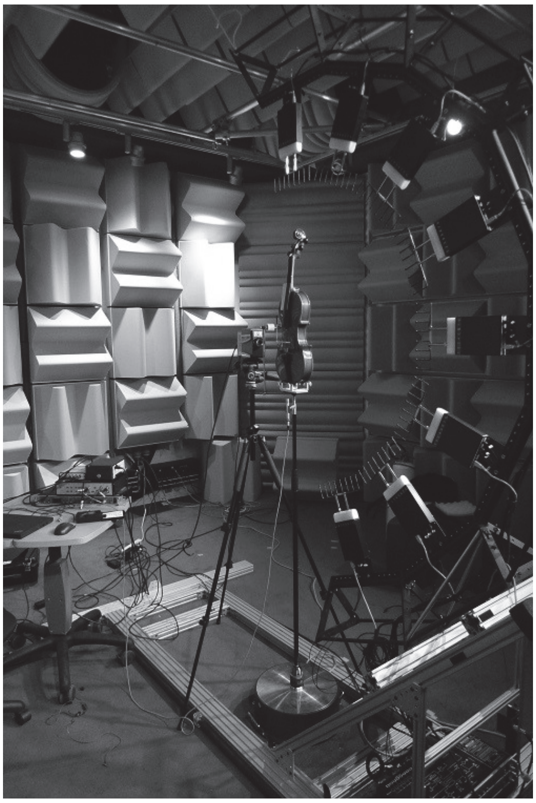

Figure 1. Semi-circular microphone array, rotating base, and support rig used to measure sound pressure signals at 4320 points on a one-meter-radius sphere around the violin. The laser Doppler vibrometer (on the tripod) was only used not used during the sound pressure measurements.

2 MEASUREMENT

2.1 Acoustic violin

In a similar fashion as performed for violin sound synthesis by digital waveguides [10], we define the frequency-domain radiativity transfer function of an acoustic violin by relating the force exerted by the strings on the bridge and the sound pressure radiated at a far-field distance from the instrument. Here, instead of considering a single external microphone position, we use a microphone array to measure the complete frequency-dependent directivity pattern on a sphere around the instrument, assuming far-field conditions.

In a hemi-anechoic chamber (with a carpeted floor and extremely low reflectivity), we carried out radiativity measurements on a violin from the Schulich School of Music at McGill University. The instrument was held vertically, with the neck pointing up, on a rotating base. Cushioned clamps were used in conjunction with a purposely machined shoulder rest to naturally fix the end of the body of the instrument to a vertical pole attached to the rotating base. Rubber bands were used to damp the strings. A semi-circular, one-meter-radius array of 60 high-precision, calibrated Sennheiser KE4-211-2 microphones was placed to cover 15/16 of elevation angle span of a sphere around the violin position, whose center was defined as the midpoint between the F-holes at an equal distance between the back and top plates. The measurement setup is shown in Figure 1. The laser Doppler vibrometer (Polytec LDV-100), mounted on the tripod, was used to initially measure the admittance of the violin but not for the subsequent radiativity measurements.

The impact hammer, which has been long used in the context of vibratory analysis or modeling [11, 12], provides a simple and effective method to drive stringed instruments with great repeatability. For our measurements, a calibrated miniature impact hammer (PCB Piezotronics 086E80) was used to excite the corner of the bass side of the bridge in the direction corresponding to the horizontal transverse motion of the strings, parallel to the bow motion. The radiated sound, together with the hammer force, was measured by each of the 60 microphones for rotating base angle increments of 5 degrees, leading to $72 \times 60 = 4320$ signal measurement combinations. For each combination, three distinct measurements were made and later averaged. The spherical sector defined by the microphones covered 95% of the sphere. In our modeling framework, the strings are assumed to meet at a single point representing a common excitation position, so for practical matters, we could also have chosen to measure on the treble side. We chose to measure on the bass-bar side because of the higher efficiency of the bridge there in driving the top plate, as observed from previous experimental studies of violin acoustics [13]. Time-domain signals of force and sound pressure were collected, delay-compensated, and stored before using frequency-domain deconvolution to obtain directivity frequency responses. Signals were sampled at a rate of 48 kHz, and coherence analysis revealed strong consistency up to approximately 7 kHz.

2.2 Silent electric violin

We measured the response of a high-end commercially available silent electric violin, which we assume can be modeled as a linear, time-invariant system with a frequency response determined from input-output measurements. As with the acoustic violin, the strings were damped with rubber bands and the miniature impact hammer was used to excite the corner of the bass side of the bridge in the direction corresponding to the horizontal transverse motion of the strings. The electrical output signal provided by the violin was recorded simultaneiously with the hammer force. Both signals were recorded at a sample rate of 48 kHz. By way of frequency-domain averaging over 3 distinct measurements, the frequency response of the electric violin was computed by deconvolution. Coherence analysis revealed strong consistency up to approximately 12 kHz.

3 ANALYSIS & MODELING

3.1 Acoustic violin directivity

We use State Wave Synthesis (SWS) [14] to model and simulate the frequency-dependent directivity of the acoustic violin. To do so, we design a mutable state-space model of 58 state variables, one non-mutable input (bridge excitation force) and an indefinite number of mutable outputs (sound pressure), each corresponding to an outwards direction expressed by two angles in vertical polar coordinates on a spherical coordinate system determined by the measurement sphere center. Assuming minimum-phase, a set of 58 common eigenvalues are estimated from the measured input admittance of the instrument. The specific number of eigenvalues was determined somewhat arbitrarily based on the quality of the frequency-domain fit. Alternatively, a similarly representative set of common eigenvalues could be obtained by performing modal analysis on a subset of the radiation measurements, though the input admittance tends to have a better signal to noise ratio. The output coordinate space of the output-mutable state-space model is defined as a bounded two-dimensional Euclidean space, with dimensions being the azimuth θ and elevation φ angles of the microphone measurement positions. In a first step, the state-to-output projection coefficients corresponding to the 4320 measurements are estimated by least-squares, leading to a matrix of 4320×58 projection coefficients. Then, estimated projection coefficients are arranged as 58 matrices of 72×60 entries each, to perform smoothing and re-sampling of the output coordinate space to obtain 58 matrices of 64×64 coefficients each (again, the specific size of the matrices is arbitrary). Finally, an output projection function is devised to perform bilinear interpolation of output projection coefficients over the space of output coordinates. Note that the mutable state-space model resulting from this modeling procedure can be equivalently expressed in real form by combining complex-conjugate pairs of eigenvalues into real second-order parallel sections whose numerator coefficients are provided by an output mapping function by bilinear interpolation. Example models of radiation frequency responses are displayed in Figure 2 along with their corresponding measured responses.

To demonstrate the dynamic behavior of the radiation model, we synthesize the input-output frequency re-

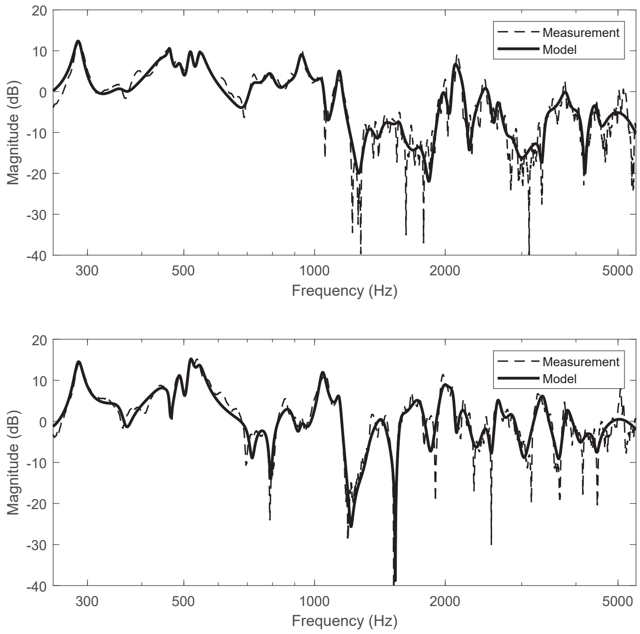

Figure 2. Detail of the radiation frequency response model. Input-output magnitude frequency responses of two individual measurements and their corresponding modeled responses, as obtained from the model. Top graph coordinates: azimuth $\theta = 1.97$ rad, elevation $\varphi = -0.21$ rad; bottom graph coordinates: azimuth $\theta = 1.02$ rad, elevation $\varphi = 0.26$ rad.

sponse as obtained from exciting the model in time-varying conditions. For 512 consecutive steps, we modify the output coordinates of an outgoing wave as captured by an ideal microphone lying on the sphere surrounding the source object. Assuming ideal excitation of the violin bridge, we simulate a continuous linear motion of the ideal microphone on the sphere, from initial position at ($\theta = 0.69$ rad, $\varphi = 4.71$ rad) to a final position at ($\theta = -1.48$ rad, $\varphi = -0.52$ rad). To illustrate the quality and smoothness of the achieved result, in Figure 3 we compare the measured frequency responses (nearest-neighbor) and the model frequency responses as obtained from bilinear interpolation of processed output projection coefficient vectors.

This modeling procedure, for which more details can be found in [14], allows the interactive simulation of the radiation properties of the acoustic violin given the time-varying position and orientation of the virtual instrument. To do so, the mutable state-space model is used to efficiently render multiple outgoing wavefronts representing the direct field and reflections, and propagating them to a listener in a virtual space. The frequency-dependent directivity of the listener, represented as a binaural HRTF, can be also simulated by a mutable state-space model as described in [14], with inter-aural time differences realized by fractional delay lines.

3.2 Electric violin equalization

In order to obtain an approximation of the bridge force signal $F(t)$ of the silent electric violin, which is needed to excite the radiation model, we "whiten" the electric violin output signal $E(t)$. This is achived by using the electric violin transfer function measurement to design a matched minimum-phase, recursive parallel filter. As well, an inversion formula that preserves the parallel configuration of the designed filter is derived. First, a minimum-phase, magnitude-only specification technique is used to design an order-30 recursive parallel filter $H(z) = c + \sum_{m=1}^{M} H_m(z)$ comprising a real constant c and real-single or complex-conjugate poles spread over M parallel first-order sections $H_m(z) = r_m/(1 - p_m z^{-1})$ (the order M is arbitrarily determined based on quality of

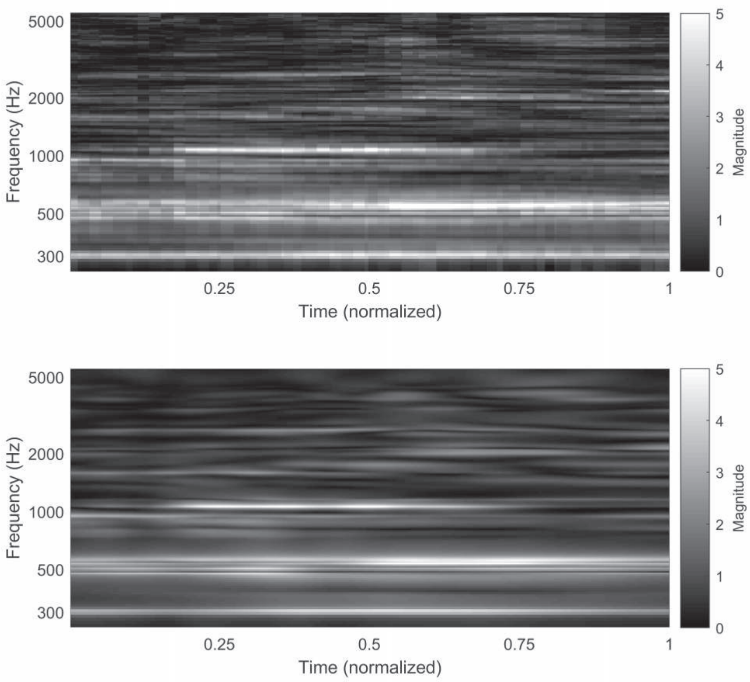

Figure 3. Input-output magnitude frequency response as obtained from exciting the radiation model in time-varying conditions: continuous linear motion of an ideal microphone on the sphere, from initial position at ($\theta = -0.69$ rad, $\varphi = -0.34$ rad) to final position at ($\theta = 5.06$ rad, $\varphi = 1.39$ rad). Top graph: nearest-neighbor measurement; bottom graph: bilinear interpolation of processed output projection coefficients.

the frequency-domain fit). Then, we express each $H_m(z)$ as $H_m(z) = r_m + z^{-1}G_m(z)$, with $G_m(z) = r_m p_m/(1 - p_m z^{-1})$. With this, the parallel filter $H(z)$ becomes $H(z) = g + z^{-1}G(z)$, where $g = c + \sum_{m=1}^{M} r_m$ and $G(z) = \sum_{m=1}^{M} G_m(z)$. Now it is possible to invert the transfer function $H(z)$ and obtain the input force signal $F(z)$ from the output electrical signal $E(z)$ via $F(z) = g^{-1}(E(z) - z^{-1}G(z)F(z))$ while preserving the parallel architecture. The resulting model and equalization are depicted in Figure 4.

4 OUTLOOK

The work reported here represents the early stages of a project intended to allow virtual acoustic rendering of acoustic violins (characterized from measured responses) using a silent electric violin. Complete measurements on a McGill-owned violin, as well as a Bergonzi from the Montreal area, have been performed. Subsequent use of less complete measurements (substantially lower number of external microphone positions, more reverberant room conditions, ...) of the Stradivari *Messiah* violin has previously been investigated [15] and is still under development. Other aspects of the project include the virtual reality rendering, motion tracking, room response modeling, perceptual testing with players and ultimately the staging of a performance demonstrating the resulting technologies.

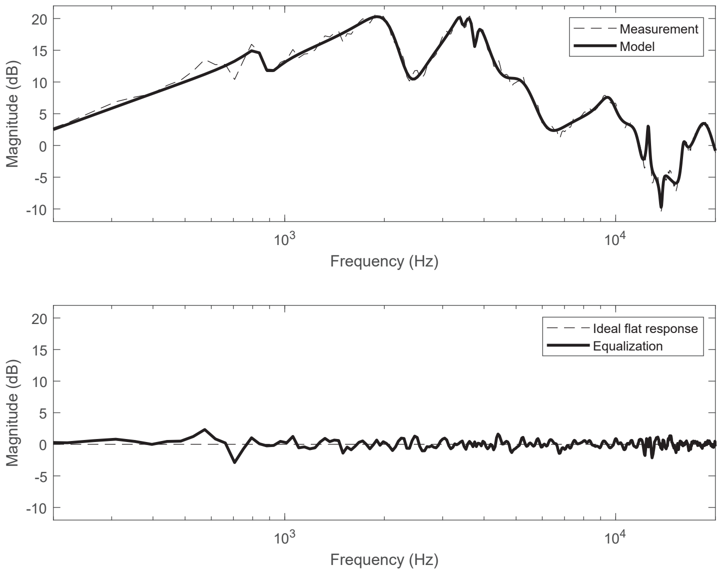

Figure 4. Silent violin digital equalization (full-band). Top graph: magnitude frequency response of the silent violin along with the response of a correspondingly designed order-30 recursive parallel filter. Bottom graph: magnitude frequency response of the equalized silent violin signal, as obtained from a parallel-inverted recursive filter.

ACKNOWLEDGEMENTS

We would like to thank Julius O. Smith for fruitful discussions on the digital filter structures and digital filter design methods applied in this work, and Harish Venkatesan for his assistance in the directivity measurements.

REFERENCES

[1] http://www.oxfordtoday.ox.ac.uk/features/caged-messiah

[2] http://tarisio.com/cozio-archive/property/?ID=40111

[3] Meyer, J. Directivity of bowed stringed instruments and its effect on orchestral sound in concert halls. Journal of the Acoustical Society of America, Vol. 51 pp. 1994–2009. 1973.

[4] Cremer, L.; Lehringe, F. Radiation of closed body surfaces. Acustica, Vol. 29 pp. 137–147. 1973.

[5] Bissinger, G.; Keiffer, J. Radiation damping, efficiency, and directivity for violin normal modes below 4 kHz. Acoustics Resesearch Letters, Vol. 4, pp. 7–12. 2003.

[6] Jansson, E. V.; Molin, N. E.; Sundin, H. Resonances of a violin studied by hologram interferometry and acoustical methods. Physica Scripta, Vol. 2(6), pp. 243–56. 1970.

[7] Marshall, K. D. Modal analysis of a violin, Journal of the Acoustical Society of America, VOl. 77, pp. 695–709. 1985.

[8] Woodhouse, J. The acoustics of the violin: a review. Reports on Progress in Physics, Vol. 77(11). 2014.

[9] Perez-Carrillo, A.; Bonada, J.; Patynen, J.; Valimaki, V. Method for measuring violin sound radiation based on bowed glissandi and its application to sound synthesis. Journal of the Acoustical Society of America, Vol. 130(2), pp. 1020–1029. 2011.

[10] Maestre, E.; Scavone, G. P.; Smith J. O. Joint Modeling of Bridge Admittance and Body Radiativity for Efficient Synthesis of String Instrument Sound by Digital Waveguides, IEEE/ACM Transactions on Audio, Speech, and Language Processing, Vol. 25 (5), pp. 1128-1139, 2017.

[11] Jansson E. V. Admittance Measurements of 25 High Quality Violins, Acta Acustica United with Acustica, Vol. 83 (2), pp. 337-341, 1997.

[12] Bissinger, G. Structural Acoustics Model of the Violin Radiativity Profile, Journal of the Acoustical Society of America, Vol 124 (6), pp. 4013-4023, 2008.

[13] Alonso, J.; Jansson E. V. Input Admittance Eigenmodes and Quality of Violins, Proceedings of the 103rd Meeting if the Acoustical Society of America, pp. 60-75, 1982.

[14] Maestre, E.; Scavone G. P; Smith ,J. O. Virtual Acoustic Rendering by State Wave Synthesis, Proceedings of EAA Spatial Audio Signal Processing Symposium, Paris, France, 2019.

[15] Chafe, C.; Maestre, E.; Sarti, A.; Canclini, A.; Scavone, G.; Smith, J.; Antonacci, F. The Return of the Messiah: Modal Analysis and Bridge Admittance Modeling. Proceedings of the 2017 International Symposium on Musical Acoustics, Montreal, Canada, 18-22 June, p. 70, 2017.

PROCEEDINGS of ISMA 2019
International Symposium on Music Acoustics

13 - 17 September 2019 in Detmold, Germany

Generation and conception of measuring tools for geometrical and acoustic properties for modern Almenräder-Heckel system bassoons.

Vincent HOUDE-TURCOTTE

(1)Montreal University, Canada, E-mail 1

(2)Institut technologique européen de la musique, France, E-mail 2

(3)Laboratoire d'acoustique de l'Université du Mans, France, E-mail 3

4Observatoire interdisciplinaire de création et de recherche en musique, Canada, E-mail 4

5Centre for interdisciplinary reaserch in music media and technology, Canada, E-mail 5

June 2019

Abstract

The bassoon is a complicated instrument that is still requiring a large quantity of research[1]. As a result, data on the instrument's design is scarce [7]. The main objective of this project is to create tools capable to provide trustful and detailed information on different structural and acoustical characteristics of modern bassoons that will be included in a database. Different types of data are included such as precise bore measurements obtained with a new measuring bench, tone hole measurements, impedance measurements, sound recording with an artificial mouth and description of the instrument's timbre from the owners. The geometry is then entered on the PAFI (Plateforme d'Aide à la Facture Instrumentale), where impedance calculation can be compared to measured ones. We want to trace the evolution of the Almenräder-Heckel bassoon over the last century through a cross reference of all the acoustic data gathered.

Keywords: Bassoon, Measurement, Acoustics

1 INTRODUCTION

This presentation takes place as part of a doctorate study at Montreal University. The goal of this study is to obtain diversified acoustical properties of modern professionally played bassoons. We target a large quantity of Almenräder-Heckel system, typically know as the "German" bassoon. This presentation will focus on the methodological aspect of the study, therefore the choice of acoustical properties, their chosen measurement methods and protocols. As of today, some tools have been tested on a single bassoon, in preparation for larger scaled data acquisition.

2 THE BASSOON

2.1 Historic

The history of the bassoon is vast, but a major turn took place in the 19th century. At the time, the acoustic world became familiar with new concepts which will also lead to changes in instrument making. Such evolution includes the addition of register holes and the removal of forked fingerings. Around 1795, the first register clefs appears on what will become the "Buffet system" bassoon (or the french bassoon). Buffet, with Jancourt's major contributions, will slowly work toward meeting new musical expectations. On a different path, we find the acoustical publication of Gottfried Weber, which will be used by Charles Almenräder. In 1824, Almenräder will publish a study on the perfecting of the bassoon. In 1831, he will join Johann Adams Heckel, wich will mark the beginning of today's leading German bassoon maker, Wilhelm Heckel GmbH. As pointed out by multiple studies on the bassoon, this change goes toward Boehm's theories of the "right tone-hole placements" principle, and the key system to hold open all subsequent keys principle. As pointed out by Jean Kergomard [1], the bassoon is actually a hybrid-semi-Boehm instrument. The first principle is applied, but only in the lower register of the instrument, mostly in the lower extension. The second principle is used only partly, with the low Bb key help open, the adding of correction holes and "resonance" holes, opened by ring keys. Around 1905, we see a bassoon with a full key system, including a separately operated bocal key (whisper key).

Both instruments were successful on a professional scale, mostly until the passing of the renowned french player and teacher Maurice Allard in 2004. The popularity of the "French bassoon" began to fall. This tendency is the reason why this project will solely focus on acoustical characteristics of the Almenräder-Heckel system. Is the "German bassoon" design still being pushed by science? Most German bassoon makers seems to share a more traditional approach. Are there anyone trying to make another bassoon revolution? There are lists of experimental bassoons, or other instruments that were given birth trough trials, prototyping and application of parallel ideas. There are many instruments that are different variations of the bassoon: the heckelphone, the sarrusophone and the logical-bassoon are simple examples of them. You would never see one of those replacing a first chair bassoon in any major classical orchestra, unless specifically requested. The famous instrument makers seems rather sceptic a introducing any drastic changes. Does the bassoon need to evolve? The instrument has many issues and solving them could help musicians.

2.2 Fundamental acoustic properties

What is the bassoon? This project will try to answer this question. We need to know what has to be adapted or kept in order to know what can change. We think that the answer lies within the bassoon itself, within its evolution. We will record the sound of the instrument, measure its geometry, measure and calculate its impedance response and finally, we will collect a description of the sound by the owner. We hope that, through the analysis of these characteristics, we will be able to find tendencies. Those tendencies should evolve toward certain line that should correspond with the growing needs of performance. Therefore, we should be able to correlate sound characteristics with geometric changes. These correlation will help us understand what is the essence of the bassoon, and at some point, propose an idea of what it could become if these tendencies are preserved.

3 METHODOLOGY

3.1 Acoustical properties measured

3.1.1 Sound recording

As mentioned, we want to have a recording of all the measured instruments. This recording isn't meant to represent and exact playing situation, but to confer comparable data between instruments. As such, we have decided to change the musician with an artificial mouth. We also have decided to use a "Légère" reed. These decisions are all taken in order to respect a proper degree of repeatability.

3.1.2 Geometry

We need a proper geometrical representation of the instrument. At first, we taught of the use of tomodensitometry (CT-scan), but the need of mobility makes it less practical. We have opted for a measuring bench recommended by Patricio de la Cuadra, whom has made one for the traditional flute. This bench will be able to measure the bore and tone-hole placements. Tone hole sizes and length will be measured with a set of graduated mandrels. The bocal's bore, being too small for this kind of measuring tool, will have his impedance measures and it's geometry calculated.

3.1.3 Impedance

The addition of the impedance in this study is not as straight forward as recording of the sound or geometric measurements. We would like to find relations between say; a specific sound characteristic, it's geometric reason, and an impedance trace of the phenomenon. We would like to gather these relations and eventually use them in prototyping.

3.1.4 Inner bore recording

It was proposed to include recordings of vibration inside the bore, in order to avoid influence by the environment. We dismissed the idea. To realize the project of collecting data on a large quantity of instrument professionally used, we need to shorten the amount of time the whole process will take. Also, we try to avoid as much intrusive manipulations are necessary.

3.2 Tools and protocol

3.2.1 The artificial mouth

With the contribution of the Jean-Pierre Dalmond at LAUM, we have designed an artificial mouth for the bassoon. It firstly runs on an input of pressurized air going through a gas regulator. Next, the air goes to a rotameter to measure the flow of gas. The line is then split, where one part is connected to a water tower. The air comes from the top section of a tube bent in a "U" shape, with the second end opened at the top. The pipe is filled halfway with water. The air will then exhort a force on the water, which will push it through the pipe. We measure the difference of the water level on both parallel sides of the tube, giving us the ΔP. Each cm of water level difference corresponds to 0,1kPa (1mBar) of air pressure. Changes are then made on the regulator until the desired pressure is reached.

The other side of the split is connected to an overpressure valve. This device was added to prevent potential surges of pressure provoked by the start of oscillation of the reed, or it's changes of oscillation regime. This design has the benefits to be cheap, sufficiently precise and easily re-creatable. A major counter part is that the water in the tower moves rather slowly. If a major change is made too swiftly to the air pressure, the air will compress until a balance is regained from the force of the water pressing on the other side of the tower. If too much pressure was allowed, the water can sprinkle from its free top end.

Following the valve is a fibreglass cylinder, closed at both ends, fitted with a removable sealing cap that is made of a pliable rubber able to squeeze around an object (the reed). The pressured air pass through the reed that is covered by a pair of artificial lips. A technician creates the desired fingerings. A microphone is set at exactly the same position for every recordings, that sends a calibrated signal to a sound card, connected to a computer to save all data.

The main reasons for using this design are: 1. We can transport all the equipment to the musicians, which will allow for a greater number of participants. 2. Most parts are widely available, allowing for easy repairs/adjustments. 3. It gives a consistent and repeatable playing situation. We do not recreate the exact sound of a musician but will not get any modification/correction either. We have also found that 4,3kPa was an optimal air pressure that allowed the tested bassoon to easily reach its whole register (from B$\flat$1 to E5). Any lower than this amount was not sufficient to hold higher oscillation regime where any higher than this amount forced the second oscillation regime while attempting the low register (mostly from F2 downward).

3.2.2 The reed

It is mandatory to choose and calibrate the excitation method. In this case, we avoid potential instability of the wood by using the "Légère" reed. We focused on the calibration of the artificial lips installed on the reed. This diagram shows three spectrum curves of the sound of a reed that was set for the low register and connected to a bocal. As the reed was held by a rubber surface, the holding of the reed by a bocal helped stabilizing the movement of the reed that was unbalanced by the weight of the artificial lips. It also lowered the emitted fundamental frequency. A first signal was recorded and set as a goal, while the other two were the results of a setup dismantle and reassemble with about 5 minutes of calibration each.

There are three main characteristics on the pressure applied to the reed, excluding the air. The first is the placement of the lips on the reed in a front-back axis. Second is the pressure applied by those lips. Finally, the "shape", or the distribution of the force applied on the reed, whether evenly or irregularly applied. We have to set the lips properly in order to recreate the same signal for every instruments. As shown in the repeatability figure, we were able to recreate a very similar excitation source that allows comparison of different

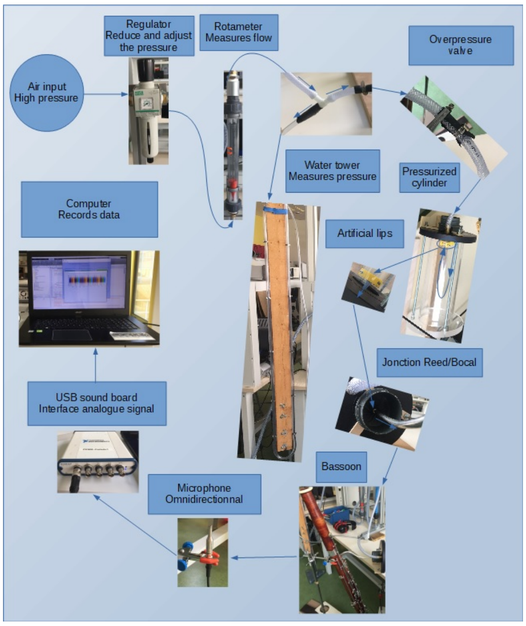

Figure 1. Diagram of the artificial mouth's configuration

instruments. While we physically move the lips ever so slightly, we were able to see great changes in the calibration measurements. This results makes the adjustments efficient since it means that, for the signal to be similar, it required a great physical resemblance. We could hardly find a difference between the analysed results multiple recordings with out without dismantling the reed. Therefore, we do not think necessary to measure the physical pressure with any sensor. We have yet to establish the off-set limits that would cause a perceivable differences in results (how close do we need to be from the original signal). We mostly rely on the fundamental frequency, the hight of the first peak and the spectral gravity center to guide the changes needed.

As shown above, a lip placement toward the tip will help reaching the lower register of the instrument, while a placement closer to the shoulder will allow changes in regimes. It is important to note that, the very tip isn't suggested with artificial lips, since their control isn't as precise as real lips (a musician's lips does not need pressure on the reed to be held in place). Thus, the optimal placement is to leave 1mm of the tip free of material. The pressure needed to obtain the low register was so low that silicon was opted out as a lip material. We replaced it with pieces of foam. The reed was almost able to vibrate properly but, the contact friction was so low that the lips would slide and fall out of position while the system was vibrating. We added a small layer of sticky patty to enhance the placement stability of the lips. This test revealed that the patty could help altering the shape of the pressure applied on the reed. Therefore, we changed from an even layer for the addition of two spots near the "magic windows" of the reed, recreating an "O" shape of embouchure. The distribution of the force (the shape of the contact surface) and the placement of the lips mostly affect the brightness of the sound, measurable with the SGC, while higher pressure will mostly rise the fundamental frequency.

3.2.3 Measuring bench

We gather information on the diameter of the bore (y) at all positions (x) of the air column with a specialized measuring bench. The bench holds a bassoon part, while a tool head slowly moves along the inside of the bore. This head is screwed at the end of a tube, used as an extension made to fit through the smallest bore diameter at the top end of the wing join and long enough to cover the longest part of a traditional long joint. The tool head has two arms installed opposed to each other, fitted with a roller to serve as contact point with

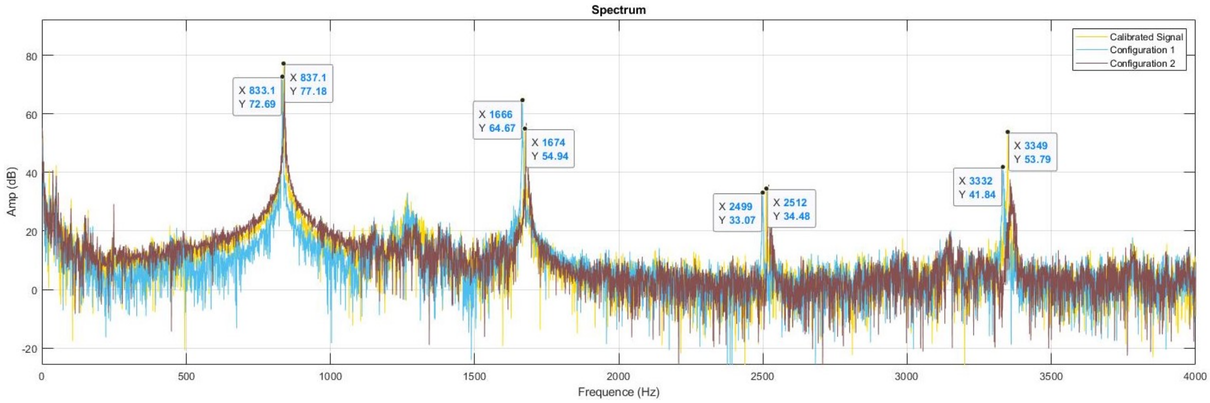

Figure 2. Repeatability test of artificial lip configurations

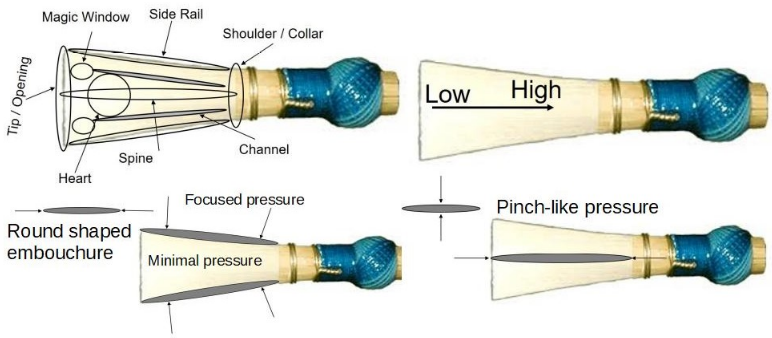

Figure 3. Diagram of characteristics of a bassoon double reed

the instrument. The use of a roller prevents any potential markings. The two arms have a pointy shape towards the center, pressing against a triangle piece. While the arms moves toward the center (in the case of the bore getting smaller), they push the triangle outside, thus transforming the y dimension into a transversal movement. The following picture is an early version of an enlarged head prototype showing the basic principle used.

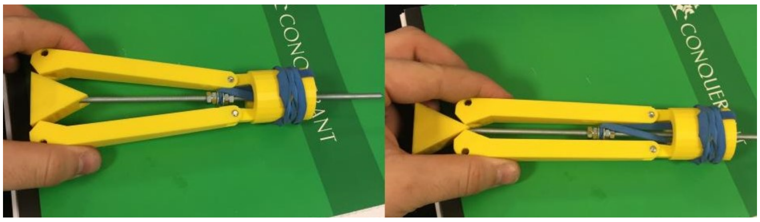

Figure 4. Picture of enlarged example of the tool head

A rod installed through the tube carries this movement to a digital indicator installed on a table. This table moves along the x axis, controlled by a threaded rod. Its position is measured by a meter long digital calliper. Both the calliper and the indicator have a data output, they are automatically synchronised and are able to efficiently record both (x,y) data every 0,7s. We are able to take specific measurements, such as the sides of every tone holes. We are also able to take measurements on two axis of the bore by rotating the bassoon's piece by 90°in cases there are indication of local modifications or warping in the bore where it could have a slightly oval shape.

Before starting the measurements, the comparator will required to be zeroed while the tool head is fitted in an industrial calibration cylinder. The diameter of the cylinder will need to be set as an offset. The calliper's offset will be the value displayed at the first recorded diameter by the comparator at contact with the instrument's bore. The operation has to be as steady as possible since any shock may cause both measuring tools to require recalibration.

3.2.4 Impedance captor

We will use the *Centre de Transfert de Technologie du Mans* (CTTM) impedance captor.

Figure 5. Picture of impedance captor's installation

It is imperative to have a proper connexion without leaks. The swipe configuration we use starts at 20Hz and goes up to 6000Hz, split 5 sections with 3 repeats each. The readings are taken with every notes, covering the whole register. A normalized fingering chart was chosen to represent the most commonly used fingerings. We will then be able to compare the measured and calculated impedance.

3.2.5 Description

We will collect information of the perception of the owners of these bassoons. We expect varied results on this subject, therefore will need to take a psychoacoustic approach. We will hand out a survey enquiring on the perceived sound of their instrument. This survey will describe two major axis of description of the sound often referred by the bassoon community, which are the brightness and the projection. The brightness should appear as a variation proportion of amplitude of harmonic partials. The projection refers to the capacity to maintain a controlled sound while altering the loudness. Since the bassoon shown a large difference of timber in its scale, we will direct the question to compare the instrument with other models of bassoon (of the same maker when possible).

4 Results

4.1 Impedance comparison

The figure bellow compared a measured impedance curve calculated by the wind version of the *Plateforme d'aide à la facture instrumentale* (PAFI) hosted by the ITEMM and a measured impedance. The F2 is the only fingerless fingering on the bassoon. There are significant similarities under 2000Hz.

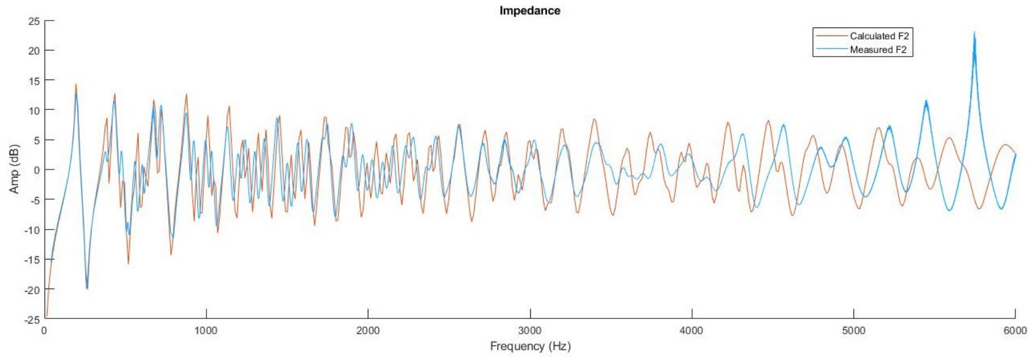

Figure 6. Comparison of Calculated and Measured Impedance of a F2

Although, notes sharing the same register key and oscillation regime (non for the low register) follows almost an exact curve above the 2000Hz, with the exception of the forked E♭2.

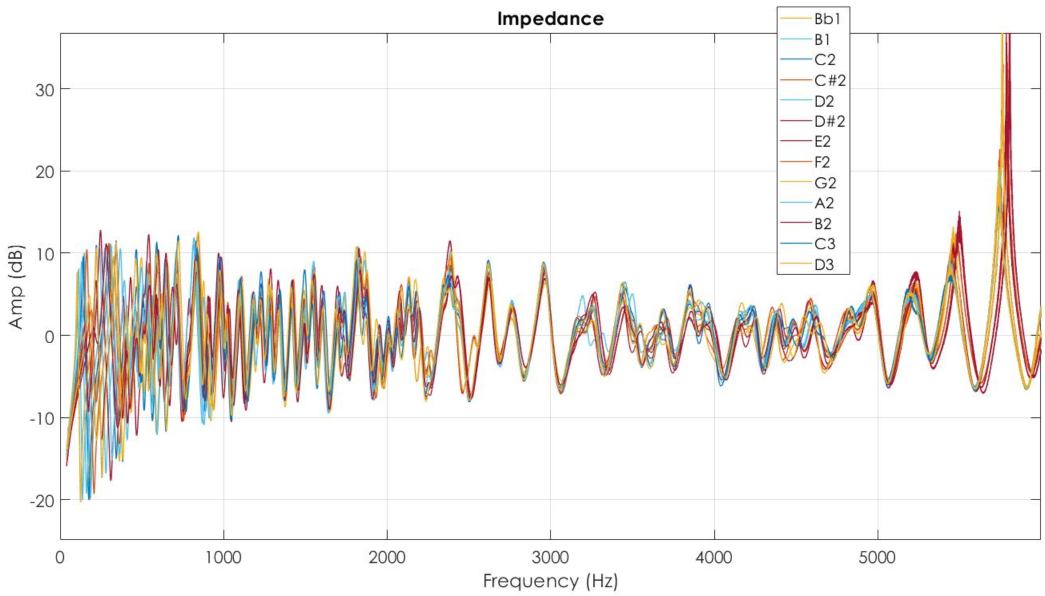

Figure 7. Comparison of Calculated and Measured Impedance of a F2

4.2 Sound analysis

With the use of the recordings acquired with the artificial mouth, we were able to calculate the fundamental frequency, then find harmonic partial peaks and calculate its spectral gravity center. We find that from the middle F3 (opened fingerings) to the lowest note, that the SGC gets considerably higher, well above the 18th harmonic partial for the low B1. It is also important to notice the inconsistency. C#3 being low does correspond to a poor tone fingering, where the G#2 is usually brighter and require adjustment.

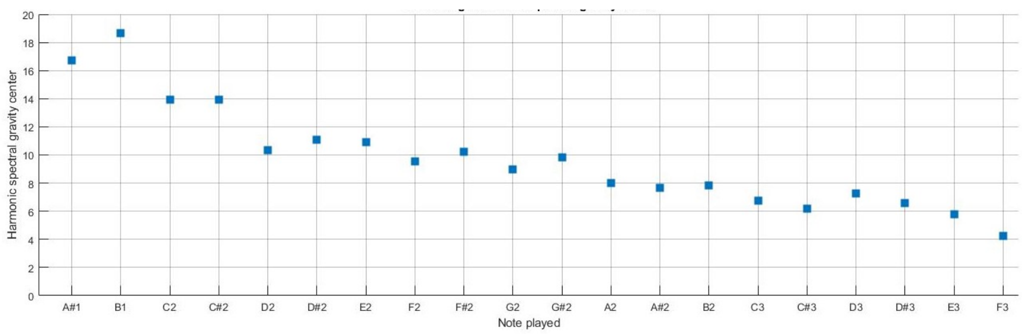

Figure 8. Low register harmonic spectral gravity center

5 CONCLUSIONS

While the development of the measuring tools have been successfully adopted and tested, there are still a number of testing left to do. Mainly, we require much more information on the acceptable range of each protocol in order to assure repeatability. In order to achieve this, the next step is put a pilot project that will take 10 participants and will focus on securing any loose ends left.

ACKNOWLEDGEMENTS

I would like to acknowledge the considerable support and guidance of both Jean-Pierre Dalmont and Marthe Curtit that guided 3 months of study in France. I would also like to thank the Université de Montréal, the CIRMMT that offered considerable support and continue to support multidisciplinary studies. A special thanks to the Perras Cholette & Cholette society for their financial support and trust.

References

[1] Kergomard, J.; Heinrich, J.M. Le basson, histoire, acoustique, l'anche. Bulletin du groupe d'acoustique musicale, 82-83, 1976, 107.

[2] Castellango, M. Écoute musicale et acoustique, Eyrolles, Paris (France), 1st edition, 2015.

[3] Langwill, L.G. The Bassoon and Contrabassoon, Ernest Benn Limited, Toronto (Canada), 1st edition, 1965.

[4] Kopp, J.B. The Bassoon, Yale University Press, Cornwall (England), 1st edition, 2012.

[5] Neverdeen, C.J. Acoustical aspects of woodwind instruments, Northern Illinois University Press, Dekald (U.S.A.), revised edition, 1969.

[6] Chaigne, A.; Kergomard, J. Acoustique des instruments de musique, Belin, Paris (France), 1st edition, 2008.

[7] Campbell, M.; Greated, C. The Musician's Guide to Acoustics, Oxford University Press, New York (U.S.A.), reprinted edition, 2001.

PROCEEDINGS of ISMA 2019
International Symposium on Music Acoustics

13 - 17 September 2019 in Detmold, Germany

Optimization of marimba bar geometry by 3D finite element analysis

Douglas BEATON *, Gary SCAVONE †

Computational Acoustic Modeling Laboratory
Centre for Interdisciplinary Research in Music Media and Technology
Schulich School of Music, McGill University, Canada

Abstract

The natural frequencies of marimba bars are tuned by removing material from the bottom of the bar. Three partials are typically tuned, though less are tuned for higher notes. With only three or fewer partials to tune, many different bar geometries may produce the desired frequencies. As a result, bar geometries can show significant variation between brands, with each manufacturer employing their own tuning approach, honed over many years of experience.

This work uses 3D finite element analysis to investigate tuning marimba bar geometry, with an aim to inform manufacturing methods. Optimization techniques, including genetic algorithms, are employed to evaluate and improve bar geometries. The preferred geometries tune the desired frequencies, while also scoring well on secondary evaluation criteria. These secondary criteria include: separating the frequencies of torsional modes from those of the tuned modes, prioritizing symmetry, and producing shapes similar to professional marimba bars.

Models are developed using the open-source finite element program *Calculix*. Optimization routines are written in Python. The programs are interfaced to coordinate model execution. Functions are created to identify mode shapes based on displaced geometry. These functions provide resilience against any modal reordering, allowing the optimization routines to run unsupervised over significant changes in geometry.

Keywords: Marimba, Finite Element Analysis, Geometry Optimization

1 INTRODUCTION

The objective of this ongoing work is to produce computer algorithms capable of tuning 3D finite element models of marimba bars for desired qualities. Tuning the nominal overtone ratio of $(1:4:10)$ is of primary importance. Secondary objectives include: separating the frequencies of tuned overtones from those of untuned torsional modes, and producing smooth, largely symmetric geometry. These secondary objectives are under investigation at the time of writing.

Previous reports of percussion bar shape optimization in the literature have focussed on 1D models with abrupt changes in bar thickness [1] [2]. Some works have considered 3D models but did not seek to produce optimized geometry [3], [4]. This work seeks to employ 3D finite element models with smooth surfaces to optimize the modal behaviour of marimba bars.

2 METHODOLOGY

2.1 Geometry definition

Structured finite element meshes were generated parametrically and used in tuning the models. Inputs include the number of elements along each axis and their type (eight-node or twenty-node). Bar geometry was defined in one of two manners, as described in the following sections.

2.1.1 Cross-section interpolation

In this approach, bar geometry is controlled by interpolation between defined cross-sections along the bar's longitudinal axis. Figure 1 gives an example. For any position across the bar's width, a cubic spline is used to

*douglas.beaton@mail.mcgill.ca
†gary.scavone@mcgill.ca

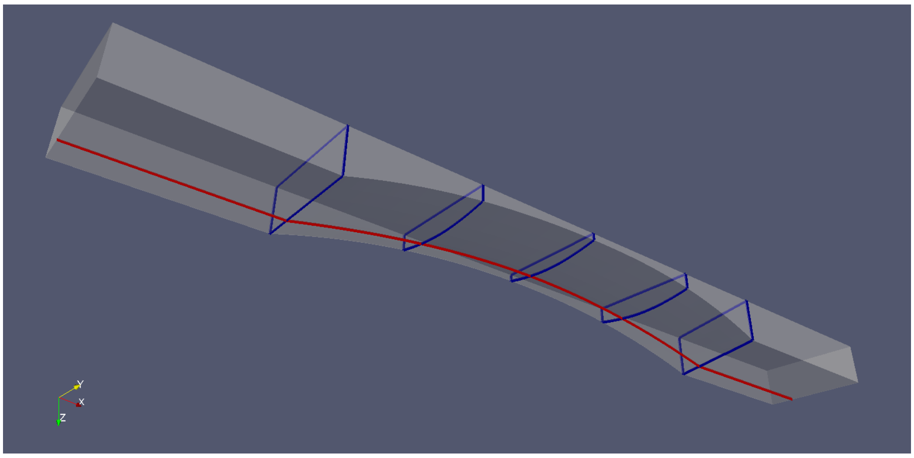

Figure 1. Bar geometry with cross-section interpolation. Cross-sections are outlined in blue. Red line exemplifies spline interpolation for bar thickness between cross-sections.

interpolate the bar's thickness between the cross-sections. Two types of cross-sections were considered: simple rectangular cross-sections (as shown at the ends of the cutaway in Figure 1), and cross-sections with a bottom surface defined by a parabola (e.g. the three middle cross-sections in Figure 1). The ability to rotate these cross-sections provided additional versatility.

2.1.2 Point grid surface interpolation

For this approach, a bar's cutaway geometry is defined by specifying thicknesses over a grid of points. A two-dimensional interpolation scheme determines thicknesses between the grid points. A uniform thickness is defined for locations outside of the cutaway. Figure 2 gives an example.

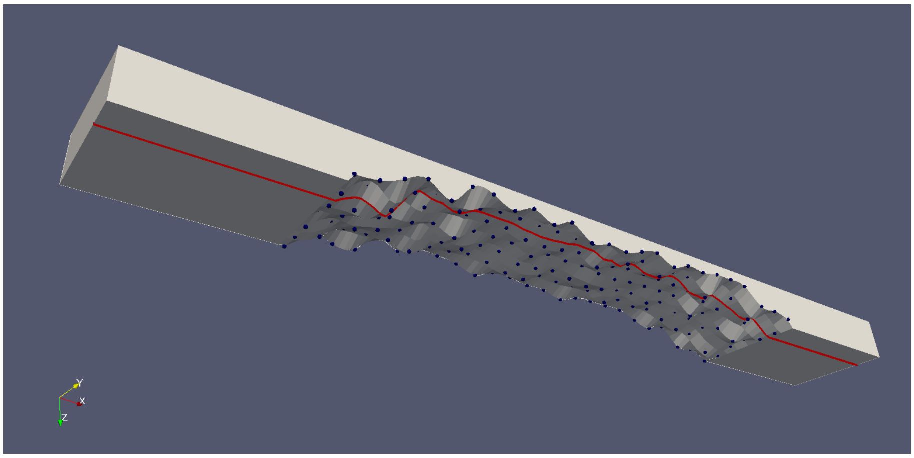

Figure 2. Bar geometry with point grid surface interpolation. Blue dots indicate surface definition points. Red line exemplifies interpolation at a given lateral coordinate. The model shown has exaggerated surface roughness for illustrative purposes.

2.2 Tuning approaches

Two approaches to tuning bar geometry are under investigation, as described below.

2.2.1 Multidimensional Newton-Raphson iteration

In this approach, bar geometry is defined using cross-section interpolation. A fixed number of cross-sections are defined. The thicknesses of these cross-sections serve as the inputs to be adjusted. Frequencies of the bar's fundamental mode and tuned overtones are the outputs to be tuned. If the number of cross-sections is greater than the number of tuned modes, multiple cross-sections may be constrained to have equal or proportional thicknesses. With this constraint in place, the Newton-Raphson iterations determine the next set of input value estimates as:

$$\mathbf{t}_{i+1} = \mathbf{t}_i - \mathbf{J}_i^{-1}\mathbf{f}_i, \tag{1}$$

where $\mathbf{t}$ is a vector of cross-section thickness inputs, i is the iteration number, $\mathbf{f}$ is a vector of modal frequencies compared to their target values and:

$$\mathbf{J} = \begin{bmatrix} \frac{\partial f_1}{\partial t_1} & \frac{\partial f_1}{\partial t_2} & \frac{\partial f_1}{\partial t_3} \\ \frac{\partial f_2}{\partial t_1} & \frac{\partial f_2}{\partial t_2} & \frac{\partial f_2}{\partial t_3} \\ \frac{\partial f_3}{\partial t_1} & \frac{\partial f_3}{\partial t_2} & \frac{\partial f_3}{\partial t_3} \end{bmatrix}. \tag{2}$$

Note that the partial derivatives in $\mathbf{J}$ are estimated numerically for each iteration.

2.2.2 Genetic algorithm

In this approach, bar geometry is defined using point grid surface interpolation. A vector of the thicknesses at each grid point forms the chromosome for a given candidate model. An initial population of candidate models is generated. The cutaway geometry of each candidate is set to a shape roughly approximating a typical marimba bar. Independent random perturbations are added to each grid point in each candidate. The random nature of these adjustments makes every candidate in the initial population unique.

The fitness of each candidate is evaluated as:

$$F = -\sum_{h=1}^{H} \left(\frac{100(f_{h,t} - f_{h,m})}{f_{h,t}} \right)^2, \tag{3}$$

where F is the fitness score, H is the number of modes being tuned, $f_{h,t}$ is the target frequency for mode h and, $f_{h,h}$ is the frequency of mode h from the candidate model under evaluation. The factor of 100 is applied to avoid excessively small fitness magnitudes.

Once the fitness of each candidate is calculated, candidate models are paired for crossover reproduction using tournament selection. New child candidates are produced by selecting a random number of grid point thicknesses from each of the parent candidate's chromosomes. Random mutation is applied to a small portion of the new candidate models. A portion of the current generation of candidate models with top fitness scores are combined with the new child candidate models to form the next generation. The process is repeated for a selected number of generations, or until the top performing candidate in a generation satisfies some established convergence criteria.

3 RESULTS

3.1 Suite of bars tuned by Newton-Raphson iterations

Measurements of bar outer dimensions were taken from a Yamaha 5.0 octave marimba. Models with these measured outer dimensions were generated for notes C2 through C4. Bar cutaways were set to be 64% of the overall bar length, centred at the midpoint. This suite of bar models was tuned to have appropriate modal frequencies using Newton-Raphson iterations. Figure 3 plots the resulting frequency ratios for the first nine modes of each model.

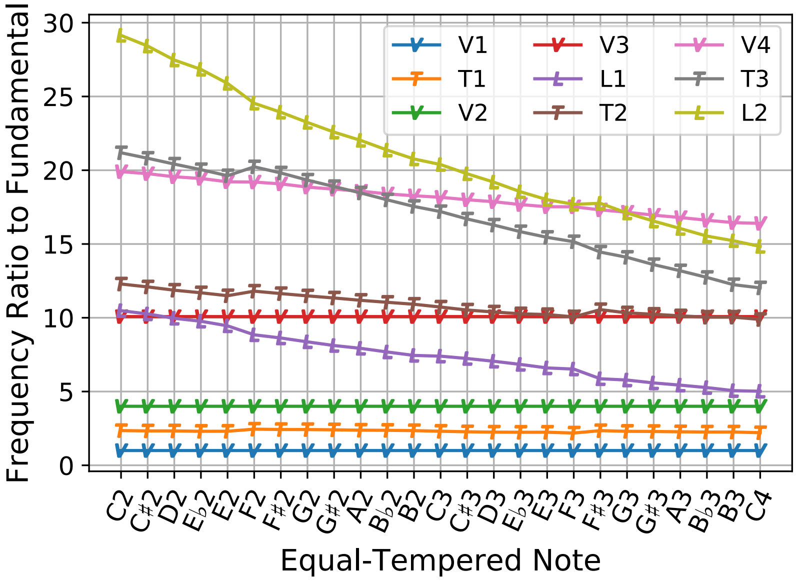

Figure 3. Modal frequency ratios from the suite of bars tuned using Newton-Raphson iterations. Symbols: V - flexural mode in a vertical plane; L - flexural mode in a lateral plane; T - torsional mode.

Note that measured bar widths decreased between notes E2 and F2, as well as between F3 and F♯3. As shown in Figure 3, the second torsional mode moves closer in frequency to the third vertical mode as the musical note increases from C2 to C4. The two modes appear quite close over the range D3 to C4. These results were used to determine notes to model when investigating separating torsional mode frequencies from tuned flexural mode frequencies.

3.2 Bar tuned via genetic algorithm

A bar of note C3 was selected for investigation using a genetic algorithm. Outer bar dimensions and material properties were set equal to those from Bork et al. [3]. A population of 50 candidate models was generated. The algorithm was arbitrarily set to run for over 500 generations. Table 1 provides the errors in modelled modal frequencies after multiples of one hundred generations. Figure 4 compares cutaway geometry for the fittest model of the intial population, and the fittest model from 400 generations onward.

As shown in Table 1 the maximum tuning error of any of the three tuned modes is around one cent after 100 iterations. After 300 iterations this error is well below one cent. No further improvement is observed between 400 and 500 iterations. Comparing parts (a) and (b) of Figure 4, it is observed that surface roughness along the fittest candidate bar's cutaway increased from the initial population to the final population.

4 SUMMARY

Newton-Raphson and genetic algorithm techniques have been implemented with the goal of tuning virtual marimba bars for their desired fundamental and overtone modal frequencies. Both techniques successfully tune the three vertical flexural modes of interest to within reasonable tolerances of their target values. At the time

Table 1. Modal tuning errors in fittest candidate models from specified generations.

Generation Number	Modal Tuning Error (cents)		
	Fundamental	Overtone 1	Overtone 2
0	53.9	122.6	47.8
100	-1.09	1.26	-0.32
200	-1.05	0.29	-0.68
300	0.13	0.12	-0.24
400	0.10	0.02	-0.23
500	0.10	0.02	-0.23

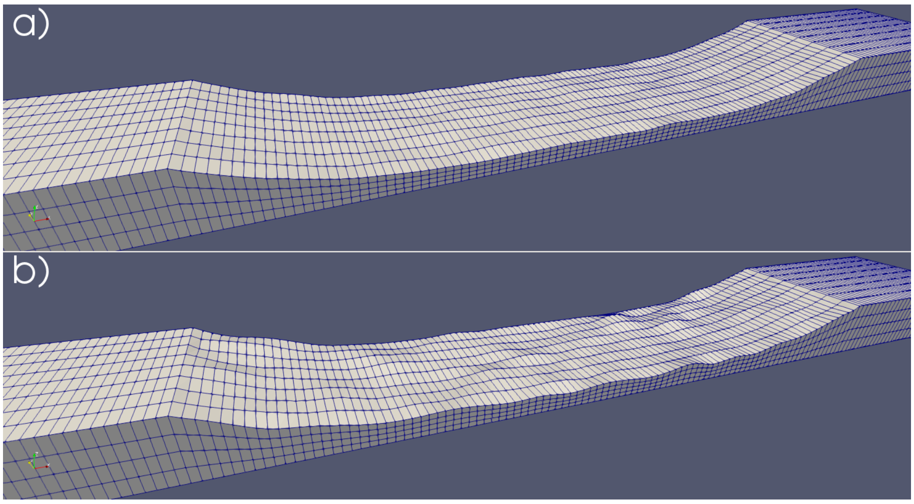

Figure 4. Geometry of bar tuned via genetic algorithm. a) cutaway of fittest candidate from initial population. b) cutaway of fittest candidate from final population.

of writing, work is underway to investigate separation of torsional mode frequencies from tuned flexural mode frequencies using both methods. Work is also underway investigating fitness functions that favour smooth, symmetric cutaway geometry with the genetic algorithm technique.

ACKNOWLEDGMENTS

This work was made possible through financial support from the Vanier Canada Graduate Scholarships Program, the Schulich School of Music, and the Centre for Interdisciplinary Research in Music Media and Technology (CIRMMT). The authors would also like to thank Fabrice Marandola, Martin Daigle and David Brongo at the Schulich School of Music for their insights into marimba performance and access to instruments.

REFERENCES

[1] Petrolito, J.; Legge, KA. Optimal undercuts for the tuning of percussive beams. The Journal of the Acoustical Society of America, 102 (4), 1997, pp 2432-2437.

[2] Henrique, LL.; Antunes, J. Optimal design and physical modelling of mallet percussion instruments. Acta Acustica United With Acustica, 89, 2003, pp 948-963.

[3] Bork, I.; Chaigne, A.; Trebuchet, LC.; Kosfelder, M.; Pillot, D. Comparison between modal analysis and finite element modelling of a marimba bar. Acta Acustica United With Acustica, 85, 1999, pp 258-266.

[4] Bretos, J.; Santamaría, C.; Alonso, MJ. Finite element analysis and experimental measurements of natural eigenmodes and random responses of wooden bars used in musical instruments. Applied Acoustics, 56 (3), 1999, pp 141-156.

PROCEEDINGS of ISMA 2019
International Symposium on Music Acoustics

13 - 17 September 2019 in Detmold, Germany

How to include several acoustic characteristics in the design of woodwind instruments?

Augustin ERNOULT[(1)], Samy MISSOUM[(2)], Philippe GUILLEMAIN[(1)], Christophe VERGEZ[(1)], Michael JOUSSERAND[(3)]

[(1)]Laboratoire de Mécanique et d'Acoustique, Aix Marseille Univ, CNRS, Centrale Marseille, UMR 7031, 4 impasse Nikola Tesla CS 40006, 13453 Marseille Cedex 13, France

[(2)]Aerospace and Mechanical Engineering Department, University of Arizona, Rm. N639, Tucson, Arizona, 85721, USA

[(3)]Buffet Crampon, 5 rue Maurice Berteaux, 78711 Mantes-La-Ville, France

Abstract

When manufacturers design woodwind instruments, they must simultaneously adjust multiple aspects of the resonator response. The same resonator is used to play several notes by opening or closing tone-holes, and, for some instruments, the same fingering is used to play several registers. From an acoustic point of view, it means that several characteristics of the input impedance must be simultaneously adjusted: at least the first two resonance frequencies of each fingering. The acoustic models can predict the input impedance from the geometry of an instrument with good confidence. This suggests the possibility to solve the inverse problem through optimization algorithm: obtain the geometry having the desired input impedance. However, this inverse problem necessitates the optimization of several acoustic characteristics by modifying dozens geometric parameters (radius and position of the tone holes, chimney height, etc). A specific strategy is therefore necessary to solve this problem. A collaboration between manufacturers from Buffet Crampon and acousticians led to the development of an optimization tool to aid in the design of new woodwind instruments. The strategy adopted in this tool will be presented and applied to an illustrative problem: the construction of a pentatonic clarinet.

Keywords: wind instrument, optimization, virtual prototyping

PROCEEDINGS of ISMA 2019
International Symposium on Music Acoustics

13 - 17 September 2019 in Detmold, Germany

Model-based quantification of the effect of wood modifications on the dynamics of the violin *

Romain Viala(1), Sarah Lämmlein(2), Vincent Placet(1), Scott Cogan(1)

(1)Univ. Bourgogne Franche-Comté, FEMTO-ST Institute, CNRS/UFC/ENSMM/UTBM, Department of Applied Mechanics, 25000 Besançon, France

(2)Swiss Federal Laboratories for Materials Science and Technology (Empa), Cellulose & Wood Materials, Dübendorf, Switzerland

Abstract

In this study, a finite element model is used to simulate the impact of wood modifications on the dynamical behaviour of a violin. Chemical and fungal modifications of the wood selected for violins (tonewood) are considered. In addition, the impact of spruce indented rings anatomic singularities is also studied. Models are used to compute modal bases up to 4000 Hz, and eigenfrequencies, eigenvectors and bridge admittance are used to compare different dynamical behaviours. The impact of wood modifications over the geometric tolerances inherent to instrument makers methods is discussed. This study shows that some modifications or anatomic singularities are not sufficiently efficient to be observed reliably over the geometric uncertainties. In contrary the fungal treatment method also known as mycowood sufficiently modifies the dynamical behaviour to to overcome the luthiers tolerances. Moreover, results give a wood modifications threshold, which can be used as a support for further wood modification methods.

Keywords: Wood modifications, Geometric tolerances, Instrument making, Violin modelling, Violin Dynamics

1 INTRODUCTION

The building of musical instruments is traditionally based on craftsmanship and selection of materials. Instrument makers generally attribute a dominant role to the material properties in regard with the acoustics of the musical instruments. Numerous methods to modify the physical and mechanical properties of tonewood are studied by both researchers. Their densities and elastic and damping parameters are of particular interest. Most of the studies aim at tailoring specific rigidities and acoustic conversion efficiency (ACE) [1], based on the assumption that high ACE is better for the quality of an instrument. Wood properties can be modified through chemical treatments [17], [9], fungal incubation [11] [10], or climatic artificial ageing [8], [7]. Moreover, anatomical singularities like spruce with indented rings also impact the mechanical properties [14], and can be used by instruments makers for this purpose. Meanwhile, all these methods increase the cost of wood preparation. Nevertheless, the objective assessment of the impact of these wood modifications on the perception of musical instruments, and especially the improvement of their "quality" remains a subject to discussion.

The perception of an instrument is subjected to numerous subjective and objective assessments. The link between the attribution of a specific quality or sonority by musicians and measurable features like vibro-acoustical behaviour has still to be established. In this study, it is proposed to study the violin through its dynamical behaviour, prior to acoustical features. The dynamical behaviour of a violin is a result of the choices of the makers in term of design and assembly prestresses, but also depends on the wood properties, relative humidity and temperature conditions. The impact of each of these variables will be studied through dynamical features computed by the numerical models, such as eigenfrequencies, eigenvectors and bridge admittances.

Physics-based models of musical instruments are now able to simulate these dynamical features for a complex geometry and material implementation. Among their capability for virtual prototyping aims, they can also be

*romain.viala@univ-fcomte.fr

used as a support for conservation of musical instruments and, furthermore, for material studies.

The main objective is to evaluate if a wood modification can overcome the luthiers geometrical uncertainities in regard to the dynamical behaviour, which is part of the acoustical performance and sound perception.

For this purpose, a numerical model is developed and driven to investigate the impact of wood property modifications on the dynamics of a violin while taking into account irreducible uncertainties in the material properties and geometrical tolerances. The aim is to establish a threshold for wood treatments that will insure an observable impact on the dynamic behaviour of instrument.

In the next section, the model, material and geometrical implementation, and analyses are described. Results, discussions and conclusions are given in the last sections.

2 MODEL AND METHODS

In this section, the computer aided design (CAD) of the violin and the finite element model are described. Subsequently, the material parameters implementation is given. Finally, the different dynamical features that have been computed are described.

2.1 Numerical model of violin

The computer aided design of the violin is shown in figure 1, which also gives the nomenclature. The geometry is parametrised using a SOLIDWORKS® feature called family tree. Once the CAD is prepared, parametrised, updated and exported, a detailed numerical model is constructed using the finite elements method based on the commercially available software MSC-PATRAN®. The mesh is created using quadratic tetrahedral elements of 5 mm as global edge length, and orthotropic material parameters are defined.

The different geometrical parameters that have been considered as uncertain are detailed in the table 1. The Relative tolerances are comprised between 0.7 and 9 %, depending on craftsman gesture.

Table 1. Sum up of the relative changes of geometry correpsonding to making tolerances and habits. Relative humidity and temperature changes.

Geometric parameter	Nominal value (mm)	Consider variance [%]
F-hole length	72.5	-1.4 +1.4
F-hole width	4.25	-2.3 +2.3
Bass bar length	270	-0.7 +0.7
Bass bar position	35	-2.8 +2.8
Bass bar width	6.1	-6.5 +6.5
Bass bar height	11	-9 +9
Soundboard averaged thickness	2.8	-3.5 +3.5
Back averaged thickness	2.95	-3.4 +3.4
Relative humidity	45	[-45 +67]
Temperature	21	[-50 +67]

2.2 Material parameters

Tonewood is implemented in the numerical model as a linear elastic orthotropic material. For each solid, wood is oriented in adequation with orientation in real instruments. Mechanically, the wood is described with three main directions, longitudinal (L), radial (R) and tangentail (T). Table 2 gives the initial material properties for all the elements of the violin in their respective local coordinate frame. These parameters are taken from

Figure 1. Scheme of the violin elements and their nomenclature.

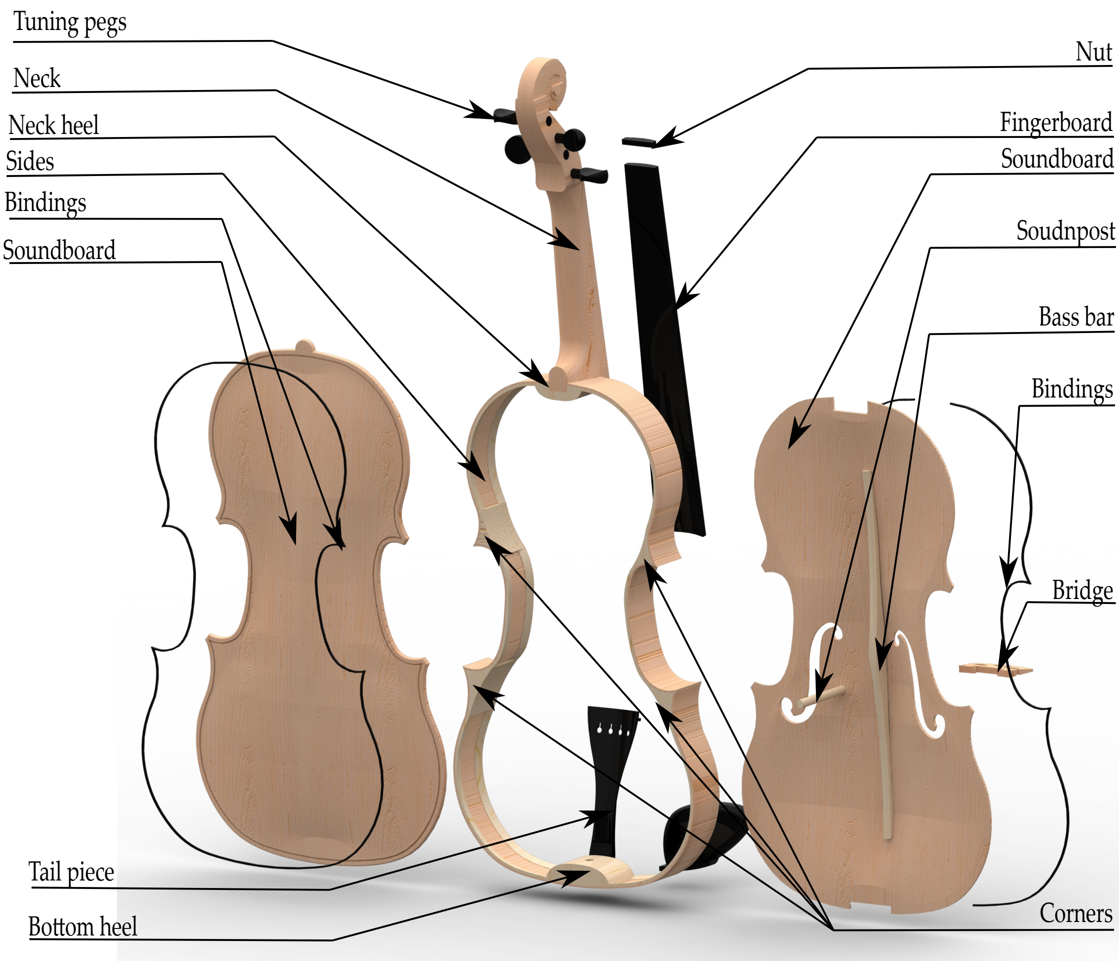

[5], [14] and [3]. Numerous different orientations are implemented, and the violin is generally made of solid materials, consisting of three wood species, with five different orientations. The orientation has to be finely taken into account, since wood is highly anisotropic, reaching ratios up to 20.

Table 2. Fixed material parameters values for different wood species and orientations. The values are taken from [5], [14] and [3]

LRT Ebony

Material parameter	Value
E_L (MPa)	17000
E_R (MPa)	1960
E_T (MPa)	1110
ν_{LR}	0.37
ν_{RT}	0.65
ν_{TL}	0.032
G_{LR} (MPa)	1370
G_{RT} (MPa)	360
G_{TL} (MPa)	950
ρ (g/cm3)	1

LRT Spruce

Material parameter	Value
E_L (MPa)	13350
E_R (MPa)	1080
E_T (MPa)	680
ν_{LR}	0.38
ν_{RT}	0.49
ν_{TL}	0.02
G_{LR} (MPa)	930
G_{RT} (MPa)	40
G_{TL} (MPa)	812
ρ (g/cm3)	0.44

LRT Maple

Material parameter	Value
E_L(MPa)	14920
E_R (MPa)	1960
E_T (MPa)	1110
ν_{LR}	0.37
ν_{RT}	0.65
ν_{TL}	0.032
G_{LR} (MPa)	1370
G_{RT} (MPa)	360
G_{TL} (MPa)	950
ρ (g/cm3)	0.64

The large number of material parameters associated with the different parts of the violin are implemented in the model and a screening analysis has been performed in an earlier study [15] to determine the most influential material parameters. These parameters include the longitudinal and radial (L and R) Young's moduli, the LR shear modulus and density for the soundboard, the bottom plate, the neck and the fingerboard. The moisture content, which is driven by the relative humidity, is related to the water absorbed by the wood. It is potentially one of the most influential material parameters as it affects stiffness, density, geometric dimensions and damping. The variability is modelled with an equi-probabilistic definition of the density, the Young's moduli in longitudinal and radial direction and the shear modulus in LR plane. The hygroscopicity of the wood is implemented as an analytical model that links the relative humidity RH and temperature to the density and mechanical properties for each species. Eq 1 gives the moisture content of the wood samples as a function of the relative humidity, based on [14]. the RH and temperature changes are given in the table 1.

$$MC = 8 + 0.16 \times (RH - 41.5) - 0.03 \times (T - 21) \tag{1}$$

Eq. 2 gives the evolution of the density as a function of the moisture content, based on the results of [13]:

$$\rho_{MC} = \rho_0 \times (1 + 0.01 \times (MC - 10)) \tag{2}$$

Most of the pieces are carved, thus, the orientation of the material properties is quite easy. The local coordinate frames of the elements inside each solid is oriented to match the correct orientation in the global coordinate frame. The sides and linings of a violin are made of bended wood. The ribs of the sides are made with maple and the linings with spruce. The orientation of the material changes along the curvature of the parts. For 3D tetrahedral elements, the correct orientation of the material constituting the bended parts is taken into account.

2.3 Wood modifications

Numerous methods to treat tonewood have been proposed for years. Their effect on the material properties is summarized in the table 3. In LR plane, the evolution of the shear modulus is generally not specified, despite its impact on the dynamical behaviour of the violin [15]. In the computations, each line of the table with data for L and R directions are considered, and modal bases are computed with given deterministic parameters.

Table 3. Summary of relative changes of mechanical properties of spruce and maple for different studies.

Ref.	Specie, treatment	$\Delta\rho$[%]	ΔE_L [%]	ΔE_R [%]	$\Delta\eta_L$ [%]	$\Delta\eta_R$ [%]	$\Delta\frac{E_L}{\rho}$ [%]	$\frac{E_R}{\rho}$ [%]
[11]	Spruce (fungi, 12 weeks)	-11	-17	-30	+20	+70	-6.7	-21
[11]	Maple (fungi, 12 weeks)	-10	-16	-21	0	10	-6.7	-12.2
[12]	Spruce (fungi, 6 months)	-2.1	-3.5	-4.1	+4.1	+5	-1.4	-2
[17]	Spruce, phenolic resin	+4.1	9.4	42.9	-29.1	-43	+5.1	+37.3
[18]	Spruce, Saligenin/formaldehyde	+4.3	6.4	30	-37.6	-46.6	+2.0	+24.6
[14]	Spruce, indented rings	-4	-15	25	-4	-5	-12.7	+33
[8]	Spruce, ageing	-	-	-	-2.5	-	+3	-

2.4 Analyses

The model is used to perform computations with varying material and geometrical parameters. For this application, the design space is explored based both on Morris method [6] and Monte Carlo sampling. For each of these analyses, 240 computations have been performed. The average duration of a run is generally equal to 1 hour, which leads to a total duration for each study of 10 days on an office computer. The eigenmodes of each modal bases of the study are compared with the nominal modal basis of the violin with initial geometrical, material and climatic parameters. The eigenmodes are correlated with a MAC criterion [2]. The minimum value that is retained for the matching of two modes is 0.6. The matched eigenvector error (MEVE) is used to compare the eigenvectors of a given mode of a modal basis to an other. In this case, this gives a normalised evaluation of the difference in the shape of the modes, through the evaluation of the MAC criterion value.

The bridge admittance is synthesised using modal superposition method based on the modal bases of each case. The bridge admittance is a frequency response function giving the displacement normalised by a force as a function of the frequency. The evaluation is located on the bass side of the bridge, in the direction perpendicualr to the strings and coplanar with the soundboard. This is usually measured using an accelerometer or a vibrometer and excited with an impact hammer. The bridge admittance is computed between 20 and 4000 Hz, and is based on nearly 150 modes. The usual increase of the bridge admittance value between 2300 and 3000 Hz is known as the bridge hill and has been widely studied and measured [16], but barely synthesised before [14].

3 RESULTS

This section describes the dynamical results. At first, the modal bases comparisons for each study cases are given, secondly the bridge admittances of each wood modifications are shown together with the bridge admittance dispersion for geometrical uncertainties.

3.1 Modal bases comparison

As an example of the 150 modes computed, several well-known modes are displayed in the figure 2 . The values of the frequencies of the CBR, B1- and B1+ modes are in accordance with the values usually obtained by experimental means [4].

Figure 2. Numerical modes of the violin body in the low frequency domain. The values in the brackets indicate common experimental values [4].

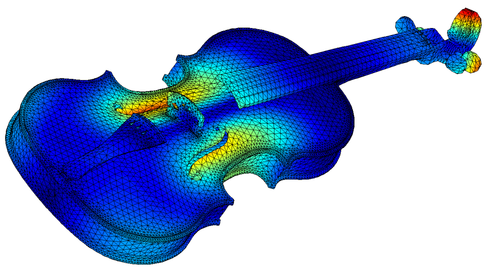

(a) CBR 390 Hz (380-430)

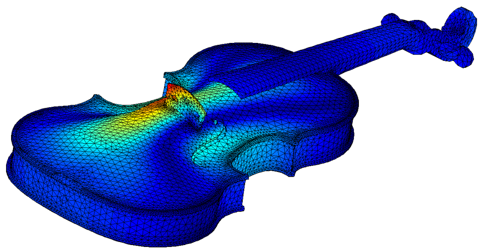

(b) B1- 432 Hz (430-480)

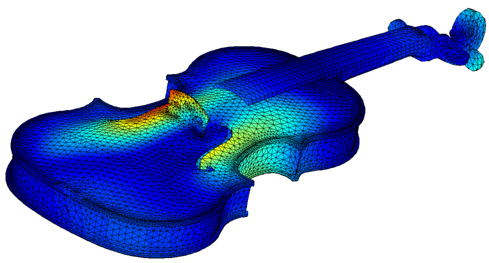

(c) B1+ 492 Hz (510-580)

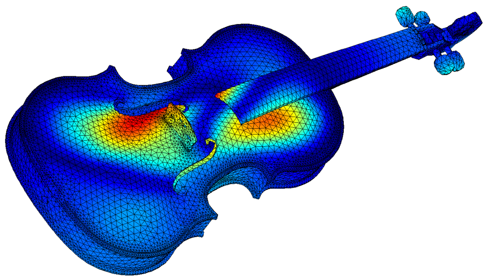

(d) C4 top 680 Hz (700)

In the table 4, it is shown that geometrical uncertainties lead to an average of the coefficient of variation of the eigenfrequencies equal to 1.1 % for 150 modes computed. Moreover, the MAC drops to 77 % as average for the same number of modes. The impact of the material variability leads to a coefficient of variation equal to 2.0 %, and the MAC value drops to 70 %. These results suggest an higher impact of material variability and moisture content when compared with the geometric tolerances.

Keeping the geometry and wood moisture content constant, the treatment using fungi for soundboard and back leads to a shift in the eigenfrequencies of 5.7 %. Being three times the coefficient of variation that is due to geometric tolerances. This is a strong argument for the observability of such modifications. It has to be noticed that the impact on both soundboard and back together is not equal to the sum of the impact of soundboard and back treatments taken separately, which can be explained by compensation effects when the parts are coupled.

The phenolic treatment leads to an evolution of the eigenfrequencies equal to 2.1 %, which is only two times higher than the coefficient of variation due to geometric uncertainties. This result indicates that, following the "68–95–99.7 rule", it can remain an error equal to 5 % when comparing dynamical behaviour with treated and non treated wood. This error is similar for the indented rings spruce.

Table 4. Evolutions of the modal bases for different cases of uncertainties and wood modifications.

Wood modifications	Frequencies error vs nominal (%)	MAC vs nominal (%)	Number of matched modes Initial: 150 modes
Geometric tolerances	1.1	77	130
Material and MC variability	2.0	70	120
Fungi Sb and B	5.7	61.8	105
Fungi Sb	4.3	68.5	102
Fungi Back	3.6	70.2	105
Phenolic	2.1	72.9	115
Indented rings spruce	2.2	72.8	112

3.2 Bridge admittance Comparison

In this subsection, the bridge admittance of each wood modifications is juxtaposed on all the bridge admittances of the different cases of geometric uncertainties in figure 3. It can be observed that, in accordance with the previous subsection, only the fungi treatments are emerging from the geometric tolerances "noise". But this is not the case for the full frequency band, especially above 3000 Hz. Generally, fungi treatment suggests a general shift to the low frequencies, with a bridge hill center frequency value that decreases from 2600 Hz to 2400 Hz.

For the remaining treatments, no clear trends are observed outside the geometric tolerances' "noise". therefore, it seems difficult to attribute a specific modifications in dynamical behaviour to weakly influential wood modifications, even in the considered case, that is very optimistic in regard with the variability of the material parameters of the other parts, that has not been considered for this study.

4 DISCUSSION AND CONCLUSION

The objective of this study was to investigate the impact of geometric tolerances and uncertainties on the vibratory behaviour, and to define a threshold of wood modifications to be reliably measured in the dynamical domain. Results have shown that, depending on the wood modifications means, some methods are not sufficiently efficient on the mechanical behaviour of wood to be measured. The coefficient of variation due to geometrical uncertainties is defined to equal to 1.1%, and it is proposed that a wood modifications changes the eigenfrequencies of at least three times the coefficient of variation, in this case 3.3%, which is outreached by the fungal treatment method (mycowood) but not by phenolic treatment and indented rings spruce selection.

Despite these encouraging results for several wood modifications, it is necessary to point out that this study doesn't take into account at the same time the effects full geometric uncertainties like the arching shape, heterogeneities, interfaces parameters and, especially, the remaining material variability. This last effect prevents the possibility to make two identical violins, due to the variability of their constitutive materials. Taking into account these different sources of variability and uncertainty, it can be argued that the modifications to outreach this residual noise in term of violin dynamical behaviour should be higher, but an analysis taking into account

Figure 3. Bridge admittances corresponding to each dimensions tolerances cases and nominal and modified material parameters.

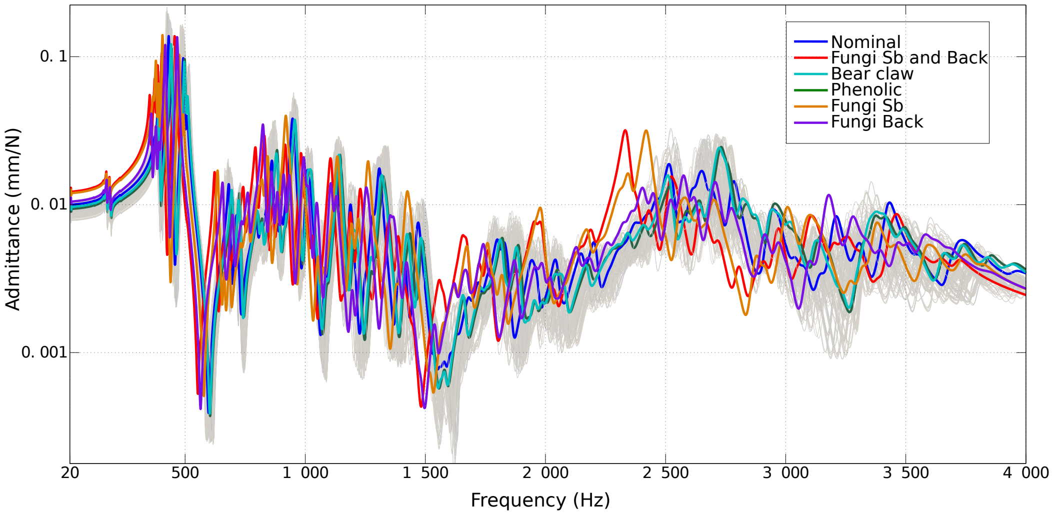

all these sources has yet to be performed. Prior to such study, and considering the high number of potential sources of uncertainties, it should be necessary to reduce the number of material and geometrical parameters using a full screening analysis.

ACKNOWLEDGEMENTS

Funding: This work has been performed in the Framework of EUR EIPHI (ANR-17-EURE-0002). The authors acknowledge Bernard Michaud, from the sawmill “Le bois de lutherie", Fertans, FRANCE.

REFERENCES

[1] H. Aizawa, E. Obataya, T. Ono, and M. Norimoto. Acoustic Converting Efficiency and Anisotropic Nature of Wood. *Wood research*, 85:1–4, 1998.

[2] R. J. Allemang and D. L. Brown. A correlation coefficient for modal vector analysis. In *First International Modal Analysis Conference*, pages 110–116, Orlando, 1982.

[3] I. Brémaud, J. Gril, and B. Thibaut. Anisotropy of wood vibrational properties: Dependence on grain angle and review of literature data. *Wood Science and Technology*, 45(4):735–754, 2011.

[4] B. Elie. *Caractérisation vibratoire et acoustique des instruments à cordes*. PhD thesis, Université du Maine, 2012.

[5] D. Guitard and F. El Amri. Modèles prévisionnels de comportement élastique tridimensionnel pour les bois feuillus et les bois résineux. *Annales des sciences forestières*, 44(3):335–358, 1987.

[6] M. D. Morris. Factorial Sampling Plans for Preliminary Computational Experiments. *Technometrics*, 33(2):161–174, 1991.

[7] T. Noguchi, E. Obataya, and K. Ando. Effects of aging on the vibrational properties of wood. *Journal of Cultural Heritage*, 13(3 SUPPL.):S21–S25, 2012.

[8] E. Obataya. Effects of natural and artificial ageing on the physical and acoustic properties of wood in musical instruments. *Journal of Cultural Heritage*, 27:S63–S69, 2016.

[9] K. Sakai, M. Matsunaga, K. Minato, F. Nakatsubo, K. Sakai, M. Matsunaga, K. Minato, and F. Nakatsubo. Effects of impregnation of simple phenolic and natural polycyclic compounds on physical properties of wood. *Journal of Wood Science*, 45(3):227–232, 1999.

[10] F. W. M. R. Schwarze and M. Schubert. Physisporinus vitreus: A versatile white rot fungus for engineering value-added wood products. *Applied Microbiology and Biotechnology*, 92(3):431–440, 2011.

[11] F. W. M. R. Schwarze, M. Spycher, and S. Fink. Superior wood for violins–wood decay fungi as a substitute for cold climate. *The New phytologist*, 179(4):1095–1104, 2008.

[12] M. Sedighi-Gilani, J. Neuenschwander, M. Heeb, R. Furrer, S. J. Sanabria, B. C. Stoel, and F. W. M. R. Schwarze. Influence of incubation time on the vibration and mechanic properties of mycowood. *Holzforschung*, 70(6):557–565, 2016.

[13] W. T. Simpson. Predicting equilibrium moisture content of wood by mathematical models. *Wood and Fiber*, 5(1):41–49, 1973.

[14] R. Viala. *Towards a model-based decision support tool for stringed musical instrument making*. PhD thesis, Université Bourgogne Franche-comté, 2018.

[15] R. Viala, V. Placet, S. Cogan, and E. Foltête. Model-based effects screening of stringed instruments. In *Conference Proceedings of the Society for Experimental Mechanics Series*, volume 3, pages 151–157, 2016.

[16] J. Woodhouse. On the Bridge-Hill of the Violin. *Acta acustica united with acustica*, 91(1):155–165, 2005.

[17] H. Yano, H. Kajita, and K. Minato. Chemical treatment of wood for musical instruments. *Journal of the Acoustical Society of America*, 99(3):1795–1796, 1996.

[18] H. Yano and K. Minato. Controlling the timbre of wooden musical instruments by chemical modification. *Wood Science and Technology*, 27(4):287–293, 1993.

PROCEEDINGS of ISMA 2019
International Symposium on Music Acoustics

13 - 17 September 2019 in Detmold, Germany

Influence of tonewood parameters on the perceived sound quality of a steel-string acoustic guitar

Sebastian MERCHEL[1]; David OLSON[2]; M. Ercan ALTINSOY[3]

(1) TU Dresden, Germany, sebastian.merchel@tu-dresden.de

(2) Pacific Rim Tonewoods, USA, d.olson@pacificrimtonewoods.com

(3) TU Dresden, Germany, ercan.altinsoy@tu-dresden.de

Abstract

Wood is one of the preferred materials for building stringed music instruments. Because wood is a naturally grown resource, there is large variability regarding material properties, even within species. Therefore, luthiers select their tonewoods very carefully. In this project, listening tests were performed to investigate whether the objective testing of physical parameters of the tonewood can help to make an appreciable and reproducible impact on the sonic quality of the resulting instrument. Nine steel string guitars of the same model were produced by the Taylor Guitar Company, with strict control of all production parameters. The guitars varied only in two parameters: the density and the modulus of elasticity of the soundboard and bracewood, both made of Sitka spruce. The variability was representative of the range of the spruce wood currently produced by Pacific Rim Tonewoods, a supplier of tonewood to the acoustic guitar market. A short music sequence was used for pairwise preference evaluation in a double-blind listening test. The results suggest that, for this particular model (the Taylor 814ce Grand Auditorium), low density and stiffness of the guitar top have a positive impact on the overall preference of the instruments. More generally, the results underscore the importance of integrating the design with physical characteristics of the component wood.

PROCEEDINGS of ISMA 2019
International Symposium on Music Acoustics

13 - 17 September 2019 in Detmold, Germany

The Bilbao project : How violin makers match backs and tops to produce particular sorts of violins

Claudia Fritz [(1)], George Stoppani [(2)], Unai Igartua [(3)], Roberto Jardón Rico [(4)], Ander Arroitajauregi [(3)], Luis Artol [(3)]

[(1)] Institut Jean Le Rond d'Alembert, Sorbonne Université / CNRS, Paris, France
[(2)] Violin and string maker, Manchester, United Kingdom
[(3)] Bele, Conservatorio de Musica – Juan Crisostomo de Arriaga, Bilbao, Spain
[(4)] Jardón Rico Luthier, Avilés, Spain

Abstract

The Bilbao project aims at answering this question by relating intrinsic characteristics of the materials (wood density and stiffness) and some geometric characteristics of the violin's constituent parts (thicknesses of the plates) with the tonal qualities of the complete violins. To this end, six instruments were carefully built: three instruments with normal backs, each paired with a pliant (thin), normal, or resistant (thick) top ; similarly, three with normal tops, each paired with a pliant, normal, or resistant back. The two examples of normal top paired with normal back serve as a control. Wood for tops and backs were closely matched in density and sound speeds – all tops and backs from the same trees. Greater control was achieved by having all plates and scrolls cut by CNC routers. The outside surface was not changed during the experiment, as the graduation was performed entirely on the inside surface. In addition, structural measurements were taken at many steps during the building process and the instruments were then assessed during playing and listening tests. These six instruments constitute therefore an unprecedented set of carefully controlled and documented violins, and offer an incredible opportunity for conducting various analyses and correlations.

Keywords: Violin, lutherie, perception

PROCEEDINGS of ISMA 2019
International Symposium on Music Acoustics

13 - 17 September 2019 in Detmold, Germany

Metamaterials in Musical Instruments *

Bader, R., Fischer, J., Münster, M. & Kontopidis, P.(1)

(1)Institute of Systematic Musicology, University of Hamburg, Germany, R_Bader@t-online.de

Abstract

Acoustic metamaterials are complex geometries leading to acoustic behavior not found in natural material, like negative stiffness or refraction, cloaking or spectral bandgaps. Indeed musical instruments are complex structures and some may already qualify as metamaterials. Still altering the instrument geometries and adding metamaterial behavior can increase the instruments sound variability and articulatory possibilities or lead to sounds not expected from mechanical instruments at all. The paper presents such examples. When modifying a frame drum by adding additional point masses forming a ring, the frame drum shows cloaking behavior when struck in the middle of the ring, where frequencies within a certain frequency band cannot leave the ring. This leads to a bandgap in the spectrum in the mid frequency range. Still when striking the drum outside the ring a normal drum sound is achieved. Therefore a drummer can produce sounds not known from drums before while with the same instrument can also play regular sounds. Other examples are modified guitar top plates with added point masses or waveguide structures.

Keywords: Sound, Music, Acoustics

1 INTRODUCTION

Metamaterials have not explicitly been used in musical instruments to this point. Still the complex geometry of musical instruments might lead to reconsider them as such. Although the fan bracing of guitars or the bracing of piano soundboards is built mainly for the purpose of stability, such regular substructures might lead to a behaviour meeting conditions of the concept of metamaterials. Indeed pitch glides of Chinese gongs [1], the brassiness of crash cymbals [2] or tam-tams [3], or the increased brightness of Balinese *gamelan gender* bronze plate [4] are caused by complex geometries.

Metamaterials in musical instruments can be used to change the instrument sound considerably. Changing existing instrument geometries can lead to added band gaps in their spectrum, and using several of such band gaps will lead to a designed sound. With percussion instruments musical articulation is realized by striking or knocking at different positions on e.g. drums or cymbals. By adding metamaterial structures to them the variability of such sounds can be increased considerably.

Membranes used in Rock or Jazz drum kits, as well as with *tablas* of Indian music or the *pat wain* or the Myanmar *hsain wain* orchestra often show additional masses attached to them. They are used for different purpose. Jazz drummers use tape and other material to damp especially the snare drum. Also tom-toms are taped to reduce the loudness as well as the length of their tone. Detuning of these drums play a minor role since these drums are tuned by tuning pegs at the drum head rim. *tabla* [4, 5] and *pat wain* [6] drums are tuned by adding a plate or a special tuning paste respectively. The aim is twofold, the drum is tuned with respect to its pitch and moreover the overtone spectrum of the drums is changed to arrive at a more harmonic overtone spectrum of the fundamentally inharmonic spectrum of these percussion instruments. The advantage of a more harmonic spectrum is to increase pitch perception of the drums to use them in melody performance.

Metamaterials have been used with membranes to achieve damping over a large bandwidth [7, 8], for a review see [9]. With massive rings attached concentric on the membrane one or only a few resonance frequencies exist up to 1 kHz, which leads to strong damping of the membrane within this range with large peaks at the resonance frequencies. Such applications differ from the concept proposed in this paper in its aims. There a strong overall damping is aimed for, where with musical applications only a partial damping is needed to maintain an audible sound. Also with such heavy masses the membrane between the mass and the membrane boundary, as well as the membrane between two rings can mainly be considered as a spring. As with concentric

*https://rolfbader.de/metamaterial-drum

rings the distances between the rings outer boundary and the membrane boundary is a constant for all angles, only one spring length and strength is present. So these applications differ in principle from the construction and the aims of the dot masses attached asymmetrically on a membrane present in this study.

Circular or more complex shaped geometries might result in a cloaking behaviour, where a traveling incoming wave looks the same in both cases, with the structure and without the structure in its way. Therefore for an observer behind the structure this structure is invisible [10]. Such geometries can also act as cages, where waves in them cannot travel out and vice versa. This has been found in optics [11] and has been applied in acoustics like in [12, 13] next to others. This behaviour is frequency dependent and a way to built a musical metamaterial, enhancing the articulatory ability of a musical instrument.

In this paper an example of applying metamaterial behaviour to musical instruments is demonstrated using a frame drum. It results bring on highly interesting new sounds and increased articulatory ability for players. After introducing the constructed instruments, the paper discusses the measurement techniques applied, microphone array and laser interferometry. Increased articulatory possibilities of the new instrument are discussed together with further design possibilities.

2 Methods

2.1 Frame Drum

A frame drum with a BoPET (biaxially-oriented polyethylene terephthalate) also called mylar drum membrane and a diameter of 40 cm was used. At the drumhead a ring-shaped area (m) with a diameter of 10 cm is separated using a set of 2×10 Neodymium magnets sticking at the front and the back of the membrane. The magnets are circular with a diameter of 5 mm and a height of 5 mm (see Fig. 4).

The magnet were chosen as they add a heavy mass to the membrane at distinctive points. When two magnets are attached to each other from the top and bottom side of the membrane the vibrations on the membrane are never strong enough to make the magnets move or fall off, no matter how hard the drum is struck. Additionally magnets are not damaging the membrane during attachment or when removing. They are also quite heavy with respect to their size. Yet a fourth advantage is that they can easily be moved by hand forming new structures. So musicians would be able to handle them easily. Still there is a lower distance limit between the magnets, as they will align magnetically. After experimenting with different adhesive fastening techniques, magnets were found to outperform other methods.

The area separated by the magnets is assumed to act as cloaking, separating vibrations inside and outside this area. Therefore it is expected that waves originating outside the ring will not enter and vice versa. In this case the frequencies and modes of one of the membrane areas are cloaked and do not contribute to the radiated sound. We therefore expect a band gap to appear in some cases where certain frequencies regions are not present. The cloaking of a frequency band, the band gap is then caused by a cloaking of regions on the membrane.

2.2 3D printed plates

Five square plates of dimension $40 \times 40cm$ were printed using a BigRep Studio-3D printer loaded with PLA-filament, a polylactic acid material printed at 205°C . The density of the raw material is $1.24g/cm^3$, the tensile strength (ISO 527) is $60MPa$, the impact strength (ISO 179) is $7.5KJ/m^2$, flexural modulus (ISO 178) of $3800MPa$. All the plates have a continuous thickness of 2mm with additional geometries printed on them. The five versions are described as followed:

1. Plain square plate, $40 \times 40cm$
2. Plate with two cups attached, open side oriented to -x-direction, with diameters of 5.5cm, 5.25cm depth, 3mm wall thickness, positioned at x=11-16.25cm, y=25cm and x=21-26.25cm, y=15cm respectively, relatively to the $40 \times 40cm$ dimension of the plate.

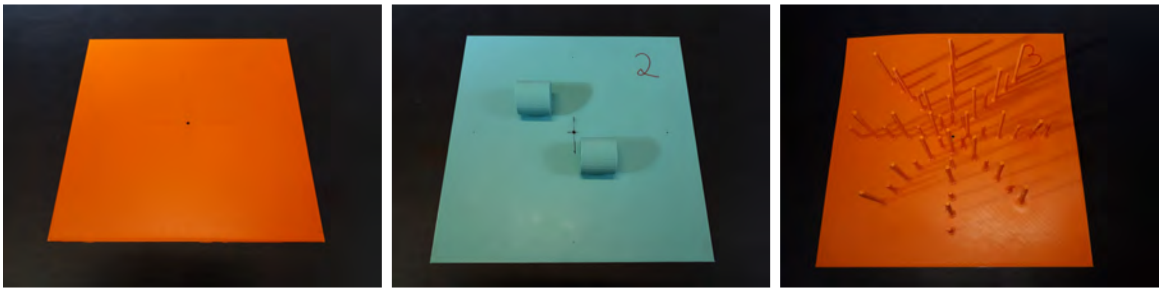

Figure 1. Square plates 1,2 and 3, from left to right.

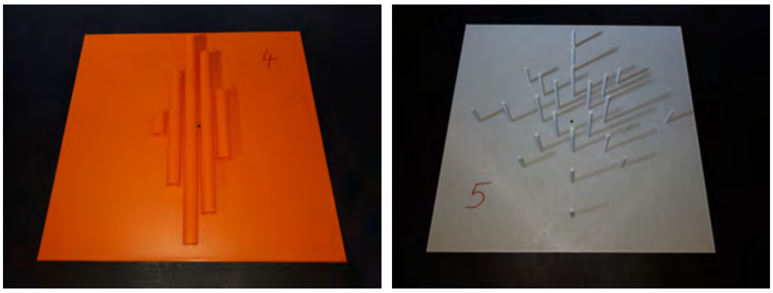

Figure 2. Square plates 4 and 5, from left to right.

3. Plate with 48 small rods arranged in z-direction, equally in line on medians and diagonals with a distance of 3cm, starting in the middle. There are 24 rods à $10cm$ and 24 rods à $5cm$, each have a diameter of 5mm.

4. Plate with five tubes lengthways an imaginary y-axis. The tubes are of different lengths: $3cm, 20cm, 36cm, 28cm$ and $12cm$ have a diameter of $2cm$ and $3mm$ thick walls. The longest tube is placed in the middle of the plate at $x = 20cm$, $y = 2$ to $38cm$. All the rest is arranged centered with a distance of 3cm to the adjacent tube.

5. Plate with twenty rods: 8 à $4cm$, 7 à $6cm$, 8 à $8cm$ each with a diameter of $5mm$. They are equally in line on medians and diagonals with a distance of $3cm$, starting in the middle of the plate.

The idea is to build geometries with spectral band gaps or enhanced spectral regions. The tubes and bars attached to the plain plate are assumed to resonate with discrete frequencies. Such vibrations can either take energy out of the plate or increase the radiation of these frequencies.

The bars are expected to take energy out, as their vibration is mainly in-plain, where the radiating area is only the top end area of the bars. This area is so small that no considerable radiation is expected. As the vibrations are damped in the bars due to internal damping, band-gaps in the radiation spectrum of the whole plate are expected at the discrete bar frequencies.

The tubes are expected to also take over energy from the plate, where the air inside the tube are driven by the plate. These frequencies are expected to radiate strongly. Theoretically, tubes with open ends have no radiation, except for the radiation caused by the end-correction of the tube. Here tubes with larger diameter have considerable larger radiation. Therefore two kinds of tube diameters were realized. The radiation due to the end-correction is also frequency-dependent, where lower frequencies radiate considerably louder than higher ones. Therefore considerable radiation is expected for the lowest few modes. Therefore different tube length were used to address different fundamental frequencies. The radiation is also strongly directional-dependent, as the tubes were only added to one side of the plate.

2.3 Laser interferometry

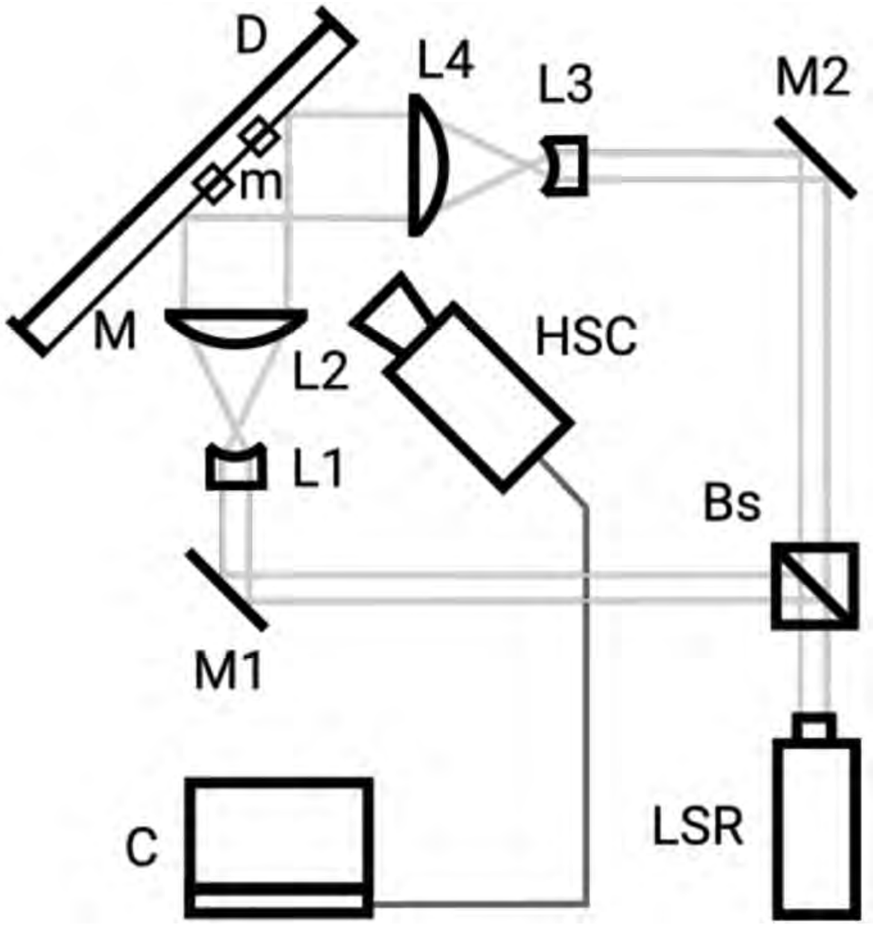

Figure 3. The experimental set-up. (LSR) laser, (Bs) Beam splitter, (M1, M2) planar mirrors, (L1, L3) semi-concave lenses $(f_{L1,L3} = -16\,mm, d_{L1,L3} = 10\,mm)$, (L2, L3) semi-convex lenses $(f_{L2,L4} = 300\,mm, d_{L1,L3} = 100\,mm)$, (M) drumhead of the frame drum (D), (m) circle-shaped part of the drumhead, separated utilizing a set of 2×10 Neodynium magnets. (HSC) high-speed camera, (C) analysis using a PC. The beam pathes are marked by green lines.

The experimental laser set-up is depicted in Fig. 3. A Verdi Single FAP (fiber array package) diode-pumped solid state frequency doubled Neodynium Vanadate $((\mathrm{Nd} : \mathrm{YPO_4})$ laser (LSR) source radiates a beam of wavelength $532\,nm$ and beam diameter of $d_{LSR} = 2.25 \pm 10\%\,mm$. The beam is splitted by a beam splitter (Bs). The splitted beams are directed to planar mirrors (M1) and (M2). Subsequently the beams are expanded via an optical lens system, consisting of a semi-concave lens with focal distance of $f_{L1,L3} = -16\,mm$ and a diameter of $d_{L1,L3} = 10\,mm$ and a semi-convex lens with focal distance of $f_{L2,L4} = 300\,mm$ and a diameter $d_{L2,L4} = 100\,mm$. The drumhead was manually excited by an impulse hammer. The excitation has been applied outside as well as inside the separated area of the drumhead. The splitted and widened beams are directed to the drumhead (M) of a frame drum (D). The impulse response leads to a characteristic interference pattern at the drumhead. The pattern is recorded using a high-speed camera (HSC) with a frame rate solution of 10000 fps. The received data are analyzed utilizing Mathematica on a PC by subtracting adjacent recorded frames [14].

Additionally, the drum head was excited by an actuator, a Brüel & Kjaer Vibration Exciter 4809, again in the middle of the ring and outside with a low frequency of 65 Hz and a high frequency of 918 Hz, two eigenfrequencies of the drum head with magnets on.

2.4 Microphone Array

The sound pressure field of the frame drum was recorded with a microphone array in the near-field, 3 cm in front of the membrane (see Fig. 4). The grid constants of the array are 5cm in x-direction and 4cm in y-direction. The microphone array records sound fields with up to 128 microphones with a sampling frequency of 48kHz and a sample depth of 24 bit simultaneously.

The recorded sound fields are back-propagated to the surface of the membrane using the Minimum Energy Method (MEM) [15], a multipole-method assuming as many radiation sources as microphones. It has successfully been used to measure the vibrations of musical instruments [16, 17] (for a review on microphone arrays and back-propagation methods see [18].

For the recordings with the microphone array the drum was struck at three positions only, recorded with a single microphone placed 50cm in front of the membrane opposite, pointing to the drum center in an unechoic enviroment. Each recording resulted in 120 sound files at the microphone positions. From these the frequency spectra were calculated and all peaks up to 1 kHz were determined. For each of these frequencies the recorded sound field was back-propagated to the surface of the drum.

3 Results

3.1 Drum modes and traveling waves

The drum was struck at three different positions as it is expected that the ring acts as a cloaking effect to the sound and therefore striking within the ring should keep most of the vibrations within this ring, while striking outside the ring would lead to a strongly reduced energy in the ring. In Fig. 5 and Fig. 6 the results of the microphone array recordings and back-propagations are shown considering this point.

The results in Fig. 5 are calculated by first detecting the maximum absolute amplitude of each mode. The local positions of these maxima are accumulated on the membrane for all strikes. Then all points on the membrane showing more than 20% of accumulated maximum points are displayed.

At the top of Fig. 5 the case of striking in the ring is shown. Clearly most maximum points are within the ring. When striking at the ring rim, shown in the middle graph, the distribution of maximum amplitudes is more widespread over the membrane. Finally with the case of striking outside the ring, shown as the bottom plot in the figure, no considerable maxima are within the ring.

To differentiate this finding with respect to frequency, the amount of absolute amplitude within the ring is shown in Fig. 6 as a fraction of the whole absolute amplitude on the drum. The three curves show the three cases of striking in the ring, at the ring rim and outside the ring. Again striking in the ring leads to a strong increase of amplitudes within the ring, compared to the cases of striking at the ring rim and outside the ring. Still this increase only appears above about 400 Hz. As the fundamental frequency of the drum is 34 Hz we can conclude that the low frequencies are not much effected by the ring, while the higher ones clearly are.

Still the relative high fraction of amplitudes in the ring at very low frequencies are again remarkable. The lowest peak detected at 7 Hz is not audible and most likely refers to the motion of the drum as a whole, so including the wooden frame. This motion is unavoidable as frame drums only sound when the wooden frame is free. Fixing it strongly, which would avoid this low vibration would lead to a very much damped sound and can therefore not be implemented in an experimental setup.

Figure 4. Modified frame drum positioned in frot of the microphone array.

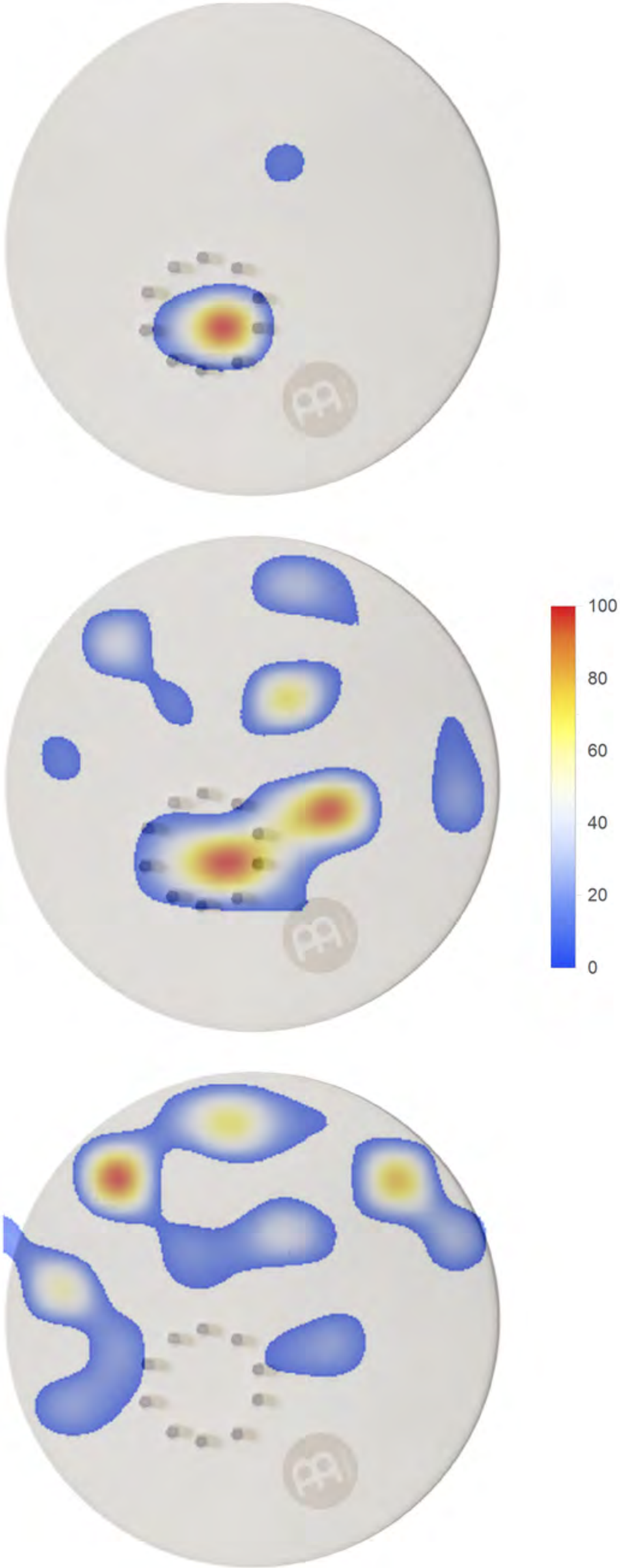

Figure 5. Density distribution of maximum amplitude values of modes on the drum up to 1 kHz for three hammer strike positions, showing densities above 20%. Top: strike in the circle, Middle: strike at circle rim, Bottom: strike outside the circle at the opposite side of the circle. While most maximum values for the strike in the circle are in the circle, very few are within the circle when the drum is struck outside the circle. A medium case is found when striking at the circle rim.

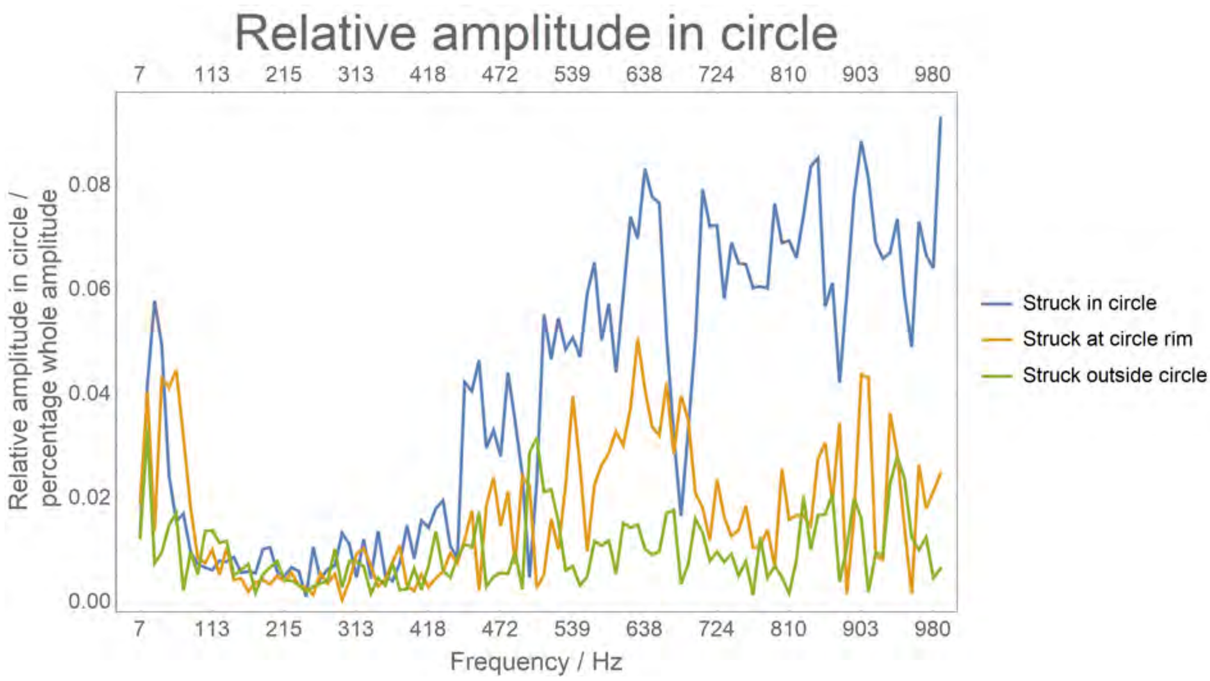

Figure 6. Frequency-dependent absolute amplitude within the circle compared to total absolute amplitude on the whole drum for three strike cases a) in the circle (blue), b) at the circle rim (orange), and c) outside the circle (green). While for frequencies below around 400 Hz the amplitude strength of the three cases are about the same, above about 400 Hz the amplitude strength within the circle strongly depends on the strike position. Strikes in the circle have stronger amplitudes there than strike at the rim with strike outside the circle showing least amplitudes in the circle.

Still the very low frequencies at 34 Hz, the 'monopole' vibration and around 65 Hz, the 'dipole' vibration again show much more relative amplitude within the ring in the cases of striking in the ring and striking at its rim, compared to the case of striking outside the ring.

The reason for this behaviour can be found when examining the modes more closely. The very low modes need to make the ring region move, too, as the anti-node regions are large, with 34 Hz it basically covers the whole membrane, with the 65 Hz 'dipole' case the membrane is split into two regions about half the membrane each. Of course due to the ring no monopole and dipole modes exist as in the case of a isotropic membrane.

The higher modes above the dipole, quadrupole, octopole and many other more complex modes with an integer number of axial and circular nodal lines, these modes can deform in such a way to avoid the motion of the ring region nearly completely. This holds for all three strike cases. It seems that even when striking in the ring, the ring is not able to maintain a vibration of these frequencies. The small leakage of vibrations leaving the ring is then taken over by the rest of the membrane leading to very similar motion compared to the case when striking outside the membrane.

To confirm these findings in Fig. 7 laser interferometry measurements for the case of striking in the ring are shown. The strike's transient is displayed as six snapshots at 0 ms, 0.2 ms, 0.6 ms, 1 ms, 3 ms, and 6 ms. Each black/while line indicate an amplitude increase of one wavelength of the used laser light. Therefore many rings do not indicate an amplitude ripple but a steep slope of the amplitude.

Starting at 0 ms, the strike leads to a circular wavefront leaving the strike point, shown at 0.2 ms. At about 0.6 ms this circular wavefront meets the ring rim. Here is is scattered and at the open rim positions new wavefronts

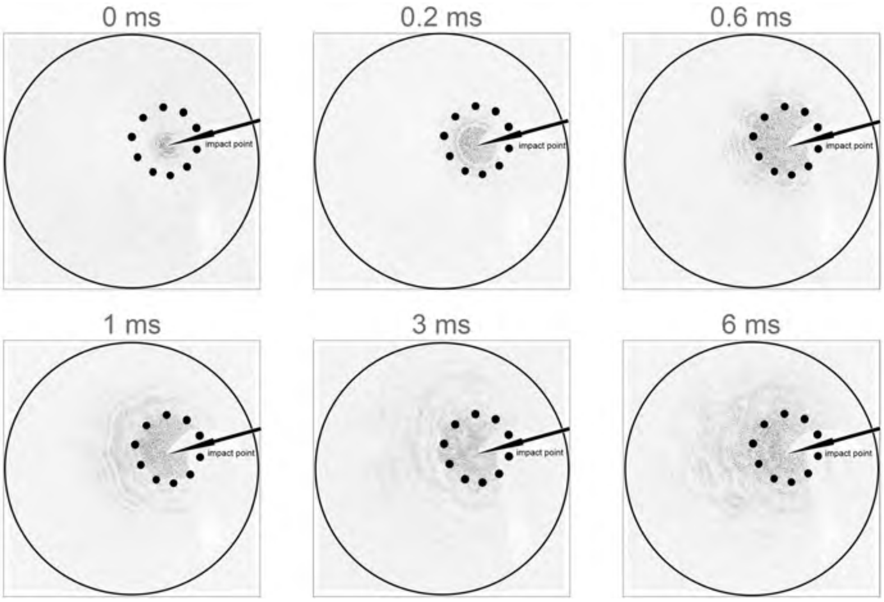

Figure 7. Laser interferometry time-dependent measurement of the initial transient of a hammer strike on a drum with a separated cirular area for several time steps. At 0 ms a circular wave leaves the strike point which meets the circle boundary at about 0.2 ms. The boundary elements lead to a split of the circle and the appearance of Huygens wave fronts outside the circle beyond 0.6 ms. At 3 ms the reflected waves on the membrane lead to complex vibrations.

start, as expected. At 1 ms these wavefronts form another wavefront outside the ring, slightly ripped as this wavefront is formed from a finite number of elementary waves according to the Huygens principle. Two cases at 1 ms and 3 ms show the wavefront outside the ring becoming more and more complex as the wavefront is then already reflected at the drum boundaries and leads to a complex waveform.

Still it can be seen at 1 ms that the ring still has a strong amplitude, much stronger than that leaving the ring. This picture continues at 3 ms and 6 ms supporting the findings fr om above. Again most vibrations are overall kept out of the ring when striking.

The same transient time development when striking outside the ring is shown in Fig. 8. Again at 0 ms a circular wave leaves the impact point which arrives at the ring at about 0.6 ms. At 1 ms it can be seen that the strong amplitude is still present outside the ring while only a small fraction enters the ring. This continues at 3 ms. At 6 ms there is some energy left in the ring likewise, which is expected from the above findings, namely that for very low frequencies at 34 Hz and 65 Hz, the ring region is also moving with some amplitude. Still again overall most vibrations keep out of the ring when striking.

To differentiate the low / high frequency difference further, the drum is driven by a shaker in and outside the ring at two frequencies, 65 Hz and 918 Hz. In Fig. 9 snapshots of the vibrations are shown at maximum amplitudes of the sinusoidal vibrations. On the top row the 65 Hz cases are shown, at the left the case when driving in the ring, at the right when driving at outside the ring. Clearly in both cases broad vibrations can be seen, indicating a distorted dipole motion. Although when driving inside the ring the amplitude is stronger inside than outside, some amplitude is still outside. When driving outside, the amplitude is about equally distributed. This is in accordance with the findings of the microphone array, especially with that of Fig. 6. There in all striking cases energy in the ring was present, still when striking in the ring the energy was even stronger.

The two lower plots in Fig. 9 show the laser interferometry measurements for sinusoidal excitation at 918Hz

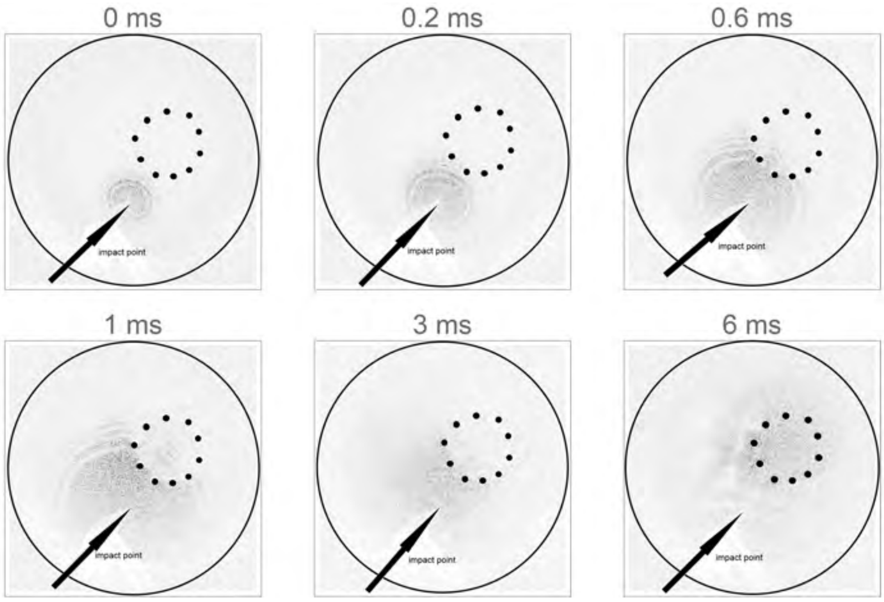

Figure 8. Laser interferometry measurement of a hammer strike on a membrane with a separated circle area, striking outside the circle. A circular wavefront leaves the strike position and reaches the circle boundary at 0.2 ms. The boundary leads to a formation of a Huygens wavefront inside the circle from about 0.6 ms. From 1 ms on the vibrations inside the circle are much less than those outside. Still after about 6 ms there is motion inside the circle, still at small wave vectors and therefore at low frequencies only.

inside the ring on the left and outside on the right. Clearly when driving inside the ring nearly all amplitude are within the ring, while when driving outside nearly all amplitudes are outside the ring, while the ring boundary cloaks the inner ring area.

Clearly the ring is cloaking vibrations in both directions, from within the ring to its outside and vice versa for frequencies above about 400 Hz. For frequencies below 400 Hz it is cloaking in a way that vibrations from outside do not enter the ring. Still when driving the ring some vibrations escape the ring and form modes outside. But also in this case the ring is not taking part in the vibrations considerably. For very low frequencies the cloaking becomes uneffective which is caused by large anti-nodal areas on the membrane.

3.2 Example sounds

The drum sounds considerably different when struck inside or outside the ring. Within the ring a sound is produced not known from regular drums, while when struck outside a normal drum sound appears. To display this aural finding the drum was struck at three positions only recording the sound with a single microphone 50 cm in front of the membrane opposite to the drum center in an unechoic chamber. With a wooden hammer the drum was struck right at the center of the ring, at the ring boundary between the magnets at a place most close to the membrane center, and outside the ring opposite to it, still with the same distance to the membrane boundary as the ring center, which is 13.5 cm.

Additionally, to test the influence of different ring diameters, next to the 10 cm diameter used for the measurements above, two additional rings were built, one with 8 cm and one with 12 cm in diameter. All had the same center point of the ring as the 10 cm ring, i.e. 13.5 cm in radial distance to the membrane boundary.

The here produced sounds are exemplary. A vast variaty of sounds can be produced utilizing hammers of different geometries, elasticities and hardnesses. The test strikes were performed with musical accuracy providing

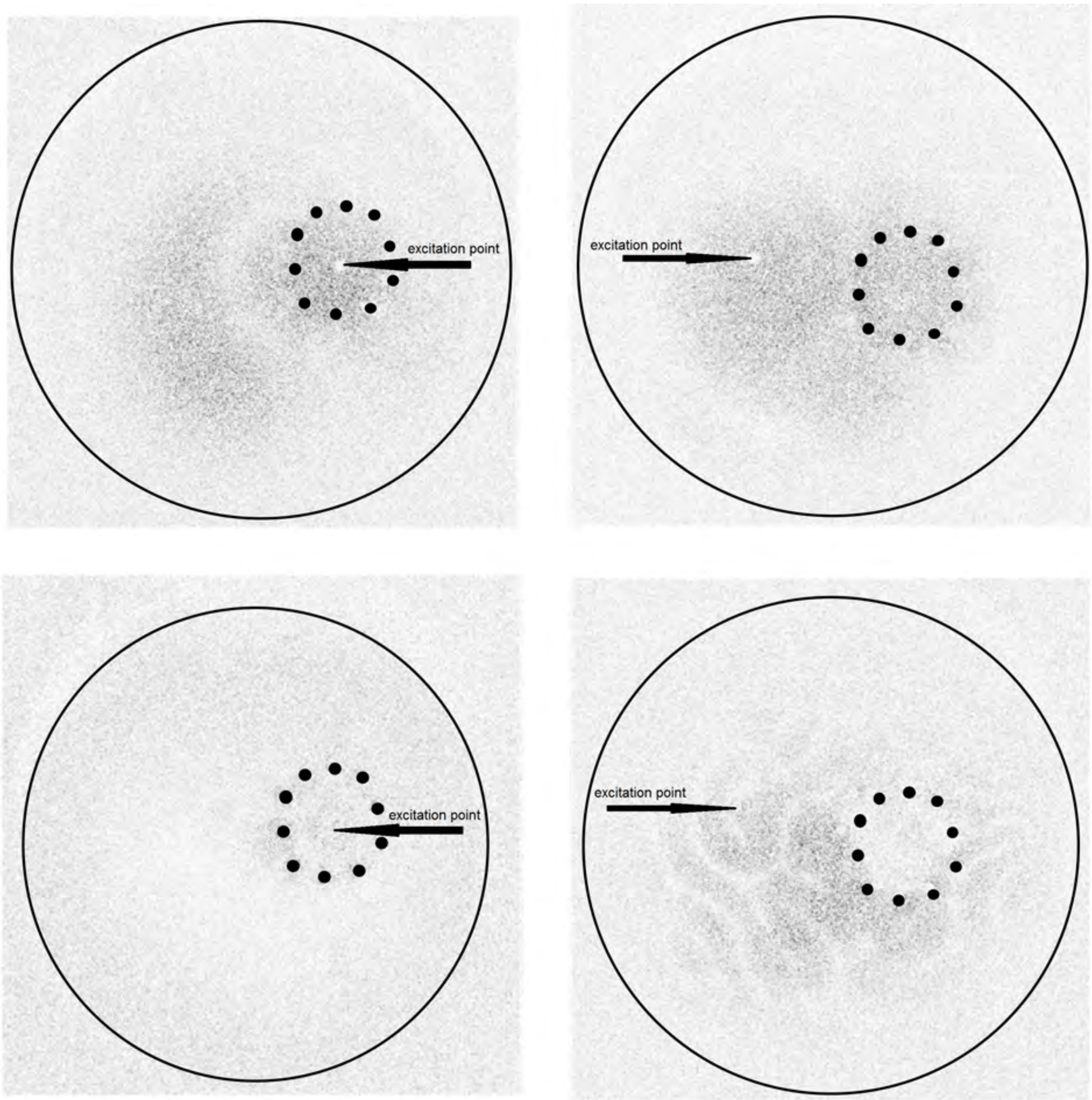

Figure 9. Snapshots of forced oscillations at 65 Hz (top row) and 918 Hz (bottom row) inside (left column) and outside (right column) the circle. At the low frequency at 65 Hz the vibrations are strong both, inside and outside the circle. At the high frequency of 918 Hz the driving of the membrane inside the circle only leads to a vibration inside, while driving the membrane outside the circle the movement is only outside the circle and very low amplitudes are present in the circle. Therefore the circle at this frequency of 918 Hz acts as a cloaking of waves in both directions. Comparing with Fig. 6 allows the conclusion that above about 400 Hz the circle acts as a cloaking element.

best possible uniformity in speed, strength and impact position.As the resulting sounds were so considerably different and this difference maintained when using different striking strength, the overall sound difference between the striking points is clearly documented by this method.

Fig. 10 shows the nine strikes, three diameters combined with the three striking positions. Each spectrum was calculated with a Fourier transform of the first 50 ms of the sound. As the drum is a percussion instrument the sound character is mainly heard during this initial sound phase. So the results presented here only refer to the initial transient.

In the top plot the spectra for the strikes inside the drum are displayed. They show a band gap starting from about $\sim$ 300 Hz - $\sim$ 700 Hz. The low frequencies are still strong, which also holds for the higher ones.

Contrary, the strikes outside the membrane displayed at the bottom of Fig. 8 show no such band gap but rather a regular spectrum exponentially decaying with frequency. The strike at the ring boundary displayed in the middle plot shows a mixture of both plots, again with an unusual flat spectrum, not considerably decaying towards the higher frequencies.

Both, the spectra of the strike inside the ring and that at its boundary cannot be produced by a regular drum. But as the drum can still be played outside the ring with regular spectral shape, it can still produce normal drum sounds. So adding the ring increases the articulatory possibilities of the drum considerably.

3.3 Theoretical Considerations

From this parametric study we can make estimations on the frequency on- and offset of the band gap.

3.3.1 Band gap upper cut-off frequency

From the lowest frequency of the membrane without the ring of $f_0 = 78$ Hz one finds a wave speed $c = f_0/J^0/(2\pi r) = 44.8$ m/s, where $J^0 = 2.405$ is the first zero crossing of the Bessel function as radial solution of the circular membrane wave equation with boundary conditions of zero displacement and drum radius $r = .2$ m. The wavelength λ fitting between two adjacent magnets of the ring is

$$\lambda_i = 2\pi r_i/m_n - m_d \tag{1}$$

with index i=1,2,3 for the three rings with radii $r_1 = .04$ m, $r_2 = .05$ m and $r_3 = .06$ m. Here $m_d = 0.005$ m is the magnet diameter subtracted from a $1/m_n$ of the ring circumference, with $m_n = 10$ the amount of magnets. The frequencies of these wavelength then are $f_i = c/\lambda_i$, and therefore $f_1 = 2027$ Hz, $f_2 = 1545$ Hz, and $f_3 = 1247$ Hz.

These frequencies are about twice the upper cut-off frequency of the band gap at about 700 Hz - 800 Hz. Therefore the cloaking behaviour disappears when the gap between the magnets is half the wavelength of the respective frequency. In Fig. 5 (top plot) the tendency of smaller ring diameters to have a larger band gap can clearly be seen. The 8 cm ring has a much larger band gap up to about 800 Hz, the 10 cm ring has a spectral peak at about 550 Hz and the 12 cm ring has also a peak at about 550 Hz but is much less damped before this frequency range. Indeed the band gap has a small amplitude slope in and out and is not a straight cut at the cutoff-frequencies (has a low Q when taken as a filter). This is expected as the calculated frequencies assume perfectly rigid magnets with infinite mass which is not the case. Still clearly the higher cut-off frequency is determined by the ring size.

As found with the microphone array and the laser interferometry data, the magnets prevent the waves within the band gap to leave or to enter the ring. The corresponding wavelengths are much longer than the distances between the magnets. Therefore the magnet geometry is sub-wavelength and therefore the effect is not a simple scattering but a cloaking of waves. When struck in the ring these band gap frequencies stay within the ring and therefore have a much smaller radiation area compared to waves traveling over the whole membrane, the lower and higher frequencies. This leads to lowered amplitudes of the band gap frequencies in the radiated sound.

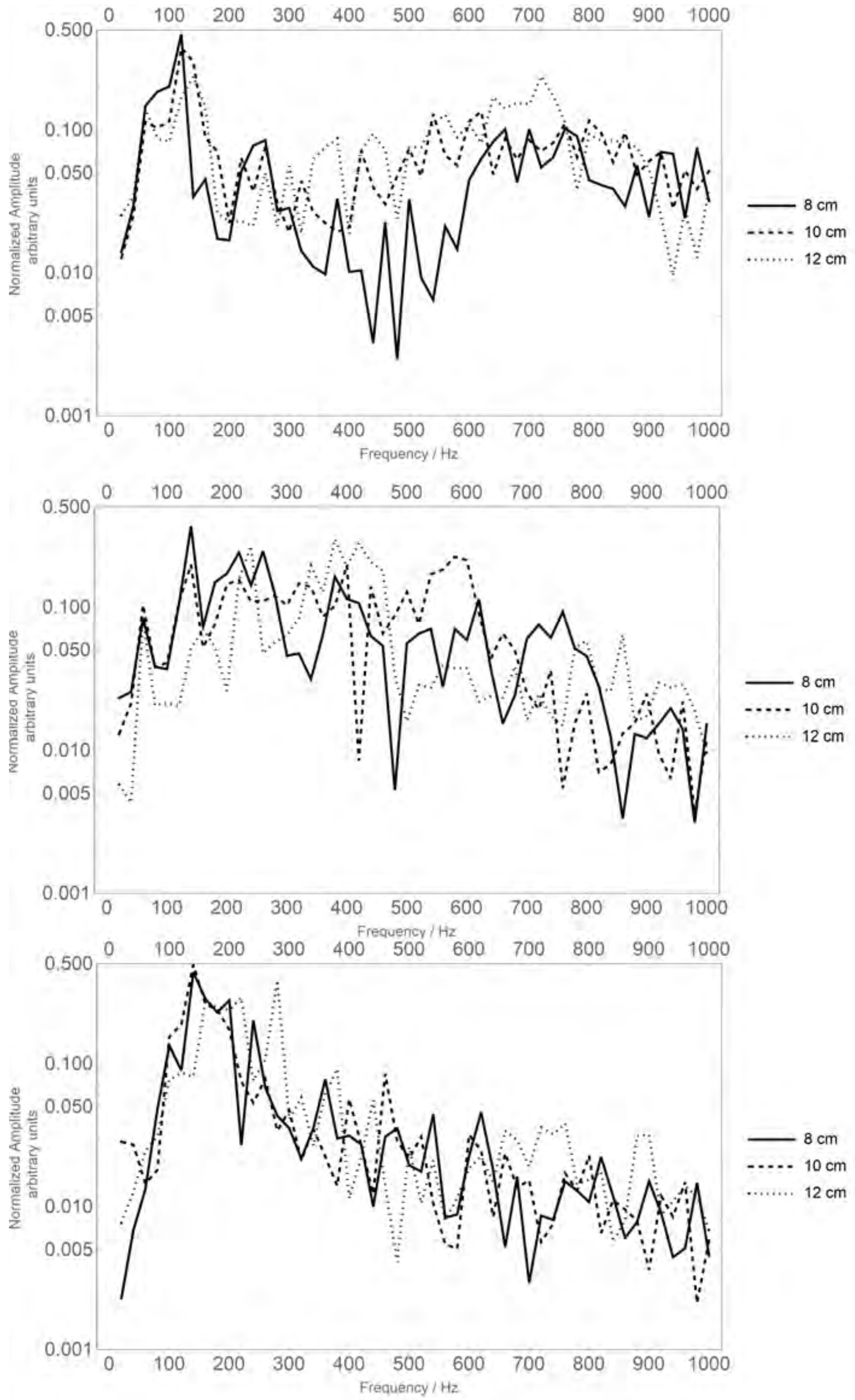

Figure 10. Spectra of example strikes on the modified membrane for three ring diameters, 8 cm, 10 cm, and 12 cm, as Fourier analysis of the first 50 ms of sound, top: strike position at the ring center, middle: strike position at the ring boundary, bottom: strike position outside the ring. The strikes inside the ring show a band gap between 300/400 - 700/800 Hz, the strikes outside the ring show regular decaying overtone strectra, the strike at the ring boundary are in the middle between inside and outside strikes.

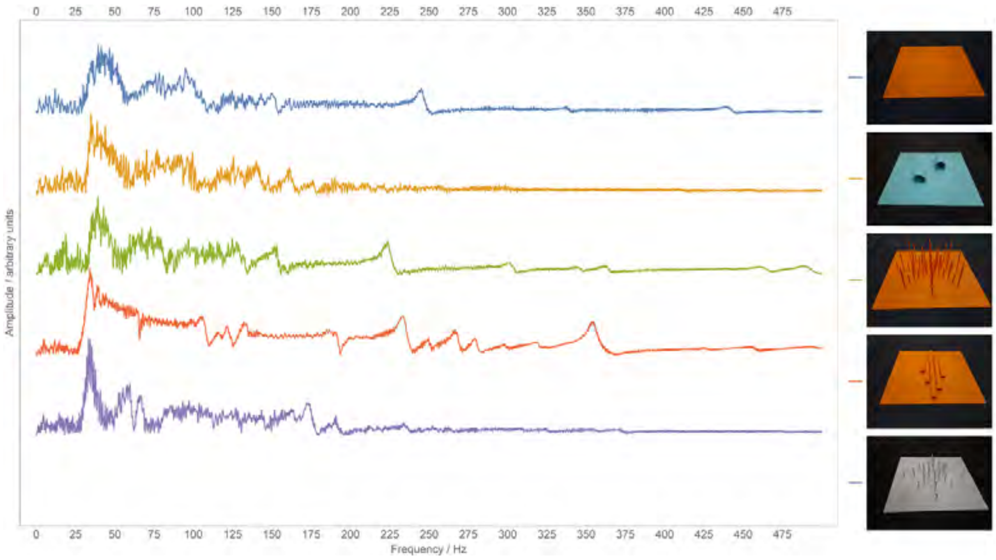

Figure 11. Spectra of five metamaterial plates of 40×40 cm, the elevation is arbitrary to have a better display, the amplitude axis is linear. From top to bottom: a) plain plate, b) plate with two large tubes, c) plate with bars, d) plate with five tubes, e) plate with bars (see text for details). The spectra of the modified plates show frequency regions of in- or decreased energy, as expected.

3.3.2 Band gap lower cut-off frequency

Estimating the frequencies within the rings by taking the magnets as boundary conditions of zero displacement we find $f_1^0 = 390$ Hz, $f_2^0 = 312$ Hz, and $f_3^0 = 260$ Hz. This is not perfectly true of course and the movement present at the magnets might be taken as an enlargement of the radii to come closer to the real values. Still the values are around the frequency range where the band gap start. This confirms the finding of the microphone array data and the laser data. Frequencies below the eigenresonance of the ring appear over the whole membrane and are therefore not damped in the spectrum as those above the fundamental frequencies of the ring.

The ring diameter does not change this overall behaviour, still the 8 cm diameter has the strongest band gap, while the 10 cm and 12 cm rings perform similar (Fig. 8 top). This also holds for the strike at the ring boundary. Aurally, indeed the ring with the smallest diameter of 8 cm showed this band gap effect most clearly.

3.4 Metamaterial plates

The plates were investigated using the actuator driving recording the acceleration with a single piezo Fourier transforming the time series, as well as using the recording of a 128 microphone array and analyzing the decay with a T60.

3.4.1 Comparison using the actuator

Fig. 11 shows the spectra of the five plates using the actuator. All have a strong frequency range below 50 Hz, still with different sharpness. The plate 2 (second from top) with two large tubes have a smoothed spectra compared to plate 1. Plate 4 (second from bottom) with five tubes on the other side has a much more complicated spectrum. Plate 3 (third from top) with many bars is more lively in its spectrum compared to plate 5 (bottom) with only a few bars. Still this last plate has the sharpest peak at the lowest frequencies.

Fig. 12 shows comparisons of the spectra. The reference spectrum of plate 1 (top) has been kept like in Fig. 11. From all other spectra that of plate 1 was subtracted. The baselines for each spectrum is platted as a

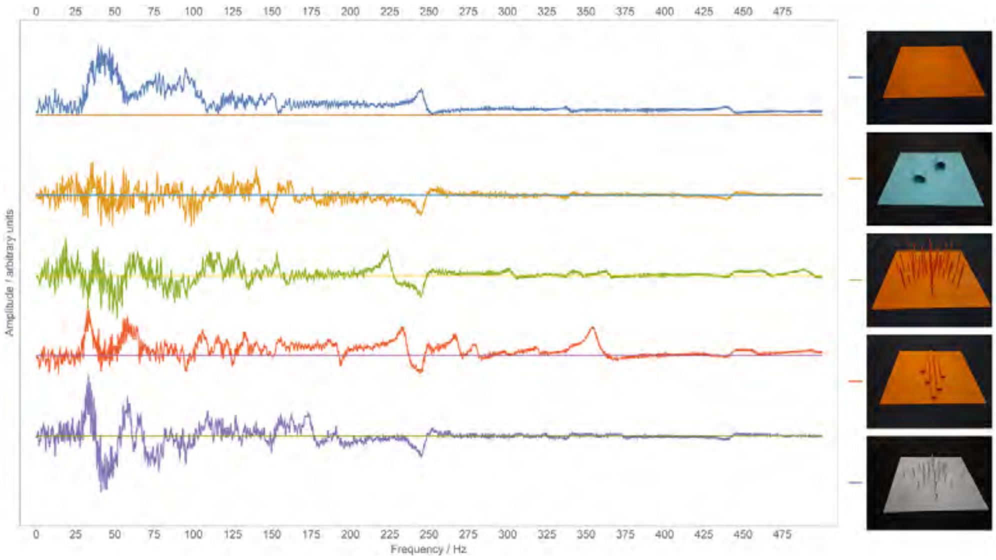

Figure 12. Comparison of spectra from Fig. 11. Plate 1 on the top is left like in the precious figure, all other are subtractions of spectrum of plate 1 from the respective spectra of plate 2 - 5. The lines are the zero line. Plate 4 (second from bottom) shows considerably more energy, while the other plates are more or less equal. Integrating the spectrum of plate 1 and weighting all other difference spectra with it plate 4 has 0.481% more energy than plate 1 within this frequency range. Contrary, plate 3 has only a 0.0556% increase, and plate 2 with -0.018% and plate 5 with -0.042% show a slight decrease.

horizontal line in the figure.

Plate 4 (second from bottom) shows considerably more energy, while the other plates are more or less equal. Integrating the spectrum of plate 1 and weighting all other difference spectra with it plate 4 has 0.481% more energy than plate 1 within this frequency range. Contrary, plate 3 has only a 0.0556% increase, and plate 2 with -0.018% and plate 5 with -0.042% show a slight decrease.

This is pointing to the tubes to be very effective. Indeed plate 4 shows the most lively spectrum and is considerably different from that of plate 1. This is most likely caused by the resonances in the air columns of the tubes.

Still the other spectra are different too. Plate 5 (bottom) shows strong deviations especially in the low frequency range around 50 Hz in both directions. Plate 3 (third from top) is much smoother , still considerable also in the low frequency range.

All plates sound very different aurally, when knocking on them. So all deviations are audible.

It is interesting to see that the impact appears strongly in the low frequency range, although the added geometries are all small, where impact in higher frequency regions is expected. Still the influence of many small geometries on frequencies in the sub-wavelength range of these geometries is a major aspect of metamaterials. Still other behaviour might play a role too, like the stiffening of the plate by the tubes.

4 Conclusions

The cloaking of the ring is frequency-dependent because the ring is not in a free-field but on a membrane which again has boundaries leading to eigenmodes of the whole system. For high frequencies above 300/400 Hz the eigenmode shapes outside the ring are complex enough that the membrane acts very much like a free field and therefore the regular cloaking behaviour appears. For lower frequencies, here below 300/400 Hz, cloaking still works in one direction that waves from outside do enter the ring not considerable, still when driving within the ring waves can leave to the outside area. For very low frequencies the cloaking then nearly vanishes. Above about 700/800 Hz the waves again travel freely over the ring boundary as the wavelength are smaller than the distances between the magnets.

The transient laser interferometry measurements also show that when striking the drum in the ring, at the very beginning of the sound some energy leaves the ring. These vibrations trigger the modes between about 100 Hz and 400 Hz outside the ring and those above the upper cut-off frequency of the band gap. This offers another musical option to decide which frequency range to drive when striking in or outside the ring.

It also appears that when striking at the rim of the ring a mixture of the two extremes, striking outside the ring or at the very center of it can be achieved. This holds for both, the frequency range up to about 400 Hz and that above this range.

Furthermore the cloaking of the ring leads to a different radiation behaviour of the drum compared to when struck outside the ring. When at higher frequencies only the ring area vibrates, it acts like a monopole and radiates sound from a clearly defined point. When striking outside the ring complex modes appear with a completely different radiation behaviour. Therefore depending on the driving point the same frequency might have two completely different radiation patterns. As a monopole radiation is perceived as a loudspeaker-like source, while a complex radiation pattern is perceived as a musical instrument played live a musician has a new kind of articulation with such a manipulated drum.

The drum shows a much higher amount of timbre variability compared to a regular drum. With regular drums the drummer can only vary the sound by striking at different positions, where striking in the middle leads to a sound dominated by low frequencies and striking more to the edge increases the amount of energy at higher frequencies making the sound more bright. Although when striking outside the ring with the presented manipulated drum these articulations are still possible, additionally the drummer is able to produce completely new sounds, when striking the membrane at different positions within the ring.

When striking at the very center, even very strongly, the sound has only energy in the low frequencies, with a band gap from 300/400 Hz - 700/800 Hz. Higher frequencies appear only in the initial transient as they decay naturally very fast. The amplitude attenuation in the band gap incrases with smaller ring diameters. This sound is not known from a regular drum struck in its middle as due to the transient behaviour of such a strike and the band gap discussed above at the very beginning of the tone higher partials are present more than with a regular drum struck at the drum center. Therefore such a sound is not possible to produce for drummers with regular drums.

The metamaterial plates show a considerably different frequency-dependent mobility. Especially plate 4 with the long tubes have amplitude peaks at small-band frequency ranges between 225-300 Hz. This plate is also resonating stronger than the reference plate 1 nearly all over the range up to 500 Hz. Therefore this plate construction is expected to be both, louder than the reference plate and enhancing special small-band frequency bands. These frequency bands need to be related to the resonance frequencies of the tubes, which is subject to further studies.

Plates 3 and 5 with the added bars show in- and decreased mobility, especially in the low frequency range around 30-50 Hz. Again this is a typical behaviour of metamaterials, where small scale geometries in the sub-wavelength size of lower frequencies effect these low frequencies. The plate with the shorter bars shows a stronger influence compared to the plate with the longer bars.

Plate 2 with the short tubes with large diameter smooth the spectrum from about 200 Hz on. Also in the low range it smoothes the spectrum compared to the reference spectrum of plate 1.

It appears that metamaterial plates are able to effect plate mobility, produce small-band gaps and peaks and effect very low frequency ranges around 20-40 Hz.

5 Acknowledgements

Many thanks to those helping with the measurements of the plates: Niko Plath, Paul Testa, Jakob Schenke, Carola Ohlsen, Pascal Brunet, Bela Wiener and Simon Mayrshofer.

References

[1] M. Jossic, O. Thomas, V. Denis, B. Chomette, A. Manmou-Mani, and D. Roze, D., "Effects of internal resonances in the pitch glide of Chinese gonsg," J. Acoust. Soc. Am. **114**, 431-442 (2018).

[2] C. Touzé, and A. Chaigne, "Lyapunov Exponents from Experimental Time Series: Application to Cymbal Vibrations," Acustica **86**, 557-567 (2000).

[3] Th. D. Rossing, *The Science of Percussion Instruments,* World Scientific, Singapore (2001).

[4] S. Tiwari and A. Gupta, "Effects of air loading on the acoustics of an Indian musical drum," J. Acoust. Soc. Am. **141** (4), 2611-2621 (2016).

[5] G. Sathej, and R. Adhikari, "The eigenspectra of Indian musical drums," J. Acoust. Soc. Am. **126** (2), 831-838 (2009).

[6] R. Bader, "Finite-Difference model of mode shape changes of the Myanmar pat wain drum ring using tuning paste," Proc. Mtgs. Acoust. **29**, 035004 (2016).

[7] Ch. J. Naify, Ch.M. Chang, G. McKnight, and S. Null, "Transmission loss of membrane-type acoustics metamaterials with coaxial ring masses," J. of Applied Physics **110**, 124903-1-8 (2011).

[8] H. Tian, X. Wang, and Y.-H. Zhou, "Theoretical model and analytical approach for a circular membrane–ring structure of locally resonant acoustic metamaterial," Applied Physics A. Materials Science & Processing, **114**, 985-990 (2014).

[9] T.-Y. Huang, Ch. Shen, and Y. Jing, "Membrane- and plate-type acoustic metamaterials," J. Acoust. Soc. Am. **139**, 3240-50 (2016).

[10] M.R. Haberman and A.N. Norris, "Acoustic Metamaterials," Acoustics Today **12** (3), 31-39, (2016).

[11] A. Mirzaei, A.E. Miroshnichenko, I.V. Shadrivov, and Y.S. Kivshar, "Optical Metacages," Physical Review Letters **115**, 215501-1-5 (2015).

[12] A. Colombi,Ph. Roux, S. Guenneau and M. Rupin, "Directional cloaking of flexural waves in a plate with a locally resonant metamaterial," J. Acoust. Soc. Am. **137** (4), 1783-89 (2015).

[13] M. Dubois, Ch. Shi, Y. Wang and X. Zhang, "A thin and conformal metasurface for illusion acoustics of rapidly changing profiles," Applied Physics Letters **110** 151902-1-5, (2017).

[14] Th. Moore, "Measurement Techniques," In: Bader R. (eds) *Springer Handbook of Systematic Musicology*, Springer, Berlin, Heidelberg, 81-103 (2018).

[15] R. Bader, "Reconstruction of radiating sound fields using minimum energy method," J. Acoust. Soc. Am. **127** (1), 300-308 (2010).

[16] R. Bader, "Characterizing Classical Guitars Using Top Plate Radiation Patterns Measured by a Microphone Array," Acta Acustica united with Acustica **97**, 830-839 (2011).

[17] R. Bader, "Radiation characteristics of multiple and single sound hole vihuelas and a classical guitar," J. Acoust. Soc. Am. **131** (1), 819-828 (2012).

[18] R. Bader, "Microphone Array," In: T. Rossing (ed.): *Springer Handbook of Acoustics*, 1179-1207 (2014).

[19] P.A. Deymier (ed.), *Acoustic Metamaterials and Phononic Crystals.* Springer Berlin Heidelberg (2013).

[20] D. Diderot, *Encyclopédie, Ou Dictionnaire Raisonné,* Vol. **66**: Suite Du Recueil De Planches. Cap.: Luthier, Planche I, Figure 8, (1779).

[21] R. Bader, "Additional modes in a Balinese gender plate due to its trapezoid shape," In: R. Bader, Ch. Neuhaus, and U. Morgenstern (eds.), *Concepts, Experiments, and Fieldwork: Studies in Systematic Musicology,* Peter Lang Verlag, Frankfurt a.M., 95-112 (2009).

PROCEEDINGS of ISMA 2019
International Symposium on Music Acoustics

13 - 17 September 2019 in Detmold, Germany

Influence of playing on the tonal characteristics of a concert piano - an observational study

Niko PLATH[(1)]

[(1)]Institute for Systematic Musicology, University of Hamburg, Germany *

Abstract

Well-maintained pianos are said to "mature" and to "change for the better" over the first years. When auditioning concert pianos for purchase, technicians do often not choose the best sounding instrument but the one with the greatest potential for future development. The present work addresses the following questions: Are structural changes measurable on a piano after one year of operation in a concert house? Are these changes perceivable by listeners? Measurements are performed on two occasions: First, on a brand new instrument prepared for sale. Second, on the same piano after having been played for one year in a concert hall. Single notes are recorded with dummy-head-microphones in player position in an anechoic chamber. An extended ABX listening test engaging 100 players, tuners, and builders, addresses the questions whether a variation in tonal quality is audible and if so, what sound properties could lead to a perceived difference. Semantic sub-grouping allows for indication on the vocabulary listeners of varying expertise use to verbalize their sensation. The statements give hints on what could have changed over the year and are used as a basis for the analysis of corresponding physical properties and psychoacoustic parameters related to the described sensations.

Keywords: Piano, Playing, ABX

1 INTRODUCTION

Instrument builders, tuners, as well as players often are certain, that new musical instruments have to be 'played in' and that older instruments can even change for worse if not played. Furthermore, it is known that wood degenerates over time, often accelerated by certain periodic climate conditions, which can affect the tonal characteristics of an instrument. The investigation at hand was prompted by indications that when auditioning brand new pianos for purchase, technicians try to 'hear the potential for future development behind the voicing' instead of just choosing the best sounding instrument. Well-maintained concert pianos are said to have their peak after five years and then gradually decrease in quality. The present work tries to establish a better understanding of what could lead to a change in tonal quality for a concert piano within a relatively short time frame of one year.

2 THEORY: INFLUENTIAL FACTORS

Possible influential factors for a change in tonal characteristics are listed and discussed for musical instruments and, in particular, for pianos in concert business. The issue is approached with regard to three main influences:

Aging: When addressing the long-term development of musical instruments, most published works focus on the time-conditioned degeneration of wood, eventually accelerated by periodic humidity alterations. For a piano, this might be relevant for material properties and geometry of the wooden soundboard with bridge and ribs. In connection with aging, the influence of climate conditions on wooden instrument parts has to be taken into account. In regard to other instrument parts, aging could show up as material fatigue of strings or mechanical parts in the action. Aging might be a crucial factor for the preservation of an instrument, particularly when dealing with historical instruments within the museum context. However, since this work attempts to address the possible changes in tonal quality for only the first year of a concert instrument under intensive supervision, other aspects gain in importance:

Playing: The vibrational properties of wood change when it is subject to vibrations for extended periods of

*niko.plath@uni-hamburg.de

time. Thereby, regular playing could cause an audible change in vibrational characteristics of piano soundboards [27]. For other instrument parts the influence of playing could show up as wear-out of mechanical connections in the action or as localized plastic deformations of hammer felt.

Maintenance: A grand piano at a concert hall is intensively monitored by a technician. It is tuned several times a week and prior to a concert, substantial adjustments to keys, action, and hammers might be made in consultation with the player to achieve a certain requested playing feel and tonal character. Since the purpose of maintenance work is to adjust the tonal characteristics, an impact in the context of this work can certainly be expected.

This section follows the tone production through the piano and describes the respective factors which presumably contribute to a difference in tonal quality of a piano. The suspected proportion of impact by each factor is estimated. The extent and interrelation of identified influential factors leads to considerations regarding the type of study design. Presented information about maintenance work on grand pianos is in part based on conversations and informal interviews with piano technicians. Furthermore, Reblitz [22] gives a comprehensive overview of service work on pianos.

2.1 Keys and Action

An important part of maintenance work on the piano is adjusting the interrelation of keys, action, and pedals, so-called *regulating*. The keys are adjusted to have certain weights needed to descend when depressed, called *down weight* and to rise back up, called *up weight*. The average down weight is approx. 50-55 grams, but professional players often have their own preference of a lighter or heavier playing feel. A possible way to change the touch weight of a key is to add or to remove lead weights from the key body. Due to a changed inertia, a different touch weight leads to a different acceleration of the key per input force and thereby will produce a different spectral distribution. Since the recorded examples are compared according to a similar key bed force, the implemented maintenance work on the keys is expected to have an impact on a potentially perceivable difference in tonal quality of the piano. For the instrument under observation the touch weight has been decreased for several keys by counterboring lead weights behind the balance rail axis. Comparable to the keys, maintenance work on the action mechanism could lead to an altered resulting acceleration of the hammer per input force. Again, this would modify the resulting spectral composition, as the string would face a hammer with different elastic properties. Thereby, maintenance on the action can be expected to have impact on the tonal quality of the piano.

2.2 Hammers

Brand new hammers (but also old worn hammers) are often considered to be too hard and the produced tone is too bright and harsh. If they were too soft, the tone would be too dull. The technician can influence hammer properties in several ways: One way is to needle the felt in certain areas, which separates felt fibers and thereby soften a hammer region. To harden a hammer, acetone or nitrocellulose lacquer can be applied to the felt. The lacquer soaks into the felt and hardens a certain region.

The piano under observation has had several so-called *hammer voicings* within the year. Since the only purpose of these adjustments is to change the tonal behavior of a note, it clearly can have impact on a perceived difference.

Since the instrument is revised several times a week during the year, an impact by material aging or mechanical wear-out is not expected for keys, action, and hammers.

2.3 Strings

Under beneficial conditions piano strings degenerate within a period of decades. Under heavy workload e.g. at a conservatory, the average lifespan decreases to 8-10 years with possible tears and breaks after approx. 5-6 years. Old strings are said to gain a clinking sound which may originate from the string itself, but is often also associated with loose bridge pins.

A possible explanation for the degeneration of steel strings is strengthening by plastic deformation (work-hardening). The increase in string stiffness could have the unwanted effect of increasing the inharmonicity of the string. However at least for wound strings, Houtsma [11] shows that the long-term increase of string inharmonicity can be explained by changes in mass distribution due to repeated stretching. Within one year the effect of the strings on the tonal quality of the piano is expected to be negligible.

2.4 Soundboard

A possible change of wood properties could be caused by two, often inter-working, factors: a) the aging of wood under certain climate conditions, and b) changes of material properties due to regular playing.

The effects of aging of wooden instrument parts on the vibrational behavior are studied mainly for violins, an overview is given by Bucur [5]. In particular, the gradual loss of hemicellulose is found to decrease the density but not to affect the Young's modulus. This raises the sound radiation coefficient E/ρ. For instruments in static high relative humidity the greatest change of vibrational properties is found in radial direction, increasing the degree of anisotropy [4]. The time-dependent deformation under constant load (so-called *creep*) is enhanced by periodic humidity alterations and leads to changes in the radiated spectrum [2]. Furthermore, vibrations accelerate the creep [24].

As known from conversations with the responsible technician, the piano soundboard curvature decreases and increases with a periodicity of one year. In autumn and winter the concert hall is artificially heated which decreases the relative humidity down to 20% at the extreme. As a result the moisture content in the soundboard wood decreases. The wood shrinks and the soundboard 'sinks in'. This has far-reaching consequences: With the soundboard also the bridge sinks in, which changes the angles between strings and bridge. With the angles also the static bridge pressure decreases with all implications on the pre-stressed vibrational behavior of the soundboard [16]. With the bridge also the strings sink in which changes the spatial alignment between strings and hammers. Thereby, as a compensation for changing climate conditions, the technician has to readjust the regulation.

When the heating is disabled in spring and summer, moisture content in the soundboard wood increases and the soundboard rises up again. The static bridge pressure and thereby the pre-stress conditions increase, the strings misalign with the hammers and the action has to be readjusted again. In that respect, technicians speak of 'artificial aging through air conditioning'.

Hunt and Balsan find that playing at generally high humidities leads to increased stiffness and decreased loss coefficient. As a consequence, 'old fiddles (are said to) sound sweeter' than new ones [12]. Hutchins [13] finds that long term playing (5-8 years) of violin family instruments leads to increased amplitudes of body cavity air modes. Bissinger [3] reports a general decrease of modal frequencies for a violin after approx. 250 hours of professional playing. Clemens et al. [8] find no evidence for changes of the vibrational behavior of guitars due to artificial vibration treatment.

Structural modifications on the soundboard are not part of regular maintenance work. In very rare cases, the static bridge pressure might be modified as a one-time adjustment by changing the angle between strings and bridge but this is by no means part of the daily work in a concert hall.

2.5 Disturbances determined by the Experimental Design

Prior to the measurements a technician (the same person in both states) has been asked to tune the instrument with the only instruction to give the piano a regular concert tuning with the same chamber tone. The technician could have influenced the tonal quality of the piano just by tuning in two ways:

1. Pianos are tuned with stretched octaves to compensate for the inharmonic overtone spectrum (*Railsback stretch*) [21]. The degree of tuned octave stretch relies on the judgment of the technician. Following Martin [17], deviations from the Railsback curve could be the tuners handling of soundboard resonances. In this regard different octave stretches could be the technicians response to a change in the vibrational behavior of the piano. In the same course, different octave stretches could lead to perceivable pitch differences between *State 1* and

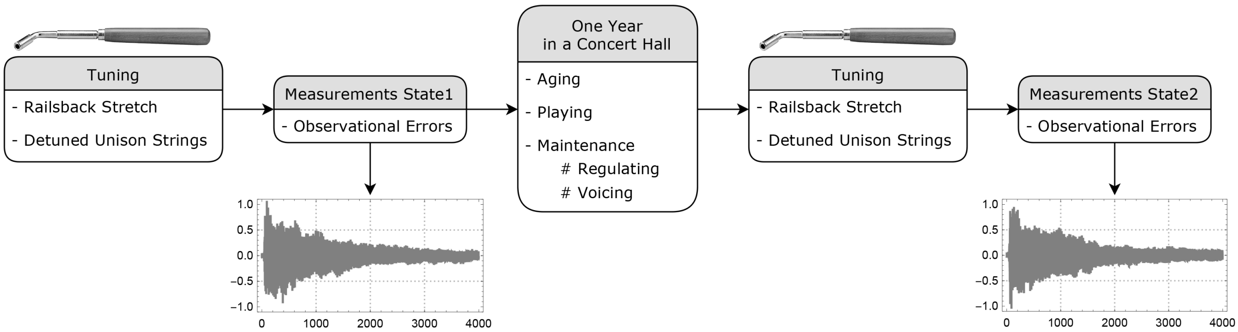

Figure 1. Influential factors and disturbances for the experimental design.

State 2 for the bass and treble range.

2. Technicians usually detune the unison strings by 1-2 cents to give the decay of the tone a complex varying structure [14]. A different degree of detuning of the unison strings for *State 1* and *State 2* could lead to a perceivable difference in the temporal development of the tones harmonic composition.

Thus, the technician who tuned the piano prior to the measurements could have strongly influenced the resulting sound. Both aspects of tuning could have crucial impact on the test because if the piano tones could be discriminated based on effects of a different tuning in the worst case listeners would only discriminate the impact of tuning the instrument and not the impact of aging, playing, and maintenance.

2.6 Study Design Considerations

The decision for a study design depends on the research question in work and is always a trade-off between two contrastive approaches with their respective advantages and drawbacks: On one side an artificial but highly controlled investigation in the laboratory where in an ideal case one independent variable is manipulated and its effect on one or more dependent variable(s) is measured. If well realized, an *experiment* can provide definitive evidence by causal relationships between individual independent- and dependent factors. Nevertheless, these abstracted studies often simplify the problem and thereby lack real relevance to the actual environment.

On the opposite side is the observation of an instrument 'in the field'. The investigation is much closer to real use and practice but control of the influential factors is limited or, in extreme cases, impossible. Randomized assignment to a control group by the researcher is not possible or a control group does not even exist. Although *observational studies* cannot provide definitive evidence by causal relationships due to the possible presence of confounding, they can show correlations between factors. Interpreted with care, these can provide valuable information about real life use and practice [23].

Maintenance work by the piano technician is an inseparable part of 'playing' in concert business. It is unlikely that an instrument would be chosen for concert use if it wasn't finely adjusted. Furthermore, many professional players demand substantial adjustments to be made on the instrument they choose for concert.[1] As described in the previous section, there are numerous influential factors for the tonal characteristics (summarized in Figure 1) which potentially are highly correlated. Moreover, most certainly there are confounding factors, e.g. the periodic curvature change of the soundboard as an independent variable affects dependent variables (psychoacoustic parameters derived from the recordings) but also affects other influential factors like the timing in the action mechanism. Furthermore, for financial as well as logistic reasons it is not possible to have a 'control group' in form of a brand new grand piano with a value of more than 100.000 euro placed into the same concert hall and not be touched or played. And it is not possible to externally control the independent variables, e.g. the

[1] Extensively documented in the awarded documentary film 'Pianomania' from 2009, which covers the work of tuner and technician Stefan Knüpfer from Vienna preparing pianos for concerts: http://www.wildartfilm.com/new/index.php?lang=en&Itemid=136, accessed in June 2019.

author could not instruct the technician to adjust parts with a certain frequency. Thus, the examination can not be conducted under 'controlled' conditions, since the influence of the technician can neither be quantified nor eliminated.

The influence of playing a piano in concert business on it's tonal characteristics can therefore not be reduced to an artificial experiment where it is 'just played'. An examination can only be done with all its disturbances in the field as an observational study.

3 EXPERIMENTAL ARRANGEMENT

Measurements are performed on a concert grand piano after manufacture has been finished and subsequent to regulating, voicing and tuning (further denoted as *State 1*). Subsequently, the instrument is employed by the manufacturer as a rental piano, leased out to a concert hall in Munich, Germany. After having been played for one year and at approx. 40 concerts, the instrument is brought back to Hamburg. The previous measurements are rerun with the exact same conditions (*State 2*). For the recordings the instrument is carried into an anechoic room and the lid is dismounted. For each state a set of 440 *forte* played single notes is recorded (88 keys $\times$ 5 takes).[2] Unfortunately, a standardized mechanical finger could not be used for the study at hand. The sensor head of an impact hammer (*Kistler 9722 A 500*) is used instead to press the keys. As a pre-processing step for the analysis the 5 $\times$ 5 pairs per key are filtered with regard to a maximum difference of key bed contact forces. Based on a pre-test, a maximum possible difference of 0.6 N is chosen for the analysis. This reduces the data base to 1 $\times$ 1 for 74 keys but ensures a highly standardized input. A calibrated artificial head (*Head HSU 3.2*) is placed in player position. A piezoelectric ICP accelerometer (*PCB 352C23*) is attached to the bridge at the corresponding string termination point in direction normal to the soundboard.

4 LISTENING TEST

The aim of the implemented listening test is to answer the following questions: 1. Is a tonal difference audible for a played grand piano before and after a year of concert business? 2. What sound properties lead to a perceivable difference? How do listeners verbalize these differences?

The latter question is approached by analyzing free text input with natural language processing methods. For the first question, the following hypothesis is stated:

- **Null hypothesis** H_0**:** No difference is noticeable for played tones of a concert grand piano before and after the first year of concert business. Results of the listening test are due to chance alone.
- **Alternative hypothesis** H_1**:** Results are due to a factor other than chance.

4.1 Design and Implementation

The ABX double-blind comparison scheme after Clark [7] is an established method to identify differences between stimuli, often used for the evaluation of audio codecs or loudspeaker quality but it also has been used frequently to evaluate research questions in piano acoustics [10, 19]. Each participant receives a randomized sample of 25 unique trials out of 74 possible comparisons. After each discrimination task the participant is asked to describe the 'property which led to a possible discrimination'. The corresponding answer for each trial is typed into a free form data entry field limited to 50 characters. Subsequent to the 25 trials, the following participant variables are inquired: Years of experience as a piano builder, ... as a piano technician, ... as a piano player, or playing a different instrument. The listening test is implemented using *BeaqleJS*, an HTML5/JavaScript framework developed by Kraft and Zölzer [15]. The test is hosted on a website and can

[2] The recordings are available for download as an open access dataset: http://doi.org/10.5281/zenodo.3274772

therefore be reached worldwide[3]. For the statistical analysis cumulative binomial probabilities are used after Burstein [6].

4.2 Results

100 participants from 12 countries completed the listening test. The number of trial completions per key varies from 25 to 50. For the following analysis three sub-groups (disjoint sets) are defined regarding their experience as non-experts, players and builders/tuners (see Table 1). With a hit ratio of 96.3% the builders/tuners sub-group

Table 1. Definition and hit ratio for sub-groups (disjoint sets) with participants i, completed trials n and correct answers c.

Sub-Group	Qualification	Σi	n	c	$c/n \times 100$
Non-Experts	one or less years experience accumulated in building, tuning and playing.	8	185	167	90.3
Builders / Tuners	more than one year experience in building or tuning pianos.	22	544	524	96.3
Players	more than one year experience in playing piano or other instruments and not member of Builders/Tuners sub-group.	70	1708	1593	93.3

has the highest result, followed by the players group with a hit ratio of 93.3%. The non-experts still have a high hit ratio of 90.3%. Statistics for the listening test are calculated according to keys as well as to participants: With an average probability p_{chance} that chance alone is operating of approx. 1e-9, H_0 has to be rejected for both confidence level $> 95\%$ ($CL_{95\%}$) and confidence level $> 99\%$ ($CL_{99\%}$) for all measured keys. In other words, participants can distinguish between the two piano tones for all keys due to one or more factor(s) other than chance. With an average probability p_{chance} that chance alone is operating of approx. 1e-7, H_0 has to be rejected under $CL_{95\%}$ conditions for all but one out of 100 participants. When utilizing the stricter $CL_{99\%}$, H_0 has to be rejected for all but 5 out of 100 participants. In other words, 99% (or 95% for $CL_{99\%}$) of the participants can distinguish between the two piano tones due to one or more factor(s) other than chance. As an intermediate result a strong ceiling effect is observable. Regarding the sub-groups the following statements can be made: H_0 has to be rejected for all participants in the builders/tuners group, in other words, no builder/tuner fails in the listening test. Two out of five participants failing the listening test under $CL_{99\%}$ conditions are non-experts with 0.5 and 1 year experience in piano playing. Three out of five participants failing the listening test under $CL_{99\%}$ conditions are players with 54, 40 and 16 years of experience in instrument playing. The participant failing the test even under $CL_{95\%}$ conditions is a non-expert.

4.3 Verbalizations

After pre-processing the free text input with tokenization, stop word removal, and stemming, the data set contains 2267 total words and 776 unique word forms. A classification of the given word forms is performed and each word is assigned to one of the domains *Timbre*, *Temporal*, *Pitch*, *Loudness*, and *Spatial*. The most dominant key words are related to *Timbre*, *Pitch*, and *Temporal* domain. Examining the data set, a second possible approach of classification becomes apparent: A similar auditory event may be described in terms of three types of foreknowledge, hereafter denoted as *descriptive*, *technical*, and *causal* (compare Table 2). On the

[3] http://musicalinstruments.digital/listeningtest/, accessed in May 2019.

Table 2. Classification of the 50 most frequent words into perceptual domains (average usage percentage in brackets) and levels of foreknowledge.

	Timbre (36%)	Pitch (16%)	Temporal (11%)	Spatial (3%)	Loudness (1%)
causal	*strings, unisons, hammer, needling*				
technical	*partials, beating harmonics, intonation, obertonreicher, resonanz, chorrein*	*pitch, tuning frequency detuned*	*attack, onset sustain, puls decay, nachhall*	*panning stereo, envelope*	*volume loudness*
descriptive	*cleaner, brillanter harder, rounder clearer, metallischer stronger, darker sharper, brighter dumpfer, softer*	*higher lower*	*longer, shorter faster, duration shifting*	*direkter farther*	*louder leiser*

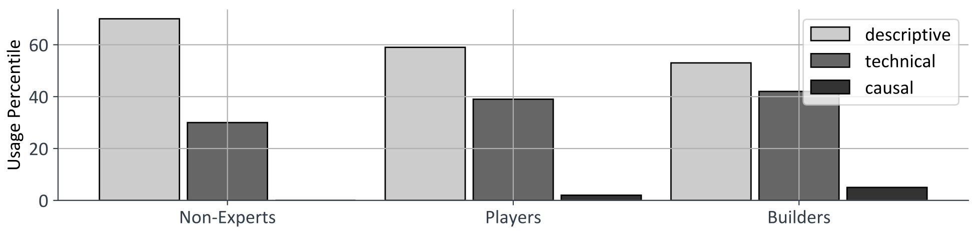

Figure 2. Percentage of used words per sub-group and category.

descriptive level one would verbalize a sensation in terms of descriptive, often metaphoric adjectives, e.g. as *'rough'* or *'dirty'*. On the *technical* level the used terms would presume a certain educational background, e.g. one would write about *'temporal development of higher partials'*, where the term 'partial' would imply a certain music-theoretical or scientific education. On the *causal* level, participants would not describe the acoustical sensation but the instrument component they hold accountable for the sensation. E.g. they would only write *'unison strings'*. The described categories moreover can be understood as representations of different concepts of knowledge: The *technical* vocabulary requires a form of education where technical terms are taught, often related to science and engineering. In contrast, the *causal* vocabulary does not require any theoretical knowledge but a high degree of empirical knowledge which can be informal, and hardly verbalisable but needs years (or sometimes generations) to establish [20].

Figure 2 shows the proportional usage of defined categories for non-experts, players and builders, which can be summarized as follows: *descriptive* vocabulary is most frequently used by non-experts (70%), but even builders and technicians use it to a high degree (53%). The proportion of *technical* vocabulary increases from non-experts over players to builders and tuners. Non-experts do not use *causal* vocabulary at all. Builders have the highest, yet only a 5% proportion of used *Causal* vocabulary.

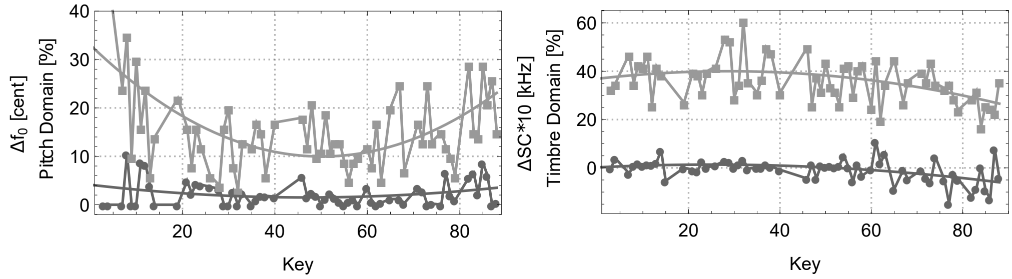

Figure 3. left: f_0 difference between *State 1* and *State 2* in cent (dark circles) vs. usage percentile of *Pitch* domain verbalizations (bright squares).
right: Spectral centroid development $\Delta SC \times 10$ between *State 1* and *State 2* (dark circles) vs. usage percentile of *Timbre* domain verbalizations (bright squares).

5 COMPARISON WITH PSYCHOACOUSTIC AND STRUCTURAL METRICS

5.1 Timbre Domain

The spectral centroid (SC) as a well established indicator for the perception of brightness of complex tones is calculated for all keys. Figure 3 shows the SC difference between *State 1* and *State 2* vs. the percentage of used Timbre domain verbalizations. For the highest octaves SC values decrease from *State 1* to *State 2* which is in accordance with statements by the responsible technician that the treble was too harsh when the piano was delivered which he had to adjust within the following months by needling the hammer felts. Nevertheless, a comparison with the proportion of timbre related verbalizations does not reflect this development: The treble range with the highest SC difference has the lowest proportion of used timbre related words. Calculations of *Roughness* after Sethares [25] and *Sharpness* after Zwicker and Fastl [9] do not show general differences between *State 1* and *State 2*.

5.2 Pitch Domain

Fundamental frequencies (f_0) are estimated for all keys by automated peak picking in the frequency domain.[4] Figure 3 shows the f_0 difference between *State 1* and *State 2* in cent. The differences can be summarized as follows: Apart from three strong outliers, the keys on the bass bridge (key 1-20) are tuned without measurable differences. In the mid range deviations of approx 2.5 cent are observable. In the highest octave deviations of up to 10 cent are observable. These notes are also the hardest to tune properly. The greatest average detuning in the bass and treble range with the minimum in the midrange could be explained with a differently tuned octave stretch since this would be most pronounced in bass and treble range. Professional musicians are able to differentiate pitch differences of a few cents [26], therefore pitch could be a cue in the listening test at least for some keys. A comparison of the measured f_0 differences and the pitch related verbalizations shows some remarkable results (compare Figure 3): For the general trend there is good agreement between measurements and verbalizations with higher values in bass and treble range. However, when looking at the relations in detail, the highest proportion of pitch related verbalizations is given for keys with no measurable difference in f_0 values. For the lowest bass notes this could be explained with the general difficulty to determine a pitch due to the quantity of audible transversal partials, a high degree of inharmonicity, and audible longitudinal partials. But also for some higher notes, 20%-30% of the verbalizations are pitch related with corresponding measured f_0 differences of 0-1 cent. In other words, participants hear a pitch difference, where there is at least no f_0 difference. This could be explained by the fact that for complex tones participants have difficulties to ignore

[4] Note that the lowest measurable harmonic does not always have to coincide with the perceived pitch. For the lowest bass notes the soundboard is not capable to project f_0 and the first measurable frequency component is the octave. Nevertheless, due to the periodicity implied by the quasi-harmonic overtone structure the pitch of the tone is perceived at the *missing fundamental* frequency.

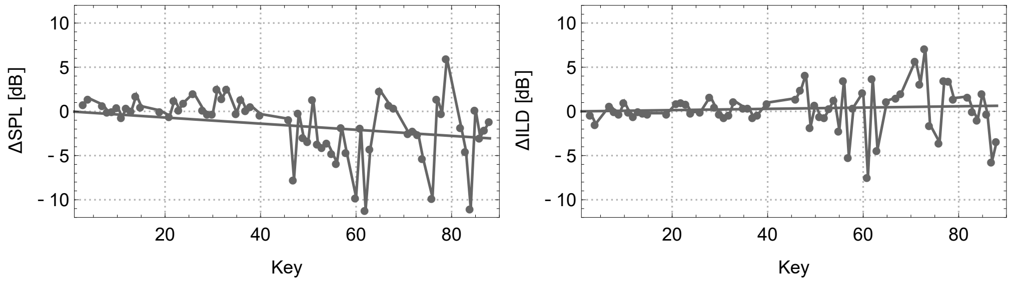

Figure 4. SPL (left) and ILD (right) development between *State 1* and *State 2*.

alterations in brightness (due to changes in the spectral distribution) when making pitch judgments (due to changes of the fundamental frequency) [18].

5.3 Temporal Domain

Notwithstanding the frequent use of words from the temporal domain (11% average per key) like e.g. *attack, onset, faster, shorter,* and *decay*, no general difference is observable, neither for the attack time, nor the decay as reverberation time RT_{60}.

5.4 Spatial and Loudness Domain

The sound pressure level (SPL) is calculated for both dummy head ear channels with reference pressure p_0 = 20 μPa. Up to the chamber tone no difference is observable for SPL or interaural level difference (ILD) (see Figure 4). For the mid- to treble range SPL values decrease within the year which can be explained with softer hammers due to several voicings. For single keys in the treble range SPL values vary up to 10 dB, ILD values vary up to 7 dB, which both should be perceivable. In the same course, with 3% and 1% usage, spatial and loudness attributes may not play an important role for discrimination when differences in more dominant domains like timbre or pitch can be used for the evaluation.

5.5 Driving Point Mobility / Soundboard Crowning

Driving point mobility measurements are performed at the bridge in direction normal to the soundboard plane for both states. The same impact hammer and accelerometer as mentioned in Section 3 are utilized. The soundboard is excited at 10 string termination points on the bridge, all strings are damped, 10 takes per input are recorded. Figure 5 shows an exemplary comparison between *state 1* and *2* for key *F4*. The mean mobility for *state 2* lies within the standard deviation of the *state 1* measurement. Therefore, no significant difference can be observed.

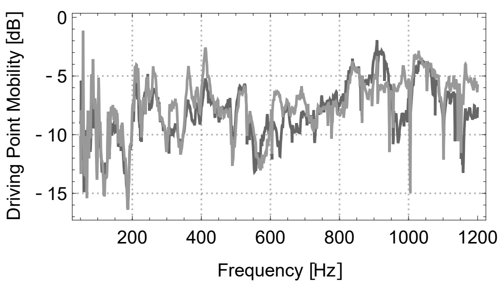

Figure 5. Driving point mobility for state *1* (dark) and *2* (bright) at key *F4*.

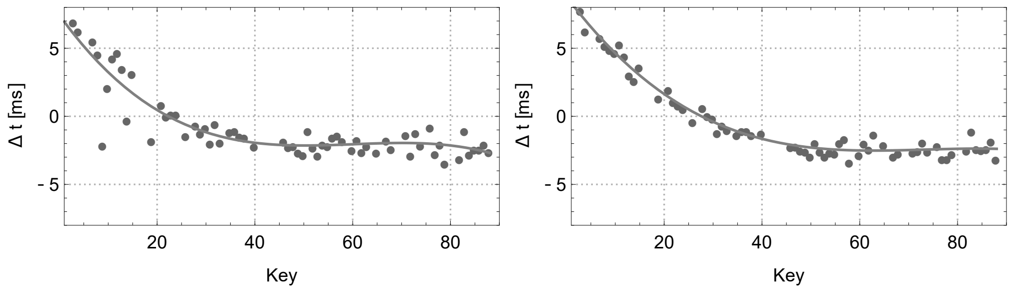

Figure 6. Time delay (Δt) between key bed contact and vibrational activation at the bridge for *State 1* (left) and *State 2* (right).

The soundboard crowning height is measured at several points on the bridge for both states with a laser rangefinder. The maximum crowning difference between states is 1 ± 0.5 mm. As described in Section 2.4, the crowning is expected to vary within a year with amplitudes of up to several millimeters. However, both measurements have been performed in the same season (winter) and therefore the soundboard should have a similar equilibrium moisture content.

5.6 Action Timing

The time delay Δt between key bed contact and vibrational activation of the piano is crucial for the sensation of how 'fast' the piano feels for the player [1]. Although this feature should not have impact for the listening test, it is a good example showing empirical proof for the work of the technician. Figure 6 shows Δt measurements for *State 1* and *State 2*. A general trend is observable with positive delays in the bass range decreasing to the mid range and a constant negative delay in the treble range. Comparison of *state 1* and *2* shows that the outliers in the bass range are leveled and the general variance decreases. This can be explained with maintenance work by the technician who diminished the outliers by regulating to yield a more consistent playing feel.

6 CONCLUSIONS

With regard to the listening test it can be noted that a difference in tonal quality is perceivable for a piano after one year in concert usage even for non-experts. Despite an observable ceiling effect for the test, builders and tuners have the highest competence to make a distinction between piano tones, which is a conclusive result, since this is one of their main professional skills. The most stated properties used to distinguish between piano tones are timbre related, followed by pitch and temporal attributes. Even experts in piano playing or building use descriptive and metaphoric vocabulary to a high degree in describing their sensations. The vocabularies of non-experts, players, and builders differ far less than assumed. In comparison a contrast becomes apparent between clear perceptibility of tonal differences on one hand, and insufficient representability with well established psychoacoustic metrics on the other hand. Although even non-experts seem to perceive small differences in tonal quality of similar piano tones, individual well established psychoacoustic parameters do not seem to be capable to reflect these differences. Due to the study design, no causal relationships can be revealed but within the time frame of one year, the technician can be expected to have much more impact on the tonal development of the piano than the effects of wood aging or playing. The presented findings give the technician to the same extent the responsibility, but also the opportunity to turn a good concert instrument into an excellent one.

ACKNOWLEDGMENTS

This work has been funded by the *Deutsche Forschungsgemeinschaft (DFG)*.

REFERENCES

[1] A. Askenfelt and E. V. Jansson. From touch to string vibrations. I: Timing in the grand piano action. *The Journal of the Acoustical Society of America*, 88(1):52–63, 1990.

[2] A. Beavitt. Humidity cycling. *Strad*, (November):916–920, 1996.

[3] G. Bissinger. Modal Analysis Comparison of New Violin Before and After 250 Hours of Playing. *Proc.13th Intern. Modal Analysis Conf.- Soc. Exp. Mechanics*, (July):822–827, 1995.

[4] I. Brémaud and J. Gril. Effect of transitional moisture change on the vibrational propoerties of violin-making wood. In *Cost FP1302 WoodMusICK annual conference "Effects of playing on early and modern musical instruments"*, 2015.

[5] V. Bucur. *Acoustics of Wood*. Springer Series in Wood Science. Springer-Verlag, Berlin, 2006.

[6] H. Burstein. Approximation Formulas for Error Risk and Sample Size in ABX Testing. *Journal of the Audio Engineering Society*, 36(11):879–883, 1988.

[7] D. Clark. High-Resolution Subjective Testing Using a Double-Blind Comparator. *Journal of the Audio Engineering Society*, 30(5):330–336, 1982.

[8] B. M. Clemens, J. Kadis, D. M. Clemens, E. Pollack, P. Clark, and J. R. Groves. Effect of Vibration Treatment on Guitar Tone: A Comparative Study. *Savart Journal*, pages 1–9, 2014.

[9] H. Fastl and E. Zwicker. *Psychoacoustics: Facts and models*. Springer, 2007.

[10] A. Galembo, A. Askenfelt, L. L. Cuddy, and F. a. Russo. Effects of relative phases on pitch and timbre in the piano bass range. *The Journal of the Acoustical Society of America*, 110(3):1649–1666, sep 2001.

[11] A. J. M. Houtsma. Inharmonicity of wound guitar strings. *The Journal of the Acoustical Society of America*, 71(S1):S9–S9, apr 1982.

[12] D. G. Hunt and E. Balsan. Why old fiddles sound sweeter. *Nature*, 379(6567):681–681, 1996.

[13] C. M. Hutchins. A Measurable Effect of Long-term Playing on Violin Family Instruments. *Catgut Acoustical Society Journal*, 3(5):38–40, 1998.

[14] R. E. Kirk. Tuning Preferences for Piano Unison Groups. *The Journal of the Acoustical Society of America*, 31(12):1644–1648, dec 1959.

[15] S. Kraft and U. Zölzer. BeaqleJS : HTML5 and JavaScript based Framework for the Subjective Evaluation of Audio Quality. *Linux Audio Conference (LAC-2014)*, (May), 2014.

[16] A. Mamou-Mani, S. Le Moyne, F. Ollivier, C. Besnainou, and J. Frelat. Prestress effects on the eigenfrequencies of the soundboards: Experimental results on a simplified string instrument. *The Journal of the Acoustical Society of America*, 131(1):872–877, jan 2012.

[17] D. W. Martin and W. D. Ward. Subjective Evaluation of Musical Scale Temperament in Pianos. *The Journal of the Acoustical Society of America*, 33(5):582–585, 1961.

[18] B. C. J. Moore and B. R. Glasberg. Frequency discrimination of complex tones with overlapping and non overlapping harmonics. *The Journal of the Acoustical Society of America*, 87(5):2163–2177, may 1990.

[19] F. Öberg and A. Askenfelt. Acoustical and perceptual influence of duplex stringing in grand pianos. *The Journal of the Acoustical Society of America*, 131(1):856–871, jan 2012.

[20] S. Petersen. *Vom "Schwachstarktastenkasten" und seinen Fabrikanten - Wissensräume im Klavierbau 1830 bis 1930*. Waxmann Verlag, 2011.

[21] O. Railsback. Scale temperament as applied to piano tuning. *The Journal of the Acoustical Society of America*, 37:2013, 1938.

[22] A. A. Reblitz. *Piano Servicing, Tuning, and Rebuilding*. Vestal Press Inc., 1993.

[23] P. R. Rosenbaum. *Design of Observational Studies*, volume 27 of *Springer Series in Statistics*. Springer New York, New York, NY, 2010.

[24] E. Segerman. Some aspects of wood structure and function. *Catgut Acoustical Society Journal*, 4(3):5–9, 2001.

[25] W. A. Sethares. Local consonance and the relationship between timbre and scale. *The Journal of the Acoustical Society of America*, 94(3):1218–1228, sep 1993.

[26] M. Tervaniemi, V. Just, S. Koelsch, A. Widmann, and E. Schröger. Pitch discrimination accuracy in musicians vs nonmusicians: an event-related potential and behavioral study. *Experimental Brain Research*, 161(1):1–10, 2005.

[27] G. Weldert. Sound Enhancement of Musical Instruments by ’ Playing them in ’: Fact or Fiction? *Europiano*, (9):0–7, 2017.

Perception-based classification of Expressive Musical Terms: Toward a parameterization of musical expressiveness

Aviel Sulem[1], Ehud Bodner[2], Noam Amir[3]

[1] Music & Technology Program, Music Department, Bar-Ilan University, Israel
[2] Department of Music and Interdisciplinary Department of Social Sciences, Bar-Ilan University, Israel
[3] Department of Communication Disorders, Sackler Faculty of Medicine, Tel-Aviv University, Israel

Abstract

Expressive Musical Terms (EMTs) are commonly used by composers as verbal descriptions of musical expressiveness and characters that performers are requested to convey. We suggest a classification of 55 of these terms, based on the perception of professional music performers who were asked (i) to organize the considered EMTs in a two-dimensional plane in such a way that proximity reflects similarity; (ii) to rate these EMTs according to *valence*, *arousal*, *extraversion* and *neuroticism*, using 7-level Likert scales. Using a minimization procedure, we found that a satisfactory partition requires these EMTs to be organized in four clusters (whose centroids are associated with *tenderness*, *happiness*, *anger* and *sadness*) located in the four quarters of the *valence-arousal* plane of the *circumplex model of affect* developed by Russell (1980). In terms of the related *positive-negative activation* parameters, introduced by Watson and Tellegen (1985), we obtained a significant correlation between *positive activation* and *extraversion* and between *negative activation* and *neuroticism*. This demonstrates that these relations, previously observed in personality studies by Watson & Clark (1992a), extend to the musical field.

PROCEEDINGS of ISMA 2019
International Symposium on Music Acoustics
13 - 17 September 2019 in Detmold, Germany

Perception of violin soundpost height differences

Lei FU [(1)]; Claudia FRITZ [(2)]; Gary SCAVONE [(1)]

[(1)] Computational Acoustic Modeling Laboratory, Centre for Interdisciplinary Research in Music Media and Technology, Schulich School of Music, McGill University, Canada, lei.fu2@mail.mcgill.ca; gary@music.mcgill.ca

[(2)] Lutheries-Acoustique-Musique, Institut Jean Le Rond d'Alembert, Unité Mixte de Recherche 7190, Sorbonne Université / Centre National de la Recherche Scientifique, France, fritz@lam.jussieu.fr

Abstract

This experiment explores how changes in soundpost height affect the perceptual qualities of the violin and whether there is a threshold of change below which players and luthiers do not perceive differences. A violin installed with a height-adjustable carbon fibre soundpost was employed. The experiment was designed as a sequence of playing tests. An experimenter was present to change the soundpost height. Thirteen professional violinists and six luthiers participated. The experiment involved two phases. During the first phase, subjects played and described their feelings about the violin with different soundpost settings in order to find their optimal soundpost height. During the second phase, the experimenter randomly increased, decreased or did not change the soundpost height in ten trials within a range of approximately ±0.1 mm around their optimal height. For each trial, subjects were asked to play the violin, comparing it with the previous setting, and to decide whether they were the same or different. Initial results indicate that each subject's optimal soundpost height varies within an interquartile range of 0.3 mm and the smallest height variation that could be recognized above chance level is about 0.04 mm.

Keywords: Soundpost height, Violin, Perception

1 INTRODUCTION

The soundpost (SP) of a violin is an essential component of the instrument. According to luthiers, subtle changes to the soundpost dimensions or position can result in significant variations in the violin sound and playing qualities. The soundpost is typically made of the same wood as the top plate, and it is a cylinder of approximately 0.7 g, 6 mm diameter and a bit longer than 50 mm (1). It provides structural support between the top and back plates and also a means of adjustment in the assembled instruments. As stated by Savart in 1840 (2), the soundpost can help transmit the vibrations from the top plate to the back plate. Through properly interpreted experiments, he also proved that the first acoustical purpose of the soundpost is to introduce asymmetry to the violin.

Jansson et al. (3), Schelleng (4) and Bissinger (1) studied the function of the soundpost through comparison between the violin with soundpost and without soundpost. Jansson et al. (3) employed hologram interferometry to study the resonances of the violin body. They designed an artificial immovable soundpost for observing the interferograms of the plates. A nodal line or a nodal area appeared on the interferograms of the plates around the position of the soundpost when the soundpost was in place and the resonance frequencies increased with a soundpost compared to without a soundpost. The appearance of the modes changed more on the top plate than the back plate when the soundpost was installed. Double exposure holograms on the complete instrument while pressing strings against the fingerboard showed that the maximum deformation of the back plate is at the soundpost. Schelling (4) approximated the violin body as a closed cigar box and the soundpost as immovable to explain the effect of the soundpost in enhancing the sound radiation. Without the soundpost, the strongest radiating mode is not excited. Also, he explained that the appearance of a new body mode with the soundpost installed depends on the adjacent modes without soundpost that do not have a null at the soundpost position. He then abandoned the assumption of the immovable soundpost and found that the admittance of the contact point of the soundpost and back plate is the smallest compared to the top plate and the ribs, i.e., it is unnecessary to assume all motion of the back plate is ascribed to the soundpost. Bissinger (1) employed a modal analysis method to test an unvarnished violin. The peaks in the accelerance spectra did not show a substantial shift in frequency with soundpost or without soundpost, and the large peaks usually stayed large. About one-third of the peaks in the no-SP spectrum did not correlate easily to the SP spectrum, and the correlation reliability generally dropped with increasing mode frequency. Using the modal analysis data, he calculated the radiation efficiency of the violin. He observed a very considerable radiation efficiency enhancement of SP over no-SP in the region of 500-800 Hz, in which there are some very important peaks in the response or radiativity curves. Overall, the average radiation efficiency increased by 17% with the soundpost installed. Simulated response curves and Fourier spectra of bowed slide tones of this violin showed that removing the soundpost weakened the frequency response as well as the overall acoustical response from 0 to 2 kHz, and this effect is much more substantial in the frequency range of 400 to 800 Hz.

Saldner et al. (5) studied the action of the soundpost by employing a TV-holography technique to visualize the modal patterns of an unvarnished violin in real time and measuring bridge admittance of the violin. They compared the violin without soundpost, with soundpost in normal position and with soundpost 10 mm closer to the centerline. Through the bridge admittance measurements, they found that the magnitude of the B1- peak stays about the same with soundpost in normal position or 10 mm closer toward the centerline; the frequency of the B1- peak increases by 25 Hz (5%) when moving the soundpost closer to the centerline. The magnitude of the B1+ mode however increased considerably when shifting the soundpost closer to the centerline, with the frequency of the B1+ mode remaining about the same. In observing the holographic vibration distributions for the B1- mode, they found a similar frequency shift as in the bridge admittance measurements. Compared to without soundpost, they found that the main vibrations in the top plates are shifted to the opposite side to the soundpost. There are small vibrations or a nodal line at the soundpost position. The soundpost makes it possible for the symmetric vibration modes to be excited by the bridge.

Jansson (6) measured the bridge admittance to compare the violin with soundpost and without soundpost as well. He found that the magnitude of the “bridge hill” (BH) is the highest with soundpost in the bridge admittance measurement, while without the soundpost, the magnitude of a peak at approximately 550 Hz is the highest. He also explored the effect of the soundpost position on the violin timbre. The soundpost was moved closer toward the bridge or further away from the bridge, and closer to the centerline or towards the nearby f-hole by 5 mm. The BH was attenuated when the soundpost was moved closer to the bridge, and the timbre turned shaper; the BH was increased when the soundpost was moved away, and the timbre became softer. The magnitude of the B1+ peak increased with the soundpost moved towards the centerline, and the timbre turned darker; the magnitude of the B1+ peak decreased with the soundpost moved towards the nearby f-hole, and the timbre became lighter. However, no formal perceptual evaluation of the violin timbre variation was conducted.

Most of the previous research studying the role of the soundpost is from physics and acoustics aspects. How the soundpost affects the perceptual qualities of the violin, however, has not been properly investigated. As often described by luthiers or players, a very subtle change to the soundpost dimension or position can result in significant variations in the violin quality, especially when the changes are around the optimal soundpost condition. Therefore, the aim of this study was to investigate correlations between a change in height of the soundpost and variations of the quality of the violin, as evaluated by players.

We decided to focus on soundpost height variations, as it is difficult to specify repeated position changes with sufficient accuracy and speed during a playing experiment. A height-adjustable soundpost was employed for this experiment. Violinists and luthiers were invited to evaluate the violin with different soundpost heights through playing tests with controlled experimental conditions. The first question to be explored is how big of a change in the soundpost height could result in perceivable variations in the violin qualities by violinists and luthiers. In addition, the changes of interest should be around each subject’s optimal soundpost height. Detailed materials and method are described in Section 2. Section 3 presents the results and discussion. Conclusions are given in the final section.

2 MATERIALS AND METHOD

2.1 General design

This experiment explores how changes in soundpost height affect the perceptual qualities of the violin and whether there is a threshold of change below which players do not perceive differences. A violin installed with a height-adjustable carbon fibre soundpost was employed. The experiment was designed as a sequence of playing tests. An experimenter was present to change the soundpost height. Violinists and luthiers were invited to participate. The experiment involved two phases. During the first phase, subjects played and described their feelings about the violin with different soundpost settings in order to find their optimal soundpost height. During the second phase, the experimenter randomly increased, decreased or did not change the soundpost height in ten trials around their optimal height. For each trial, subjects were asked to play the violin, comparing it with the previous setting, and to decide whether they were the same or different.

Players were asked to use their own bows to play the violin and evaluate, as they typically use their own bows when testing violins in real life. Luthiers were given the option of either using their own bow if they play violin or to use a bow provided by us. This experiment took place in a room free of strong resonances and a relatively low reverberation time. The area of the experiment room was approximately 26.7 m^2.

2.2 Soundpost and violin

A height adjustable carbon fibre soundpost (Anima Nova) was employed for this study, as shown in Figure 1. According to the description by the manufacturer (Anima Nova), the soundpost has flexible ball-and-socket joints at its two ends, which allow the soundpost to adjust automatically to every contour of the violin whilst distributing the pressure evenly over the contact area. The upper cylinder shell possessing a scale on its bottom is sheathed with the lower cylinder through an internal thread, and one can increase or decrease the soundpost height by turning the upper cylinder shell anticlockwise or clockwise. A vertical line indicated on the surface of the lower cylinder acts as the pointer of the scale. A height change is specified by a number of graduations. The minimum graduation value is 0.02 millimeter and the scale employs an octal number system. By turning one complete revolution, the soundpost height varies 0.64 mm. There are 5 numbers ranging from 0 to 4 on the scale. Between adjacent numbers, there are 8 minimum graduations. Through the special tools provided by Anima Nova, one can change the soundpost height without taking it out of the violin body. Two adjacent numbers can always be seen simultaneously from the f-hole.

Figure 1. Anima Nova height-adjustable soundpost

The violin used in this experiment is a performance-level violin borrowed from Schulich School of Music, McGill University. We asked a local luthier to help replace the original wooden soundpost (around 53.77 mm high) with the Anima Nova height-adjustable soundpost. The height-adjustable soundpost was placed about 3.5-4 mm below the bridge and centered with the treble foot of the bridge according to the soundpost manufacturer’s instruction. The soundpost was set initially at a relatively low height, approximately 53 mm.

2.3 Participants

Thirteen experienced violinists and six skilled luthiers participated in this experiment. Among the players, there were 8 females, 5 males; 7 native English speakers, 3 native Chinese speakers and 3 other native speakers. Their average age was 30 yrs (SD=9 yrs, range=21-54 yrs). They had at least 16 years of playing experience (mean=23 yrs, SD=7 yrs, range=16-40 yrs), and at least 8 years of training (mean=18 yrs, SD=4 yrs, range=8-26 yrs). They reported to play 23 hours per week on average (SD=10 hrs, range=6-37.5 hrs). Eleven players described themselves as professional violinists. One of the players was a doctoral candidate in music performance, 2 had master's degrees in music performance, 4 were master students in music performance, 3 had bachelor's degrees in music performance, 1 had a bachelor's degree in arts, and 2 were currently undergraduate students in music. They reported to play various types of music [classical (100%), contemporary (69%), jazz/pop (38.5%), baroque (23.1%), and folk (15%)]. 85% of them play in chamber music, symphonic orchestra or solo, respectively. One of the players play in Folk/Jazz band, pop band, chamber orchestra or work as a private music teacher, respectively. Among the luthiers, there were 4 males, 2 females; 3 native English speakers and 3 native French speakers. Their average age was 48.5 yrs (SD=11 yrs, range=36-61 yrs). They had at least 15 years of experience being a violin maker. Five luthiers played violin, among them there were 1 professional violinist, 2 advanced players and 2 beginners. All subjects were paid for their participation.

2.4 Detailed procedure

This experiment consisted of two phases and lasted about 1 hour. Subjects were scheduled individually. Two experimenters were present during the experiment. One experimenter, who made adjustments to the soundpost, sat behind a table, with a screen in front to prevent subjects from observing the adjustments. The other experimenter helped with facilitating the experiment and taking notes for the subjects. During the first phase, the soundpost was initially set at a relatively low height, around 53 mm. Subjects were then asked to play the violin with this initial setting and describe their feelings. Then the experimenter increased the soundpost height by 8 graduations, or about 0.16 mm and the subjects repeated the playing and describing process. Depending on the subjects' descriptions, the experimenter decided to increase or decrease the soundpost height by different graduations in order to find their most preferred setting, which required from 5 to 9 trials. Each soundpost height adjustment took about a minute to complete.

There was a 5-minute break between phase 1 and phase 2. During the second phase, the experimenter randomly increased, decreased or did not change the soundpost height in ten trials within a range of approximately ±0.1 mm around their optimal height. Subjects were asked to play the violin during each trial and compare it with the previous setting, to decide whether they were the same or different. At the beginning of phase 2, subjects were asked to play the violin with their optimal soundpost heights again. Then the experimenter increased, decreased, or did not change the soundpost height by different graduations over ten trials according to a plan determined in advance, which was unknown to subjects. The height variations are ΔH=0, 0, 2, -2, 3, -3, 4, -4, 5, -5 graduations (actual height of ΔH = 0, 0, 0.04, -0.04, 0.06, -0.06, 0.08, -0.08, 0.1, -0.1 mm). They were randomized differently for each subject, while keeping the variations approximately within ±0.1 mm around the subjects' optimal height. To minimize subject fatigue, there was a 5-minute break after five trials.

Thresholds were estimated using detection theory (7). As shown in Table 1, we have two stimulus classes. Height variations of ΔH=0 are class S1, and ΔH=2, -2, 3, -3, 4, -4, 5, -5 are different cases of the S2 class. A "Hit" is defined as a correct identification of an S2 class element (participants recognize a height change). A "False alarm" is defined as an incorrect identification of an S1 class element (they think the height changed when no variation of the soundpost height was made). Table 1 summarizes the four possible cases. The hit and false-alarm rates can be written as the following probabilities:

$$H = P(\text{“Different”} \mid S2) \quad (1)$$

$$F = P(\text{“Different”} \mid S1) \quad (2)$$

The perceptual sensitivity is estimated using the d' measure: d' is defined in terms of the inverse of the normal distribution function z:

$$d' = z(H) - z(F) \quad (3)$$

Thus, when H=F, d'=0 and the performance is at chance; when H>F, d'>0, which means that subjects are able to recognize a difference in height. The sensitivity of detection increases as d' increases. When H=0.99, F=0.01, d'=0.465: this is considered as an effective ceiling by many experimenters. By calculating d' for each ΔH, we can estimate the sensitivity in soundpost height variation.

Table 1. Different responses for different stimulus classes

Stimulus Class	Response	
	"Different"	"Same"
Different soundpost height (S2)	Hits	Misses
Same soundpost height (S1)	False alarms	Correct rejections

3 RESULTS AND DISCUSSION

3.1 Optimal soundpost heights

During the first phase of the experiment, we found an optimal soundpost height for each subject. The optimal soundpost heights were represented relative to the original soundpost height (around 53 mm). Figure 2 shows the relative optimal soundpost height of each subject sorted from smallest to largest. Figure 3 displays the boxplots of the relative optimal soundpost height for all subjects, players and makers separately. The interquartile ranges of the relative optimal soundpost height for these three groups are 0.3 mm, 0.32 mm and 0.26 mm, respectively. The interquartile range for makers is smaller than players, the median relative optimal soundpost height for makers (0.28 mm) is also lower than for players (0.36 mm). The mean relative optimal soundpost height and SD for all subjects are 0.34 mm and 0.156 mm. The corresponding mean and SD for players and makers are 0.36 mm, 0.163 mm and 0.3 mm, 0.143 mm, respectively. Players had a higher mean relative optimal soundpost height than makers. Figure 4 displays the mean relative optimal soundpost height for all subjects, players and makers separately. Error bars of two-sided 95% confidence interval of the means are also displayed. The confidence interval error bar of the means for makers is very high, which might be partially due to the small number of maker participants. We compared the relative optimal soundpost height for players and makers by performing the independent-samples Mann-Whitney U test. The results showed that the null hypothesis that the distribution of the relative soundpost height was the same across players and makers could not be rejected, $U=28$, $z=-0.969$, $p=0.368$.

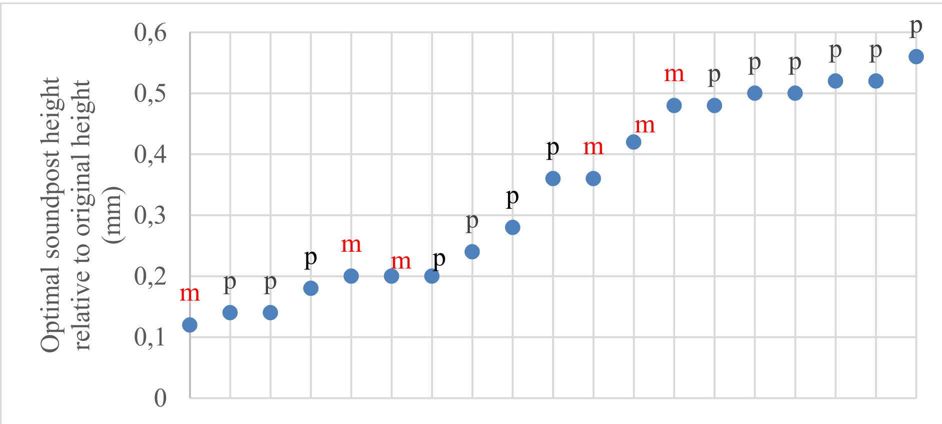

Figure 2. Optimal soundpost height relative to original height for each subject (m: makers; p: players)

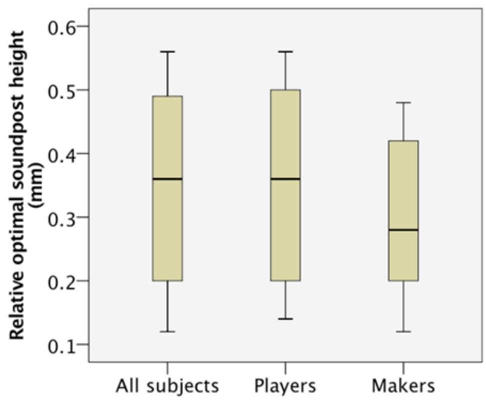

Figure 3. Boxplot of the optimal soundpost height relative to original height for all subjects, players and makers

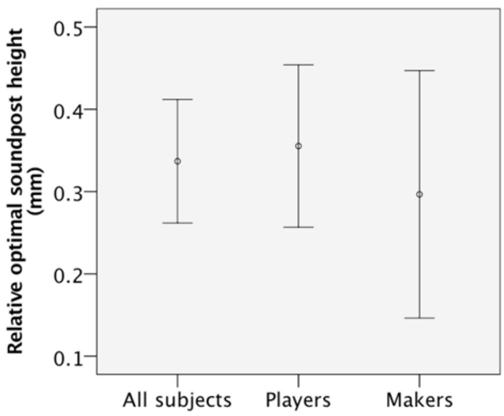

Figure 4. Mean optimal soundpost height relative to original height for all subjects, players and makers (error-bar = 95% confidence interval of the mean)

3.2 Perceptual threshold of soundpost height differences

As described in the detailed procedure, we can estimate the threshold of the soundpost height differences by calculating a sensitivity measure d' for each ΔH. During phase 2 of this experiment, positive ΔH and negative ΔH were counterbalanced by randomizing the presentation of positive ΔH and corresponding negative ΔH for subjects. In addition, in order to increase the number of test trials (sample size) and estimate the threshold more precisely, we calculated d' for each |ΔH| instead of each ΔH. Figure 5(a) shows the probabilities that subject considered the two soundpost heights with a height difference of |ΔH| as "different". We can see that the false alarm rate, which corresponds to P ("different") for ΔH=0 mm is very high: 0.71. It is even higher than the hit rate for |ΔH| =0.06 mm: 0.68. The highest hit rate is for |ΔH| =0.08 mm: P ("different") =0.84. The d' for each |ΔH| is shown in figure 5(b). d' for |ΔH| =0.04, 0.08, 0.1 mm are bigger than 0, implying that subjects could recognize soundpost height changes of 0.04, 0.08 and 0.1 mm at greater than chance level. It is however surprising that d' is negative for |ΔH| =0.06 mm as, in this range of |ΔH|, an increase of the sensitivity would have been expected with an increase of |ΔH|.

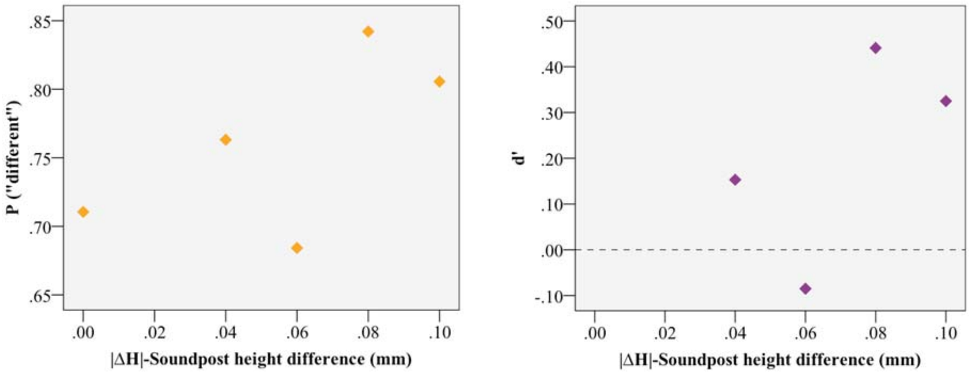

(a) (b)

Figure 5. (a) Probabilities subjects considered the two soundpost heights with a height difference of |ΔH| as "different"; (b) perceptual sensitivity d' for each |ΔH|

In figure 6, we compare the results for players and makers. Dividing the population into two groups can be problematic because it reduces the amount of data in each group (which was already low), especially in the group of makers. The following results may only be indicative. Figure 6(a) displays the probabilities that players and makers considered the two soundpost heights with a height difference of |ΔH| as "different". We can see that the false alarm rate for makers (0.75) is higher than for players (0.69). The hit rates for makers vary more with |ΔH| than for players. The hit rates for |ΔH| =0.04 mm and 0.06 mm are much lower for makers than players, while the hit rate for |ΔH| =0.08 mm is much higher for makers (1) than players (0.77). The corresponding d' for each |ΔH| of makers and players are shown in figure 6(b). All d' for |ΔH| ≥0.04 mm is greater than 0 for players, while only d' for |ΔH| =0.08 mm and 0.1 mm are greater than 0 for makers.

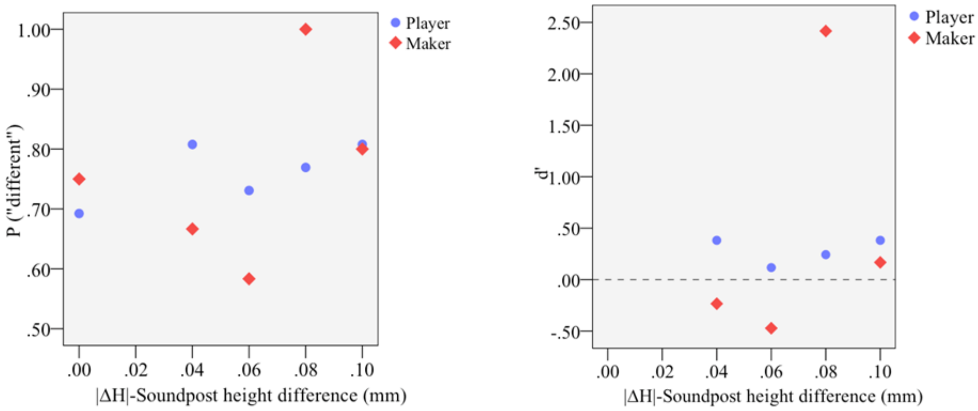

(a) (b)

Figure 6. (a) Probabilities players or makers considered the two soundpost heights with a height difference of |ΔH| as "different"; (b) perceptual sensitivity d' of each |ΔH| for players and makers, respectively

4 CONCLUSIONS

In this experiment, we explored violinists' and luthiers' perception of violin soundpost height differences through a playing test. By employing a height-adjustable soundpost, we were able to find the optimal soundpost height for each subject and investigate the perceptual sensitivity to soundpost height differences around each subject's optimal soundpost height.

The results showed that the optimal soundpost height for each subject varies within an interquartile range of

0.3 mm. The variation interquartile range is higher for players (0.32 mm) than for makers (0.26 mm). The mean relative optimal soundpost height is also higher for players (0.36 mm) than for makers (0.3 mm). Statistical analysis showed that the differences of the relative optimal soundpost height for players and makers were not significant. The perceptual threshold of the soundpost height differences around each subject's optimal soundpost height was estimated through calculating a perceptual sensitivity measure of d'. The results for all subjects showed that subjects could recognize height changes of 0.04 mm, 0.08 mm and 0.1 mm at better than chance levels, but couldn't recognize the height change of 0.06 mm. Further investigation showed that the biggest fluctuation came from the makers' results. Players could recognize height changes of 0.04 mm and greater at above chance levels, but makers could only recognize the height changes of 0.08 mm and greater.

Overall, the subjects performed at only a little bit greater than chance level in recognizing the differences we presented. And the false alarm rate was very high, i.e., subjects tended to say "different" even though there was no change at all in the soundpost height. That might partly be due to the sequential nature of the trials (they could not compare the different settings at the same time) and thus they might forget what the previous setting was like (though it only took a minute or less to make the soundpost changes). As well, there was a significant amount of variation in their organization approach to violin evaluation. Some subjects used a very consistent set of playing materials for each trial, while others used either very limited or changing materials between trials. Makers were in general significantly less skilled than players and thus may not have been able to "explore" the full range and capabilities of the violin. Additionally, the variation of soundpost height was quite small (within ±0.1 mm), which made the task very difficult and could have contributed to player fatigue, so perhaps the true perceptual threshold is beyond that range. Finally, there was some imprecision in soundpost adjustments, with an absolute average error of 0.007 mm. All these factors could have had an effect on our results.

ACKNOWLEDGEMENTS

We acknowledge support and funding from the Centre for Interdisciplinary Research in Music Media and Technology, the Natural Sciences and Engineering Research Council of Canada, Hector and Ada Ma China Scholarship Council and the China Scholarship Council. We would like to thank the inventor of the Anima Nova height-adjustable soundpost, Pal Molnar, for generously loaning the soundpost to us, as well as for instructions on the installation and use of the soundpost. We thank the Schulich School of Music for loaning the violin for the experiment. We are also grateful to Tom Wilder for helping with the installation of the soundpost to the violin.

REFERENCES

[1] Bissinger, G. Some mechanical and acoustical consequences of the violin soundpost. The Journal of the Acoustical Society of America, Vol 97 (5), 1995, pp 3154-3164.

[2] F. Savart, ‘‘The violin,’’ L'Institut 8, 1840, pp 54–56. [English translation by D. A. Fletcher and printed in Musical Acoustics, Part I, Violin Family Functions, Vol 5, Benchmark Papers in Acoustics, edited by C. M. Hutchins, Dowden, Hutchinson, and Ross (Stroudsburg, PA, 1975), pp 323 – 327.]

[3] Jansson, E., Molin, N. E., & Sundin, H. Resonances of a violin body studied by hologram interferometry and acoustical methods. Physica scripta, Vol 2(6), 1970, pp 243-256.

[4] Schelleng, J. C. The action of the soundpost. Catgut Acoust. Soc. Newsletter No. 16, 1971. 11-15.

[5] Saldner, H. O., Molin, N. E., & Jansson, E. V. Vibration modes of the violin forced via the bridge and action of the soundpost. The Journal of the Acoustical Society of America, Vol 100 (2), 1996. pp 1168-1177.

[6] Jansson, E. Acoustics for Violin and Guitar Makers. Kungl. Tekniska högskolan, Department of Speech, Music and Hearing, 4th edition. Retrieved from http://www.speech.kth.se/music/acviguit4/ (Accessed: 27 June 2019).

[7] Macmillan, N. and Creelman, C. Detection Theory: A User's Guide. Mahwah (America): Lawrence Erlbaum Associates, 2nd edition, 2005.

AUTHOR INDEX